The GROMOS Software for (Bio)Molecular Simulation

Volume 2: Algorithms and Formulae for Modelling of Molecular Systems

January 9, 2021

Contents

Chapter 1. Introduction 2-1

Chapter 2. Basic choices in the definition of a molecular model 2-3
2.1. Introduction 2-3
2.2. Choice of degrees of freedom 2-4
2.3. Choice of the description of the interaction 2-5
2.4. Choice of method for configuration generation 2-6
2.5. Choice of the boundary conditions 2-8

Chapter 3. Scope of the GROMOS package 2-9
3.1. Introduction 2-9
3.2. Choice of the degrees of freedom 2-9
3.3. Choice of the description of the interaction 2-9
3.3.1. Charge groups, searching neighbours 2-10
3.3.2. Twin-range method for long-range interactions 2-11
3.3.3. Pairlist construction 2-11
3.4. Choice of the method for the configuration generation 2-12
3.5. Choice of the boundary conditions 2-12

Chapter 4. Spatial boundary conditions 2-13
4.1. Introduction 2-13
4.2. Vacuum boundary conditions (VBC) 2-13
4.3. Fixed boundary conditions (FBC) 2-14
4.4. Periodic boundary conditions (PBC) 2-15
4.4.1. Triclinic computational box under PBC 2-16
4.4.2. Special periodic boundary conditions 2-21
4.4.3. Multiple unit-cell simulations under PBC 2-22
4.4.4. Rectangular-brickwall box 2-23

Chapter 5. Bonded interaction force-field terms 2-25
5.1. Bond stretching force-field term 2-25
5.2. Bond-angle bending force-field term 2-26
5.3. Improper dihedral-angle bending force-field term 2-26
5.4. Proper dihedral-angle torsion force-field term 2-27

Chapter 6. van der Waals interactions 2-31
6.1. Introduction 2-31
6.2. Excluded neighbours 2-31
6.3. Normal van der Waals interactions 2-31
6.4. Third-neighbour van der Waals interaction 2-32
6.5. Soft-core interactions 2-33

Chapter 7. Electrostatic interactions 2-35
7.1. Introduction 2-35
7.2. Common features 2-35
7.3. Reaction-field (RF) interactions 2-36
7.4. Lattice-sum (LS) interactions 2-36
7.4.1. Introduction 2-36
7.4.2. Real-space interactions in LS electrostatics 2-44

7.4.3. Ewald reciprocal-space interactions in LS electrostatics 2-44
7.4.4. PPPM reciprocal-space interactions in LS electrostatics 2-46
7.5. Polarization 2-55
7.5.1. Introduction 2-55
7.5.2. Theory 2-56
7.5.3. Off-atom sites 2-58
7.5.4. Non-linear polarizability 2-59

Chapter 8. Coarse-grained models and multi-resolution simulation 2-61
8.1. Introduction 2-61
8.2. Multi-resolution simulation 2-64

Chapter 9. Special force-field terms 2-65
9.1. Introduction 2-65
9.2. Atom-position restraining or fixed atoms 2-65
9.3. Distance restraining 2-66
9.4. Virtual and pseudo atoms 2-70
9.4.1. CH1-group (aliphatic) 2-72
9.4.2. CH1-group (aromatic) 2-72
9.4.3. CH2-group (two virtual protons) 2-73
9.4.4. CH2-groups (one pseudo site) 2-74
9.4.5. CH3-group (one pseudo site) 2-74
9.4.6. Two CH3-groups (one pseudo site) 2-74
9.4.7. Three CH3-groups (one pseudo site) 2-74
9.4.8. Center of geometry (one pseudo site) 2-75
9.4.9. Center of mass (one pseudo site) 2-75
9.5. Bond-angle restraining 2-75
9.6. Dihedral-angle restraining 2-75
9.7. ^3J-coupling constant restraining 2-76
9.8. S^2-order parameter restraining 2-82
9.9. X-ray structure factor amplitude restraining 2-84
9.10. X-ray electron density restraining 2-85
9.11. X-ray crystallographic symmetry restraining 2-85
9.12. Distance-field distance restraining 2-86
9.13. Biasing energy functions 2-88
9.13.1. Local elevation biasing 2-88
9.13.2. Umbrella sampling 2-89
9.13.3. Local elevation umbrella sampling (LEUS) 2-89
9.13.4. Ball and stick LEUS 2-90

Chapter 10. Constraints 2-95
10.1. Introduction 2-95
10.2. Position Constraints 2-96
10.3. Constraints using the SHAKE method and its derivatives 2-96
10.3.1. Constraints using the SHAKE method 2-96
10.3.2. Constraints using the SETTLE method 2-99
10.3.3. Constraints using the LINCS method 2-100
10.3.4. Constraints using the M-SHAKE method 2-101
10.3.5. Constraints using the FLEXSHAKE method 2-102
10.3.6. Constrained positions 2-102
10.3.7. Constrained velocities 2-102
10.3.8. Constrained forces 2-103
10.4. Bond-length constraints in the solute 2-103
10.5. Bond-length and bond-angle constraints in solvent 2-104
10.6. Dihedral-angle constraints 2-104
10.7. Translational and rotational constraints 2-107

Chapter 11. Energy Minimization 2-111

11.1. Introduction 2-111
11.2. Steepest-descent minimization 2-112
11.3. Conjugate-gradient minimization 2-112
11.4. Steepest-descent minimization with constraints (SHAKE) 2-114
11.5. Conjugate-gradients minimization with constraints (SHAKE) 2-115

Chapter 12. Molecular Dynamics 2-119
12.1. Introduction 2-119
12.2. Temperature scaling 2-120
12.2.1. Temperature calculation in MD++ 2-120
12.2.2. Thermostat algorithms in MD++ 2-121
12.2.3. Use of temperature groups, sets of degrees of freedom and thermostats 2-124
12.3. Number of degrees of freedom 2-125
12.4. Calculation of the virial 2-126
12.5. Pressure scaling 2-128
12.6. MD algorithms 2-130
12.7. Initialization, equilibration and sampling 2-131

Chapter 13. Stochastic Dynamics 2-137
13.1. Introduction 2-137
13.2. Leap-frog SD algorithm 2-137
13.3. Choice of atomic friction coefficient 2-141

Chapter 14. Free Energy Determination 2-143
14.1. Introduction 2-143
14.2. Parameterization of the Hamiltonian 2-144
14.2.1. Covalent bond forces 2-145
14.2.2. Covalent bond forces (soft potential energy function) 2-147
14.2.3. Covalent bond-angle forces 2-149
14.2.4. Covalent bond-angle forces (soft potential energy function) 2-151
14.2.5. Improper dihedral-angle forces 2-151
14.2.6. Improper dihedral-angle forces (soft potential energy function) 2-153
14.2.7. Dihedral-angle torsion forces 2-154
14.2.8. Non-bonded forces 2-156
14.2.9. Polarization 2-158
14.2.10. Perturbed atom-atom distance restraints 2-161
14.2.11. Perturbed dihedral angle restraints 2-164
14.2.12. Perturbed distance-field distance restraints 2-165
14.3. Constraints 2-166
14.4. Assigning different $\lambda-$dependences for specific groups of atoms 2-167
14.5. Choice of pathway and states A and B 2-170
14.6. Thermodynamic integration 2-172
14.7. Thermodynamic perturbation and extrapolation 2-173
14.8. Umbrella sampling 2-174
14.9. Enveloping Distribution Sampling 2-176
14.9.1. EDS with smoothness parameter s 2-176
14.9.2. Accelerated EDS 2-178
14.9.3. Twin-system EDS 2-180
14.9.4. Configurational EDS 2-180

Chapter 15. QM/MM simulation 2-185
15.1. Introduction 2-185
15.2. Hamiltonian 2-185
15.3. Initialization, simulation and analysis 2-187

Chapter 16. Replica Exchange (RE) Molecular Dynamics 2-189
16.1. Introduction 2-189
16.2. Temperature replica exchange MD 2-190

16.2.1. Simulation checks 2-191
16.2.2. Factors determining the efficiency 2-192
16.3. Hamiltonian replica exchange MD 2-192
16.4. Initialization, simulation and analysis 2-192
16.4.1. Set up of a RE simulation 2-192
16.4.2. Analysis of a RE trajectory 2-193

Chapter 17. Derivatives of the force-field terms 2-195
17.1. Bond stretching force-field term 2-195
17.2. Bond-angle bending force-field term 2-195
17.3. Improper dihedral-angle bending force-field term 2-196
17.4. Proper dihedral-angle torsion force-field term 2-196
17.5. LJ interaction terms 2-197
17.6. Electrostatic interaction terms: Coulomb plus reactive field 2-197
17.7. Electrostatic interaction terms: lattice sum 2-197

Chapter 18. Appendices 2-199
18.1. Conversion of force constants: bond-stretching and bond-angle bending interactions 2-199

Bibliography 2-i

CHAPTER 1

Introduction

In this volume, the molecular model, the molecular interactions, and the computational procedures used in GROMOS are described. Chap. 2 discusses the basic choices in the definition of a molecular model in a general way. The application of these choices within GROMOS are outlined in Chap. 3. Chap. 4 discusses various aspects of the spatial boundary conditions implemented in GROMOS. Chaps. 5, 6 and 7 deal with the description of molecular interactions divided into covalent interactions (Chap. 5), nonbonded van der Waals interactions (Chap. 6) and nonbonded electrostatic interactions (Chap. 7). Chap. 8 describes coarse-grained interactions between supra-molecular particles representing sets of identical molecules. Chaps. 9 and 10 deal with geometrical boundary conditions, which may be either imposed on the system in a soft way, using restraints (Chap. 9) or enforced in a hard way, defined as constraints (Chap. 10). The next three chapters involve searching and sampling of conformational space using energy minimization (Chap. 11), molecular dynamics (Chap. 12), or stochastic dynamics (Chap. 13). Chap. 14 deals with the calculation of free-energy differences and QM/MM simulations are described in Chap. 15. In Chap. 16 the implementation of replica exchange methods in GROMOS is discussed. In Chap. 17 all contributions to the molecular forces and the virial due to the interactions described in Chaps. 5 - 8 are collected and Chap. 18 forms an appendix with mathematical details on the conversion between different types of force constants.

CHAPTER 2

Basic choices in the definition of a molecular model

2.1. Introduction

The four *basic choices*[1–3] involved in the definition of a molecular model are (Fig. 2.1) :

A. Choice of the *degrees of freedom*[3,4] (Sec. 2.2) :
What are the variables of the model, *i.e.* those uniquely defining a system configuration in this model. Most commonly, this choice is equivalent to that of the elementary particles, *i.e.* smallest entities, considered by the model, *i.e.* the model resolution. The selected degrees of freedom are treated explicitly by the model. In contrast, degrees of freedom internal to the selected elementary particles are handled implicitly.

B. Choice of the description of the *interaction*[4] (Sec. 2.3) :
What is the Hamiltonian operator for quantum-mechanical degrees of freedom or the Hamiltonian function for classical degrees of freedom describing the interaction and kinetic energy associated with the selected degrees of freedom. This interaction must incorporate the mean effect of the implicit degrees of freedom on the explicit ones.

C. Choice of method for the *configuration generation*[5,6] (Sec. 2.4) :
What method will be used to generate configurations of the system *i.e.* values for the variables defining the degrees of freedom of the model, generally based on information from the corresponding interaction. The selection of a method, e.g., MC, MD or SD, affects the properties of the resulting set of configurations in terms of structural, thermodynamic and dynamic properties.

D. Choice of the *boundary conditions*[7] (Sec. 2.5) :
What are the global restrictions imposed on the system during the configuration generation. These restrictions may represent the interface of the internal degrees of freedom of the system to the outside world and are typically of a spatial/geometric, thermodynamic or alchemical nature.

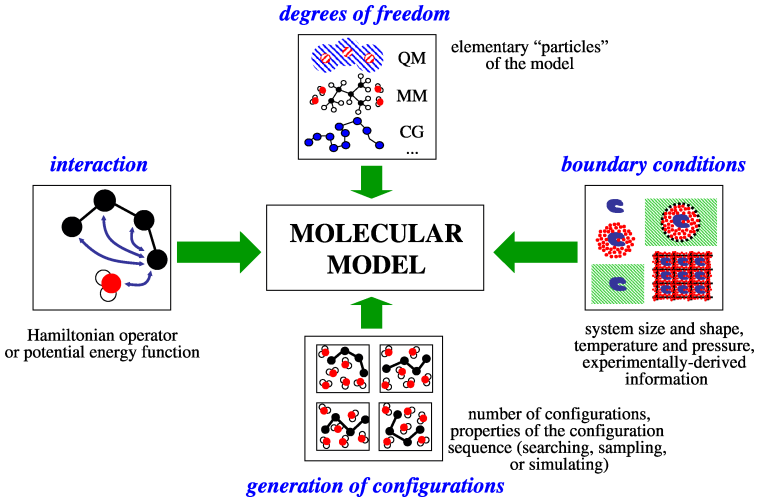

FIGURE 2.1. Four basic choices involved in the definition of a molecular model

Two important considerations typically precede the definition of a molecular model. First, most molecular models result in equations that are too complex or too numerous for an analytical solution. They must thus be solved numerically on a computer. Because the computing power is limited, one is always compelled to strike a balance between the required accuracy of the process or property of interest, the quality of the

models and the size of the relevant, accessible configurational space of the system that is to be probed in a tractable amount of computer time.

2.2. Choice of degrees of freedom

The possible physical choices of degrees of freedom in the context of the modelling of molecular systems, from the highest to the lowest resolution, can be broadly classified as[4] (Fig. 2.2) :

A. Nuclei and electrons of atoms
B. Nuclei and valence electrons of atoms
C. Nuclei and (valence) electrons of solute atoms
D. Atoms
E. United-atoms
F. Solute atoms
G. Beads representing atom groups
H. Rigid bodies representing molecules
I. Local properties of finite volume elements

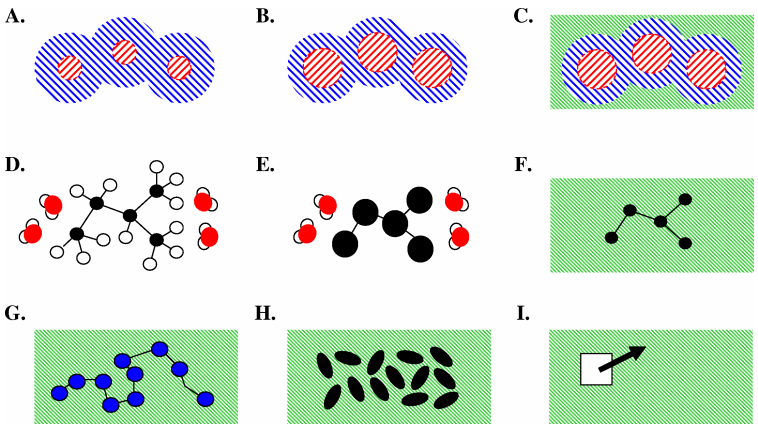

FIGURE 2.2. Broad classification of the possible levels of resolution or choice of the degrees of freedom in the modelling of molecular systems.

Each lower level of resolution turns a set of degrees of freedom that were handled explicitly at the previous level into implicit degrees of freedom at the next level. Models at the levels of resolution of Pts. A-C are commonly referred to as *Quantum Mechanical* (QM) models. Models at the levels of resolution of Pts. D-F are commonly referred to as *Atomistic* (AA for All Atoms) models. Models at the level of resolution of Pt. G are commonly referred to as *Coarse Grained* (CG) models. A number of *hybrid methods* attempt to merge different levels of resolution for different parts of a molecular system.

The selected level of resolution determines what should be referred to as the *configuration* or microstate of a corresponding system of $\mathcal{N}_d$ degrees of freedom. At the levels of resolution of Pts. A-C, a *quantum-mechanical* description is the most appropriate. In this case, a configuration of a system of particles is defined in the position representation by a wavefunction $\Psi \doteq \Psi(\boldsymbol{r})$, where $\boldsymbol{r}$ is the $\mathcal{N}_d$-dimensional vector characterizing the $\mathcal{N}_d = 3\mathcal{N}_a$ positional degrees of freedom associated with the $\mathcal{N}_a$ quantum-mechanical particles considered. At the levels of resolution of Pts. D-G, a *classical* description is the most appropriate. In this case, a configuration of a system of particles is defined by two $\mathcal{N}_d$-dimensional vectors $\boldsymbol{q}$ and $\boldsymbol{p_q}$, containing $\mathcal{N}_d = 3\mathcal{N}_a$ generalized coordinates and momenta associated with the $\mathcal{N}_a$ classical particles considered, respectively. In the special case where a Cartesian coordinate system is adopted, $\boldsymbol{q}$ is written as $\boldsymbol{r}$ and contains the components of the Cartesian particle coordinates as triplets, while $\boldsymbol{p_q}$ is written $\boldsymbol{p}$ and contains the components of the Cartesian particle momenta as triplets. This situation may be noted

$$\boldsymbol{r}^N \doteq \{\mathbf{r}_i \mid i = 1..\mathcal{N}_a\} \quad \text{and} \quad \boldsymbol{p}^N \doteq \{\mathbf{p}_i \mid i = 1..\mathcal{N}_a\} \ , \tag{2.1}$$

where $\mathbf{r}_i$ and $\mathbf{p}_i$ are the three-dimensional Cartesian coordinate and momentum vectors of a particle i. For simplicity and unless otherwise specified, a Cartesian coordinate description will be used systematically throughout this manual. At the level of resolution of Pt. H, there are twelve degrees of freedom per rigid

molecule (position, orientation, translational velocity, rotational velocity). Finally, at the level of resolution of Pt. I, a *continuous-material* description is adopted and the number of degrees of freedom per volume element depends on the (scalar or vector) properties that are considered.

In many cases, the choice of the degrees of freedom included in a model is not physical, *i.e.* matching exactly the real degrees of freedom of a molecular system. Important examples include :

J. The *Car Parrinello* (CP) approach[8] :
Here the electronic degrees of freedom in the form of the coefficients of the electronic wavefunction are treated as classical degrees of freedom and evolved in time simultaneously with the classically treated nuclei.

K. The *Charge On Spring* (COS) approach[9] :
Here, the instantaneous dipoles associated with electronic polarization effects are accounted for by means of artificial point charges connected to the atoms by means of harmonic springs.

L. The *Path Integral* (PI) approach[10] :
Here, a system of particles treated at the classical level is used to emulate the statistical-mechanical properties of a corresponding quantum-mechanical system a single quantum-mechanical particle being assigned to a given number of the classical particles, connected by harmonic springs in a ring topology.

M. Various *extended-system* methods :
Here, one or a few additional degrees of freedom are added to those of the physical system and evolved simultaneously, *e.g.* thermostat or barostat variables,[7,11] force-field parameters to be refined,[12] atomic charges to account for polarization effects[9] as in the fluctuating charge model, Hamiltonian coupling parameters.

N. Ensemble propagation approaches[5,13] :
Here the degrees of freedom do not correspond to those of a single molecular system, but to the coefficients of an ensemble probability distribution of such systems (as projected in a given basis set).[13]

The choice of the degrees of freedom or particles that are handled explicitly in the model automatically implies a definition of the implicit degrees of freedom, the internal degrees of freedom of the selected particles that are not considered explicitly in the model.

The possibilities in the domain of application of the GROMOS package in terms of degrees of freedom are discussed in Sec. 3.2.

2.3. Choice of the description of the interaction

When the degrees of freedom of the model are to be treated according to the laws of quantum mechanics, the interaction associated with the selected degrees of freedom is described by a *Hamiltonian operator* $\hat{\mathcal{H}}$. Assuming that this operator is constant *i.e.* not explicitly dependent on any external parameter or on time, and that all elementary, subatomic, particles are explicitly included in the model, the expectation value $\langle\hat{\mathcal{H}}\rangle$ of the Hamiltonian operator in terms of the wavefunction $\Psi \doteq \Psi(\boldsymbol{r})$ representing a system configuration represents the total, kinetic plus potential, energy of the system in this configuration, *i.e.*

$$\langle\hat{\mathcal{H}}\rangle[\Psi] \doteq \langle\Psi \mid \hat{\mathcal{H}} \mid \Psi\rangle \ , \tag{2.2}$$

where the square brackets indicate a functional dependence and it is assumed that Ψ is normalized. The Hamiltonian operator is itself the sum of a *kinetic energy operator* $\hat{\mathcal{K}}$ and a *potential energy operator* $\hat{\mathcal{V}}$, *i.e.*

$$\hat{\mathcal{H}} \doteq \hat{\mathcal{K}} + \hat{\mathcal{V}} \tag{2.3}$$

with

$$\hat{\mathcal{K}} \doteq -\sum_{i=1}^{\mathcal{N}_a} \frac{\hbar^2}{2m_i}\nabla_i^2 \ , \tag{2.4}$$

where m_i is the mass of particle i and $\hbar \doteq (2\pi)^{-1}h$, h being Planck's constant. The potential energy operator accounts for the proper interaction between the different quantum-mechanical particles. When the quantum-mechanical degrees of freedom included in the model do not encompass all particles in the system, the interaction may still tentatively be formulated using an effective Hamiltonian operator that encompasses the mean effect of the implicit degrees of freedom on the explicit ones, e.g. as in the use of pseudo-potentials

accounting for the implicit core electrons or of effective solvation terms for the implicit solvent in the potential energy operator.

When the degrees of freedom of the model are to be treated according to the laws of classical mechanics, the interaction associated with the selected degrees of freedom is described by a *Hamiltonian function* $\mathcal{H}$. Assuming that this function is constant, i.e. not explicitly dependent on any external parameter or on time, that all elementary particles or atoms are explicitly included in the model, and using a Cartesian coordinate system, the Hamiltonian function can be written $\mathcal{H}(\boldsymbol{r}^N, \boldsymbol{p}^N)$, and its value is equal to the total, kinetic plus potential, energy of the system in the configuration $(\boldsymbol{r}^N, \boldsymbol{p}^N)$. The Hamiltonian function is the sum of a *kinetic energy function* $\mathcal{K}$ that solely depends on the Cartesian momenta of the particles and a *potential energy function* $\mathcal{V}$ that solely depends on the Cartesian coordinates of the particles, *i.e.*

$$\mathcal{H}(\boldsymbol{r}^N, \boldsymbol{p}^N) \doteq \mathcal{K}(\boldsymbol{p}^N) + \mathcal{V}(\boldsymbol{r}^N) \tag{2.5}$$

with

$$\mathcal{K}(\boldsymbol{p}^N) \doteq \sum_{i=1}^{\mathcal{N}_a} \frac{1}{2m_i} \mathbf{p}_i^2 \ . \tag{2.6}$$

When a generalized coordinate system is employed, the kinetic energy is in the general case a function of both coordinates and momenta. The potential energy function accounts for the proper interaction between the different classical particles. When the classical degrees of freedom included in the model do not encompass all particles in the system, the interaction may still tentatively be formulated using an effective Hamiltonian function that encompasses the mean effect of the implicit degrees of freedom on the explicit ones. According to classical statistical mechanics, the ensemble properties of the reduced system will be identical to those of a corresponding all-particle system if the potential energy function involved in the effective Hamiltonian is defined as a *potential of mean force*, *i.e.* a potential energy term or function, the derivative of which is equal to the force on the explicit degrees of freedom ensemble-averaged over the compatible values of the implicit degrees of freedom. In this situation, the notation $\overline{\mathcal{V}}$ (potential of mean force) instead of $\mathcal{V}$ (all-particle potential energy term or function) will sometimes be used when the distinction is important.

Finally, when the degrees of freedom of the model are to be treated according to a continuous-material description, the interaction is typically described in terms of *gradients* of specific intensive properties and *conservation equations* for specific extensive properties.

When modelling aims at emulating the physical behaviour of a molecular system as closely as possible, the approximations employed to define the interaction should be as representative as possible for the real physical situation. In some cases, however, alterations are performed, typically in the form of extra unphysical and possibly time-dependent terms included into the potential energy function to serve specific purposes, *e.g.* enhanced probing of the configurational space, inclusion of experimental data as a boundary condition. The possibilities in the domain of application of the GROMOS package in terms of interactions are discussed in Sec. 3.3.

2.4. Choice of method for configuration generation

The possible choices of methods to generate configurations of a molecular system can be broadly classified as:[6]

A. *Search methods*:
   Generation of a set of relevant configurations within the configurational space of the system, typically configurations representing local energy minima, without any further requirement on the distribution or time sequence of these configurations.
B. *Sampling methods*:
   Generation of a set of system configurations obeying a well-defined probability distribution in terms of energy, a configurational ensemble.
C. *Simulation methods*:
   Generation of a time sequence of system configurations obeying a particular probability distribution both governed by the chosen equation of motion.

Both sampling and simulation methods permit the evaluation of *thermodynamic properties* from the generated configurational ensemble. Only simulation methods permit the evaluation of *dynamical properties* from the generated trajectory.

At the quantum-mechanical level assuming that the Hamiltonian operator is constant, the simulation of a molecular system involves the integration of the *time-dependent Schrödinger equation*

$$\hat{\mathcal{H}}\Psi(\boldsymbol{r},t) = i\hbar\frac{\partial}{\partial t}\Psi(\boldsymbol{r},t) \ , \tag{2.7}$$

where $\Psi(\boldsymbol{r},t)$ represents the instantaneous state of the system at time t. Integrating this equation numerically forward in time on a computer to simulate quantum-dynamical behaviour of a molecular system is called *quantum molecular dynamics* (QMD) simulation. Two simplifying approximations are often made in QMD : (i) A molecule is built up from just two types of particles, nuclei with negligible size and irrelevant internal structure and electrons, the motion of which can be separated using the Born-Oppenheimer approximation. Thus, a complex molecular system can be described as a system of point masses moving in an effective potential field; (ii) Some particles, e.g. the nuclei, obey the laws of classical mechanics. This is a reasonable assumption at room temperature and for all but the lightest atoms. For the latter the path-integral formalism can be used to obtain the quantum equilibrium distribution using classical equations of motion.

At the classical level, using a Cartesian coordinate system, the simulation of a molecular system involves the integration of the *Newtonian equations of motion*

$$\dot{\boldsymbol{p}}^N(t) = -\nabla\mathcal{V}(\boldsymbol{r}^N(t)) \quad \text{and} \quad \dot{\boldsymbol{r}}^N(t) = \underline{\mathbf{m}}^{-1}\boldsymbol{p}^N(t) \tag{2.8}$$

where $\underline{\mathbf{m}}$ is a $\mathcal{N}_d$-dimentional (diagonal) mass matrix of a system of $\mathcal{N}_a$ particles containing the mass of the atoms by triplets along its diagonal and $(\boldsymbol{r}^N(t),\boldsymbol{p}^N(t))$ represents the instantaneous configuration of the system at time t. These equations represent a particular case of the more general Hamiltonian equations of motion in the special case of a Cartesian coordinate system. Two relevant quantities entering in Eq. 2.8 are the $\mathcal{N}_d$-dimensional force and velocity vectors, *i.e.*

$$\boldsymbol{v}^N(t) \doteq \underline{\mathbf{m}}^{-1}\boldsymbol{p}^N(t) = \dot{\boldsymbol{r}}^N(t) \tag{2.9}$$

and

$$\boldsymbol{f}^N(t) \doteq -\nabla\mathcal{V}(\boldsymbol{r}^N(t)) = \dot{\boldsymbol{p}}^N(t) \ , \tag{2.10}$$

with the notation

$$\boldsymbol{v}^N \doteq \{\mathbf{v}_i \mid i = 1..\mathcal{N}_a\} \quad \text{and} \quad \boldsymbol{f}^N \doteq \{\mathbf{f}_i \mid i = 1..\mathcal{N}_a\} \ . \tag{2.11}$$

where $\mathbf{v}_i$ and $\mathbf{f}_i$ are the three-dimensional Cartesian velocity and force vectors of a particle i. In terms of these quantities, the first equation in Eq. 2.8 may equivalently be written

$$\underline{\mathbf{m}}\dot{\boldsymbol{v}}^N(t) = \boldsymbol{f}^N(t) \ . \tag{2.12}$$

Integrating Eq. 2.8 numerically forward in time on a computer to simulate classical-dynamical behaviour of a molecular system is called classical *molecular dynamics* (MD) simulation.

An alternative to *Newtonian equations of motion* are the *Langevin equations of motion*

$$\underline{\mathbf{m}}\dot{\boldsymbol{v}}^N(t) = \overline{\boldsymbol{f}}^N(t) + \boldsymbol{f}^{st,N}(t) - \underline{\mathbf{m}}\underline{\gamma}\boldsymbol{v}^N(t) \ , \tag{2.13}$$

where

$$\overline{\boldsymbol{f}}(t) \doteq -\nabla\overline{\mathcal{V}}(\boldsymbol{r}(t)) \ . \tag{2.14}$$

The mean force $\overline{\boldsymbol{f}}$ is the negative gradient of the potential of mean force $\overline{\mathcal{V}}$, *i.e.* it includes the forces between the explicit particles but also accounts in an effective fashion for the average forces exerted by the implicit particles.

The *stochastic force* is denoted by $\boldsymbol{f}^{st}(t)$ and the *frictional force* is proportional to the velocities $\mathbf{v}_i$ with the proportionality factor $\underline{\mathbf{m}}\underline{\gamma}$, in which $\underline{\gamma}$ is a diagonal matrix containing the atomic friction coefficients γ_i. A stochastic force introduces energy into the system, and a frictional force removes energy from it. The condition of zero energy loss on average will relate the two forces. If the stochastic force $\mathbf{f}_i^{st}$ obeys a Gaussian probability distribution with zero mean, if it is not correlated with prior velocities or forces, and if the friction coefficient γ_i is independent of time, this condition reads

$$< (\mathbf{f}_i^{st})^2 > \ = \ 6m_i\gamma_i \ k_B \ T_{ref} \tag{2.15}$$

where a time average is denoted by $<...>$, k_B is Boltzmann's constant, and T_{ref} is the reference temperature of the system. Numerical integration of the stochastic equations of motion is called *stochastic dynamics (*SD*) simulation*. Different approximations to this purpose are *Stochastic Dynamics* (SD), *high viscosity* SD *or Brownian Dynamics* (BD) or *Diffusive Particle Dynamics* (DPD).

Finally, when the degrees of freedom of the model are to be treated according to a continuous-material description, the equations of motion are typically formulated in terms of *transport equations* that relate the flow of specific extensive properties to the gradients of specific intensive properties.

A molecular system can be coupled to external quantities in different ways (see also Sec. 2.5):

1. Inclusion of an extra term $\mathcal{V}^{(res)}(\boldsymbol{r})$, a *penalty function*, in the interaction function of the system that restrains the motion of the particles such that the simulated value approaches the prescribed value of the given external quantity.
2. The prescribed value of the external quantity can be imposed as a *constraint* on to the system, such that it is satisfied by every configuration.
3. A first-order equation can be added to the particle equations of motion that drives the simulated value of the external quantity towards the prescribed value: the so-called *weak-coupling method*.

The latter two methods imply modification of the classical equations of motion of the molecular system.

We note that the total energy of the system will only be conserved in an MD simulation if the potential energy $\mathcal{V}$ is only a function of the current configuration. When applying weak coupling or a penalty function with time-averaged parameter values, this condition is not fulfilled.

The possibilities in the domain of application of the GROMOS package in terms of configuration generation are discussed in Sec. 3.4.

When performing *energy minimization*, the potential energy $\mathcal{V}$ molecular system is minimized using the negative gradient of this function.

2.5. Choice of the boundary conditions

The term *boundary condition* refers to global restrictions imposed on the system during the configuration generation. A restriction may be *hard*, a constraint affecting all individual configurations, or *soft*, a constraint on the average value of an observable over the generated configurations or a restraint biasing this average value towards a specified target value. One may distinguish the following types of boundary conditions:

A. *Spatial* boundary conditions
   These concern the nature of the confinement or periodicity applied to the molecular system. Typical examples are: *Vacuum Boundary Conditions* (VBC), a set of molecules in vacuum, *Fixed Boundary Conditions* (FBC), a system confined to a fixed region of space by means of a wall, and *Periodic Boundary Conditions* (PBC), a periodic system defined by the replication of a computational box of space-filling shape.

B. *Geometric* boundary conditions
   These concern the possible presence of constraints or restraints on specific internal coordinates within the system. Typical examples are the use of rigid bond lengths, the use of experiment-based restraints affecting specific internal coordinates or averages thereof, the use of artificial constraints or restraints on a specific internal coordinate, *e.g.* to avoid structural distortions during the equilibration phase of a simulation, or to bias the generation of configurations towards specific regions of the configurational space.

C. *Thermodynamic* boundary conditions
   These concern the thermodynamic state point associated with the generated configurational ensemble. Typical examples are a constant *number of particles vs* a constant *chemical potential*, a constant *volume vs* a constant *pressure*, a constant *energy* or enthalpy *vs* a constant *temperature*. In specific cases, other variables may be required for the definition of the thermodynamic state point.

The possibilities in the domain of application of the GROMOS package in terms of boundary conditions are discussed in Sec. 3.5.

CHAPTER 3

Scope of the GROMOS package

3.1. Introduction

The GROMOS package for molecular simulation currently consists of two subpackages that are tightly linked together but can largely be compiled and used as separate entities.

a. GROMOS++ is a library of supporting programs for pre- and post-MD tasks. It mainly consists of programs to facilitate the setup of simulations and of programs to analyze trajectories that are the results of such simulations.
b. MD++ is an energy minimizer and simulator, written in *C++* in an object oriented manner.

This chapter discusses the options offered by the two subpackages regarding the four basic aspects of molecular simulation.

3.2. Choice of the degrees of freedom

GROMOS can only consider degrees of freedom behaving according to the laws of classical mechanics. These are usually atoms or united atoms with two exceptions : (*i*) beads assumed to behave classically in a coarse-grained representation of molecular systems; (*ii*) beads connected by harmonic springs in a ring topology as a path-integral representation of a quantum-mechanical system. GROMOS is primarily intended for simulations of condensed-phase systems, solutions, pure liquids and crystals, with an explicit representation of the solvent molecules in the case of solutions. However, the simulation of systems in the gas phase and of solutions with an implicit-solvent representation are also possible. Since GROMOS was originally developed for atomic degrees of freedom, particles are generally named atoms, although they actually may be groups of atoms or path-integral beads.

3.3. Choice of the description of the interaction

In classical simulations, the Hamiltonian of a molecular system has the form

$$\mathcal{H}(\boldsymbol{p}^N, \boldsymbol{r}^N) \quad = \quad \mathcal{K}(\boldsymbol{p}^N) + \mathcal{V}(\boldsymbol{r}^N) \tag{3.1}$$

The first term is the *kinetic energy* term

$$\mathcal{K}(\boldsymbol{p}^N) = \sum_{i=1}^{N} \frac{\mathbf{p}_i{}^2}{2m_i} = \sum_{i=1}^{N} \tfrac{1}{2} m_i \mathbf{v}_i{}^2 \ , \tag{3.2}$$

which is independent of the particle coordinates $\boldsymbol{r}^N$ in the absence of geometric positional constraints. If constraints are imposed, the components of the momenta $\mathbf{p}_i$ or the velocities $\mathbf{v}_i$ along the constrained degrees of freedom must be zero. The second term is the *potential energy* term or interaction function, which describes the interaction energy in terms of particle coordinates $\mathbf{r}$

$$\mathcal{V}(\boldsymbol{r};\mathbf{s}) \quad \equiv \quad \mathcal{V}(\mathbf{r}_1, \mathbf{r}_2, \ldots, \mathbf{r}_N; \mathbf{s}_1, \mathbf{s}_2, \ldots, \mathbf{s}_M). \tag{3.3}$$

Here $\boldsymbol{r}^N$ denotes the $3\mathcal{N}_a$-dimensional Cartesian coordinate vector of the system (periodic copies of the atoms within the reference box if PBC is applied). Generally, such a potential energy function $\mathcal{V}(\boldsymbol{r}^N;\mathbf{s})$ depends on a number (M) of parameters, also called force-field parameters, here indicated by $\mathbf{s} \equiv (\mathbf{s}_1, \mathbf{s}_2, \ldots, \mathbf{s}_M)$. In practice, the interaction function $\mathcal{V}(\boldsymbol{r}^N)$ consists of a sum of terms which represent different types of interactions. We distinguish two types of interactions or forces:

1. The standard *physical* atomic *interaction* function $\mathcal{V}^{(phys)}(\boldsymbol{r}^N, \mathbf{s})$, e.g. the GROMOS force field.

2. The *non-physical* atomic *interaction* function terms $\mathcal{V}^{(spec)}(\boldsymbol{r}^N)$, which are included to serve a special purpose, e.g. atomic position restraining, distance restraining, dihedral-angle restraining, etc.

So, we have

$$\mathcal{V}(\boldsymbol{r};\mathbf{s}) \quad = \quad \mathcal{V}^{(phys)}(\boldsymbol{r}^N;\mathbf{s}) + \mathcal{V}^{(spec)}(\boldsymbol{r}^N) \tag{3.4}$$

The physical potential energy term $\mathcal{V}^{(phys)}$ is further divided into a term $\mathcal{V}^{(cov)}$ corresponding to *covalent interactions* and a term $\mathcal{V}^{(nbd)}$ corresponding to *non-bonded interactions*. This results in

$$\mathcal{V}^{(phys)}(\boldsymbol{r}^N;\mathbf{s}) \doteq \mathcal{V}^{(cov)}(\boldsymbol{r}^N;\mathbf{s}) + \mathcal{V}^{(nbd)}(\boldsymbol{r}^N;\mathbf{s}) \ . \tag{3.5}$$

The covalent term is further partitioned as a sum of contributions from *bond stretching*, *bond-angle bending*, *improper dihedral-angle bending* and *proper dihedral-angle torsion* interactions, namely

$$\mathcal{V}^{(cov)}(\boldsymbol{r}^N;\mathbf{s}) \doteq \mathcal{V}^{(b)}(\boldsymbol{r}^N;\mathbf{s}) + \mathcal{V}^{(\theta)}(\boldsymbol{r}^N;\mathbf{s}) + \mathcal{V}^{(\xi)}(\boldsymbol{r}^N;\mathbf{s}) + \mathcal{V}^{(\varphi)}(\boldsymbol{r}^N;\mathbf{s}) \ . \tag{3.6}$$

The non-bonded term is further partitioned as a sum of contributions from *van der Waals* and *electrostatic* interactions, namely

$$\mathcal{V}^{(nbd)}(\boldsymbol{r}^N;\mathbf{s}) \doteq \mathcal{V}^{(vdw)}(\boldsymbol{r}^N;\mathbf{s}) + \mathcal{V}^{(ele)}(\boldsymbol{r}^N;\mathbf{s}) \ . \tag{3.7}$$

The different terms involved in Eqs. 3.5-3.7 are described in Chaps. 5, 6 and 7. The force $\mathbf{f}_i$ on particle i due to a particular interaction term is given by the relation

$$\mathbf{f}_i \quad = \quad -\frac{\partial}{\partial \mathbf{r}_i}\, \mathcal{V}(\mathbf{r}_1, \mathbf{r}_2, ..., \mathbf{r}_N), \tag{3.8}$$

which can also be used to obtain the interaction energy difference that corresponds to a given force $\mathbf{f}_i$. We note that a MD trajectory only depends on the forces on the atoms, not on the energies.

The derivatives of the potential energy terms with respect to atomic coordinates, box or coupling parameters are provided in Chap. 17, while the parameters involved in these terms are included as part of the GROMOS force-field description in Vol. 3.

3.3.1. Charge groups, searching neighbours. The bulk of the computer time required by a simulation time step is used for calculating the non-bonded interactions, that is, for finding the nearest neighbour atoms and subsequently evaluating the van der Waals and electrostatic interaction terms for the obtained atom pairs. Therefore, various schemes for performing this task as efficiently as possible are available.[14]

Since the non-bonded interaction between atoms decreases with the distance between them, only interactions between atoms closer to each other than a certain cut-off distance R_c are generally taken into account in simulations.

When the (partial) atomic charges of a group of atoms add up to exactly zero, the leading term of the electrostatic interaction between two such groups of atoms is of dipolar ($1/r^3$) character. The sum of the 1/r monopole contributions of the various atom pairs to the group-group interaction will be zero. Therefore, the range of the electrostatic interaction can be considerably reduced when atoms are assembled in so-called charge groups, which have a zero net charge, and for which the electrostatic interaction with other (groups of) atoms is either calculated for all atoms of the charge group or for none.

The GROMOS force fields make use of this *concept of charge groups*. The atoms that belong to a charge group are chosen such that their partial atomic charges add up to zero. For groups of atoms with a total charge of $+e$ or $-e$, like the sidechain atoms of Arg or Asp, the partial atomic charges of the charge group may add up to $+e$ or $-e$. When a cut-off radius is used, one can choose to base this cutoff on the atomic positions (AT) or to use a charge group based cutoff. The *position of a charge group* is defined differently for a charge group belonging to the "solute" part of the molecular topology and one in the "solvent" part of the molecular topology.

- The position of a "solute" charge group is taken to be its centre of geometry:

$$R_{cg} = \sum_{i=1}^{N_{cg}} \mathbf{r}_i / N_{cg} \tag{3.9}$$

  where the number of atoms belonging to the charge group is denoted by N_{cg}.
- The position of a "solvent" charge group is taken to be the position of the first atom of a solvent molecule. A "solvent" molecule may only contain one charge group.

Therefore, in the GROMOS non-bonded interaction subroutines the cut-off radius R_c , denoted by RCUTP, is used to select nearest-neighbour charge groups.

The simplest way to find the neighbouring charge groups of a charge group, that is, the charge groups that lie within R_c , is to scan all possible charge group pairs in the system. For a system consisting of N_{CG} charge groups, the number of pairs amounts to $1/2{N_{CG}}^2$, which makes the computer time required for finding the neighbours in this way proportional to ${N_{CG}}^2$. Faster neighbour-search algorithms do exist, see Sec. 3.3.3. Once the neighbours have been found, the time required for calculating the non-bonded interaction is proportional to N_{CG} . We note that non-bonded interactions within a charge group may need to be calculated, when the charge group contains many atoms.

3.3.2. Twin-range method for long-range interactions. In order to evaluate the non-bonded interaction (Eq. 3.7) with sufficient accuracy, a long cut-off radius R_{cl} has to be used; for molecular systems a value of at least 1.4 nm seems necessary. But such a range is very expensive if pair interactions are evaluated; the number of neighbour atoms within 1.4 nm will exceed 300. Therefore, in GROMOS the non-bonded interaction can be evaluated using a *twin-range method.*[15] Secondly, the electrostatic interactions beyond the long-range cutoff R_{cl} can be approximated by a Poisson-Boltzmann generalized *reaction field* term.

The non-bonded interactions in Eq. 3.7 are evaluated at every simulation step using the charge group pair list that is generated with a short range cut-off radius R_{cp} (=RCUTP). The longer range non-bonded interactions, that is, those between charge groups at a distance longer than R_{cp} and smaller than R_{cl} (=RCUTL), are evaluated less frequently, viz. only at every n-th (=NSNB) simulation step when also the pair list is updated. They are kept unchanged between these updates. In this way the long-range non-bonded forces can be approximately taken into account, without increasing the computing effort significantly, at the expense of neglecting the fluctuation of the forces beyond R_{cp} during n simulation steps.

The long-range interaction, which is calculated for charge group pairs at distances between R_{cp} and R_{cl}, is evaluated by using the electrostatic term in Eq. 3.7 and the normal van der Waals parameters in the Lennard-Jones term. It is assumed that no excluded neighbours, no third-neighbour or 1,4-interactions and no intra-charge-group interactions exist at these distances. So R_{cp} must not be chosen too small.

The evaluation of the nonbonded interactions in GROMOS relies on the application of the twin-range method.[1,16–18] The GROMOS implementation of this approach relies on the definition of: (1) a short-range pairlist and cutoff distance R_{cp}; (2) an intermediate-range pairlist and cutoff distance R_{cl}; (3) anupdate frequency N_s for the short-range pairlist and for the intermediate range interactions; Short-range interactions are computed every time step based on a short-range pairlist containing pairs in the distance range [0; R_{cp}].

The short-range pairlist is reevaluated every N_s time steps. It can be generated either on the basis of distances between charge groups (groups of covalently linked atoms defined in the system topology) or of distances between individual atoms. Intermediate range interactions are computed every N_s time steps based on all pairs in the distance range [R_{cp}; R_{cl}] at the time of the evaluation of these interactions. The energy, forces, and virial contributions associated with intermediate-range interactions are assumed constant between two updates (i.e., during N_s steps).

The evaluated interaction includes Lennard-Jones and electrostatic components. The latter component may include a reaction-field contribution or the real-space contribution to a lattice-sum method. Note that the real-space contribution to a lattice-sum method may only be computed within the short-range contribution to the interaction.

3.3.3. Pairlist construction. Pairlist construction may be performed in three different ways:

1. using the standard double-loop algorithm;
2. using a grid-based pairlist algorithm[19];
3. using a slight variation of the grid-based algorithm, which permits easier parallelization and avoids periodicity corrections during the interaction evaluation.

The standard double-loop algorithm is selected by setting the `algorithm` flag in the `PAIRLIST` block to 0. A grid-based pairlist algorithm is implemented to allow for a fast construction of cutoff-based nonbonded pairlists in molecular simulations under periodic boundary conditions based on an arbitrary box shape (rectangular, truncated-octahedral, or triclinic).[19] The key features of this algorithm are: (1) the use of a one-dimensional mask array (to determine which grid cells contain interacting atoms) that incorporates the effect of periodicity, and (2) the grouping of adjacent interacting cells of the mask array into stripes, which

permits the handling of empty cells with a very low computational overhead. Testing of the algorithm on water systems of different sizes (containing about 2000 to 11,000 molecules) has shown that the method: (1) is about an order of magnitude more efficient compared to a standard (double-loop) algorithm, (2) achieves quasi-linear scaling in the number of atoms, (3) is weakly sensitive in terms of efficiency to the chosen number of grid cells. This grid-based algorithm is set by setting the `algorithm` parameter in the `PAIRLIST` block to 2.

Furthermore, MD++ includes a slightly modified version of this grid-based pairlist algorithm following ideas similar to those of a published pairlist algorithm.[20] In an effort to reduce the number of nearest image determinations during the pairlist generation and the nonbonded force calculation, the system gets extended on all sides before the pairlist construction. The additional atom or charge-group positions are obtained by simple shifts of the original positions by the box vectors. To allow for more efficient (distributed- memory) parallelization and to save time, the central computational box is divided into N layers. Each of the P parallel processes only has to extend over N/P layers. After every extension, the atom pairs consisting of one atom within the layer and a second atom from one of the above (not extended) layers are added to the respective pairlist (using a one-dimensional mask array). Filtering or energy and force evaluation can then be carried out right away (without nearest image determinations owing to the preshifted atomic positions), or at a later stage with the information on the shift vectors encoded into the pairlist, thus enabling a fast reconstruction of the shifted positions. This version of the grid-based algorithm is selected by setting the `algorithm` flag of the `PAIRLIST` block to 1.

3.4. Choice of the method for the configuration generation

The GROMOS program MD++ may be used to perform energy minimizations, molecular dynamics simulations or stochastic dynamics simulations. Details of the algorithms that are implemented and considerations to be kept in mind when setting up the calculations are given in Chaps. 11, 12 and 13 respectively.

3.5. Choice of the boundary conditions

GROMOS offers a wide range of algorithms to apply boundary conditions to an energy minimization, molecular or stochastic dynamics simulation. Spatial boundary conditions are limited to vacuum boundary conditions, fixed boundary conditions or periodic boundary conditions in various shapes. Details for spatial boundary conditions are described in Chap. 4. Geometric boundary conditions may be applied in the form of restraints through the use of special force-field terms (Chap. 9) or as constraints through a direct adaptation of the equations of motion (Chap. 10). GROMOS currently cannot perform simulations in a grand-canonical ensemble, *i.e.* with constant chemical potential rather than constant number of particles.

CHAPTER 4

Spatial boundary conditions

4.1. Introduction

When simulating a system of finite size, some thoughts must be given to the way how the boundary of the system will be treated. Spatial boundary conditions define the shape, size and confinement of the simulated system. GROMOS can handle the following types of spatial boundary conditions:

A. *Vacuum boundary conditions* (VBC) describe a system of particles surrounded by vacuum.
B. *Fixed boundary conditions* (FBC) describe a system of particles confined within a finite volume.
C. *Periodic boundary conditions* (PBC) describe a system of particles within a reference computational box of space-filling shape surrounded by an infinite lattice of periodic replicas of itself.

The simplest choice is the *vacuum* boundary condition, which is discussed in Sec. 4.2. The *fixed* boundary conditions (Sec. 4.3) are not implemented separately in GROMOS and are treated like a special case of a vacuum simulation. Periodic boundary conditions are useful in simulations of solutions, to remove surface effects when dealing with microscopic samples, and in simulations of crystals based on the periodicity determined by the crystallographic unit cell. When periodic boundary conditions are applied, the shape, size and orientation of the computational box must be defined. Sec. 4.4 discusses the use of periodic boundary conditions in GROMOS.

4.2. Vacuum boundary conditions (VBC)

Simulating a molecular system in vacuo, that is, without any wall or boundary, corresponds to the gas phase at pressure zero. When the vacuum boundary is used for a molecule in solution, properties of atoms near or at the surface of the system will be distorted[21, 22]. The vacuum boundary condition may also distort the shape of a non-spherical molecule, since it generally tends to minimize the surface area. Moreover, the shielding effect of a solvent with high dielectric permittivity, such as water, on the electric interaction between charges or dipoles in a molecule is missed in vacuo. Therefore, simulation of a charged extended molecule *e.g.* DNA in vacuo is a precareous undertaking. The best results in vacuo are obtained for relatively large globular macromolecules.

The vacuum boundary condition is selected using the switch NTB = 0 in the input block BOUNDCOND. When the molecular system contains groups of atoms with a total net charge not equal to zero, it is advised to use the *GROMOS 45B4 or 54B7 force field* in which charged charge groups are neutralized and some van der Waals parameters are modified in order to maintain the hydrogen binding capacity of the charge group that is neutralized.

When simulating a system in vacuo, the translational momentum and the angular momentum are conserved quantities. Therefore, it is common practice to *stop* the *translational* motion of the centre of mass and the *rotational motion* around the centre of mass at the start of such a simulation. This is done by using NTICOM=2 in the input block INITIALISE at the start of a simulation. In vacuo these motions will remain absent (zero), except in the case of long simulations, when the numerical noise may build up a sizeable centre of mass translation or rotational motion, especially when the system is coupled to a temperature bath. Therefore, it is advisable to stop the centre of mass motion regularly, e.g. by setting the number of steps after which centre of mass motion is stopped, NSCM = 10000 in the input block COMTRANSROT in MD++. By specifying a negative number for NSCM, the centre of mass rotation is stopped additionally.

The temperature T of a system is calculated using the relation

$$\sum_{i=1}^{\mathcal{N}_a} 1/2 m_i \mathbf{v}_i^2 \quad = \quad \tfrac{1}{2}\mathcal{N}_d k_B T \tag{4.1}$$

where k_B is Boltzmann's constant and the number of degrees of freedom in the system is denoted by

$$\mathcal{N}_d \quad = \quad 3\mathcal{N}_a - N_c - NDFMIN \tag{4.2}$$

Here the number of atoms is $\mathcal{N}_a$ and the number of geometric constraints is N_c. The choice of the value for NDFMIN in input block BOUNDCOND should depend on the boundary condition chosen and on whether the centre of mass motion is regularly stopped.

When the overall translational and rotational motion has been stopped and the system is in vacuo, six degrees of freedom have to be subtracted from the total in Eq. 4.2, so NDFMIN = 6, in order to obtain the correct kinetic energy per degree of freedom.

4.3. Fixed boundary conditions (FBC)

When simulating crystals or solutions of large molecules, the application of periodic boundary conditions may require many atoms to be included in the computational box and so may become very expensive. In that case the number of atoms in the simulation can be limited by simulating only part of the molecular system. For example, only the atoms within a spherical region around a specific atom or point in the system are retained, while all atoms lying beyond a radius R_2 are removed from the system. Edge effects, due to the presence of vacuum beyond R_2, can be minimized by restraining the motion of the atoms in the outer shell, viz. between radii R_1 and R_2. This shell is called the extended wall region (see Fig. 4.1). The atoms in this *wall region* can be kept fixed or near given stationary reference positions by the technique of *position restraining*, which is discussed in Sec. 9.2. Atoms in the inner region, within R_1, are simulated without any restraints.

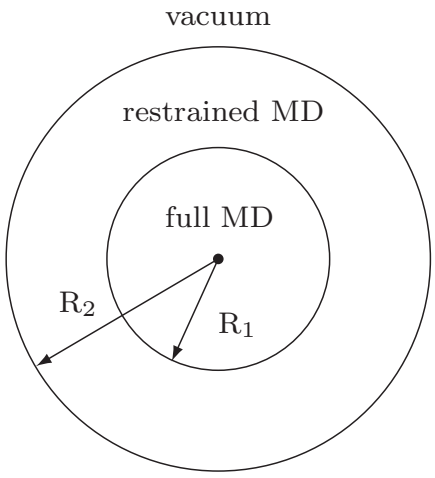

FIGURE 4.1. Spherical wall region with restrained atomic motion

When applying the extended wall region boundary condition, the *molecular topology* (Vol. 4) can be *reduced* to one containing only atoms, *i.e.* charge groups, that lie within a distance R_2 from a given point. The subset of atoms within the simulation sphere and in the extended wall region may be obtained from a complete system using the GROMOS++ program *pairlist* (Sec. 5-5.5), the molecular topology may subsequently be reduced using the program *red_top* (Sec. 5-2.27). The coordinate file can be modified using the GROMOS++ program filter (Sec. 5-4.29). The reduced system is not restricted to be of spherical shape. During a simulation the vacuum boundary condition should be selected (NTB = 0) and position

restraining applied to the atoms forming the wall region. Again, the restrained region is not restricted to being a spherical shell.

In order to avoid distorting effects of the vacuum beyond R_2 on the atomic motion within R_1 , one should choose these radii such that

$$R_c \quad < \quad R_2 - R_1 \tag{4.3}$$

that is, the thickness of the shell of restrained atoms should be larger than the nonbonded *cut-off radius* R_c .

4.4. Periodic boundary conditions (PBC)

The classical way to minimize edge effects in a finite system is to use periodic boundary conditions. The atoms of the system that is to be simulated are put into a periodic, space filling box, cubic, rectangular, triclinic, truncated octahedral, which is surrounded by identical translated images of itself (Fig. 4.2).

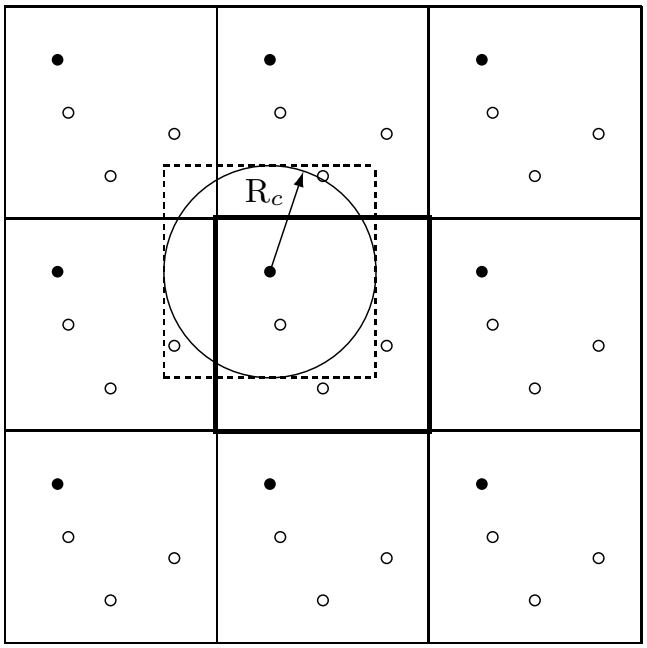

FIGURE 4.2. Periodic boundary conditions.

When an atom leaves the central box at one side, it enters it with identical velocity at the opposite side at the translated image position. Application of periodic boundary conditions means that in fact a crystal is simulated. For a molecule in solution the periodicity is an artifact of the computation, so the effects of periodicity on the forces on the atoms should not be significant. Possible distorting effects of the periodic boundary condition may be traced by simulating systems of different sizes.

When simulating a system using periodic boundary conditions, the translational momentum is a conserved quantity, but the *angular momentum* of the system is *not conserved*. As in vacuo, it is common practice to stop the translational motion of the centre of mass of the system and also the rotational motion around the centre of mass at the start of a simulation. However, the rotational degrees of freedom will pick up energy when the system evolves, and the translational energy should remain zero. Therefore, when the temperature of the system is calculated using Eqs. 4.1-4.2 three degrees of freedom have to be subtracted from the total in Eq. 4.2, so NDFMIN = 3, in order to obtain the correct kinetic energy per degree of freedom. As in the case of vacuum boundary condition, the centre of mass motion should be stopped now and then to avoid build-up of translational motion due to numerical noise in long simulations.

As all space filling boxes, *i.e.* cube, rectangular box, triclinic box, truncated octahedron, used in GROMOS can be expressed as triclinic boxes, this case is discussed in more detail in the following section. Periodic boundary conditions are switched on when NTB $\neq 0$. If NTB=1 rectangular periodic boundary conditions will be applyied, triclinic periodic boundary conditions for NTB=2, and truncated-octahedral periodic boundary condition for NTB=-1.

4.4.1. Triclinic computational box under PBC**.** The spatial properties, including position, shape, size and orientation, of an arbitrary triclinic box relative to a *reference coordinate system* $\{O, \hat{\mathbf{e}}_x, \hat{\mathbf{e}}_y, \hat{\mathbf{e}}_z\}$, assumed Cartesian and right-handed, can be specified by 12 real numbers.

In the *matrix* representation, the spatial properties are specified by the position vector $\mathbf{T}$ of one reference corner of the box (relative to the origin O), along with the three edge vectors $\mathbf{a}$, $\mathbf{b}$ and $\mathbf{c}$ of the box, chosen so as to define a right-handed set, *i.e.* $\mathbf{a} \cdot (\mathbf{b} \times \mathbf{c}) > 0$. The elements of these vectors will be assumed to represent the corresponding components in the reference coordinate system $\{\hat{\mathbf{e}}_x, \hat{\mathbf{e}}_y, \hat{\mathbf{e}}_z\}$.

In the *angular* representation, the spatial properties are specified by the position vector $\mathbf{T}$, along with the box edge lengths a, b and c, the edge angles α between $\mathbf{b}$ and $\mathbf{c}$, β between $\mathbf{a}$ and $\mathbf{c}$ and γ between $\mathbf{a}$ and $\mathbf{b}$, and the Euler angles ϕ, θ and ψ defining the orientation of the box relative to the reference coordinate system. In the definition of the Euler angles, the three edge vectors are used to define a box-linked right-handed Cartesian coordinate system $(\hat{\mathbf{e}}_{x'}, \hat{\mathbf{e}}_{y'}, \hat{\mathbf{e}}_{z'})$ in the following way : (i) the x'-axis is chosen along and in the direction of $\mathbf{a}$; (ii) the y'-axis is chosen orthogonal to $\mathbf{a}$ in the plane defined by $\mathbf{a}$ and $\mathbf{b}$, and oriented in the direction of $\mathbf{b}$; (iii) the z'-axis is chosen orthogonal to both $\mathbf{a}$ and $\mathbf{b}$, and oriented in the direction of $\mathbf{c}$. The reference coordinate system can be rotated onto the box-linked coordinate system by the following series of rotations : (i) a rotation by an angle ϕ around the z-axis ; (ii) a rotation by an angle θ around the new y-axis ; (iii) a rotation by an angle ψ around the new x-axis. The angles ϕ, θ and ψ thus represent the three Euler rotation angles in the zyx or yaw-pitch-roll convention. At any time during a simulation, the box angles α, β and γ are restricted to the range $]0; \pi[$, the Euler angles ϕ and ψ to the range $]-\pi; \pi]$, and the Euler angle θ to the range $[-\pi/2; \pi/2]$. The condition on θ follows from the observation that the changes $\theta \rightarrow \pi - \theta$, $\phi \rightarrow \pi + \phi$ and $\psi \rightarrow \pi + \psi$ always lead to an equivalent description of the box orientation. When $\theta = \pm\pi/2$, the angles ϕ and ψ are individually undefined only $\phi - \psi$ or $\phi + \psi$ are defined when $\theta = \pi/2$ and $-\pi/2$, respectively. In this situation, ϕ is arbitrarily set to zero. For both rectangular and truncated-octahedral boxes, the conditions $\alpha = \beta = \gamma = \pi/2$ and $\phi = \theta = \psi = 0$ are also enforced at any time during the simulation. For a truncated-octahedral box, the condition $a = b = c$ is enforced in addition.

4.4.1.1. *Coordinate transformations: triclinic box.* Based on a general triclinic box in an arbitrary orientation, as introduced in Sec. 4.4.1 the coordinates of an atom can be specified in four distinct ways : (i) through oblique fractional coordinates $\check{\mathbf{r}} = (q, s, t)$ with reference to the box-edge vectors ; (ii) through oblique coordinates $\check{\mathbf{r}} = (u, v, w)$ with reference to the box-edge vectors ; (iii) through coordinates $\mathbf{r}' = (x', y', z')$ within the box-linked Cartesian coordinate system ; (iv) through coordinates $\mathbf{r} = (x, y, z)$ within the reference Cartesian coordinate system. The different sets of coordinates are related through

$$u = qa \ , v = sb \ , w = tc \ , \tag{4.4}$$

$$\mathbf{r}' = ua^{-1}\mathbf{a}' + vb^{-1}\mathbf{b}' + wc^{-1}\mathbf{c}' \ , \tag{4.5}$$

$$\mathbf{r} = x'\hat{\mathbf{e}}_{x'} + y'\hat{\mathbf{e}}_{y'} + z'\hat{\mathbf{e}}_{z'} \tag{4.6}$$

and

$$\mathbf{r} = ua^{-1}\mathbf{a} + vb^{-1}\mathbf{b} + wc^{-1}\mathbf{c} \ , \tag{4.7}$$

where $\mathbf{a}$, $\mathbf{b}$ and $\mathbf{c}$ are the components of the edge vectors in the reference Cartesian coordinate system, and $\mathbf{a}'$, $\mathbf{b}'$ and $\mathbf{c}'$ the corresponding components in the box-linked Cartesian coordinate system.

Defining the matrix $\underline{\mathbf{B}}$ as the diagonal matrix containing the box-edge lengths a, b and c as its elements, *i.e.*

$$\underline{\mathbf{B}} = \begin{pmatrix} a & 0 & 0 \\ 0 & b & 0 \\ 0 & 0 & c \end{pmatrix} \ , \tag{4.8}$$

Eq. 4.4 may be rewritten

$$\check{\mathbf{r}} = \underline{\mathbf{B}}\check{\mathbf{r}} \ . \tag{4.9}$$

Defining the transformation matrix $\underline{\mathbf{S}}$ as the matrix containing $a^{-1}\mathbf{a}'$, $b^{-1}\mathbf{b}'$ and $c^{-1}\mathbf{c}'$ in its columns, *i.e.*

$$\underline{\mathbf{S}} = \begin{pmatrix} a^{-1}a_x{}' & b^{-1}b_x{}' & c^{-1}c_x{}' \\ a^{-1}a_y{}' & b^{-1}b_y{}' & c^{-1}c_y{}' \\ a^{-1}a_z{}' & b^{-1}b_z{}' & c^{-1}c_z{}' \end{pmatrix} = \begin{pmatrix} 1 & \cos\gamma & \cos\beta \\ 0 & \sin\gamma & \sin\beta\cos\delta \\ 0 & 0 & \sin\beta\sin\delta \end{pmatrix} , \tag{4.10}$$

where

$$\cos\delta = \frac{\cos\alpha - \cos\beta\cos\gamma}{\sin\beta\sin\gamma} \quad \text{with} \quad \delta \in]0;\pi[, \tag{4.11}$$

Eq. 4.5 may be rewritten as

$$\mathbf{r}' = \underline{\mathbf{S}}\check{\mathbf{r}} . \tag{4.12}$$

The inverse transformation is performed through the matrix

$$\underline{\mathbf{S}}^{-1} = \begin{pmatrix} 1 & -\cot\gamma & \cot\gamma\cot\delta - \cot\beta\sin^{-1}\delta \\ 0 & \sin^{-1}\gamma & -\cot\delta\sin^{-1}\gamma \\ 0 & 0 & \sin^{-1}\beta\sin^{-1}\delta \end{pmatrix} . \tag{4.13}$$

In MD++ the matrix $\underline{\mathbf{S}}$ is defined as `math::Matrixl math::smat`.

Defining the transformation matrix $\underline{\mathbf{R}}$ as the matrix containing $\hat{\mathbf{e}}_{x'}$, $\hat{\mathbf{e}}_{y'}$ and $\hat{\mathbf{e}}_{z'}$ in its columns, *i.e.*

$$\underline{\mathbf{R}} = \begin{pmatrix} \cos\theta\cos\phi & \sin\psi\sin\theta\cos\phi - \cos\psi\sin\phi & \cos\psi\sin\theta\cos\phi + \sin\psi\sin\phi \\ \cos\theta\sin\phi & \sin\psi\sin\theta\sin\phi + \cos\psi\cos\phi & \cos\psi\sin\theta\sin\phi - \sin\psi\cos\phi \\ -\sin\theta & \sin\psi\cos\theta & \cos\psi\cos\theta \end{pmatrix} , \tag{4.14}$$

Eq. 4.6 may be rewritten as

$$\mathbf{r} = \underline{\mathbf{R}}\mathbf{r}' . \tag{4.15}$$

The inverse transformation is performed through the matrix $\underline{\mathbf{R}}^{-1} = {}^t\underline{\mathbf{R}}$. In MD++ the matrix $\underline{\mathbf{R}}$ is defined by `math::Matrixl math::rmat` which can be inverted by transposition.

Finally, Eq. 4.7 corresponds to the combined transformation

$$\mathbf{r} = \underline{\mathbf{T}}\check{\mathbf{r}} \tag{4.16}$$

with

$$\underline{\mathbf{T}} = \underline{\mathbf{R}}\,\underline{\mathbf{S}} . \tag{4.17}$$

The inverse transformation is obtained through $\underline{\mathbf{T}}^{-1} = \underline{\mathbf{S}}^{-1}\underline{\mathbf{R}}^{-1} = \underline{\mathbf{S}}^{-1}\,{}^t\underline{\mathbf{R}}$. In MD++ the matrices `math::Matrixl math::mmat` and `math::Matrixl math::minvmat` can be used.

It is also convenient to define the matrix $\underline{\mathbf{L}}'$ as the matrix containing $\mathbf{a}'$, $\mathbf{b}'$ and $\mathbf{c}'$ in its columns, *i.e.*

$$\underline{\mathbf{L}}' = \begin{pmatrix} a_x{}' & b_x{}' & c_x{}' \\ a_y{}' & b_y{}' & c_y{}' \\ a_z{}' & b_z{}' & c_z{}' \end{pmatrix} = \underline{\mathbf{S}}\,\underline{\mathbf{B}} , \tag{4.18}$$

and the matrix $\underline{\mathbf{L}}$ as the matrix containing containing $\mathbf{a}$, $\mathbf{b}$ and $\mathbf{c}$ in its columns, *i.e.*

$$\underline{\mathbf{L}} = \begin{pmatrix} a_x & b_x & c_x \\ a_y & b_y & c_y \\ a_z & b_z & c_z \end{pmatrix} = \underline{\mathbf{R}}\,\underline{\mathbf{L}}' = \underline{\mathbf{R}}\,\underline{\mathbf{S}}\,\underline{\mathbf{B}} = \underline{\mathbf{T}}\,\underline{\mathbf{B}} . \tag{4.19}$$

Obviously,

$$\mathbf{r}' = \underline{\mathbf{L}}'\check{\mathbf{r}} \quad \text{and} \quad \mathbf{r} = \underline{\mathbf{L}}\check{\mathbf{r}} . \tag{4.20}$$

In some cases, it may be necessary to calculate the Euler angles ϕ, θ and ψ from the components of the $\mathbf{a}$, $\mathbf{b}$ and $\mathbf{c}$ vectors. This may be done by constructing the unit vectors of the box-linked Cartesian coordinate system as

$$\begin{aligned} \hat{\mathbf{e}}_{x'} &= a^{-1}\,\mathbf{a} , \\ \hat{\mathbf{e}}_{y'} &= \parallel \mathbf{b} - (a\,b)^{-1}(\mathbf{a}\cdot\mathbf{b})\mathbf{a} \parallel^{-1} \; [\mathbf{b} - (a\,b)^{-1}(\mathbf{a}\cdot\mathbf{b})\mathbf{a}] , \\ \hat{\mathbf{e}}_{z'} &= \hat{\mathbf{e}}_{x'} \times \hat{\mathbf{e}}_{y'} . \end{aligned} \tag{4.21}$$

Identifying the matrix containing $\hat{\mathbf{e}}_{x'}$, $\hat{\mathbf{e}}_{y'}$ and $\hat{\mathbf{e}}_{z'}$ in its columns with the matrix $\underline{\mathbf{R}}$ of Eq. 4.14, one has

$$\begin{aligned} \theta &= -\text{sign}(\underline{\mathbf{R}}_{31})\text{acos}[(\underline{\mathbf{R}}_{11}^2 + \underline{\mathbf{R}}_{21}^2)^{1/2}] && (4.22) \\ \psi &= \text{sign}(\underline{\mathbf{R}}_{32}\cos^{-1}\theta)\text{acos}(\underline{\mathbf{R}}_{33}\cos^{-1}\theta) \\ \phi &= \text{sign}(\underline{\mathbf{R}}_{21}\cos^{-1}\theta)\text{acos}(\underline{\mathbf{R}}_{11}\cos^{-1}\theta) && (4.23) \end{aligned}$$

if $R_{11}^2 + R_{21}^2 \neq 0$, or

$$\begin{aligned} \theta &= -\text{sign}(\underline{\mathbf{R}}_{31})\pi/2 && (4.24) \\ \psi &= 0 \\ \phi &= -\text{sign}(\underline{\mathbf{R}}_{12})\text{acos}(\underline{\mathbf{R}}_{22}) \ , && (4.25) \end{aligned}$$

otherwise. The function $sign(x)$ delivers the sign of x.

4.4.1.2. *Nearest image and gathering.* When calculating the forces on the black atom in the central box in Fig. 4.2, all interactions with atoms in the central box or images in the surrounding boxes that lie within the spherical cut-off radius R_c are taken into account. To avoid artificial periodicity effects, an atom should not simultaneously interact with another atom and its image. Therefore, in GROMOS only the *interaction between nearest images* is evaluated. Consequently, the smallest wall-to-wall distance R_{box} *must exceed twice the cut-off radius* R_c:

$$R_{box} > 2R_c \qquad (4.26)$$

that is, the *cut-off radius* (RCUTP or RCUTL) must be smaller than half the smallest edge of the box. Since the cut-off radii RCUTP and RCUTL are applied to charge groups one should choose

$$RCUTP \leqslant RCUTL \leqslant R_c - R^{cg} \qquad (4.27)$$

with R_c satisfying Eq. 4.26 and where R^{cg} is the charge group radius.

This condition can be met by choosing the system large enough, e.g. in a crystal the computational box may contain more than one unit cell. The application of non-bonded neighbour search techniques in periodic systems is discussed in[14]. Possible distorting effects of the periodic boundary condition may be traced by simulating systems of different size.

Applying periodic boundary conditions implies that when an atom leaves the central box through one of its walls, it enters at the opposite image position with the same velocity. However, in GROMOS this *periodic translation* is not performed for single atoms, but for all *atoms of a charge group*. Solute charge group atoms and solvent molecules are translated, applying periodic boundary conditions such that the first atom of a solute charge group or of a solvent molecule lies within the central periodic box.

For an arbitrary molecular configuration the atoms of a charge group may lie far apart in the central box, close to opposite walls, while their nearest images are close to each other. In that case the atoms of a charge group must first be gathered by applying periodic boundary conditions, such that the atoms of a charge group lie within $R_{box}/2$ of each other. It is always assumed that the atoms of a solvent molecule lie within $R_{box}/2$ of each other, viz. that the *solvent atom coordinates are generated without mixing different periodic images in one solvent molecule*.

When a solute molecule consists of a chain of covalently bound atoms, this chain may be cut into different segments by the periodic boundaries. Following the chain one may leave the central box through one wall and enter it at the opposite wall at the image position. This means that when the various contributions to the potential energy in Eq. 3.5 are computed, nearest images of atoms involved in bonds, bond angles, dihedral angles, etc. have to be used.

In a triclinic box, the direction of the edges are denoted by **a**, **b** and **c** and lengths a, b, and c. The atom or charge group i with position $\mathbf{r}_i$ can be *kept in the computational box* that lies in the positive quadrant with respect to an origin at $\mathbf{r}_0$, by applying the translation

$$\mathbf{r}_i' = \mathbf{r}_i - NINT((z_i - z_0 - c/2)/c)\mathbf{c}$$

$$\begin{aligned}
\mathbf{r}_i'' &= \mathbf{r}_i' - NINT((y_i' - y_0 - b/2)/b)\mathbf{b} \\
\mathbf{r}_i''' &= \mathbf{r}_i'' - NINT((x_i'' - x_0 - a/2)/a)\mathbf{a} \\
\mathbf{r}_i &= \mathbf{r}_i'''. \qquad (4.28)
\end{aligned}$$

where the function NINT(x) delivers the integer number that is nearest to x. When calculating in oblique coordinates, Eq. 4.53 can be used. For two atoms or charge groups i and j the vector

$$\mathbf{r}_{ij} = \mathbf{r}_i - \mathbf{r}_j \qquad (4.29)$$

can be transformed to the vector $\mathbf{r}_{ij}^{NI}$ *connecting nearest images* by the transformation

$$\begin{aligned}
\mathbf{r}_{ij}' &= \mathbf{r}_i - NINT((z_{ij}/c)\mathbf{c} \\
\mathbf{r}_{ij}'' &= \mathbf{r}_i' - NINT((y_{ij}'/b)\mathbf{b} \\
\mathbf{r}_{ij}''' &= \mathbf{r}_i'' - NINT((x_{ij}''a)\mathbf{a} \\
\mathbf{r}_{ij}^{NI} &= \mathbf{r}_i'''. \qquad (4.30)
\end{aligned}$$

4.4.1.3. *Geometric properties.* In a general triclinic box, the square length of a vector is given in terms of the corresponding oblique coordinates by

$$\begin{aligned}
r^2 &= x^2 + y^2 + z^2 = (x')^2 + (y')^2 + (z')^2 \qquad (4.31) \\
&= u^2 + v^2 + w^2 + 2uv\cos\gamma + 2uw\cos\beta + 2vw\cos\alpha \ .
\end{aligned}$$

The volume of a triclinic box is given by

$$\mathcal{V} = abc[1 - \cos^2\alpha - \cos^2\beta - \cos^2\gamma + 2\cos\alpha\cos\beta\cos\gamma]^{1/2} \ . \qquad (4.32)$$

The acceptable cutoff value within a triclinic box is restricted to half the minimum distance between any two opposite walls of the cell, *i.e.* the restriction Eq. 4.26 becomes

$$R_c \leq \frac{1}{2}\,\mathrm{MIN}((ab\sin\gamma)^{-1}\mathcal{V}; (ac\sin\beta)^{-1}\mathcal{V}; (bc\sin\alpha)^{-1}\mathcal{V}), \qquad (4.33)$$

The function MIN(x,y,z) delivers the smallest of its arguments x, y, z. In principle, the condition

$$R_c \leq \frac{1}{2}\mathrm{MIN}\{\parallel n_1\mathbf{a} + n_2\mathbf{b} + n_3\mathbf{c} \parallel \mid \ n_1, n_2, n_3 = 0 \text{ or } 1 \ , \ \mathbf{n} \neq \mathbf{0}\} \qquad (4.34)$$

would be sufficient to ensure that at most one periodic copy of each particle is within the cutoff distance of any other. However, this closest periodic copy is not necessarily the minimum image as determined by Eq. 4.52. To avoid this complication, the more restrictive condition of Eq. 4.33 is required.

The checking whether the box parameters are in allowed ranges (Sec. 4.4.1) and that the cutoff values are compatible with these is performed by `math::boundary_check_cutoff` in MD++.

4.4.1.4. *Reciprocal-lattice.* In the triclinic case, the reciprocal-lattice vectors $\tilde{\mathbf{a}}$, $\tilde{\mathbf{b}}$ and $\tilde{\mathbf{c}}$ associated with the edge vectors $\mathbf{a}$, $\mathbf{b}$ and $\mathbf{c}$ are defined by

$$\tilde{\mathbf{a}} = \mathcal{V}^{-1}\mathbf{b}\times\mathbf{c} \quad , \quad \tilde{\mathbf{b}} = \mathcal{V}^{-1}\mathbf{c}\times\mathbf{a} \quad \text{and} \quad \tilde{\mathbf{c}} = \mathcal{V}^{-1}\mathbf{a}\times\mathbf{b} \ . \qquad (4.35)$$

The matrix containing in its columns the components of $\tilde{\mathbf{a}}'$, $\tilde{\mathbf{b}}'$ and $\tilde{\mathbf{c}}'$ in the box-linked Cartesian coordinate system is easily shown to be

$$\begin{pmatrix} \tilde{a}_{x'} & \tilde{b}_{x'} & \tilde{c}_{x'} \\ \tilde{a}_{y'} & \tilde{b}_{y'} & \tilde{c}_{y'} \\ \tilde{a}_{z'} & \tilde{b}_{z'} & \tilde{c}_{z'} \end{pmatrix} = ({}^t\underline{\mathbf{L}}')^{-1} = {}^t\underline{\mathbf{S}}^{-1}\,\underline{\mathbf{B}}^{-1} \ . \qquad (4.36)$$

Similarly, the matrix containing in its columns the components of $\tilde{\mathbf{a}}$, $\tilde{\mathbf{b}}$ and $\tilde{\mathbf{c}}$ in the reference Cartesian coordinate system is given by

$$\begin{pmatrix} \tilde{a}_x & \tilde{b}_x & \tilde{c}_x \\ \tilde{a}_y & \tilde{b}_y & \tilde{c}_y \\ \tilde{a}_z & \tilde{b}_z & \tilde{c}_z \end{pmatrix} = {}^t\underline{\mathbf{L}}^{-1} = \underline{\mathbf{R}}\,({}^t\underline{\mathbf{L}}')^{-1} = \underline{\mathbf{R}}\,{}^t\underline{\mathbf{S}}^{-1}\,\underline{\mathbf{B}}^{-1} = {}^t\underline{\mathbf{T}}^{-1}\,\underline{\mathbf{B}}^{-1} \ . \qquad (4.37)$$

A reciprocal-space vector $\mathbf{k}$ is defined by

$$\mathbf{k} = 2\pi(l_a\tilde{\mathbf{a}} + l_b\tilde{\mathbf{b}} + l_c\tilde{\mathbf{c}}) \ , \qquad (4.38)$$

where $\mathbf{l} = (l_a, l_b, l_c)$ is a vector with integer, positive or negative, components. A reciprocal-space vector can be specified in five distinct ways : (*i*) through the integer vector $\mathbf{l}$; (*ii*) through oblique fractional

reciprocal space vectors $\breve{\mathbf{k}} = (\chi_q, \chi_s, \chi_t)$ with reference to the reciprocal-lattice vectors ; (iii) through oblique reciprocal space vectors $\breve{\mathbf{k}} = (\kappa_u, \kappa_v, \kappa_w)$ with reference to the reciprocal-lattice vectors ; (iv) through reciprocal space vectors $\mathbf{k}' = (rlk_{x'}', rlk_{y'}', rlk_{z'}')$ within the box-linked Cartesian coordinate system ; (v) through reciprocal space vectors $\mathbf{k} = (rlk_x, rlk_y, rlk_z)$ within the reference Cartesian coordinate system. The different coordinates are related through

$$\breve{\mathbf{k}} = 2\pi \mathbf{l} \; , \tag{4.39}$$

$$\breve{\mathbf{k}} = \underline{\mathbf{B}}^{-1} \breve{\mathbf{k}} = 2\pi \underline{\mathbf{B}}^{-1} \mathbf{l} \; , \tag{4.40}$$

$$\mathbf{k}' = {}^t\underline{\mathbf{S}}^{-1} \breve{\mathbf{k}} = ({}^t\underline{\mathbf{L}}')^{-1} \breve{\mathbf{k}} = 2\pi ({}^t\underline{\mathbf{L}}')^{-1} \mathbf{l} \; , \tag{4.41}$$

and

$$\mathbf{k} = \underline{\mathbf{R}} \mathbf{k}' = {}^t\underline{\mathbf{T}}^{-1} \breve{\mathbf{k}} = {}^t\underline{\mathbf{L}}^{-1} \breve{\mathbf{k}} = 2\pi {}^t\underline{\mathbf{L}}^{-1} \mathbf{l} \; . \tag{4.42}$$

At this point, it is also useful to state a number of important relationships. First, scalar products between real- and reciprocal-space vectors can be formulated similarly in the different coordinate representations, *i.e.*

$$\mathbf{k} \cdot \mathbf{r} = \mathbf{k}' \cdot \mathbf{r}' = \breve{\mathbf{k}} \cdot \breve{\mathbf{r}} = \breve{\mathbf{k}} \cdot \breve{\mathbf{r}} \; , \tag{4.43}$$

which follow immediately from the coordinate transformations given above. Second, a few useful differential relationships can be stated. For differentiating a reciprocal-space vector with respect to the box parameters, given in the form of the matrix $\underline{\mathbf{L}}$, one has

$$\frac{\partial \mathbf{k}}{\partial \underline{\mathbf{L}}_{\mu\nu}} = -\mathbf{k}_\mu \, {}^t\underline{\mathbf{L}}^{-1} \hat{\mathbf{e}}_\nu \; . \tag{4.44}$$

Following from this result, the differentiation of a scalar product of two reciprocal-space vectors with respect to the box parameters leads to

$$\frac{\partial (\mathbf{k}_1 \cdot \mathbf{k}_2)}{\partial \underline{\mathbf{L}}_{\mu\nu}} = -\mathbf{k}_{1,\mu} \, [\underline{\mathbf{L}}^{-1} \mathbf{k}_2]_\nu - \mathbf{k}_{2,\mu} \, [\underline{\mathbf{L}}^{-1} \mathbf{k}_1]_\nu \; . \tag{4.45}$$

Introducing the differentiation with respect to a matrix as a differentiation on a component-by-component basis, this may be rewritten as

$$\frac{\partial (\mathbf{k}_1 \cdot \mathbf{k}_2)}{\partial \underline{\mathbf{L}}} = -(\mathbf{k}_1 \otimes \mathbf{k}_2 + \mathbf{k}_2 \otimes \mathbf{k}_1) {}^t\underline{\mathbf{L}}^{-1} \; . \tag{4.46}$$

For differentiating the box volume $\mathcal{V} = | \, \underline{\mathbf{L}} \, |$ with respect to the box parameters, one has

$$\frac{\partial \mathcal{V}}{\partial \underline{\mathbf{L}}} = V \, {}^t\underline{\mathbf{L}}^{-1} \; . \tag{4.47}$$

4.4.1.5. *Tensor transformations.* It may be necessary to transform rank-two tensors, 3×3 matrices, among the various coordinate representations. If a tensor is written as $\underline{\mathbf{\Omega}}$ in terms of real-space oblique coordinates, $\underline{\mathbf{W}}'$ in the box-linked Cartesian coordinate system and $\underline{\mathbf{W}}$ in the reference Cartesian coordinate system, the conversion between the different representations is given by

$$\underline{\mathbf{W}}' = \underline{\mathbf{S}} \, \underline{\mathbf{\Omega}} \, {}^t\underline{\mathbf{S}} \tag{4.48}$$

and

$$\underline{\mathbf{W}} = \underline{\mathbf{R}} \, \underline{\mathbf{W}}' \, {}^t\underline{\mathbf{R}} = \underline{\mathbf{T}} \, \underline{\mathbf{\Omega}} \, {}^t\underline{\mathbf{T}} \; . \tag{4.49}$$

These three types of transformations can be easily checked by considering the simple tensors $\underline{\mathbf{W}} = \mathbf{r} \otimes \mathbf{r}$, $\underline{\mathbf{W}}' = \mathbf{r}' \otimes \mathbf{r}'$ and $\underline{\mathbf{\Omega}} = \breve{\mathbf{r}} \otimes \breve{\mathbf{r}}$ with $\mathbf{r}' = \underline{\mathbf{S}} \breve{\mathbf{r}}$ and $\mathbf{r} = \underline{\mathbf{R}} \mathbf{r}'$.

If the tensor is written $\underline{\tilde{\mathbf{\Omega}}}$ in terms of reciprocal-space oblique coordinates, the conversion between the different representations becomes

$$\underline{\mathbf{W}}' = {}^t\underline{\mathbf{S}}^{-1} \, \underline{\tilde{\mathbf{\Omega}}} \, \underline{\mathbf{S}}^{-1} \tag{4.50}$$

and

$$\underline{\mathbf{W}} = \underline{\mathbf{R}} \, \underline{\mathbf{W}}' \, {}^t\underline{\mathbf{R}} = {}^t\underline{\mathbf{T}}^{-1} \, \underline{\tilde{\mathbf{\Omega}}} \, \underline{\mathbf{T}}^{-1} \tag{4.51}$$

The transformation corresponding to the last equality can be checked by considering the simple tensors $\underline{\mathbf{W}} = \mathbf{k} \otimes \mathbf{k}$, $\underline{\mathbf{W}}' = \mathbf{k}' \otimes \mathbf{k}'$ and $\underline{\tilde{\mathbf{\Omega}}} = \breve{\mathbf{k}} \otimes \breve{\mathbf{k}}$ with $\mathbf{k}' = {}^t\underline{\mathbf{S}}^{-1} \breve{\mathbf{k}}$ and $\mathbf{k} = \underline{\mathbf{R}} \mathbf{k}'$.

In practice, these transformations are used to interconvert the various representations of the virial tensor.

4.4.1.6. *Application of periodicity.* In the triclinic case, the periodicity requirements apply to the oblique coordinates $\check{\mathbf{r}}$. The Cartesian components of the minimum-image vector $\overline{\mathbf{r}} = (\overline{x}, \overline{y}, \overline{z})$ associated with a vector $\mathbf{r} = (x, y, z)$ are obtained by

$$\begin{aligned} \overline{u} &= u - a\,\mathrm{NINT}\left(\frac{x-a}{a}\right) \\ \overline{v} &= v - b\,\mathrm{NINT}\left(\frac{y-b}{b}\right) \\ \overline{w} &= w - c\,\mathrm{NINT}\left(\frac{z-c}{c}\right) , \end{aligned} \tag{4.52}$$

where (u, v, w) are obtained from (x, y, z) through the inverse of Eq. 4.16 and $(\overline{x}, \overline{y}, \overline{z})$ from $(\overline{u}, \overline{v}, \overline{w})$ through Eq. 4.16. For the calculation of $\overline{r}^2$, the second operation may be replaced by Eq. 4.31.

4.4.2. Special periodic boundary conditions.

4.4.2.1. *Periodic rectangular box.* The simplest case of a periodic box is a rectangular box (NTB = 1). The lengths of the edges in the $x-$, $y-$ and $z-$directions are denoted by a, b and c and $\alpha = \beta = \gamma = \pi/2$. The atom or charge group i can be *kept in the computational box* that lies in the positive quadrant with respect to an origin at $\mathbf{r}_0$, by applying the translation

$$\begin{aligned} x_i &= x_i - NINT((x_i - x_0 - a/2)/a)a \\ y_i &= y_i - NINT((y_i - y_0 - b/2)/b)b \\ z_i &= z_i - NINT((z_i - z_0 - c/2)/c)c \end{aligned} \tag{4.53}$$

For two atoms or charge groups i and j the vector

$$\mathbf{r}_{ij} = \mathbf{r}_i - \mathbf{r}_j \tag{4.54}$$

can be transformed to the vector $\mathbf{r}_{ij}^{NI}$ *connecting nearest images* by the transformation

$$\begin{aligned} x_{ij}^{NI} &= x_{ij} - NINT(x_{ij}/a)a \\ y_{ij}^{NI} &= y_{ij} - NINT(y_{ij}/b)b \\ z_{ij}^{NI} &= z_{ij} - NINT(z_{ij}/c)c \end{aligned}$$

For a reactangular computational box the *requirement* Eq. 4.26 becomes

$$R_c < 1/2MIN(a, b, c) \tag{4.55}$$

4.4.2.2. *Truncated-octahedral computational box under* PBC. When simulating a spherical solute, use of a more spherically shaped computational box instead of a rectangular one may considerably reduce the number of solvent molecules that is needed to fill the remaining empty space in the box. A more spherically shaped space filling periodic box is a truncated octahedron, shown in Fig. 4.3. For a truncated-octahedral box, the vectors **a**, **b**, **c** correspond to the edges of the cube based on which the truncated octahedron is constructed with $a = b = c$ and $\alpha = \beta = \gamma = \pi/2$. The distance between the square planes is a, and between the six-sided planes it is $\frac{\sqrt{3}}{2}a$. The volume of the truncated octahedron is $\frac{1}{2}a^3$.

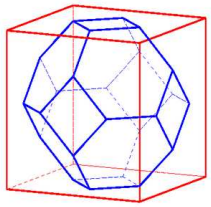

FIGURE 4.3. Truncated octahedron

The atom or charge group i can be *kept in the computational box* that lies in the positive quadrant with respect to an origin at $\mathbf{r}_0$, by applying the rectangular periodicity check Eq. 4.53 with $a = b = c$ followed by the translation

$$\text{if} \qquad |x_i - x_0 - a/2| + |y_i - y_0 - a/2| + |z_i - z_0 - a/2| > 3a/4$$

$$\text{then} \qquad \left\{ \begin{array}{rcl} x_i &=& x_i - \text{sign}(x_i - x_0 - a/2)a/2 \\ y_i &=& y_i - \text{sign}(y_i - y_0 - a/2)a/2 \\ z_i &=& z_i - \text{sign}(z_i - z_0 - a/2)a/2 \end{array} \right\} \tag{4.56}$$

The vector $\mathbf{r}_{ij}^{NIto}$ connecting nearest images of atoms or charge groups i and j is obtained by applying the rectangular periodicity check Eq. 4.55 with $a = b = c$ followed by the transformation

$$\text{if} \qquad |x_{ij}^{NI}| + |y_{ij}^{NI}| + |z_{ij}^{NI}| > 3a/4$$

$$\text{then} \quad \left\{ \begin{array}{rcl} x_{ij}^{NIto} &=& x_{ij}^{NI} - \text{sign}(x_{ij}^{NI})a/2 \\ y_{ij}^{NIto} &=& y_{ij}^{NI} - \text{sign}(y_{ij}^{NI})a/2 \\ z_{ij}^{NIto} &=& z_{ij}^{NI} - \text{sign}(z_{ij}^{NI})a/2 \end{array} \right\} \tag{4.57}$$

If *only* $(\mathbf{r}_{ij}^{NIto})^2$ *is required*, the last step, after applying Eq. 4.53 is replaced by calculating

$$(\mathbf{r}_{ij}^{NIto})^2 = (x_{ij}^{NI})^2 + (y_{ij}^{NI})^2 + (z_{ij}^{NI})^2 + a\ MIN(0,\ 3a/4 - |x_{ij}^{NI}| - |y_{ij}^{NI}| - |z_{ij}^{NI}|) \tag{4.58}$$

For a truncated octahedron the *requirement* Eq. 4.26 becomes

$$R_C \leq \frac{\sqrt{3}}{4}\, a \approx 0.433a\ . \tag{4.59}$$

that is, the *cut-off radius* must be smaller than half the distance between opposite planes that are defining the truncated octahedron. However, if the truncated-octahedron is mapped to an equivalent triclinic box (Sec. 4.4.2.3), Eq. 4.33 leads to the more restrictive condition

$$R_c \leq \frac{1}{2\sqrt{2}}\, a \approx 0.354a\ . \tag{4.60}$$

4.4.2.3. *Coordinate transformations: truncated-octahedral to triclinic box.* A simulation performed in a truncated-octahedral box can equivalently be performed in a special type of triclinic box, by applying an appropriate coordinate transformation.[23] If the edge vectors of the cube based on which the truncated-octahedron is constructed are $\mathbf{a}$, $\mathbf{b}$ and $\mathbf{c}$ (recall that $a = b = c$, $\alpha = \beta = \gamma = \pi/2$ and $\phi = \theta = \psi = 0$ in this case), a possible choice for the edges $\mathbf{a}_t$, $\mathbf{b}_t$ and $\mathbf{c}_t$ of the transformed triclinic box is

$$\mathbf{a}_t = \mathbf{a}\ , \quad \mathbf{b}_t = (1/2)(\mathbf{a} + \mathbf{b} + \mathbf{c}) \quad \text{and} \quad \mathbf{c}_t = (1/2)(-\mathbf{a} - \mathbf{b} + \mathbf{c})\ . \tag{4.61}$$

The corresponding box-edge lengths, box angles and Euler angles are $a_t = a$, $b_t = c_t = (\sqrt{3}/2)a$, $\alpha_t = \text{acos}(-1/3) \approx 109.5^o$, $\beta_t = \text{acos}(-1/\sqrt{3}) \approx 125.3^o$, $\gamma_t = \text{acos}(1/\sqrt{3}) \approx 54.8^o$, $\phi_t = \theta_t = 0$, and $\psi_t = 45°$. The mapping of atomic coordinates within a truncated-octahedral box to atomic coordinates within the transformed triclinic box is performed by applying shifts along the $\mathbf{a}_t$, $\mathbf{b}_t$ and $\mathbf{c}_t$ vectors. This transformation is performed by `math::truncoct_triclinic` in MD++. This formalism is applied for the generalization of grid-based pairlist algorithms (Sec. 3.3.3) and lattice-sum electrostatics (Sec. 7.4) to truncated-octahedral boxes.

4.4.3. Multiple unit-cell simulations under PBC**.** It is possible to simulate a periodic computational box consisting of multiple identical periodic copies, M_a, M_b and M_c along the three edge vectors, of a smaller unit cell. This option may be useful when trying to simulate a single unit cell of a crystal that is too small to allow for the application of a reasonably large cutoff value. The application of such multiple-unit-cell simulations is restricted to rectangular or triclinic periodic boundary conditions.

In MD++ the topology is constructed using `multicell_topo` where the normal topology is multiplied by M. Every timestep, before interactions are calculated, the configuration, that is coordinates and velocities, is prepared using `expand_configuration` where copies j of the original configuration $\boldsymbol{r}_i$ are added to the

original coordinate $\boldsymbol{r}_i$ using $\boldsymbol{r}_j = \boldsymbol{r}_i + (M_a M_b m_c \mathbf{a} + M_a m_b \mathbf{b} + m_c \mathbf{c})$ with m_a ranging from 1 to M_a, m_b from 1 to M_b, and m_c from 1 to M_c. The simulation time step is then performed. After that only the configuration of the original box is kept.

Note that the removal of the center of mass motion whenever required, is applied to charge groups and solvent molecules gathered in the individual subcells. Note also that the application of particle-mesh methods to evaluate electrostatic interactions (Sec. 7.4.4) will only give rise to exactly periodic forces if the number of P^3M grid subdivisions along each axis is an integer multiple of the corresponding number of subcell boundaries.

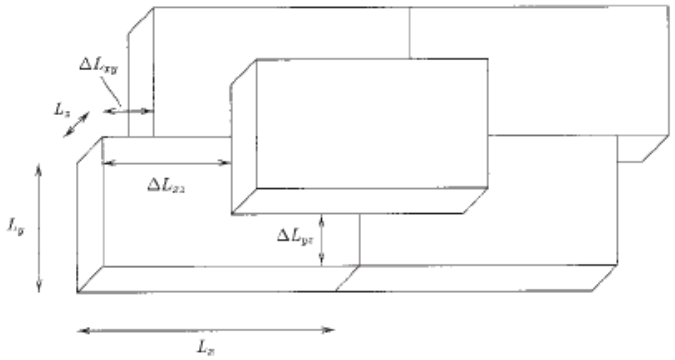

FIGURE 4.4. Rectangular-brickwall

4.4.4. Rectangular-brickwall box. A simulation performed in a triclinic box under triclinic periodic boundary conditions can equivalently be performed in a rectangular box using brickwall boundary conditions.[23] Under brickwall boundary conditions, the periodic copies of the reference box no longer systematically share common faces, but are staggered as depicted in Fig. 4.4. This transformation is applied to the triclinic box in the box-linked coordinate system, *i.e.* after rotation of the box and coordinates. The box edges of the rectangular-brickwall box will be noted $L_{x'}$, $L_{y'}$, $L_{z'}$, and the three corresponding offsets as $\Delta L_{x'y'}$, $\Delta L_{x'z'}$ and $\Delta L_{y'z'}$, primed because they refer to the Cartesian axes of the box-linked coordinate system. Out of three possible definitions, it will be further specified here that the periodic boxes only share, in the general case, common y' z' -faces and common x' -directed edges of their x' z' -faces. The edges $L_{x'}$, $L_{y'}$, and $L_{z'}$ of the rectangular box, together with the offsets $\Delta L_{x'y'}$, $\Delta L_{x'z'}$ and $\Delta L_{y'z'}$ determining the relative positions of neighboring boxes, are dictated by the lattice parameters, *i.e.* three edges and three angles, of the original triclinic box, so that the center of each rectangular box is located at a point of this triclinic lattice. To define these offsets in a unique fashion, it is further imposed that

$$-\frac{L_{x'}}{2} < \Delta L_{x'y'},\ \frac{L_{x'}}{2} \geq \Delta L_{x'z'}\ and\ -\frac{L_{y'}}{2} < \Delta L_{y'z'} \leq \frac{L_{y'}}{2} \tag{4.62}$$

Under brick-wall boundary conditions, the minimum-image function is not separable into Cartesian components, and must operate directly on a vector, that is, one has

$$\begin{aligned} z''_{ij} &= \tilde{z}'_{ij} - NINT((\tilde{z}'_{ij}/L_{z'})L_{z'}\ with\ \tilde{z}'_{ij} = z'_{ij} \\ y''_{ij} &= \tilde{y}'_{ij} - NINT((\tilde{y}'_{ij}/L_{y'})L_{y'}\ with\ \tilde{y}'_{ij} = y'_{ij} + (z''_{ij} - z''_{ij})/L_{z'} \\ x''_{ij} &= \tilde{x}'_{ij} - NINT((\tilde{x}'_{ij}/L_{x'})L_{x'} \\ with\ & \tilde{x}'_{ij} = x'_{ij} + (z''_{ij} - z''_{ij})/L_{z'} + (y''_{ij} - y''_{ij})/L_{y'} \end{aligned} \tag{4.63}$$

This formalism is applied for the generalization of grid-based pairlist algorithms (Sec. 3.3.3) to triclinic boxes and truncated-octahedral boxes, after transformation to the equivalent triclinic box, see Sec. 4.4.2.2. In the special case of a simulation performed in a regular rectangular box, the rectangular-brickwall box is identical to the original computational box and one has $L_{x'} = a$, $L_{y'} = b$, $L_{y'} = c$, $\Delta L_{x'y'} = 0$, $\Delta L_{x'z'} = 0$ and $\Delta L_{y'z'} = 0$.

The volume of the rectangular-brickwall box is equal to that of the triclinic box (Sec. 4.4.2.2) and is also identical to that of the original box.

Finally, if a triclinic box is mapped to an equivalent rectangular-brickwall box, the condition for the cut-off radius (Eq. 4.26) becomes

$$R_c \leq \frac{1}{2} \min(L_{x'}, L_{y'}, L_{z'}) \ . \tag{4.64}$$

When using a grid-based pairlist algorithm (Sec. 3.3.3), the condition is slightly more restrictive, namely

$$R_c \leq \frac{1}{2} \min(L_{x'}(1 - {G_{x'}}^{-1}), L_{y'}(1 - {G_{y'}}^{-1}), L_{z'}(1 - G_{z'})^{-1}) \ , \tag{4.65}$$

where $G_{x'}$, $G_{y'}$ and $G_{z'}$ represent the number of grid-cell subdivisions along the three axes of the box-linked coordinate system. These restrictions only apply to the specific, short- or long-range, cutoff values involved in the grid-based algorithm.

CHAPTER 5

Bonded interaction force-field terms

The potential energy or force-field term associated with *covalent interactions* is the term $\mathcal{V}^{(cov)}(\boldsymbol{r}^N;\mathbf{s})$ in Eq. 3.5. The four contributions to this term as defined by Eq. 3.6 are described in the following sections.

5.1. Bond stretching force-field term

The potential energy term associated with *bond-stretching interactions* is the term $\mathcal{V}^{(b)}(\boldsymbol{r}^N;\mathbf{s})$ in Eq. 3.6. It is given by

$$\mathcal{V}^{(b)}(\boldsymbol{r}^N;\mathbf{s}) = \sum_{n=1}^{N^{(b)}} V^{(b)}(b_n;k_n^{(b)},b_n^0) \ , \tag{5.1}$$

where $N^{(b)}$ is generally equal to the total number of all covalent bonds present in the system *i.e.* each covalent bond is associated with one and only one stretching term in the GROMOS force field, and $V^{(b)}$ is the function describing the potential energy associated with the stretching of a single bond. The quantity $b_n \doteq b_n(\boldsymbol{r}^N)$ represents the length of bond n in the given system configuration, *i.e.* the distance $\mathbf{r}_{ij}$ between the two atoms $i \doteq i(n)$ and $j \doteq j(n)$ connected by the covalent bond n, *i.e.* the minimum-image distance if PBC is applied, namely

$$b_n \doteq r_{ij} \tag{5.2}$$

with

$$\mathbf{r}_{ij} \doteq \mathbf{r}_i - \mathbf{r}_j \tag{5.3}$$

and

$$r_{ij} \doteq (\mathbf{r}_{ij}\cdot\mathbf{r}_{ij})^{1/2} \ . \tag{5.4}$$

The quantities $k_n^{(b)}$ and b_n^0 represent force-field parameters, force constant and reference length, respectively, characteristic for the specific bond n, as encoded by a corresponding *bond type code* $M_n^{(b)}$, *i.e.* one may write $k_n^{(b)} \doteq k^{(b)}(M_n^{(b)})$ and $b_n^0 \doteq b^0(M_n^{(b)})$.

Two different expressions can be used for the function $V^{(b)}$ in GROMOS. The *quartic* bond stretching interaction form $V^{(b)} = V^{(b,q)}$, the default, as used in GROMOS96, is defined as[24]

$$V^{(b,q)}(b;k^{(b,q)},b^0) \doteq \tfrac{1}{4}k^{(b,q)}(b^2-(b^0)^2)^2 \ . \tag{5.5}$$

The *harmonic* bond stretching interaction form $V^{(b)} = V^{(b,h)}$ is defined as

$$V^{(b,h)}(b;k^{(b,h)},b^0) \doteq \tfrac{1}{2}k^{(b,h)}(b-b^0)^2 \ . \tag{5.6}$$

The quartic form is computationally less expensive, since it avoids the square-root operation in the calculation of b from b^2. However, the efficiency gain is moderate for most systems, where computational costs are dominated by the calculation of the non-bonded interactions, and the harmonic form is more common and conceptually simpler. The procedure for interconverting the quartic and harmonic force constants is described in Sec. 18.1. We note that this procedure is not of immediate relevance to the users of GROMOS, since both force constants are explicitly included in the force-field files. The selection of one or the other form for bond stretching interactions can be made using the COVALENTFORM block of the MD++ input (Vol. 4).

The derivatives of the bond stretching term are described in Sec. 17.1 and the GROMOS parameters involved in this term are provided in Sec. 3-2.2.

5.2. Bond-angle bending force-field term

The potential energy term associated with *bond angle bending interactions* is the term $\mathcal{V}^{(\theta)}(\boldsymbol{r}^N;\mathbf{s})$ in Eq. 3.6. It is given by

$$\mathcal{V}^{(\theta)}(\boldsymbol{r};\underline{\mathcal{B}};\mathbf{s}) = \sum_{n=1}^{N^{(\theta)}} V^{(\theta)}(\theta_n; k_n^{(\theta)}, \theta_n^0) \ , \tag{5.7}$$

where $N^{(\theta)}$ is generally equal to the total number of all covalent bond angles present in the system *i.e.* each definable covalent bond angle is associated with one and only one bending term in the GROMOS force field, and $V^{(\theta)}$ is the function describing the potential energy associated with the bending of a single bond angle. The quantity $\theta_n \doteq \theta_n(\boldsymbol{r}^N)$ represents the value of bond angle n in the given system configuration, *i.e.* the angle formed by the three atoms $i \doteq i(n)$, $j \doteq j(n)$ and $k \doteq k(n)$ defining the covalent bond angle n, *i.e.* the minimum-image triplet if PBC is applied, namely

$$\theta_n \doteq \arccos\left(\frac{\mathbf{r}_{ij}\cdot\mathbf{r}_{kj}}{r_{ij}r_{kj}}\right) \quad \text{with} \quad 0 \le \theta_n \le \pi \tag{5.8}$$

where

$$\mathbf{r}_{ij} \doteq \mathbf{r}_i - \mathbf{r}_j \quad \text{and} \quad \mathbf{r}_{kj} \doteq \mathbf{r}_k - \mathbf{r}_j \ , \tag{5.9}$$

and

$$r_{ij} \doteq (\mathbf{r}_{ij}\cdot\mathbf{r}_{ij})^{1/2} \quad \text{and} \quad r_{kj} \doteq (\mathbf{r}_{kj}\cdot\mathbf{r}_{kj})^{1/2} \ . \tag{5.10}$$

The quantities $k_n^{(\theta)}$ and θ_n^0 represent force-field parameters, force constant and reference bond angle, respectively, characteristic for the specific bond angle n, as encoded by a corresponding *bond-angle type code* $M_n^{(\theta)}$, *i.e.* one may write $k_n^{(\theta)} \doteq k^{(\theta)}(M_n^{(\theta)})$ and $\theta_n^0 \doteq \theta^0(M_n^{(\theta)})$.

Two different expression can be used for the function $V^{(\theta)}$ in GROMOS. The *cosine-harmonic* bond angle bending interaction form $V^{(\theta)} = V^{(\theta,c)}$, the default, as used in GROMOS96, is defined as

$$V^{(\theta,c)}(\theta; k^{(\theta,c)}, \theta^0) \doteq \tfrac{1}{2}k^{(\theta,c)}(\cos\theta - \cos\theta^0)^2 \ . \tag{5.11}$$

The *angle-harmonic* bond-angle bending interaction form $V^{(\theta)} = V^{(\theta,h)}$ is defined as

$$V^{(\theta,h)}(\theta; k^{(\theta,h)}, \theta^0) \doteq \tfrac{1}{2}k^{(\theta,h)}(\theta - \theta^0)^2 \ . \tag{5.12}$$

The cosine-harmonic form is computationally less expensive, since it avoids the arc-cosine operation in the calculation of θ from $\cos\theta$. However, the efficiency gain is moderate for most systems, where computational costs are dominated by the calculation of the non-bonded interactions, and the harmonic form is more common and conceptually simpler. Furthermore, the cosine-harmonic form may pose problems in cases where the reference bond angle is close to 0 or π, *e.g.* in linear molecules or functional groups, since the curve described by $V^{(\theta,h)}$ then becomes flat around $\theta \approx \theta^0$, *i.e.* very high force constants are required to maintain the linear bond angle geometry.

The procedure for interconverting the cosine-harmonic and harmonic force constants is described in Sec. 18.1. We note that this procedure is not of immediate relevance to the users of GROMOS, since both force constants are explicitly included in the force-field files. The selection of one or the other form for bond-angle bending interactions can be made using the COVALENTFORM block of the MD++ input (Vol. 4).

The derivatives of the bond-angle bending term are described in Sec. 17.2 and the GROMOS parameters involved in this term are provided in Sec. 3-2.3.

5.3. Improper dihedral-angle bending force-field term

The potential energy term associated with *improper dihedral-angle bending interactions*, typically controlling out-of-plane or out-of-tetrahedron distortions, is the term $\mathcal{V}^{(\xi)}(\boldsymbol{r}^N;\mathbf{s})$ in Eq. 3.6. It is given by

$$\mathcal{V}^{(\xi)}(\boldsymbol{r}^N;\mathbf{s}) = \sum_{n=1}^{N^{(\xi)}} V^{(\xi)}(\xi_n; k_n^{(\xi)}, \xi_n^0) \ , \tag{5.13}$$

where $N^{(\xi)}$ generally corresponds to a subset of all possibly definable improper dihedral angles in the system, and $V^{(\xi)}$ is the function describing the potential energy associated with the bending of a single improper

dihedral angle. The quantity $\xi_n \doteq \xi_n(\boldsymbol{r}^N)$ represents the value of improper dihedral angle n in the given system configuration, *i.e.* the dihedral angle formed by the four atoms $i \doteq i(n)$, $j \doteq j(n)$, $k \doteq k(n)$ and $l \doteq l(n)$ defining the covalent improper dihedral angle n, *i.e.* the minimum-image quadruplet if PBC is applied, namely

$$\xi_n \doteq \text{sign}(\mathbf{r}_{ij} \cdot \mathbf{r}_{nk}) \arccos\left(\frac{\mathbf{r}_{mj} \cdot \mathbf{r}_{nk}}{r_{mj} r_{nk}}\right) \quad \text{with} \quad -\pi < \mid \xi_n \mid \leq \pi \tag{5.14}$$

where

$$\mathbf{r}_{mj} \doteq \mathbf{r}_{ij} \times \mathbf{r}_{kj} \quad \text{and} \quad \mathbf{r}_{nk} \doteq \mathbf{r}_{kj} \times \mathbf{r}_{kl} \tag{5.15}$$

and

$$r_{mj} \doteq (\mathbf{r}_{mj} \cdot \mathbf{r}_{mj})^{1/2} \quad \text{and} \quad r_{nk} \doteq (\mathbf{r}_{nk} \cdot \mathbf{r}_{nk})^{1/2} \ . \tag{5.16}$$

Note that the sign of the dihedral angle as defined by Eq. 5.14 follows the IUPAC-IUB convention,[25] and that the improper dihedral angle is undefined if either $r_{mj} = 0$ or $r_{nk} = 0$. The quantities $k_n^{(\xi)}$ and ξ_n^0 represent force-field parameters, force constant and reference improper dihedral angle, respectively, characteristic for the specific improper dihedral angle n, as encoded by a corresponding *improper dihedral angle type code* $M_n^{(\xi)}$, *i.e.* one may write $k_n^{(\xi)} \doteq k^{(\xi)}(M_n^{(\xi)})$ and $\xi_n^0 \doteq \xi^0(M_n^{(\xi)})$.

The function $V^{(\xi)}$ is always a *harmonic* function in GROMOS, *i.e.*

$$V^{(\xi)}(\xi; k^{(\xi)}, \xi^0) \doteq {}^1\!/_2 k^{(\xi)}(\xi - \xi^0)^2 \quad \text{with} \quad -\pi < \xi - \xi^0 \leq \pi \ . \tag{5.17}$$

Note that since improper dihedral angles are periodic variables, of period 2π, the interval selected for evaluating the difference $\xi - \xi^0$ must be specified, *i.e.* the interval $]-\pi; \pi]$ as indicated.

Unlike for bond-stretching and bond-angle bending terms, the summation in Eq. 5.13 only involves a subset of $N^{(\xi)}$ terms selected by considering all possibly definable improper dihedral angles in the system, *i.e.* only some among all definable improper dihedral angles are associated with a single improper dihedral-angle term in GROMOS. These improper dihedral angles are selected to keep groups of atoms close to a specified spatial configuration, typically planar or tetrahedral. For example, in an amino acid residue, the atoms CA, C, O and N are kept near a planar configuration by defining an improper dihedral C-CA-N-O with $\xi^0 = 0°$. As another example, if the CA atom of an amino acid residue carries no explicit hydrogen, *i.e.* it is a united-atom of type CH1, the atoms CA, N, C and CB are kept near a tetrahedral configuration by defining an improper dihedral angle CA-N-C-CB (L-amino acid) or CA-C-N-CB (D-amino acid) with $\xi^0 = 35.26°$. A third example is that of an aromatic ring, like in the phenylalanine amino acid residue, which is kept close to planarity by defining 6 improper dihedral angles (CG-CD1-CE1-CZ, CD1-CE1-CZ-CE2, CE1-CZ-CE2-CD2, CZ-CE2-CD2-CG, CE2-CD2-CG-CD1 and CD2-CG-CD1-CE1), all with $\xi^0 = 0°$.

The derivatives of the improper dihedral-angle bending term are described in Sec. 17.3 and the GROMOS parameters involved in this term are provided in Sec. 3-2.4.

5.4. Proper dihedral-angle torsion force-field term

The potential energy term associated with *torsional dihedral-angle bending interactions*, typically controlling, together with non-bonded interactions, the rotational barriers around covalent bonds, is the term $\mathcal{V}^{(\varphi)}(\boldsymbol{r}^N; \mathbf{s})$ in Eq. 3.6. It is given by

$$\mathcal{V}^{(\varphi)}(\boldsymbol{r}^N; \mathbf{s}) = \sum_{n=1}^{N^{(\varphi)}} V^{(\varphi)}(\varphi_n; k_n^{(\varphi)}, \varphi_n^0, m_n^{(\varphi)}) \ , \tag{5.18}$$

where $N^{(\varphi)}$ generally corresponds to a subset of all possibly definable proper, torsional dihedral angles in the system. We note that multiple terms may be associated to the covalent proper dihedral angle in the GROMOS force field. $V^{(\varphi)}$ is the function describing the potential energy contribution of the term to the torsion of the corresponding proper dihedral angle. The quantity $\varphi_n \doteq \varphi_n(\boldsymbol{r}^N)$ represents the value of proper dihedral angle n in the given system configuration, *i.e.* the dihedral angle formed by the four atoms $i \doteq i(n)$, $j \doteq j(n)$, $k \doteq k(n)$ and $l \doteq l(n)$ defining the covalent proper dihedral angle n, *i.e.* the minimum-image quadruplet if PBC is applied, namely

$$\varphi_n \doteq \text{sign}(\mathbf{r}_{ij} \cdot (\mathbf{r}_{kj} \times \mathbf{r}_{kl})) \arccos\left(\frac{\mathbf{r}_{im'} \cdot \mathbf{r}_{ln'}}{r_{im'} r_{ln'}}\right) \quad \text{with} \quad -\pi < \varphi_n \leq \pi \tag{5.19}$$

where

$$\mathbf{r}_{im'} \doteq \mathbf{r}_{ij} - \frac{\mathbf{r}_{ij} \cdot \mathbf{r}_{kj}}{r_{kj}^2} \cdot \mathbf{r}_{kj} \quad \text{and} \quad \mathbf{r}_{in'} \doteq -\mathbf{r}_{kl} + \frac{\mathbf{r}_{kl} \cdot \mathbf{r}_{kj}}{r_{kj}^2} \cdot \mathbf{r}_{kj} \tag{5.20}$$

and

$$r_{im'} \doteq (\mathbf{r}_{im'} \cdot \mathbf{r}_{im'})^{1/2} \quad \text{and} \quad r_{in'} \doteq (\mathbf{r}_{in'} \cdot \mathbf{r}_{in'})^{1/2} \; . \tag{5.21}$$

Note that Eq. 5.19 is readily shown to be equivalent to Eq. 5.14. The sign of the dihedral angle as defined by Eq. 5.19 follows the IUPAC-IUB convention,[25] and the proper dihedral angle is undefined if either $r_{im'} = 0$ or $r_{in'} = 0$. The quantities $k_n^{(\varphi)}$, φ_n^0 and $m_n^{(\varphi)}$ represent force-field parameters, force constant, reference dihedral angle, and multiplicity, respectively. The reference dihedral angle is also called the phase shift. The multiplicity is a positive non-zero integer. These parameters are characteristic for the specific proper dihedral angle term n, as encoded by a corresponding *proper dihedral-angle type code* $M_n^{(\varphi)}$, *i.e.* one may write $k_n^{(\varphi)} \doteq k^{(\varphi)}(M_n^{(\varphi)})$, $\varphi_n^0 \doteq \varphi^0(M_n^{(\varphi)})$ and $m_n^{(\varphi)} \doteq m^{(\varphi)}(M_n^{(\varphi)})$

Two different expression can be used for the function $V^{(\varphi)}$ in GROMOS. These expressions do not differ in the resulting value of the interaction, but only in their range of application. The *symmetric* proper dihedral-angle torsion interaction form, the default, as used in GROMOS96, is defined as

$$V^{(\varphi)}(\varphi; k^{(\varphi)}, \varphi^0, m^{(\varphi)}) \doteq k^{(\varphi)}(1 + \cos\varphi^0 \cos m^{(\varphi)}\varphi) \quad \text{with} \quad \varphi^0 = 0, \pi \; . \tag{5.22}$$

In this form, the value of the phase shift is restricted to 0 or π, which leads to a potential that is symmetric with respect to the eclipsed conformation, either corresponding to a minimum or a maximum, depending on the sign of $\cos\varphi^0$. In addition, considering practical usefulness and computational efficiency, the multiplicity $m^{(\varphi)}$ may not exceed a value of six here. The *generalized* proper dihedral-angle torsion interaction form is defined as

$$V^{(\varphi)}(\varphi; k^{(\varphi)}, \varphi^0, m^{(\varphi)}) \doteq k^{(\varphi)} \left[1 + \cos(m^{(\varphi)}\varphi - \varphi^0)\right] \quad \text{with} \quad \varphi^0 \in [0, 2\pi[\; . \tag{5.23}$$

Here, no restrictions are made on the values of the phase shift and multiplicity. It is easily verified that Eqs. 5.22 and 5.23 are equivalent, within the domain of validity of the former expression. The symmetric form is computationally less expensive, since it avoids the arc-cosine operation in the calculation of φ from $\cos\varphi$, owing to the expansions

$$\begin{aligned}
\cos(1\varphi) &= \cos\varphi \\
\cos(2\varphi) &= 2\cos^2\varphi - 1 \\
\cos(3\varphi) &= 4\cos^3\varphi - 3\cos\varphi \\
\cos(4\varphi) &= 8\cos^4\varphi - 8\cos^2\varphi + 1 \\
\cos(5\varphi) &= 16\cos^5\varphi - 20\cos^3\varphi + 5\cos\varphi \\
\cos(6\varphi) &= 32\cos^6\varphi - 48\cos^4\varphi + 18\cos^2\varphi - 1 \; .
\end{aligned} \tag{5.24}$$

However, the efficiency gain is moderate for most systems, where computational costs are dominated by the calculation of the non-bonded interactions, and the generalized form offers the advantage of being more flexible. In particular, it may be useful in cases where a potential that is not symmetric with respect to the eclipsed conformation may permit an improved fitting of rotational profiles against experimental or theoretical data.

Note that since proper dihedral angles are periodic variables, of period 2π, the interval selected for evaluating the φ should in principle be specified. However, this selection has no influence of the result of Eqs. 5.22 and 5.23.

Unlike for bond-stretching and bond-angle bending terms, the summation in Eq. 5.18 only involves a subset of $N^{(\varphi)}$ terms selected by considering all possibly definable proper dihedral angles in the system, *i.e.* only some among all definable proper dihedral angles are associated with a single, or few proper dihedral-angle terms in GROMOS. These proper dihedral-angles are selected to control, in combination with non-bonded interactions, the rotational barriers around covalent bonds for this selection. The following guidelines can be given:

1. In general, for any bond between atoms j and k, only one set of atoms i, j, k and l is chosen to define a proper dihedral angle.
2. For bonds between atoms j and k in rigid, planar rings (aromatics), no proper torsional dihedral angle is defined, but rather improper dihedrals are used to maintain the planarity of the ring.

3. To obtain correct torsional-angle energy profiles, several torsional dihedral angles with different parameters can be defined on the same set of atoms i, j, k and l. This is for instance done for the protein backbone ϕ and ψ angles (in the GROMOS parameter set 54A7), in sugar rings or along the backbone of a nucleotide sequence.

The selection of one or the other form for proper dihedral torsion interactions can be made using the COVALENTFORM block of the MD++ input (Vol. 4).

The derivatives of the proper dihedral-angle torsion term are described in Sec. 17.4 and the GROMOS parameters involved in this term are provided in Sec. 3-2.5.

CHAPTER 6

van der Waals interactions

6.1. Introduction

In GROMOS, the van der Waals (vdW) interaction term, $\mathcal{V}^{(vdw)}(\boldsymbol{r}^N;\mathbf{s})$ in Eq. 3.7, is represented by a Lennard-Jones function, and the term is partitioned as a sum of two contributions.

$$\mathcal{V}^{(vdw)}(\boldsymbol{r}^N;\mathbf{s}) = \sum_{i}^{\mathcal{N}_a-1} \sum_{j=i+1}^{\mathcal{N}_a} \left[\frac{C_{12}(i,j)}{\mathbf{r}_{ij}^6} - C_6(i,j) \right] \cdot \frac{1}{\mathbf{r}_{ij}^6} \tag{6.1}$$

where $C_{12}(i,j)$ is the van der Waals repulsion coefficient for the interaction between atoms or sites i and j, $C_6(i,j)$ is the dispersion coefficient, and $\mathbf{r}_{ij}$ the distance between the two sites.

$$C_{12}(i,j) = 4\epsilon\sigma^{12} \tag{6.2}$$

and

$$C_6(i,j) = 4\epsilon\sigma^{6} \tag{6.3}$$

in which ϵ is the depth of the potential well, σ is the corresponding distance between the two sites where $\mathcal{V}^{(vdw)} = 0$. The minimum-energy distance is $2^{1/6}\sigma$.

The total van der Waals interaction of all particles is in principle obtained from a summation of all pairs of atoms within the pairlist (Sec. 3.3). However, in practice a number of pairs are excluded from the summation. These pairs are defined as excluded neighbour atom pairs. This is discussed in Sec. 6.2.

The derivatives of the van der Waals interaction term are described in Sec. 17.5.

6.2. Excluded neighbours

Atoms i and j that are covalently bound are called first neighbour atoms and if they are each covalently bound to one common neighbour atom, they are called second neighbours. Due to the short distance $\mathbf{r}_{ij}$ between first or second neighbours, the non-bonded interaction (Eq. 6.1) between such neighbour atoms i and j will be very large. In addition, first and second neighbour interactions are represented by bond-stretching and bond-angle bending interaction terms. Therefore, *first and second neighbours are excluded* from the summation. *Third neighbours* are only in special cases excluded, e.g. between atoms in or attached to aromatic rings, or between specific atoms in certain carbohydrate building blocks.

Lists of excluded atoms are kept in the molecular topology file, see Vol. 4. The atom sequence numbers j of the excluded neighbours of a solute atom i are listed in ascending order and i<j. In the solvent part of the molecular topology all atoms that form a solvent molecule are excluded neighbours of each other.

For the GROMOS force fields the excluded atom information can be found in the molecular topology building block files *.mtb.

6.3. Normal van der Waals interactions

The non-bonded interaction van der Waals parameters C_{12}(i,j) and C_6(i,j) in formula (Eq. 6.1) depend on the atom type or more specifically the integer atom codes I = IAC[i] and J = IAC[j] of the atoms with atom sequence numbers i and j. The integer atom codes of the various types of atoms are listed in Chap. 3-3. Lists of integer atom codes are kept in the molecular topology file Vol. 4. The molecular topology file contains the full matrix of interaction parameters for all combinations of integer atom types. In this way it is possible to change the van der Waals interaction between each pair of atom types independently. In practice, the

GROMOS van der Waals parameters for an atom pair with integer atom codes I and J are derived from single atom van der Waals parameters using the relations

$$C_6(I,J) = {C_6}^{1/2}(I,I){C_6}^{1/2}(J,J) \tag{6.4}$$

and

$$C_{12}(I,J) = {C_{12}}^{1/2}(I,I){C_{12}}^{1/2}(J,J) \tag{6.5}$$

For the GROMOS force fields, the single atom van der Waals parameters $C_6(I,I)^{1/2}$ and $C_{12}(I,I)^{1/2}$ are given in the third and fourth columns of Tabs. 3-3.7 (45A4 and 45B4) and 3-3.22 (54A7 and 54B7) as a function of integer atom code or non-bonded atom type.

The GROMOS force fields do not contain a special term in the interaction function (Eq. 3.4) that mimics hydrogen bonding. The hydrogen bonding capacity of molecules is the result of a balance between Coulomb and van der Waals attraction and repulsion. In order to mimic correctly the hydrogen bonding properties of polar atoms, their van der Waals repulsion has been increased over the value resulting from the use of ${C_{12}}^{1/2}$ from the fourth column in Tabs. 3-3.7 and 3-3.22. The fifth column of these tables contains the ${C_{12}}^{1/2}$(I,I) values to be used between polar atoms. For correct modelling of hydrogen bonds between atoms that are part of a charged moiety, like the OM atom in a COO^- group and a NL atom in a NH_3^+ group, the repulsive part of the van der Waals interaction has been increased even more. The sixth column in Tabs. 3-3.7 and 3-3.22 contains the ${C_{12}}^{1/2}$(I,I) values to be used between oppositely charged atoms. In Tabs. 3-3.10 and 3-3.24 it is denoted which values for ${C_{12}}^{1/2}$(I,I) and ${C_{12}}^{1/2}$(J,J) are to be used in formula (Eq. 6.5) for obtaining C_{12}(I,J).

If another combination rule than formulae Eqs. 6.4 and 6.5 is to be used to obtain C_6(I,J) and C_{12}(I,J) or if these mixed atom type pair parameters are not related to the single atom type van der Waals parameters ${C_6}^{1/2}$(I,I) and ${C_6}^{1/2}$(J,J) or ${C_{12}}^{1/2}$(I,I) and ${C_{12}}^{1/2}$(J,J), the interaction parameters for the pair of atom types (I,J) must be explicitly given as C_6(I,J) and C_{12}(I,J). In the GROMOS force field this is the case for the van der Waals parameters for the solvent chloroform. The non-standard mixed atom type pair van der Waals parameters are listed in Tab. 3-3.9. Furthermore, exceptions for individual pairs of atoms i,j may be defined at the building block level, using the LJEXCEPTION listings (see Vol. 4).

For the GROMOS force fields the non-bonded atom type information and the normal van der Waals interaction parameters can be found in the interaction function parameter files *.ifp.

The van der Waals parameters of the 45B4 force field which is to be used for in vacuo calculations, are identical to those of the 45A4 force field which is to be used for calculations including solvent, except for the repulsive parameters of the OM and NL atoms of which the charge has been reduced when deriving the 45B4 force field from the 45A4 one.

For an atom pair with integer atom codes I and J, the ${C_{12}}^{1/2}$(I,I) value in formula (Eq. 6.5) is taken from the fourth column in Tabs. 3-3.7 and 3-3.22 if the matrix element (I,J) equals 1; it is taken from the fifth column if the matrix element is equal to 2 and from the sixth element if it is equal to 3. Similarly, the ${C_{12}}^{1/2}$(J,J) value in formula (Eq. 6.5) is selected using the matrix element (J,I).

6.4. Third-neighbour van der Waals interaction

When the van der Waals parameters for the united atoms (CH1, CH2, CH3, CR1) are applied to atoms that are separated by three covalent bonds, so-called third neighbours, they induce a too large repulsion in gauche conformations.

In order to avoid this effect, the smaller van der Waals parameters that are given in Tab. 3-3.11 (45A4, 45B4) and Tab. 3-3.26 (53A5, 53B5, 54A7, 54B7) are used for united atoms when obtaining C_6(I,J) and C_{12}(I,J) from (Eq. 6.4-Eq. 6.5) for third-neighbour atoms. The van der Waals parameters for *third-neighbour or 1-4 interactions* are kept in the molecular topology file (Vol. 4).

Lists of third-neighbour atoms are kept in the molecular topology file (Vol. 4). The sequence numbers j of an atom that is a third neighbour of the atom with sequence number i, are listed in ascending order and $i < j$. In the solvent part of the molecular topology all atoms that form a solvent molecule are excluded neighbour atoms of each other, so will have neither normal nor third-neighbour van der Waals interaction.

The list of third neighbours can be derived from the list of covalent bonds occurring in the "solute". This is done in program *make_top* upon construction of a molecular topology file from the molecular building blocks.

For the GROMOS force fields the third-neighbour van der Waals interaction parameters can be found in the interaction function parameter files (*.ifp). GROMOS offers a possibility to specify the van der Waals parameters for a specific atom pair, thereby overruling the interaction parameters as derived from the normal (or third-neighbour) interaction parameters. This can be done by introducing a LJEXCEPTIONS block in the molecular topology file (see Sec. 4-3.2).

6.5. Soft-core interactions

The van der Waals interaction in Eq. 6.1 and the electrostatic interaction between charges of equal sign in Eq. 7.2 become infinitely large for $\mathbf{r}_{ij}$ approaching zero. Using interactions Eqs. 6.1 and 7.2 the atoms have a so-called hard core, which restricts the sampling of configurational space. By smoothening the potential energy surface $\mathcal{V}^{(vdw)}(\boldsymbol{r}^N;\mathbf{s})$ the sampling can be considerably enhanced. Using a so-called *soft-core interaction* function for the interactions between particles i and j of the form[26]

$$\mathcal{V}_{ij}^{(vdw),sc}(\boldsymbol{r}^N;\mathbf{s}) = \left[\frac{C_{12}(i,j)}{\alpha_{LJ}(i,j)\lambda^2 C_{126}(i,j)+(r_{ij})^6} - C_6(i,j)\right]\cdot\frac{1}{\alpha_{LJ}(i,j)\lambda^2 C_{126}(i,j)+(r_{ij})^6} \tag{6.6}$$

and

$$\mathcal{V}^{(ele)}(\boldsymbol{r};\underline{\mathcal{B}};\mathbf{s}) = \frac{q_i q_j}{4\pi\epsilon_0\epsilon_1}\left[\frac{1}{[\alpha_C(i,j)\lambda^2+(\mathbf{r}_{ij})^2]^{1/2}} - \frac{\frac{1}{2}C_{rf}(\mathbf{r}_{i,j})^2}{\left[\alpha_C(i,j)\lambda^2+R_{rf}^2\right]^{3/2}} - \frac{(1-\frac{1}{2}C_{rf})}{R_{rf}}\right] \tag{6.7}$$

The singularity at $r_{ij}=0$ is removed and the interaction function is smoothened for $\lambda\neq 0$. α_{LJ} (i,j) is a softness parameter and C_{126} is defined in Eq. 14.79.

In GROMOS, the soft-core interaction Eq. 6.6 can only be selected in the framework of a so-called perturbation molecular topology required for free energy calculations using the λ-coupling parameter approach. Therefore, the soft-core interaction is described further in Chap. 14.

CHAPTER 7

Electrostatic interactions

7.1. Introduction

In this chapter, we provide the possible forms employed in GROMOS for the term $\mathcal{V}^{(ele)}(\boldsymbol{r}^N;\mathbf{s})$ in Eq. 3.7. In all cases, this quantity can be further partitioned as a sum of contributions from a *pairwise*, a *self* and a *surface* term, namely

$$\mathcal{V}^{(ele)}(\boldsymbol{r}^N;\mathbf{s}) \doteq \mathcal{V}^{(ele,pws)}(\boldsymbol{r}^N;\mathbf{s}) + \mathcal{V}^{(ele,slf)}(\mathbf{s}) + \mathcal{V}^{(ele,srf)}(\boldsymbol{r}^N;\mathbf{s}) \; . \tag{7.1}$$

The expressions defining these three contributions differ whether one decides to employ a *reaction-field* (RF) or a *lattice-sum* (LS) scheme to evaluate the long-distance electrostatic interactions. The RF scheme is applicable under either FBC or PBC, while the LS scheme is only applicable under PBC. The features common to the two schemes are summarized in Sec. 7.2. The specifics of the RF and LS schemes are then provided in Secs. 7.3 and 7.4, respectively.

7.2. Common features

The pairwise contribution $\mathcal{V}^{(ele,pws)}$ in Eq. 7.1 can be written in the form

$$\mathcal{V}^{(ele,pws)}(\boldsymbol{r}^N;\mathbf{s}) \doteq (4\pi\epsilon_0\epsilon_{cs})^{-1} \sum_{i=1}^{\mathcal{N}_a-1} \sum_{j=i+1}^{\mathcal{N}_a} q_i q_j [\Psi_{ij}^{(ele)}(\boldsymbol{r}^N;\mathbf{s}) - \delta_{ij}^{(exc)}(\mathbf{s})\overline{r}_{ij}{}^{-1}] \tag{7.2}$$

where ϵ_0 is the permittivity of vacuum, and ϵ_{cs} the relative permittivity of the medium in which the simulation is performed. In simulations with explicit solvent we generally set $\epsilon_{cs} = 1$. q_i and q_j are the charges of particles i and j, respectively, $\overline{\mathbf{r}}_{ij}$ the (minimum-image, under PBC) vector connecting j to i (norm $\overline{r}_{ij}$), $\Psi_{ij}^{(ele)}(\boldsymbol{r}^N;\mathbf{s})$ is the *electrostatic influence function* associated with the particle pair $i-j$, $\delta_{ij}^{(exc)}$ is the *non-bonded exclusion indicator* for the particle pair $i-j$, 1 if the atoms are excluded, 0 otherwise. In the GROMOS force field, first- and second covalent neighbours are normally excluded from electrostatic interactions, as well as some specific pairs of atoms that are separated by three or more covalent bonds, as described in Sec. 6.2. The definition of excluded pairs is assumed to be encompassed in the force-field parameter vector $\mathbf{s}$. Although Coulomb's law would suggest that $\Psi_{ij}^{(ele)}(\boldsymbol{r}) = r_{ij}^{-1}$, this choice is almost never directly applicable in practice (except for systems under FBC and in the absence of exclusions; see below).

The self contribution $\mathcal{V}^{(ele,slf)}$ in Eq. 7.1 can be written in the form

$$\mathcal{V}^{(ele,slf)}(\boldsymbol{r}^N;\mathbf{s}) \doteq (8\pi\epsilon_0\epsilon_{cs})^{-1} \sum_{i=1}^{\mathcal{N}_a} q_i^2 \Psi^{(ele,slf)} \tag{7.3}$$

where $\Psi^{(ele,slf)}$ is the *electrostatic self influence function*, defined by

$$\Psi^{(ele,slf)} \doteq \lim_{\mathbf{r}_i \to \mathbf{r}_o} \Psi_{oi}^{(ele)}(\boldsymbol{r};\mathbf{s}) \; . \tag{7.4}$$

The fact that $\Psi^{(ele,slf)}$ solely depends on the boundary conditions and associated parameters will be explicited in the following sections.

Finally, the surface contribution $\mathcal{V}^{(ele,srf)}$ in Eq. 7.1 arises from the definition of the medium surrounding an infinite periodic system (under PBC). It can be written in the form

$$\mathcal{V}^{(ele,srf)}(\boldsymbol{r}^N;\mathbf{s}) \doteq [2\pi\epsilon_0(2\epsilon_{ls}+1)\mathcal{V}]^{-1}\mathbf{M}^2 \tag{7.5}$$

where ϵ_{ls} is the relative permittivity of the medium surrounding the infinite periodic system, $\mathcal{V}$ is the volume of the computational box, and $\mathbf{M}$ the box dipole moment.

The exact forms of taken by the functions $\Psi_{ij}^{(ele)}$ and $\Psi^{(ele,slf)}$ in Eqs. 7.2 and 7.4, respectively, will be detailed in Secs. 7.3 and 7.4, respectively.

7.3. Reaction-field (RF) interactions

The RF scheme is applicable under either FBC or PBC. The electrostatic influence function $\Psi_{ij}^{(ele)}$ (Eq. 7.2) in the RF case, which is a cutoff-based scheme, may take two different forms depending on whether a *particle (atom)* (AT) or a *charge-group* (CHG) cutoff truncation is applied.

In the AT case, this function reads

$$\Psi_{ij}^{(ele)}(\boldsymbol{r}) \doteq H(R_C - \overline{r}_{ij})\psi^{(RF)}(\overline{r}_{ij}) \ , \tag{7.6}$$

(independent of $\mathbf{s}$ here) while in the CHG case, it reads

$$\Psi_{ij}^{(ele)}(\boldsymbol{r};\mathbf{s}) \doteq H(R_C - \overline{R}_{ij}(\boldsymbol{r}))\psi^{(RF)}(\overline{r}_{ij}) \ , \tag{7.7}$$

where $\overline{\mathbf{r}}_{ij}$ is the (minimum-image, under PBC) vector vector connecting particle j to particle i (norm $\overline{r}_{ij}$), $\overline{\mathbf{R}}_{ij}$ the (minimum-image, under PBC) vector connecting the centers of the CHG to which the two particles belong (norm $\overline{R}_{ij}$), R_C is the cutoff distance and H the Heaviside step function (1 if its argument is positive, 0 otherwise). In the two above equations, the function $\psi^{(RF)}$ is the same and reads

$$\psi^{(RF)}(r) \doteq \frac{1}{r} - \frac{C_{RF}}{2{R_{RF}}^3}r^2 - \frac{1-(1/2)C_{RF}}{R_{RF}} \tag{7.8}$$

with

$$C_{RF} \doteq \frac{(2\epsilon_{cs}-2\epsilon_{RF})(1+\kappa_{RF}R_{RF}) - \epsilon_{RF} * (\kappa_{RF}R_{RF})^2}{(\epsilon_{cs}+2\epsilon_{RF})(1+\kappa_{RF}R_{RF}) + \epsilon_{RF} * (\kappa_{RF} * R_{RF})^2} \ , \tag{7.9}$$

where ϵ_{RF} is the RF permittivity, κ_{RF} the inverse Debye screening length and R_{RF} the RF cutoff.

The three terms resulting from the insertion of Eqs. 7.6 or 7.7 into Eq. 7.2 are termed *coulombic*, *distance-dependent* and *distance-independent*, namely

$$\mathcal{V}^{(ele,pws,RF-CB)} \doteq (4\pi\epsilon_0)^{-1}\sum_i\sum_j \frac{q_iq_j}{\overline{r}_{ij}} \tag{7.10}$$

$$\mathcal{V}^{(ele,pws,RF-RF)} \doteq (4\pi\epsilon_0)^{-1}\sum_i\sum_j -\frac{q_iq_jC_{RF}{\overline{r}_{ij}}^2}{2{R_{RF}}^3} \tag{7.11}$$

and

$$\mathcal{V}^{(ele,pws,RF-RC)} \doteq (4\pi\epsilon_0)^{-1}\sum_i\sum_j -\frac{q_iq_j(1-(1/2)C_{RF})}{R_{RF}} \tag{7.12}$$

In GROMOS, Eq. 7.10 is not evaluated for excluded atoms (Sec. 6.2), while Eqs. 7.11 and 7.12 are evaluated for these atoms as well, unless the simulation is performed in the GROMOS96 compatibility mode, see Vol. 4.

Inserting $\Psi_{ij}^{(ele)}$ from Eqs. 7.6 or 7.7 into Eq. 7.4, one finds that the self influence function is in both cases given by

$$\Psi^{(ele,slf)} = -\frac{1-(1/2)C_{RF}}{R_{RF}} \tag{7.13}$$

The fact that $\Psi^{(ele,slf)}$ solely depends on the boundary conditions and associated parameters will be explicited in the following sections.

The surface term is as in Eq. 7.5 - if we decide to add it.

7.4. Lattice-sum (LS) interactions

7.4.1. Introduction. Lattice-sum (LS) methods rely on two key principles : (*i*) the treatment of electrostatic interactions as exactly periodic within the simulated system ; (*ii*) the splitting of the interaction into a short-range component, evaluated by direct summation over the pairs of atoms, and a long-range component, evaluated by Fourier series.

To ensure overall neutrality of the system, each "charge" is actually represented by a charge density defined by a periodic point charge plus a homogeneous neutralizing background charge density filling the infinite periodic system. This background charge has absolutely no influence for overall neutral systems. For charged systems, it permits the calculation of a finite electrostatic energy, containing a self-interaction (Wigner) term, but has no influence on the forces.

The box dipole moment comes into the definition of the surface term (Eq. 7.30). In the general case, this quantity is not translationally invariant. Different definitions of the reference computational box (*i.e.* of $\mathbf{r}_c$) may lead to different values of $\mathbf{M}$.

Lattice sum methods rely on the use of a charge-shaping function with a width a to split the electrostatic potential into a real-space contribution and a reciprocal-space contribution, plus a constant. The width parameter a should be smaller than the short-range cutoff R_{cp} (input parameter RCUTP). Otherwise, an error will be issued. When the shaping function is a TP function (N_γ=1...10 in Tab. 7.1), the real-space interaction may be computed exactly provided that all atom pairs within a distance a or smaller are at any time included in the pairlist. When all atom pairs within a distance R_{cp} or smaller are at any time included in the pairlist, the optimal value of a is R_{cp}. When the shaping function is a Gaussian (N_γ=-1 in Tab. 7.1), the real-space interaction is not computed exactly, because the Gaussian is infinite-ranged. In this case, the real-space interaction is computed for all atom pairs within the pairlist, and will be accurate when a/R_{cp} is small enough. In many cases, $a \approx R_{cp}/3$ is a reasonable choice.

The two lattice-sum methods available differ in the way they evaluate the reciprocal-space contribution to the electrostatic energy and forces (Secs. 7.4.2, 7.4.3 and 7.4.4) : the Ewald method is based on direct summation over reciprocal-space lattice vectors while the particle-particle-particle-mesh (PPPM) method makes use of a fast Fourier transform (FFT) algorithm.

It will be useful to make the following definitions.

We consider a periodic system of Nq charges q_i at positions $\mathbf{r}_i$ within a general triclinic computational box with arbitrary orientation (Sec. 4.4.1). We further define the box dipole moment

$$\mathbf{M} = \sum_{i=1}^{Nq} q_i \left(\mathbf{r}_i - \mathbf{r}_c\right) , \tag{7.14}$$

where $\mathbf{r}_c$ is the center of the computational box, the box overall charge

$$S = \sum_{i=1}^{Nq} q_i , \tag{7.15}$$

and the box overall square charge

$$\tilde{S}^2 = \sum_{i=1}^{Nq} q_i^2 . \tag{7.16}$$

The electrostatic influence function $\Psi_{ij}^{(ele)}$ (Eq. 7.2) in the LS case, which is a periodic scheme (no cutoff), may formally be written

$$\Psi_{ij}^{(ele)}(\boldsymbol{r}) \doteq \psi^{(LS)}(\mathbf{r}_{ij}) = 4\pi \mid \underline{\mathbf{L}} \mid^{-1} \sum_{\mathbf{l},l\neq 0} k^{-2} \exp[i\mathbf{k}\cdot\mathbf{r}_{ij}] , \tag{7.17}$$

where $\underline{\mathbf{L}}$ is a matrix containing the Cartesian component of the box edge vectors in its columns (triclinic computational box), $\mathbf{l}$ a *lattice vector* with (positive or negative) integer components, $\mathbf{k} = 2\pi\underline{\mathbf{L}}^{-1}\mathbf{l}$ the associated *reciprocal-lattice vector*, and $\mathbf{r}_{ij} \doteq \mathbf{r}_i - \mathbf{r}_j$ the vector connecting sites i and j (in the computational box). The influence function $\psi^{(LS)}(\mathbf{x})$ describes the (periodic) electrostatic influence at position $\mathbf{x}$ relative to a point charge screened by a homogeneous neutralizing background charge density of opposite magnitude. Here, the electrostatic influence is just the electrostatic potential divided by $(4\pi\epsilon_0)^{-1}q$.

Because the summation over reciprocal-lattice vectors involved in this equation converges very slowly, in practice, $\Psi_{ij}^{(ele)}$ is partitioned into two contributions, termed the *real-space* and the *reciprocal-space* contributions (Ewald splitting).

7.4.1.1. *Charge-shaping function.* Lattice-sum methods rely on the use of a charge-shaping function $a^{-3}\gamma(a^{-1}r)$ of width a to split the electrostatic potential into a real-space contribution and a reciprocal-space contribution, plus a constant. In practice, it is assumed that the charge-shaping function satisfies the condition

$$\gamma(a^{-1}r) = 0 \quad \text{for} \quad r \geq R_{cp} , \quad \text{with} \quad R_{cp} \leq (1/2)\min\{L_x, L_y, L_z\} , \tag{7.18}$$

where R_{cp} is the real-space cutoff distance (input parameter RCUTP), which implies that the switch function $\eta(a^{-1}r)$ also vanishes beyond R_{cp}. This condition can be enforced in a strict fashion for all truncated-polynomial charge-shaping functions (Tab. 7.1; $N_\gamma = 0...10$) by setting a (input parameter ASHAPE) equal to R_{cp}. It can be enforced in an approximate manner for the Gaussian charge-shaping function (Tab. 7.1;

$N_\gamma = -1$) by setting $a \ll R_{cp}$. In many cases, $a \approx R_{cp}/3$ is a reasonable choice. If $a > R_{cp}$, an error will be issued in the FORCE routine. If $R_{cp} > (1/2)\min\{L_x, L_y, L_z\}$, an error will be issued.

The charge-shaping function is normalized to satisfy the condition

$$4\pi\, a^{-3} \int_0^\infty dr\, r^2\, \gamma(a^{-1}r) = 1 \ . \tag{7.19}$$

The following definitions are related to the charge-shaping function. The Fourier coefficients of (a lattice sum of) the charge-shaping function are given by

$$\hat{\gamma}(ak) = \begin{cases} 4\pi k^{-1}\, a^{-3} \int_0^\infty dr\, r\, \sin(kr)\, \gamma(a^{-1}r) & \text{for } \ k \neq 0 \\ 1 & \text{for } \ k = 0 \end{cases} \ , \tag{7.20}$$

where reciprocal-lattice vectors are defined as $\mathbf{k} = 2\pi \underline{\mathbf{L}}^{-1}\mathbf{l}$ with $\mathbf{l} \in \mathbb{Z}^3$.

The switch function $\eta(a^{-1}r)$ associated with the charge-shaping function is defined by

$$\eta(a^{-1}r) = 4\pi\, a^{-3} \int_r^\infty d\rho\, \rho\, (\rho - r)\, \gamma(a^{-1}\rho) \ . \tag{7.21}$$

Finally, the constants A_1, A_2 and A_3 are defined as

$$A_1 = -4\pi\, \mathcal{V}^{-1} \int_0^\infty dr\, r\, \eta(a^{-1}r) \ , \tag{7.22}$$

$$A_2 = 4\pi\, \mathcal{V}^{-1} \sum_{\mathbf{l}\in\mathbb{Z}^3\,,\, l\neq 0} k^{-2}\, \hat{\gamma}(ak) \ , \tag{7.23}$$

and

$$A_3 = \lim_{r\to 0} [\, \sum_{\mathbf{n}\in\mathbb{Z}^3} \parallel \mathbf{r} + \underline{\mathbf{L}}\,\mathbf{n} \parallel^{-1} \eta(a^{-1} \parallel \mathbf{r} + \underline{\mathbf{L}}\,\mathbf{n} \parallel) \quad - \quad r^{-1}\,] \ . \tag{7.24}$$

This limit becomes independent of the direction of $\mathbf{r}$ when $\mathbf{r} \to \mathbf{0}$.

The shaping functions ccurrently implemented and indexed by N_γ, and the related Fourier coefficients, switch functions and A-constants are listed in Tabs. 7.1 - 7.6. The charge-shaping function is selected through the value of NSHAPE in the LONGRANGE block.

The complementary error function required for the Gaussian charge-shaping function is calculated via the Chebyshev approximation (see ref.[27]). The evaluation of the exponential function for both $\eta(\xi)$ and $\hat{\gamma}(\kappa)$ might lead to computational underflows when their argument is negative and large. We did not encounter such cases for now, but if underflows are flagged at run time, they are likely to come from there.

7.4.1.2. *Electrostatic energy.* Due to self-interactions (Wigner term) and interactions with the dielectric continuum outside the infinite periodic system (surface term; this term vanishes only in the limit $\epsilon_{LS} \to \infty$, referred to as conducting or tinfoil boundary conditions), $\mathcal{V}^{(ele)}$ is actually a free energy. However, within the force field, it plays the role of a normal energy term. Note also that both E_γ and E_A also contain self energies. However, these cancel out and $E_\gamma + E_\eta + E_A$ is truly a pairwise energy (*i.e.* this quantity vanishes for a system consisting of a single charge). This is not the case of $\mathcal{V}^{(ele,slf)}$ and $\mathcal{V}^{(ele,srf)}$.

The electrostatic (reversible-charging) energy $\mathcal{V}^{(ele)}$ of the periodic system of charges can now be written as[28]

$$\mathcal{V}^{(ele)} = \mathcal{V}^{(ele,pws,LS-KS)} + \mathcal{V}^{(ele,pws,LS-RS)} + \mathcal{V}^{(ele,srf)} + \tag{7.25}$$

with

$$E_\gamma = (2\epsilon_0\epsilon_{ls}\, V)^{-1} \sum_{i=1}^{N_q} \sum_{j=1}^{N_q} q_i q_j \sum_{\mathbf{l}\in\mathbb{Z}^3\,,\, l\neq 0} k^{-2} \hat{\gamma}(ak)\, \cos(\mathbf{k}\cdot\mathbf{r}_{ij}) \ , \tag{7.26}$$

$$E_\eta = (4\pi\epsilon_0\epsilon_{ls})^{-1} \sum_{i=1}^{N_q} \sum_{j=1\,,\, j>i}^{N_q} q_i\, q_j \sum_{\mathbf{n}\in\mathbb{Z}^3} \parallel \mathbf{r}_{ij} + \underline{\mathbf{L}}\,\mathbf{n} \parallel^{-1} \eta(a^{-1} \parallel \mathbf{r}_{ij} + \underline{\mathbf{L}}\,\mathbf{n} \parallel) \ , \tag{7.27}$$

$$E_A = (8\pi\epsilon_0\epsilon_{ls})^{-1} \left[A_1\, S^2 - (A_1 + A_2)\, \tilde{S}^2\right] \ , \tag{7.28}$$

$$\mathcal{V}^{(ele,slf)} = (8\pi\epsilon_0\epsilon_{ls})^{-1}\, (A_1 + A_2 + A_3)\, \tilde{S}^2 \ , \tag{7.29}$$

N_γ	m	$\pi\gamma(\xi)$
-1	∞	$\pi^{-1/2}\, e^{-\xi^2}$
0	0	$(3/4)\, H(1-\xi)$
1	1	$3(1-\xi)\, H(1-\xi)$
2	2	$(15/2)\, (1-\xi)^2\, H(1-\xi)$
3	2	$(15/4)\, (1-\xi)^2(1+2\xi)\, H(1-\xi)$
4	3	$(105/16)\, (1-\xi)^3(3\xi+1)\, H(1-\xi)$
5	4	$(21/2)\, (1-\xi)^4(4\xi+1)\, H(1-\xi)$
6	4	$(63/8)\, (1-\xi)^4(5\xi^2+4\xi+1)\, H(1-\xi)$
7	5	$(45/4)\, (1-\xi)^5(8\xi^2+5\xi+1)\, H(1-\xi)$
8	6	$(165/32)\, (1-\xi)^6(35\xi^2+18\xi+3)\, H(1-\xi)$
9	6	$(165/64)\, (1-\xi)^6(64\xi^3+69\xi^2+30\xi+5)\, H(1-\xi)$
10	7	$(2145/128)\, (1-\xi)^7(21\xi^3+19\xi^2+7\xi+1)\, H(1-\xi)$

TABLE 7.1. Charge-shaping functions currently implemented. Related quantities are listed in Tabs. 7.2-7.6. N_γ : code of the function (input switch NSHAPE ; $N_\gamma = 0...10$: optimal TP-function of order N_γ; $N_\gamma = -1$: Gaussian) ; m : convergence rate of $\hat{\gamma}(\kappa)$ towards zero (convergence is as $\kappa^{-(m+2)}$ when $\kappa \to \infty$) ; $\pi\gamma(\xi)$: charge-shaping function amplified by π (the actual shaping function is $a^{-3}\gamma(a^{-1}r)$) ; $H(\xi)$: Heaviside function ($H(\xi) = 1$ when $\xi \geq 0$, zero otherwise). Note that the Gaussian function is infinite-ranged.

N_γ	$\eta(\xi)$
-1	erfc(ξ)
0	$(1/2)\, (1-\xi)^2(\xi+2)\, H(1-\xi)$
1	$(1-\xi)^3(\xi+1)\, H(1-\xi)$
2	$(1/2)\, (1-\xi)^4(3\xi+2)\, H(1-\xi)$
3	$(1/4)\, (1-\xi)^4(4\xi^2+7\xi+4)\, H(1-\xi)$
4	$(1/8)(1-\xi)^5(15\xi^2+19\xi+8)\, H(1-\xi)$
5	$(1-\xi)^6(3\xi^2+3\xi+1)\, H(1-\xi)$
6	$(1/16)\, (1-\xi)^6(35\xi^3+66\xi^2+51\xi+16)\, H(1-\xi)$
7	$(1/8)(1-\xi)^7(32\xi^3+49\xi^2+31\xi+8)\, H(1-\xi)$
8	$(1/16)\, (1-\xi)^8(105\xi^3+136\xi^2+73\xi+16)\, H(1-\xi)$
9	$(1/32)\, (1-\xi)^8(160\xi^4+335\xi^3+312\xi^2+151\xi+32)\, H(1-\xi)$
10	$(1/128)(1-\xi)^9(1155\xi^4+2075\xi^3+1665\xi^2+697\xi+128)\, H(1-\xi)$

TABLE 7.2. Switch functions corresponding to the charge-shaping functions currently implemented (see Tab. 7.1). N_γ : code of the function ; $\eta(\xi)$: switch function (the real-space interaction function is $r^{-1}\eta(a^{-1}r)$) ; erfc : complementary error function.

and

$$\mathcal{V}^{(ele,srf)} = [2\epsilon_0\epsilon_{ls}\,(2\epsilon_{LS}+1)\,\mathcal{V}]^{-1}\,\mathbf{M}^2\ , \tag{7.30}$$

where $\mathbf{r}_{ij} = \mathbf{r}_i - \mathbf{r}_j$, ϵ_0 is the dielectric permittivity of vacuum, and ϵ_{LS} (input parameter EPSLS) the relative permittivity of the medium "surrounding" the infinite periodic system. If the switch EPSLS is set to 0.0, conducting boundary conditions will be used, *i.e.* $\epsilon_{LS} \to \infty$. The expression for the surface term is obtained by assuming that the infinite periodic system is built by assembling a (roughly) spherical assembly of N periodic cells centered at $\mathbf{r}_c$, the center of the reference computational box, with $N \to \infty$. In this case, if the medium outside the assembly is a continuum of permittivity ϵ_{LS}, the Onsager self energy reads (for N

N_γ	$-\eta'(\xi)$
-1	$2\pi^{-1/2}e^{-\xi^2}$
0	$(3/2)\,(1-\xi)(\xi+1)\,H(1-\xi)$
1	$2(1-\xi)^2(2\xi+1)\,H(1-\xi)$
2	$(5/2)\,(1-\xi)^3(3\xi+1)\,H(1-\xi)$
3	$(3/4)\,(1-\xi)^3(8\xi^2+9\xi+3)\,H(1-\xi)$
4	$(21/8)(1-\xi)^4(5\xi^2+4\xi+1)\,H(1-\xi)$
5	$3(1-\xi)^5(8\xi^2+5\xi+1)\,H(1-\xi)$
6	$(9/16)\,(1-\xi)^5(35\xi^3+47\xi^2+25\xi+5)\,H(1-\xi)$
7	$(5/8)(1-\xi)^6(64\xi^3+69\xi^2+30\xi+5)\,H(1-\xi)$
8	$(55/16)\,(1-\xi)^7(21\xi^3+19\xi^2+7\xi+1)\,H(1-\xi)$
9	$(15/32)\,(1-\xi)^7(128\xi^4+203\xi^3+141\xi^2+49\xi+7)\,H(1-\xi)$
10	$(65/128)(1-\xi)^8(231\xi^4+312\xi^3+186\xi^2+56\xi+7)\,H(1-\xi)$

TABLE 7.3. Derivative of the switch functions corresponding to the charge-shaping functions currently implemented (see Tabs. 7.1 and 7.2). N_γ : code of the function ; $-\eta'(\xi)$: derivative switch function amplified by -1 ($\eta'(\xi) = d\eta(\xi)/d\xi$).

N_γ	$\kappa^{N_\gamma+3}\hat{\gamma}(\kappa)$
-1	$\kappa^2 e^{-\kappa^2/4}$
0	$3[-\kappa C + S]$
1	$12[2 - 2C - \kappa S]$
2	$60[2\kappa + \kappa C - 3S]$
3	$90[8 + (\kappa^2-8)C - 5\kappa S]$
4	$630[8\kappa + 7\kappa C + (\kappa^2-15)S]$
5	$5040[4(\kappa^2-6) - (\kappa^2-24)C + 9\kappa S]$
6	$7560[48\kappa - (\kappa^2-57)\kappa C + 3(4\kappa^2-35)S]$
7	$75600[24(\kappa^2-8) - 3(5\kappa^2-64)C - (\kappa^2-87)\kappa S]$
8	$831600[8\kappa(\kappa^2-24) + (\kappa^2-123)\kappa C - (18\kappa^2-315)S]$
9	$1247400[192(\kappa^2-10) + (\kappa^4-207\kappa^2+1920)C - (22\kappa^2-975)\kappa S]$
10	$16216200[64\kappa(\kappa^2-30) + (26\kappa^2-1545)\kappa C + (\kappa^4-285\kappa^2+3465)S]$

TABLE 7.4. Fourier coefficients corresponding to the shaping functions currently implemented (see Tab. 7.1). N_γ : code of the function ; $\kappa^{N_\gamma+3}\hat{\gamma}(\kappa)$: Fourier coefficient amplified by $\kappa^{N_\gamma+3}$ (the actual Fourier coefficient is $\hat{\gamma}(ak)$) ; C : short notation for $\cos(\kappa)$; S : short notation for $\sin(\kappa)$.

large)

$$\Delta G_o(\epsilon_{LS}) = -(8\pi\epsilon_0)^{-1}\frac{2(\epsilon_{LS}-1)}{2\epsilon_{LS}+1}\frac{N\mathbf{M}^2}{[(3/4)\pi^{-1}NV]^{1/3}}$$

The quantity $\mathcal{V}^{(ele,srf)}$ being a correction from conducting (tinfoil) boundary conditions to finite-permittivity is then given by $\mathcal{V}^{(ele,srf)} = \Delta G_o(\epsilon_{LS}) - \Delta G_o(\infty)$.

The interpretation of the different contributions to $\mathcal{V}^{(ele)}$ in Eq. 7.25 is given below, with reference to the following terminology for charge densities (which can be added to or subtracted from one another): point charge (p), γ-shaped charge (γ), and homogeneous background charge (b). The term E_γ represents the electrostatic energy (including self interaction) of a set of $(p-b)$-charges of magnitude $\{q_i\}$ at positions $\{\mathbf{r}_i\}$ in the potential generated by the corresponding periodic system of $(\gamma-b)$-charges. Since the potential is a non-singular and generally smooth function of position, E_γ is conveniently evaluated in reciprocal

N_γ	$\kappa^{N_\gamma+4}\hat{\gamma}'(\kappa)$
-1	$-(1/2)\kappa^4 e^{-\kappa^2/4}$
0	$3[3\kappa C + (\kappa^2-3)S]$
1	$12[-8-(\kappa^2-8)C + 5\kappa S]$
2	$60[-8\kappa - 7\kappa C - (\kappa^2-15)S]$
3	$90[-48-(9\kappa^2-48)C - (\kappa^2-33)\kappa S]$
4	$630[-48\kappa + (\kappa^2-57)\kappa C - 3(4\kappa^2-35)S]$
5	$5040[-24(\kappa^2-8) + 3(5\kappa^2-64)C + (\kappa^2-87)\kappa S]$
6	$7560[-384\kappa + 3(6\kappa^2-187)\kappa C + (\kappa^4-141\kappa^2+945)S]$
7	$75600[-192(\kappa^2-10) - (\kappa^4-207\kappa^2+1920)C + (22\kappa^2-975)\kappa S]$
8	$831600[-64\kappa(\kappa^2-30) - (26\kappa^2-1545)\kappa C - (\kappa^4-285\kappa^2+3465)S]$
9	$1247400[-1920(\kappa^2-12) - 15(2\kappa^4-203\kappa^2+1536)C - (\kappa^4-405\kappa^2+12645)\kappa S]$
10	$16216200[-640\kappa(\kappa^2-36) + (\kappa^4-545\kappa^2+22005)\kappa C - 5(7\kappa^4-936\kappa^2+9009)S]$

TABLE 7.5. derivative of the Fourier coefficients corresponding to the shaping functions currently implemented (see Tabs. 7.1 and 7.4). N_γ : code of the function ; $\kappa^{N_\gamma+4}\hat{\gamma}'(\kappa)$: derivative Fourier coefficient amplified by $\kappa^{N_\gamma+4}$ (the actual derivative of the Fourier coefficient is $\hat{\gamma}'(ak)$).

-1	$-(1/2)\kappa^4 e^{-\kappa^2/4}$	
0	$3[3\kappa C + (\kappa^2-3)S]$	
N_γ	$-V\pi^{-1}a^{-2}A_1$	$-aA_3$
-1	1	$2\pi^{-1/2}$
0	2/5	3/2
1	4/15	2
2	4/21	5/2
3	3/14	9/4
4	1/6	21/8
5	2/15	3
6	8/55	45/16
7	4/33	25/8
8	4/39	55/16
9	10/91	105/32
10	2/21	455/128

TABLE 7.6. A-constants corresponding to the shaping functions currently implemented (see Tab. 7.1). N_γ : code of the function ; $-V\pi^{-1}a^{-2}A_1$: constant A_1 amplified by $-V\pi^{-1}a^{-2}$; $-aA_3$: constant A_3 amplified by $-a$. These results are derived using Eq. 7.31, and thus valid exactly when $a \leq \min\{L_x, L_y, L_z\}$ (TP functions) or as an approximation when $a \ll \min\{L_x, L_y, L_z\}$ (Gaussian).

space, using the Ewald method[29] or the PPPM method[30] (see Sec. 7.4.3 and Sec. 7.4.4). The term E_η represents the electrostatic energy (excluding self interaction) of a set of $(p-b)$-charges of magnitude $\{q_i\}$ at positions $\{\mathbf{r}_i\}$ in the potential generated by the corresponding periodic system of $(p-\gamma)$-charges. With an appropriate choice of charge-shaping function, the function $\eta(a^{-1}r)$ can be made a quickly decreasing function of distance, in which case E_η is conveniently evaluated by direct (real-space) summation over the charge pairs (Sec. 7.4.1). The terms E_A and $\mathcal{V}^{(ele,slf)}$ (Sec. 7.4.1.3) are configuration-independent. The term E_A eliminates the self-energies present in E_γ and contains a small correction due to the constraint of zero average potential within the periodic system. The term $\mathcal{V}^{(ele,slf)}$ accounts for the self-energy of set

of $(p-b)$-charges of magnitude $\{q_i\}$ in the potential generated by the corresponding periodic system of $(p-b)$-charges (Wigner term[31–33]). Finally, the term $\mathcal{V}^{(ele,srf)}$ accounts for the interaction of the infinite periodic system with a dielectric continuum of relative permittivity ϵ_{LS} surrounding it. In the absence of the surface term, lattice-sum methods lead to conducting or tinfoil boundary conditions, which corresponds to $\epsilon_{LS} \to \infty$. The surface term is thus a correction to account for a medium of finite permittivity instead.

Only three energy contributions are reported by GROMOS : the pairwise energy $\mathcal{V}^{(ele,pws)} = E_\gamma + E_\eta + E_A$, the self-energy term $\mathcal{V}^{(ele,slf)}$, and the surface term $\mathcal{V}^{(ele,srf)}$. These quantities are stored in the arrays normally for the Coulomb, distance-dependent reaction field and distance-independent reaction field contributions. The splitting between $\mathcal{V}^{(ele,pws)}$ and $\mathcal{V}^{(ele,slf)}$ is only meaningful when the constant A_2 is calculated (switch NA2CLC≠0). Otherwise, it is arbitrary and only the sum is correct.

7.4.1.3. *Constant and self-energy terms.* The constant term E_A and the self-energy term $\mathcal{V}^{(ele,slf)}$ are given by Eqs. 7.28 and 7.29, respectively, where the A-constants are defined by Eqs. 7.22, 7.23 and 7.24. When Eq. 7.18 is satisfied the $\mathbf{n}$-sum in Eq. 7.24 can be restricted to the $\mathbf{n} = \mathbf{0}$ term, leading to

$$A_3 = \lim_{r \to 0} r^{-1} \left[\eta(a^{-1}r) \quad - \quad 1 \right] . \tag{7.31}$$

Because the Gaussian charge-shaping function is infinite-ranged, Eq. 7.18 is never exactly satisfied, and Eq. 7.31 only applies here as an approximation. In this case, A_1 and A_3 have analytical expressions for a given charge-shaping function (Tab. 7.6). In the general case, the constant A_2 must be computed numerically by direct summation. In practice, this is done by evaluating

$$A_2(l_{max}) = 4\pi\, V^{-1} \sum_{\mathbf{l} \in \mathbb{Z}^3\,,\, l \neq 0\,,\, l_x, l_y, l_z \leq l_{max}} k^{-2}\, \hat{\gamma}(ak) \tag{7.32}$$

for increasing values of l_{max}, until a user-specified relative tolerance (input parameter TOLA2) is reached. In the specific case of a cubic unit cell ($L_x = L_y = L_z = L$), this evaluation is replaced by[28,33] $A_2 \approx \xi_{EW} L^{-1} - A_1 - A_3$ with $\xi_{EW} = -2.83792748$ (macro WIGNER_CUBE in define.inc). The quantity A_2 is calculated (input switch NA2CLC≥2) either (*i*) once at the beginning of the simulation (constant-volume simulation), (*ii*) whenever an energy output (input switches NTPR and NTWE) is required (constant-pressure simulation and NA2CLC=2) or (*iii*) every step (constant-pressure simulation and NA2CLC=3 or 4). When NA2CLC=0, the value of A_2 is set to zero. When NA2CLC=2, only the energies are affected by the calculation, not the virial. Thus, the estimation of A_2 is not required unless an energy output is needed. The value of A_2 is assumed constant between updates. When NA2CLC≥ 3, both the energies and the virial are affected by the calculation. Thus, the estimation of A_2 is required at every step in a constant-pressure simulation.

The quantity A_2 calculated through Eq. 7.32 represents the exact (in the limit of large l_{max}) value of A_2 entering into $\mathcal{V}^{(ele,slf)}$ (Eq. 7.29). However, because the reciprocal-space interaction energy is evaluated with a finite precision (*i.e.* through the Ewald or PPPM method), this value of A_2 will only approximately remove the reciprocal-space self-energy when included in E_A (Eqs. 7.28). In particular, using this A_2 value in the expression for E_A will lead to a pairwise energy $E_\eta + E_\gamma + E_A$ that will not exactly vanish for a system consisting of a single charge. Although for most practical purposes, this approximation (corresponding to NA2CLC=2) is sufficient, it is possible to compute a more accurate method-dependent value $\tilde{A}_2$ to be used in the evaluation of E_A, *i.e.*

$$E_A = (8\pi\epsilon_0)^{-1} \left[A_1\, S^2 - (A_1 + \tilde{A}_2)\, \tilde{S}^2 \right] , \tag{7.33}$$

The calculation of this quantity is feasible for the the Ewald (input switch NA2CLC=1 or 3) or PPPM (input switch NA2CLC=3 or 4).

The E_A and $\mathcal{V}^{(ele,slf)}$ terms give rise to no force contribution. The corresponding virial contributions are given in Sec. 17.7. Although the A_2 term in E_A is configuration-dependent, the corresponding force on the atoms is neglected

The calculation of the A_2 term may be entirely skipped (input switch NA2CLC=0). In this case, A_2 is set to zero and the A_2 contributions are omitted in the evaluation of both E_A and $\mathcal{V}^{(ele,slf)}$ (Eqs. 7.28 and 7.29). As a consequence, the splitting between pairwise and self contributions becomes arbitrary, but the sum of the two quantities (and thus the overall electrostatic energy) remains correct within the approximation $A_2 \approx \tilde{A}_2$. Skipping the calculation of A_2 (and/or $\tilde{A}_2$) may be advantageous in constant-pressure simulations, where these quantities must be recalculated at every step.

The surface term $\mathcal{V}^{(ele,srf)}$ is given by Eq. 7.30 where $\mathbf{M}$ is defined by Eq. 7.14 and ϵ_{LS} is the relative permittivity of the medium surrounding the infinite periodic system (input parameter EPSLS; a value of 0.0 selects an infinite permittivity, *i.e.* conducting or tinfoil boundary conditions). The corresponding force on atom i is given by

$$\mathbf{f}_{srf,i} = -[\epsilon_0 (2\epsilon_{LS} + 1) V]^{-1} q_i \mathbf{M} . \tag{7.34}$$

The corresponding virial contribution is discussed in Sec. 17.7.

Energy partitioning. The partitioning of the E_γ (Eq. 7.26; for PPPM: Eq. 7.72) term into energy groups requires multiple reciprocal-space evaluations. For N_e (N_e>1) energy groups, the $N_e(N_e+1)/2-1$ quantities

$$(E_\gamma)_{IJ}(2\epsilon_0 \mathcal{V})^{-1} \sum_{\mathbf{l}\in G\,,\, l\neq 0} \hat{G}_g(\mathbf{k_l}) \mid (\hat{s}_g(\mathbf{k_l}))_{IJ} \mid^2 \tag{7.35}$$

with $I = 1..N_e - 1$ and $J = I..N_e$ are evaluated. $(E)_{N_eN_e}$ is obtained by subtracting the sum of the other terms from E_γ.

The splitting of the E_A and $\mathcal{V}^{(ele,slf)}$ into energy groups is based on the splitting of the quantities S^2 and $\tilde{S}^2$ (Eqs. 7.15 and 7.16) as

$$\tilde{S}^2_{IJ} = \delta_{IJ} \sum_{i\in I} q_i^2 \tag{7.36}$$

and

$$S^2_{IJ} = (2 - \delta_{IJ})(\sum_{i\in I} q_i)(\sum_{j\in J} q_j) \tag{7.37}$$

where I and J denote two energy groups with $I < J$. These definitions ensure

$$\sum_I \sum_{J\geq I} \tilde{S}^2_{IJ} = \tilde{S}^2 \quad \text{and} \quad \sum_I \sum_{J\geq I} S^2_{IJ} = S^2 .$$

In this case, the pairwise group contributions to E_A and $\mathcal{V}^{(ele,slf)}$ (Eqs. 7.28 and 7.29) read

$$(E_A)_{IJ} = (8\pi\epsilon_0)^{-1} [A_1 S^2_{IJ} - (A_1 + A_2) \tilde{S}^2_{IJ}] , \tag{7.38}$$

$$(\mathcal{V}^{(ele,slf)})_{IJ} = (8\pi\epsilon_0)^{-1} (A_1 + A_2 + A_3) \tilde{S}^2_{IJ} , \tag{7.39}$$

If Eq. 7.33 is used instead for E_A together with an exact evaluation of $\tilde{A}_2$ (input switch NA2CLC=3), the splitting must be done by evaluating separately $(\tilde{A}_2)_{II}$ for each group based on Eq. 7.104 (with $\tilde{S}^2_{II}$ instead of $\tilde{S}^2$). In this case, one has

$$(E_A)_{IJ} = (8\pi\epsilon_0)^{-1} \{A_1 [(S^2)_{IJ} - (\tilde{S}^2)_{IJ} - \delta_{IJ}(\tilde{A}_2)_{II}(\tilde{S}^2)_{II}\} . \tag{7.40}$$

The splitting of the $\mathcal{V}^{(ele,srf)}$ term into energy groups is based on the splitting of the quantity $\mathbf{M}^2$ (Eqs. 7.14) as

$$(\mathbf{M}^2)_{IJ} = (2 - \delta_{IJ})[\sum_{i\in I} q_i (\mathbf{r}_i - \mathbf{r}_c)][\sum_{j\in J} q_j (\mathbf{r}_j - \mathbf{r}_c)] , \tag{7.41}$$

In this case, the pairwise group contributions to $\mathcal{V}^{(ele,srf)}$ (Eq. 7.30) reads

$$(\mathcal{V}^{(ele,srf)})_{IJ} = [2\epsilon_0 (2\epsilon_{LS} + 1) V]^{-1} (\mathbf{M}^2)_{IJ} . \tag{7.42}$$

When perturbation is applied, the soft core is only applied to the 1/r component of the real-space interaction, but not to the complement $\eta - r^{-1}$.

7.4.2. Real-space interactions in LS electrostatics. In the most general form, the real-space contribution to the electrostatic interactions is given by Eq. 7.27. The switch functions η corresponding to the charge-shaping functions implemented are listed in Tab. 7.2. In practice, it is assumed that the charge-shaping function satisfies the condition

$$\gamma(a^{-1}r) = 0 \quad \text{for} \quad r \geq R_{cp} \ , \quad \text{with} \quad R_{cp} \leq (1/2)\min\{L_x, L_y, L_z\} \ , \tag{7.43}$$

where R_{cp} is the real-space cutoff distance (input parameter RCUTP), which implies that the switch function $\eta(a^{-1}r)$ also vanishes beyond R_{cp}. This condition can be enforced in a strict fashion for all truncated-polynomial charge-shaping functions (Tab. 7.1; $N_\gamma = 0...10$) by setting a (input parameter ASHAPE) equal to R_{cp}. It can be enforced in an approximate manner for the Gaussian charge-shaping function (Tab. 7.1; $N_\gamma = -1$) by setting $a \ll R_{cp}$. In many cases, $a \approx R_{cp}/3$ is a reasonable choice. If $a > R_{cp}$, an error will be issued in the FORCE routine. If $R_{cp} > (1/2)\min\{L_x, L_y, L_z\}$, an error will be issued. In this case, and taking into account that Coulombic interaction between excluded covalent neighbours should be removed, one may rewrite Eq. 7.27 as

$$\begin{aligned} E_\eta \quad = \quad & (4\pi\epsilon_0)^{-1} \sum_{i=1}^{N_q} \sum_{j=1\,,\,j>i\,,\,\overline{r}_{ij}<R_{cp}\,,\,j\notin Exc(i)}^{N_q} q_i\, q_j\, \overline{r}_{ij}^{-1}\, \eta(a^{-1}\overline{r}_{ij}) \\ & +(4\pi\epsilon_0)^{-1} \sum_{i=1}^{N_q} \sum_{j=1\,,\,j>i\,,\,j\in Exc(i)}^{N_q} q_i\, q_j\, \overline{r}_{ij}^{-1}\, [\eta(a^{-1}\overline{r}_{ij}) - 1] \ , \end{aligned} \tag{7.44}$$

where $\overline{\mathbf{r}}_{ij}$ is the minimum-image vector corresponding to $\mathbf{r}_{ij} = \mathbf{r}_i - \mathbf{r}_j$ and the notation $j \in Exc(i)$ indicates that atom j belongs to the exclusion list of atom i. First and second covalent neighbours are excluded from electrostatic interactions. Only the interaction between atom i and the nearest periodic copy of atom j must be removed, not the interaction of i with the other periodic copies of j. Therefore, a contribution in $\overline{r}_{ij}^{-1}$ must be subtracted. It is also assumed that all pairs of excluded neighbours are within a minimum-image distance smaller than R_{cp}.

When using truncated-polynomial charge-shaping functions, the evaluation of E_η will only be exact provided that all atom pairs within a distance smaller than a are included into the short-range (charge-group or atomic) pairlist. This may not be the case because (i) charge-group pairs which are too far away to be in a molecular pairlist may still contain atom pairs at a distance smaller than R_{cp}, and (ii) the charge-group or molecular pairlist may not be updated every step. To alleviate the first source of inaccuracy if using a molecular pairlist, it is recommended to define each solute atom as its own charge group in the topology and to set $a = R_{cp} - d$ where d is the maximal distance between the first atom and any other atom within a solvent molecule. To alleviate the second source of inaccuracy, it is recommended either to update the pairlist very frequently or to use a slightly extended pairlist with R_n (input parameter RCUTN) larger than R_{cp}.

When using a Gaussian, the evaluation of E_η is always approximate. If care is taken that the pairlist contains all atom pairs within a minimum-image distance smaller than R_{cp} (previous footnote), it is likely that it will also contain pairs with distances slightly above R_{cp}. To avoid the inclusion of such arbitrariness in the calculation, these additional pairs are ignored and the interaction is restricted solely to pairs within R_{cp}. This restriction can be removed by setting the macro GAUSSIAN_LOOSE_CUTOFF in define.inc. The same restriction to pairs within R_{cp} is applied to Lennard-Jones interactions and can be removed by setting the macro VDW_LOOSE_CUTOFF in define.inc.

Note that no real-space interaction is calculated in intermediate range of charge-group or atom pairs with distances between R_{cp} and R_{cl} (input parameter RCUTL).

The corresponding atomic forces (Eq. 17.32) and contributions to the virial are discussed in Sec. 17.7.

7.4.3. Ewald reciprocal-space interactions in LS **electrostatics.** In the Ewald method, the reciprocal-space energy E_γ defined by Eq. 7.26, as well as the corresponding forces and virial, are evaluated by direct summation over reciprocal-lattice vectors.

For improved computational speed the triple-sum (over $\mathbf{l}$, i and j) in Eq. 7.26 is rewritten as a double-sum (over $\mathbf{l}$ and i)

$$E_\gamma = (2\epsilon_0 V)^{-1} \sum_{\mathbf{l}\in\mathbb{W}\,,\,l\neq 0} k^{-2}\, \hat{\gamma}(ak)\, [\, C^2(\mathbf{k}) + S^2(\mathbf{k})\,] \ , \tag{7.45}$$

with the definitions

$$C(\mathbf{k}) = \sum_{i=1}^{N_q} q_i \cos \mathbf{k} \cdot \mathbf{r}_i \qquad \text{and} \qquad S(\mathbf{k}) = \sum_{i=1}^{N_q} q_i \sin \mathbf{k} \cdot \mathbf{r}_i \ . \tag{7.46}$$

The equivalence between the two equations follows from writing

$$\sum_{i=1}^{N_q} \sum_{j=1}^{N_q} q_i q_j \sum_{\mathbf{l} \in \mathbb{W}, l \neq 0} k^{-2} \hat{\gamma}(ak) \cos(\mathbf{k} \cdot \mathbf{r}_{ij}) = \mathrm{Re} \{ \sum_{\mathbf{l} \in \mathbb{W}, l \neq 0} k^{-2} \hat{\gamma}(ak) \mid \sum_{i=1}^{N_q} q_i e^{i \mathbf{k} \cdot \mathbf{r}_i} \mid^2 \} \ ,$$

and noting that the square norm of a real number is always real. Note that the use of Eq. 7.45 rather than Eq. 7.26 is considerably more efficient, but does no longer allow for a pairwise decomposition of the contributions to E_γ (and to the corresponding forces and virial).

The force on atom i corresponding to Eq. 7.45 can be found in Eq. 17.33, and the corresponding virial contribution is given in Sec. 17.7.

The reciprocal-lattice vectors are defined as $\mathbf{k} = 2\pi^t \underline{\mathbf{L}}^{-1} \mathbf{l}$, where $\underline{\mathbf{L}}$ is the matrix $\underline{\mathbf{L}}$ containing as columns the Cartesian components of the box vectors (Sec. 4.4.1) and $\mathbf{l}$ is a vector with integer components. In the general case of a triclinic box, it is conveninent to introduce the oblique fractional coordinates $\check{\mathbf{r}}_i = \underline{\mathbf{L}}^{-1} \mathbf{r}_i$, and the oblique reciprocal-lattice vector $\check{\mathbf{k}} = 2\pi \mathbf{l}$. In this case, it is easily seen that any occurrence of the scalar product $\mathbf{k} \cdot \mathbf{r}_i$ can be replaced by $\check{\mathbf{k}} \cdot \check{\mathbf{r}}_i$.

The summation in Eq. 7.45 is restricted to the subset $\mathbb{W}$ of integer vectors $\mathbf{l}$ defined by components l_x, l_y, and l_z in the ranges $[-l_{x,max}; l_{x,max}]$, $[-l_{y,max}; l_{y,max}]$, and $[-l_{z,max}; l_{z,max}]$, and by a norm of k smaller or equal to a cutoff value k_c.

7.4.3.1. *Implementation.* The trigonometric functions involved in the two latter quantities in Eq. 7.46 can be written as

$$\begin{aligned} \cos \mathbf{k} \cdot \mathbf{r}_i \quad = \quad & c_{x,i,l_x} c_{y,i,l_y} c_{z,i,l_z} - c_{x,i,l_x} s_{y,i,l_y} s_{z,i,l_z} \\ & - s_{x,i,l_x} c_{y,i,l_y} s_{z,i,l_z} - s_{x,i,l_x} s_{y,i,l_y} c_{z,i,l_z} \end{aligned} \tag{7.47}$$

and

$$\begin{aligned} \sin \mathbf{k} \cdot \mathbf{r}_i \quad = \quad & - s_{x,i,l_x} s_{y,i,l_y} s_{z,i,l_z} + s_{x,i,l_x} c_{y,i,l_y} c_{z,i,l_z} \\ & + c_{x,i,l_x} s_{y,i,l_y} c_{z,i,l_z} + c_{x,i,l_x} c_{y,i,l_y} s_{z,i,l_z} \ , \end{aligned} \tag{7.48}$$

with

$$c_{\mu,i,l} = \cos 2\pi L_\mu^{-1} l r_{i,\mu} \quad \text{and} \quad s_{\mu,i,l} = \sin 2\pi L_\mu^{-1} l r_{i,\mu} \ . \tag{7.49}$$

In practice, the quantities defined by Eq. 7.49 are precomputed by recursion and stored into an array for all the allowed positive values of l_x, l_y, and l_z. The corresponding recursion equations are

$$c_{\mu,i,l} = \begin{cases} 1 & \text{if} \ \ l = 0 \\ \cos 2\pi L_\mu^{-1} r_{i,\mu} & \text{if} \ \ l = 1 \\ c_{\mu,i,l-1} c_{\mu,i,1} - s_{\mu,i,l-1} s_{\mu,i,1} & \text{otherwise} \end{cases} \tag{7.50}$$

and

$$s_{\mu,i,l} = \begin{cases} 0 & \text{if} \ \ l = 0 \\ \sin 2\pi L_\mu^{-1} r_{i,\mu} & \text{if} \ \ l = 1 \\ c_{\mu,i,l-1} s_{\mu,i,1} + s_{\mu,i,l-1} c_{\mu,i,1} & \text{otherwise} \end{cases} \ . \tag{7.51}$$

The results for $l > 1$ follow from expansion into complex exponentials. The corresponding quantities for negative l values are not stored into the array, since they are simply given by

$$c_{\mu,i,-l} = c_{\mu,i,l} \quad \text{and} \quad s_{\mu,i,-l} = -s_{\mu,i,l} \ . \tag{7.52}$$

The maximal values for l_x, l_y, and l_z corresponding to wavectors of $\mathbb{W}$ are $\max\{l_{x,max}; k_d L_x\}$, $\max\{l_{y,max}; k_d L_y\}$, and $\max\{l_{z,max}; k_d L_z\}$.

In a rectangular box, an increase in computational efficiency can be obtained by noting that the terms in the $\mathbf{l}-$sum involved in Eq. 7.45 are invariant upon changing $\mathbf{k}$ to $-\mathbf{k}$. Thus, the summation can be restricted to the half-space with $l_x \geq 0$, and the resulting energies and forces (and virial contribution) multiplied by two. More precisely, to avoid double counting, the half-space should include the (i) vectors with $l_x > 0$, (ii) the vectors with $l_x = 0$ and $l_y > 0$, and (iii) the vectors with $l_x = 0, l_y = 0$ and $l_z > 0$. The zero wavevector is in any case excluded from the summations.

An alternative way is to observe that, due the symmetry properties of the trigonometric functions, the quantities $C^2(\mathbf{k})$ and $S^2(\mathbf{k})$ in Eq. 7.46 do not contain any cross-terms when expanded through Eqs. 7.47 or 7.48, *i.e.*

$$C^2(\mathbf{k}) = C_o^2(\mathbf{k}) + C_x^2(\mathbf{k}) + C_y^2(\mathbf{k}) + C_z^2(\mathbf{k}) \tag{7.53}$$

and

$$S^2(\mathbf{k}) = S_o^2(\mathbf{k}) + S_x^2(\mathbf{k}) + S_y^2(\mathbf{k}) + S_z^2(\mathbf{k}) \ , \tag{7.54}$$

with

$$\begin{array}{lll} C_o(\mathbf{k}) = \sum_{i=1}^{N_q} q_i c_{x,i,l_x} c_{y,i,l_y} c_{z,i,l_z} & , & C_x(\mathbf{k}) = \sum_{i=1}^{N_q} q_i c_{x,i,l_x} s_{y,i,l_y} s_{z,i,l_z} \\ C_y(\mathbf{k}) = \sum_{i=1}^{N_q} q_i s_{x,i,l_x} c_{y,i,l_y} s_{z,i,l_z} & , & C_z(\mathbf{k}) = \sum_{i=1}^{N_q} q_i s_{x,i,l_x} s_{y,i,l_y} c_{z,i,l_z} \end{array} \tag{7.55}$$

and

$$\begin{array}{lll} S_o(\mathbf{k}) = \sum_{i=1}^{N_q} q_i s_{x,i,l_x} s_{y,i,l_y} s_{z,i,l_z} & , & S_x(\mathbf{k}) = \sum_{i=1}^{N_q} q_i s_{x,i,l_x} c_{y,i,l_y} c_{z,i,l_z} \\ S_y(\mathbf{k}) = \sum_{i=1}^{N_q} q_i c_{x,i,l_x} s_{y,i,l_y} c_{z,i,l_z} & , & S_z(\mathbf{k}) = \sum_{i=1}^{N_q} q_i c_{x,i,l_x} c_{y,i,l_y} s_{z,i,l_z} \end{array} \ . \tag{7.56}$$

Due to symmetry Eq. 7.45 is then easily rewritten as a sum over the positive octant

$$\begin{aligned} E_\gamma \ = \ & 4(\epsilon_0 V)^{-1} \sum_{\mathbf{l}\in\mathbb{W}',\, l\neq 0} k^{-2}\, \hat{\gamma}(ak)\, \sigma_{\mathbf{k}} [\, C_o^2(\mathbf{k}) + C_x^2(\mathbf{k}) + C_y^2(\mathbf{k}) + C_z^2(\mathbf{k}) \\ & + S_o^2(\mathbf{k}) + S_x^2(\mathbf{k}) + S_y^2(\mathbf{k}) + S_z^2(\mathbf{k}) \,] \ , \end{aligned} \tag{7.57}$$

where $\mathbb{W}'$ denotes the restriction of $\mathbb{W}$ to wavevectors with positive or zero components, and $\sigma_{\mathbf{k}}$ is a symmetry factor equal to 2^{-n}, where n is the number of vanishing wavevector components. The force is given in Eq. 17.34.

The reciprocal-space Ewald contribution to the atomic virial W_μ (corresponding to the energy term E_γ defined by Eq. 7.26 and evaluated as Eq. 7.45) is given in Eq. 17.38.

7.4.3.2. *Calculation of the $\tilde{A}_2$ self term.* In the Ewald case, the quantity $\tilde{A}_2$ is evaluated as

$$\tilde{A}_2 = (\epsilon_0 \epsilon_{ls} V)^{-1} \sum_{\mathbf{l}\in\mathbb{W},\, l\neq 0} k^{-2}\, \hat{\gamma}(ak) \ . \tag{7.58}$$

As discussed above, an increase in computational efficiency can be obtained by restricting the summation to a half-space and doubling the result, or even, summing over an octant and multiplying the result by eight. Because the calculation of $\tilde{A}_2$ in the Ewald case is inexpensive, while this quantity generally represents a reasonably-accurate estimate for A_2, it is possible to suppress the calculation of A_2 by Eq. 7.32 and set $A_2 = \tilde{A}_2$ in this case (input switch NA2CLC=1, only allowed for Ewald).

7.4.4. PPPM **reciprocal-space interactions in** LS **electrostatics.** The reciprocal-space contribution E_γ to the total electrostatic energy evaluated through the LS method (Eq. 7.26) may be calculated via the particle-particle particle-mesh (PPPM) algorithm of Hockney and Eastwood.[30] Alternatively, this algorithm may be applied to the calculation of the reciprocal-space contribution E_ω to the total electrostatic energy evaluated through the LSERF method.

For a general triclinic computational box, the PPPM algorithm relies on the discretization of the box by means of a grid (mesh). The number of grid subdivisions along each of the box axes must be even. The algorithm consists of six steps : (*i*) assignment of the charge density associated with the atomic partial charges to the grid points by means of an assignment function ; (*ii*) conversion of the charge density grid to reciprocal space by means of a three-dimensional fast Fourier transform (3D-FFT) ; (*iii*) solution for the reciprocal-space electrostatic potential via multiplication by an optimized influence function ; (*iv*) conversion of the reciprocal-space potential grid to real space by means of a 3D-FFT ; (*v*) evaluation of the electrostatic field on the grid by means of a finite-difference operator ; (*vi*) interpolation of the field at the location of the atomic partial charges by means of the same assignment function used in the first step. In the *ik*-differentiation variant, the fifth and sixth steps are replaced by : (*v*) evaluation of the reciprocal-space field through multiplication by $i\mathbf{k}$; (*iv*) conversion of the reciprocal-space field grid to real space by means of three 3D-FFTs, one for each field component.

The influence function describes the electrostatic potential generated at the different grid points by a unit $(\gamma - b)$-charge at the origin (Sec. 7.4). It is stored in reciprocal-space as its corresponding value at each of the reciprocal-space grid points. A key to the accuracy of the algorithm is to preoptimize this function so that it compensates for errors inherent to the discretization process, the use of an approximate assignment function and the use of an approximate finite-difference operator. When the virial is to be calculated or

when the box dimensions may vary in the course of a simulation, six grids are computed simultaneously, containing the relevant derivatives of the optimal influence function with respect to the box parameters. The optimization of the influence function (and the evaluation of its derivatives when required) is computationally expensive. In simulations without variations of the box parameters, however, this function is constant (as well as its derivatives) and the calculation needs to be performed only once at the beginning of a simulation. In simulations involving a variation of the box parameters, the accuracy of the influence function may progressively deteriorate with time as the box changes shape and size. Two mechanisms are then used to improve the accuracy of the current influence function at reasonable computational costs. First, the derivative information computed together with the optimized influence function is used to apply a first-order correction to the current influence function upon variation of the box parameters. Second, the accuracy of the algorithm may be reevaluated at periodic intervals, and a reoptimization of the influence function (and recalculation of its derivatives) undertaken when this accuracy falls below a user-specified threshold. If desired, the optimal influence function (and its derivatives, whenever required) may be read from file in the first step of a simulation, and may be written to file in the last step of a simulation.

The 3D-FFTs are performed using the FFTW libraries.

The use of the PPPM method is restricted to systems under periodic boundary conditions and in three dimensions only. The implementation for truncated-octahedral boxes results from the coordinate transformation described in Sec. 4.4.2.3, so that only the general triclinic case will be discussed in detail. The special case of a rectangular box results in minor simplifications at the level of the calculation of the influence function, which will be mentioned in this context.

7.4.4.1. *Discretization of the computational box.* A general triclinic box may be discretized by means of a grid G, defined by the number of subdivisions N_a, N_b and N_c along the $\mathbf{a}$, $\mathbf{b}$ and $\mathbf{c}$ box-edge vectors. The three numbers must be even. It will be convenient to introduce the diagonal matrix $\underline{\mathbf{N}}$ with elements N_a, N_b and N_c, *i.e.*

$$\underline{\mathbf{N}} = \begin{pmatrix} N_a & 0 & 0 \\ 0 & N_b & 0 \\ 0 & 0 & N_c \end{pmatrix} . \tag{7.59}$$

The matrices $\underline{\mathbf{H}}'$ and $\underline{\mathbf{H}}$ are then defined as

$$\underline{\mathbf{H}}' = \begin{pmatrix} N_a^{-1}a'_x & N_b^{-1}b'_x & N_c^{-1}c'_x \\ N_a^{-1}a'_y & N_b^{-1}b'_y & N_c^{-1}c'_y \\ N_a^{-1}a'_z & N_b^{-1}b'_z & N_c^{-1}c'_z \end{pmatrix} = \underline{\mathbf{L}}'\,\underline{\mathbf{N}}^{-1} = \underline{\mathbf{S}}\,\underline{\mathbf{B}}\,\underline{\mathbf{N}}^{-1} , \tag{7.60}$$

and

$$\underline{\mathbf{H}} = \begin{pmatrix} N_a^{-1}a_x & N_b^{-1}b_x & N_c^{-1}c_x \\ N_a^{-1}a_y & N_b^{-1}b_y & N_c^{-1}c_y \\ N_a^{-1}a_z & N_b^{-1}b_z & N_c^{-1}c_z \end{pmatrix} = \underline{\mathbf{L}}\,\underline{\mathbf{N}}^{-1} = \underline{\mathbf{R}}\,\underline{\mathbf{H}}' = \underline{\mathbf{T}}\,\underline{\mathbf{B}}\,\underline{\mathbf{N}}^{-1} . \tag{7.61}$$

The volume of a grid cell is noted $V_G = \mid \underline{\mathbf{H}}' \mid = \mid \underline{\mathbf{H}} \mid$.

Each point of the real-space grid G is associated with an index $\mathbf{n} = (n_a, n_b, n_c)$, with $n_a \in [0; N_a - 1]$, $n_b \in [0; N_b - 1]$ and $n_c \in [0; N_c - 1]$. Points outside this range are periodic copies of points within the range. The corresponding real-space vector may be written in the different representations (Sec. 4.4.1.1)

$$\check{\mathbf{r}}_\mathbf{n} = \underline{\mathbf{N}}^{-1}\mathbf{n} \; , \breve{\mathbf{r}}_\mathbf{n} = \underline{\mathbf{B}}\,\underline{\mathbf{N}}^{-1}\mathbf{n} \; , \mathbf{r}'_\mathbf{n} = \underline{\mathbf{H}}'\mathbf{n} \; , \mathbf{r}_\mathbf{n} = \underline{\mathbf{H}}\mathbf{n} . \tag{7.62}$$

Similarly, each point of the reciprocal-space grid G is associated with an index $\mathbf{l} = (l_a, l_b, l_c)$, with $l_a \in [-N_a/2 + 1; N_a/2]$, $l_b \in [-N_b/2 + 1; N_b/2]$ and $l_c \in [-N_c/2 + 1; N_c/2]$. The corresponding reciprocal-space vector may be written in the different representations (Sec. 4.4.1.4)

$$\check{\mathbf{k}}_\mathbf{l} = 2\pi\mathbf{l} \; , \breve{\mathbf{k}}_\mathbf{l} = 2\pi\underline{\mathbf{B}}^{-1}\mathbf{l} \; , \mathbf{k}'_\mathbf{l} = 2\pi({}^t\underline{\mathbf{L}}')^{-1} \; , \mathbf{k}_\mathbf{l} = 2\pi\,{}^t\underline{\mathbf{L}}^{-1}\mathbf{l} . \tag{7.63}$$

All gridded functions, *i.e.* real- or reciprocal-space functions that only take a value at a grid point of G, will be indicated with a g subscript.

The forward 3D-FFT operation converts a gridded function $f_g(\mathbf{r}_\mathbf{n})$ on the grid G into its finite Fourier coefficients $\hat{f}_g(\mathbf{k}_\mathbf{l})$ on the same grid

$$\hat{f}_g(\mathbf{k}_\mathbf{l}) = V_G \sum_{\mathbf{n}\in G} f_g(\mathbf{r}_\mathbf{n}) \; e^{-i\mathbf{k}_\mathbf{l}\cdot\mathbf{r}_\mathbf{n}} \; , \tag{7.64}$$

where $\mathbf{k_l} = 2\pi {}^t\underline{\mathbf{L}}^{-1}\mathbf{l}$ with $\mathbf{l} \in G$. The backward 3D-FFT performs the reverse operation, namely

$$f_g(\mathbf{r_n}) = V^{-1} \sum_{\mathbf{l}\in G} \hat{f}_g(\mathbf{k_l})\, e^{i\mathbf{k_l}\cdot\mathbf{r_n}} \ . \tag{7.65}$$

7.4.4.2. PPPM *potential.* The PPPM algorithm starts by distributing the N_q atomic partial charges q_i at locations $\mathbf{r}_i$ within the computational box onto the neighbouring grid points (taking periodicity into account), so as to generate the charge-density grid s_g. This assignment is performed as

$$s_g(\mathbf{r_n}) = \sum_{i=1}^{N_q} q_i\, \sigma_g(\mathbf{r_n}; \mathbf{r}_i) \tag{7.66}$$

with

$$\sigma_g(\mathbf{r_n}; \mathbf{r}) = P(\mathbf{r_n} - \mathbf{r}) \ , \tag{7.67}$$

where P is a so-called assignment function discussed in Sec. 7.4.4.4. Note that s_g is a real quantity. The charge density grid is converted to its (complex) reciprocal-space representation $\hat{s}_g(\mathbf{k_l})$ by applying a forward 3D-FFT to $s_g(\mathbf{r_n})$.

The reciprocal-space potential, *i.e.* the potential generated by the corresponding gridded (γ-b)-charges (Sec. 7.4) is then computed in reciprocal space as

$$\hat{\Phi}_{\gamma,g}(\mathbf{k_l}) = (\epsilon_0 \epsilon_{ls})^{-1}\, \hat{G}_g^{\dagger}(\mathbf{k_l})\, \hat{s}_g(\mathbf{k_l}) \ , \tag{7.68}$$

where $\hat{G}_g^{\dagger}$ represents the Fourier coefficients of the influence function. If all charges were located exactly at grid points or if the grid spacing was infinitesimal, the quantity $\hat{G}_g$ would be given by $k_{\mathbf{l}}^{-2}\, \hat{\gamma}(ak_{\mathbf{l}})$. However, since this is generally not the case, a significant gain in accuracy is reached by optimizing $\hat{G}_g^{\dagger}$ to compensate for errors linked with the discretization procedure, taking into account possible variations in the shape and size of the computational box. To this purpose, the influence function $\hat{G}_g^{\dagger}$ is defined as

$$\hat{G}_g^{\dagger}(\mathbf{k_l}) = \hat{G}_g^{o}(\mathbf{k_l}) - \mathrm{Tr}[\widehat{\underline{\mathbf{\Gamma}}}_g^{o}(\mathbf{k_l})({}^t\underline{\mathbf{L}}^{o})^{-1}({}^t\underline{\mathbf{L}} - {}^t\underline{\mathbf{L}}^{o})] \tag{7.69}$$

where $\hat{G}_g^{o}$ is the influence function optimized for a given set $\underline{\mathbf{L}}^{o}$ of box parameters and $\widehat{\underline{\mathbf{\Gamma}}}_g^{o}$ contains the corresponding first-order derivative information in the form

$$\widehat{\underline{\mathbf{\Gamma}}}_g^{o}(\mathbf{k_l}) = -\frac{\partial \hat{G}_g^{o}(\mathbf{k_l})}{\partial \underline{\mathbf{L}}^{o}}\, {}^t\underline{\mathbf{L}}^{o} \ . \tag{7.70}$$

The calculation of the quantities $\hat{G}_g^{o}$ and $\widehat{\underline{\mathbf{\Gamma}}}_g^{o}$ is described below. The optimal influence function $\hat{G}_g^{o}$ is only optimal for a specific set $\underline{\mathbf{L}}^{o}$ of box parameters $\underline{\mathbf{L}}$. When the shape and size of the computational box may vary, the second term in Eq. 7.69 includes a first-order correction to the influence function optimized at $\underline{\mathbf{L}}^{o}$, based on the derivative information calculated simultaneously. In practice, because $\widehat{\underline{\mathbf{\Gamma}}}_g^{o}$ is symmetric, the storage of the two quantities requires seven grids of reals. This evaluation (but not the storage requirement) is omitted for simulations not involving the calculation of the virial or the variation of the box parameters.

7.4.4.3. PPPM *energy and forces.* The reciprocal-space contribution E_γ to the total electrostatic energy (Eq. 7.26) is given by

$$E_\gamma = (2\epsilon_0 \epsilon_{ls}\, \mathcal{V})^{-1} \sum_{i=1}^{N_q} \sum_{j=1}^{N_q} \sum_{\mathbf{l}\in G\,,\, l\neq 0} q_i\, \hat{\sigma}_g(\mathbf{k_l}; \mathbf{r}_i)\, q_j\, \hat{\sigma}_g^{*}(\mathbf{k_l}; \mathbf{r}_j)\, \hat{G}_g^{\dagger}(\mathbf{k_l}) \ . \tag{7.71}$$

For computational efficiency, this pairwise sum is evaluated as a single sum, through

$$E_\gamma = (2\epsilon_0 \epsilon_{ls}\, \mathcal{V})^{-1} \sum_{\mathbf{l}\in G\,,\, l\neq 0} \hat{G}_g^{\dagger}(\mathbf{k_l}) \mid \hat{s}_g(\mathbf{k_l}) \mid^2 \ . \tag{7.72}$$

The (approximate) forces associated with the energy contribution E_γ (Eq. 7.72) are obtained through the evaluation of the gridded field $\mathbf{E}_g$ and its interpolation at the location of the charges. The reciprocal-space force on atom i is then written

$$\mathbf{F}_{\gamma,i} = q_i\, \mathbf{E}(\mathbf{r}_i) \tag{7.73}$$

with

$$\mathbf{E}(\mathbf{r}) = V_G \sum_{\mathbf{n}\in G} P(\mathbf{r} - \mathbf{r_n})\, \mathbf{E}_g(\mathbf{r_n}) \ . \tag{7.74}$$

The same assignment function P should be used here and for the charge assignment (Eq. 7.67), to ensure conservation of the total linear momentum during the dynamics. The gridded field $\mathbf{E}_g$ to be used in Eq. 7.74 can be obtained in either of two ways.

The first method (finite-difference) relies on performing a backward 3D-FFT of the potential to obtain the (real) real-space potential, and using a finite-difference approximation to compute the gridded field as

$$\mathbf{E}_g(\mathbf{r_n}) = -\sum_{\mathbf{n}'\in G} i\,V_G\,\mathbf{D}_g(\mathbf{r_n}-\mathbf{r_{n'}})\,\Phi_{\gamma,g}(\mathbf{r_{n'}}) \tag{7.75}$$

where $i\,V_G\,\mathbf{D}_g$ is is a so-called finite-difference operator, discussed below.

The second method (ik-differentiation) relies on computing the exact gridded field in reciprocal-space

$$\widehat{\mathbf{E}}_g(\mathbf{k_l}) = -i\mathbf{k_l}\,\hat{\Phi}_{\gamma,g}(\mathbf{k_l})\ , \tag{7.76}$$

One then performs three backward 3D-FFTs (one for each Cartesian component) to obtain the corresponding (real) quantity $\mathbf{E}_g$ in real-space. Note that the choice of $\mathbf{k_l}$ in Eq. 7.76 leaves room for some ambiguity. This is because the gridded potential can be mapped to a continuous function (of which the gradient is to be taken) in an infinite number of ways. Accordingly, $\mathbf{k_l}$ in Eq. 7.76 can be any alias vector $\mathbf{k_{l+m\underline{N}}}$ of $\mathbf{k_l}$ with $\mathbf{m}\in\mathbb{Z}^3$. The most realistic mapping of the potential is the one avoiding the introduction of spurious oscillations, which corresponds to the $\mathbf{k_l}$ vectors with the smallest norms. The convention adopted here is to select the alias vectors with $\mathbf{l}$ components are in the ranges $[-N_x/2+1; N_x/2]$, $[-N_y/2+1; N_y/2]$, and $[-N_z/2+1; N_z/2]$.

In principle, the use of $ik-$differentiation requires the storage of three complex grids. In the program, this storage is reduced to two by recycling the charge density / potential grid for the field component along the z-axis.

The virial associated with the energy contribution E_γ (Eq. 7.72) is given in Eqs. 17.40 and 17.41.

7.4.4.4. *Assignment function.* The assignment function P of order p (Eqs. 7.67 and 7.74) performs the distribution (interpolation) of a continuous function at an arbitrary location onto (from) values at the neighbouring p^3 grid points. This function is defined as[28]

$$P(\mathbf{r}) \;=\; V_G^{-1}\sum_{\mathbf{n}\in\mathbb{Z}^3}\tilde{P}(\mathbf{r}+\underline{\mathbf{L}}\mathbf{n}) \tag{7.77}$$

with

$$\tilde{P}(\mathbf{r}) = w_p([\underline{\mathbf{H}}^{-1}\mathbf{r}]_a)w_p([\underline{\mathbf{H}}^{-1}\mathbf{r}]_b)w_p([\underline{\mathbf{H}}^{-1}\mathbf{r}]_c)\ . \tag{7.78}$$

Here, $w_p(\xi)$ is a normalized one-dimensional function vanishing for $\mid\xi\mid\geq p/2$. These functions are listed in Tab. 7.7. The assignment scheme is formulated in terms of oblique coordinates. Thus, in the general case, the distribution (interpolation) of the function from (at) an arbitrary location onto (from) the neighbouring grid points is not necessarily correlated with the Cartesian distance between the points (this is only the case for a rectangular computational box). Note that P is a real quantity.

p	$w_p(\xi)$	range
1	1	$\mid\xi\mid< 1/2$
2	$1-\mid\xi\mid$	$\mid\xi\mid< 1$
3	$3/4-\xi^2$	$\mid\xi\mid< 1/2$
	$(1/8)(2\mid\xi\mid-3)^2$	$1/2<\mid\xi\mid< 3/2$
4	$(1/6)(3\mid\xi\mid^3-6\xi^2+4)$	$\mid\xi\mid< 1$
	$-(1/6)(\mid\xi\mid-2)^3$	$1<\mid\xi\mid< 2$
5	$(1/192)(48\xi^4-120\xi^2+115)$	$\mid\xi\mid< 1/2$
	$-(1/96)(16\xi^4-80\mid\xi\mid^3+120\xi^2-20\mid\xi\mid-55)$	$1/2<\mid\xi\mid< 3/2$
	$(1/384)(2\mid\xi\mid-5)^4$	$3/2<\mid\xi\mid< 5/2$

TABLE 7.7. One-dimensional functions $w_p(\xi)$ used to define the charge-assignment functions (Eq. 7.78). The functions $w_p(\xi)$ vanish for $\mid\xi\mid\geq p/2$.

In practice, the assignment is performed as follows. For p odd, one finds the grid point $\mathbf{n}_i$ closest to the location of charge q_i. For p even, one finds the grid-cell center closest to the location of charge q_i. In this

case, $\mathbf{n}_i$ has half-integer components. With the definitions $\boldsymbol{\zeta}_i = \mathbf{n}_i - \underline{\mathbf{H}}^{-1}\mathbf{r}_i$ and $\Delta\mathbf{n}_i = \mathbf{n} - \mathbf{n}_i$, the fraction of charge allocated to the periodic copy of the grid point $\mathbf{n}$ inside the computational box is given by

$$P(\mathbf{r_n} - \mathbf{r}_i) = V_G^{-1}\, w_p(\zeta_{i,a} + \Delta n_{i,a}) w_p(\zeta_{i,b} + \Delta n_{i,b}) w_p(\zeta_{i,c} + \Delta n_{i,c}) \ . \tag{7.79}$$

Because, by construction, the components of $\boldsymbol{\zeta}_i$ are smaller than 1/2 in absolute value while $w_p(\xi) = 0$ for $\mid \xi \mid \geq p/2$, $w_p(\zeta + \Delta n)$ vanishes for $\mid \Delta n \mid \geq p/2$. The $w_p(\xi)$ functions reexpressed as $w_p(\zeta + \Delta n)$ are listed in Tab. 7.8.

p	Δn	$w_p(\zeta + \Delta n)$
1	0	1
2	$\pm 1/2$	$-(1/2)(\pm 2\zeta - 1)$
3	0	$-(1/4)(4\zeta^2 - 3)$
	± 1	$(1/8)(\pm 2\zeta - 1)^2$
4	$\pm 1/2$	$(1/48)[32 - 12(\pm 2\zeta + 1)^2 + 3(\pm 2\zeta + 1)^3]$
	$\pm 3/2$	$-(1/48)(\pm 2\zeta - 1)^3$
5	0	$(1/192)(48\zeta^4 - 120\zeta^2 + 115)$
	± 1	$(1/96)[-16\zeta^4 \pm 16\zeta^3 + 24\zeta^2 - (\pm 44\zeta) + 19]$
	± 2	$(1/384)(\pm 2\zeta - 1)^4$

TABLE 7.8. One-dimensional functions $w_p(\xi)$ (Tab. 7.7) represented as $w_p(\zeta + \Delta n)$ with Δn integer (p odd) or half-integer (p even), and $\mid \zeta \mid \leq 1/2$. The functions $w_p(\zeta + \Delta n)$ vanish for $\mid \Delta n \mid \geq p/2$.

The Fourier coefficient $\hat{P}$ of the assignment function P are given by

$$\hat{P}(\mathbf{k}) = \hat{w}_p([^t\underline{\mathbf{H}}\mathbf{k}]_a)\hat{w}_p([^t\underline{\mathbf{H}}\mathbf{k}]_b)\hat{w}_p([^t\underline{\mathbf{H}}\mathbf{k}]_c) \ , \tag{7.80}$$

with ${}^t\underline{\mathbf{H}}\mathbf{k} = 2\pi\underline{\mathbf{N}}^{-1}\mathbf{l}$, where $\hat{w}_p(\kappa)$ is the continuous Fourier transform of $w_p(\xi)$, which evaluate to

$$\hat{w}_p(\kappa) = [2\kappa^{-1}\sin(\kappa/2)]^p(1 - \delta_\kappa) \quad + \quad \delta_\kappa \ . \tag{7.81}$$

Note that $\hat{P}$ is a real quantity, that is non-periodic, and odd (p odd) or even (p even) with respect to a change in the sign of any component of $\mathbf{l}$

7.4.4.5. *Finite- and exact-difference operators.* The finite-difference operator $iV_G\mathbf{D}_g$ of order q (Eq. 7.75) estimates the gradient of a given function at a grid point based on the value of the function at the $6q$ neighbouring grid points along the three box axes. The operator $\mathbf{D}_g$ is defined as[28]

$$\mathbf{D}_g(\mathbf{r_n}) = \sum_{j=1}^{q} c_j\, d_{vg,j}(\mathbf{r_n}) \ . \tag{7.82}$$

In this expression, the centered-difference operator $iV_G d_{vg,j}$ generates the gradient contribution evaluated from the function at the 6 neighbouring points distant from the grid point by $\pm jN_a^{-1}a$, $\pm jN_b^{-1}b$ and $\pm jN_c^{-1}c$ along the the three box axes. The operator $d_{vg,j}$ is given by

$$d_{vg,j}(\mathbf{r_n}) = \underline{\mathbf{R}}\,\underline{\mathbf{S}}\mathbf{e}_{g,j}(\mathbf{r_n}) \ , \tag{7.83}$$

where $\mathbf{e}_{g,j}$ is the corresponding operator in terms of oblique coordinates, *i.e.*

$$e_{g,j,a}(\mathbf{r_n}) = i\, V_G^{-1}\, (2jN_a^{-1}a)^{-1}\, \delta_{n_b}\delta_{n_c} \sum_{m\in\mathbb{Z}} (\delta_{n_a - j + N_a m} - \delta_{n_a + j + N_a m}) \ , \tag{7.84}$$

with similar expressions for the b and c components. Note that $iV_G\mathbf{D}_g$ is a real quantity.

The Fourier coefficients $\widehat{\mathbf{D}}_g$ of the operator $\mathbf{D}_g$ are given by

$$\widehat{\mathbf{D}}_g(\mathbf{k_l}) = \sum_{j=1}^{q} c_j\, \widehat{\mathbf{d}}_{g,j}(\mathbf{k_l}) \ , \tag{7.85}$$

where

$$\widehat{\mathbf{d}}_{g,j}(\mathbf{k_l}) = \underline{\mathbf{R}}\,{}^t\underline{\mathbf{S}}^{-1}\,\hat{\mathbf{e}}_{g,j}(\mathbf{k_l}) \tag{7.86}$$

and

$$\hat{e}_{g,j,a}(\mathbf{k_l}) = (jN_a^{-1}a)^{-1}\sin(j[{}^t\underline{\mathbf{H}}\mathbf{k_l}]_a) \ , \tag{7.87}$$

with similar expressions for the b and c components. Taken together, Eqs. 7.85, 7.86 and 7.87 may be written

$$\widehat{\mathbf{D}}_g(\mathbf{k_l}) = {}^t\underline{\mathbf{H}}^{-1}\sum_{j=1}^{q} c_j\, j^{-1} \begin{pmatrix} \sin(j[{}^t\underline{\mathbf{H}}\mathbf{k_l}]_a) \\ \sin(j[{}^t\underline{\mathbf{H}}\mathbf{k_l}]_b) \\ \sin(j[{}^t\underline{\mathbf{H}}\mathbf{k_l}]_c) \end{pmatrix} \tag{7.88}$$

with ${}^t\underline{\mathbf{H}}\mathbf{k_l} = 2\pi\underline{\mathbf{N}}^{-1}\mathbf{l}$. Note that $\widehat{\mathbf{D}}_g$ is a real quantity, periodic in the components of $\mathbf{l}$ (with periods N_a, N_b and N_c), and characterized by the same symmetry properties as $\mathbf{k_l}$ with respect to $\mathbf{l}$ (central antisymmetry in the general case, antisymmetry with respect to changing the sign of any component for a rectangular box). In addition, any component of ${}^t\underline{\mathbf{H}}\widehat{\mathbf{D}}_g(\mathbf{k_l})$ vanishes when the corresponding l component is a half-integer multiple of the corresponding number of grid subdivisions. This implies in particular that $\widehat{\mathbf{D}}_g(\mathbf{k_l}) = \mathbf{0}$ for the vectors $\mathbf{l}$ with components equal to $n_aN_a/2$, n_bN_b and n_cN_c with $\mathbf{n} \in \mathbb{Z}^3$

In reciprocal space, Eq. 7.75 can be written

$$\widehat{\mathbf{E}}_g(\mathbf{k_l}) = -i\widehat{\mathbf{D}}_g(\mathbf{k_l})\,\hat{\Phi}_{\gamma,g}(\mathbf{k_l}) \ . \tag{7.89}$$

Comparing this expression with Eq. 7.76 shows that the exact difference operator corresponds to

$$\widehat{\mathbf{D}}_g(\mathbf{k_l}) = \mathbf{k_l} \ . \tag{7.90}$$

In this specific case, $\widehat{\mathbf{D}}_g$ retains the same symmetry properties as the finite-difference operators with respect to the components of $\mathbf{l}$, but is no longer periodic.

For a given finite-difference operator of order q, the coefficients c_j in Eq. 7.82 may be selected so as to minimize the difference between the corresponding finite-difference operator and the exact-difference operator[28,34]. In reciprocal space, this leads to the requirement

$${}^t\underline{\mathbf{H}}^{-1}\sum_{j=1}^{q} c_j\, j^{-1} \begin{pmatrix} \sin(2\pi jN_a^{-1}l_a) \\ \sin(2\pi jN_b^{-1}l_b) \\ \sin(2\pi jN_c^{-1}l_c) \end{pmatrix} \approx \mathbf{k_l} \tag{7.91}$$

for any $\mathbf{l}$ or, equivalently,

$$\sum_{j=1}^{q} c_j\, j^{-1}\sin(2\pi jx) \approx 2\pi x \tag{7.92}$$

for any x. Differentiating with respect to x and dividing by 2π gives

$$\sum_{j=1}^{q} c_j\cos(2\pi jx) \approx 1 \ . \tag{7.93}$$

Expanding the left-hand side in Taylor series around $x = 0$ up to order $2q - 2$, equating the coefficients of power m to δ_m, and solving the resulting system of equations results in the optimal coefficients listed in Tab. 7.9.

q	c_1	c_2	c_3	c_4	c_5
1	1				
2	4/3	-1/3			
3	3/2	-3/5	1/10		
4	8/5	-4/5	8/35	-1/35	
5	5/3	-20/21	5/14	-5/63	1/12

TABLE 7.9. Optimal weighting coefficients c_j ($j \leq q$) for the finite-difference operator (Eq. 7.82).

7.4.4.6. *Optimal influence function and derivatives.* For a given set of box parameters characterized by the matrix $\underline{\mathbf{L}}^o$, the influence function that optimally compensates for discretization errors can be computed as

$$\hat{G}_g^o(\mathbf{k_l}) = \frac{\widehat{\mathbf{D}}_g(\mathbf{k_l}) \cdot [\sum_{\mathbf{m}\in\mathbb{Z}^3} \mathbf{k_{l,m}} k_{\mathbf{l,m}}^{-2} \hat{\gamma}(a k_{\mathbf{l,m}}) \hat{P}^2(\mathbf{k_{l,m}})]}{\widehat{\mathbf{D}}_g^2(\mathbf{k_l}) [\sum_{\mathbf{m}\in\mathbb{Z}^3} \hat{P}^2(\mathbf{k_{l,m}})]^2} \ , \tag{7.94}$$

where

$$\mathbf{k_{l,m}} = \mathbf{k_{l+\underline{N}\,m}} = \mathbf{k_l} + 2\pi^t \underline{\mathbf{H}}^{-1} \mathbf{m} \tag{7.95}$$

with $\mathbf{m} \in \mathbb{Z}^3$ is an alias vector of $\mathbf{k}$. This is valid for $\mathbf{l} \in G$ and $\mathbf{l} \neq \mathbf{0}$, together with $\hat{G}_g(\mathbf{0}) = 0$. In practice, the summation over alias vectors is restricted to $\mathbf{m}$ vectors with integer components in the range $[-m_{max}...m_{max}]$. A value of 2 or 3 for m_{max} is usually sufficient to reach convergence. The quantity $\hat{P}$ is given in by Eq. 7.80, the quantity $\widehat{\mathbf{D}}_g$ by Eqs. 7.88 (finite-difference) or 7.90 (ik-differentiation), and the quantity $\hat{\gamma}$ by Eq. 7.20. Note that $\hat{G}_g^o$ is a real quantity.

Due to the summation over alias vectors, the second terms in both the numerator and denominator of Eq. 7.94 are periodic in the components of $\mathbf{l}$ (with periods N_a, N_b and N_c, respectively). The second term in the numerator is also characterized by the same symmetry properties as $\mathbf{k_l}$ with respect to these components (central antisymmetry in the general case, antisymmetry with respect to changing the sign of any component for a rectangular box). Due to the properties of $\widehat{\mathbf{D}}_g$ (Sec. 7.4.4.5) one observes that : (i) $\hat{G}_g^o$ is periodic when using a finite-difference operator (but not when using ik-differentiation) ; (ii) in the general triclinic case, $\hat{G}_g^o$ is even with respect to a change in the sign of $\mathbf{l}$; (iii) in the rectangular case, $\hat{G}_g^o$ is even with respect to a change in the sign of any component of $\mathbf{l}$. Thus, for a triclinic box, the calculation of the influence function may be simplified by evaluating it over a half-space ($l_c \in [0; N_c/2]$) and symmetrizing the function afterwards. When using a finite-difference operator and a triclinic box, some care must be taken in regard to the boundary points. For example, if the points $(N_a/2, l_b, l_c)$ and $(-N_a/2, -l_b, -l_c)$ share the same value of $\hat{G}_g^o$, the points $(-N_a/2, -l_b, -l_c)$ and $(N_a/2, -l_b, -l_c)$ do not. Therefore, symmetry cannot be applied to the boundary point, which still must be calculated only over the entire space to enforce the convention for the definition of $\mathbf{k_l}$ in Eq. 7.76. This problem does not arise when using a finite-difference operator ($\hat{D}_g$ is then periodic), or using a rectangular computational box (where the points $(-N_a/2, -l_b, -l_c)$ and $(N_a/2, -l_b, -l_c)$ share the same value of $\hat{G}_g^o$ due to symmetry). For a rectangular box, the calculation may be further limited to an single octant ($l_a \in [0; N_a/2]$, $l_b \in [0; N_b/2]$ and $l_c \in [0; N_c/2]$) and symmetrizing the function afterwards. The quantity $k_{\mathbf{l,m}}$ can never be zero (and is thus not invertible) because $\hat{G}_g^o$ is not needed for $l = 0$ (Eq. 7.72). However, when using a finite-difference operator, the numerator and denominator vanish for the vectors $\mathbf{l}$ with components equal to $n_a N_a/2$, $n_b N_b$ and $n_c N_c$ with $\mathbf{n} \in \mathbb{Z}^3$, in which case $\hat{G}_g^o$ should be separately set to zero.

In practice, the sum in the denominator of Eq. 7.94 is evaluated analytically as

$$\sum_{\mathbf{m}\in\mathbb{Z}^3} \hat{P}^2(\mathbf{k_{l,m}}) = \prod_{\mu=x,y,z} \omega_p(H_{\mu k_\mu}) \tag{7.96}$$

with

$$\omega_p(\kappa) = -[\sin(\kappa/2)]^{2p} \frac{1}{(2m-1)!} \frac{d^{2p-1}}{dx^{2p-1}} \cot\theta \mid_{\theta=\kappa/2} \ . \tag{7.97}$$

The values of the $\omega_p(\kappa)$ functions are reported in Tab. 7.10

p	$\omega_p(\kappa)$
1	1
2	$1 - (2/3)s^2$
3	$1 - s^2 + (2/15)s^4$
4	$1 - (4/3)s^2 + (2/5)s^4 - (4/315)s^6$
5	$1 - (5/3)s^2 + (7/9)s^4 - (17/189)s^6 + (2/2835)s^8$

TABLE 7.10. Functions used in the analytical evaluation of the denominator in Eq. 7.94 (Eq. 7.97), with $s = \sin(\kappa/2)$.

The negative derivative of the optimal influence function with respect to the box parameters $\underline{\mathbf{L}}^o$, amplified on the right by ${}^t\underline{\mathbf{L}}^o$ (Eq. 7.70) may be calculated simultaneously with the influence function using Eq. 4.46 and noting that $\hat{P}$ is independent of $\underline{\mathbf{L}}^o$

$$\begin{aligned}
\widehat{\underline{\mathbf{\Gamma}}}^o_g(\mathbf{k_l}) \;=\; & \frac{1}{\widehat{\mathbf{D}}^2_g(\mathbf{k_l})\,[\sum_{\mathbf{m}\in\mathbb{Z}^3}\hat{P}^2(\mathbf{k_{l,m}})]^2}\sum_{\mathbf{m}\in\mathbb{Z}^3}\frac{\hat{P}^2(\mathbf{k_{l,m}})}{k^2_{\mathbf{l,m}}}\Big\{ \\
& \big\{k_{\mathbf{l,m}}\otimes\widehat{\mathbf{D}}_g(\mathbf{k_l})+\widehat{\mathbf{D}}_g(\mathbf{k_l})\otimes k_{\mathbf{l,m}} \quad -\frac{2[\mathbf{k_{l,m}}\cdot\widehat{\mathbf{D}}_g(\mathbf{k_l})]\mathbf{k_{l,m}}\otimes\mathbf{k_{l,m}}}{k^2_{\mathbf{l,m}}} \\
& -\frac{2[\mathbf{k_{l,m}}\cdot\widehat{\mathbf{D}}_g(\mathbf{k_l})]\widehat{\mathbf{D}}_g(\mathbf{k_l})\otimes\widehat{\mathbf{D}}_g(\mathbf{k_l})}{\widehat{\mathbf{D}}^2_g(\mathbf{k_l})}\big\}\hat{\gamma}(ak_{\mathbf{m}}) \\
& +\frac{[\mathbf{k_{l,m}}\cdot\widehat{\mathbf{D}}_g(\mathbf{k_l})]k_{\mathbf{l,m}}\otimes k_{\mathbf{l,m}}}{k^2_{\mathbf{l,m}}}\;ak_{\mathbf{l,m}}\,\hat{\gamma}'(ak_{\mathbf{l,m}})\Big\}
\end{aligned} \tag{7.98}$$

with $\hat{\gamma}'(\kappa)=d\hat{\gamma}(\kappa)/d\kappa$ (Tab. 7.5), valid for $\mathbf{l}\in G$ and $\mathbf{l}\neq\mathbf{0}$, together with $\widehat{\underline{\mathbf{\Gamma}}}^o_g(\mathbf{0})=\underline{\mathbf{0}}$. Note that $\widehat{\underline{\mathbf{\Gamma}}}^o_g$ is a real quantities. One further observes that : (i) $\widehat{\underline{\mathbf{\Gamma}}}^o_g$ is periodic when using a finite-difference operator (but not when using ik-differentiation) ; (ii) in the general triclinic case, $\widehat{\underline{\mathbf{\Gamma}}}^o_g$ is even with respect to a change in the sign of $\mathbf{l}$; (iii) in the rectangular case, the components of $\widehat{\underline{\mathbf{\Gamma}}}^o_g$ are odd with respect to a change in the sign of any component of $\mathbf{l}$ involved in their definition. Thus, as for the influence function, the calculation of $\widehat{\underline{\mathbf{\Gamma}}}^o_g$ can be restricted to a half-space (triclinic box) or to an octant (rectangular box), followed by symmetrization.

7.4.4.7. *Accuracy estimate.* When the charge-shaping function and the real-space cutoff are chosen so that Eq. 7.43 is satisfied, which implies that the real-space force evaluation is exact, and under the assumptions that (i) the force error is a sum of pairwise contributions and (ii) the system is homogeneous and disordered, the PPPM root-mean-square force error ΔF can be estimated as[35],

$$\Delta F=\big[\,\frac{1}{N_q}\sum_{i=1}^{N_q}(\mathbf{F}_i-\mathbf{F}_i^{exact})^2\,\big]^{1/2}\approx\frac{1}{4\pi\epsilon_0}\tilde{S}^2\,(\frac{Q}{N_qV})^{1/2}\;, \tag{7.99}$$

where $\mathbf{F}_i^{exact}$ is the the reference (exact) force, with

$$\begin{aligned}
Q \;=\; & 16\pi^2V^{-1}\sum_{\mathbf{l}\in G\,,\,\mathbf{l}\neq\mathbf{0}}\Big\{\sum_{\mathbf{m}\in\mathbb{Z}^3}k^{-2}_{\mathbf{l,m}}\,\hat{\gamma}^2(ak_{\mathbf{l,m}}) \\
& +[\hat{G}^\dagger_g]^2(\mathbf{k_l})\,\widehat{\mathbf{D}}^2_g(\mathbf{k_l})\,[\sum_{\mathbf{m}\in\mathbb{Z}^3}\hat{P}^2(\mathbf{k_{l,m}})]^2 \\
& -2\,\hat{G}^\dagger_g(\mathbf{k_l})\,\widehat{\mathbf{D}}_g(\mathbf{k_l})\cdot\sum_{\mathbf{m}\in\mathbb{Z}^3}\mathbf{k_{l,m}}\,k^{-2}_{\mathbf{l,m}}\,\hat{\gamma}(ak_{\mathbf{l,m}})\,\hat{P}^2(\mathbf{k_{l,m}})\Big\}\;.
\end{aligned} \tag{7.100}$$

Note that Eq. 7.100 is valid for any influence function (not necessary the optimal one defined in Eq. 7.94) so that it can be used to estimate accuracy losses upon using the first-order corrected influence function of Eq. 7.69 upon variations of the box dimensions. As for the influence function and its derivatives (Sec. 7.4.4.6) the calculation can be restricted to a half-space (triclinic box) or to an octant (rectangular box), and amplified by a symmetry weighting factor. Note that the vectors $\mathbf{l}$ with components equal to $n_aN_a/2$, n_bN_b and n_cN_c with $\mathbf{n}\in\mathbb{Z}^3$, for which $\hat{G}^o_g$ was set to zero (Sec. 7.4.4.6) must be included here.

This estimate is generally an upper bound to the error for realistic molecular systems. It is excellent for random distribution of charges, but generally provides an upper bound in realistic molecular systems with charge compensation (dipolar molecules, configurations favouring charge-charge, charge-dipole and dipole-dipole cancellations).

In the special case where $\hat{G}^\dagger_g=\hat{G}^o_g$, inserting Eq. 7.94 into Eq. 7.100 gives

$$\begin{aligned}
Q=16\pi^2V^{-1}\sum_{\mathbf{l}\in G\,,\,l\neq0}\Big\{\sum_{\mathbf{m}\in\mathbb{Z}^3}k^{-2}_{\mathbf{l,m}}\,\hat{\gamma}^2(k_{\mathbf{l,m}}) \\
-\frac{\big[\widehat{\mathbf{D}}_g(\mathbf{k_l})\;\cdot\;[\sum_{\mathbf{m}\in\mathbb{Z}^3}\mathbf{k_{l,m}}k^{-2}_{\mathbf{l,m}}\hat{\gamma}(k_{\mathbf{l,m}})\hat{P}^2(\mathbf{k_{l,m}})]\big]^2}{\widehat{\mathbf{D}}^2_g(\mathbf{k_l})\,[\sum_{\mathbf{m}\in\mathbb{Z}^3}\hat{P}^2(\mathbf{k_{l,m}})]^2}\Big\}\;.
\end{aligned} \tag{7.101}$$

An accuracy reevaluation through Eqs. 7.100 occurs every N_{ev} steps in MD simulations (including step zero if the influence function is read from file). If the estimated r.m.s. force error is larger than the threshold ΔF_{ev}, the influence function is reoptimized (together with its derivatives if required). In addition, any calculation

of the influence function (in the first step unless the function was read from file, or subsequent during reoptimizations after accuracy reevaluation) is accompanied by an accuracy evaluation through Eq. 7.101. In this case, if the estimated r.m.s. force error is larger than ΔF_{ev}, the program stops with an error message.

7.4.4.8. *Calculation of the $\tilde{A}_2$ self term in* PPPM. In the PPPM case, the quantity $\tilde{A}_2$ is evaluated as follows. In a first step, one constructs the grid $R_g(\mathbf{r_n})$ using the assignment-like equation

$$R_g(\mathbf{r_n}) = V_G^{-1} \sum_{i=1}^{N_q} q_i^2 \sum_{\mathbf{m}\in\mathbb{Z}^3} \prod_{\mu=x,y,z} f_p(L_\mu m_\mu + n_\mu; s_{i,\mu}) \tag{7.102}$$

where

$$f_p(n;s) = \sum_{n'=-(p-1)/2}^{(p-1)/2} w_p(s+n'-n) w_p(s+n'), \tag{7.103}$$

the n'-sum running over integers (p odd) or half integers (p even). For each charge, $\mathbf{s}_i$ is defined as follows. For p odd, one finds the grid point $\mathbf{n}_i$ closest to the location of charge q_i. For p even, one finds the grid-cell center closest to the location of charge q_i. In this case, $\mathbf{n}_i$ has half-integer components. Introducing the definition $\mathbf{s}_i = \mathbf{n}_i - \underline{\mathbf{H}}^{-1}\mathbf{r}_i$, one easily sees that the components of $\mathbf{s}_i$ satisfy the condition $\mid s_{i,\mu} \mid \leq 1/2$. The functions w_p in Eq. 7.103 are those used to construct the assignment function of order p (Tab. 7.8). Because $w_p(s+n)$ with $\mid s \mid \leq 1/2$ vanishes for $\mid n \mid \geq p/2$, $f_p(n;s)$ vanishes for $\mid n \mid \geq p$. Thus, the assignment of Eq. 7.102 distributes the square charge onto the $(2p-1)^3$ grid points neighbouring the origin of the grid (taking periodicity into account). The functions f_p are listed in Tab. 7.11. In a second step, one performs a fast Fourier transform of $R_g(\mathbf{r_n})$ to obtain $\hat{R}_g(\mathbf{k_l})$. The time required for this FFT is included in the timing information for the A2 calculation, not for the PPPM FFT. Note also that due to the symmetry of $f_p(n;s)$, a cosine transform would be sufficient here.

In a third step, one computes A_2 as

$$\tilde{A}_2 = \frac{4\pi}{V\tilde{S}^2} \sum_{\mathbf{l}\in G} \hat{G}_g^*(\mathbf{k_l})\, \hat{R}_g(\mathbf{k_l}) \ , \tag{7.104}$$

where $\hat{G}_g^*(\mathbf{k_l})$ is the first-order corrected influence function. Due to the properties of $\mathbf{s}_i$, the reciprocal-space self-energy of a charge is a function of its relative position to the nearest grid point (or grid-cell center). For large enough systems, these relative positions will be randomly distributed, and an estimate of the average self-energy can be obtained by replacing $f_p(n;s)$ by

$$\overline{f}_p(n) = \int_{-1/2}^{1/2} ds\, f_p(n;s) \tag{7.105}$$

in Eq. 7.102. The functions $\overline{f}_p$ are listed in Tab. 7.11. Using f_p (input switch NA2CLC=3), the self-energy term is configuration-dependent and needs to be recalculated every step of the simulation, except for $p=1$ ($f_1(n;s) = \overline{f}_1$) where the two choices lead to the same (configuration-independent) result. Using $\overline{f}_p$ (input switch NA2CLC=4), this calculation needs only be done once (if the volume is constant). In practice, the quantity $\tilde{A}_2$ is calculated (input switch NA2CLC=3 or 4) either (*i*) once at the beginning of the simulation (constant-volume simulation and NA2CLC=4), (*ii*) whenever an energy output (input switches NTPR and NTWE) is required (constant-volume simulation and NA2CLC=3), or (*iii*) every step (constant-pressure simulation). The value of $\tilde{A}_2$ is assumed constant between updates. These choices, together with the updating mode of A_2 (see above), ensure that the constant-pressure dynamics is always correct, and the energies and virial correct whenever printed into an energy output (they are only approximate in-between).

7.4.4.9. *Reading and writing of the influence function and derivatives.* If desired, the optimal influence function $\hat{G}_g^o$ (and its derivatives $\hat{\Gamma}_g^o$ whenever required), together with the corresponding reference edge lengths $\underline{\mathbf{L}}^o$, can be read from file at the beginning of a simulation. They can also be written to file at the end of a simulation. The file is unformatted and contains : 3 integers N_a, N_b and N_c ; 6 reals for the box parameters $\underline{\mathbf{L}}^o$; 1 logical indicating whether the six derivative grids are in the file ; 1 grid $\hat{G}_g^o$; 6 grids $\hat{\Gamma}_g^o$ in the order *aa*, *ab*, *ac*, *bb*, *bc* and *cc* (if the corresponding logical is set). Upon reading the file, the values of N_a, N_b and N_c are checked against the corresponding current parameters, the value $\underline{\mathbf{L}}^o$ against the current $\underline{\mathbf{L}}$ (within an acceptably small tolerance, $\underline{\mathbf{L}}^o$ is then exactly equalized to $\underline{\mathbf{L}}$), and the logical against the current need for derivatives. Any incompatibility results in an error message.

p	$\mid n \mid$	$f_p(n;s)$	$\overline{f}_p(n)$
1	0	1	1
2	0	$1/2(1+4s^2)$	$2/3$
	1	$1/4(1-4s^2)$	$1/6$
3	0	$1/32(19-24s^2+48s^4)$	$11/20$
	1	$1/16(3+8s^2-16s^4)$	$13/60$
	2	$1/64(1-8s^2+16s^4) = 1/64(1-4s^2)^2$	$1/120$
4	0	$1/576(265+204s^2-528s^4+320s^6)$	$151/315$
	1	$1/2304(575-564s^2+1488s^4-960s^6)$	$397/1680$
	2	$1/1152(23+84s^2-240s^4+192s^6)$	$1/42$
	3	$1/2304(1-12s^2+48s^4-64s^6) = 1/2304(1-4s^2)^3$	$1/5040$
5	0	$1/73728(32227-9520s^2+28960s^4-29440s^6+8960s^8)$	$15619/36288$
	1	$1/18432(4389+1792s^2-5472s^4+5632s^6-1792s^8)$	$44117/181440$
	2	$1/36864(1559-1456s^2+4512s^4-4864s^6+1792s^8)$	$913/22680$
	3	$1/18432(19+128s^2-416s^4+512s^6-256s^8)$	$251/181440$
	4	$1/147456(1-16s^2+96s^4-256s^6+256s^8) = 1/147456(1-4s^2)^4$	$1/362880$

TABLE 7.11. The functions $f_p(n;s)$ and $\overline{f}_p(n)$ required for the evaluation of the exact PPPM self energy term $\tilde{A}_2$ (Eqs. 7.103 and 7.105). The variable s must satisfy $\mid s \mid \leq 1/2$, and both functions vanish for $\mid n \mid \geq p/2$.

7.5. Polarization

7.5.1. Introduction. Polarisability allows for a more accurate description of the non-bonded interactions in classical atomistic simulations and must be implemented in the software when using polarisable force fields[9].

Several methods have been described in the literature that explicitly treat electronic polarization. GROMOS uses the charge on spring (COS) model[36] (also called Drude oscillator[37] or shell model[38]) where an inducible dipole $\boldsymbol{\mu}_i$ is modeled by attaching a massless, virtual site with a point-charge q_i^v to the polarisable center i, via a spring with harmonic force constant $k^{ho}{}_i$,

$$k^{ho}{}_i = \frac{(q_i^v)^2}{\alpha_i}. \tag{7.106}$$

The inducible dipole $\boldsymbol{\mu}_i$ adapts its size and direction according to its polarisability α_i and the electric field $\mathbf{E}'_i$ at the COS of the polarisable center i (assuming isotropic α_i and linear dependence of $\boldsymbol{\mu}_i$ on $\mathbf{E}'_i$) according to

$$\boldsymbol{\mu}_i = \alpha_i \mathbf{E}'_i. \tag{7.107}$$

The charge at the polarisable center with position $\mathbf{r}_i$, which may have a permanent charge q_i, is then $(q_i - q_i^v)$. Thus, the induced dipoles $\boldsymbol{\mu}_i$ are represented by

$$\boldsymbol{\mu}_i = q_i^v(\mathbf{r}'_i - \mathbf{r}_i) \tag{7.108}$$

where $\mathbf{r}'_i$ is the position of the charge-on-spring. There is no electrostatic interaction between the virtual charge q_i^v at $\mathbf{r}'_i$ and the charge $(q_i - q_i^v)$ at $\mathbf{r}_i$. In COS based schemes in which the charges-on-spring are not explicitly treated as additional degrees of freedom, the sum of the forces acting on any charge-on-spring should be zero, and the virtual charge q_i^v must be positioned such that

$$\mathbf{f}'^{ho}_i + \mathbf{f}'^{coul}_i = 0 \tag{7.109}$$

with the force $\mathbf{f}'^{ho}_i$ due to the spring given by

$$\mathbf{f}'^{ho}_i = -k^{ho}{}_i(\mathbf{r}'_i - \mathbf{r}_i) = -\frac{(q_i^v)^2}{\alpha_i}(\mathbf{r}'_i - \mathbf{r}_i) \quad , \tag{7.110}$$

and $\mathbf{f}_i'^{coul}$ due to the (Coulombic) electric field at the charge-on-spring ($\mathbf{E}_i'$) given by

$$\mathbf{f}_i'^{coul} = q_i^v \mathbf{E}_i' \quad . \tag{7.111}$$

To satisfy eq Eq. 7.109, the $\boldsymbol{\mu}_i$, i.e., the $\mathbf{r}_i'$, must be determined from the $\mathbf{E}_i'$s where the field $\mathbf{E}_i'$ does not contain a contribution from the charge $(q_i - q_i^v)$ at $\mathbf{r}_i$. However, since the displacement $|\mathbf{r}_i' - \mathbf{r}_i|$ of the charge-on-spring from the polarisable center is nonzero upon polarisation, an approximation of the ideal inducible dipole $\boldsymbol{\mu}_i$ at site i would require to determine $\mathbf{r}_i'$ from the electric field $\mathbf{E}_i$ at the polarisable center itself[39],

$$\mathbf{r}_i' = \mathbf{r}_i + \frac{\alpha_i \mathbf{E}_i}{q_i^v} \tag{7.112}$$

Using this approximation, the total force acting on the charge-on-spring is only zero if

$$\mathbf{E}_i = \mathbf{E}_i' \tag{7.113}$$

which is usually not the case for the induced dipole due to the nonzero values for $|\mathbf{r}_i' - \mathbf{r}_i|$. By choosing q_i^v large enough, $|\mathbf{r}_i' - \mathbf{r}_i|$ adopts relatively small values, resulting in small differences between $\mathbf{E}_i$ and $\mathbf{E}_i'$. On the other hand, the size of q_i^v is limited to values for which $|\mathbf{r}_i' - \mathbf{r}_i|$ is significant enough with respect to interatomic distances such that numerical precision is ensured when calculating, e.g. interaction energies involving induced dipoles.[36,39] The COS method has been employed in combination with iterative procedures to minimize the energy of the COS with respect to its position $\mathbf{r}_i'$, *i.e.* solving Eq. 7.109. In GROMOS q_i^v is generally set to $-8e$.

7.5.2. Theory. The COS method treats the induced dipole moments via additional point charges only, which allows for an easy introduction of polarisability into schemes to compute long-range electrostatic forces, such as the reaction-field, Ewald-summation, Particle-Particle- Particle-Mesh (PPPM) and Particle-Mesh-Ewald (PME) techniques or into a quantum-mechanical Hamiltonian for the electronic degrees of freedom of a (solute) molecule. The electrostatic potential ϕ_i at the polarisable centers i due to the charges in the system can be expressed using Coulombic terms

$$\phi_i(\mathbf{r}, \mathbf{r}') = \frac{1}{4\pi\epsilon_0\epsilon_{cs}} \sum_{\substack{j \neq i \\ j \text{ inside cut-off } i \\ (i,j) \text{ not excluded}}}^{N} \left[\frac{(q_j - q_j^v)}{|\mathbf{r}_i - \mathbf{r}_j|} + \frac{q_j^v}{|\mathbf{r}_i - \mathbf{r}_j'|} \right] \tag{7.114}$$

where the positions of the N atoms and corresponding virtual charges denoted by $\boldsymbol{r}^N = (\mathbf{r}_1, \mathbf{r}_2, \ldots, \mathbf{r}_N)$ and $\boldsymbol{r}'^N = (\mathbf{r}_1'\mathbf{r}_2', \ldots, \mathbf{r}_N')$, and ϵ_{cs} is the relative dielectric permittivity used for the model interactions. Because of the dependence of the $\mathbf{r}_i'$ on the $\mathbf{r}_j$s (and $\mathbf{r}_i'$s) via $\mathbf{E}_i$ in eq Eq. 7.112, the relation between ϕ_i and the electric field $\mathbf{E}_i$ is given by

$$\mathbf{E}_i = -\nabla_i \phi_i(\mathbf{r}, \mathbf{r}') = -\left(\frac{\partial \phi_i}{\partial \mathbf{r}_i} + \sum_{k \neq i}^{N} \frac{\partial \phi_i}{\partial \mathbf{r}_k'} \cdot \frac{\partial \mathbf{r}_k'}{\partial \mathbf{r}_i} \right) \tag{7.115}$$

When applying a Born-Oppenheimer-like iterative self-consistent field (SCF) procedure, however, the $\mathbf{r}_i$s are at every iteration step determined in the fixed electric field due to the other q_js and q_j^vs. When using a convergence criterion which minimizes the ϕ_is with respect to the positions $\mathbf{r}_i'$, the second term in eq Eq. 7.115 is zero at convergence because $\partial\phi_i/\partial\mathbf{r}_k' = 0$. Thus

$$\mathbf{E}_i = -\frac{\partial \phi_i}{\partial \mathbf{r}_i} = \frac{1}{4\pi\epsilon_0\epsilon_{cs}} \sum_{\substack{j \neq i \\ j \text{ inside cut-off } i \\ (i,j) \text{ not excluded}}}^{N} \left[\frac{(q_j - q_j^v)(\mathbf{r}_i - \mathbf{r}_j)}{|\mathbf{r}_i - \mathbf{r}_j|^3} + \frac{q_j^v(\mathbf{r}_i - \mathbf{r}_j')}{|\mathbf{r}_i - \mathbf{r}_j'|^3} \right] \tag{7.116}$$

The electrostatic part $\mathcal{V}^{(ele)}$ of the potential energy can also be expressed in terms of Coulomb interactions. The only non-Coulombic term to be added to $\mathcal{V}^{(ele)}$ is the selfpolarization energy V^{self}, which in the COS model can be expressed in terms involving point charges as well

$$\mathcal{V}^{(ele)} = V^{coul} + V^{self} \tag{7.117}$$

with

$$V^{coul}(\mathbf{r},\mathbf{r}') = \frac{1}{4\pi\epsilon_0\epsilon_{cs}} \sum_{\substack{i=1}}^{N-1}\sum_{\substack{j>i \\ j \text{ inside cut-off } i \\ (i,j) \text{ not excluded}}}^{N} \left[\frac{(q_i-q_i^v)(q_j-q_j^v)}{|\mathbf{r}_i-\mathbf{r}_j|} + \frac{(q_i-q_i^v)q_j^v}{|\mathbf{r}_i-\mathbf{r}'_j|} + \frac{(q_j-q_j^v)q_i^v}{|\mathbf{r}'_i-\mathbf{r}_j|} + \frac{q_i^v q_j^v}{|\mathbf{r}'_i-\mathbf{r}'_j|}\right] \tag{7.118}$$

and

$$V^{self}(\mathbf{r},\mathbf{r}') = \frac{1}{2}\sum_{i=1}^{N}\frac{(q_i^v)^2}{\alpha_i}|\mathbf{r}'_i-\mathbf{r}_i|^2 \tag{7.119}$$

Next we consider the expression for the forces $\mathbf{f}_i$ that act on (polarisable) atomic centers i

$$\mathbf{f}_i = -\nabla_i V_i^{ele}(\mathbf{r},\mathbf{r}') = -\left(\frac{\partial\mathcal{V}^{(ele)}}{\partial\mathbf{r}_i} + \sum_{k\neq i}^{N}\frac{\partial\mathcal{V}^{(ele)}}{\partial\mathbf{r}'_k}\cdot\frac{\partial\mathbf{r}'_k}{\partial\mathbf{r}_i}\right). \tag{7.120}$$

Note again the dependence of the $\mathbf{r}'_k$s on the $\mathbf{r}_i$s that appears in the second term on the right in eq Eq. 7.120, which might adopt nonzero values because $\mathcal{V}^{(ele)}$ not only contains terms due to the ϕ_is (first two terms on the right in Eq. 7.118) but also due to the ϕ_is (last two terms on the right in Eq. 7.118) and V^{self}, whereas when using eq Eq. 7.112 only the ϕ_is have been minimized with respect to the $\mathbf{r}'_i$s. When nevertheless using assumptions Eqs. 7.109 and 7.113, Eq. 7.120 reduces to

$$\mathbf{f}_i^{red} = -\frac{\partial\mathcal{V}^{(ele)}}{\partial\mathbf{r}_i} = -\left(\frac{\partial V^{coul}}{\partial\mathbf{r}_i} + \frac{\partial V^{self}}{\partial\mathbf{r}_i}\right) \quad . \tag{7.121}$$

From the assumptions in Eqs. 7.109 and 7.113 we have

$$-\frac{\partial V^{self}}{\partial\mathbf{r}_i} = \mathbf{f}_i^{ho} = -\mathbf{f}_i'^{ho} = \mathbf{f}_i'^{coul} = -\frac{\partial V^{coul}}{\partial\mathbf{r}_i} \tag{7.122}$$

and the reduced expression $\mathbf{f}_i^{red}$ for the atomic forces

$$\begin{aligned}
\mathbf{f}_i^{red} &= \frac{1}{4\pi\epsilon_0\epsilon_{cs}} \sum_{\substack{i=1}}^{N-1}\sum_{\substack{j>i \\ j \text{ inside cut-off } i \\ (i,j) \text{ not excluded}}}^{N} \left[\frac{(q_i-q_i^v)(q_j-q_j^v)(\mathbf{r}_i-\mathbf{r}_j)}{|\mathbf{r}_i-\mathbf{r}_j|^3}\right. \\
&+ \frac{(q_i-q_i^v)q_j^v(\mathbf{r}_i-\mathbf{r}'_j)}{|\mathbf{r}_i-\mathbf{r}'_j|^3} \\
&+ \frac{(q_j-q_j^v)q_i^v(\mathbf{r}'_i-\mathbf{r}_j)}{|\mathbf{r}'_i-\mathbf{r}_j|^3} \\
&+ \left.\frac{q_i^v q_j^v(\mathbf{r}'_i-\mathbf{r}'_j)}{|\mathbf{r}'_i-\mathbf{r}'_j|^3}\right].
\end{aligned} \tag{7.123}$$

If the COS model is used with reaction field, a reaction-field term is to be added to $\mathcal{V}^{(ele)}$

$$\begin{aligned}
V^{RF}(\boldsymbol{r}^N) &= \frac{1}{4\pi\epsilon_0\epsilon_{cs}} \sum_{\substack{i=1}}^{N-1}\sum_{\substack{j>i \\ j \text{ inside cut-off } i}}^{N} (q_i-q_i^v)(q_j-q_j^v)\left(-\frac{\frac{1}{2}C_{rf}|\mathbf{r}_i-\mathbf{r}_j|^2}{{R_{rf}}^3} - \frac{1-\frac{1}{2}C_{rf}}{R_{rf}}\right) \\
&+ (q_i-q_i^v)q_j\left(-\frac{\frac{1}{2}C_{rf}|\mathbf{r}_i-\mathbf{r}'_j|^2}{{R_{rf}}^3} - \frac{1-\frac{1}{2}C_{rf}}{R_{rf}}\right) \\
&+ q_i^v(q_j-q_j^v)\left(-\frac{\frac{1}{2}C_{rf}|\mathbf{r}'_i-\mathbf{r}_j|^2}{{R_{rf}}^3} - \frac{1-\frac{1}{2}C_{rf}}{R_{rf}}\right) \\
&+ q_i^v q_j^v\left(-\frac{\frac{1}{2}C_{rf}|\mathbf{r}'_i-\mathbf{r}'_j|^2}{{R_{rf}}^3} - \frac{1-\frac{1}{2}C_{rf}}{R_{rf}}\right) \qquad (7.124) \\
&- \frac{1}{4\pi\epsilon_0\epsilon_{cs}}\sum_{i=1}^{N}\frac{q_i^2}{2}\frac{1-\frac{1}{2}C_{rf}}{R_{rf}} \qquad (7.125)
\end{aligned}$$

where R_{rf} is the reaction-field cutoff and C_{rf} is the reaction-field constant defined as

$$C_{rf} = \frac{2(\epsilon_{cs} - \epsilon_{rf})(1 + \kappa_{rf}R_{rf}) - \epsilon_{rf}(\kappa_{rf}R_{rf})^2}{(\epsilon_{cs} + 2\epsilon_{rf})(1 + \kappa_{rf}R_{rf}) + \epsilon_{rf}(\kappa_{rf}R_{rf})^2} \tag{7.126}$$

where κ_{rf} is the inverse Debye screening length and ϵ_{rf} is the reaction-field dielectric permittivity outside the reaction-field cutoff radius R_{rf}. The reaction field term makes the electrostatic force and interaction zero at the reaction-field cut-off distance. Using a cut-off radius plus reaction field the summation over j in Eq. 7.123 is over sites j inside the cut-off of site i, and omits the covalently bound nearest neighbours j of atom i that are excluded from the non-bonded interaction. These neighbours j of i must not be excluded in the summation over j in Eq. 7.124 because they contribute to the reaction field[40]. The last term in Eq. 7.124 is a constant that is added to represent the self-interaction of the permanent, i.e. non-COS, charges.

The Coulomb contribution $\mathbf{E}_i^{coul}$ to the electrc field $\mathbf{E}_i$ is given by Eq. 7.116. The reaction field contribution $\mathbf{E}_i^{RF}$ is

$$\mathbf{E}_i^{RF} = \frac{C_{rf}}{4\pi\epsilon_0\epsilon_{cs}} \sum_{\substack{j \neq i \\ j \text{ inside cut-off } i}}^{N} \left[\frac{(q_j - q_j^v)(\mathbf{r}_i - \mathbf{r}_j)}{{R_{rf}}^3} + \frac{q_j^v(\mathbf{r}_i - \mathbf{r}'_j)}{{R_{rf}}^3} \right] . \tag{7.127}$$

Since iteratively solving Eqs. 7.112, 7.116 and 7.127 is costly, the number of iterations to be carried through till

$$\mathbf{E}_i = \mathbf{E}_i^{coul} + \mathbf{E}_i^{RF} \tag{7.128}$$

does not change significantly anymore should be kept low *i.e.* lower than a few. Since the molecular configuration will not change much between subsequent MD time steps Δt, one may use previous consistent values for the displacement of the virtual charge q_i^v

$$\Delta\mathbf{r}_i^v = \mathbf{r}'_i - \mathbf{r}_i, \tag{7.129}$$

i.e. iterated till $\Delta\mathbf{r}_i^v$ and $\mathbf{E}_i$ reach consistency, to obtain a good prediction of the next $\Delta\mathbf{r}_i^v$ to be used to start the iteration at $t + \Delta t$,

$$\Delta\mathbf{r}_i^v(predicted) = 2\Delta\mathbf{r}_i^v(t) - \Delta\mathbf{r}_i^v(t - \Delta t). \tag{7.130}$$

On average, two to three iterations are required at every time step to calculate the consistent fields with the convergence criterion of[41,42]

$$max_{i,x,y,z}(|\Delta E_{i,x}|, |\Delta E_{i,y}|, |\Delta E_{i,z}|)|q_O|d_{OH} < \Delta U \tag{7.131}$$

with $\Delta U = 2.5$ kJ mol^{-1}, and where $\Delta E_{i,x}$, $\Delta E_{i,y}$ and $\Delta E_{i,z}$ are the changes between consecutive iteration steps in the electric field component at the COS site i along the x-, y- and z- axes, q_O denotes the non-polarisable part of the charge of an oxygen atom (typically of a water molecule) and d_{OH} is the length of the OH bond of water molecule.

7.5.3. Off-atom sites. For certain polarisable models[43] it is necessary to add an additional virtual atomic center M. The position of this virtual site M is defined in terms of the positions of three non-virtual atoms i, j and k,

$$\mathbf{r}_M = \mathbf{r}_i + \frac{\gamma^{pol}}{2}(\mathbf{r}_{ji} + \mathbf{r}_{ki}) \tag{7.132}$$

where γ^{pol} is a constant, which determines the distance $d_{iM} = r_{iM}$ as a function of the distances $d_{ij} = r_{ij}$ and $d_{ik} = r_{ik}$. For example, in a model for H_2O, i would denote the oxygen atom and j and k the hydrogen atoms. The addition of the massless site M defined by Eq. 7.132 does not introduce any extra degrees of freedom into the molecule in the calculation of the kinetic energy of the system. The " pseudo-force" $\mathbf{f}_M$ that acts on the virtual-atom site M is redistributed to the non-virtual atoms i, j and k according to

$$\begin{aligned} &\mathbf{f}_i + (1 - \gamma^{pol})\mathbf{f}_M \\ &\mathbf{f}_j + \frac{\gamma^{pol}}{2}\mathbf{f}_M \\ &\mathbf{f}_k + \frac{\gamma^{pol}}{2}\mathbf{f}_M \end{aligned} \tag{7.133}$$

7.5.4. Non-linear polarizability. A problematic feature of many polarisable models, apart from their larger demand for computing power than nonpolarisable ones, is their tendency to allow for overpolarisation in the presence of strong local electric fields, leading to the polarisation catastrophe and a too large static dielectric permittivity. There are several approaches to resolve this problem. Using the GROMOS force fields the polarisation catastrophe is avoided by a big enough repulsive Lennard-Jones interaction between non-hydrogen atoms leading to dipole-dipole distances larger than $(4\alpha_i^2)^{1/6}$. Additionally the GROMOS simulation software allows the linear dependence of the induced dipole $\boldsymbol{\mu}_{ind,i}$ on the electric field $\mathbf{E}_i$ to be substituted by a sublinear dependence for large field strengths[44,45] which can be achieved by making the polarisability α_i electric field dependent. For example, α_i is replaced by $\alpha_{D,i} = \alpha_{D,i}(E)$ for large $\mathbf{E}_i$ using

$$\alpha_{D,i} = \begin{cases} \alpha_i & for\ E_i \le E_{0,i} \\ \frac{\alpha_i E_{0,i}}{p_i E}\left[p_i + 1 - \left(\frac{E_{0,i}}{E_i}\right)^{p_i}\right] & for\ E_i > E_{0,i}. \end{cases} \tag{7.134}$$

where p_i is a polarisation damping parameter. The induced dipole is then defined as

$$\boldsymbol{\mu}_i^{ind} = \begin{cases} \alpha_i \mathbf{E}_i & for\ E_i \le E_{0,i} \\ \frac{\alpha_i E_{0,i}}{p_i}\left[p_i + 1 - \left(\frac{E_{0,i}}{E_i}\right)^{p_i}\right]\frac{\mathbf{E}_i}{E_i} & for\ E_i > E_{0,i}. \end{cases} \tag{7.135}$$

This change also influences the self-polarisation contribution to the potential energy

$$V^{self,i} = \begin{cases} \frac{1}{2}\alpha_i E_i^2 & for\ E_i \le E_{0,i} \\ \frac{1}{2}\alpha_i E_{0,i}^2 & \\ \quad + \frac{\alpha_i E_{0,i}^2}{p_i(p_i-1)}\left[-p_i^2 + (p_i^2-1)\left(\frac{E_i}{E_{0,i}}\right) + \left(\frac{E_{0,i}}{E_i}\right)^{p_i-1}\right] & for\ E_i > E_{0,i} \end{cases} \tag{7.136}$$

with $V^{self} = \sum_i V^{self,i}$ where i runs over all polarisable centers.

CHAPTER 8

Coarse-grained models and multi-resolution simulation

8.1. Introduction

In chemistry, different levels of modelling, i.e. involving different types of degrees of freedom, can be chosen (Tab. 8.1). At the second most fine-grained level, one considers nuclei and electrons, as done in quantum chemistry. If one is not interested in breaking or forming chemical bonds or excited states of molecules, for example, one may eliminate the electronic degrees of freedom from the model and only consider atoms. In other words, the fine-grained model is coarse-grained by elimination of electronic degrees of freedom. This coarse-graining procedure can be applied between any two levels of modelling and thus any model in chemistry can be viewed as a coarse-grained model with respect to the eliminated degrees of freedom. However, the term coarse-grained modelling has predominately been used to indicate models in which the particles that constitute the degrees of freedom of the model represent more than one non-hydrogen atom.

Level	Particles	Size of bead /nm	Scaling effort	CG reduction N_{df}	CG reduction comput. effort
I	Nucleons + electrons	10^{-6}	$N_n^{\geq 3}$		
				10-100	$> 10^3$
II	Nuclei + electrons	$10^{-6} - 10^{-5}$	$N_e^{\geq 3}$		
				10-100	$> 10^3$
III	Atoms	0.03-0.3	N_a^{1-2}		
				2-5	2-25
IV	Supra-atomic beads	0.5-1.0	N_b^{1-2}		
				2-10	2-100
V	Supra-molecular beads	0.5-1.0	N_b^{1-2}		

TABLE 8.1. Characteristic sizes of particles at different levels of resolution of modelling, scaling of the computational effort as a function of the number of nucleons (N_n), electrons (N_e), atoms (N_a) or beads (N_b), and the reduction of the number of degrees of freedom or interactions N_{df} and the reduction of computational effort that can be achieved by coarse-graining to the next level of modelling

If these atoms belong to one molecule, such a model is a supra-atomic, or molecular, coarse-grained model. If the particles that constitute the degrees of freedom represent more than one molecule, such a model is a supra-molecular coarse-grained model.

The interactions governing the motion of the particles of the different levels are: (I) strong interaction, Coulomb and Pauli principle (II) Coulomb and Pauli principle (III) Coulomb, van der Waals, repulsive and bonded terms (IV) Coulomb, van der Waals, repulsive and bonded terms (V) Coulomb, van der Waals, repulsive terms The interactions of levels I and II are governed by quantum mechanics, while the interactions

of levels III-V are governed by classical statistical mechanics. The number of degrees of freedom, particles or interaction sites will determine, together with the applicable equations of motion (quantum- or classical-mechanical), the computational effort required, and thus the reduction of the latter that can be reached by coarse-graining (Tab. 8.1). Coarse-graining from level II to level III has different characteristics and problematic issues than coarse-graining from level III to level IV or V, because of the limited compatibility of quantum and classical mechanical concepts. Therefore, here we only consider coarse-graining in the realm of classical mechanics, i.e. between levels III, IV and V. For coarse-graining from level II to level III we refer to Ref.[3] and Chap. 15.

Coarse-graining implies eliminating degrees of freedom. This leads inevitably to a decrease of the applicability of the model. For example, when coarse-graining from level II (nuclei and electrons) to level III (atoms), relaxation of electronically excited states of molecules is not covered by the model any more. Generally, coarse-graining leads to a loss of accuracy of the model, although for particular properties and types of models this need not be the case. For example, the properties of liquid water at ambient temperature are more accurately described by the SPC model,[46] a level III model, than by level II ab initio models based on density-functional theory, due to the limited accuracy of the functionals used. In general, the choice of degrees of freedom to be eliminated depends on the property and phase of the substance of interest.

The conditions that must be fulfilled by degrees of freedom in order that they may be eliminated in a physically correct manner in the coarse-graining process, such that a computationally efficient and yet accurate coarse-grained model is obtained, are:

1. they must be non-essential for the process or property of interest.
2. they must be large in number or computationally intensive, so that the computational gain is substantial enough to offset the loss in accuracy.
3. the interactions governing these degrees of freedom to be eliminated should be largely decoupled from the interactions governing the other degrees of freedom of the system which are to be maintained. This means that the frequency components of the motion along the degrees of freedom to be eliminated must be well separated from the other frequencies occurring in the system, and that the coupling between the two types of motion is weak.[47]
4. their elimination should allow a simple, efficient representation of the interaction governing the other, remaining degrees of freedom.

Two examples of coarse-graining between levels III and IV are discussed: the use of so-called united atoms and of bond-length constraints. By treating the aliphatic CH, CH2 and CH3 groups as united atoms, the number of atomic interaction sites is substantially reduced, up to almost a factor of 10 fewer pairwise non-bonded interactions for lipids, at the cost of losing the dipolar interactions of the CH moieties and the van der Waals interactions of the H atoms. The intra-moiety motions of these CHn groups are largely decoupled from the motions of the other atoms and the torsional interactions involving these H atoms can be incorporated into the corresponding interactions for the torsional angle that does not involve an aliphatic H atom. If the positions of these H atoms are needed, i.e. when calculating quantities such as nuclear Overhauser effects (NOE s), residual dipolar couplings (RDCs) or S^2 order parameters measurable by NMR, the H atom positions can be easily recovered based on the positions of the carbon atom and its non-hydrogen covalently bound neighbours. Thus, all four conditions for appropriate coarse-graining are largely met in this case.

The other example of coarse-graining is the use of geometric constraints for small molecules without intra-molecular torsional-angle degrees of freedom, such as the solvents water, methanol or chloroform, or bond-length constraints in macromolecules.[47] The latter are standardly used in biomolecular simulations, because they satisfy conditions 1 to 4 and allow, through the use of SHAKE or other similar techniques to maintain such constraints, a gain of about a factor of four in computational efficiency.

An example of coarse-graining that does not satisfy conditions 3 and 4 is the use of an implicit solvent model, *i.e.* the attempt to mimic the effect of the solvent by a function that is only dependent on the solute coordinates. If the solvent is water, this leads to severe distortions of the energy surface of the solute. Although the motions of a large solute may cover time scales ranging from femtoseconds to milliseconds and the relaxation times of water molecules are of the order of picoseconds, their motions on picosecond to nanosecond time scales are not decoupled, and thus condition 3 is not satisfied for particular processes.

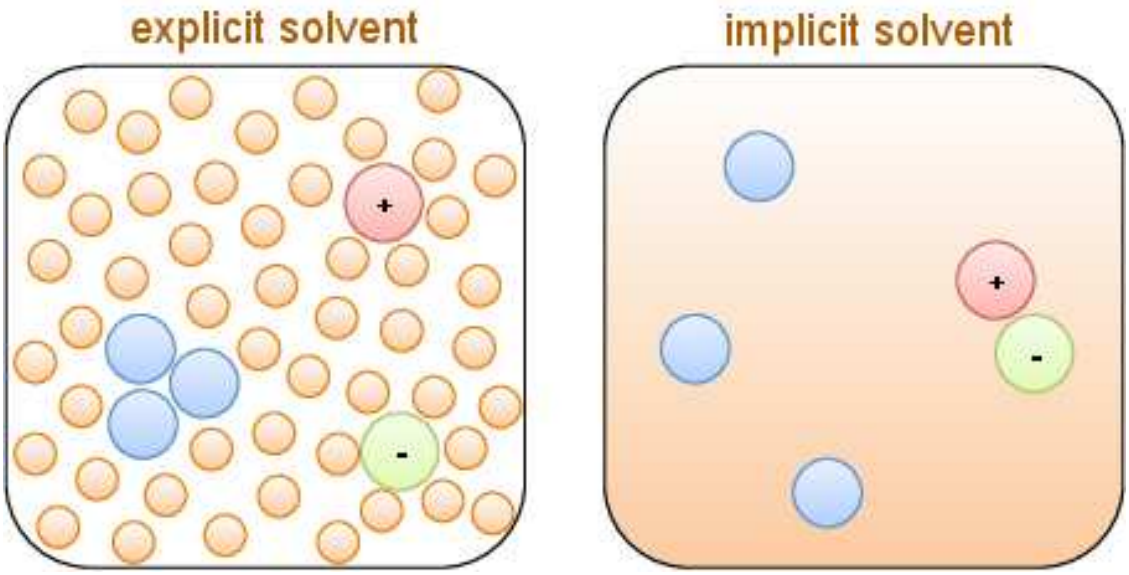

FIGURE 8.1. Illustration of the hydrophobic effect and the adverse effect of eliminating solvent degrees of freedom in the process of coarse-graining. The solvent is shown in orange, the hydrophobes in blue, and the ions in red (positively charged) and green (negatively charged).

In explicit solvents (orange particles in the left panel of Fig. 8.1), the non-polar particles (blue) aggregate, and the electrostatic interaction between ions (red and green) is reduced, leading to dissolution. So-called hydrophobic or non-polar particles do like water, but their interaction with water is less strong than the interaction of water with itself, leading to water excluding the hydrophobes and their subsequent aggregation. Ions with opposite charges do like water more than each other, which leads to water surrounding the ions and dissolution of ion pairs. The "hydrophobic effect", the apparent attraction between non-polar molecules or repulsion between ions in aqueous solution due to the stronger interaction between the water molecules or between water molecules and ions, cannot be properly modelled in terms of solute and ion coordinates only (right panel Fig. 8.1), because the effective interaction between solute atoms and their entropy is a complex function of the distribution of solvent coordinates. Thus, condition 4 is difficult to meet.

Coarse-graining from level III to IV for biomolecules is a challenge because of the heterogeneity of biomolecules. The scale invariance that lies at the heart of the renormalisation group approach to coarse-graining of largely homogeneous polymers is not observed for biopolymers, which are composed of many different, complex structural units that are connected through different types of interactions. In the coarse-graining process, the basic geometry and the balance between the various interactions must be preserved in order to avoid losing characteristic features of these molecules. In addition, entropy plays a non-negligible role in biomolecular processes, which means that the loss of entropy in the process of coarse-graining must be compensated for by a loss in energy in order to maintain the relevant free energy differences. Finally, the reduction of the computational effort between levels III and IV is rather modest compared to that between other levels (Tab. 8.1). These considerations lead us to the conclusion that coarse-graining from level III to level IV does not pay off for biomolecules such as proteins, DNA, RNA and sugars. Only a limited decrease in the number of interaction sites is reached at the cost of losing the essential characteristics of such molecules in terms of intra-molecular interactions, interactions with the solvent and entropy. Only lipids, which have relatively long homogeneous aliphatic tails, may be able to retain the dominant characteristics of an amphiphilic molecule with a particular geometry and flexibility upon coarse-graining from level III to level IV. Due to the abundance of lipids in membranes, the reduction in computational cost may off-set the loss of accuracy.

Since the inclusion of solvent degrees of freedom is essential to properly represent the hydrophobic effect and because the calculation of the solvent-solvent interactions in a simulation of a biomolecule such as a

protein or a fragment of DNA in aqueous solution dominates the computational effort, coarse-graining of the solvent degrees of freedom holds much promise to reduce the computational costs, in particular when more than one solvent molecule is subsumed into a supra-molecular bead. In the case of water, such coarse-graining from level III to level V should retain the thermodynamic and dielectric screening properties and hydrogen-bonding capacity of water as much as possible, and a proper ratio between entropy and energy.[48,49] This is not the case if a water bead is modelled as a Lennard-Jones particle without charge. Coarse-graining of solvent degrees of freedom in a biomolecular simulation has a good chance of meeting conditions 1 to 4, depending on how the coarse-grained interaction is modelled.

When coarse-graining from level III to level V, a few technical issues emerge that are generally not present in atomic-level models.

1. Atomic biomolecular force fields generally use a relative dielectric constant ϵ_{cs} of 1 in the Coulomb interaction, because there is vacuum between the atoms and the polarisability of atoms is neglected. The supra-molecular beads should represent the polarisability or dielectric screening capability of Nmol molecules. This is accounted for by using values of $\epsilon_{cs} > 1$ in the direct Coulomb interaction.
2. When comparing the pressure calculated for the supra-molecular beads with the desired experimental value, one should account for the fact that this pressure will be N_{mol} times smaller than in an atomic-level simulation by using a scaling factor $S_{SM} = N_{mol}$.
3. For thermodynamic quantities such as the heat of vaporisation, the excess free energy of a liquid or the free energy of solvation that are defined by a difference of an energy or free energy between the gas phase and the liquid phase, a meaningful comparison of values calculated with a supra-molecular model ($N_{mol} > 1$) and experimental ones is not possible, because it would require a reliable calculation of the (free) energy of cluster decomposition in the gas phase.

8.2. Multi-resolution simulation

Generally, a model developed for a particular level of modelling is only used at the same level of modelling. For example, models for small molecular compounds in the liquid phase are used to study the properties of mixtures of such compounds. However, this may limit the accessible time and length scales in biomolecular simulations. Because of the heterogeneity of biomolecular systems in terms of their relaxation time scales and the different types of interactions present it is of interest to combine different levels of modelling in one simulation or system.
The combination of different levels of modelling or resolution, *i.e.* multi-graining, can take different forms.[50]

1. The simulation switches between the two levels of modelling in time: multi-graining in time. This can be done in two ways:
   a. the simulation is performed at the coarse-grained level and particular configurations are later mapped back to the fine-grained level;
   b. a coupling parameter λ is introduced that defines a path between the fine-grained (*e.g.* $\lambda = 0$) and the coarse-grained (*e.g.* $\lambda = 1$) representation of the particles, which allows a smooth switching between different levels of modelling in *e.g.* a Hamiltonian replica-exchange simulation.[51]
2. The system contains a mixture of fine-grained and coarse-grained particles: multi-graining in space. This can be done in two ways:
   a. the space occupied by the system is divided into a fine-grained and a coarse-grained region with a small buffer region in which the particles change from one resolution to the other. The resolution of the particles thus depends on their position in space;
   b. the particles of the system are either fine-grained or coarse-grained and can freely mix. The resolution of the particles is thus fixed.[45,52,53]

Multi-graining of type 2(b) is for example also applied between level II and level III in so-called hybrid QM/MM simulations in which the electrons are treated quantum-mechanically (level II) and the nuclei and surrounding atoms classically (level III). See Chap. 15.

CHAPTER 9

Special force-field terms

9.1. Introduction

The interaction function $\mathcal{V}(\boldsymbol{r};\mathbf{s})$ as given in Eq. 3.4 may contain special terms indicated as $\mathcal{V}^{(spec)}(\boldsymbol{r};\mathbf{s})$, which are only used under special circumstances. In GROMOS, the following special interaction terms have been implemented.

A. *atom position restraining* (Sec. 9.2)
B. *atom-atom distance restraining* (Sec. 9.3)
C. *bond-angle restraining* (Sec. 9.5)
D. *dihedral-angle restraining* (Sec. 9.6)
E. ^3J*-coupling constant restraining* (Sec. 9.7)
F. S^2*-order parameter restraining* (Sec. 9.8)
G. *crystallographic structure-factor amplitude restraining* (Sec. 9.9)
H. *crystallographic electron-density restraining* (Sec. 9.10)
I. *crystallographic symmetry restraining* (Sec. 9.11)
J. *distance-field restraining* (Sec. 9.12)
K. *local-elevation biasing* (Sec. 9.13)

In cases Pts. A-F, the motion along a particular type of degree of freedom is restrained. Therefore, these special terms are often called *restraining interaction terms*, $\mathcal{V}^{(res)}(\boldsymbol{r};\mathbf{s})$. They are commonly used in structure refinement based on NMR data and can also be employed as so-called umbrella functions to focus the sampling of configuration space when determining a free energy profile along a given coordinate (Sec. 14.8). Case K is an example of the use of a repulsive restraint, which diverts the system away from the parts of configuration space it has already visited. This technique is useful when searching conformational space and can also be used as an alternative to restraining. One may also choose to remove all motion for specific atoms or along certain degrees of freedom. Such hard boundary conditions are referred to constraints and will be the topic of Chap. 10.

When the interaction function $\mathcal{V}^{(spec)}(\boldsymbol{r};\mathbf{s})$ refers to non-atomic sites as centres of interaction, it is still possible to decompose the force on a non-atomic site into forces on those atoms, of which the atomic positions are used to define the position of the non-atomic site. The use of such non-atomic interaction sites, also called *virtual* or *pseudo atoms*, is discussed in Sec. 9.4. It has only been implemented in GROMOS in the context of atom-atom distance restraining special interaction terms.

When restraining an atom-atom distance or a ^3J-coupling constant or an S^2 order parameter to experimental values obtained from NMR experiments, which generally represent an average over time and space, one should *restrain* only the *time-average* of the function r^{-3} of the distance r or the *time average* of the ^3J-coupling constant or S^2 order parameter. This is discussed in Secs. 9.3, 9.7 and 9.8, respectively.

9.2. Atom-position restraining or fixed atoms

When simulating a molecular system, it may be desirable to fix specific atoms or parts of the system. In MD simulation it is in general not advisable to immobilize atoms completely, because this may reduce the flexibility of the system such that transitions and motions that are normally occurring in the system, are completely inhibited by the rigidity of the atoms. Therefore, a better way to keep specific atoms approximately at given reference positions is to restrain the motion of those atoms around these positions by applying a harmonic restraining force, which still leaves room for flexibility and mobility. The application of position constraints will be discussed in Sec. 10.3.

The special interaction term in $\mathcal{V}^{(spec)}(\boldsymbol{r};\mathbf{s})$ in Eq. 3.4 that performs *atom position restraining* reads

$$\begin{aligned}\mathcal{V}^{(pr)}(\boldsymbol{r};\mathbf{s}) &= \sum_{n=1}^{\mathcal{N}^{(pr)}} \mathcal{V}^{(pr)}{}_n(\mathbf{r}_n; k^{(pr)}{}_n; \mathbf{r}_n^0) \\ &= \sum_{n=1}^{\mathcal{N}^{(pr)}} \tfrac{1}{2} k^{(pr)}{}_n [\mathbf{r}_n - \mathbf{r}_n^0]^2 \end{aligned} \tag{9.1}$$

The summation runs over a set of $\mathcal{N}^{(pr)}$ selected atoms. The fixed reference positions are denoted by $\mathbf{r}_n^0$. The harmonic oscillator force constant $k^{(pr)}{}_n$ can be chosen

- to be equal for all selected atoms, $k^{(pr)}{}_n = CPOR$, $(NTPOR = 1)$, or
- to be inversely proportional to the atomic B-factors of the selected atoms, $k^{(pr)}{}_n = CPOR/BFAC[n]$, $(NTPOR = 2)$,

where CPOR, NTPOR and BFAC[n] are user specified (see Vol. 4).

The actual position of the n-th restrained atom is denoted by $\mathbf{r}_n$.

The force on atom n due to the n-th term in Eq. 9.1 is

$$\mathbf{f}_n = -k^{(pr)}{}_n [\mathbf{r}_n - \mathbf{r}_n^0] \tag{9.2}$$

The atom sequence numbers of the restrained atoms are stored in JRC[1..NRC], $NRC = \mathcal{N}^{(pr)}$. These are used to select atom reference position coordinates from $XC[1..3 * \mathcal{N}_a]$, where $\mathcal{N}_a$ denotes the total number of atoms in the system. Reading of the reference positions in program MD++ is controlled by the switch NTPORB. The reference positions can either be read from a startup file $(NTPORB = 0)$ or from a special file $(NTPORB = 1)$. The specification of atoms and reference positions for atom position restraining is discussed in Secs. 4-3.11 and 4-4.2. Position restraining can be applied to any atom of solute or solvent. The switch NTPOR controls the atom position restraining or fixed atom option:

NTPOR	$= 0$,	no atom position restraining
	$= 1$,	harmonic atom position restraining, $k^{(pr)}{}_n = CPOR$
	$= 2$,	harmonic atom position restraining, $k^{(pr)}{}_n = CPOR/BFAC[n]$
	$= 3$,	position constraining

The reference positions can be scaled upon pressure scaling by using the switch NTPORS.

Applications of atom position restraining are the following.

- When a solute is placed in a box with solvent molecules, the solute-solvent atomic contacts may be very unfavourable. When performing energy minimization or molecular dynamics starting from such a configuration the solute conformation may be distorted by the bad non-bonded contacts with the solvent molecules. By applying atom position restraining to the solute atoms the unfavourable contacts can be relaxed without changing the solute conformation.
- When only a part of a molecular system is simulated under fixed boundary conditions (FBC), it is necessary to restrain the atoms in the wall region in order to avoid distortion of the system due to the vacuo boundary condition, see Sec. 4.3.

9.3. Distance restraining

When simulating a molecular system it may be desirable to restrain the distance between selected atoms to a given value or to only a minimum value or maximum value.[54] This can be performed by using as a special term $\mathcal{V}^{(spec)}(\boldsymbol{r};\mathbf{s})$ in the interaction function (Eq. 3.4) a harmonic oscillator or one half of a harmonic oscillator for lower or upper bound. However, when the actual distance $r_{nn'}$ between atoms n and n' is very different from the reference distance $r^0_{nn'}$ the energy and force due to a harmonic function may become very large. Therefore, the special interaction term for atom-atom distance restraining is chosen to become linear beyond a specified deviation $\Delta r^h = r^1 - r^0$ of $r_{nn'}$ from $r^0_{nn'}$[55] (see Fig. 9.1).

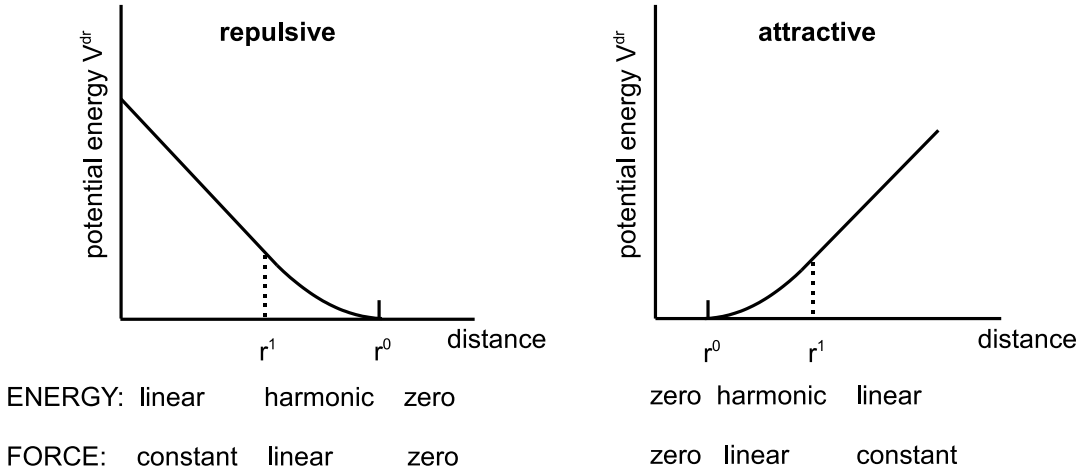

FIGURE 9.1. Potential energy term for atom-atom distance restraining. The function and its derivative are continuous at $r = r^0$ and $r = r^1$.

The special interaction term in $\mathcal{V}^{(spec)}(\boldsymbol{r};\mathbf{s})$ in Eq. 3.4 that performs *atom-atom distance restraining* reads

$$\mathcal{V}^{(dr)}(\boldsymbol{r};\mathbf{s}) \quad = \quad \sum_{m=1}^{N^{(dir)}} \mathcal{V}^{(dr)}{}_m(r_{nn'};k^{(dr)}{}_m,r^0_m,\Delta r^h) \tag{9.3}$$

where the m-th atom-atom distance restraint involves atoms denoted by n and n'. The summation runs over a set of $N^{(dir)}$ distance restraints. An *attractive distance restraint* m with length r^0_m between atoms n and n' is represented by[56]

$$\begin{aligned}
&\mathcal{V}^{(dr)}{}_m(r_{nn'};k^{(dr)}{}_m,r^0_m,\Delta r^h) \\
&\quad = 0 && 0 < r_{nn'} < r^0_m \\
&\quad = \tfrac{1}{2}k^{(dr)}{}_m[r_{nn'}-r^0_m]^2 && r^0_m < r_{nn'} < r^0_m + \Delta r^h \\
&\quad = +k^{(dr)}{}_m[r_{nn'}-r^0_m-\tfrac{1}{2}\Delta r^h]\Delta r^h && r^0_m + \Delta r^h < r_{nn'}
\end{aligned} \tag{9.4}$$

The actual distance between atoms n and n' is denoted by $r_{nn'}$ and $r^1_m = r^0_m + \Delta r^h$ is the distance at which $\mathcal{V}^{(dr)}{}_m$ changes from a quadratic (harmonic) to a linear function of $r_{nn'}$

The forces on atoms n and n' due to $\mathcal{V}^{(dr)}{}_m$ in Eq. 9.4 are

$$\begin{aligned}
\mathbf{f}_n \quad &= \quad -\frac{\partial \mathcal{V}^{(dr)}{}_m}{\partial r_{nn'}}\frac{\partial r_{nn'}}{\partial \mathbf{r}_n} \\
&= \quad 0 && 0 < r_{nn'} < r^0_m \\
&= \quad -k^{(dr)}{}_m[r_{nn'}-r^0_m]\cdot[\mathbf{r}_{nn'}/r_{nn'}] && r^0_m < r_{nn'} < r^0_m + \Delta r^h \\
&= \quad -k^{(dr)}{}_m\cdot\Delta r^h\cdot[\mathbf{r}_{nn'}/r_{nn'}] && r^0_m + \Delta r^h < r_{nn'}
\end{aligned} \tag{9.5}$$

and

$$\mathbf{f}_{n'} \quad = \quad -\mathbf{f}_n \tag{9.6}$$

A *repulsive distance restraint* m with length r^0_m between atoms n and n' is represented by

$$\begin{aligned}
&\mathcal{V}^{(dr)}{}_m(r_{nn'}, k^{(dr)}{}_m, r^0_m, \Delta r^h) \\
&= -k^{(dr)}{}_m[r_{nn'} - r^0_m + \tfrac{1}{2}\Delta r^h]\Delta r^h \qquad 0 < r_{nn'} < r^0_m - \Delta r^h \\
&= \tfrac{1}{2}k^{(dr)}{}_m[r_{nn'} - r^0_m]^2 \qquad r^0_m - \Delta r^h < r_{nn'} < r^0_m \\
&= 0 \qquad r^0_m < r_{nn'}
\end{aligned} \tag{9.7}$$

where$r^1_m = r^0_m - \Delta r^h$ is the distance at which $\mathcal{V}^{(dr)}{}_m$ changes from a linear to a quadratic (harmonic) function of $r_{nn'}$.

The forces on atoms n and n' due to $\mathcal{V}^{(dr)}{}_m$ in Eq. 9.7 are

$$\begin{aligned}
\mathbf{f}_n &= -\frac{\partial \mathcal{V}^{(dr)}{}_m}{\partial r_{nn'}}\frac{\partial r_{nn'}}{\partial \mathbf{r}_n} \\
&= +k^{(dr)}{}_n \cdot \Delta r^h \cdot [\mathbf{r}_{nn'}/r_{nn'}] \qquad 0 < r_{nn'} < r^0_m - \Delta r^h \\
&= -k^{(dr)}{}_m[r_{nn'} - r^0_m] \cdot [\mathbf{r}_{nn'}/r_{nn'}] \qquad r^0_m - \Delta r^h < r_{nn'} < r^0_m \\
&= 0 \qquad r^0_m < r_{nn'}
\end{aligned} \tag{9.8}$$

and

$$\mathbf{f}_{n'} = -\mathbf{f}_n \tag{9.9}$$

The specification of the atoms n and n' is given in a distance restraints file as discussed in Sec. 9.4, of this volume and in Sec. 4-3.4 and Sec. 4-4.10. The force constants $k^{(dr)}{}_n$ can be chosen

- to be equal for all specified distance restraints, $k^{(dr)}{}_m = CDIR$, ($|NTDIR| = 1$), or
- to be proportional to a distance restraint weight factor W0[1..NB], $k^{(dr)}{}_m = CDIR * W0[m]$, ($|NTDIR| = 2$).

The factor CDIR is read from the input by program MD++. The reference distances r^0_m are denoted by $B0[1..NB] = R0[1..NDR]$, where $NB = NDR = N^{(dir)}$. Attractive restraining is selected when $B0 = R0 > 0$, whereas repulsive restraining is selected by changing the sign of B0 = R0 (< 0). Of course, $r^0_m = |R0|$ is used in the formulae. The distance Δr^h is denoted by $DB0 = DIR0$.

When the given atom-atom distance restraints r^0_m in Eq. 9.3 have been derived from NOE cross-peak intensities originating from nuclei n and n', they represent an average over space and time,

$$< r^{-p}_{nn'} >^{-\frac{1}{p}} . \tag{9.10}$$

This means that in the restraining interaction $\mathcal{V}^{(dr)}{}_m(r_{nn'}; k^{(dr)}{}_m, r^0_m, \Delta r^h)$, the instantaneous distance $r_{nn'}$ should be replaced by the average Eq. 9.10, so that only this average is restrained. The ensemble average Eq. 9.10 can be taken as a time (trajectory) average

$$< r^{-p}_{nn'} >= \overline{r^{-p}_{nn'}(t)} \equiv t^{-1}\int_0^t r^{-p}(t')dt' \tag{9.11}$$

or as an average over space, that is, different molecules[57]. In MD or SD simulations, the use of the time average Eq. 9.11 is the natural choice. When averaging over relatively short times, the angular correlation in the vector $\mathbf{r}_{nn'}$ should be neglected, which gives $p = 3$. The true average Eq. 9.11 is not suitable for use in Eq. 9.3, from which the restraining force is obtained during a simulation: the rate of change of $\overline{r^{-3}_{nn'}(t)}$

depends on the length of the averaging period, t. This problem is avoided by building a decay into the summation over time with a characteristic decay time or *memory relaxation time* τ_{dr}, so that[58]

$$< r_{nn'}^{-3} >= \overline{r_{nn'}^{-3}(t;\tau_{dr})} \equiv \frac{\int_0^t \exp(-(t-t')/\tau_{dr}) r_{nn'}^{-3}(t')dt'}{\tau_{dr}[1-exp(-t/\tau_{dr})]} \tag{9.12}$$

This time average is easily obtained in a simulation using discrete time steps Δt. When

$$t \gg \tau_{dr} \tag{9.13}$$

we have

$$\begin{aligned} \overline{r_{nn'}^{-3}(t;\tau_{dr})} &= [1-\exp(-\Delta t/\tau_{dr})] r_{nn'}^{-3}(t) \\ &+ \exp(-\Delta t/\tau_{dr}) \overline{r_{nn'}^{-3}(t-\Delta t;\tau_{dr})}. \end{aligned} \tag{9.14}$$

Upon insertion of

$$\overline{r}_{nn'} \equiv \left[\overline{r_{nn'}^{-3}(t;\tau_{dr})}\right]^{-\frac{1}{3}} \tag{9.15}$$

into the distance restraining interaction Eq. 9.3 we obtain for the force on atom n due to ${\mathcal{V}^{(dr)}}_m$ at time t

$$\mathbf{f}_n = -\frac{\partial {\mathcal{V}^{(dr)}}_m(\overline{r}_{nn'}; {k^{(dr)}}_m, r_m^0, \Delta r^h)}{\partial \overline{r}_{nn'}} \frac{\partial \overline{r}_{nn'}}{\partial r_{nn'}} \frac{\mathbf{r}_{nn'}}{r_{nn'}} \tag{9.16}$$

The second factor in Eq. 9.16 is

$$\frac{\partial \overline{r}_{nn'}}{\partial r_{nn'}} = [1-\exp(-\Delta t/\tau_{dr})] \left(\frac{\overline{r}_{nn'}}{r_{nn'}}\right)^4 \tag{9.17}$$

and causes large fluctuations in the force. The switch FORCESCALE in the DISTANCERES block of MD++ allows the selection of approximations. Setting FORCESCALE = 0, leads to the approximation

$$\frac{\partial \overline{r}_{nn'}}{\partial r_{nn'}} = 1 \tag{9.18}$$

and setting FORCESCALE = 1, leads to the approximation

$$\frac{\partial \overline{r}_{nn'}}{\partial r_{nn'}} = [1-\exp(-\Delta t/\tau_{dr})] \tag{9.19}$$

while when using FORCESCALE = 2, equation Eq. 9.17 is used in formula Eq. 9.16. We note that the total energy will not be conserved when applying time averaging due to the approximation Eq. 9.18 and the dependence of the restraining interaction Eq. 9.3 on time points before time t[59].

At the start of a simulation, the value of the average Eq. 9.15 is set such as to satisfy the restraint distance,

$$\left[\overline{\mathbf{r}_{nn'}^{-3}(t=0;\tau_{dr})}\right]^{-\frac{1}{3}} = r_m^0 \tag{9.20}$$

At the end of a simulation the value of the average Eq. 9.15 is stored with the final configuration for use in a continuation simulation (Sec. 4-4.10)

The choice of the values for the parameters ${k^{(dr)}}_m$ and τ_{dr} = TAUDIR is discussed in[60]. The latter should satisfy the condition

$$\tau_{dr} \ll t_{MD} \tag{9.21}$$

where t_{MD} is the length of the simulation.

The switch NTDIR in program MD++ controls the atom-atom distance restraining options:

NTDIR	=	0,	no atom-atom distance restraining
	>	0,	atom-atom distance restraining, no time averaging
	<	0,	atom-atom distance restraining with time averaging
|NTDIR|	=	1,	force constants equal, ${k^{(dr)}}_m = CDIR$
	=	2,	force constants proportional to the individual distance restraint weight factors, ${k^{(dr)}}_m = CDIR * W0[m]$

Applications of atom-atom distance restraining are the following.

- When a molecular structure is to be obtained that satisfies a set of given interatomic distances, atom-atom distance restraining can be used during EM or MD simulation to force the molecular conformation in the desired direction.
- When a part of a molecule is required to keep its form during a simulation, atom-atom distance restraining can be used to fix relative atom positions of a group of atoms without restraining the mobility of the group.
- When a free energy (profile) as a function of the distance between two atoms is to be determined by MD or SD simulation, the atom-atom distance restraining term can serve as umbrella function to focus the sampling (Sec. 14.8).
- In mixed fine-grained / coarse-grained simulations, a layer of fine-grained solvent molecules may be kept around the solute by applying the appropriate atom-atom distance restraints. Note that for this application, a contribution to the virial due to the special interaction energy terms is appropriate, which can be selected using option VDIR = 1 in the MD++ input file.

9.4. Virtual and pseudo atoms

In the GROMOS force fields most aliphatic hydrogen atoms are not explicitly treated, but are incorporated in the carbon atom to which they are attached forming united atoms (Vol. 3). However, an atom-atom distance restraint which is derived from proton NMR experiments, may refer to such a hydrogen atom, which is called here a *virtual atom.* In that case the distance restraint interaction (Eq. 9.3) refers to a *non-atomic site as a centre of interaction.* A proton-proton distance restraint may also refer to non-atomic sites when a stereospecific assignment of a resonance to a proton cannot be obtained, e.g. C_β protons in proteins or methyl groups in the amino acid residues Leu and Val, or when dynamic effects such as rotation of methyl group hydrogens and flipping of aromatic rings influence the NMR signal. In these cases the distance restraint must refer to a *pseudo atom* and a *correction term* Δr_n^{ps} must be added to the restraint distance $r_{nn'}^0$

$$r_{nn'}^0(pseudo) = r_{nn'}^0(real) + \Delta r_n^{ps} + \Delta r_{n'}^{ps} \tag{9.22}$$

The value of Δr_n^{ps}depends on the geometry of construction of the pseudo atom site and is given in Tab. 9.1. So, virtual and pseudo sites or atoms are massless points, whose positions are rigorously related to the positions of the masses in the molecule.

When using pseudo or virtual sites, two additional steps are added to the calculation of the forces on the real atoms.

group	configuration	atom type	correction term Δr^{ps} on distance restraint r^0 *(nm)*	geometric code TYPE1 or TYPE2 *)
CH1 (aliphatic)	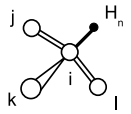	virtual	.00	1
CH1 (aromatic)	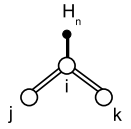	virtual	.00	2
CH2 (stereospecific)	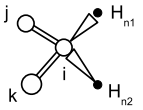	virtual	.00	4
CH2 (non-stereospecific)	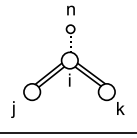	pseudo	.09	3
CH3		pseudo	.10	5
CH3 (non-stereospecific, Val, Leu)	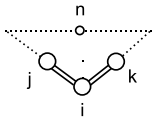	pseudo	.22	6
CH3 (non-stereospecific, t-butyl)	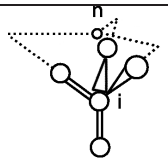	pseudo	.23	7
COG (center of geometry)	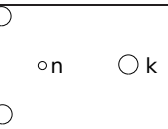	pseudo	.00	-1
COM (center of mass)	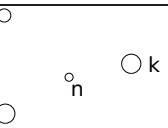	pseudo	.00	-2

TABLE 9.1. Virtual and pseudo hydrogen atoms and distance restraint correction terms.
*) see Sec. 4-3.4

1. Before the interaction terms Eqs. 9.3, 9.4, 9.7 involving virtual or pseudo sites can be evaluated, the virtual or pseudo site n must be constructed using the positions of those atoms (i,j,k,l) that define the virtual or pseudo atom n.
2. The force $\mathbf{f}_n$ acting on the virtual or pseudo site n must be redistributed over the atoms (i,j,k,l) that define the virtual or pseudo atom n. The contribution of $\mathbf{f}_n$ to the force on atom i is *e.g.*

$$\mathbf{f}_i = \mathbf{f}_{nx}\frac{\partial x_n}{\partial \mathbf{r}_i} + \mathbf{f}_{ny}\frac{\partial y_n}{\partial \mathbf{r}_i} + \mathbf{f}_{nz}\frac{\partial z_n}{\partial \mathbf{r}_i} \tag{9.23}$$

or in matrix notation

$$\begin{pmatrix} \mathbf{f}_{ix} \\ \mathbf{f}_{iy} \\ \mathbf{f}_{iz} \end{pmatrix} = \begin{pmatrix} \partial x_n/\partial x_i & \partial y_n/\partial x_i & \partial z_n/\partial x_i \\ \partial x_n/\partial y_i & \partial y_n/\partial y_i & \partial z_n/\partial y_i \\ \partial x_n/\partial z_i & \partial y_n/\partial z_i & \partial z_n/\partial z_i \end{pmatrix} \begin{pmatrix} \mathbf{f}_{nx} \\ \mathbf{f}_{ny} \\ \mathbf{f}_{nz} \end{pmatrix} \tag{9.24}$$

Corresponding formulae hold for atoms j, k and l. The matrices of partial derivatives in Eq. 9.24 can easily be derived from the definition of $\mathbf{r}_n$ in terms of $\mathbf{r}_i$, $\mathbf{r}_j$, $\mathbf{r}_k$ and $\mathbf{r}_l$. These definitions have been kept as simple as possible in order to avoid too complex derivatives.

The virtual and pseudo atoms that can be used when the distance restraining potential energy term (Eqs. 9.3, 9.4, 9.7) is applied, are displayed in Tab. 9.1 (see also[55]). Three types of virtual atoms and six types of pseudo atoms are distinguished:

9.4.1. CH1-group (aliphatic). The position vector of the hydrogen H_n is given by

$$\mathbf{r}_n = \mathbf{r}_i + d_{CH}\mathbf{s}/s \tag{9.25}$$

with

$$\mathbf{s} = 3\mathbf{r}_i - \mathbf{r}_j - \mathbf{r}_k - \mathbf{r}_l \tag{9.26}$$

and

$$\begin{aligned} s &= (\mathbf{s}\cdot\mathbf{s})^{\frac{1}{2}} \\ &= [{s_x}^2 + {s_y}^2 + {s_z}^2]^{\frac{1}{2}} \end{aligned} \tag{9.27}$$

The carbon-hydrogen distance d_{CH} is stored in DISH. The partial derivatives are

$$\frac{\partial \mathbf{r}_n}{\partial \mathbf{r}_i} = \begin{pmatrix} [1+3d_{CH}(s^2-{s_x}^2)/s^3] & -3d_{CH}s_ys_x/s^3 & -3d_{CH}s_zs_x/s^3 \\ -3d_{CH}s_xs_y/s^3 & [1+3d_{CH}(s^2-{s_y}^2)/s^3] & -3d_{CH}s_zs_y/s^3 \\ -3d_{CH}s_xs_z/s^3 & -3d_{CH}s_ys_z/s^3 & [1+3d_{CH}(s^2-{s_z}^2)/s^3] \end{pmatrix} \tag{9.28}$$

and

$$\frac{\partial \mathbf{r}_n}{\partial \mathbf{r}_j} = \begin{pmatrix} -d_{CH}(s^2-{s_x}^2)/s^3 & d_{CH}s_ys_x/s^3 & d_{CH}s_zs_x/s^3 \\ d_{CH}s_xs_y/s^3 & -d_{CH}(s^2-{s_y}^2)/s^3 & d_{CH}s_zs_y/s^3 \\ d_{CH}s_xs_z/s^3 & d_{CH}s_ys_z/s^3 & -d_{CH}(s^2-{s_z}^2)/s^3 \end{pmatrix} \tag{9.29}$$

and $\partial\mathbf{r}_n/\partial\mathbf{r}_k$ and $\partial\mathbf{r}_n/\partial\mathbf{r}_l$ are identical to Eq. 9.29.

9.4.2. CH1-group (aromatic). The position vector of the hydrogen H_n is given by

$$\mathbf{r}_n = \mathbf{r}_i + d_{CH}\mathbf{s}/s \tag{9.30}$$

with

$$\mathbf{s} = 2\mathbf{r}_i - \mathbf{r}_j - \mathbf{r}_k \tag{9.31}$$

and s defined by Eq. 9.27. Again, the carbon-hydrogen distance is denoted by d_{CH}. The partial derivatives are

$$\partial\mathbf{r}_n/\partial\mathbf{r}_i = \begin{pmatrix} [1+2d_{CH}(s^2-{s_x}^2)/s^3] & -2d_{CH}s_ys_x/s^3 & -2d_{CH}s_zs_x/s^3 \\ -2d_{CH}s_xs_y/s^3 & [1+2d_{CH}(s^2-{s_y}^2)/s^3] & -2d_{CH}s_zs_y/s^3 \\ -2d_{CH}s_xs_z/s^3 & -2d_{CH}s_ys_z/s^3 & [1+2d_{CH}(s^2-{s_z}^2)/s^3] \end{pmatrix} \tag{9.32}$$

and $\partial\mathbf{r}_n/\partial\mathbf{r}_j$ and $\partial\mathbf{r}_n/\partial\mathbf{r}_k$ are given by Eq. 9.29.

9.4.3. CH2-group (two virtual protons). The position vector of the hydrogen H_{n1} is given by

$$\mathbf{r}_{n_1} = \mathbf{r}_i + \alpha\mathbf{s}/s + \beta\mathbf{q}/q \tag{9.33}$$

with $\mathbf{s}$ defined by Eq. 9.31, s by Eq. 9.27 and $\mathbf{q}$ by

$$\mathbf{q} = (\mathbf{r}_i - \mathbf{r}_j) \times (\mathbf{r}_i - \mathbf{r}_k) \tag{9.34}$$

with

$$q = ({q_x}^2 + {q_y}^2 + {q_z}^2)^{\frac{1}{2}} \tag{9.35}$$

The values of α and β are derived from

$$\begin{aligned} \alpha &= d_{CH}\cos(\theta/2) \\ \beta &= d_{CH}\sin(\theta/2) \end{aligned} \tag{9.36}$$

where θ is the tetrahedral angle and the carbon-hydrogen distance is d_{CH}. The partial derivatives are (for $n = n_1$):

$$\partial\mathbf{r}_n/\partial\mathbf{r}_i = \mathbf{A} + \mathbf{B} + \mathbf{C} \tag{9.37}$$

with

$$\mathbf{A} = \begin{pmatrix} [1 + 2\alpha(s^2 - {s_x}^2)/s^3] & -2\alpha s_y s_x/s^3 & -2\alpha s_z s_x/s^3 \\ -2\alpha s_x s_y/s^3 & [1 + 2\alpha(s^2 - {s_y}^2)/s^3] & -2\alpha s_z s_y/s^3 \\ -2\alpha s_x s_z/s^3 & -2\alpha s_y s_z/s^3 & [1 + 2\alpha(s^2 - {s_z}^2)/s^3] \end{pmatrix} \tag{9.38}$$

and

$$\mathbf{B} = \begin{pmatrix} -\beta q_x a_x/q^3 & -\beta q_y a_x/q^3 & -\beta q_z a_x/q^3 \\ -\beta q_x a_y/q^3 & -\beta q_y a_y/q^3 & -\beta q_z a_y/q^3 \\ -\beta q_x a_z/q^3 & -\beta q_y a_z/q^3 & -\beta q_z a_z/q^3 \end{pmatrix} \tag{9.39}$$

and

$$\mathbf{C} = \begin{pmatrix} 0 & +\beta b_z/q & -\beta b_y/q \\ -\beta b_z/q & 0 & +\beta b_x/q \\ +\beta b_y/q & -\beta b_x/q & 0 \end{pmatrix} \tag{9.40}$$

where $\boldsymbol{a} = \mathbf{q} \times \mathbf{r}_{kj} = \begin{pmatrix} a_x \\ a_y \\ a_z \end{pmatrix}$ and $\boldsymbol{b} = \mathbf{r}_{kj}$, and

$$\partial\mathbf{r}_n/\partial\mathbf{r}_j = \mathbf{D} + \mathbf{E} + \mathbf{F} \tag{9.41}$$

where

$$\mathbf{D} = \begin{pmatrix} -\alpha(s^2 - {s_x}^2)/s^3 & \alpha s_y s_x/s^3 & \alpha s_z s_x/s^3 \\ \alpha s_x s_y/s^3 & -\alpha(s^2 - {s_y}^2)/s^3 & \alpha s_z s_y/s^3 \\ \alpha s_x s_z/s^3 & \alpha s_y s_z/s^3 & -\alpha(s^2 - {s_z}^2)/s^3 \end{pmatrix} \tag{9.42}$$

and $\mathbf{E}$ is identical to $\mathbf{B}$ in Eq. 9.39 but with $\boldsymbol{a} = \mathbf{q} \times \mathbf{r}_{ik}$ and $\mathbf{F}$ is identical to $\mathbf{C}$ in Eq. 9.40 but with $\boldsymbol{b} = \mathbf{r}_{ik}$, and

$$\partial\mathbf{r}_n/\partial\mathbf{r}_k = \mathbf{D} + \mathbf{G} + \mathbf{H} \tag{9.43}$$

where $\mathbf{G}$ is identical to $\mathbf{B}$ in Eq. 9.39 but with $\boldsymbol{a} = \mathbf{q} \times \mathbf{r}_{ji}$ and $\mathbf{H}$ is identical to $\mathbf{C}$ in Eq. 9.40 but with $\boldsymbol{b} = \mathbf{r}_{ji}$.

The position vector $\mathbf{r}_{n2}$ of the second virtual proton H_{n2} can be obtained from the same formulae by interchanging j and k.

9.4.4. CH2-groups (one pseudo site). When a distance restraint refers to one proton of a CH2-group of which no stereospecific assignment is known, the restraint is referred to a pseudo site between the two protons. The position vector of the pseudo atom n is defined by

$$\mathbf{r}_n = \mathbf{r}_i + \alpha\mathbf{s}/s \tag{9.44}$$

where α is given by Eq. 9.36 and $\mathbf{s}$ is defined by Eq. 9.31 and s by Eq. 9.27. The partial derivatives are

$$\partial\mathbf{r}_n/\partial\mathbf{r}_i = \mathbf{A} \tag{9.45}$$

and

$$\partial\mathbf{r}_n/\partial\mathbf{r}_j = \partial\mathbf{r}_n/\partial\mathbf{r}_k = \mathbf{D} \tag{9.46}$$

9.4.5. CH3-group (one pseudo site). For a single methyl group and for a methyl group of a diastereotopic pair for which the stereospecific assignment is known, the pseudo atom n is defined to be in the middle of the three hydrogens:

$$\mathbf{r}_n = \mathbf{r}_i + \gamma\mathbf{s}/s \tag{9.47}$$

with

$$\gamma = d_{CH}\cos(\pi - \theta) \tag{9.48}$$

and

$$\mathbf{s} = \mathbf{r}_i - \mathbf{r}_j \tag{9.49}$$

Again, θ is the tetrahedral angle and the carbon-hydrogen distance is d_{CH}.

The partial derivatives are

$$\frac{\partial\mathbf{r}_n}{\partial\mathbf{r}_i} = \begin{pmatrix} [1+\gamma(s^2-{s_x}^2)/s^3 & -\gamma s_y s_x/s^3 & -\gamma s_z s_x/s^3 \\ -\gamma s_x s_y/s^3 & [1+\gamma(s^2-{s_y}^2)/s^3] & -\gamma s_z s_y/s^3 \\ -\gamma s_x s_z/s^3 & -\gamma s_y s_z/s^3 & [1+\gamma(s^2-{s_z}^2)/s^3] \end{pmatrix} \tag{9.50}$$

and $\partial\mathbf{r}_n/\partial\mathbf{r}_j$ is identical to $\mathbf{D}$ in Eq. 9.42 but with α replaced by γ.

9.4.6. Two CH3-groups (one pseudo site). When a restraint involves a methyl group of a stereotopic pair for which no stereospecific assignments are known, the restraint is referred to a pseudo atom n at the geometric mean position of the 6 hydrogens of the pair:

$$\mathbf{r}_n = \mathbf{r}_i + \delta\mathbf{s}/s \tag{9.51}$$

with

$$\delta = -\cos(\theta/2)[d_{CC} + \gamma] \tag{9.52}$$

where $\mathbf{s}$ is defined by Eq. 9.31, the carbon-carbon distance d_{CC} is stored in DISC, θ is tetrahedral and γ is given by Eq. 9.48. The partial derivative $\partial\mathbf{r}_n/\partial\mathbf{r}_i$ is identical to $\mathbf{A}$ in Eq. 9.38, but with α replaced by δ, $\partial\mathbf{r}_n/\partial\mathbf{r}_j$ and $\partial\mathbf{r}_n/\partial\mathbf{r}_k$ are identical to $\mathbf{D}$ in Eq. 9.42 but with α replaced by δ.

9.4.7. Three CH3-groups (one pseudo site). When a distance restraint refers to a t-butyl for which no stereospecific assignments are known, the restraint is referred to a pseudoatom n at the geometric mean position of the 9 hydrogens of the three CH3 groups:

$$\mathbf{r}_n = \mathbf{r}_i + \varepsilon\mathbf{s}/s \tag{9.53}$$

with

$$\varepsilon = (d_{CC} + \gamma)\cos(\pi - \theta) \tag{9.54}$$

where $\mathbf{s}$ is defined by Eq. 9.49, the carbon-carbon distance d_{CC} is stored in DISC, γ is given by Eq. 9.48, and θ is the tetrahedral angle. The partial derivative $\partial\mathbf{r}_n/\partial\mathbf{r}_i$ is identical to Eq. 9.50, but with γ replaced by ε, and $\partial\mathbf{r}_n/\partial\mathbf{r}_j$ is identical to $\mathbf{D}$ in Eq. 9.42 but with α replaced by ε.

9.4.8. Center of geometry (one pseudo site). For the δ and ε protons of tyrosine and phenylalanine rings that are displaying fast 180^o ring flips, or for the protons i and j of a planar NH2 group, a pseudo atom can be constructed at the center of geometry of these atoms.

$$\mathbf{r}_n = N_{ps}^{-1} \sum_{i=1}^{N_{ps}} \mathbf{r}_i \tag{9.55}$$

where N_{ps} denotes the number of non-virtual atoms with position vector $\mathbf{r}_i$ the centre of geometry of which is to serve as pseudo atom n. The partial derivative $\partial \mathbf{r}_n / \partial \mathbf{r}_i$ is

$$\partial \mathbf{r}_n / \partial \mathbf{r}_i \quad = \quad \begin{pmatrix} N_{ps}^{-1} & 0 & 0 \\ 0 & N_{ps}^{-1} & 0 \\ 0 & 0 & N_{ps}^{-1} \end{pmatrix} \tag{9.56}$$

9.4.9. Center of mass (one pseudo site). Alternatively, one may choose to define a pseudo atom at the centre of mass of given atoms using

$$\mathbf{r}_n = M_{ps}^{-1} \sum_{i=1}^{N_{ps}} m_i \mathbf{r}_i \tag{9.57}$$

with

$$M_{ps} = \sum_{i=1}^{N_{ps}} m_i \tag{9.58}$$

where N_{ps} denotes the number of non-virtual atoms with position vector $\mathbf{r}_i$ and mass m_i the centre of mass of which is to serve as pseudo atom n. The partial derivative $\partial \mathbf{r}_n / \partial \mathbf{r}_i$ is

$$\partial \mathbf{r}_n / \partial \mathbf{r}_i \quad = \quad \begin{pmatrix} m_i/M_{ps} & 0 & 0 \\ 0 & m_i/M_{ps} & 0 \\ 0 & 0 & m_i/M_{ps} \end{pmatrix} \tag{9.59}$$

The various atom types are selected using the code shown in Tab. 9.1. For the first atom n_1 of the pairs these codes are listed in TYPE1[1..NB] = TYPE1[1..NDR] and the atom sequence numbers of the atoms i, j, k and l that define atom n_1 are given in I1, J1, K1, L1[1..NB] see Sec. 4-3.4. For the second atom n_2 of the pairs the corresponding arrays are denoted by TYPE2, etc. The carbon-hydrogen distance is denoted by DISH and the carbon-carbon distance by DISC.

We note that the correction terms Δr_n^{ps} which are listed in Tab. 9.1 are *not* automatically incorporated into the specified restraint distance r_m^0 by applying Eq. 9.22. The user must incorporate the correction terms Δr_n^{ps} into B0[1..NB] = R0[1..NDR]. The GROMOS++ program *prep_noe* may help to prepare the correct distance restraints for virtual and pseudo atoms commonly encountered in biomolecular systems.

9.5. Bond-angle restraining

One may wish to restrain a bond angle to a given value. For this case of restraining no special subroutines have been made in GROMOS. The *bond angle* $\theta(ijk)$ between atoms i, j and k can be restrained by applying distance restraints (Sec. 9.3) to the three distances ij, jk and ik. An alternative is to add to the molecular topology of a molecular system the bond angle $\theta(ijk)$ and to choose appropriate values for $K_{\theta n}$ and θ_{0n} (Sec. 5.2).

9.6. Dihedral-angle restraining

The special interaction term $\mathcal{V}^{(spec)}(\boldsymbol{r};\mathbf{s})$ in Eq. 3.4 that performs *dihedral-angle restraining* reads

$$\mathcal{V}^{(tr)}(\boldsymbol{r};\mathbf{s}) \quad = \quad \sum_{n=1}^{\mathcal{N}^{(tr)}} {\mathcal{V}^{(tr)}}_n(\varphi_n; k^{(tr)}, \varphi_n^0, \Delta\varphi^h) \tag{9.60}$$

The summation runs over a set of $\mathcal{N}^{(tr)}$ selected dihedral angles φ_n , which are defined by specifying the atom sequence numbers i, j, k and l of the atoms forming dihedral angle $\varphi_n(i-j-k-l)$. The ${\mathcal{V}^{(tr)}}_n$ reads

$${\mathcal{V}^{(tr)}}_n(\varphi_n; k^{(tr)}, \varphi_n^0, \Delta\varphi^h)$$
$$= \quad -{k^{(tr)}}_n(\Delta\varphi_n + \tfrac{1}{2}\Delta\varphi^h)\Delta\varphi^h \qquad\qquad \Delta\varphi_n < \Delta\varphi^h$$

$$
\begin{aligned}
&= \tfrac{1}{2}k^{(tr)}{}_n(\Delta\varphi_n)^2 && -\Delta\varphi^h < \Delta\varphi_n < \Delta\varphi^h \\
&= k^{(tr)}{}_n(\Delta\varphi_n - \tfrac{1}{2}\Delta\varphi^h)\Delta\varphi^h && \Delta\varphi_n > \Delta\varphi^h
\end{aligned}
\tag{9.61}
$$

where $\Delta\varphi_n = \varphi_n - \varphi_n^0 + 2m\pi$, where m is chosen such that φ_n is within the range $[\varphi_n^0 + \delta_n - 2\pi, \varphi_n^0 + \delta_n]$. Using this dihedral angle restraint formulation δ_n determines at which position the direction of the rotation around the dihedral angle inverts. Typically, δ_n is set to 180^o. The interaction $\mathcal{V}^{(tr)}(\boldsymbol{r};\mathbf{s})$ has the same form as the improper dihedral angle interaction $V^{(\xi)}(\boldsymbol{r};\mathbf{s})$ described in Sec. 5.3. So, the formulae Eq. 17.11-Eq. 17.14 give the forces on atoms i, j, k and l due to the interaction (Eq. 9.60), if ξ_n is replaced by φ_n, $k_n^{(\xi)}$ by $k^{(tr)}{}_n$ and ξ_n^0 by φ_n^0.

The atom sequence numbers of the atoms i, j, k and l that define φ_n and the force constant $k^{(tr)}{}_n$ and reference dihedral angle φ_n^0 are to be specified in a dihedral angle restraints file and stored in the arrays IPLR, JPLR, KPLR, LPLR, WPLR, PDLR, DELTA[1..NDLR], with NDLR $= \mathcal{N}^{(tr)}$, as described in Sec. 4-3.5. The dihedral angle restraining interaction (Eq. 9.60) can be multiplied by an overall weight factor, CDLR, which is read from the input by program MD++. The switch NTDLR controls the dihedral angle restraining option:

NTDLR	$= 0$,	no dihedral-angle restraining
	$= 1$,	dihedral-angle restraining with equal force constants, $k^{(tr)}{}_n = CDLR$
	$= 2$,	dihedral angle restraining with force constants proportional to the individual dihedral angle weight factors, $k^{(tr)}{}_n = CDLR * WDLR[n]$
	$= 3$,	dihedral angle constraining

Dihedral angle restraining may be *applied* as umbrella function when a free energy (profile) as a function of a dihedral angle is to be determined by MD or SD simulation.[61,62] The implementation of dihedral angle constraints will be discussed in Sec. 10.6.

9.7. ^3J-coupling constant restraining

When simulating a molecular system, it may be desirable to restrain the spin-spin ^3J-coupling constant, $^3J_{mm'}$, between two nuclei m and m', to a given value $^3J^0$. If $^3J^0$ is an experimental value, measured as an average over time and space in an NMR experiment, then the time-average should be restrained.

The ^3J-coupling constant $^3J_{mm'}$ depends on the value of the dihedral angle $\zeta_n(m-j-k-m')$ involving the three covalent bonds connecting the atoms m and m' through atoms j and k according to the Karplus relation (see, e.g. Fig. 9.2)

$$
\begin{aligned}
{}^3J_{mm'} &= a\cos^2(\zeta_n(m-j-k-m')) \\
&\quad + b\cos(\zeta_n(m-j-k-m')) + c.
\end{aligned}
\tag{9.62}
$$

The coefficients a, b and c will depend on the types of the atoms m, j, k and m' (Tab. 9.2).

The special interaction term $\mathcal{V}^{(spec)}(\boldsymbol{r};\mathbf{s})$ in Eq. 3.4 that performs ^3J*-coupling constant restraining* reads

$$
\mathcal{V}^{(Jr)}(\boldsymbol{r};\mathbf{s}) = \sum_{n=1}^{N_{Jr}} \mathcal{V}^{(Jr)}{}_n(J(\zeta_n); k_n^{(Jr)}, J^0{}_n)
\tag{9.63}
$$

where the dihedral angle $\zeta(m-j-k-m')$ is denoted by ζ_n, the reference $^3J^0{}_{mm'}$ value by $J^0{}_n$ and the superscript 3 has been dropped from the J.

In the case of experimentally measured ^3J-couplings, which are averages over space and time, it is preferable to apply the restraint to the time-averaged ^3J-couplings. The special interaction term then becomes

$$
\mathcal{V}^{(Jr)}(\boldsymbol{r};\mathbf{s}) = \sum_{n=1}^{N_{Jr}} \mathcal{V}^{(Jr)}{}_n(\overline{J(\zeta_n)}; k_n^{(Jr)}, J^0{}_n)
\tag{9.64}
$$

where the horizontal bar denotes a time-average.

The functional form of ${\mathcal{V}^{(Jr)}}_n$ may be harmonic, half-harmonic attractive, half-harmonic repulsive, biquadratic or periodically scaled. Whilst using a single half-harmonic potential energy term makes little sense in the case of a periodic structural feature such as a dihedral angle, two half-harmonic potential energy terms may be combined to form a full harmonic potential energy term that is asymmetric with respect to ${J^0}_n$ (in contrast to standard flat-bottomed restraining, see Eqs. 9.75 and 9.76).

For instantaneous restraining, the harmonic form is defined as

$$ {\mathcal{V}^{(Jr)}}_n(J(\zeta_n);k_n^{(Jr)},{J^0}_n) = \frac{1}{2}k_n^{(Jr)}\left[J(\zeta_n)-{J^0}_n\right]^2, \tag{9.65} $$

the half-harmonic attractive form as

$$ \begin{aligned} {\mathcal{V}^{(Jr)}}_n(J(\zeta_n);k_n^{(Jr)},{J^0}_n) &= 0 & J(\zeta_n)<{J^0}_n \\ &= \frac{1}{2}k_n^{(Jr)}\left[J(\zeta_n)-{J^0}_n\right]^2 & J(\zeta_n)>{J^0}_n, \end{aligned} \tag{9.66} $$

and the half-harmonic repulsive form as

$$ \begin{aligned} {\mathcal{V}^{(Jr)}}_n(J(\zeta_n);k_n^{(Jr)},{J^0}_n) &= \frac{1}{2}k_n^{(Jr)}\left[J(\zeta_n)-{J^0}_n\right]^2 & J(\zeta_n)<{J^0}_n \\ &= 0 & J(\zeta_n)>{J^0}_n. \end{aligned} \tag{9.67} $$

For standard time-averaging, the harmonic form is

$$ {\mathcal{V}^{(Jr)}}_n(\overline{J(\zeta_n)};k_n^{(Jr)},{J^0}_n) = \frac{1}{2}k_n^{(Jr)}\left[\,\overline{J(\zeta_n)}-{J^0}_n\right]^2 \tag{9.68} $$

and the half-harmonic forms are easily derived from Eqs. 9.66 and 9.67.

A further option with time-averaging is to use a biquadratic penalty function[63]

$$ {\mathcal{V}^{(Jr)}}_n(\overline{J(\zeta_n)};k_n^{(Jr)},{J^0}_n) = \frac{1}{2}k_n^{(Jr)}\left[\,J(\zeta_n)-{J^0}_n\right]^2\cdot\left[\,\overline{J(\zeta_n)}-{J^0}_n\right]^2. \tag{9.69} $$

This functional form avoids the large structural fluctuations that occur when standard time-averaging is used with ${}^3J$-value restraints.[64,65]

When using time-averaging, it is possible to periodically scale the potential energy function for the dihedral angles related to the ${}^3J$-couplings and the ${}^3J$-coupling restraint itself by the introduction of an oscillating factor $\cos^2(\omega^{Jr}t)$. During the scaling period, $\tau_{Jr}^s=\frac{180^\circ}{\omega^{Jr}}$, the restraining function is given by[66]

$$ \begin{aligned} {\mathcal{V}^{(Jr)}}_n(\overline{J(\zeta_n)};k_n^{(Jr)},{J^0}_n) &= \cos^2(\omega^{Jr}t)\cdot \\ &\quad \left[V^{(\varphi)}(\varphi_n;k^{(\varphi)},\varphi_n^0)+{\mathcal{V}^{(Jr)}}_n(\overline{J(\zeta_n)};k_n^{(Jr)},{J^0}_n)\right]. \end{aligned} \tag{9.70} $$

and $V^{(\varphi)}\ (\varphi_n\ ;\ k^{(\varphi)}\ ,\ \varphi_n^0\ )$ is taken out of the sum in Eq. 5.18.

The oscillating factor is switched on as soon as the average ${}^3J$-value deviates more than a certain threshold (ΔJ^0, see below) from the target value. After one oscillating period, τ_{Jr}^s, is completed, the scaling is suspended for a time period Δt_ω. This allows the system to deviate from the reference value for some time, which may be useful to overcome the degeneracy of the Karplus curve, as in the following example. Consider the Karplus curve in Fig. 9.2 and assume that a reference ${J^0}_n$ value of 9 Hz is used. For dihedral angle values around $\phi=60^\circ$, the restraint may get stuck in the local minimum with maximum ${}^3J$ values of 7 Hz.

A further possibility is to use local-elevation (LE) biasing rather than restraining the ${}^3J$-couplings. In this case, ${\mathcal{V}^{(Jr)}}_n$ is a sum of N_{le} LE terms

$$ {\mathcal{V}^{(Jr)}}_n(\overline{J(\zeta_n)};k_n^{(Jr)},{J^0}_n) = \sum_{i=1}^{N_{le}}{\mathcal{V}^{(Jr)}}_{ni}(\overline{J(\zeta_n)};k_n^{(Jr)},{J^0}_n). \tag{9.71} $$

Only the Gaussian functional form is currently implemented, giving

$$ {\mathcal{V}^{(Jr)}}_{ni}(\overline{J(\zeta_n)};k_n^{(Jr)},{J^0}_n) = k_n^{(Jr)}w_{\zeta ni}\exp\left(-(\zeta_n-{\zeta_{ni}}^0)^2/2(\Delta\zeta^0)^2\right). \tag{9.72} $$

In Eq. 9.72, $w_{\zeta ni}$ is the weight of the ith penalty term, the centres ${\zeta_{ni}}^0$ of the Gaussian functions ${\mathcal{V}^{(Jr)}}_{ni}$ are equally distributed over the range of possible values of ζ_n (${\zeta_{ni}}^0 = 360°i/N_{le}$ with $i = 1, \ldots, N_{le}$) and the width is given by $\Delta\zeta^0 = 360°/N_{le}$.

The weight, $w_{\zeta ni}$, is calculated according to

$$w_{\zeta ni} = t^{-1} \int_0^t \delta_{\zeta_n {\zeta_n}^0} \Big[\overline{J(\zeta_n)} - {J^0}_n \Big]^2 \tag{9.73}$$

for time-averaging and

$$w_{\zeta ni} = t^{-1} \int_0^t \delta_{\zeta_n {\zeta_n}^0} \big[J(\zeta_n) - {J^0}_n \big]^2 \cdot \Big[\overline{J(\zeta_n)} - {J^0}_n \Big]^2 \tag{9.74}$$

for biquadratic time-averaging. The Kronecker delta, $\delta_{\zeta_n {\zeta_n}^0}$, is defined using finite differences

$$\delta_{\zeta_n {\zeta_n}^0} = \begin{array}{ll} 1 & \text{if } {\zeta_{ni}}^0 - \Delta\zeta^0/2 \le \zeta_n < {\zeta_{ni}}^0 + \Delta\zeta^0/2 \\ 0 & \text{otherwise.} \end{array}$$

It is often desirable to allow for some uncertainty in the reference ${}^3J$-values, ${J^0}_n$. This can be done by using flat-bottomed restraining, where the restraint penalty function is only applied if the calculated ${}^3J$-values deviate by more than a given value ΔJ^0 from ${J^0}_n$. The instantaneous contribution to the special interaction function (Eqs. 9.63, 9.65, 9.66 and 9.67) then depends on

$$\begin{array}{ll} [J(\zeta_n) - {J^0}_n - \Delta J^0]^2 & \text{for } J(\zeta_n) > {J^0}_n + \Delta J^0 \\ [J(\zeta_n) - {J^0}_n + \Delta J^0]^2 & \text{for } J(\zeta_n) < {J^0}_n - \Delta J^0 \\ 0 & \text{otherwise} \end{array} \tag{9.75}$$

and, likewise, the time-averaged factor (Eqs. 9.64 and 9.67) depends on

$$\begin{array}{ll} [\overline{J(\zeta_n)} - {J^0}_n - \Delta J^0]^2 & \text{for } \overline{J(\zeta_n)} > {J^0}_n + \Delta J^0 \\ [\overline{J(\zeta_n)} - {J^0}_n + \Delta J^0]^2 & \text{for } \overline{J(\zeta_n)} < {J^0}_n - \Delta J^0 \\ 0 & \text{otherwise.} \end{array} \tag{9.76}$$

A slight complication arises when one or both of the atoms m and m' defining the angle $\zeta_n(m-j-k-m')$ are not explicitly treated in the simulation. This is, for example, the case for the GROMOS force fields, in which most hydrogen atoms that are attached to carbon atoms are not explicitly treated, but are instead incorporated into the carbons, forming united atoms (Sec. 3.2). In such a case, when atom m is incorporated into atom j or atom m' is incorporated into atom k, the dihedral angle $\zeta_n(m-j-k-m')$ is not defined in terms of atomic coordinates of real atoms. However, if another (real, non-H) atom i is bound to atom j, or another (real, non-H) atom l is bound to atom k, the dihedral angle $\zeta_n(m-j-k-m')$ can be related to the dihedral angle $\eta_n(i-j-k-l)$ by the relation

$$\zeta_n(m-j-k-m') = \eta_n(i-j-k-l) + \delta_n \tag{9.77}$$

where δ_n is a phase shift. Examples of the relation Eq. 9.77 are given in Tab. 9.2 and a Karplus curve is shown in Fig. 9.2.

The true time-averaged ${}^3J$-coupling constant is defined as a trajectory average

$$\begin{aligned} \overline{J_n(t)} &\equiv t^{-1} \int_0^t J_n(t')dt' \\ &= a\ \overline{\cos^2(\eta_n(t) + \delta_n)} + b\ \overline{\cos(\eta_n(t) + \delta_n)} + c. \end{aligned} \tag{9.78}$$

As for distance restraining, the true average (Eq. 9.78) is not suitable for use in Eq. 9.64 to derive the forces on atoms i, j, k and l. A characteristic decay time or memory relaxation time τ_{Jr} is therefore introduced, so that[64]

$$\overline{J_n(t;\tau_{Jr})} \equiv \frac{\int_0^t \exp(-(t-t')/\tau_{Jr}) J_n(t')dt'}{[\tau_{Jr}[1 - \exp(-t/\tau_{Jr})]]}$$

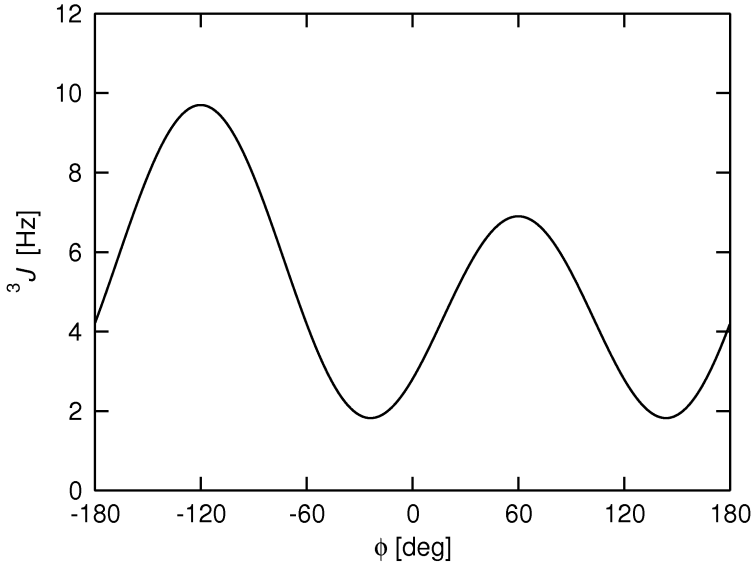

FIGURE 9.2. The Karplus curve (Eq. 9.62) for the angle ζ_n (H-N-C_α-H_α) given as a function of the angle $\eta_n = \phi$(C-N-C_α-C) (Eq. 9.77). The phase shift $\delta_n = \zeta_n - \eta_n = -60°$ for an L-amino acid has been applied and the calibration of Pardi *et al.*[67], with $a = 6.4$ Hz, $b = -1.4$ Hz and $c = 1.9$ Hz, was used.

ζ_n	η_n	δ_n (degrees)	a (Hz)	b (Hz)	c (Hz)
H - N - C_α - H_α[67]	C - N - C_α - C	- 60 (L) +60 (D)	6.4	-1.4	1.9
H_α - C_α - C_β - $H_{\beta 2}$[68]	N- C_α - C_β - C_γ	-120 (L) 0 (D)	9.5	-1.6	1.8
H_α - C_α - C_β - $H_{\beta 3}$[68]	N - C_α - C_β - C_γ	0 (L) +120 (D)	9.5	-1.6	1.8
N - C_α - C_β - $H_{\beta 2}$[69]	N - C_α - C_β - C_γ	120 (L) -120 (D)	4.4	-1.2	-0.1
N - C_α - C_β - $H_{\beta 3}$[69]	N - C_α - C_β - C_γ	-120 (L) 0 (D)	4.4	-1.2	-0.1
H - N - C_α- C_β[70]	C - N - C_α - C	+60 (L) - 60 (D)	4.7	-1.5	-0.2
H - N - C_α- C[70]	C - N - C_α- C	-180 (L,D)	5.7	-2.7	0.1

TABLE 9.2. Relations between ^3J-coupling constants and dihedral angles $\zeta_n = \eta_n + \delta_n$ occurring in polypeptides. The dihedral angles and atom names are defined according to the IUPAC-IUB convention.[25] L- and D-amino acid residues are indicated by L and D respectively.

$$= \quad a\ \overline{\cos^2(\eta_n + \delta_n)(t;\tau_{Jr})} + b\ \overline{\cos(\eta_n + \delta_n)(t;\tau_{Jr})} + c. \tag{9.79}$$

The time averages of $\cos^m(\eta_n(t) + \delta_n)$ in Eq. 9.79 are easily obtained in a simulation using discrete time steps Δt. When

$$t \quad \ll \quad \tau_{Jr} \tag{9.80}$$

we have

$$\begin{aligned} \overline{\cos^m(\eta_n + \delta_n)(t;\tau_{Jr})} \quad &= \quad [1 - \exp(-\Delta t/\tau_{Jr})]\cos^m(\eta_n(t) + \delta_n) \\ &\quad + \exp(-\Delta t/\tau_{Jr})\ \overline{\cos^m(\eta_n + \delta_n)(t - \Delta t;\tau_{Jr})}. \end{aligned} \tag{9.81}$$

The force on an atom i due to an instantaneous ^3J-value restraint in Eq. 9.63 can be written as

$$\mathbf{f}^{inst} \quad = \quad -\frac{\partial \mathcal{V}^{(Jr)}{}_n(J(\zeta_n); k_n^{(Jr)}, J^0{}_n)}{\partial J} \cdot \frac{\partial J_n}{\partial \eta_n} \cdot \frac{\partial \eta_n}{\partial \mathbf{r}_i}. \tag{9.82}$$

where the first factor in Eq. 9.82 is

$$\frac{\partial \mathcal{V}^{(Jr)}{}_n}{\partial J_n} \quad = \quad k_n^{(Jr)} \; [J_n \; - \; J^0{}_n]. \tag{9.83}$$

for the harmonic function (Eq. 9.65) and corresponding expressions are obtained for the half-harmonic cases (Eq. 9.66 and Eq. 9.67).

Using the relation

$$cos(\eta_n + \delta_n) \quad = \quad cos\eta_n cos\delta_n \; - \; sin\eta_n sin\delta_n \tag{9.84}$$

we find for the second factor in Eq. 9.82

$$\begin{aligned} \frac{\partial J_n}{\partial \eta_n} \quad &= \quad (2a \; cos(\eta_n + \delta_n) + b) \cdot (-sin(\eta_n + \delta_n)) \\ &= \quad (2a \; (cos\eta_n cos\delta_n \; - \; sin\eta_n sin\delta_n) + b) \cdot (-sin\eta_n cos\delta_n - cos\eta_n sin\delta_n). \end{aligned} \tag{9.85}$$

The third factor in Eq. 9.82, the derivative of the angle η_n (i-j-k-l) with respect to the positions $\mathbf{r}_i, \mathbf{r}_j, \mathbf{r}_k$ and $\mathbf{r}_l$ can be obtained from the expressions and definitions in Sec. 17.4 with the angle ξ_n replaced by η_n.

$$\frac{\partial \eta_n}{\partial \mathbf{r}_i} \quad = \quad \frac{r_{kj}}{r_{mj}^2} \mathbf{r}_{mj} \quad , \tag{9.86}$$

$$\frac{\partial \eta_n}{\partial \mathbf{r}_l} \quad = \quad -\frac{r_{kj}}{r_{nk}^2} \mathbf{r}_{nk} \quad , \tag{9.87}$$

$$\frac{\partial \eta_n}{\partial \mathbf{r}_k} \quad = \quad -\frac{\partial \eta_n}{\partial r_i} - \frac{\partial \eta_n}{\partial \mathbf{r}_j} - \frac{\partial \eta_n}{\partial \mathbf{r}_l} \quad , \tag{9.88}$$

$$\frac{\partial \eta_n}{\partial \mathbf{r}_j} \quad = \quad \left[\; \frac{(\mathbf{r}_{ij} \cdot \mathbf{r}_{kj})}{\mathbf{r}_{kj}^2} - 1 \right] \frac{\partial \eta_n}{\partial \mathbf{r}_i} - \frac{(\mathbf{r}_{kl} \cdot \mathbf{r}_{kj})}{r_{kj}^2} \frac{\partial \eta_n}{\partial \mathbf{r}_l} \quad . \tag{9.89}$$

For time averaged ${}^3J$-value restraints we use the short-hand notation

$$\overline{J_n} \quad = \quad \overline{J_n(t; \tau_{Jr})}, \tag{9.90}$$

and find the force on atom i due to $\mathcal{V}^{(Jr)}{}_n$ in Eq. 9.64 at time t to be

$$\mathbf{f}_i \quad = \quad -\frac{\partial \mathcal{V}^{(Jr)}{}_n(\overline{J_n}; k_n^{(Jr)}, J^0{}_n)}{\partial \overline{J_n}} \cdot \frac{\partial \overline{J_n}}{\partial \eta_n} \cdot \frac{\partial \eta_n}{\partial \mathbf{r}_i}. \tag{9.91}$$

The first factor in Eq. 9.91 is

$$\frac{\partial \mathcal{V}^{(Jr)}{}_n}{\partial \overline{J_n}} \quad = \quad k_n^{(Jr)} \; \left[\; \overline{J_n} - J^0{}_n \right] \tag{9.92}$$

for the harmonic function (Eq. 9.65) and corresponding expressions are obtained for the half-harmonic cases (Eqs. 9.66 and 9.67).

Using the relation Eq. 9.84

$$\cos(\eta_n + \delta_n) \quad = \quad \cos\eta_n \cos\delta_n - \sin\eta_n \sin\delta_n \tag{9.93}$$

we find for the second factor in Eq. 9.91

$$\begin{aligned} \frac{\partial \overline{J_n}}{\partial \eta_n} \quad &= \quad [1 - \exp(-\Delta t/\tau_{Jr})] \, [2a \cos(\eta_n + \delta_n) + b] \, [-\sin(\eta_n + \delta_n)] \\ &= \quad [1 - \exp(-\Delta t/\tau_{Jr})] \cdot [2a[\cos\eta_n \cos\delta_n - \sin\eta_n \sin\delta_n] + b] \cdot \end{aligned}$$

$$[-\sin\eta_n\cos\delta_n - \cos\eta_n\sin\delta_n]. \tag{9.94}$$

As for distance restraining, the factor $[1-\exp(\Delta t/\tau_{Jr})]$ may be set to one when inserting Eq. 9.94 into Eq. 9.91. This may be done for practical reasons: to avoid having to choose the values for $k_n^{(Jr)}$ proportional to $[1-\exp(\Delta t/\tau_{Jr})]^{-1}$.

When using the biquadratic functional form the force on atom i becomes the sum of equations Eq. 9.82 and Eq. 9.91, where

$$\mathbf{f}_i^{bi} = \mathbf{f}_i^{tav} + \mathbf{f}_i^{inst} \tag{9.95}$$

And

$$\frac{\partial \mathcal{V}^{(Jr)}{}_n}{\partial J_n} = k_n^{(Jr)}\,(\overline{J_n} - J^0{}_n)^2(J_n - J^0{}_n). \tag{9.96}$$

and

$$\frac{\partial \mathcal{V}^{(Jr)}{}_n}{\partial \overline{J_n}} = k_n^{(Jr)}\left[\overline{J_n} - J^0{}_n\right](J_n - J^0{}_n)^2. \tag{9.97}$$

As for normal time averaging the term on the right hand side of (Eq. 9.97) is multiplied with the factor $[1-\exp(\Delta t/\tau_{Jr})]$. Alternatively this factor can be set to one or to zero, respectively. The latter option means that there will be no contribution of (Eq. 9.97) to the restraining force.

We note that the total energy will not be conserved when applying time-averaging due to the dependence of the restraining interaction (Eq. 9.64) on time points before time t.[64]

At the start of a simulation the value of the average (Eq. 9.79) is set equal to the ^3J-value calculated from the starting configuration

$$\begin{aligned}\overline{J_n(t=0;\tau_{Jr})} &= J_n(t=0)\\ &= a\cos^2(\eta_n(t=0)+\delta_n) + b\cos(\eta_n(t=0)+\delta_n) + c.\end{aligned} \tag{9.98}$$

At the end of a simulation the values of the averages (Eq. 9.79) are stored with the final configuration for use in a continuation simulation (Sec. 4-4.11).

The type of restraining applied to the ^3J-couplings (NTJVR: instantaneous, time-averaged or biquadratic time-averaged or with local-elevation (LE) (only with time-averaging)), whether or not this is a continuation run (NTJVRA), the value of the overall force constant, $k_n^{(Jr)}$ = CJVR, the coupling time, τ_{Jr} = TAUJVR, the option to omit the factor $[1-\exp(\Delta t/\tau_{Jr})]$, i.e. set it to one, in case of normal time-averaging (NJVRTARS), the option to weight the contribution of (Eq. 9.97) to the force in case of biquadratic restraining (NJVRBIQW), the number of grid points for the local-elevation potential (NGRID), the tolerance to deviation from the experimental value, ΔJ^0 (DELTA) and whether to write the ^3J-value data to a special trajectory are specified in the JVALUERES block of the MD input file (see Chap. 4-8).

The use of periodic scaling is controlled by setting RESTYPE=jrest in the PERSCALE block of the MD input file (see Chap. 4-8). Within this block, the maximum scaling factor for the dihedral angle potential energy term (KDIH) and for the ^3J-value restraint potential energy term (KJ), the period τ_{Jr}^s of the cosine scaling function (T), the minimum deviation ΔJ^0 from the target value to start a scaling period (DIFF), the minimum fraction of τ_{Jr}^s that needs to be passed before starting a new scaling period (RATIO) and the reading of the scaling parameters (READ) can be specified. An example of ^3J-coupling constant restraining using this method is given in[66].

An application of ^3J-coupling constant restraining using time-averaging, including a discussion of the choice of the values for CJVR and TAUJVR, is given in[64]. The latter should satisfy the condition

$$\tau_{Jr} \ll t_{\mathrm{MD}} \tag{9.99}$$

where t_{MD} is the length of the simulation. The overall force constant CJVR can be multiplied by individual weight factors WJVR specific to each ^3J-coupling constant (see below).

The choices for NGRID, DELTA and TAUJVR when local-elevation is used are discussed in[71], which contains an example of ^3J-value restraining using time-averaging and local-elevation.

The atom sequence numbers of the atoms i, j, k and l that define η_n (IPJV, JPJV, KPJV, LPJV [1..NDJV]), the individual restraint weights (WJVR[1..NDJV]), the reference ^3J-values $J^0{}_n$ (PJR0[1..NDJV]), the phase shifts $\delta_n = \zeta_n - \eta_n$ (PSJR[1..NDJV]) the Karplus parameters a, b and c (AJV, BJV, CJV[1..NDJV]) belonging

to the angles ζ_n and the type of restraining potential energy term (NHJV: harmonic, half-harmonic attractive or half-harmonic repulsive) are specified in the JVALRESSPEC block of a ^3J-coupling constant restraints file (see Sec. 4-3.6).

9.8. S^2-order parameter restraining

The special interaction term $\mathcal{V}^{(spec)}(\boldsymbol{r};\mathbf{s})$ in Eq. 3.4 that performs S^2-*order parameter restraining* reads[72]

$$\mathcal{V}^{(Sr)}(\boldsymbol{r};\mathbf{s}) \;=\; \sum_{n=1}^{N_{Sr}} \mathcal{V}^{(Sr)}{}_n(\overline{S(\mathbf{r}_{XY})};k_n^{(Sr)},S_n^0,\Delta S_n^0) \tag{9.100}$$

where the horizontal bar denotes a time-average and the n-th S^2-order parameter restraint restrains the motion of atoms X and Y. The summation runs over a set of N_{Sr} S^2-order parameter restraints. The functional form of $\mathcal{V}^{(Sr)}$ reads

$$\begin{aligned}
&\mathcal{V}^{(Sr)}{}_n(\overline{S(\mathbf{r}_{XY})};k_n^{(Sr)},S_n^0,\Delta S_n^0)\\
&= \tfrac{1}{2}k_n^{(Sr)}[\overline{S(\mathbf{r}_{XY})}-S_n^0-\Delta S_n^0]^2 \quad \text{for} \quad \overline{S(\mathbf{r}_{XY})} > S_n^0+\Delta S_n^0\\
&= \tfrac{1}{2}k_n^{(Sr)}[\overline{S(\mathbf{r}_{XY})}-S_n^0+\Delta S_n^0]^2 \quad \text{for} \quad \overline{S(\mathbf{r}_{XY})} < S_n^0-\Delta S_n^0\\
&= 0 \quad \text{otherwise.}
\end{aligned} \tag{9.101}$$

where the value ΔS_n^0 allows for some uncertainty in the reference S_n^0 -values. The time-averaged order parameter is calculated from[72,73]

$$\overline{S(\mathbf{r}_{XY}(t))} = \frac{1}{2}\left\{3\sum_{\alpha=1}^{3}\sum_{\beta=1}^{3}\left[\overline{Q_{\alpha\beta}(t)}\right]^2 - \left[\overline{D(t)}\right]^2\right\}\cdot(r_{\mathrm{XY}}^{\mathrm{eff}})^6 \tag{9.102}$$

where $r_{\mathrm{XY}}^{\mathrm{eff}}$ is an effective internuclear distance between atoms X and Y. The time averaged quantities $\overline{Q_{\alpha\beta}(t)}$ and $\overline{D(t)}$ are calculated in the usual damped memory manner[58] with the memory relaxation time τ_{sr},

$$\overline{Q_{\alpha\beta}(t)} = \frac{1}{\tau_{\mathrm{sr}}[1-e^{-t/\tau_{\mathrm{sr}}}]}\int_0^t e^{-(t-t')/\tau_{\mathrm{sr}}}Q_{\alpha\beta}(t')dt' \tag{9.103}$$

and

$$\overline{D(t)} = \frac{1}{\tau_{\mathrm{sr}}[1-e^{-t/\tau_{\mathrm{sr}}}]}\int_0^t e^{-(t-t')/\tau_{\mathrm{sr}}}D(t')dt' \tag{9.104}$$

and

$$Q_{\alpha\beta}(t') = \frac{(r_{\mathrm{X}\alpha}(t')-r_{\mathrm{Y}\alpha}(t'))(r_{\mathrm{X}\beta}(t')-r_{\mathrm{Y}\beta}(t'))}{(r_{\mathrm{XY}}(t'))^5} \tag{9.105}$$

and

$$D(t') = \frac{1}{r_{\mathrm{XY}}(t')^3} \tag{9.106}$$

with

$$\mathbf{r}_{XY} = \mathbf{r}_X - \mathbf{r}_Y \quad \text{and} \quad r_{\mathrm{XY}} = [(\mathbf{r}_X-\mathbf{r}_Y)\cdot(\mathbf{r}_X-\mathbf{r}_Y)]^{1/2} \tag{9.107}$$

and

$$\begin{aligned}
r_{\mathrm{X1}} &= \mathrm{x-component\ of\ vector}\ \mathbf{r}_X\\
r_{\mathrm{X2}} &= \mathrm{y-component\ of\ vector}\ \mathbf{r}_X\\
r_{\mathrm{X3}} &= \mathrm{z-component\ of\ vector}\ \mathbf{r}_X
\end{aligned} \tag{9.108}$$

and likewise for $\mathbf{r}_Y$. The discretized form, applicable to atomic trajectories, in which configurations are separated by a time interval Δt, is

$$Q_{\alpha\beta}(m\Delta t) = \frac{(r_{\mathrm{X}\alpha}(m\Delta t) - r_{\mathrm{Y}\alpha}(m\Delta t))(r_{\mathrm{X}\beta}(m\Delta t) - r_{\mathrm{Y}\beta}(m\Delta t))}{(r_{\mathrm{XY}}(m\Delta t))^5} \tag{9.109}$$

and

$$\overline{Q_{\alpha\beta}(n\Delta t)} = Q_{\alpha\beta}(n\Delta t)\left\{1 - e^{-\Delta t/\tau_{\mathrm{sr}}}\right\} + e^{-\Delta t/\tau_{\mathrm{sr}}}\overline{Q_{\alpha\beta}((n-1)\Delta t)} \tag{9.110}$$

and

$$\overline{S^2_{\mathrm{XY}}(n\Delta t)} = \frac{1}{2}\left\{3\sum_{\alpha=1}^{3}\sum_{\beta=1}^{3}\left[\overline{Q_{\alpha\beta}(n\Delta t)}\right]^2 - \left[\overline{D(n\Delta t)}\right]^2\right\}\cdot (r^{\mathrm{eff}}_{\mathrm{XY}})^6 \tag{9.111}$$

with

$$D(m\Delta t) = \frac{1}{r_{\mathrm{XY}}(m\Delta t)^3} \tag{9.112}$$

and

$$\overline{D(n\Delta t)} = D(n\Delta t)\left\{1 - e^{-\Delta t/\tau_{\mathrm{sr}}}\right\} + e^{-\Delta t/\tau_{\mathrm{sr}}}\overline{D((n-1)\Delta t)}. \tag{9.113}$$

The restraining force on atom X then becomes

$$\begin{aligned}\mathbf{f}_X(t) &= -\frac{\partial V^{\mathrm{restr}}(\vec{r}^N(t))}{\partial \vec{r}_{\mathrm{X}}(t)} \\ &= -K^{\mathrm{sr}}\left[\overline{S^2_{\mathrm{XY}}(\vec{r}^N(t))} - S^2_{\mathrm{XY}}(\mathrm{exp})\right] \\ &\quad \cdot\frac{1}{2}\left\{3\sum_{\alpha=1}^{3}\sum_{\beta=1}^{3}2\overline{Q_{\alpha\beta}(t)}\frac{\partial\overline{Q_{\alpha\beta}(t)}}{\partial Q_{\alpha\beta}(t)}\frac{\partial Q_{\alpha\beta}(t)}{\partial \vec{r}_{\mathrm{X}}(t)} - 2\overline{D(t)}\frac{\partial\overline{D(t)}}{\partial D(t)}\frac{\partial D(t)}{\partial \vec{r}_{\mathrm{X}}(t)}\right\}\cdot (r^{\mathrm{eff}}_{\mathrm{XY}})^6\end{aligned} \tag{9.114}$$

and the restraining force on atom Y becomes

$$\begin{aligned}\mathbf{f}_Y(t) &= -\frac{\partial V^{\mathrm{restr}}(\vec{r}^N(t))}{\partial \vec{r}_{\mathrm{Y}}(t)} \\ &= -K^{\mathrm{sr}}\left[\overline{S^2_{\mathrm{XY}}(\vec{r}^N(t))} - S^2_{\mathrm{XY}}(\mathrm{exp})\right] \\ &\quad \cdot\frac{1}{2}\left\{3\sum_{\alpha=1}^{3}\sum_{\beta=1}^{3}2\overline{Q_{\alpha\beta}(t)}\frac{\partial\overline{Q_{\alpha\beta}(t)}}{\partial Q_{\alpha\beta}(t)}\frac{\partial Q_{\alpha\beta}(t)}{\partial \vec{r}_{\mathrm{Y}}(t)} - 2\overline{D(t)}\frac{\partial\overline{D(t)}}{\partial D(t)}\frac{\partial D(t)}{\partial \vec{r}_{\mathrm{Y}}(t)}\right\}\cdot (r^{\mathrm{eff}}_{\mathrm{XY}})^6\end{aligned} \tag{9.115}$$

although using 9.110 we have

$$\frac{\partial\overline{Q_{\alpha\beta}(t)}}{\partial Q_{\alpha\beta}(t)} = \frac{\partial\overline{Q_{\alpha\beta}(n\Delta t)}}{\partial Q_{\alpha\beta}(n\Delta t)} = \left[1 - e^{-\Delta t/\tau_{\mathrm{sr}}}\right] \tag{9.116}$$

the approximation[63]

$$\frac{\partial\overline{Q_{\alpha\beta}(t)}}{\partial Q_{\alpha\beta}(t)} = 1 \tag{9.117}$$

is often used, which only leads to a rescaling of K^{sr} in practice, and likewise

$$\frac{\partial\overline{D(t)}}{\partial D(t)} = 1. \tag{9.118}$$

For the derivatives $\frac{\partial Q_{\alpha\beta}(t)}{\partial \vec{r}_{\mathrm{X}}(t)}$ we find using 9.105, where we omit the variable t and denote the three components of the position vector $\vec{r}_{\mathrm{X}}$ of atom X by $r_{\mathrm{X}\gamma}$ with $\gamma = 1, 2, 3$,

$$\begin{aligned}\frac{\partial Q_{\alpha\beta}}{\partial r_{\mathrm{X}_\gamma}} &= \frac{(r_{\mathrm{XY}})^5\left\{\delta_{\gamma\alpha}(r_{\mathrm{X}\beta} - r_{\mathrm{Y}\beta}) + \delta_{\gamma\beta}(r_{\mathrm{X}\alpha} - r_{\mathrm{Y}\alpha})\right\}}{(r_{\mathrm{XY}})^{10}} \\ &\quad -\frac{(r_{\mathrm{X}\alpha} - r_{\mathrm{Y}\alpha})(r_{\mathrm{X}\beta} - r_{\mathrm{Y}\beta})\cdot 5(r_{\mathrm{XY}})^4(r_{\mathrm{X}\gamma} - r_{\mathrm{Y}\gamma})(r_{\mathrm{XY}})^{-1}}{(r_{\mathrm{XY}})^{10}} \\ &= \frac{(r_{\mathrm{XY}})^2\left\{\delta_{\gamma\alpha}(r_{\mathrm{X}\beta} - r_{\mathrm{Y}\beta}) + \delta_{\gamma\beta}(r_{\mathrm{X}\alpha} - r_{\mathrm{Y}\alpha})\right\} - 5(r_{\mathrm{X}\alpha} - r_{\mathrm{Y}\alpha})(r_{\mathrm{X}\beta} - r_{\mathrm{Y}\beta})(r_{\mathrm{X}\gamma} - r_{\mathrm{Y}\gamma})}{(r_{\mathrm{XY}})^7}\end{aligned} \tag{9.119}$$

where δ_{ij} is the Kronecker delta. For the derivatives $\frac{\partial Q_{\alpha\beta}(t)}{\partial \vec{r}_{\rm Y}(t)}$ we find likewise

$$\frac{\partial Q_{\alpha\beta}}{\partial r_{{\rm Y}\gamma}} = -\frac{\partial Q_{\alpha\beta}}{\partial r_{{\rm X}\gamma}}. \tag{9.120}$$

Thus the restraining force on atom Y is the negative of the restraining force on atom X for this restraining function. For the derivatives $\frac{\partial D(t)}{\partial \vec{r}_{\rm X}(t)}$ we find using 9.106 likewise

$$\frac{\partial D}{\partial r_{{\rm X}\gamma}} = \frac{-3(r_{{\rm X}\gamma} - r_{{\rm Y}\gamma})}{(r_{\rm XY})^5} \tag{9.121}$$

and

$$\frac{\partial D}{\partial r_{{\rm X}\gamma}} = -\frac{\partial D}{\partial r_{{\rm Y}\gamma}}. \tag{9.122}$$

Note that the use of order parameters to bias MD simulations is conceptually different from the use of other properties such as nuclear Overhauser enhancement (NOE) atom-atom distance bounds or ^3J-coupling constants, because order parameters are not instantaneous observables, i.e. the order parameter for a single configuration is by definition equal to unity. Therefore, $\tau_{\rm sr}$ represents not only the memory relaxation but also the experimentally determined averaging period. Thus it should be chosen larger than the decay time of the internal autocorrelation function of the vector connecting the two atoms, but not larger than the sensitivity time window of the NMR experiment.

At the start of a simulation the values of the averages 9.103 and 9.104 are set to their instantaneous values calculated from the starting configuration. At the end of a simulation the values of the averages (9.103 and 9.104) are stored with the final configuration for use in a continuation simulation.

9.9. X-ray structure factor amplitude restraining

In GROMOS a five Gaussian parametrisation[74] of the atomic scattering factor f_i is used,

$$f_i(\mathbf{k}) = O_i \exp\left(-\frac{B_i}{4k^2}\right)\left[\sum_{j=1}^{5}\left[a_{ij}\exp\left(-\frac{b_{ij}}{4k^2}\right)\right] + c_i\right]. \tag{9.123}$$

Here, O_i and B_i are the atomic occupancy and the atomic B-factor, a, b and c are coefficients which depend on the type and charge of the atom i[74]. The atomic electron density ρ_i is given by the analytical Fourier backwards transform of the scattering factor f_i. The global electron density is then computed as the sum of the atomic densities

$$\rho(\mathbf{r}; \boldsymbol{r}\mathcal{N}_a) = \sum_{i=1}^{\mathcal{N}_a} \rho_i(\mathbf{r}; \boldsymbol{r}^{\mathcal{N}_a}) \tag{9.124}$$

on a grid whose resolution is an adjustable parameter. The structure factor is obtained by Fourier transform of the electron density of the system

$$F(\mathbf{k}; \boldsymbol{r}^{\mathcal{N}_a}) = \mathcal{F}\{\rho(\mathbf{r}; \boldsymbol{r}^{\mathcal{N}_a})\}. \tag{9.125}$$

The structure factors obtained by the procedure described above are denoted as the *calculated* structure factors. Their amplitudes $\mid F \mid$ can be compared to the observed structure-factor amplitudes $\mid F^0 \mid$, derived from the scattering intensities, through the R-factor which is given by

$$R = \frac{\sum_{i=1}^{N_F} \mid \mid F_i^0 \mid - s \mid F_i \mid \mid}{\sum_{i=1}^{N_F} \mid F_i^0 \mid}, \tag{9.126}$$

where N_F is the number of observed structure-factor amplitudes. As $\mid F^0 \mid$ is generally on an arbitrary scale, the calculated amplitudes are fitted to the observed ones by means of a weighted linear regression, leading to the scaling factor

$$s = \frac{\sum_{i=1}^{N_F} w_i \mid F_i^0 \mid\mid F_i \mid}{\sum_{i=1}^{N_F} w_i \mid F_i \mid^2}. \tag{9.127}$$

The weight w_i of an individual reflection is generally taken as the inverse of the variance of the structure-factor amplitude.

As for ^3J-couplings, a harmonic potential energy term for the structure-factor amplitude can be used to restrain the computed structure-factor amplitudes to the observed ones

$$\mathcal{V}^{(Fxr)}(\boldsymbol{r}^{N_F};\mid F^0 \mid) = \frac{1}{2}\frac{k^{xr}}{\sum_{i=1}^{N_F} w_i \mid F_i^0 \mid^2}\sum_{i=1}^{N_F} w_i \left(\mid F_i^0 \mid -s \mid F_i(\boldsymbol{r}^{N_F}) \mid\right)^2. \tag{9.128}$$

The weight factor or force constant k^{xr} is made resolution independent by the factor $\frac{1}{\sum_{i=1}^{N_F} w_i |F_i^0|^2}$. Time-averaging is introduced by substitution of $\mid F_i \mid$ by $\langle \mid F_i \mid \rangle_t$ in 9.128[75]. In addition to the instantaneous and time-averaging restraining term, a biquadratic term is available

$$\begin{aligned}\mathcal{V}^{(Fxr)}(\boldsymbol{r}^{N_F};\mid F^0 \mid) &= \frac{1}{2}\frac{k^{xr}}{\sum_{i=1}^{N_F} w_i \mid F_i^0 \mid^4} \\ &\sum_{i=1}^{N_F} w_i \left(\mid F_i^0 \mid -s_{\text{inst}} \mid F_i(\boldsymbol{r}^{N_F}) \mid\right)^2 \left(\mid F_i^0 \mid -s_{\text{avg}} \left\langle \mid F_i(\boldsymbol{r}^{N_F}) \mid \right\rangle_t\right)^2.\end{aligned} \tag{9.129}$$

We note that two individual scaling constants s_{inst} and s_{avg} are used. s_{inst} is computed using 9.127, while s_{avg} is calculated using the same relation, where the calculated amplitudes $\mid F_i \mid$ were replaced by the time-averaged ones $\langle \mid F_i \mid \rangle_t$.

9.10. X-ray electron density restraining

In X-ray crystallography, the electron density ρ^0 is not an experimentally observable quantity. As the phase of F^0 is generally not observable, it is taken from the structure factor F computed from an atomic model. The electron density ρ^0 is then computed as

$$\rho^0(\mathbf{r}) = \mathcal{F}^{-1}\{\left(2 \mid F^0(\mathbf{k}) \mid -s \mid F(\mathbf{k}) \mid\right) \exp\left[i \arg\left(F(\mathbf{k})\right)\right]\}, \tag{9.130}$$

where $\arg(F)$ is the phase computed from the model. In analogy to 9.126, a real-space R-factor[76] can be defined

$$R = \frac{\sum_{\mathbf{r}} \mid \beta\rho^0(\mathbf{r}) + \alpha - \rho(\mathbf{r}) \mid}{\sum_{\mathbf{r}} \mid \beta\rho^0(\mathbf{r}) + \alpha + \rho(\mathbf{r}) \mid}. \tag{9.131}$$

Summation is only carried out over the extent of the atoms of interest. α and β are scaling constants computed using a linear regression of

$$\rho(\mathbf{r}) = \beta\rho^0(\mathbf{r}) + \alpha. \tag{9.132}$$

These values can be calculated for an arbitrary set of atoms. Fitting is carried out using only the grid points lying within spheres with a radius R_{cut} centered at the positions of these atoms.

The electron density computed using 9.130 can be used for restraining. The penalty function[77] is defined as

$$\mathcal{V}^{(exr)}(\boldsymbol{r}^{\mathcal{N}_a};\rho^0) = \frac{1}{2}k^{xr}\sum_{\mathbf{r}}\left(\beta\rho^0 + \alpha - \rho(\boldsymbol{r}^{\mathcal{N}_a})\right)^2. \tag{9.133}$$

The summation is carried out over all grid points of the unit cell. Time-averaging is not available for electron density restraints, neither is a biquadratic penalty function.

9.11. X-ray crystallographic symmetry restraining

In a crystal, having a space group different from P1, multiple identical asymmetric units (ASUs) are assembled to construct the unit cell. The relationship between the ASUs is fully defined by the space group and the size of the unit cell. A space group S contains N_{sym} number of symmetry operations $\mathbb{S}_i$. Every atom position in the first asymmetric unit $\mathbf{r}_i$ has $N_{\text{sym}} - 1$ images $\mathbf{r}_i^{(j)}$ defined as

$$\mathbf{r}_i^{(j)} = \mathbb{S}_j\mathbf{r}_i. \tag{9.134}$$

Note that $\mathbb{S}_1$ is the identity symmetry operation and thus $\mathbf{r}_i^{(1)}$ and $\mathbf{r}_i$ are identical. Symmetry operations can be described in terms of a rotation followed by a translation,

$$\mathbb{S}_j\mathbf{r}_i = \mathbf{R}_j\mathbf{r}_i + \mathbf{t}_j. \tag{9.135}$$

Here, the rotation matrix $\mathbf{R}_j$ of the symmetry operation j is, in contrast to the translation vector $\mathbf{t}_j$, independent of the size of the unit cell. The inverse symmetry operation $symop^{-1}$ can be formulated as

$$\mathbb{S}_j{}^{-1}\mathbf{r}_i = \mathbf{R}_j{}^{-1}\left(\mathbf{r}_i - \mathbf{t}_j\right). \tag{9.136}$$

When simulating a unit cell, one may want to impose restraints on the symmetry of the system as, in many cases, insufficient experimental data for refinement of the whole unit cell is available. An easy way of achieving this is by adding harmonic potential energy terms for every symmetry-related pair. For every atom i in the first asymmetric unit, the term

$$\mathcal{V}^{(sxr)}\left(\mathbf{r}_i; k^{sym}\right) = \frac{1}{2}k^{sym}\sum_{i'=1}^{N_{\mathrm{sym}}-1}\sum_{j'=i'+1}^{N_{\mathrm{sym}}}\left[\mathbb{S}_{j'}{}^{-1}\mathbf{r}_i^{(j')} - \mathbb{S}_{i'}{}^{-1}\mathbf{r}_i^{(i')}\right]^2 \tag{9.137}$$

is added. The term can be interpreted as follows: all possible symmetry pairs are transformed to their position in the first asymmetric unit and a set of springs between corresponding atoms is introduced for each pair of molecules.

9.12. Distance-field distance restraining

The calculation of protein-ligand binding free energy energies is an important goal in the field of computational chemistry. Applying path-sampling methods for this purpose involves calculating the associated potential of mean force (PMF) and gives insight into the binding free energy along the binding process. Without a priori knowledge about the binding path, sampling reversible binding can be difficult to achieve. To alleviate this problem, the distance field (DF) has been introduced as reaction coordinate for such calculations.[78] DF is a grid-based method in which the shortest distance between the binding site and a ligand is determined avoiding routes that pass through the protein. Combining this reaction coordinate with Hamiltonian replica-exchange molecular dynamics (REMD) allows for the reversible binding of the ligand to the protein.

In the case of protein ligand binding, a DF restraint can be applied between (virtual) atom i and (virtual) atom j, representing the active site and the ligand, respectively. At the start of a simulation employing a DF restraint, a 3-dimensional grid is created with the grid spacing, g_s, as set by the user (input parameter GRID in the DISTANCEFIELD block). The minimal DF distance from a (virtual) atom i to each of the grid points is then assigned by applying Dijkstra's algorithm.[79]

1. The DF distance at every grid point is initialized to a large value that cannot be reached during the simulation. Here, we have chosen this value to be $4 \times a \times b \times c$ where a, b and c are the box edge lengths. The grid points that are positioned within a user-specified cutoff distance (PROTEINCUTOFF in block DISTANCEFIELD) of any protein atom are flagged by a large value (PROTEINOFFSET in block DISTANCEFIELD).
2. All grid points are marked as unvisited. The initial node is the grid point closest to (virtual) atom i. This grid point is assigned as the current node and a DF distance of 0 is assigned to it.
3. The unvisited nodes that are neighboring the current node are subsequently considered.
   - A new DF distance for the neighboring grid point is initially calculated as the DF distance assigned to the current node plus the distance between the two grid points (g_s). If a neighboring node is flagged as protein, an additional user-specified protein penalty is added to the distance.
   - When the new DF distance is less than the previously assigned preliminary distance, the latter is overwritten. Otherwise the distance does not change. In both cases, the neighbors are still marked 'unvisited' and the assigned DF distances are still preliminary.
4. When all neighbors are considered, the current node is marked as 'visited'. With this marking, the preliminary distance becomes final and this node will not be considered anymore.
5. The unvisited grid point with the lowest preliminary distance becomes the current node. Go back to step 3 and continue until all grid points are marked 'visited'.

Using this approach, periodic boundary conditions are taken fully into account and grid points are not revisited. Once the updating step is completed, all grid points are assigned the shortest DF distance from atom i. The DF distances are updated (by applying steps 1-5) every UPDATE steps (in block DISTANCEFIELD). Not updating every time step speeds up the simulation significantly and is allowed as long as the protein does not change its conformation too much between the updates, even though this will come at the expense of a slight loss of energy conservation. Using an UPDATE value of 100, the simulations are slowed down by 20 percent with respect to regular distance restraint simulations.

To avoid simulation artifacts, several extra features are implemented.

1. If (virtual) atom i is flagged as being within the protein, the DF distances of the grid points are not updated. It sometimes happens that this virtual atom temporarily gets buried in the active site due to the flexibility of the protein. If an update step would be performed, all DF distances are very large, because each of them has the additional protein penalty which was added to the first point. The forces induced by a DF restraint will thus get very large and may disrupt the structure. Also, because each grid point has the additional penalty, the DF distance converges to a normal radial distance with an initial offset.
2. The user can specify the number of smoothening rounds that are applied after each updating step (input parameter SMOOTH in the DISTANCEFIELD block). In a smoothening round, we loop over all non-protein grid points and check if one of its neighbors is flagged as protein. If this is the case, we are dealing with a grid point that is at the edge of the protein. In order to avoid large forces pointing away from the protein, the DF distance on the flagged protein grid point is determined again based on its direct neighbors, but now without the protein penalty. In this way, the large forces arising from the protein penalty on the grid are buried within the protein, and the regular van der Waals repulsion will ensure that the ligand never reaches these grid points. The DF distances of other grid points and the optimal route for atom j are not affected as this smoothening step is performed after the normal updating steps (1-5) have finished.

Once the DF distances are defined for all grid points, we can impose a DF restraint on the distance between atoms i and j. The forces and energies due to the DF restraint are calculated at each time step. We start this process by determining the 8 grid points that are closest to atom j, to which DF distances have been determined in the updating step. In order to be able to calculate the forces, the derivatives of the DF distance, l in the x, y and z directions have to be determined for each of the 8 neighboring grid points. This is done using a finite differences approach as illustrated in Eq. 9.138 for grid point k, in the x direction.

$$\frac{dl}{dx_k} = \frac{l(x_k - 1, y_k, z_k) - l(x_k + 1, y_k, z_k)}{2g_s} \tag{9.138}$$

Here, $l(x_k - 1, y_k, z_k)$ is the DF distance assigned to the neighbor of grid point k with the smaller x coordinate and g_s is the grid spacing. In order to interpolate the DF distance and its derivatives from the neighboring points to atom j, an assignment function of order 2 is used, similar to the one used for charges in the PPPM method (see Sec. 7.4.4.4).

The potential energy associated with the DF restraint, $\mathcal{V}^{(df)}$, can now be calculated using

$$\begin{aligned}
&\mathcal{V}^{(df)}(l_{ij}, k^{(df)}, l^0, \Delta l^h) \\
&= -k^{(df)}[l_{ij} - l^0 + \tfrac{1}{2}\Delta l^h]\Delta l^h && l_{ij} \leq l^0 - \Delta l^h \\
&= \tfrac{1}{2}k^{(df)}[l_{ij} - l^0]^2 && l^0 - \Delta l^h < l_{ij} \leq l^0 + \Delta l^h \\
&= k^{(df)}[l_{ij} - l^0 - \tfrac{1}{2}\Delta l^h]\Delta l^h && l_{ij} > l^0 + \Delta l^h
\end{aligned} \tag{9.139}$$

$k^{(df)}$ is the force constant of the harmonic DF restraint, l^0 is the reference DF distance and l_{ij} is the current DF distance between atoms i and j. The interaction term is linearized after a certain deviation Δl^h to prevent too large energy and forces for larger deviations (input parameter RL in the DISTANCEFIELD block). The forces on atom i and j are calculated with

$$\begin{aligned}
\mathbf{f}_j &= -\frac{\partial \mathcal{V}^{(df)}}{\partial l_{ij}} \frac{\partial l_{ij}}{\partial \mathbf{r}_j} \\
&= k^{(df)} \Delta l^h \frac{\partial l_{ij}}{\partial \mathbf{r}_j} && l_{ij} \leq l^0 - \Delta l^h
\end{aligned}$$

$$
\begin{aligned}
&= -k^{(df)}(l_{ij}-l^0)\frac{\partial l_{ij}}{\partial \mathbf{r}_j} \qquad l^0-\Delta l^h < l_{ij} \le l^0+\Delta l^h \\
&= -k^{(df)}\Delta l^h \frac{\partial l_{ij}}{\partial \mathbf{r}_j} \qquad\qquad\qquad\qquad l_{ij} > l^0+\Delta l^h
\end{aligned} \tag{9.140}
$$

and

$$
\mathbf{f}_i = -\mathbf{f}_j \tag{9.141}
$$

9.13. Biasing energy functions

The force field may be combined with a bias energy, so as to penalise or favour specified parts of conformational space. Such a bias energy may be time-dependent, such as in the local elevation method (Sec. 9.13.1) or time-independent, such as in the umbrella sampling method (Sec. 9.13.2) or may be a combination of these, such as in the local elevation umbrella sampling methods (Sec. 9.13.3 and Sec. 9.13.4). GROMOS allows a specification of a bias energy based on the following steps:

1. definition of a set of N_{LE} coordinates, collectively noted by the vector $\boldsymbol{Q} = \{\mathcal{Q}_n, n = 1..N_{LE}\}$, of which the bias energy will depend. The chosen set of coordinates will be named local elevation- or LE-coordinates. These coordinates are assumed to be well defined and differentiable functions of the vector $\boldsymbol{r}$ encompassing the Cartesian coordinates of all particles in the system, *i.e.* the vector function $\boldsymbol{Q} = \boldsymbol{Q}(\boldsymbol{r})$ must be defined for any $\boldsymbol{r}$ and its derivative must be non-singular. Examples of possible internal coordinates include *e.g.* distances between atom pairs, angles between atom triples, dihedral angles between atom quadruples, root-mean-square atomic positional deviations from given reference structures, extended-system variables (*e.g.* λ-variables in λ-dynamics[80–82]), or any (differentiable) mathematical combination of these. Currently implemented is dihedral angle [VARTYPE=1], distance [VARTYPE=2] and distance-field distance [VARTYPE=6].
2. a specification of one (or more) grid(s) within the space of the LE-coordinates consisting of $\Gamma+1$ grid points and a memory force-constant vector $\boldsymbol{M}_k = \{M_{k,i}, i = 0..\Gamma_k\}$ giving the force constants at each grid point. Three types of grid may be specified, (*i*) a full-dimensional grid, used in the LE and LEUS methods; (*ii*) a spherical grid and (*iii*) a line grid, the latter two used in the B&S − LEUS[83] method.
3. a set of basis functions γ to give a continuous interpolation between grid points. Various LE basis functions are available for the use in GROMOS, and a discussion of the different functions can be found in[84]. The LE basis function may be of Gaussian type

   $$
   \gamma^{Gauss}(x) = H(r_{cut}-|x|)\exp\Big[-\frac{(x)^2}{2\sigma^2}\Big] \tag{9.142}
   $$

   or of polynomial form with continuous 1st derivative ($NTLEFU = 0$)

   $$
   \gamma^{Poly_1}(x) = H(r_{cut}-|x|)[1-3\frac{|x|^2}{\sigma^2}+2\frac{|x|^3}{\sigma^3}] \tag{9.143}
   $$

   or with continuous second derivative

   $$
   \gamma^{Poly_2}(x) = H(r_{cut}-|x|)[1-10\frac{|x|^3}{\sigma^3}+15\frac{|x|^4}{\sigma^4}-6\frac{|x|^5}{\sigma^5}]\ , \tag{9.144}
   $$

   where σ describes the width of the basis functions $WLES$. For the polynomial forms σ equals the grid spacing of the defined grid.

9.13.1. Local elevation biasing. MD or SD simulation can also be used as a method to search the conformational space of a molecule for conformations of low energy. Due to the presence of relatively high barriers on the energy surface, MD and SD simulations have the tendency to repeatedly visit a small set of local energy minima. To avoid resampling of conformations, we may add a penalty potential energy to energetically penalise conformations already sampled. The local elevation method[85] offers a way to produce such a penalty potential energy by gradually adding small, local, repulsive potential energy terms (LE basis function γ) during the simulation. In practice, this is performed by increasing the values of the memory force-constant vector $\boldsymbol{M}$ according to the grid point visited at the current time, giving a time-dependent bias energy. The local elevation method can also be used in combination with time-averaging to bias a simulation towards conformations that, on average, satisfy a set of experimental data such as ^3J-couplings (Sec. 9.7).

If the number of LE coordinates is low ($N_{le} \approx\leq 5$), one may enhance the sampling in the complete LE-subspace. This can be done by using a full-dimensional grid (NTLES), where the special interaction term ($\mathcal{V}^{(spec)}(\boldsymbol{r};\mathbf{s})$ in Eq. 3.4) defining the *local elevation bias* reads

$$\begin{aligned}\mathcal{V}^{(spec)}(\boldsymbol{r};\mathbf{s}) &= \mathcal{V}^{(le)}(\boldsymbol{Q};\boldsymbol{M}(t)) \\ &= \sum_{k=0}^{\Gamma} M_k(t) \prod_{i=1}^{N_{le}} \gamma_i(\boldsymbol{Q}_i - \boldsymbol{Q}^0_{k,i}) \end{aligned} \tag{9.145}$$

where the sum k goes over the $\Gamma + 1$ grid points (in practice over visited grid points), the product i runs over the N_{le} local elevation (LE) coordinates $\boldsymbol{Q}_i$, γ_i is the LE basis function and $\boldsymbol{M}(t)$ describes a (time-dependent) memory force-constant vector. In the LE method, the time dependence of the memory force-constant vector is simply given as

$$M_k(t) = M_k(t - \Delta t) + k^{(le)} \tag{9.146}$$

where $k^{(le)}$ is the LE force constant $CLES$ and $\boldsymbol{Q}_i(t)$ is within the range of grid point k. We note that the total energy will not be conserved when applying the LE interaction due to the change of the memory force-constant vector $\boldsymbol{M}(t)$ as a function of time[85]. Under specific conditions of the memory force-constant vector $\boldsymbol{M}(t)$, the bias potential energy generated by the LE procedure will, together with the physical potential energy, create an approximately flat free energy surface[86,87], thus we can in principle approximate the free energy surface as the negative of the LE bias potential energy. However, to obtain accurate free energies (and other ensemble properties), it is highly recommended to freeze the build up and use the LE bias potential energy as an (time-independent) umbrella potential energy term, as done in the LEUS method.

At the end of a simulation, the information concerning the definition of LE conformations, which LE conformations have been visited and how many times (ILEPOT), are stored with the final configuration for use in a continuation simulation.

Whether or not to apply LE (NTLES) and the build-up or freezing of each potential energy term (NTLEFR) are read from the LOCALELEV block of the MD input file. Parameters to describe the form of the potential energy term may be read from the LOCALELEV block (NTLESA=0, starting with $\mathcal{V}^{(le)} = 0$), or together with the potential energy from the coordinate file (NTLESA=1) or a LEUS database file (NTLESA=2). The atom sequence numbers defining the LE coordinate and the identifiers of the potential energy are given in the LOCALELEVSPEC block of the LE input file. An application of LE search is given in[85].

9.13.2. Umbrella sampling. According to the umbrella sampling method[88], one can recover the ensemble properties of an unbiased ensemble by means of reweighting as

$$A = \frac{< A(\boldsymbol{q},\boldsymbol{p_q}) \exp[\frac{\mathcal{V}^{(spec)}}{k_B T}] >_B}{< \exp[\frac{\mathcal{V}^{(spec)}}{k_B T}] >_B} \tag{9.147}$$

A suitable bias energy may therefore be specified, so as to calculate ensemble properties such as free energy, ^3J-couplings and occurrences of hydrogen bonds at a higher efficiency than a normal MD simulation. One example may be the application of an energy bias that cancels out the potential of mean force, giving uniform sampling in the space of the selected LE-coordinates. The potential of mean force is however in most cases unknown and is often the sought result of the simulation, and a manual specification of the bias potential energy term is therefore in most cases not possible.

9.13.3. Local elevation umbrella sampling (LEUS**).** As described in Sec. 9.13.1, an energy bias as built by the LE method will approximate the negative of the free energy surface. In practice however, the quality of the approximation is depending on the chosen build-up parameters and includes a certain amount of statistical uncertainty. To get accurate free energies and other ensemble properties one may either attempt to optimise the build-up procedure itself, or correct for the uncertainties by freezing the LE-build up and run an umbrella sampling procedure where the bias energy is time-independent. In practice, the second choice is simpler to accomplish, as uncertainties in the bias energy up to approximately $k_B T$ will be corrected for. This is the principle of the LEUS method: first a relatively short LE run is performed to create a biasing term that allows an approximate uniform sampling in the space of LE-coordinates and secondly a US run is performed with the LE bias energy term frozen to obtain accurate simulation results.

The build-up or freezing of the bias potential energy terms (NTLEFR) are read from the LOCALELEV block of the MD input file.

An application of LEUS is given in Ref.[89].

9.13.4. Ball and stick LEUS**.** In the case where the LE-space is of a high dimension, the application of a full-dimensional grid becomes unpractical. A solution to this problem for systems with well-defined conformational states is presented in the *ball-and-stick* local elevation umbrella sampling method (B&S − LEUS)[83], where sampling is restricted to and enhanced within a prespecified subspace of the chosen LE coordinates.

The B&S − LEUS method consists of seven steps.

1. Choice of a LE subspace permitting the definition of the relevant conformational states. Note that periodic internal coordinates (*e.g.* dihedral angles) should not be $''refolded''$ to a reference period, *i.e.* their time evolution must be continuous. Furthermore it is assumed that the definition of any internal coordinate (with a specified unit) is associated with the selection of a corresponding reference value σ_n (with the same unit), and that $\mathcal{Q}_n$ is defined by the unitless ratio of the two quantities. It is important to stress that the results of a B&S − LEUS simulation depend on a given choice of the σ_n factors, so that these factors must be clearly specified as an integral part of the definition of the conformational subspace.
2. Representation of the relevant conformational states by means of K centered volumes within the reduced conformational subspace. One possible type of centered volume is the sphere. The biasing potential energy function $\mathcal{B}_k(\boldsymbol{Q})$ corresponding to a sphere $\mathcal{S}_k$ associated with a state k is defined by the following parameters: a sphere center $\boldsymbol{Q}_k$, a radius R_k, a restraining force constant c_k, a number of radial grid points $\Gamma_k + 1$, and a memory force-constant vector $\boldsymbol{M}_k = \{M_{k,i}, i = 0..\Gamma_k\}$. The corresponding expression is (for $k = 1..K$)

$$\mathcal{B}_k(\boldsymbol{Q}) = \begin{cases} M_{k,\Gamma_k} + \frac{1}{2}c_k(r_k - R)^2 & \text{if } r_k \geq R_k \\ \sum_{i=0}^{\Gamma_k} M_{k,i}\gamma(d_{k,i}) & \text{if } r_k < R_k \end{cases} , \tag{9.148}$$

where γ is the LE basis function, and the quantities r_k and $d_{k,i}$ depend on $\boldsymbol{Q}$ as

$$r_k = ||\boldsymbol{Q} - \boldsymbol{Q}_k|| \tag{9.149}$$

and

$$d_{k,i} = \Gamma_k R_k^{-1} r_k - i \ . \tag{9.150}$$

Within the sphere ($r_k < R_k$), the memory vector $\boldsymbol{M}_k$ permits to enforce a radially-dependent potential energy term of arbitrary form (with an approximate resolution $\Gamma_k^{-1}R_k$), expressed as a weighted sum of $\Gamma_k + 1$ repulsive local functions γ. Outside the sphere ($r_k \geq R_k$), the potential energy term is changed to an attractive half-harmonic restraint. It is easily verified that the biasing potential energy term $\mathcal{B}_k$ defined by Equation Eq. 9.148 is continuous and differentiable[84].

A carefully adjusted one-dimensional memory may be used to obtain a biasing potential energy term enforcing a homogeneous radial sampling of the centered volume, but this potential energy term will generally not lead to a homogeneous sampling of the multi-dimensional volume itself, the directional (non-radial) dimensions remaining unbiased. Note also that such a potential energy term will guarantee that the center of the volume is sampled.

3. Definition of a set of conformational paths connecting the centers of the volumes representing the K states. Only the simplest possible type of path will be considered here, namely the line or, more precisely, the line segment. The numbering of the corresponding biasing potential energy terms will start at $K + 1$. The biasing potential energy term $\mathcal{B}_l(\boldsymbol{Q})$ corresponding to a line $\mathcal{L}_l$ is defined by the following parameters: a starting point $\boldsymbol{Q}_l$, an ending point $\boldsymbol{Q}'_l$, a width W_l, a restraining force constant c_l, a number of longitudinal grid points $\Gamma_l + 1$, and a memory force-constant vector $\boldsymbol{M}_l = \{M_{l,i}, i = 0..\Gamma_l\}$. The corresponding expression is (for $k = K + 1..K + L$)

$$\mathcal{B}_l(\boldsymbol{Q}) = \begin{cases} M_{l,0} + \frac{1}{2}c_l H(r_l - W_l)(r_l - W_l)^2 & \text{if } u_l \leq 0 \\ M_{l,\Gamma_l} + \frac{1}{2}c_l H(r'_l - W_l)(r'_l - W_l)^2 & \text{if } u_l \geq U_l \\ \sum_{i=0}^{\Gamma_k}[M_{l,i} + \frac{1}{2}c_l H(p_l - W_l)(p_l - W_l)^2]\gamma(d_{l,i}) & \text{if } 0 < u_l < U_l \end{cases} , \tag{9.151}$$

where the where γ is the LE basis function, U_l is the line length

$$U_l = ||\boldsymbol{Q}'_l - \boldsymbol{Q}_l|| \ , \tag{9.152}$$

and the quantities u_l, p_l, r_l, r'_l and $d_{l,i}$ depend on $\boldsymbol{Q}$ as

$$u_l = U_l^{-1}(\boldsymbol{Q}'_l - \boldsymbol{Q}_l)^T(\boldsymbol{Q} - \boldsymbol{Q}_l) \ , \tag{9.153}$$
$$p_l = ||(\boldsymbol{Q} - \boldsymbol{Q}_l) - U_l^{-1}u_l(\boldsymbol{Q}'_l - \boldsymbol{Q}_l)|| \ , \tag{9.154}$$
$$r_l = ||\boldsymbol{Q} - \boldsymbol{Q}_l|| \ , \tag{9.155}$$
$$r'_l = ||\boldsymbol{Q} - \boldsymbol{Q}'_l|| \ , \tag{9.156}$$

$\boldsymbol{v}^T$ indicating the transpose of a vector $\boldsymbol{v}$, and

$$d_{l,i} = \Gamma_l U_l^{-1} u_l - i \ . \tag{9.157}$$

Note that Eq. 9.151 is formulated so as to allow for displaced lines and lines with longitudinally-dependent widths or force constants. The quantity u_l represents the longitudinal distance between the starting point of the line and the current point $\boldsymbol{Q}$, while the parameter p_l represents the corresponding transverse (perpendicular) distance. Within the line ($0 < u_l < U_l$), the memory vector $\boldsymbol{M}_l$ permits to enforce a longitudinally-dependent potential energy term of arbitrary form (with an approximate resolution $\Gamma_l^{-1}U_l$), expressed as a weighted sum of $\Gamma_l + 1$ repulsive local functions γ, and applied together with a transverse attractive flat-bottom (width W_l) half-harmonic restraining potential energy term. Outside the line, *i.e.* when going past its two terminal points in terms of longitudinal distance ($u_l \leq 0$ or $u_l \geq U_l$), the potential energy term is changed to an attractive flat-bottom (width W_l) half-harmonic restraint depending on the distance to the corresponding end point. It is easily verified that the biasing potential energy term $\mathcal{B}_l$ defined by Equation Eq. 9.151 is continuous and differentiable.

GROMOS also allows a non-linear variant of the line, the displaced line, where an offset coordinate $\Delta\boldsymbol{Q}_{l,i}$ perpendicular to the line (*i.e.* with $\Delta\boldsymbol{Q}_{l,i}^T(\boldsymbol{Q}'_l - \boldsymbol{Q}_l) = 0$ and $\Delta\boldsymbol{Q}_{l,0} = \Delta\boldsymbol{Q}_{l,\Gamma_l} = 0$), and replacing p_l in Equation Eq. 9.151 by

$$p_{l,i} = ||(\boldsymbol{Q} - \boldsymbol{Q}_l) - U_l^{-1}u_l(\boldsymbol{Q}'_l - \boldsymbol{Q}_l) - \Delta\boldsymbol{Q}_{l,i}||. \tag{9.158}$$

This requires the specification of a set of orthonormal vectors, orthogonal to the defined line together with the specification of the displacement along each of these vectors for each grid point. Another possible variant involves the use of longitudinally-dependent line widths or/and restraining force constants, *i.e.* the replacement of c_l and W_l in Equation Eq. 9.151 by corresponding grid-point dependent quantities $c_{l,i}$ and $W_{l,i}$. In principle, the L paths will be chosen to connect pairs among the K centered volumes defining the states. This must be done in such a way that all states are connected to each other *via* at least one path or succession thereof. The minimum number of paths is thus $L = K - 1$ (maximum-spanning tree), but it may be advantageous in terms of convergence properties to include additional (redundant) paths. Note that the end points of the paths must be identical to the centers of the states (*e.g.* they should not connect to the periphery of the centered volumes). This is essential because independent biasing potential energy terms leading to a homogeneous radial sampling of the centered volumes and longitudinal sampling of the paths can only guarantee that these specific points are sampled (for lines, assuming sufficiently small line widths at the end points).

4. Unification of the biasing potential energy terms associated with the $M = K + L$ centered volumes and paths into a single biasing potential energy term according to the enveloping distribution sampling procedure[90]. For the ease of notation, these objects have been given the generic notation $\mathcal{B}_m$, where the index m ranges from 1 to $M = K + L$ ($1..K$ for the centered volumes, $K + 1..M$ for the paths). The various LEUS potential energy terms are combined following the EDS principle as

$$\mathcal{V}^{(bias)}(\boldsymbol{r}; \boldsymbol{M}) = -\frac{1}{\beta s} \ln \left(\sum_{m=1}^{M} \exp[-\beta s \mathcal{B}_m(\boldsymbol{Q}(\boldsymbol{r}))] \right) \ , \tag{9.159}$$

where $\beta = (k_B T)^{-1}$, k_B being Boltzmann's constant and T the absolute temperature, $\boldsymbol{r}$ represents the system configuration (Cartesian coordinates of all particles), $\boldsymbol{Q}(\boldsymbol{r})$ the corresponding representative point in the reduced subspace, s a (positive) smoothing parameter, and $\boldsymbol{M}$ the joint memories of the M objects, *i.e.* a vector containing $N_M = \sum_{m=1}^{M} \Gamma_m$ elements.

Qualitatively speaking, the exponential weighting in Equation Eq. 9.159 ensures that the combined biasing potential energy term $\mathcal{V}^{(bias)}$ is low in the regions of the conformational subspace where *any* of the $\mathcal{B}_m$ is low, and high in the regions where *all* the $\mathcal{B}_m$ are high. For the ease of

reference, the subvolume of the reduced conformational subspace where any of the $\mathcal{B}_m$ is low, *i.e.* the union of all centered volumes and paths, will be referred to as the active subspace.

The forces derived from $\mathcal{V}^{(bias)}$ in Eq. 9.159 are given by

$$\boldsymbol{f}_{bias}(\boldsymbol{r}) = -\frac{\partial \mathcal{V}^{(bias)}(\boldsymbol{r};\boldsymbol{M})}{\partial \boldsymbol{r}} = -\sum_{m=1}^{M} w_m(\boldsymbol{Q}) \frac{\mathrm{d}\mathcal{B}_m(\boldsymbol{Q})}{\mathrm{d}\boldsymbol{Q}} \frac{\partial \boldsymbol{Q}}{\partial \boldsymbol{r}} \tag{9.160}$$

where

$$w_m(\boldsymbol{Q}) = \frac{\exp[-\beta s \mathcal{B}_m(\boldsymbol{Q})]}{\sum_{m=1}^{M} \exp[-\beta s \mathcal{B}_m(\boldsymbol{Q})]} \tag{9.161}$$

can be interpreted as measuring the relative influence (weight) of a single-object biasing potential energy term m on the dynamics of the system in a conformation $\boldsymbol{Q}$. Note that the forces defined by Equation Eq. 9.160 are non-singular, because $\mathcal{B}_m(\boldsymbol{Q})$ and $\boldsymbol{Q}(\boldsymbol{r})$ are both differentiable functions of their arguments.

5. LE build-up phase to optimize the memory, leading to a biasing potential energy term enabling nearly uniform sampling (radially within the centered volumes, longitudinally within the paths) of the active subspace. The updating scheme for the memory $\boldsymbol{M}(t)$ relies on the equation

$$M_{m,i}(t+\Delta t) = M_{m,i}(t) + k^{(le)} f_{LE}^{I_{\mathcal{R}}(t;\gamma_{LE},n_{LE})} j_{m,i}(\boldsymbol{Q}) h_{m,i}(\boldsymbol{Q}) w_m(\boldsymbol{Q}) \ , \tag{9.162}$$

where $M_{m,i}$ is the memory associated with grid point i of object m, $\boldsymbol{Q} = \boldsymbol{Q}(\boldsymbol{r}(t))$, Δt is the simulation timestep, $k^{(le)}$ the basis force-constant increment, f_{LE} a force-constant reduction factor, $I_{\mathcal{R}}$ a force-constant reduction counter, associated with a defined conformational region $\mathcal{R}$, γ_{LE} a local visiting cutoff (real), n_{LE} a global visiting cutoff (integer), $j_{m,i}$ a distribution-alteration function, $h_{m,i}$ a grid-assignment function, and w_m the weight defined by Eq. 9.161. In the absence of prior knowledge concerning the form on the free-energy hypersurface, the memory will typically be initiated to $\boldsymbol{M}(0) = \boldsymbol{0}$. The different factors involved in Eq. 9.162 are explained below.

The grid-assignment function evaluates to one for a single grid point in each of the single-object biasing potential energy terms and to zero for all other grid points, namely the grid point i in object m that is (radially for centered volumes, longitudinally for paths) closest to $\boldsymbol{Q}$. For a sphere k, one has ($k = 1..K$)

$$h_{k,i}(\boldsymbol{Q}) = \begin{cases} \delta_{i,\Gamma_k} & \text{if } r_k \geq R_k \\ \delta_{i,\mathrm{NINT}(\Gamma_k R_k^{-1} r_k)} & \text{if } r_k < R_k \end{cases} \ , \tag{9.163}$$

where δ is the Kronecker symbol and the function NINT returns the nearest integer to a real number. For a line l, one has ($l = K+1..M$)

$$h_{k,i}(\boldsymbol{Q}) = \begin{cases} \delta_{i,0} & \text{if } u_l \leq 0 \\ \delta_{i,\Gamma_l} & \text{if } u_l \geq U_l \\ \delta_{i,\mathrm{NINT}(\Gamma_l U_l^{-1} u_l)} & \text{if } 0 < u_l < U_l \end{cases} \ . \tag{9.164}$$

As a result, the build-up always affects one and only one grid point in each of the M single-object memories. However, the presence of the weight factor w_m in Equation Eq. 9.162 ensures that the build-up is only significant within the objects encompassing or closest to point $\boldsymbol{Q}$ (note that the sum of w_m over all objects is one).

The distribution-alteration function is generally set to

$$j_{m,i}(\boldsymbol{Q}) = 1 \ , \tag{9.165}$$

leading to a nearly homogenous sampling (radially within the centered volumes, longitudinally within the paths) of the active subspace. However, this function may be used to enforce deviations from this homogenous sampling. As a simple example, one may observe that the volume of relevant conformational subspace accounted for by a radial grid point i within a sphere k (distance $\Gamma_k^{-1} i R_k$ from the center) increases with $(i_k+\frac{1}{2})^{N-1}$ (Jacobian factor), where N is the subspace dimensionality. One may then decide to bias the sampling of the sphere towards its periphery, which can be achieved by setting for all spheres k ($k = 1..K$)

$$j_{k,i}(\boldsymbol{Q}) = \frac{(i+\frac{1}{2})^{1-N}}{\sum_{j=0}^{\Gamma_k} (j+\frac{1}{2})^{1-N}} \ . \tag{9.166}$$

The force-constant reduction factor can be used in the context of an iterative procedure to progressively decrease the build-up rate during the searching phase. As noted previously by other authors[86,91], a high build-up rate is desired in the early stage of the searching, where the deep free-energy basins have to be "filled up" coarsely (*i.e.* without wasting computer time), while a low build-up rate (near-equilibrium situation) is preferable in the later stage, where the remaining shallower free-energy wiggles have to be "levelled off" (so as to produce a close-to-optimal biasing potential energy term). This can be achieved by a progressive reduction of the build-up rate, enforced in Equation Eq. 9.162 by using $f_{LE} < 1$ along with a force-constant reduction counter $I_{\mathcal{R}}$ progressively increasing with time (the choice $f_{LE} = 1$ switches off the force-reduction procedure). In the B&S − LEUS algorithm, the force-reduction procedure is associated with a region $\mathcal{R}$ within the active subspace, defined by a specific collection of grid points. The reduction counter $I_{\mathcal{R}}$ is propagated in time according to the following procedure. $I_{\mathcal{R}}(t)$ as well as an auxiliary counter $N_c(t)$ are set to 0 at $t = 0$. An auxiliary memory $\boldsymbol{A}(t)$ is also set to $\mathbf{0}$ at $t = 0$ and propagated in time according to the equation

$$A_{m,i}(t + \Delta t) = A_{m,i}(t) + w_m(\boldsymbol{Q})h_{m,i}(\boldsymbol{Q}) \ . \tag{9.167}$$

When $A_{m,i}(t)$ exceeds a specified local visiting cutoff γ_{LE} for all grid points $(m, i) \in \mathcal{R}$, the auxiliary counter is increased by one and the auxiliary memory reset to zero. When the auxiliary counter exceeds a global visiting cutoff n_{LE}, $I_{\mathcal{R}}$ is increased by one and the auxiliary counter reset to zero. Two possible (reasonable) choices for $\mathcal{R}$ are either: (i) the $i = 0$ (central) grid points of all centered volumes k ($k = 1..K$), a choice that will be noted $\mathcal{R} = \mathcal{C}$; (ii) all grid points i of all objects m ($m = 1..M$), a choice that will be referred to as $\mathcal{R} = \mathcal{A}$. Possible (reasonable) choices for the parameters γ_{LE} and n_{LE} are 1.0 and 2, respectively. The reasoning behind the present force-constant reduction scheme (assuming $\gamma_{LE} = 1.0$ and $n_{LE} = 2$) is that when all grid points of $\mathcal{R}$ have undergone an "effective" number of visits (auxiliary memory, *i.e.* based on the w_m weights) of one, it is still possible that the "flattened" free-energy hypersurface retains an overall "slope". However, when all these points have undergone an "effective" number of visits of one for the second time, even the points that were "uphill" have been revisited. When this condition is met, it becomes advantageous to reduce the build-up rate by incrementing $I_{\mathcal{R}}$, which in effect scales this rate by a factor f_{LE}.

Finally, the constant $k^{(le)}$ in Equation Eq. 9.162 represents the basic force-constant increment (units of energy) and determines the initial rate of the build-up. Note that the above force-reduction procedure also presents the advantage of permitting a convergence assessment of the build-up phase, by monitoring the time evolution of $I_{\mathcal{R}}$. The build-up phase can, for example, be terminated whenever $I_{\mathcal{R}}$ reaches a threshold value $I_{\mathcal{R}}^{max}$. In this case, the procedure guarantees that all grid points of $I_{\mathcal{R}}$ have undergone an "effective" number of visits of at least $n_{LE}\gamma_{LE}I_{\mathcal{R}}^{max}$, while the energetic resolution of the biasing potential energy term is of the order of $f_{LE}^{I_{\mathcal{R}}^{max}} k^{(le)}$. Alternatively, the termination may be based on the time interval separating successive incrementations of $I_{\mathcal{R}}$. In the initial stage of the build-up, the diffusion of the system within the active subspace will be accelerated (hill surfing). However, as the free-energy hypersurface becomes increasingly "flat" and the build-up rate is decreased, this diffusion will progressively slow down towards a "natural" regime (as determined by the physical system after removal of the free-energy bias). Thus, the force-reduction procedure could also be terminated when the interval separating successive increments of $I_{\mathcal{R}}$ has increased and leveled off to an approximately constant time.

6. US sampling phase to generate of a biased ensemble of configurations, using the biasing potential energy term pre-optimized during the LE build-up phase. Owing to Eq. 9.159 the biased sampling during this phase should be approximately homogeneous (radially within the centered volumes, longitudinally along the paths) within the active subspace.
7. Reweighting and state assignment so as to calculate the relative free energies of the states in the physical ensemble. For each state k, the free energy can be written (for $k = 1...K$)

$$G_k = -\beta^{-1} \ln \left\langle \exp[\beta \mathcal{V}^{(bias)}(\boldsymbol{r}; \boldsymbol{M})] \right\rangle_{\boldsymbol{Q}(\boldsymbol{r}) \in \mathcal{S}'_k} + C_G \tag{9.168}$$

where C_G is an offset constant and $\langle .. \rangle_{\boldsymbol{Q}(\boldsymbol{r}) \in \mathcal{S}'_k}$ denotes ensemble (trajectory) averaging over the biased ensemble (sampling phase), restricted to conformations belonging to state k (see also Sec. 14.8 and Eq. 14.162). The symbol $\mathcal{S}'_k$ has been used rather than $\mathcal{S}_k$ to underline the fact that the regions

used to assign the states need not necessarily be exactly identical to the centered volumes involved in the construction of the biasing potential energy term.

CHAPTER 10

Constraints

10.1. Introduction

This chapter will discuss various kinds of hard geometric boundary conditions that are implemented in GROMOS. These may concern the position of atoms, the distance between pairs of atoms, the dihedral angle defined by four atoms or the overall translation and rotation of a set of atoms. The *application* of holonomic geometric *constraints* in molecular simulation may have the following *advantages*.

1. When constructing a molecular model in which certain degrees of freedom are ill-defined, one may optimize or sample these degrees of freedom under the constraint that the other degrees of freedom do not change.

2. If a degree of freedom is characterized by vibrational frequencies ν, for which

   $$h\nu \gg k_B T \tag{10.1}$$

   the motion will be of quantum-mechanical nature. In equilibrium at room temperature, condition Eq. 10.1 is fulfilled for e.g. the bond-stretching vibrations. Treating the bonds as constraints is probably a better approximation of their quantum behaviour than treating them as classical harmonic oscillators[92].

3. When the range of frequencies in a molecular simulation is very broad, this may cause the energy relaxation between high-frequency and low-frequency modes to be slow. If the forces for the different modes are computed with different accuracies, the different modes will suffer from different heating rates. When the latter are faster than the energy relaxation rate of the system, the system will not reach equilibrium, but remain in a stationary state. This problem can be solved by coupling the degrees of freedom of different frequency and heating rate to separate temperature baths (Sec. 12.2). However, the application of constraints generally reduces the range of frequencies in the system and thus alleviates this problem.

4. The application of constraints will generally save computing effort. The length of the time step Δt in a MD or SD simulation is limited by the highest frequency ν_{max} occurring in the molecular system of interest,

   $$\Delta t \gg \nu_{\mathrm{max}}^{-1}. \tag{10.2}$$

   By constraining the degrees of freedom with the highest frequencies the time step Δt can generally be lengthened, which reduces the computer time required for a simulation of a given length. For molecular systems one may think of reducing computational effort by constraining bond lengths or additionally bond angles, the latter only for molecules without internal torsional degrees of freedom.

5. A potential of mean force along a degree of freedom can be obtained by applying a constraint along the degree of freedom and performing a thermodynamic integration in which the derivative of the free energy with respect to a modification of the constraint is calculated from the constraint forces.

6. In order to minimize the amount of solvent needed to solvate a large molecular system, one may constrain the overall translation and rotation of a given set, allowing for a smaller computational box, but ensuring that the cutoff criterion (Eq. 4.26) will not be violated due to a rotation of the system within the box.

The application of *constrained dynamics* makes physical sense only when[47]

1. the frequencies of the frozen degrees of freedom are (considerably) higher than those of the remaining ones, thereby allowing a (considerable) increase of Δt, and when
2. the frozen degrees of freedom are only weakly coupled to the remaining ones, viz. when the motion of the molecules is not affected by application of the constraints[93], and when
3. metric tensor effects due to constraining the molecules to a hypersurface in configuration space, play a minor role.[94]

For biomolecules the effect of constraining bond lengths and bond angles has been evaluated[93]. It turns out that the application of *bond-length constraints* saves about a factor of 2 in computer time when hydrogen atoms are explicitly treated and a factor of 3 when the united-atom model is used[47]. Metric tensor corrections play no role when only bond-length constraints are applied[94]. The use of *bond-angle constraints* is not allowed in flexible (viz. with rotational internal degrees of freedom) molecules, since it affects the dynamics of such molecules considerably[93]. Moreover, metric tensor effects are non-negligible in this case[94]. The bond-angle degrees of freedom appear to be coupled to the other molecular degrees of freedom, such as the torsional-angle ones. However, for completely rigid molecules, that is, without internal degrees of freedom, metric tensor effects play no role, and the application of bond-length and bond-angle constraints is common practice.

The application of position constraints is described in Sec. 10.2. For application of distance constraints GROMOS uses the *SHAKE-method*[95] and its derivatives (viz. SETTLE[96], M-SHAKE[97], and LINCS[98], and FLEXSHAKE[99]), which will be described in Sec. 10.3. The application of bond-length constraints to a solute molecule is described in Sec. 10.4, and the use of constraints in rigid solvent molecules is discussed in Sec. 10.5. Dihedral-angle constraints are described in Sec. 10.6, and overall translational and rotational constraints in Sec. 10.7.

10.2. Position Constraints

In certain cases, it may be advantageous to prevent certain atoms from moving completely. GROMOS allows the user to apply position constraints to selected atoms. The selection of the atoms which are to be kept fixed at given reference positions during a simulation or energy minimization is done as for harmonic position restraining (Sec. 9.2), except that the switch $NTPOR = 3$. Solvent atom positions cannot be kept fixed.

Atoms can be kept at their initial positions $\mathbf{r}_i = \mathbf{r}_i^0$ by setting their velocities $\mathbf{v}_i$ and forces $\mathbf{f}_i$ equal to zero before every MD or EM integration (time) step. When applying constraints using the SHAKE method, see Sec. 10.3.1, the atomic position of an atom i involved in a constraint is changed with m_i^{-1} as weight factor. If such an atom is selected for position fixing, its mass is increased such that the atom position is effectively not changed when applying SHAKE. If two atoms i and j are involved in a distance (bond-length) constraint $r_{ij} = d_{ij}^0$ to be imposed by SHAKE ($NTC > 1$) and they are *both* selected as atoms to be kept fixed, the constraint d_{ij}^0 will be skipped when the constraint list is handled by SHAKE.

If one or more atoms of the molecular system are kept fixed, removal of centre of mass motion is disabled (even though $NSCM > 0$).

Fixing of atom positions should not be used in a free energy perturbation calculation.

When calculating a temperature, the total kinetic energy of the degrees of freedom for which the temperature is to be determined, is divided by the number of these degrees of freedom multiplied by $\frac{1}{2}k_B$(k_B = Boltzmann's constant). When $\mathcal{N}^{(pr)}$ atoms are kept fixed, the system contains $3\mathcal{N}^{(pr)}$ less degrees of freedom. If atoms are kept fixed, the choice of temperature bath coupling is restricted: i) solute internal/rotational degrees of freedom should be coupled to the same bath as solute translational degrees of freedom, ii) if the whole molecule is positionally constrained, temperature coupling makes no sense.

10.3. Constraints using the SHAKE method and its derivatives

10.3.1. Constraints using the SHAKE method. The SHAKE method[95] can be used to impose distance constraints onto the molecular system. Bond-length and bond-angle constraints can be put in the form of *distance constraints* between atoms k_1 and k_2,

$$\sigma_k(\mathbf{r}^N) \equiv r_{k_1k_2}^2 - \left(d_{k_1k_2}^0\right)^2 = 0 \quad k = 1, 2, ..., N^{(c)} \tag{10.3}$$

where $k \equiv (k_1,k_2)$, the constraint distance is given by $d^0_{k_1k_2}$ and the actual distance between atoms k_1 and k_2 by $r_{k_1k_2}$. The equations of motion Eqs. 2.8, 2.9, 2.10 and 2.12 (Newtonian equations of motion) or 2.13 (Langevin equations of motion) have to be integrated while satisfying conditions Eq. 10.3. This can be accomplished by applying *Lagrange's* method of undetermined *multipliers*. A zero term, expression Eq. 10.3, is added to the potential energy function $\mathcal{V}(\mathbf{r})$ in Eq. 2.10, which then yields the equations of motion (Newton)

$$m_i \frac{d^2\mathbf{r}_i(t)}{dt^2} = -\frac{\partial}{\partial \mathbf{r}_i}\left[\mathcal{V}(\mathbf{r}) + \sum_{k=1}^{N^{(c)}} l_k(t)\sigma_k(\mathbf{r})\right]. \tag{10.4}$$

The time-dependent multipliers $l_k(t)$ are to be determined such that the conditions Eq. 10.3 are satisfied. The first term on the right hand side of Eq. 10.4 represents the *unconstrained force* $\mathbf{f}^{uc}_i(t)$ derived from the interaction function, and the second term represents the yet unknown *constraint force*

$$\mathbf{f}^{(c)}_i(t) = -\sum_{k=1}^{N^{(c)}} l_k(t)\frac{\partial \sigma_k(\mathbf{r}(t))}{\partial \mathbf{r}_i(t)} \tag{10.5}$$

which compensates the components of $\mathbf{f}^{uc}_i(t)$ that act along the directions of the constraints.

In the leap-frog MD or SD algorithm, which is used in GROMOS, solving for $l_k(t)$ is done as follows. The leap-frog equation (see Sec. 12.1) for the atomic positions with the unconstrained forces gives the unconstrained positions at time $t + \Delta t$,

$$\mathbf{r}^{uc}_i(t+\Delta t) = \mathbf{r}_i(t) + \mathbf{v}_i(t-\Delta t/2)\Delta t + m_i^{-1}\mathbf{f}^{uc}_i(t)(\Delta t)^2 \tag{10.6}$$

Since the constrained positions at $t + \Delta t$,

$$\mathbf{r}_i(t+\Delta t) = \mathbf{r}^{uc}_i(t+\Delta t) + m_i^{-1}\mathbf{f}^{(c)}{}_i(t)(\Delta t)^2 \tag{10.7}$$

must satisfy the constraint equation Eq. 10.3, we find

$$\left(\left[\, \mathbf{r}^{uc}_{k_1}(t+\Delta t) + m_{k_1}^{-1}\mathbf{f}^{(c)}_{k_1}(t)(\Delta t)^2 - \mathbf{r}^{uc}_{k_2}(t+\Delta t) - m_{k_2}^{-1}\mathbf{f}^{(c)}_{k_2}(t)(\Delta t)^2\right]\right)^2$$

$$-\left(d^0_{k_1k_2}\right)^2 = 0. \qquad with\ k = 1,2,...,N^{(c)} \tag{10.8}$$

Substituting

$$\mathbf{f}^{(c)}_i(t) = -2\sum_{k=1}^{N^{(c)}} l_k(t)(\delta_{ik_1} - \delta_{ik_2})\mathbf{r}_{k_1k_2}(t) \tag{10.9}$$

into Eq. 10.8 we find

$$\left[\, \mathbf{r}^{uc}_{k_1k_2}(t+\Delta t) - 2l_k(t)(m_{k_1}^{-1} + m_{k_2}^{-1})\mathbf{r}_{k_1k_2}(t)(\Delta t)^2\right]^2 - \left(d^0_{k_1k_2}\right)^2 = 0 \qquad k = 1,2,...,N^{(c)} \tag{10.10}$$

which is a set of $N^{(c)}$ quadratic equations from which the $N^{(c)}$ multipliers $l_k(t)$ are to be solved and used to obtain the constrained positions $\mathbf{r}$ $(t + \Delta t)$ through Eqs. 10.7 and 10.9. In the SHAKE method, the equations Eq. 10.10 are linearized by neglecting the terms quadratic in $l_k(t)$, which yields

$$l_k(t) = \frac{\left(d^0_{k_1k_2}\right)^2 - (\mathbf{r}^{uc}_{k_1k_2}(t+\Delta t))^2}{-4(\Delta t)^2(m_{k_1}^{-1} + m_{k_2}^{-1})(\mathbf{r}_{k_1k_2}(t)\cdot\mathbf{r}^{uc}_{k_1k_2}(t+\Delta t))} \tag{10.11}$$

Since the atoms may be involved in more than one constraint, the set of equations Eq. 10.10 is solved iteratively, where the corrections to the unconstrained positions are given by

$$\Delta\mathbf{r}^{uc}_{k_1}(t+\Delta t) = -2(\Delta t)^2 m_{k_1}^{-1} l_k(t)\mathbf{r}_{k_1k_2}(t)$$

$$= m_{k_1}^{-1} g_k(t)\mathbf{r}_{k_1k_2}(t) \tag{10.12}$$

and

$$\Delta\mathbf{r}^{uc}_{k_2}(t+\Delta t) = +2(\Delta t)^2 m_{k_2}^{-1} l_k(t)\mathbf{r}_{k_1k_2}(t)$$

$$= -m_{k_2}^{-1} g_k(t)\mathbf{r}_{k_1k_2}(t) \tag{10.13}$$

This implies that corrections due to the distance constraint $d^0_{k_1k_2}$ to the positions of atoms k_1 and k_2 are applied in the direction of the vector $\mathbf{r}_{k_1k_2}$, and are in opposite direction, weighted by the inverse mass of atoms k_1 and k_2. This is illustrated in Fig. 10.1. The iterations over all $N^{(c)}$ constraints in SHAKE are terminated,

1. if all $N^{(c)}$ distance constraints are satisfied within a given relative tolerance *tol* (TOL), or
2. if an excessive (1000) number of iterations is required, or
3. if the positional shift in the unconstrained step, $\mathbf{r}^{uc}_{k1}$ - $\mathbf{r}_{k_1}$ or $\mathbf{r}^{uc}_{k_2}$ - $\mathbf{r}_{k_2}$ is so big that no corrections (Eq. 10.12, Eq. 10.13) along $\mathbf{r}_{k_1k_2}$ can be found that will produce a distance $d^0_{k_1k_2}$ between the corrected positions of atoms k_1 and k_2 , see Fig. 10.2.

The *application* of the procedure *SHAKE* will be denoted by

$$SHAKE\ (\mathbf{r}(t); \mathbf{r^{uc}}(t+\Delta t); \mathbf{r}(t+\Delta t)). \tag{10.14}$$

This means that the positions $\mathbf{r}^{uc}(t+\Delta t)$ that result from the non-constrained time step, will be reset to give the constrained positions $\mathbf{r}(t+\Delta t)$. The direction of the correction vectors is determined by the *reference positions* $\mathbf{r}(t)$, that is, for each individual distance constraint involving atom k_1 and k_2 , the correction vector is parallel to the vector $\mathbf{r}_{k_1k_2}(t)$ of the reference configuration.

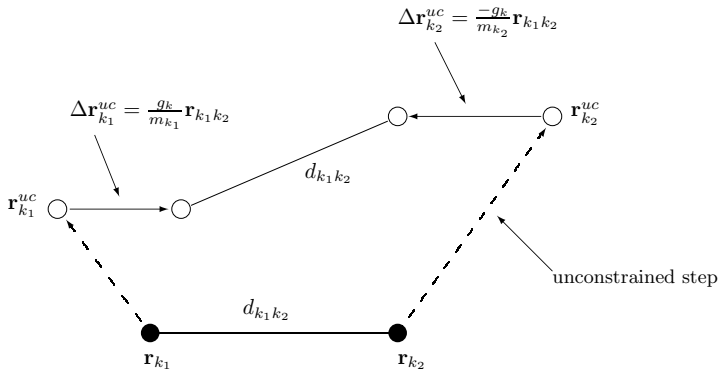

FIGURE 10.1. Positional corrections $\Delta\mathbf{r^{uc}}$ induced by SHAKE.

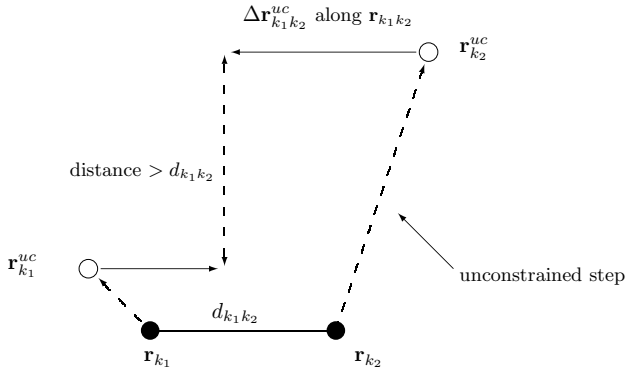

FIGURE 10.2. Situation in which SHAKE fails due to a too large unconstrained step.

When using SHAKE in combination with the GROMOS force field the *geometric tolerance* (TOL) should be chosen such that the noise in the simulation due to SHAKE is much smaller than that due to other sources, such as the application of a nonbonded interaction cutoff radius, etc. When applying energy minimization

(EM), we choose TOL = 10^{-3}, whereas in MD a value of at least TOL = 10^{-4} is used, based on the observation that MD is more sensitive to the accumulation of errors when moving through configuration space.

10.3.2. Constraints using the SETTLE method. The time derivatives of Eq. 10.3 give constraints on the velocities,

$$\mathbf{r}_{ij} \cdot \mathbf{v}_{ij} \quad = \quad 0 \tag{10.15}$$

This suggests that the component of the relative velocity along the bond should be zero. This constraint can be applied to both the position constraint, similar to the SHAKE method, and the velocity constraint, similar to the RATTLE method.

In the SETTLE method, the determination of $\mathbf{r}_i(t_0 + \delta t)$ is through the use of quasi-Euler angles thus the explicit calculation of constraint forces is avoided.

Taking a rigid water molecule as an example, a triangle ABC is defined with the oxygen and the two hydrogen atoms corresponding to A, B, and C respectively. $\Delta A_0 B_0 C_0$, $\Delta A_1 B_1 C_1$, and $\Delta A_3 B_3 C_3$ are the triangles at time t_0, $t_0 + \delta t$ in the absence of constraints, and $t_0 + \delta t$ with constraints. Ideally, triangles $\Delta A_0 B_0 C_0$ and $\Delta A_3 B_3 C_3$ should overlap each other after proper rotation (about the y' axis by ψ ($-\pi/2 \leq \psi \leq \pi/2$, about the x' axis by ϕ ($-\pi < \phi \leq \pi$) and about the z' axis by θ ($-\pi < \phi \leq \pi$)), assuming zero centre of mass motion.

By introducing an orthogonal coordinate system $x'y'z'$ which the origin coincides with the center of mass d_0 and the $x'y'$ plane is parallel to the plane of $\Delta A_0 B_0 C_0$, the angles ψ, ϕ are determined uniquely from $\Delta A_1 B_1 C_1$. The angle θ can then be calculated analytically by using the condition that constraint forces directed along the bond at time t_0 are of equal magnitudes and opposite orientations.

In the case of velocity constraints, the solution of the constrained velocity is

$$\mathbf{v}_i(t_0 + \delta t) \quad = \quad \mathbf{v}_i^{uc}(t_0 + \delta t) + \delta \mathbf{v}_i^0(t_0 + \delta t) \tag{10.16}$$

where $\mathbf{v}_i^{uc}(t_0 + \delta t)$ is the velocity after an unconstraint step (δt) and $\delta \mathbf{v}_i(t_0 + \delta t)$ is the correction velocity necessary to satisfy the constraints,

$$\begin{aligned} \delta \mathbf{v}_i(t_0 + \delta t) &= 1/2 \cdot \delta t / m_i \cdot \sum \mathbf{g}_{ij}(t_0 + \delta t) \\ &= 1/2 \cdot \delta t / m_i \cdot \sum l_{ij}(t_0 + \delta t) \mathbf{r}_{ij}(t_0 + \delta t). \end{aligned} \tag{10.17}$$

where the Lagrangian multipliers, $l_{ij}(t_0)$, ($l_{ij} = l_{ji}$) are chosen so that the constraint Eq. 10.3 are satisfied at time $t_0 + \delta t$.

A physical picture of this is that constraint forces $[\mathbf{f}^{(c)}{}_{ij}(t_0)]$ of equal magnitudes and opposite orientations are applied to the atoms i and j and are directed along the bond vectors $[\mathbf{r}_{ij}(t_0)]$ at time t_0. In the conventional method a set of quadratic equations for l_{ij} is obtained by substitution of Eq. 10.16 and Eq. 10.17 into Eq. 10.15. The solution to the quadratic equations is given by first solving them in their linear form and subsequently iterating them until all the constraints are fulfilled to within an acceptable tolerance. The linear equations can be solved by either matrix inversion or by the SHAKE method.

The constrained velocities at time $t_0 + \delta t$ of the three vertices are:

$$\begin{aligned} \mathbf{v}_A(t_0 + \delta t) \quad = \quad & \mathbf{v}_A^{uc}(t_0 + \delta t) + \delta t / 2 m_a \cdot (\tau_{AB}(t_0 + \delta t) \\ & - \tau_{CA}(t_0 + \delta t)) \end{aligned} \tag{10.18}$$

where τ_{AB} and τ_{CA} are the Lagrangian multipliers.

According to the constraint in Eq. 10.15,

$$\mathbf{r}_{AB} \cdot \mathbf{v}_{AB} = \mathbf{r}_{AB} \cdot (\mathbf{v}_B - \mathbf{v}_A) \quad = \quad 0 \tag{10.19}$$

the rearrangement of Eq. 10.19 gives

$$\begin{aligned} & \delta t (m_a + m_b) \tau_{AB} + \delta t \cdot m_a \tau_{BC} \cdot cos\mathbf{B} + \delta t \cdot m_b \tau_{CA} \cdot cos\mathbf{A} \\ & \qquad = 2 m_a m_b \hat{\mathbf{e}}_{AB} \cdot \mathbf{v}_{AB}^{uc} \end{aligned} \tag{10.20}$$

where $cosA$ and $cosB$ are cosines of the apex angles of A and B, and $\mathbf{e}_{AB}$ is the unit vector of $\mathbf{r}_{AB}$.

Similarly,

$$\delta t(m_b + m_c)\tau_{BC} + \delta t \cdot m_b\tau_{CA}cos\mathbf{C} + \delta t \cdot m_c\tau_{AB}cos\mathbf{B} = 2m_b m_c \mathbf{e}_{BC} \cdot \mathbf{v}^{uc}_{BC} \tag{10.21}$$

$$\delta t(m_c + m_a)\tau_{CA} + \delta t \cdot m_c\tau_{AB}cos\mathbf{A} + \delta t \cdot m_a\tau_{BC}cos\mathbf{C} = 2m_c m_a \mathbf{e}_{CA} \cdot \mathbf{v}^{uc}_{CA} \tag{10.22}$$

These equations are simultaneous linear equations with respect to the variables $\tau_{AB}, \tau_{BC}, \tau_{CA}$, and they can be solved by use of Cramer's rule. The $\tau_{AB}, \tau_{BC}, \tau_{CA}$ can then be used to calculate the constrained velocities.

10.3.3. Constraints using the LINCS method. The LINear Constraint Solver (LINCS) method was developed for the treatment of bond constraints by means of two steps of projections:

1. project the new bonds onto the old directions of the bonds;
2. correction for rotational lengthening.

The equation of motion with constraints Eq. 10.4 can be rewritten as:

$$\text{-}\underline{\mathbf{m}}\frac{d^2\mathbf{r}}{dt^2} + \mathbf{B}^T\mathbf{l} + \mathbf{f}^{uc} = 0 \tag{10.23}$$

where $\mathbf{B}$ is a $K \times 3N$ matrix containing the directions of the constraints, and defined by

$$\mathbf{B}_{ki} = \frac{\partial \sigma_k}{\partial r_i} \tag{10.24}$$

Since

$$\frac{d^2\sigma_k}{dt^2} = \mathbf{B}\frac{d^2\mathbf{r}}{dt^2} + \frac{d\mathbf{B}}{dt}\frac{d\mathbf{r}}{dt} = 0 \tag{10.25}$$

The equation of motion Eq. 10.23 can be rewritten as

$$\frac{d^2\mathbf{r}}{dt^2} = (\mathbf{I} \text{ - } \mathbf{TB})\underline{\mathbf{m}}^{-1}\mathbf{f}^{uc} \text{- } \mathbf{T}\frac{d\mathbf{B}}{dt}\frac{d\mathbf{r}}{dt} \tag{10.26}$$

where $\mathbf{T} = \underline{\mathbf{m}}^{-1}B^T(B\underline{\mathbf{m}}{-}1B^T)^{-1}$ is a $3N \times K$ matrix that transforms motions in Cartesian coordinates, without changing the equations of motion of the unconstrained coordinates. **I - TB** is a projection matrix that sets the constrained coordinates to zero, $\mathbf{B}\underline{\mathbf{m}}^{-1}\mathbf{f}^{uc}$ is a $\mathbf{K}$ vector of second derivatives of the bond lengths in the direction of the bonds. The last term represents centripetal forces caused by rotating bonds.

In a leap-frog algorithm, the constrained positions at time step $n+1$ (in other words, at time $(n+1)\Delta t$),

$$\begin{aligned}
\mathbf{r}_{n+1} &= (\mathbf{I} - \mathbf{T_n}\mathbf{B_n})(\mathbf{r}_n + \Delta t\mathbf{v}_{n-\frac{1}{2}} + \Delta t^2\underline{\mathbf{m}}^{-1}\mathbf{f}^{uc}_n) + \mathbf{T}_n\mathbf{d^0} \\
&= (\mathbf{I} - \mathbf{T_n}\mathbf{B_n})\mathbf{r}^{uc}_{n+1} + \mathbf{T}_n\mathbf{d^0} \\
&= \mathbf{r}^{uc}_{n+1} - \underline{\mathbf{m}}^{-1}\mathbf{B}_n(\mathbf{B}_n\underline{\mathbf{m}}^{-1}\mathbf{B}_n^T)^{-1}(\mathbf{B}\cdot\mathbf{r}^{uc}_{n+1} - \mathbf{d^0})
\end{aligned} \tag{10.27}$$

The matrix $(\mathbf{B}_n\ \underline{\mathbf{m}}^{-1}\ \mathbf{B}_n^T)$ has diagonal elements of $1/m_{k_1} + 1/m_{k_2}$, and non-zero off-diagonal elements of $cos\phi/m_c$ when two bonds are connected by the atom with the mass of m_c and a bond angle of ϕ. Its inversion can be transformed to the following form:

$$\begin{aligned}
(\mathbf{B}_n\underline{\mathbf{m}}^{-1}\mathbf{B}_n^T)^{-1} &= \mathbf{S}\mathbf{S}^{-1}(\mathbf{B}_n\underline{\mathbf{m}}^{-1}\mathbf{B}_n^T)^{-1}\mathbf{S}^{-1}\mathbf{S} \\
&= \mathbf{S}(\mathbf{I} - \mathbf{A_n})^{-1}\mathbf{S}
\end{aligned} \tag{10.28}$$

where $\mathbf{S}$ is a $K \times K$ matrix,

$$\mathbf{S} = Diag(\sqrt{\frac{1}{m_{1_1}} + \frac{1}{m_{1_2}}}, \ldots, \sqrt{\frac{1}{m_{k_1}} + \frac{1}{m_{k_2}}}) \tag{10.29}$$

Since $\mathbf{A}_n$ is symmetric and sparse and has zeros on the diagonal, the inversion of the matrix ($\mathbf{I}$ - $\mathbf{A}_n$) can be solved efficiently through an expansion,

$$(\mathbf{I} - \mathbf{A_n})^{-1} \quad = \quad \mathbf{I} + \mathbf{A}_n + \mathbf{A}_n^2 + \mathbf{A}_n^3 + \ldots \tag{10.30}$$

10.3.4. Constraints using the M-SHAKE method. In the SHAKE procedure, two approximations are made to solve a system of $N^{(c)}$ quadratic equations for the Lagrange multipliers:

1. the system of equations is linearized by neglecting any term quadratic in the multipliers,
2. the multipliers are determined independently in sequence by omitting the coupling between distance constraints involving a common atom.

As a consequence of these approximations, the procedure must be performed iteratively until satisfaction of all constraints within a specified tolerance. Note, however, that the second approximation can easily be removed by a M-SHAKE procedure (Matrix-inversion SHAKE). In this procedure, the linearized system of coupled equations is solved exactly through the inversion of an $N^{(c)} \times N^{(c)}$ matrix.

According to Eq. 10.10, a set of $N^{(c)}$ quadratic equations is obtained and to be solved for the Lagrange multipliers $l_k(t)$

$$\begin{aligned} &\{\mathbf{r}^{uc}_{k_1k_2}(t+\Delta t) - 2(\Delta t)^2 \sum_{k'=1}^{N^{(c)}} l_{k'}(t)\mathbf{r}_{k'_1k'_2}(t) \\ &\times[m_{k_1}^{-1}(\delta_{k_1,k'_1} - \delta_{k_1,k'_2}) + m_{k_2}^{-1}(\delta_{k_2,k'_2} - \delta_{k_2,k'_1})]\}^2 \\ &\quad -(d^0_{k_1k_2})^2 = 0 \qquad k = 1, 2, ..., N^{(c)} \end{aligned} \tag{10.31}$$

After linearization, Eq. 10.31 is rewritten in the matrix form

$$\mathbf{Al} \quad = \quad \mathbf{c} \tag{10.32}$$

where l is an $N^{(c)}$-dimensional vector containing the Lagrange multipliers, and the elements of the vector $\mathbf{c}$ are given by:

$$c_k \quad = \quad \frac{[\mathbf{r}^{uc}_{k_1k_2}(t+\Delta t)]^2 - (d^0_{k_1k_2})^2}{4(\Delta t)^2} \tag{10.33}$$

and the elements of the matrix $\mathbf{A}$

$$\begin{aligned} A_{kk'} = &[m_{k_1}^{-1}(\delta_{k_1,k'_1} - \delta_{k_1,k'_2}) + m_{k_2}^{-1}(\delta_{k_2,k'_2} - \delta_{k_2,k'_1})] \\ &\times \mathbf{r}_{k'_1k'_2}(t)\mathbf{r}^{uc}_{k_1k_2}(t+\Delta t). \end{aligned} \tag{10.34}$$

It is easily seen that the diagonal elements A_{kk} characterize the force directly due to constraint k, whereas the off-diagonal elements $A_{kk'}(k' \neq k)$ account for the effect along a constraint k of the forces due to a constraint k'. These off-diagonal elements are neglected in SHAKE.

In M-SHAKE, Eq. 10.32 is solved directly by matrix inversion with the following methods:

1. Explicit (hard-coded) calculation of $\mathbf{A}^{-1}$. This was only done for water ($N^{(c)} = 3$), because the expressions quickly become very complex for larger matrices.
2. Use of Cramer's rule. In this method, each component of the vector l is calculated as $l_k = |A_k|/|A_j|$, where $\mathbf{A}_k$ is the determinant obtained by replacing the kth column of $\mathbf{A}$ by the vector $\mathbf{c}$. Here again, the expressions quickly become untractable for larger matrices and the method was only tested for water.
3. Use of the *LU*-factorization method. In this method, a square, non-singular matrix $\mathbf{A}$ is factorized into a lower triangular matrix $\mathbf{L}$ and an upper triangular matrix $\mathbf{U}$, such that $\mathbf{LU} = \mathbf{A}$. The computational cost of the factorization scales as $N^{(c)3}$, whereas the inversion of the triangular matrices only scales as $N^{(c)2}$.
4. Use of the $\mathbf{LDL}^t$-factorization method. In this case, the matrix $\mathbf{A}$ is approximated by a symmetric matrix **A'** with identical diagonal elements, but in which any occurrence of $\mathbf{r}^{uc}_{k_1k_2}(t+\Delta t)$ in the off-diagonal elements is replaced by $\mathbf{r}_{k_1k_2}(t)$. The symmetric matrix **A'** is then factorized as $\mathbf{LDL}^t = \mathbf{A}$, where $\mathbf{D}$ is a diagonal matrix, $\mathbf{L}$ a lower triangular matrix, and the t superscript denotes the

transpose. This factorization method also scales as $N^{(c)3}$, but is about twice less expensive in terms of floating-point operations compared to LU-factorization.

10.3.5. Constraints using the FLEXSHAKE method. In the FLEXSHAKE method, the ideal constrained bond lengths for every constraint are recalculated at each time step, and the total energy U^{uc} and a hypothetic harmonic bond-stretching energy $U^c = \sum_{k=1}^{N^{(c)}} U_k^c$ is minimized with respect to the bond or constraint lengths d_k^0 at each time step[99].

The Hamiltonian for a flexible constrained system is:

$$\frac{d}{dt}\boldsymbol{q} = \underline{\mathbf{m}}^{-1}\boldsymbol{p} \tag{10.35}$$

$$\frac{d}{dt}\boldsymbol{q} = -\nabla_{\boldsymbol{q}} U^c(\boldsymbol{q}) - \nabla_{\boldsymbol{q}} \sum_{k=1}^{N^{(c)}} l_k(t)\sigma_k'(\boldsymbol{q},t) \tag{10.36}$$

$$\sigma_k'(\boldsymbol{q},t) = |\mathbf{r}_k|^2 - \left(d_k^0\right)^2(t), k = 1, 2, \cdots, N^{(c)} \tag{10.37}$$

The constrained forces are given by

$$\begin{aligned}\mathbf{f}_i^{(c)}(t) &= -\nabla_{\boldsymbol{q}} \sum_{k=1}^{N^{(c)}} l_k(t)\sigma_k'(\boldsymbol{q},t) \\ &= -2\sum_{k=1}^{N^{(c)}} l_k[\mathbf{r}_k(t)(\delta_{ik_1} - \delta_{ik_2}) - d_k^0(t+\Delta t)\nabla_{\boldsymbol{q}_i} d_k^0(t+\Delta t)]\end{aligned} \tag{10.38}$$

The new constrained positions are given by

$$\begin{aligned}\mathbf{r}_i(t+\Delta t) &= \mathbf{r}_i^{uc}(t+\Delta t) - \frac{2(\Delta t)^2}{m_i}\sum_{k=1}^{N^{(c)}} l_k[(\delta_{ik_1} - \delta_{ik_2})\mathbf{r}_k(t) \\ &\quad -d_k^0(t+\Delta t)\nabla_{\boldsymbol{q}_i} d_k^0(t+\Delta t)].\end{aligned} \tag{10.39}$$

Inserting Eq. 10.39 into Eq. 10.37 and neglecting the second order terms of l_k gives the Lagrange multipliers l_k

$$\begin{aligned}l_k(t) &= \frac{d_k^0(t+\Delta t)^2 - (\mathbf{r}_k^{uc}(t+\Delta t))^2}{-4(\Delta t)^2 \cdot \mathbf{r}_k^{uc}(t+\Delta t)} \\ &\quad \cdot \frac{1}{(m_{k_1}^{-1} + m_{k_2}^{-1})\mathbf{r}_k(t) - d_k^0(t+\Delta t)[m_{k_1}^{-1}\nabla_{\boldsymbol{q}_{k_1}} d_k^0(t+\Delta t) - m_{k_2}^{-1}\nabla_{\boldsymbol{q}_{k_2}} d_k^0(t+\Delta t)]}\end{aligned} \tag{10.40}$$

The $N^{(c)}$ equations can be solved iteratively using the SHAKE method, and the l_k can be then used to calculate the new positions and constrained forces.

10.3.6. Constrained positions. When a given molecular configuration $\mathbf{r}^0$ does not satisfy a set of constraints, SHAKE or its derived methods can be used to obtain a *constrained configuration* $\mathbf{r}$, viz. that satisfies the constraints. This is done by using $\mathbf{r}^0$ as reference positions when using, e.g. SHAKE, with $\mathbf{r}^{uc} = \mathbf{r}^0$ as initial configuration:

$$SHAKE(\mathbf{r}^0; \mathbf{r^{uc}}; \mathbf{r}) \tag{10.41}$$

10.3.7. Constrained velocities. Since the unconstrained forces $\mathbf{f}^{uc}$ in Eq. 10.4 will generally contain components along the constraint directions, this will also be true for the velocities obtained from the leap-frog equation.

$$\mathbf{v}_i(t+\Delta t/2) = \mathbf{v}_i(t-\Delta t/2) + m_i^{-1}\mathbf{f}_i^{uc}(t)\Delta t, \tag{10.42}$$

When applying constraints these components have to be removed, that is, the velocities must be shaken. In the leap-frog algorithm the *constrained velocities* are simply determined by inverting the leap-frog equation for the positions

$$\mathbf{r}_i(t+\Delta t) = \mathbf{r}_i(t) + \mathbf{v}_i(t+\Delta t/2)\Delta t \tag{10.43}$$

and using constrained positions at times t and $t + \Delta t$,

$$\mathbf{v}_i(t + \Delta t/2) = [\mathbf{r}_i(t + \Delta t) - \mathbf{r}_i(t)]/\Delta t \tag{10.44}$$

If unconstrained positions $\mathbf{r}(t)$ and velocities $\mathbf{v}(t)$ are given at the same time t, the positions are made to satisfy the constraints by applying SHAKE as specified in Sec. 10.3.1. Using the constrained positions $\mathbf{r}(t)$ the velocities are constrained in three steps:

1. Compute
$$\mathbf{r}_i^{uc}(t + \Delta t) = \mathbf{r}_i(t) + \mathbf{v}_i(t + \frac{\Delta t}{2})\Delta t \tag{10.45}$$
2. Perform
$$SHAKE(\mathbf{r}(t); \mathbf{r^{uc}}(t + \Delta t); \mathbf{r}(t + \Delta t)) \tag{10.46}$$
3. Obtain the *shaken or constrained velocities* from
$$\mathbf{v}_i(t + \frac{\Delta t}{2}) = [\mathbf{r}_i(t + \Delta t) - \mathbf{r}_i(t)]/\Delta t \tag{10.47}$$

10.3.8. Constrained forces. From Eq. 10.7 it is clear that the *constraint forces* $\mathbf{f}_i^{(c)}(t)$ can be derived by saving the unconstrained configuration $\mathbf{r}^{uc}(t)$ before application of SHAKE and using

$$\mathbf{f}_i^{(c)}(t) \quad = \quad [\mathbf{r}_i(t + \Delta t) - \mathbf{r}_i^{uc}(t + \Delta t)]m_i/(\Delta t)^2 \tag{10.48}$$

We note that the *constrained forces*, that is, the forces that contain no components along the constraints, are given by $\mathbf{f}_i^{uc}$+$\mathbf{f}_i^{(c)}$, since the procedure SHAKE yields a $\mathbf{f}_i^{(c)}$ which compensates the components of $\mathbf{f}_i^{uc}$ along the directions of the constraints.

10.4. Bond-length constraints in the solute

The "solute" part of a molecular topology contains two lists of covalent bonds, one of bonds involving hydrogen atoms, and one involving the other bonds. The two lists of covalent bonds can be used to specify the constraints that are imposed on the molecular system by SHAKE or its derived methods. In addition MD++ allows the user to specify a third list in the topology with selected bonds to be considered. The *switch NTC* in MD++ controls which lists of atom pairs are to be used for constraining. The switches NTF[1] and NTF[2] in the input block FORCE are used to skip the bond interaction terms in the interaction function Eq. 3.6 when the bond lengths are constrained. A sensible choice of the longest time step is:

1. 0.0005 ps when no constraints are used;
2. 0.001 ps when only bonds with hydrogen atoms are constrained;
3. 0.002 ps when all bonds are constrained.

The usage of the switches that control the constraint lists and methods are shown below:
MD++: blockname CONSTRAINT

- NTC: controls application of constraints to bonds
  - 0: no constraints are applied
  - 1: constraints are applied to solvent only
  - 2: constraints are applied to solvent and solute bonds involving hydrogen atoms
  - 3: constraints are applied to solvent and solute bonds
  - 4: constraints are applied to bonds specified in the CONSTRAINT block in topology only
- NTCP: controls the algorithms to apply solute constraints
  - shake(1): apply SHAKE for solute
  - lincs(2): apply LINCS for solute
  - flexshake(3): apply flexible SHAKE for solute
- NTCS: controls the algorithm to apply solvent constraints
  - shake(1): apply SHAKE for solvent
  - lincs(2): apply LINCS for solvent
  - flexshake(3): apply flexible SHAKE for solvent
  - settle(4): apply SETTLE for solvent
  - m_shake(5): apply M_SHAKE for solvent
  - gpu_shake(6): apply M_SHAKE for solvent using GPU

In an MD simulation the solute temperature T is determined by the total kinetic energy of the solute molecules, $\mathcal{K}$ (solutes), and the number of degrees of freedom of the solutes,

$$\mathcal{K}(solutes) = \sum_{\substack{i=1 \\ solutes}}^{\mathcal{N}_a} \tfrac{1}{2} m_i \mathbf{v}_i^2 = \tfrac{1}{2} \mathcal{N}_d(solutes) k_B T \tag{10.49}$$

where k_B is Boltzmann's constant ($k_B = 8.31441\ 10^{-3}$ kJ mol^{-1}K^{-1}) and the number of degrees of freedom of the solutes is denoted by

$$\mathcal{N}_d(solutes) \quad = \quad 3\mathcal{N}_a(solutes) - N^{(c)}(solutes) \tag{10.50}$$

Here the number of solute atoms is $\mathcal{N}_a$(solutes) and the number of solute constraints is $N^{(c)}$ (solutes). The latter is dependent on the value of switch NTC. In an MD simulation, the size of the solute kinetic energy $\mathcal{K}$ (*solute*) and the size and direction of the atomic velocities $\mathbf{v}_i$ will depend on the value of NTC, that is, whether solute constraints are applied or not. This means that if the value of NTC is changed in the course of a MD simulation the velocities have to be rescaled in order to let them correspond to the unchanged temperature T.

For example, an MD job with NTC=3 has produced a final configuration with velocities $\mathbf{v}_i$(NTC=3). If one would continue the simulation with NTC=1 so, if one would assume $\mathbf{v}_i$(NTC=1) = $\mathbf{v}_i$(NTC=3), the temperature T (NTC=1) would become approximately 2/3 T (NTC=3). This can be understood by taking Eq. 10.49 for NTC=1 and NTC=3 and using the equality of the velocities,

$$T(NTC = 1) \quad = \quad \frac{\mathcal{N}_d(solutes; NTC = 3)}{\mathcal{N}_d(solutes; NTC = 1)} \ \cdot \ T(NTC = 3) \tag{10.51}$$

Since in a linear molecule the number of covalent bonds is approximately equal to the number of atoms, one has T (NTC=1) = 2/3 T (NTC=3).

In order to avoid this effect, the *solute velocities should be rescaled upon changing NTC* from NTC to NTC' by a factor $\frac{\mathcal{N}_d(solutes;NTC')}{\mathcal{N}_d(solutes;NTC)}$.

If two atoms i and j are involved in a bond-length constraint $\mathbf{r}_{ij} = d_{ij}^0$ to be imposed by SHAKE (NTC>1) and they are both selected as atoms to be kept at fixed positions, the constraint d_{ij}^0 will be skipped when handling the set of constraints in SHAKE.

10.5. Bond-length and bond-angle constraints in solvent

In Chap. 4-3 it is discussed that solvent molecules of which the topological properties are contained in the "solvent" part of a molecular topology file, are subject to a number of restrictions. One of these is that *a solvent molecule is assumed to be rigid*. Its internal structure is maintained by the application of distance constraint forces between its atoms using SHAKE or its derived methods. It is called with the constraint lengths taken from the SOLVENTCONSTRAINT block in the molecular topology. For examples, see Chap. 3-4.

The solvent temperature is calculated from

$$\mathcal{K}(solvent) = \sum_{\substack{i=1 \\ solvent}}^{\mathcal{N}_a} \tfrac{1}{2} m_i \mathbf{v}_i^2 = \tfrac{1}{2} \mathcal{N}_d(solvent) k_B T \tag{10.52}$$

with

$$\mathcal{N}_d(solvent) = 3\mathcal{N}_a(solvent) - N^{(c)}(solvent) = 6 \tag{10.53}$$

10.6. Dihedral-angle constraints

GROMOS also allows for dihedral-angle constraints which may be used to evaluate a potential of mean force.[100] For dihedral-angle constraints, the derivation of the expressions for the constraint forces $\mathbf{f}^{(c)}$ follows the same lines as that for the distance constraints. However, due to the not very simple dependence of a dihedral angle $\varphi_n(\mathbf{r})$ upon the positions $\mathbf{r}_i, \mathbf{r}_j, \mathbf{r}_k$ and $\mathbf{r}_l$ of its four constituting atoms i, j, k and l (*i.e.* $i - j - k - l$), the formulae become much more complicated.

Following the definition in Eq. 5.19 we have

$$\varphi_n \doteq \text{sign}(\varphi_n) \ \arccos\left(\frac{\mathbf{r}_{m'j} \cdot \mathbf{r}_{n'k}}{r_{m'j} r_{n'k}}\right) \quad \text{with} \quad -\pi < \varphi_n \leq \pi \tag{10.54}$$

where

$$\mathbf{r}_{m'j} \equiv \mathbf{r}_{ij} \times \mathbf{r}_{kj}, \tag{10.55}$$

$$\mathbf{r}_{n'k} \equiv \mathbf{r}_{kj} \times \mathbf{r}_{kl}, \tag{10.56}$$

and

$$sign(\varphi_n) = sign(\mathbf{r}_{ij} \cdot \mathbf{r}_{n'k}), \tag{10.57}$$

following the IUPAC-IUB convention.[25]

Because of the occurrence of the arccos function in the definition of the dihedral angle φ_n the constraints are to be formulated in terms of $cos(\varphi_n)$. The occurrence of the square root functions in the distances $|\mathbf{r}_{m'j}|$ and $|\mathbf{r}_{n'k}|$ in the denominator of Eq. 10.54 suggests that the use of $cos^2(\varphi_n)$ will simplify the expressions. Thus, we consider a set of N_c dihedral-angle constraints

$$\sigma_n(\varphi_n(\mathbf{r}); \varphi_n^0(\lambda)) \equiv cos^2(\varphi_n(\mathbf{r})) - cos^2(\varphi_n^0(\lambda)) = 0, \quad n = 1, 2, .., N_c \tag{10.58}$$

where the angle $\varphi_n(\mathbf{r})$ is constrained to the λ-dependent value (see Chap. 14)

$$\varphi_n^0(\lambda) = (1-\lambda)\varphi_n^{0\,A} + \lambda\varphi_n^{0\,B}, \tag{10.59}$$

in which $\varphi_n^{0\,A}$ is the φ_n-value in state A and $\varphi_n^{0\,B}$ that in state B.

Newton's equations of motion for $\mathcal{N}_a$ atoms become

$$m_m \frac{d^2\mathbf{r}_i(t)}{\Delta t^2} = -\frac{\partial}{\partial \mathbf{r}_m}\left(\mathcal{V}^{(phys)}(\mathbf{r}) + \sum_{n=1}^{N_c} l_n(t)\sigma_n(\varphi_n(\mathbf{r}); \varphi_n^0(\lambda))\right), \quad m = 1, 2, .., N \tag{10.60}$$

where the Lagrange multipliers $l_k(t)$ are to be determined such that the condition given in Eq. 10.58 is satisfied. The second term on the right in Eq. 10.60 represents the (yet unknown) constraint forces,

$$\begin{aligned} \mathbf{f}_m^{(c)}(t) &= -\sum_{n=1}^{N_c} l_n(t)\frac{\partial\sigma_n(\varphi_n(\mathbf{r}); \varphi_n^0(\lambda))}{\partial \mathbf{r}_m} \\ &= +\sum_{n=1}^{N_c} l_n(t) 2cos(\varphi_n)sin(\varphi_n)\frac{\partial\varphi_n(\mathbf{r})}{\partial \mathbf{r}_m}. \end{aligned} \tag{10.61}$$

where $\frac{\partial\varphi_n}{\partial \mathbf{r}_m}$ is given by[101–103]

$$\begin{aligned} \frac{\partial\varphi_n(\mathbf{r})}{\partial \mathbf{r}_m} &= \delta_{mi}\frac{|\mathbf{r}_{kj}|}{|\mathbf{r}_{m'j}|^2}\mathbf{r}_{m'j} \\ &+\delta_{mj}\left[\left(\frac{\mathbf{r}_{ij}\cdot\mathbf{r}_{kj}}{|\mathbf{r}_{kj}|^2} - 1\right)\frac{|\mathbf{r}_{kj}|}{|\mathbf{r}_{m'j}|^2}\mathbf{r}_{m'j} + \frac{\mathbf{r}_{kl}\cdot\mathbf{r}_{kj}}{|\mathbf{r}_{kj}|^2}\frac{|\mathbf{r}_{kj}|}{|\mathbf{r}_{n'k}|^2}\mathbf{r}_{n'k}\right] \\ &-\delta_{mk}\left[\left(\frac{\mathbf{r}_{kl}\cdot\mathbf{r}_{kj}}{|\mathbf{r}_{kj}|^2} - 1\right)\frac{|\mathbf{r}_{kj}|}{|\mathbf{r}_{n'k}|^2}\mathbf{r}_{n'k} + \frac{\mathbf{r}_{ij}\cdot\mathbf{r}_{kj}}{|\mathbf{r}_{kj}|^2}\frac{|\mathbf{r}_{kj}|}{|\mathbf{r}_{m'j}|^2}\mathbf{r}_{m'j}\right] \\ &-\delta_{ml}\frac{|\mathbf{r}_{kj}|}{|\mathbf{r}_{n'k}|^2}\mathbf{r}_{n'k}. \end{aligned} \tag{10.62}$$

To shorten the expressions we denote the four terms in Eq. 10.62, apart from the Kronecker delta's, by $\mathbf{a}_i, \mathbf{a}_j, \mathbf{a}_k$, and $\mathbf{a}_l$, respectively. Then we have

$$\mathbf{f}^{(c)}{}_m(t) = \sum_{k=1}^{N_c} l_k(t) sin(2\varphi_n(t)\left[\delta_{mi}\mathbf{a}_i(t) + \delta_{mj}\mathbf{a}_j(t) + \delta_{mk}\mathbf{a}_k(t) + \delta_{ml}\mathbf{a}_l(t)\right]. \tag{10.63}$$

The leap-frog scheme yields the unconstrained positions $\mathbf{r}_m^{uc}(t_n+\delta t)$ from Eq. 10.6. The constrained positions $\mathbf{r}_m(t_n+\delta t)$ are related to the constraint forces (Eq. 10.63) through Eq. 10.7 and should satisfy the constraint Eq. 10.58,

$$cos^2(\varphi_n(\mathbf{r}(t_n+\delta t)) - cos^2(\varphi_n^0(\lambda)) = 0, \quad k = 1, 2, .., N_c, \tag{10.64}$$

or using Eq. 10.54,

$$\left[\frac{\mathbf{r}_{m'j}(t_n+\delta t)\cdot\mathbf{r}_{n'k}(t_n+\delta t)}{|\mathbf{r}_{m'j}(t_n+\delta t)||\mathbf{r}_{n'k}(t_n+\delta t)|}\right]^2 - cos^2(\varphi_n^0(\lambda)) = 0. \tag{10.65}$$

Since $\mathbf{r}_{m'j}(t_n+\delta t)$ and $\mathbf{r}_{n'k}(t_n+\delta t)$ are each quadratic in the Lagrange multipliers $l_k(t_n)$, both the numerator and the denominator of the left term in Eq. 10.65 contain powers of up to eight of the $l_k(t_n)$. Thus a set of

N_c equations consisting of terms containing up to powers of eight of the unknowns $l_k(t_n)$ is to be solved. As for the case of distance constraints this is achieved by linearizing the equations for each constraint, omitting the coupling between the different constraints (equations), and iterating through all *ncon* equations until the $l_k(t_n)$ converge to a consistent value.

Using Eqs. 10.7 and 10.63 we find for the k-th constraint

$$\begin{aligned}\mathbf{r}_{ij}(t_n+\delta t) &= \mathbf{r}^{uc}_{ij}(t_n+\delta t)\\ &\quad +l_k(t_n)sin(2\varphi_n(t_n))(\delta t)^2\left(m_i^{-1}\mathbf{a}_i(t_n)-m_j^{-1}\mathbf{a}_j(t_n)\right)\end{aligned} \tag{10.66}$$

and likewise for $\mathbf{r}_{kj}(t_n+\delta t)$ and $\mathbf{r}_{kl}(t_n+\delta t)$. Building the cross products in Eqs. 10.55 and 10.56 and linearizing the resulting expressions yields

$$\begin{aligned}\mathbf{r}_{m'j}(t_n+\delta t) &= \mathbf{r}^{uc}_{ij}(t_n+\delta t)\times\mathbf{r}^{uc}_{kj}(t_n+\delta t)\\ &\quad +l_k(t_n)sin(2\varphi_n(t_n))(\delta t)^2\\ &\quad \Big[\mathbf{r}^{uc}_{ij}(t_n+\delta t)\times\left(m_k^{-1}\mathbf{a}_k(t_n)-m_j^{-1}\mathbf{a}_j(t_n)\right)-\\ &\quad \mathbf{r}^{uc}_{kj}(t_n+\delta t)\times\left(m_i^{-1}\mathbf{a}_i(t_n)-m_j^{-1}\mathbf{a}_j(t_n)\right)\Big]\end{aligned} \tag{10.67}$$

or using a shorter notation $\mathbf{b}_{ijk}(t_n+\delta t)$ for the last factor

$$\begin{aligned}\mathbf{r}_{m'j}(t_n+\delta t) &= \mathbf{r}^{uc}_{ij}(t_n+\delta t)\times\mathbf{r}^{uc}_{kj}(t_n+\delta t)\\ &\quad +l_k(t_n)sin(2\varphi_n(t_n))(\delta t)^2\mathbf{b}_{ijk}(t_n,t_n+\delta t),\end{aligned} \tag{10.68}$$

and

$$\begin{aligned}\mathbf{r}_{n'k}(t_n+\delta t) &= \mathbf{r}^{uc}_{kj}(t_n+\delta t)\times\mathbf{r}^{uc}_{kl}(t_n+\delta t)\\ &\quad +l_k(t_n)sin(2\varphi_n(t_n))(\delta t)^2\\ &\quad \Big[\mathbf{r}^{uc}_{kj}(t_n+\delta t)\times\left(m_k^{-1}\mathbf{a}_k(t_n)-m_l^{-1}\mathbf{a}_l(t_n)\right)-\\ &\quad \mathbf{r}^{uc}_{kl}(t_n+\delta t)\times\left(m_k^{-1}\mathbf{a}_k(t_n)-m_j^{-1}\mathbf{a}_j(t_n)\right)\Big]\end{aligned} \tag{10.69}$$

or using the shorter notation

$$\begin{aligned}\mathbf{r}_{n'k}(t_n+\delta t) &= \mathbf{r}^{uc}_{kj}(t_n+\delta t)\times\mathbf{r}^{uc}_{kl}(t_n+\delta t)\\ &\quad +l_k(t_n)sin(2\varphi_n(t_n))(\delta t)^2\mathbf{b}_{jkl}(t_n,t_n+\delta t).\end{aligned} \tag{10.70}$$

The scalar product in the numerator of the first term in Eq. 10.65 becomes after linearization

$$\begin{aligned}\mathbf{r}_{m'j}(t_n+\delta t)\ \cdot\ &\mathbf{r}_{n'k}(t_n+\delta t)=\\ &\left(\mathbf{r}^{uc}_{ij}(t_n+\delta t)\times\mathbf{r}^{uc}_{kj}(t_n+\delta t)\right)\cdot\left(\mathbf{r}^{uc}_{kj}(t_n+\delta t)\times\mathbf{r}^{uc}_{kl}(t_n+\delta t)\right)\\ &+l_k(t_n)sin(2\varphi_n(t_n))(\delta t)^2\\ &\Big[\left(\mathbf{r}^{uc}_{ij}(t_n+\delta t)\times\mathbf{r}^{uc}_{kj}(t_n+\delta t)\right)\cdot\mathbf{b}_{jkl}(t_n,t_n+\delta t)+\\ &\left(\mathbf{r}^{uc}_{kj}(t_n+\delta t)\times\mathbf{r}^{uc}_{kl}(t_n+\delta t)\right)\cdot\mathbf{b}_{ijk}(t_n,t_n+\delta t)\Big]\end{aligned} \tag{10.71}$$

or in a shorter notation

$$\begin{aligned}&\mathbf{r}_{m'j}(t_n+\delta t)\cdot\mathbf{r}_{n'k}(t_n+\delta t)=c_{ijkl}(t_n+\delta t)\\ &\quad +l_k(t_n)sin(2\varphi_n(t_n))(\delta t)^2d_{ijkl}(t_n,t_n+\delta t).\end{aligned} \tag{10.72}$$

The square becomes after linearization

$$\begin{aligned}&\Big(\mathbf{r}_{m'j}(t_n+\delta t)\cdot\mathbf{r}_{n'k}(t_n+\delta t)\Big)^2=\left(c_{ijkl}(t_n+\delta t)\right)^2\\ &+2l_k(t_n)sin(2\varphi_n(t_n))(\delta t)^2c_{ijkl}(t_n+\delta t)d_{ijkl}(t_n,t_n+\delta t).\end{aligned} \tag{10.73}$$

The factors in the denominator of the first term in Eq. 10.65 become

$$\begin{aligned}|\mathbf{r}_{m'j}(t_n+\delta t)|^2 &= \left(\mathbf{r}^{uc}_{ij}(t_n+\delta t)\times\mathbf{r}^{uc}_{kj}(t_n+\delta t)\right)^2\\ &\quad +2l_k(t_n)sin(2\varphi_n(t_n))(\delta t)^2\\ &\quad \left(\mathbf{r}^{uc}_{ij}(t_n+\delta t)\times\mathbf{r}^{uc}_{kj}(t_n+\delta t)\right)\cdot\mathbf{b}_{ijk}(t_n+\delta t)\end{aligned} \tag{10.74}$$

and

$$\begin{aligned}|\mathbf{r}_{n'k}(t_n+\delta t)|^2 &= \left(\mathbf{r}^{uc}_{kj}(t_n+\delta t)\times\mathbf{r}^{uc}_{kl}(t_n+\delta t)\right)^2\\ &\quad +2l_k(t_n)sin(2\varphi_n(t_n))(\delta t)^2\\ &\quad \left(\mathbf{r}^{uc}_{kj}(t_n+\delta t)\times\mathbf{r}^{uc}_{kl}(t_n+\delta t)\right)\cdot\mathbf{b}_{jkl}(t_n+\delta t).\end{aligned} \tag{10.75}$$

The linearized denominator of the first term in Eq. 10.65 is then

$$
\begin{aligned}
&|\mathbf{r}_{m'j}(t_n+\delta t)|^2|\mathbf{r}_{n'k}(t_n+\delta t)|^2 = \\
&\left(\mathbf{r}^{uc}_{ij}(t_n+\delta t)\times\mathbf{r}^{uc}_{kj}(t_n+\delta t)\right)^2\left(\mathbf{r}^{uc}_{kj}(t_n+\delta t)\times\mathbf{r}^{uc}_{kl}(t_n+\delta t)\right)^2 \\
&+2l_k(t_n)sin(2\varphi_n(t_n))(\delta t)^2 \\
&\Bigg[\left(\mathbf{r}^{uc}_{ij}(t_n+\delta t)\times\mathbf{r}^{uc}_{kj}(t_n+\delta t)\right)^2 \\
&\left(\mathbf{r}^{uc}_{kj}(t_n+\delta t)\times\mathbf{r}^{uc}_{kl}(t_n+\delta t)\right)\cdot\mathbf{b}_{jkl}(t_n,t_n+\delta t) \\
&+\left(\mathbf{r}^{uc}_{kj}(t_n+\delta t)\times\mathbf{r}^{uc}_{kl}(t_n+\delta t)\right)^2 \\
&\left(\mathbf{r}^{uc}_{ij}(t_n+\delta t)\times\mathbf{r}^{uc}_{kj}(t_n+\delta t)\right)\cdot\mathbf{b}_{ijk}(t_n,t_n+\delta t)\Bigg]
\end{aligned}
\tag{10.76}
$$

Finally, the equation for the Lagrange multiplier of the k-th constraint becomes

$$
\begin{aligned}
l_k(t_n) \quad = \quad & \Bigg[cos^2(\varphi^0_n(\lambda))\left(\mathbf{r}^{uc}_{ij}(t_n+\delta t)\times\mathbf{r}^{uc}_{kj}(t_n+\delta t)\right)^2 \\
& \left(\mathbf{r}^{uc}_{kj}(t_n+\delta t)\times\mathbf{r}^{uc}_{kl}(t_n+\delta t)\right)^2-\left(c_{ijkl}(t_n+\delta t)\right)^2\Bigg] \\
& \Bigg[2sin(2\varphi_n(t_n))(\delta t)^2\Big[c_{ijkl}(t_n+\delta t)d_{ijkl}(t_n+\delta t) \\
& -cos^2(\varphi^0_n(\lambda))\Big((\mathbf{r}^{uc}_{ij}(t_n+\delta t)\times\mathbf{r}^{uc}_{kj}(t_n+\delta t))^2 \\
& (\mathbf{r}^{uc}_{kj}(t_n+\delta t)\times\mathbf{r}^{uc}_{kl}(t_n+\delta t))\cdot\mathbf{b}_{jkl}(t_n,t_n+\delta t) \\
& +(\mathbf{r}^{uc}_{kj}(t_n+\delta t)\times\mathbf{r}^{uc}_{kl}(t_n+\delta t))^2 \\
& (\mathbf{r}^{uc}_{ij}(t_n+\delta t)\times\mathbf{r}^{uc}_{kj}(t_n+\delta t))\cdot\mathbf{b}_{ijk}(t_n,t_n+\delta t)\Big)\Big]\Bigg]^{-1}
\end{aligned}
\tag{10.77}
$$

The derivative of the contribution of the constraint forces to the free energy for the k-th constraint becomes

$$
\frac{d\mathbf{f}^{(c)}_k(\lambda)}{d\lambda} = <l_k>_\lambda\, sin(2\varphi^0_n(\lambda))\left(\varphi^{0\,B}_n-\varphi^{0\,A}_n\right). \tag{10.78}
$$

We note that the expressions given here for the application of dihedral-angle constraints are different from the formalism presented in Ref.[104], which is based on matrix inversion.

10.7. Translational and rotational constraints

In MD++ it is possible to apply rotational and translational constraints. These constraints, if jointly applied, are called *roto-translational constraints*. It may be advantageous to perform simulations with translational and/or rotational constraints, because: (*i*) the simulation of non-spherical solutes can be done in computational boxes whose shape is optimally adjusted to the shape of the solute, thus reducing the required amount of solvent molecules; (*ii*) it is possible to prevent the coupling of internal degrees of freedom with the roto-translational ones, which may speed up equilibration of a system; (*iii*) many interesting simulations can be performed, such as *e.g.* the modelling of solvent molecules as Langevin dipoles at fixed grid points, or ligand-binding studies involving ligands exempt of rotational degrees of freedom; (*iv*) simulations *in vacuo* may benefit from the application of statistically-mechanically rigorous roto-translational constraints rather than merely setting the angular momentum to zero.

A *translational constraint* $\mathcal{C}_t$ on a set of atoms $\mathcal{G}_{Tj}$ consisting of atoms $i=1,...,N_{\mathcal{G}_{Tj}}$ is defined as

$$
\mathcal{C}_t(\mathcal{G}_{Tj}): \quad \sum_{i=1}^{N_{\mathcal{G}_{Tj}}} m_i\mathbf{r}_i(t) = const \quad , \tag{10.79}
$$

where m_i denotes the atomic masses and $\mathbf{r}_i(t)$ the atomic Cartesian coordinates at time t in the fixed orthonormal laboratory frame. From Eq. 10.79 it is obvious that $\mathcal{C}_t(\mathcal{G}_{Tj})$ fixes the position (Cartesian

coordinates in the fixed orthonormal laboratory frame) of the centre-of-mass (COM) of $\mathcal{G}_{Tj}$,

$$\mathbf{r}_{COM}(t;\mathcal{G}_{Tj}) = \frac{1}{\sum_{i=1}^{N_{\mathcal{G}_{Tj}}} m_i} \sum_{i=1}^{N_{\mathcal{G}_{Tj}}} m_i \mathbf{r}_i(t) \quad , \tag{10.80}$$

during the simulation. In a simulation involving constant pressure (*i.e.*, involving a variation of the volume of the computational box), it is the oblique Cartesian coordinates of the COM, $\tilde{\mathbf{r}}_{COM}(t;\mathcal{G}_{Tj})$ which are fixed, *i.e.*

$$\mathcal{C}_t(\mathcal{G}_{Tj}) : \sum_{i=1}^{N_{\mathcal{G}_{Tj}}} m_i \mathbf{L}^{-1}(t)\mathbf{r}_i(t) = const \quad , \tag{10.81}$$

where $\mathbf{L}(t)$ is the box matrix at time t, and

$$\tilde{\mathbf{r}}_{COM}(t;\mathcal{G}_{Tj}) = \frac{1}{\sum_{i=1}^{N_{\mathcal{G}_{Tj}}} m_i} \sum_{i=1}^{N_{\mathcal{G}_{Tj}}} m_i \mathbf{L}^{-1}(t)\mathbf{r}_i(t) \quad . \tag{10.82}$$

Due to its more general nature, Eq. 10.81, rather than Eq. 10.79 is used in the following to describe translational constraints.
A *rotational constraint* $\mathcal{C}_r$ on a set of atoms $\mathcal{G}_{Tj}$ consisting of atoms $i = 1, ..., N_{\mathcal{G}_{Tj}}$ is defined as

$$\mathcal{C}_r(\mathcal{G}_{Tj}) : \sum_{i=1}^{N_{\mathcal{G}_{Tj}}} m_i[\ \mathbf{q}^o{}_i \times \mathbf{q}_i(t)] = \mathbf{0} \quad , \tag{10.83}$$

where $\mathbf{q}^o{}_i$ and $\mathbf{q}_i(t)$ are reference and instantaneous atomic Cartesian coordinates, respectively, in a a local orthonormal frame whose origin lies at the COM of $\mathcal{G}_{Tj}$. From Eq. 10.83 it is obvious that $\mathcal{C}_r(\mathcal{G}_{Tj})$ fixes the rotational orientation of $\mathcal{G}_{Tj}$ with respect to the reference orientation given by the set of $\mathbf{q}^o{}_i$ during the simulation.

The implementation of Eq. 10.81 and Eq. 10.83 is done in a Lagrange-multiplier formalism relying on six linear holonomic constraints captured by the corresponding $\mathcal{C}_t(\mathcal{G}_{Tj})$ and $\mathcal{C}_r(\mathcal{G}_{Tj})$, as described in Ref.[105]. The gradients of these constraint equations, $\frac{\partial \mathcal{C}_t{}^{(k)}(\mathcal{G}_{Tj})}{\partial q_{i,\alpha}}(t)$ and $\frac{\partial \mathcal{C}_r{}^{(k)}(\mathcal{G}_{Tj})}{\partial q_{i,\alpha}}(t)$, where $k = 1, 2, 3$, i denotes an atom of $\mathcal{G}_{Tj}$ and α denotes a Cartesian vector component (x, y or z), give the constraint forces as linear combinations thereof (in conjunction with the corresponding Lagrange multipliers as the coefficients of the gradients in this linear combination).
More precisely,

$$\mathcal{C}_t{}^{(1)}(t;\mathcal{G}_{Tj}) \doteq \sum_{i=1}^{N_{\mathcal{G}_{Tj}}} m_i q_{i,x}(t) = 0 \quad , \tag{10.84}$$

$$\mathcal{C}_t{}^{(2)}(t;\mathcal{G}_{Tj}) \doteq \sum_{i=1}^{N_{\mathcal{G}_{Tj}}} m_i q_{i,y}(t) = 0 \quad , \tag{10.85}$$

$$\mathcal{C}_t{}^{(3)}(t;\mathcal{G}_{Tj}) \doteq \sum_{i=1}^{N_{\mathcal{G}_{Tj}}} m_i q_{i,z}(t) = 0 \quad , \tag{10.86}$$

$$\mathcal{C}_r{}^{(1)}(t;\mathcal{G}_{Tj}) \doteq \sum_{i=1}^{N_{\mathcal{G}_{Tj}}} m_i [q^o_{i,y} q_{i,z}(t) - q^o_{i,z} q_{i,y}(t)] = 0 \quad , \tag{10.87}$$

$$\mathcal{C}_r{}^{(2)}(t;\mathcal{G}_{Tj}) \doteq \sum_{i=1}^{N_{\mathcal{G}_{Tj}}} m_i [q^o_{i,z} q_{i,x}(t) - q^o_{i,x} q_{i,z}(t)] = 0 \quad , \tag{10.88}$$

$$\mathcal{C}_r{}^{(3)}(t;\mathcal{G}_{Tj}) \doteq \sum_{i=1}^{N_{\mathcal{G}_{Tj}}} m_i [q^o_{i,x} q_{i,y}(t) - q^o_{i,y} q_{i,x}(t)] = 0 \quad , \tag{10.89}$$

and the resulting constraint forces acting on atom i are ${\mathbf{F}^{(\mathcal{C}_t)}}_i[t;\mathcal{C}_t(\mathcal{G}_{T\,j})]$ and ${\mathbf{F}^{(\mathcal{C}_r)}}_i[t;\mathcal{C}_r(\mathcal{G}_{T\,j})]$, with components $f_{i,\alpha}^{(\mathcal{C}_t)}[t;\mathcal{C}_t(\mathcal{G}_{T\,j})]$, $f_{i,\alpha}^{(\mathcal{C}_r)}[t;\mathcal{C}_r(\mathcal{G}_{T\,j})]$ given by

$$f_{i,\alpha}^{(\mathcal{C}_t)}[t;\mathcal{C}_t(\mathcal{G}_{T\,j})] = \sum_{k=1}^{3} \lambda_{t,k}(t) \frac{\partial {\mathcal{C}_t}^{(k)}(t;\mathcal{G}_{T\,j})}{\partial q_{i,\alpha}}(t) \tag{10.90}$$

and

$$f_{i,\alpha}^{(\mathcal{C}_r)}[t;\mathcal{C}_r(\mathcal{G}_{T\,j})] = \sum_{k=1}^{3} \lambda_{r,k}(t) \frac{\partial {\mathcal{C}_r}^{(k)}(t;\mathcal{G}_{T\,j})}{\partial q_{i,\alpha}}(t) \quad , \tag{10.91}$$

where the Lagrange multipliers $\boldsymbol{\lambda}_t = (\lambda_{t,1}\ \lambda_{t,2}\ \lambda_{t,3})^T$ and $\boldsymbol{\lambda}_r = (\lambda_{r,1}\ \lambda_{r,2}\ \lambda_{r,3})^T$ (with T denoting the transpose) are given as

$$\boldsymbol{\lambda}_t = -\boldsymbol{\Theta}_t^{-1}\mathbf{c}_t \tag{10.92}$$

and

$$\boldsymbol{\lambda}_r = -\boldsymbol{\Theta}_r^{-1}\mathbf{c}_r \quad , \tag{10.93}$$

with

$$\boldsymbol{\Theta}_t = \begin{pmatrix} \theta_{t,11} & 0 & 0 \\ 0 & \theta_{t,22} & 0 \\ 0 & 0 & \theta_{t,33} \end{pmatrix} \tag{10.94}$$

and

$$\boldsymbol{\Theta}_r = \begin{pmatrix} \theta_{r,11} & \theta_{r,12} & \theta_{r,13} \\ \theta_{r,21} & \theta_{r,22} & \theta_{r,23} \\ \theta_{r,31} & \theta_{r,32} & \theta_{r,33} \end{pmatrix} \quad . \tag{10.95}$$

The matrix elements $\theta_{t,ii}$ and $\theta_{r,ij}$ can be shown to be

$$\theta_{t,11} = \theta_{t,22} = \theta_{t,33} = (\Delta t)^2 \sum_{i=1}^{N_{\mathcal{G}_{T\,j}}} m_i \quad , \tag{10.96}$$

$$\theta_{r,11} = (\Delta t)^2 \sum_{i=1}^{N_{\mathcal{G}_{T\,j}}} m_i ({q_{i,y}^o}^2 + {q_{i,z}^o}^2) \quad , \tag{10.97}$$

$$\theta_{r,12} = \theta_{r,21} = -(\Delta t)^2 \sum_{i=1}^{N_{\mathcal{G}_{T\,j}}} m_i q_{i,x}^o q_{i,y}^o \quad , \tag{10.98}$$

$$\theta_{r,13} = \theta_{r,31} = -(\Delta t)^2 \sum_{i=1}^{N_{\mathcal{G}_{T\,j}}} m_i q_{i,x}^o q_{i,z}^o \quad , \tag{10.99}$$

$$\theta_{r,22} = (\Delta t)^2 \sum_{i=1}^{N_{\mathcal{G}_{T\,j}}} m_i ({q_{i,x}^o}^2 + {q_{i,z}^o}^2) \quad , \tag{10.100}$$

$$\theta_{r,23} = \theta_{r,32} = -(\Delta t)^2 \sum_{i=1}^{N_{\mathcal{G}_{T\,j}}} m_i q_{i,y}^o q_{i,z}^o \quad , \tag{10.101}$$

$$\theta_{r,33} = (\Delta t)^2 \sum_{i=1}^{N_{\mathcal{G}_{T\,j}}} m_i ({q_{i,x}^o}^2 + {q_{i,y}^o}^2) \quad , \tag{10.102}$$

where Δt is the integration time step. Note that $\theta_{r,ij}$ is dependent on the set of reference coordinates ${\mathbf{q}^o}_i$. If simulations are performed at constant pressure, these reference coordinates are scaled along with all other box-dependent quantities (box matrix, atomic Cartesian coordinates) by the appropriate scaling factors.

That is, $\mathbf{\Theta}_r = \mathbf{\Theta}_r(t)$, *i.e.* will change during the simulation.
The vectors $\mathbf{c}_t = (c_{t,1}\ c_{t,2}\ c_{t,3})^T$ and $\mathbf{c}_r = (c_{r,1}\ c_{r,2}\ c_{r,3})^T$ can be shown to be

$$c_{t,k} = \sum_{i=1}^{N_{\mathcal{G}_{T\,j}}} \sum_{\alpha=x,y,z} \frac{\partial \mathcal{C}_t{}^{(k)}(t;\mathcal{G}_{T\,j})}{\partial q_{i,\alpha}} \Delta r_{i,\alpha} \tag{10.103}$$

and

$$c_{r,k} = \sum_{i=1}^{N_{\mathcal{G}_{T\,j}}} \sum_{\alpha=x,y,z} \frac{\partial \mathcal{C}_r{}^{(k)}(t;\mathcal{G}_{T\,j})}{\partial q_{i,\alpha}} \Delta r_{i,\alpha} \quad , \tag{10.104}$$

where $k = 1, 2, 3$ and $\Delta r_{i,\alpha}$ is the α-component of the displacement vector $\Delta\mathbf{r}_i$ of atom i, with the displacement being that coordinate change since the last time step which the corresponding constraint force is correcting for, *e.g.*: (*i*) the displacement due to the conservative force in the current time step, if no other constraint forces are applied; (*ii*) the displacement due to the conservative force and a subsequent SHAKE force in the current time step, if bond constraints are enforced with the SHAKE algorithm; (*iii*) the displacement due to the conservative force and any sum of subsequently, iteratively-applied other constraint forces in the current time step.

Any input settings concerning roto-translational constraints are specified in the ROTTRANS and INITIALISE blocks of the MD++ imd file.
Roto-translational constraints are always applied on the first specified number of atoms. It is not possible to separately apply a translational or rotational constraint only. Thus, for instance, one can apply a roto-translational constraint to a solvated biomolecule (one solute molecule).
Note that, upon starting a new MD simulation, a rotational constraint on a certain temperature group can be initialised in either of two ways: The reference coordinates $\mathbf{q}_i^o$ may be read from the ROTOTRANSREFPOS block in the configuration file, or may be computed from scratch based on the set of initial coordinates given in the configuration file (POSITION block). This decision is specified in the INITIALISE block of the MD++ input file.

CHAPTER 11

Energy Minimization

11.1. Introduction

Energy minimization (EM) with an empirical energy function such as Eq. 3.4 is a widely used tool for obtaining low-energy configurations of a molecular system. Various function minimization methods can be used, which can be classified as follows:

1. *Direct search methods*, requiring only function values. They converge slowly and are therefore not considered here.
2. *Gradient methods*, requiring function and derivative values. These methods fall into three subclasses:
   a. The *steepest descent method* (SDEM) performs well far from a minimum, but converges slowly near a minimum, or when searching in a long, thin, curving valley. It is a robust method, which is easy to implement.
   b. The *conjugate gradient method*[106] (CGEM) which searches along directions corresponding to the local quadratic approximation to the function, usually converges superlinearly. Because it is the most rapidly converging minimizer that does not require manipulation and storage of matrices of dimension equal to the number of degrees of freedom, it appears to be most appropriate for very large systems, like macromolecules.
   c. The *variable metric or quasi-Newton methods*, which use various approximations to the inverse of the Hessian matrix (matrix of second partial derivatives), are also quadratically convergent, but they require storage space for the inverse Hessian and time for its manipulation. Hence, they are less suited for application to large systems.
3. *Second-order methods*, requiring function, derivative and Hessian matrix. These methods are not well suited for application to large systems for the same reason as mentioned under 2c.

For references to the different methods we refer to ref.[107]. The method of steepest descents is discussed in Sec. 11.2, the conjugate gradient technique in Sec. 11.3. In Sec. 11.4 and 11.5 it is described how the SHAKE method for constraining bond lengths and/or bond angles can be incorporated in the steepest descent and conjugate gradient energy minimization algorithm.

When applying EM algorithms one searches for a minimum energy configuration of a system by moving (approximately) along the gradient of the potential energy through configuration space,

$$\Delta \mathbf{r}_i \sim -\frac{\partial}{\partial r_i} V(\mathbf{r}_1, \mathbf{r}_2, ..., \mathbf{r}_N), \tag{11.1}$$

where $\Delta \mathbf{r}_i$ denotes the shift in position of atom i. Since in this way one basically moves only downhill over the energy hypersurface, EM yields only a *local* minimum energy configuration, which is generally not far from the initial one. Using formulae like Eq. 11.1 crossing of energy barriers is impossible. A more efficient way to find low energy configurations is to apply molecular dynamics (MD). The available kinetic energy may be used to pass over energy barriers which are not much higher than $k_B T$ (k_B = Boltzmann's constant and T = absolute temperature). It has been shown[108] that MD at elevated temperatures can be used to generate a variety of configurations. Therefore, MD searches a larger part of configuration space for an energy minimum and generally ends up in a lower energy minimum than an ordinary energy minimizer does[109]. However, the application of MD starting from a highly strained, very high potential energy configuration is not recommended, since the immediate conversion of potential energy into kinetic energy will raise the temperature to unacceptably high values. In that case, one should first perform a number of EM steps in order to reduce the high potential energy of the system. When the high potential energy is due to close non-bonded contacts or stretched bond lengths or bent bond angles in a molecular system, ten to fifty EM steps generally suffice to reduce the potential energy to values which are normal at room temperature.

The configuration at the n-th minimization step is denoted by $\boldsymbol{r}(t_n) \equiv (\mathbf{r}_1(t_n), \mathbf{r}_2(t_n), \ldots, \mathbf{r}_N(t_n))$, where t_n is used in analogy with MD simulation and the configuration consists of N atoms. The *scalar product of two configurations* $\boldsymbol{r}$ and $\boldsymbol{r}'$ is denoted by

$$< \boldsymbol{r} | \boldsymbol{r}' > \quad \equiv \quad \sum_{i=1}^{N} \mathbf{r}_i \cdot \mathbf{r}'_i \tag{11.2}$$

When a set of atoms is to be kept fixed, their positions $\mathbf{r}_i$ are not changed and the forces (negative gradients) f_i on them are kept equal to zero at each minimization step. Their inverse masses are set to zero in order to immobilize these atoms when their position might be up for resetting by the procedure SHAKE in case a fixed atom is involved in a constraint to a non-fixed atom.

11.2. Steepest-descent minimization

Energy minimization by the *steepest-descent (*SDEM*) algorithm* is simple. The *computational scheme* for the (n+1)-th minimization step reads,

1. Calculate the forces $\boldsymbol{f}(t_n) = \boldsymbol{f}(\boldsymbol{r}(t_n))$ from the interaction function $V(\boldsymbol{r})$ (see Eq. 3.4) using expression Eq. 2.10 and the configuration $\boldsymbol{r}(t_n)$.
2. Compute the next configuration from

   $$\boldsymbol{r}(t_{n+1}) = \boldsymbol{r}(t_n) + \Delta x < \boldsymbol{f}(t_n) | \boldsymbol{f}(t_n) >^{-\frac{1}{2}} \boldsymbol{f}(t_n) \tag{11.3}$$

   where the step size is denoted by Δx.

SDEM is selected by setting switch NTEM=1 in the input of MD++. The initial step size Δx is to be specified in DX0. As long as the potential energy decreases, the step size Δx is increased by 20% per step. If the potential energy increases, Δx is halved. The growth of the step size can be limited by specifying a maximum value, DXM. The energy minimization is terminated when the number of EM steps reaches the value NSTLIM or when the potential energy change between two subsequent steps is less than the value DELE. However, one may specify a minimum number of steps to take using parameter NMIN. The final configuration is saved.

At every NTPR-th minimization step a number of *quantities* (step number (TIMESTEP), various energies (ENERGY block), etc. see Sec. 12.7) are *printed*. In addition, coordinate or energy trajectories may be written (see Vol. 4).

11.3. Conjugate-gradient minimization

The *conjugate gradient (*CGEM*) algorithm* can be summarized as follows. It is started by calculating the forces or negative gradients, $\boldsymbol{f}(t_0) = \boldsymbol{f}(\boldsymbol{r}(t_0))$, from the interaction function $V(\boldsymbol{r})$ (see Eq. 3.4) using expression Eq. 2.10 and the initial configuration $\boldsymbol{r}(t_0)$, and by taking the first search directions $\boldsymbol{p}(t_0) \equiv (\mathbf{p}_1(t_0), \mathbf{p}_2(t_0), \ldots, \mathbf{p}_N(t_0))$ along the negative gradients, that is,

$$\boldsymbol{p}(t_0) = \boldsymbol{f}(t_0) \tag{11.4}$$

The *computational scheme* for the (n+1)-th minimization step reads,

1. Find the minimum of the potential energy $\mathcal{V}(\boldsymbol{r})$ on the line through $\boldsymbol{r}(t_n)$ in the direction $\boldsymbol{p}(t_n)$, that is, determine s_{min} such that

   $$\mathcal{V}(\boldsymbol{r}(t_n) + s_{min}\boldsymbol{p}(t_n)) \tag{11.5}$$

   finds its minimum, or equivalently, such that

   $$g(t_n; s_{min}) \equiv < \boldsymbol{p}(t_n) | \boldsymbol{f}(\boldsymbol{r}(t_n) + s_{min}\boldsymbol{p}(t_n)) >= 0 \tag{11.6}$$

   The determination s_{min} is done in two stages: the first establishes bounds a and b on $s_{min'}(a < s_{min} \leqslant b)$, and the second interpolates its value in the interval (a, b).

a. As a first guess for the bounds, take $a = 0$, and $b = \Delta x < \boldsymbol{p}(t_n)|\boldsymbol{p}(t_n) >^{-\frac{1}{2}}$. The step size Δx should be chosen such that no iterations are required when establishing the bound b. We already know the energy $\mathcal{V}(\boldsymbol{r}(t_n)+a\boldsymbol{p}(t_n)) = V(\boldsymbol{r}(t_n))$ and also the forces $\boldsymbol{f}(\boldsymbol{r}(t_n)+a\boldsymbol{p}(t_n)) = \boldsymbol{f}(\boldsymbol{r}(t_n))$, so $g(t_n; a)$ is easily obtained. The same quantities have to be examined at b, so we compute $\boldsymbol{r}(t_n) + b\boldsymbol{p}(t_n)$ and evaluate the energy $\mathcal{V}(\boldsymbol{r}(t_n) + b\boldsymbol{p}(t_n))$ and the forces $\boldsymbol{f}(\boldsymbol{r}(t_n) + b\boldsymbol{p}(t_n))$, and compute $g(t_n; b)$. The value b is accepted as upper bound on s_{min} if

$$g(t_n; b) \quad < \quad 0 \tag{11.7}$$

or

$$\mathcal{V}(\boldsymbol{r}(t_n) + b\boldsymbol{p}(t_n)) \geq \mathcal{V}(\boldsymbol{r}(t_n) + a\boldsymbol{p}(t_n)) \tag{11.8}$$

Otherwise s_{min} lies beyond b, so b is too small and so is Δx and the process of looking for bounds on s_{min} is to be repeated with doubled b.

b. Use a cubic interpolation formula in order to estimate s_{min} in the interval $(a,\ b)$,

$$s_{min} \quad = \quad b - \frac{[W - Z - g(t_n; b)][b - a]}{[g(t_n; a) - g(t_n; b) + 2W]} \tag{11.9}$$

in which

$$W \quad \equiv \quad \left[\ Z^2 - g(t_n; a)g(t_n; b)\right]^{1/2} \tag{11.10}$$

and

$$Z \quad \equiv \quad \frac{3[\mathcal{V}(\boldsymbol{r}(t_n) + a\boldsymbol{p}(t_n)) - \mathcal{V}(\boldsymbol{r}(t_n) + b\boldsymbol{p}(t_n))]}{[b - a]} - g(t_n; a) - g(t_n; b). \tag{11.11}$$

c. In order to improve the estimate of $s_{min,0}$ and allow for tighter convergence, it is accepted only if RMSD between the new and the previous estimate is smaller than the threshold Δr_{thres}, that is if

$$|s_{min,i+1} - s_{min,i}|\sqrt{\frac{\langle \boldsymbol{p}(t_n)|\boldsymbol{p}(t_n)\rangle}{N}} \quad < \quad \Delta r_{thres} \tag{11.12}$$

where for first iteration $s_{min,0} = a$. If RMSD is higher than Δr_{thres}, the energy $\mathcal{V}(\boldsymbol{r}(t_n) + s_{min,i+1}\boldsymbol{p}(t_n))$, forces $\boldsymbol{f}(\boldsymbol{r}(t_n)+s_{min,i+1}\boldsymbol{p}(t_n))$ and $g(t_n; s_{min,i+1})$ are calculated. If $g(t_n; s_{min,i+1})$ is less than 0 and the energy is lower than $\mathcal{V}(\boldsymbol{r}(t_n) + a\boldsymbol{p}(t_n))$, the upper bound b is moved to $s_{min,i+1}$, that is $b = s_{min,i+1}$, otherwise $a = s_{min,i+1}$. Steps **1b** and **1c** are repeated until RMSD is below Δr_{thres} or maximum number of steps i_{max} is reached. Δr_{thres} and i_{max} can be set using parameters CGIC and CGIM, respectively. By setting $i_{max} = 1$ the first estimate of s_{min} is always accepted. $i_{max} > 1$ is useful for tight convergence. With the accepted s_{min} the new configuration is

$$\boldsymbol{r}(t_{n+1}) \quad = \quad \boldsymbol{r}(t_n) + s_{\min}\boldsymbol{p}(t_n) \tag{11.13}$$

2. Calculate the new energy $\mathcal{V}(\boldsymbol{r}(t_{n+1}))$ and the forces $\boldsymbol{f}(t_{n+1}) = \boldsymbol{f}(\boldsymbol{r}(t_{n+1}))$ from the interaction function $\mathcal{V}(\boldsymbol{r})$.

3. Determine the new search directions $\boldsymbol{p}(t_{n+1})$ from

$$\boldsymbol{p}(t_{n+1}) \quad = \quad \boldsymbol{f}(t_{n+1}) + \beta_n\boldsymbol{p}(t_n) \tag{11.14}$$

where in Fletcher-Reeves method (FRCG)[106]

$$\beta_n \quad = \quad \frac{< \boldsymbol{f}(t_{n+1})|\boldsymbol{f}(t_{n+1}) >}{< \boldsymbol{f}(t_n)|\boldsymbol{f}(t_n) >}. \tag{11.15}$$

or in Polak-Ribiére method (PRCG)[110]

$$\beta_n = \frac{< \boldsymbol{f}(t_{n+1}) - \boldsymbol{f}(t_n) | \boldsymbol{f}(t_{n+1}) >}{< \boldsymbol{f}(t_n) | \boldsymbol{f}(t_n) >}. \tag{11.16}$$

Each new direction of search is partly determined by previous search directions. The weight depends on the relative size of the forces at $\boldsymbol{r}(t_{n+1})$ and $\boldsymbol{r}(t_n)$. Although both CGEM algorithms perform at least two function evaluations of $\mathcal{V}(\boldsymbol{r})$ per minimization step, they are generally more efficient than the SDEM algorithm, which performs one function evaluation per step.[107] However, the latter algorithm is more robust.

CGEM energy minimization is selected by setting the switch NTEM = 2 for FRCG or NTEM = 3 for PRCG in the input of program MD++. The CGEM step size Δx is to be specified in DX0 and should be carefully chosen. It should be just large enough to avoid interval doubling iterations when establishing bounds a and b on s_{min} (step **1a**), but small enough to allow for a good estimate of s_{min} by interpolation (step **1b**). If the estimated s_{min} was found within first 10% of the search interval, Δx is decreased by 10% in the next step. If s_{min} was found beyond the initial b, next Δx is increased by 10%. The growth of Δx can be limited by specifying a maximum value, DXM. If the energy decreases slowly near a local minimum, one may try to reach it faster by restarting the CGEM algorithm with a smaller Δx value. It may be sometimes useful to limit the number of CGEM steps taken with a given series of search direction vectors. This can be achieved by setting the variable NCYC a finite (<NSTLIM) value: after every NCYC CGEM minimization steps the algorithm will use

$$\beta_n = 0 \tag{11.17}$$

instead of β_n given by 11.15 or 11.16, thereby discarding the contribution of previous search directions to $\boldsymbol{p}(t_{n+1})$ in Eq. 11.13.

So, for NCYC = 1 the CGEM algorithm reduces to a SDEM algorithm with cubic interpolation. With NCYC = 0 the search direction vectors are reset only if the energy grows in the search direction, that is if

$$g(t_n; a) < 0 \tag{11.18}$$

The energy minimization is terminated when the number of EM steps reaches the value NSTLIM or when the RMS force is less than the value DELE

$$f_{RMS}(t_n) = \sqrt{\frac{\langle \boldsymbol{f}(t_n) | \boldsymbol{f}(t_n) \rangle}{N}} < \text{DELE} \tag{11.19}$$

However, one may also specify a minimum number of steps to take using parameter NMIN. The final configuration is saved. In addition, coordinate or energy trajectories may be written (see Vol. 4).

11.4. Steepest-descent minimization with constraints (SHAKE)

The essential feature of the SHAKE method for conserving constraints is that after each minimization step, the constraints are satisfied by adding displacement vectors to the position vectors of the atoms that result from an unconstrained minimization step. The added displacement vectors are determined such that the constraints are satisfied at the final positions (see Sec. 10.3).

The procedure *SHAKE* can be directly incorporated into the *steepest-descent* energy minimization *algorithm* in the following way. The initial configuration $\boldsymbol{r}(t_0)$ must be made satisfy the constraints as discussed in Sec. 10.3.1. Shaking of the initial configuration is selected by taking NTISHK = 1 in the input file. Then, the *computational scheme* for the (n+1)-th constrained minimization step reads,

1. Calculate the unconstrained forces $\mathbf{f}^{uc}(t_n) = \mathbf{f}^{uc}(\boldsymbol{r}(t_n))$ from the interaction function $\mathcal{V}(\boldsymbol{r})$ (see Eq. 3.4), from which the terms acting *only* along the constrained degrees of freedom are excluded (e.g. the bond length interactions), using Eq. 2.8 and the (shaken) configuration $\boldsymbol{r}(t_n)$.

2. Determine the unconstrained positions at step t_{n+1},

$$\mathbf{r}^{uc}(t_{n+1}) \quad = \quad \boldsymbol{r}(t_n) + \Delta x < \mathbf{f}^{uc}(t_n)|\mathbf{f}(t_n) >^{-1/2} \mathbf{f}^{uc}(t_n) \tag{11.20}$$

where the step size is denoted by Δx. The positions $\mathbf{r}^{uc}(t_{n+1})$ do not, in general, satisfy the constraints, as the forces normally contain components in the constrained directions.

3. The positions are made satisfy the constraints by performing

$$SHAKE(\boldsymbol{r}(t_n); \mathbf{r}^{uc}(t_{n+1}); \boldsymbol{r}(t_{n+1})) \tag{11.21}$$

Most of the parameters of the SDEM algorithm with SHAKE are identical to those discussed in Sec. 11.2 for the unconstrained SDEM algorithm. An additional feature is that the step size Δx is halved when the number of iterations in SHAKE in Eq. 11.21 exceeds 100. The constrained forces $\boldsymbol{f}(t_n) = \mathbf{f}^{uc}(t_n) + \mathbf{f}^{(c)}(t_n)$ can be obtained from solving Eq. 11.20 for $\mathbf{f}^{uc}(t_n)$ and using $\boldsymbol{r}(t_{n+1})$ instead of $\mathbf{r}^{uc}(t_{n+1})$,

$$\boldsymbol{f}(t_n) \quad = \quad \frac{\boldsymbol{r}(t_{n+1}) - \boldsymbol{r}(t_n)}{\Delta x < \mathbf{f}^{uc}(t_n)|\mathbf{f}^{uc}(t_n) >^{-1/2}}. \tag{11.22}$$

11.5. Conjugate-gradients minimization with constraints (SHAKE)

Incorporation of *SHAKE* into the *conjugate-gradients algorithm* is more complex than in the case of steepest descent, since there only the positions $\mathbf{r}^{uc}(t_{n+1})$ had to be shaken. Here, the search direction, which is composed of the force direction and previous search directions, also must be chosen such that it does not contain components along the constraints. Hence, $\mathbf{f}^{uc}(t_{n+1})$ and $\mathbf{p}^{uc}(t_{n+1})$ have to be shaken too.

The initial configuration $\boldsymbol{r}(t_0)$ must be made satisfy the constraints as discussed in Sec. 10.3.1. Shaking of the initial configuration is selected by taking NTISHK = 1 in the input block INITIALIZE. The initial unconstrained forces $\mathbf{f}^{uc}(t_0)$ can be shaken by the procedure, which was used to remove components along the constraint directions from the velocities in Sec. 10.3.7,

A. Determine

$$\mathbf{r}^{uc}(t_1) \quad = \quad \mathbf{r}(t_0) + \Delta x^{uc} \mathbf{f}^{uc}(t_0) \tag{11.23}$$

where $\Delta x^{uc} = \Delta x \, \langle \mathbf{f}^{uc}(t_0)|\mathbf{f}^{uc}(t_0)\rangle^{-\frac{1}{2}}$ and Δx is the conjugate-gradients step size.

B. Perform

$$SHAKE(\mathbf{r}(t_0); \mathbf{r}^{uc}(t_1); \mathbf{r}(t_1)). \tag{11.24}$$

C. Obtain the constrained or shaken forces $\mathbf{f}(t_0)$ from

$$\mathbf{f}(t_0) \quad = \quad \frac{\mathbf{r}(t_1) - \mathbf{r}(t_0)}{\Delta x^{uc}}. \tag{11.25}$$

The initial search direction is taken along $\boldsymbol{f}(t_0)$, that is, $\mathbf{p}(t_0) = \boldsymbol{f}(t_0)$. Then, the *computational scheme* for the (n+1)-th minimization step reads,

1. Find the minimum of the potential energy $\mathcal{V}(\boldsymbol{r})$ on the line through $\boldsymbol{r}(t_n)$ in the direction $\mathbf{p}(t_n)$, that is, determine s_{min} such that

$$\mathcal{V}(\boldsymbol{r}(t_n) + s_{\min}\mathbf{p}(t_n)) \tag{11.26}$$

finds its minimum, or such that

$$g(t_n; s_{\min}) \equiv \langle \mathbf{p}(t_n)|\mathbf{f}(r(t_n) + s_{\min}\mathbf{p}(t_n))\rangle = 0 \quad . \tag{11.27}$$

When the components along the constraints have been eliminated from $\mathbf{p}(t_n)$ and $\boldsymbol{f}(\boldsymbol{r}(t_n) + s_{min}\mathbf{p}(t_n)$, the conditions Eq. 11.26 and Eq. 11.27 are *not* equivalent and $\mathcal{V}(\boldsymbol{r}(t_n) + s_{min}\mathbf{p}(t_n))$ may have a minimum with $g(t_n; s_{min}) \neq 0$.

The determination of s_{min} is done in two stages: the first establishes bounds a and b on $s_{\min'}(a < s_{\min} \leqslant b)$, and the second interpolates its value in the interval $(a,\ b)$.

a. As a first guess for the bounds, take $a = 0$ and $b = \Delta x \langle \mathbf{p}(t_n)|\mathbf{p}(t_n)\rangle^{\frac{1}{2}}$. We already know the energy $\mathcal{V}(\boldsymbol{r}(t_n) + a\mathbf{p}(t_n)) = \mathcal{V}(\boldsymbol{r}(t_n))$ and the constrained (shaken) forces $\mathbf{f}(\boldsymbol{r}(t_n) + a\mathbf{p}(t_n)) = \mathbf{f}(\mathbf{r}(t_n))$, so $g(t_n; a)$ is easily obtained. The same quantities have to be examined at b, so we compute

$$\mathbf{r}(t_n; b) \quad \equiv \quad \mathbf{r}(t_n) + b\mathbf{p}(t_n) \tag{11.28}$$

and evaluate the energy $\mathcal{V}(\boldsymbol{r}(t_n) + b\mathbf{p}(t_n))$ and the forces

$$\mathbf{f}^{uc}(t_n; b) \quad \equiv \quad \mathbf{f}^{uc}(\mathbf{r}(t_n) + b\mathbf{p}(t_n)) \tag{11.29}$$

from the interaction function, from which the terms acting *only* along the constrained degrees of freedom are excluded. The components along the directions of the constraints are removed by the procedure Eq. 11.23-Eq. 11.25, that is, by performing

$$\mathbf{r}^{uc}(t_{n+1}; b) \quad \equiv \quad \mathbf{r}(t_n; b) + \Delta x^{uc}\mathbf{f}^{uc}(t_n; b) \tag{11.30}$$

where

$$\Delta x^{uc} \quad = \quad \frac{\mathbf{b}\,\langle \mathbf{p}(t_n)|\mathbf{p}(t_n)\rangle}{\langle \mathbf{f}^{uc}(t_n; b)|\mathbf{f}^{uc}(t_n; b)\rangle} \tag{11.31}$$

and

$$SHAKE(\mathbf{r}(t_n; b); \mathbf{r}^{uc}(t_{n+1}; b); \mathbf{r}(t_{n+1}; b)) \tag{11.32}$$

and

$$\mathbf{f}(t_n; b) \quad \equiv \quad \frac{\mathbf{r}(t_{n+1}; b) - \mathbf{r}(t_n; b)}{\Delta x^{uc}}. \tag{11.33}$$

With the shaken forces (Eq. 11.33) *g(t$_n$;b)* can be computed. The values a and b are accepted as bounds on s_{min} if

$$g(t_n; b) \quad < \quad 0 \tag{11.34}$$

or

$$\mathcal{V}(\boldsymbol{r}(t_n) + b\mathbf{p}(t_n)) \quad \geqslant \quad \mathcal{V}(\mathbf{r}(t_n) + a\mathbf{p}(t_n)) \tag{11.35}$$

Otherwise s_{min} lies beyond b, so b is too small (and so is Δx) and the process of looking for bounds on s_{min} is to be repeated with b doubled.

a. Use the cubic interpolation formulae Eqs. 11.9-11.13 in order to find s_{min} in the interval $(a,\ b)$ and determine the new unconstrained configuration

$$\mathbf{r}^{uc}(t_{n+1}) \quad = \quad \boldsymbol{r}(t_n) + s_{\min}\mathbf{p}(t_n) \tag{11.36}$$

which has to be shaken,

$$SHAKE(\boldsymbol{r}(t_n); \mathbf{r}^{uc}(t_{n+1}); \boldsymbol{r}(t_{n+1})) \tag{11.37}$$

2. Calculate the new energy $\mathcal{V}(\boldsymbol{r}(t_{n+1}))$ and the unconstrained forces $\mathbf{f}^{uc}(t_{n+1}) = \mathbf{f}^{uc}(\boldsymbol{r}(t_{n+1}))$ from the interaction function excluding the interaction terms that act *only* along the constraints. The components of the forces along the constraints are removed as above by performing

$$\mathbf{r}^{uc}(t_{n+2}) \quad = \quad \mathbf{r}(t_{n+1}) + \Delta x^{uc}\mathbf{f}^{uc}(t_{n+1}) \tag{11.38}$$

where

$$\Delta x^{uc} = \frac{s_{\min} \langle \mathbf{p}(t_n) | \mathbf{p}(t_n) \rangle^{1/2}}{< \mathbf{f}^{uc}(t_{n+1}) | \mathbf{f}^{uc}(t_{n+1}) >^{1/2}} \tag{11.39}$$

and

$$SHAKE(\mathbf{r}(t_{n+1}); \mathbf{r}^{uc}(t_{n+2}); \mathbf{r}(t_{n+2})) \tag{11.40}$$

and

$$\mathbf{f}(t_{n+1}) \equiv \frac{\mathbf{r}(t_{n+2}) - \mathbf{r}(t_{n+1})}{\Delta x^{uc}}. \tag{11.41}$$

3. The new search direction $\mathbf{p}(t_{n+1})$ could be directly obtained from Eq. 11.13. It is a linear combination of (n+2) shaken vectors. As the number of minimization steps n increases, the components of $\mathbf{p}(t_{n+1})$ along the constraint directions will grow, unless the search direction is also shaken at every minimization step. This can be achieved by solving $\mathbf{p}(t_n)$ from Eq. 11.36 with $\boldsymbol{r}(t_{n+1})$ instead of $\mathbf{r}^{uc}(t_{n+1})$,

   $$\mathbf{p}(t_n) \equiv \frac{\boldsymbol{r}(t_{n+1}) - \boldsymbol{r}(t_n)}{s_{\min}}. \tag{11.42}$$

   Then, the new search direction becomes

   $$\mathbf{p}(t_{n+1}) = \boldsymbol{f}(t_{n+1}) + \beta_n \mathbf{p}(t_n), \tag{11.43}$$

   with β_n given by Eq. 11.14).

Most of the parameters of the CGEM algorithm with SHAKE are identical to those discussed in Sec. 11.3 for the unconstrained CGEM algorithm. When applying constraints, conditions Eqs. 11.26 and 11.27 are not equivalent. This implies that it may occur that

$$Z^2 - g(t_n; a) g(t_n; b) < 0 \tag{11.44}$$

in (Eq. 11.9), in which case the minimization is terminated.

At every NTPR-th minimization step the same *quantities* as described in Chapters Secs. 11.2-11.3 for unconstrained SDEM and CGEM minimization are *printed*.

CHAPTER 12

Molecular Dynamics

12.1. Introduction

Molecular dynamics (MD) simulation with an empirical energy function such as Eq. 3.4 is a widely used tool to study the equilibrium and non-equilibrium structural, dynamical and thermodynamic properties of molecular systems. The equations of motion of classical mechanics for the atoms are integrated forward in time. When using Cartesian coordinates, these equations are Newton's equations of motion Eq. 2.8, with the forces $\boldsymbol{f}$ calculated as the negative gradient of the energy function $\mathcal{V}$, Eq. 2.10.

A simple but efficient algorithm for integration of Newton's equations of motion is the leap-frog scheme, which is obtained as follows. A Taylor expansion of the velocity $\mathbf{v}_i(t_n - \Delta t/2)$ at time point $t = t_n$ is subtracted from a Taylor expansion of $\mathbf{v}_i(t_n + \Delta t/2)$ at $t = t_n$.

Neglecting terms of third and higher order in the time step Δt and using Eq. 2.12 we obtain

$$\mathbf{v}_i(t_n + \Delta t/2) \quad = \quad \mathbf{v}_i(t_n - \Delta t/2) + m_i^{-1}\mathbf{f}_i(t_n)\Delta t, \tag{12.1}$$

the leap-frog velocity formula. Subtracting a Taylor expansion of the position $\mathbf{r}_i(t_n)$ at time point $t = t_n + \Delta t/2$ from a Taylor expansion of $\mathbf{r}_i(t_n + \Delta t)$ at $t = t_n + \Delta t/2$, neglecting terms of third and higher order in Δt and using Eq. 2.9 we obtain

$$\mathbf{r}_i(t_n + \Delta t) \quad = \quad \mathbf{r}_i(t_n) + \mathbf{v}_i(t_n + \Delta t/2)\Delta t, \tag{12.2}$$

the leap-frog position formula. Eq. 12.1 and Eq. 12.2 form the *leap-frog scheme* (Fig. 12.1).

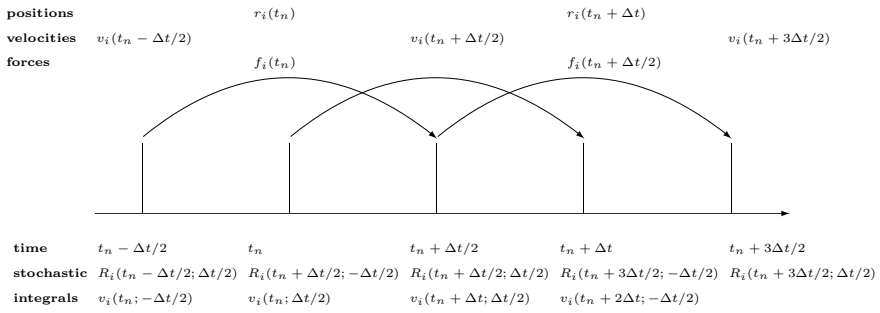

FIGURE 12.1. The leap-frog scheme.

In a standard MD simulation, the total energy E of the molecular system is a constant of motion. Since the number of atoms N and the volume of the computational (periodic) box V are standardly kept fixed, such an MD simulation is called an (N, V, E) simulation. In practice one would often prefer to keep the temperature T fixed instead of the energy, leading to an (N, V, T) simulation. In addition, one may want to keep the pressure P fixed instead of the volume, leading to an (N, P, T) simulation. Coupling of the molecular system to a temperature or pressure bath will imply a modification of the equations of motion and so of the simple leap-frog MD algorithm. In Sec. 12.2 *coupling to a temperature bath* is described and in Sec. 12.5 *coupling to a pressure bath*. The latter requires the *calculation of the virial*, which is discussed in Sec. 12.4. In Sec. 12.6 the leap-frog scheme including the modifications due to temperature scaling, pressure scaling and the presence of constraints, as it has been implemented in GROMOS, is presented. In Sec. 12.7 issues with respect to initialization, equilibration and sampling of an MD simulation are discussed.

12.2. Temperature scaling

MD simulations at constant temperature have several advantages: (*i*) the ensemble generated may be closer to the ensemble generated under experimental conditions; (*ii*) the sampling of conformations may be enhanced by performing simulations at high temperatures; (*iii*) energetic drifts caused by numerical inaccuracies or cutoff artifacts can be ameliorated; (*iv*) temperature dependent properties can be studied.

Thermostatting in MD++ relies on coupling a certain set of degrees of freedom $\{D\}_i$ to a certain temperature bath $\mathcal{B}_{Tj}(\{D\}_i)$ such that energy can "flow" between $\{D\}_i$ and $\mathcal{B}_{Tj}(\{D\}_i)$ and hence allow for the instantaneous temperature $\mathcal{T}(t;\{D\}_i)$ of the degrees of freedom set $\{D\}_i$ to be rigorously constant, or to fluctuate about the reference temperature $\mathcal{T}_o[\mathcal{B}_{Tj}(\{D\}_i)]$. (This flow of energy does, of course, not change the reference temperature $\mathcal{T}_o[\mathcal{B}_{Tj}(\{D\}_i)]$). The coupling is implemented by scaling the velocities of all atoms contained in $\{D\}_i$ with a (time-dependent) *scaling factor* $\lambda[t;\mathcal{B}_{Tj}(\{D\}_i)]$.

$\{D\}_i$ may contain translational, internal+rotational, or both types of degrees of freedom. The calculation of the corresponding instantaneous temperature $\mathcal{T}(t;\{D\}_i)$ is explained in Sec. 12.2.1. The variables characterizing $\mathcal{B}_{Tj}$, as well as the precise form of coupling between $\mathcal{B}_{Tj}$ and $\{D\}_i$ are dependent on the thermostat algorithm employed. These algorithms will be detailed in Sec. 12.2.2. The concept of temperature groups, sets of degrees of freedom and temperature baths will be discussed in more detail in Sec. 12.2.3. The precise calculation of the number of degrees of freedom is explained in Sec. 12.3.

12.2.1. Temperature calculation in MD++. Thermostatting involves the comparison of the instantaneous temperature $\mathcal{T}(t-\frac{\Delta t}{2};\{D\}_i)$ with the reference temperature $\mathcal{T}_o[\mathcal{B}_{Tj}(\{D\}_i)]$, where

$$\mathcal{T}\left(t-\frac{\Delta t}{2};\{D\}_i\right)=\frac{2\mathcal{K}(t-\frac{\Delta t}{2};\{D\}_i)}{N_{df}(\{D\}_i)k_B} \quad , \tag{12.3}$$

with $\mathcal{K}(t-\frac{\Delta t}{2};\{D\}_i)$ and $N_{df}(\{D\}_i)$ being the kinetic energy and number of degrees of freedom, respectively associated with $\{D\}_i$ and k_B being Boltzmann's constant. In the following, we use $t-\frac{\Delta t}{2}=t'$.
$\mathcal{K}(t';\{D\}_i)$ is computed as the sum of the kinetic energies pertaining to the individual temperature groups $\mathcal{G}_{Tj}$ contained in $\{D\}_i$,

$$\mathcal{K}(t';\{D\}_i)=\sum_{\mathcal{G}_{Tj}\in\{D\}_i}\mathcal{K}(t';\mathcal{G}_{Tj}) \quad . \tag{12.4}$$

The calculation of $\mathcal{K}(t';\mathcal{G}_{Tj})$, in turn, considers the type of degrees of freedom contributed by the different temperature groups:
Translational velocities $\mathbf{v}_{tr}(t';\mathcal{G}_{Tj})$ of a temperature group $\mathcal{G}_{Tj}$ are computed as

$$\mathbf{v}_{tr}(t';\mathcal{G}_{Tj})=M^{-1}(\mathcal{G}_{Tj})\sum_{k\in\mathcal{G}_{Tj}}m_k\mathbf{v}_k(t') \quad , \tag{12.5}$$

where $M(\mathcal{G}_{Tj})=\sum_{k\in\mathcal{G}_{Tj}}m_k$ is the total mass of the temperature group $\mathcal{G}_{Tj}$ and $\mathbf{v}_k(t')$ and m_k are the velocities and masses of atom k (belonging temperature group $\mathcal{G}_{Tj}$). The corresponding *translational kinetic energy* is

$$\mathcal{K}_{tr}(t';\mathcal{G}_{Tj})=\frac{1}{2}\sum_{k\in\mathcal{G}_{Tj}}\left\{m_k\mathbf{v}_k^2(t')-m_k\left[\mathbf{v}_k(t')-\mathbf{v}_{tr}(t';\mathcal{G}_{Tj})\right]^2\right\} \quad . \tag{12.6}$$

The corresponding internal+rotational kinetic energy is

$$\mathcal{K}_{ir}(t';\mathcal{G}_{Tj})=\frac{1}{2}\sum_{k\in\mathcal{G}_{Tj}}m_k\left[\mathbf{v}_k(t')-\mathbf{v}_{tr}(t';\mathcal{G}_{Tj})\right]^2 \quad . \tag{12.7}$$

Eq. 12.6 and Eq. 12.7 can be easily understood as the latter arising from atomic velocities measured with respect to the centre of mass velocity of the temperature group the atoms belong to, whereas the former merely constitutes the rest (difference of total kinetic energy and the internal+rotational contribution).

For the calculation of the instantaneous temperature according to Eq. 12.3, a set of degrees of freedom involving only translational degrees of freedom will contribute translational kinetic energies only, whereas a set of degrees of freedom involving only internal+rotational degrees of freedom will contribute internal+rotational kinetic energies only. A set of degrees of freedom involving both translational and internal+rotational degrees of freedom will contribute a sum of translational and internal+rotational kinetic

energies.
Finally, it should be emphasized that the velocities $\mathbf{v}_k(t')$ used in the temperature calculation are *constrained velocities*, that is, rather than being free-flight velocities deriving from the physical force field, they are corrected for the application of various constraints.

12.2.2. Thermostat algorithms in MD++. Algorithms that modify Newton's equation of motion in order to generate a constant-temperature (rather than a constant-energy) ensemble are called *thermostat algorithms*. Several methods for performing MD at constant temperature have been proposed in the literature.[7,111] Among non-stochastic thermostatting methods, one can distinguish between temperature *constraining* and temperature *relaxation* approaches. The latter can *e.g.* be implemented in a *weak coupling* or an *extended-system* scheme.
MD++ offers a weak coupling and an extended-sytem [Nosé-Hoover (chain)] thermostat. Here, we present the implementation of these algorithms in the context of a simple velocity-scaling scheme acting on *free-flight* velocities. Denoting the unscaled free-flight velocity of atom k pertaining to the degrees of freedom set $\{D\}_i$ with ${\mathbf{v}^{un}}_k\left(t+\frac{\Delta t}{2}\right)$, the velocity scaling obeys the following equations:

- in the case of only the translational degrees of freedom of atom k (belonging to temperature group $\mathcal{G}_{Tj}$) being coupled to a temperature bath $\mathcal{B}_{Tn}(\{D\}_i)$,

$$\begin{aligned}\mathbf{v}_k\left(t+\frac{\Delta t}{2}\right) &= \lambda[t;\mathcal{B}_{Tn}(\{D\}_i)]\mathbf{v}^{un}_{tr}\left(t+\frac{\Delta t}{2};\mathcal{G}_{Tj}\right) \\ &+ \left[{\mathbf{v}^{un}}_k\left(t+\frac{\Delta t}{2}\right)-\mathbf{v}^{un}_{tr}\left(t+\frac{\Delta t}{2};\mathcal{G}_{Tj}\right)\right] \quad ;\end{aligned} \tag{12.8}$$

- in the case of only the internal+rotational degrees of freedom of atom k (belonging to temperature group $\mathcal{G}_{Tj}$) being coupled to a temperature bath $\mathcal{B}_{Tm}(\{D\}_i)$,

$$\begin{aligned}\mathbf{v}_k\left(t+\frac{\Delta t}{2}\right) &= \mathbf{v}^{un}_{tr}\left(t+\frac{\Delta t}{2};\mathcal{G}_{Tj}\right) \\ &+ \lambda[t;\mathcal{B}_{Tm}(\{D\}_i)]\left[{\mathbf{v}^{un}}_k\left(t+\frac{\Delta t}{2}\right)-\mathbf{v}^{un}_{tr}\left(t+\frac{\Delta t}{2};\mathcal{G}_{Tj}\right)\right] \quad ;\end{aligned} \tag{12.9}$$

- in the case of the translational degrees of freedom of atom k (belonging to temperature group $\mathcal{G}_{Tj}$) being coupled to a temperature bath $\mathcal{B}_{Tn}(\{D\}_i)$ and the internal+rotational degrees of freedom of atom k (belonging to temperature group $\mathcal{G}_{Tj}$) being coupled to a temperature bath $\mathcal{B}_{Tm}(\{D\}_i)$,

$$\begin{aligned}\mathbf{v}_k\left(t+\frac{\Delta t}{2}\right) &= \lambda[t;\mathcal{B}_{Tn}(\{D\}_i)]\mathbf{v}^{un}_{tr}\left(t+\frac{\Delta t}{2};\mathcal{G}_{Tj}\right) \\ &+ \lambda[t;\mathcal{B}_{Tm}(\{D\}_i)]\left[{\mathbf{v}^{un}}_k\left(t+\frac{\Delta t}{2}\right)-\mathbf{v}^{un}_{tr}\left(t+\frac{\Delta t}{2};\mathcal{G}_{Tj}\right)\right] \quad ,\end{aligned} \tag{12.10}$$

where, in analogy to Eq. 12.5, the *unscaled* translational velocity of temperature group $\mathcal{G}_{Tj}$ is computed as

$$\mathbf{v}^{un}_{tr}\left(t+\frac{\Delta t}{2};\mathcal{G}_{Tj}\right)=M^{-1}(\mathcal{G}_{Tj})\sum_{k\in\mathcal{G}_{Tj}}m_k{\mathbf{v}^{un}}_k\left(t+\frac{\Delta t}{2};\mathcal{G}_{Tj}\right) \quad . \tag{12.11}$$

For details about the isothermal equations of motions resulting from the application of the different thermostat algorithms, the corresponding phase space metrics and conserved properties, the reader is referred to the original papers introducing these methods.

Woodcock thermostat

A temperature constraint algorithm does not allow any temperature fluctuations, *i.e.*, it enforces, at each time step, the instantaneous temperature $\mathcal{T}(t';\{D\}_i)$ to be equal to the corresponding reference temperature $\mathcal{T}_o[\mathcal{B}_{Tj}(\{D\}_i)]$. This can be done with *e.g.* the Woodcock thermostat[112], where the scaling factor at time t is computed as

$$\lambda[t;\mathcal{B}_{Tj}(\{D\}_i)]=\left[\frac{N_{df}(\{D\}_i)-1}{N_{df}(\{D\}_i)}\frac{\mathcal{T}_o[\mathcal{B}_{Tj}(\{D\}_i)]}{\mathcal{T}(t';\{D\}_i)}\right]^{\frac{1}{2}} \quad . \tag{12.12}$$

The Woodcock thermostat generates a canonical distribution of coordinates, but (due to the absence of kinetic energy fluctuations) not momenta, at $\mathcal{T}_o$.

Berendsen thermostat

A weak-coupling algorithm[11] achieves a first-order relaxation of the instantaneous temperature $\mathcal{T}(t';\{D\}_i)$ to the corresponding reference temperature $\mathcal{T}_o[\mathcal{B}_{Tj}(\{D\}_i)]$) according to

$$\frac{d\mathcal{T}(t';\{D\}_i)}{dt} = \tau^{-1}[\mathcal{B}_{Tj}(\{D\}_i)]\left\{\mathcal{T}_o[\mathcal{B}_{Tj}(\{D\}_i)] - \mathcal{T}(t';\{D\}_i)\right\} \quad . \tag{12.13}$$

The scaling factor describing this relaxation in terms of a velocity-scaling according to Eq. 12.8-Eq. 12.10 is found by expressing the change of the kinetic energy in terms of the heat capacity (per degree of freedom) at constant volume c_v^{df} as

$$\Delta\mathcal{K}(t';\{D\}_i) = N_{df}(\{D\}_i)c_v^{df}k_B\Delta T(t') \quad , \tag{12.14}$$

so that, using[11] $c_v^{df} = \frac{1}{2}k_B$, the so-called Berendsen thermostat is recovered, with

$$\begin{aligned}\lambda[t;\mathcal{B}_{Tj}(\{D\}_i)] &= \left\{1 + 2c_v^{df}k_B^{-1}\tau^{-1}[\mathcal{B}_{Tj}(\{D\}_i)]\Delta t\left[\frac{\mathcal{T}_o[\mathcal{B}_{Tj}(\{D\}_i)]}{\mathcal{T}(t';\{D\}_i)} - 1\right]\right\}^{\frac{1}{2}} \\ &= \left\{1 + \tau^{-1}[\mathcal{B}_{Tj}(\{D\}_i)]\Delta t\left[\frac{\mathcal{T}_o[\mathcal{B}_{Tj}(\{D\}_i)]}{\mathcal{T}(t';\{D\}_i)} - 1\right]\right\}^{\frac{1}{2}} \quad .\end{aligned} \tag{12.15}$$

The temperature bath-specific parameter $\tau[\mathcal{B}_{Tj}(\{D\}_i)]$ is a purely empirical quantity adjusting the strength of the coupling of the degrees of freedom set $\{D\}_i$ to the heat bath $\mathcal{B}_{Tj}(\{D\}_i)$. In the limit $\tau[\mathcal{B}_{Tj}(\{D\}_i)] = \Delta t$, the Berendsen algorithm is equivalent to the Woodcock temperature constraining algorithm, except for the reduction of degrees of freedom by one. In the limit $\tau[\mathcal{B}_{Tj}(\{D\}_i)] \to \infty$, thermostatting is disabled, and Newton's equations of motion are recovered. Note that the isothermal equations of motion given by the Berendsen thermostat will not sample canonical coordinates *and* momenta. Only if the Berendsen thermostat reduces to the Woodcock one ($\tau[\mathcal{B}_{Tj}(\{D\}_i)] = \Delta t$) will the generated configurations be canonical. Neither the Woodcock nor the Berendsen thermostat render possible canonical sampling of the momenta. This deficiency has to be considered if fluctuation-dependent properties[113] are to be computed in the analysis of simulation data.

Nosé-Hoover thermostat

The modification of Newton's equations of motion to generate an isothermal trajectory can also be done in an extended-system approach. This thermostatting method was originally developed by Nosé,[114] and subsequently cast into the more practical framework nowadays-known as the Nosé-Hoover thermostat.[115,116] The corresponding equations of motion sample a microcanonical ensemble in the extended system, and a canonical emsemble in the real system. The extension of the system is brought about by introducing an additional artificial dynamical variable $\tilde{s}_1(t)$ [with mass $Q_1 > 0$ and velocity $\dot{\tilde{s}}_1(t)$]. The velocity $\dot{\tilde{s}}_1(t)$ of the extended-system variable is equal to the function $\gamma_1(t)$ controlling the heat exchange between the thermostatted (real) system and the heat bath, such that, for atom k,

$$\dot{\mathbf{p}}_k(t) = \mathbf{f}_k(t) - \gamma_1(t)\mathbf{p}_k(t) \quad , \tag{12.16}$$

with $\mathbf{f}_k(t)$ denoting the force acting on atom k at time t and $\mathbf{p}_k(t)$ denoting the momentum corresponding to the thermostatted velocity of atom k. The time-evolution of $\tilde{s}_1(t)$ is described by a second-order equation, which implies that heat fluxes between the system and the bath, and hence the temperature evolution, are oscillatory. These oscillations can be tuned by the mass Q_1 of $\tilde{s}_1(t)$. Considering the first-order evolution of $\gamma_1(t)$ [rather than the second-order evolution of $\tilde{s}_1(t)$] for a certain temperature bath $\mathcal{B}_{Tj}$,

$$\begin{aligned}\dot{\gamma}_1[t;\mathcal{B}_{Tj}(\{D\}_i)] &= -k_B N_{df}(\{D\}_i)Q_1^{-1}[\mathcal{B}_{Tj}(\{D\}_i)]\cdot \\ &\quad \left\{\mathcal{T}_o[\mathcal{B}_{Tj}(\{D\}_i)] - \mathcal{T}(t';\{D\}_i)\right\} \quad ,\end{aligned} \tag{12.17}$$

and using $Q_1[\mathcal{B}_{Tj}(\{D\}_i)] = \tau_1^2[\mathcal{B}_{Tj}(\{D\}_i)]N_{df}(\{D\}_i)k_B\mathcal{T}_o[\mathcal{B}_{Tj}(\{D\}_i)]$, one finds

$$\dot{\gamma}_1[t;\mathcal{B}_{Tj}(\{D\}_i)] = -\tau_1^{-2}[\mathcal{B}_{Tj}(\{D\}_i)]\left\{1 - \frac{\mathcal{T}(t';\{D\}_i)}{\mathcal{T}_o[\mathcal{B}_{Tj}(\{D\}_i)]}\right\} \quad , \tag{12.18}$$

thereby introducing an effective relaxation time

$$\tau_1[\mathcal{B}_{Tj}(\{D\}_i)] = \left\{\frac{Q_1[\mathcal{B}_{Tj}(\{D\}_i)]}{N_{df}(\{D\}_i)k_B\mathcal{T}_o[\mathcal{B}_{Tj}(\{D\}_i)]}\right\}^{\frac{1}{2}} \tag{12.19}$$

instead of the less intuitive effective mass $Q_1[\mathcal{B}_{Tj}(\{D\}_i)]$ to characterize the strength of the coupling to the heat bath.

MD++ implements the Nosé-Hoover thermostat by using

$$\lambda[t;\mathcal{B}_{Tj}(\{D\}_i)] = 1 - \Delta t \gamma_1[t;\mathcal{B}_{Tj}(\{D\}_i)] \quad , \tag{12.20}$$

where $\gamma_1[t;\mathcal{B}_{Tj}(\{D\}_i)]$ is determined by discrete integration,

$$\begin{aligned} \gamma_1[t;\mathcal{B}_{Tj}(\{D\}_i)] &= \gamma_1[t-\Delta t;\mathcal{B}_{Tj}(\{D\}_i)] \\ &+ \Delta t \tau_1^{-2}[\mathcal{B}_{Tj}(\{D\}_i)] \left\{ \frac{\mathcal{T}(t';\{D\}_i)}{\mathcal{T}_o[\mathcal{B}_{Tj}(\{D\}_i)]} - 1 \right\} \quad , \end{aligned} \tag{12.21}$$

which follows from Eq. 12.16 propagating the momentum variables at (due to use of the leap-frog scheme) half-integer time steps as

$$\mathbf{p}_k(t'+\Delta t) = \mathbf{p}_k(t') + \Delta t \left[\mathbf{f}_k(t) - \gamma_1(t)\mathbf{p}_k(t')\right] = m_k \mathbf{v}^{un}{}_k \left[1 - \gamma_1(t)\Delta t\right] \quad , \tag{12.22}$$

where, again, $\mathbf{v}^{un}{}_k$ denotes the unscaled free-flight velocity of atom k.
The temperature bath-specific parameter $\tau[\mathcal{B}_{Tj}(\{D\}_i)]$ is a purely empirical quantity adjusting the strength of the coupling of the degrees of freedom set $\{D\}_i$ to the heat bath $\mathcal{B}_{Tj}(\{D\}_i)$. Too large values of $\tau[\mathcal{B}_{Tj}(\{D\}_i)]$ (loose coupling; high mass of the extended-system variable) may cause a poor temperature control (the limiting case $\tau[\mathcal{B}_{Tj}(\{D\}_i)] \to \infty$ generating the microcanonical ensemble), whereas too small values (tight coupling; low mass of the extended-system variable) may cause high-frequency temperature oscillations.

Nosé-Hoover chain thermostat

The Nosé-Hoover chain thermostat[117] aims at relaxing the instantaneous temperature $\mathcal{T}(t';\{D\}_i)$ to the reference value $\mathcal{T}_o[\mathcal{B}_{Tj}(\{D\}_i)]$ based on a chain of successive thermostat variables. In this case, the single thermostat variable $\gamma_1[t;\mathcal{B}_{Tj}(\{D\}_i)]$ of the Nosé-Hoover scheme is enhanced by a chain of variables $\gamma_c[t;\mathcal{B}_{Tj}(\{D\}_i)]$, $c = 2, ..., N_c$, applying a thermostat to each other in sequence. This algorithm has been introduced[117] to alleviate the two main drawbacks of the Nosé-Hoover algorithm: (*i*) the presence of spurious temperature oscillations; (*ii*) the non-ergodicity of the sampling for small or stiff systems, or systems at low temperatures.
MD++ implements the Nosé-Hoover chain thermostat in analogy to Eq. 12.20 and Eq. 12.21 as

$$\lambda[t;\mathcal{B}_{Tj}(\{D\}_i)] = 1 - \Delta t \gamma_1[t;\mathcal{B}_{Tj}(\{D\}_i)] \quad , \tag{12.23}$$

where $\gamma_1[t;\mathcal{B}_{Tj}(\{D\}_i)]$ is determined by discrete integration,

$$\begin{aligned} \gamma_1[t;\mathcal{B}_{Tj}(\{D\}_i)] &= \gamma_1[t-\Delta t;\mathcal{B}_{Tj}(\{D\}_i)] + \Delta t \tau_1^{-2}[\mathcal{B}_{Tj}(\{D\}_i)] \left\{ \frac{\mathcal{T}(t';\{D\}_i)}{\mathcal{T}_o[\mathcal{B}_{Tj}(\{D\}_i)]} - 1 \right\} \\ &- \Delta t \gamma_1[t-\Delta t;\mathcal{B}_{Tj}(\{D\}_i)]\gamma_2[t;\mathcal{B}_{Tj}(\{D\}_i)] \quad , \end{aligned} \tag{12.24}$$

each successive chain thermostat $\gamma_c[t;\mathcal{B}_{Tj}(\{D\}_i)]$, $c = 2, ..., N_c - 1$ is propagated according to

$$\begin{aligned} \gamma_c[t;\mathcal{B}_{Tj}(\{D\}_i)] &= \gamma_c[t-\Delta t;\mathcal{B}_{Tj}(\{D\}_i)] \\ &+ \Delta t \left\{ \tau_c^{-2}[\mathcal{B}_{Tj}(\{D\}_i)] \left[\tau_{c-1}^2[\mathcal{B}_{Tj}(\{D\}_i)]\gamma_{c-1}^2[t-\Delta t;\mathcal{B}_{Tj}(\{D\}_i)] \right.\right. \\ &\left.\left. - {N_{df}}^{-1}(\{D\}_i) \right] - \gamma_c[t-\Delta t;\mathcal{B}_{Tj}(\{D\}_i)]\gamma_{c+1}[t;\mathcal{B}_{Tj}(\{D\}_i)] \right\} \quad , \end{aligned} \tag{12.25}$$

the last one being

$$\begin{aligned} \gamma_{N_c}[t;\mathcal{B}_{Tj}(\{D\}_i)] &= \gamma_{N_c}[t-\Delta t;\mathcal{B}_{Tj}(\{D\}_i)] \\ &+ \Delta t \tau_{N_c}^{-2}[\mathcal{B}_{Tj}(\{D\}_i)] \left[\tau_{N_c-1}^2[\mathcal{B}_{Tj}(\{D\}_i)]\gamma_{N_c-1}^2[t-\Delta t;\mathcal{B}_{Tj}(\{D\}_i)] \right. \\ &\left. - {N_{df}}^{-1}(\{D\}_i) \right] \quad . \end{aligned} \tag{12.26}$$

This follows from the chain analog of Eq. 12.22

$$\mathbf{p}_k(t'+\Delta t) = \mathbf{p}_k(t') + \Delta t \left[\mathbf{f}_k(t) - \gamma_1(t)\mathbf{p}_k(t')\right] = m_k \mathbf{v}^{un}{}_k \left[1 - \gamma_1(t)\Delta t\right] \quad , \tag{12.27}$$

with the corresponding equations for the chain thermostat variables,

$$\begin{aligned} \mathbf{p}_{\gamma_1}(t'+\Delta t) &= \mathbf{p}_{\gamma_1}(t') \\ &+ \Delta t \left\{ 2\Delta\mathcal{K}(t';\{D\}_i) - N_{df}(\{D\}_i) k_B \mathcal{T}_o[\mathcal{B}_{Tj}(\{D\}_i)] \right\} \end{aligned} \tag{12.28}$$

$$- \quad \mathbf{p}_{\gamma_1}(t') \frac{\mathbf{p}_{\gamma_2}(t'+\Delta t)}{\tau_2^2[\mathcal{B}_{Tj}(\{D\}_i)] N_{df}(\{D\}_i) k_B \mathcal{T}_o[\mathcal{B}_{Tj}(\{D\}_i)]} \quad ,$$

$$\begin{aligned} \mathbf{p}_{\gamma_c}(t'+\Delta t) &= \mathbf{p}_{\gamma_c}(t') \\ &+ \Delta t \left\{ \frac{\mathbf{p}^2_{\gamma_{c-1}}(t')}{\tau_{c-1}^2[\mathcal{B}_{Tj}(\{D\}_i)] N_{df}(\{D\}_i) k_B \mathcal{T}_o[\mathcal{B}_{Tj}(\{D\}_i)]} - k_B \mathcal{T}_o[\mathcal{B}_{Tj}(\{D\}_i)] \right\} \\ &- \mathbf{p}_{\gamma_c}(t') \frac{\mathbf{p}_{\gamma_{c+1}}(t'+\Delta t)}{\tau_{c+1}^2[\mathcal{B}_{Tj}(\{D\}_i)] N_{df}(\{D\}_i) k_B \mathcal{T}_o[\mathcal{B}_{Tj}(\{D\}_i)]} \quad , \end{aligned} \tag{12.29}$$

and

$$\begin{aligned} \mathbf{p}_{\gamma_{N_c}}(t'+\Delta t) &= \mathbf{p}_{\gamma_{N_c}}(t') \\ &+ \Delta t \left\{ \frac{\mathbf{p}^2_{\gamma_{N_c-1}}(t')}{\tau_{N_c-1}^2[\mathcal{B}_{Tj}(\{D\}_i)] N_{df}(\{D\}_i) k_B \mathcal{T}_o[\mathcal{B}_{Tj}(\{D\}_i)]} - k_B \mathcal{T}_o[\mathcal{B}_{Tj}(\{D\}_i)] \right\} \quad , \end{aligned} \tag{12.30}$$

where N_c chain thermostats are used.

12.2.3. Use of temperature groups, sets of degrees of freedom and thermostats. If different parts of the molecular system are subject to different heating rates due to, for example, the use of a non-bonded interaction cut-off radius, it may be necessary to *separately couple the different parts of the system to different temperature baths*.
In the following we will explain the characterisation and definition of temperature groups, degrees of freedom sets and temperature baths in MD++. Finally, we will summarize the flexibility of temperature coupling in MD++ and provide an example of a typical thermostat setting in a biomolecular simulation.
In the following, we will use the abbreviation tr for translational, i+r for internal+rotational degrees of freedom and dof for degrees of freedom.

- **Temperature groups in MD++**
  Temperature groups are molecular entities serving to dissect tr and i+r properties, *e.g.* in the computation of degrees of freedom, velocities or kinetic energies, or in the application of translational and/or rotational constraints. Usually, one molecule forms one temperature group, *e.g.* one protein, or one water molecule. But also just one particle, *e.g.* an ion, can be one temperature group.

  Temperature groups are defined in the molecular topology file (TEMPERATUREGROUPS block) for those molecular entities contained in the solute molecular topology (SOLUTEATOM block). If the system contains solvent molecules from the solvent molecular topology (SOLVENTATOM block), each solvent molecule inevitably (*i.e.* not changeable by the user) constitutes one separate temperature group.
- **Sets of degrees of freedom in MD++**
  A dof set is a collection of atoms (MD++) that are affected by the same thermostat settings.
  A dof set I is defined and characterized in the MULTIBATH block *via* the joint specification of: (*i*) the last atom in this dof set [LAST(I)]; (*ii*) the temperature bath the tr dof of this dof set are coupled to [COM-BATH(I)]; (*iii*) the temperature bath the i+r dof of this dof set are coupled to [IR-BATH(I)].

- **Temperature baths in MD++**
  A temperature bath is a heat reservoir of constant reference temperature thermostatting one or several dof sets.

  A temperature bath I is defined and characterized in the MULTIBATH block *via* the joint specification of: (*i*) the reference temperature of this bath [TEMP0(I)]; (*ii*) the coupling time of this bath [TAU(I)]. Note that the specification of a certain thermostat algorithm, as well as of the number of chains in the Nosé-Hoover chain thermostat, thus inevitably apply to all temperature baths. In adddition, in the case of thermostatting with the Nosé-Hoover chain algorithm, each of the chain thermostat variables will have the same coupling time.

Finally, we consider the example of two peptide copies in a methanol-water mixture. More specifically, we consider a topology whose solute block consists of two peptides (2x50 atoms) and 500 methanol molecules (1500 atoms). Furthermore, we assume the system to contain 4000 water molecules, *i.e.* the coordinate file will contain 100 peptide and 1500 methanol atoms as well as 12000 water atoms. We define the following

4502 temperature groups: Peptides 1 and 2 (temperature group defined in the molecular topology file), each of methanol molecules 1-500 (temperature groups defined in the molecular topology file), and each of the water molecules 1-4000 (temperature group definitions being an immediate consequence of the solvent nature).

In a typical MD simulation, one would here employ three different temperature baths. In a physically-realistic equilibrium situation, these three baths would have equal temperatures. One would couple the tr dof of the two peptides to bath 1, the i+r dof the two peptides to bath 2, and the tr and rotational dof of all (rigid) methanol and water molecules to bath 3. We assume thermostatting at 298.15 K by the weak coupling method with a coupling time of 0.1 ps.
The MD++ MULTIBATH block reads:

```
MULTIBATH
# general thermostatting settings
# ALGORITHM
0
# NBATHS
3
# temperature bath definition and characterisation
# TEMP0(1..NBATHS)
298.15 298.15 298.15
# TAU(1..NBATHS)
0.1 0.1 0.1
# DOFSET
4
# dof set definition and characterisation
# LAST(1..DOFSET) COM-BATH(1..DOFSET) IR-BATH(1..DOFSET)
# peptides
100 1 2
# 500 methanol molecules
1600 3 3
# solvent molecules
13600 3 3
END
```

Finally, an important practical issue arises in thermostatted MD simulations: When Newton's equations of motion Eq. 2.8 are integrated, the total energy and the total translational momentum of the system are conserved. This need no longer be true when a coupling to a temperature bath is applied. The centre of mass may slowly pick up motion during an MD simulation, even when initially at rest. This motion may be regularly removed, which is described in Sec. 4.4.

12.3. Number of degrees of freedom

It is important to know exactly how many and which degrees of freedom are being simulated. For a system with $\mathcal{N}_a$ particles moving in three dimensions, the total number of degrees of freedom $\mathcal{N}_d$ is essentially $3\mathcal{N}_a$. However, the application of various boundary conditions in the form of geometric constraints will reduce this number. Each temperature group (TG) $\mathcal{G}_{Ti}$ is assigned a certain number of translational $[N^t_{df}(\mathcal{G}_{Ti})]$ and internal+rotational $[N^{ir}_{df}(\mathcal{G}_{Ti})]$ degrees of freedom (DOF). In the absence of any constraints, the values of these variables for a given TG $\mathcal{G}_{Ti}$ consisting of $N_{\mathcal{G}_{Ti}}$ atoms are $N^t_{df}(\mathcal{G}_{Ti}) = 3$, and $N^{ir}_{df}(\mathcal{G}_{Ti}) = 3(N_{\mathcal{G}_{Ti}} - 1)$, respectively. However, simulations are usually performed in ensembles involving a variety of different constraints, *e.g.* position, distance, dihedral angle, rotational and/or translational constraints, or constraints of the linear and/or angular momentum or of the temperature of the system. Any application of constraints (not redundant to already existing constraints) to a given TG I will reduce the number of degree of freedom of this TG. The following section explains how the number of degree of freedom is reduced.

If TG $\mathcal{G}_{Ti}$ contains ${N_{\mathcal{G}_T}^{poscon}}_i > 0$ posititionally-constrained atoms, $N_{df}^t(\mathcal{G}_{Ti})$ is decreased by three and $N_{df}^{ir}(\mathcal{G}_{Ti})$ by $3({N_{\mathcal{G}_T}^{poscon}}_i - 1)$. Remember that a temperature group consists of covalently bound atoms, meaning that a single position restraint on an atom in the group removes the translational degrees of freedom of the group.

If TG $\mathcal{G}_{Ti}$ contains ${N_{\mathcal{G}_T}^{discon}}_i > 0$ distance-constraints involving at least one non-positionally-constrained atom, $N_{df}^{ir}(\mathcal{G}_{Ti})$ is decreased by ${N_{\mathcal{G}_T}^{discon}}_i$. Any dof reduction arising from distance constraints between two different TG is distributed in equal amounts (one half) between the two TG.

If TG $\mathcal{G}_{Ti}$ contains ${N_{\mathcal{G}_T}^{dihcon}}_i > 0$ dihedral-angle constraints involving at least one non-positionally-constrained atom, $N_{df}^{ir}(\mathcal{G}_{Ti})$ is decreased by ${N_{\mathcal{G}_T}^{dihcon}}_i$. Any dof reduction arising from dihedral-angle constraints between two different TG $\mathcal{G}_{Ti}$, $\mathcal{G}_{Tj}$ is distributed in a ratio of $\frac{N_{dih,a}(\mathcal{G}_{Ti})}{N_{dih,a}(\mathcal{G}_{Tj})}$ between the two TG, where $1 \leq N_{dih,a}(\mathcal{G}_{Ti}) \leq 3$, $1 \leq N_{dih,a}(\mathcal{G}_{Tj}) \leq 3$ (with $N_{dih,a}(\mathcal{G}_{Ti}) + N_{dih,a}(\mathcal{G}_{Tj}) = 4$) are the numbers of dihedral-angle atoms contained in TG $\mathcal{G}_{Ti}$ and $\mathcal{G}_{Tj}$, respectively.

If TG $\mathcal{G}_{Ti}$ is translationally-constrained, $N_{df}^t(\mathcal{G}_{Ti})$ will be decreased by three. If TG $\mathcal{G}_{Ti}$ is rotationally-constrained, $N_{df}^{ir}(\mathcal{G}_{Ti})$ will be decreased by three.

When the system linear and/or angular momentum is constrained, three dof must be removed for each constrained type of momentum. After application of the previous rules, there will be M TG $\mathcal{G}_{Ti}$ for which $N_{df}^t(\mathcal{G}_{Ti}) > 0$. For these groups, $N_{df}^t(\mathcal{G}_{Ti})$ is decreased by $3/M$ if the system linear momentum is constrained and by $3/M$ if the system angular momentum is constrained. When instead the centre-of-mass motion is removed every NSCM steps, NDFMIN degrees of freedom are removed in the same way at those time points.

When temperature constraining is applied, the number of dof of TG $\mathcal{G}_{Ti}$ coupled to a temperature bath involved in temperature constraining must be decreased by one (to ensure canonical sampling in the configurational space). In this case, and after application of the previous rules and for a given translational set of DOF $\{D^t\}_j$, there will be $M(\{D^t\}_j)$ TG $\mathcal{G}_{Ti} \in \{D^t\}_j$ for which $N_{df}^t(\mathcal{G}_{Ti}) > 0$. For these groups, $N_{df}^t(\mathcal{G}_{Ti}) > 0$ is decreased by $1/M(\{D^t\}_j)$. Similarly, for a given internal+rotational set of DOF $\{D^{ir}\}_j$, there will be $N(\{D^{ir}\}_j)$ TG $\mathcal{G}_{Ti} \in \{D^{ir}\}_j$ for which $N_{df}^{ir}(\mathcal{G}_{Ti}) > 0$. For these groups, $N_{df}^{ir}(\mathcal{G}_{Ti})$ is decreased by $1/N(\{D^{ir}\}_j)$.

12.4. Calculation of the virial

In the GROMOS implementation, the way the virial is calculated can be chosen. In the PRESSURESCALE block the switch VIRIAL can be set to none(0) (no virial calculated), atomic(1) (atomic virial) or group(2) (group-based virial), and these settings equally apply to solute and solvent.

The group based instantaneous pressure tensor $\underline{\mathcal{P}}$ is related to the group-based virial and group-based internal kinetic energy tensor of the system. The word *group-based* refers to a pressure definition excluding virial and kinetic-energy contributions within user-specified groups of (covalently-linked) atoms[118,119]. These groups will be referred to as pressure groups (see Vol. 3). Single atoms can be used as pressure groups, in which case an atom-based pressure definition is recovered. In the same way molecules can be defined as pressure groups to recover a molecular-based pressure definition. The average pressure is not affected by the specific choice of groups, but the pressure fluctuations are. In practice, atom grouping is used to reduce these fluctuations. The pressure is only calculated for systems under periodic boundary conditions. Note also that the contribution of special (nonphysical) forces (e.g., atom-position or atom-distance restraining) to the pressure is generally not included, except for atom-distance restraining. The instantaneous atom-based pressure tensor is computed as

$$\underline{\mathcal{P}}^* = \frac{2}{\mathcal{V}}(\underline{\mathcal{K}}^* - \underline{\mathcal{W}}^*) \tag{12.31}$$

where

$$\underline{\mathcal{K}}^* = \tfrac{1}{2}\sum_{i=1}^{N} m_i \dot{\mathbf{r}}_i \otimes \dot{\mathbf{r}}_i \tag{12.32}$$

and

$$\underline{\mathcal{W}}^*_{\mu\nu} = \tfrac{1}{2}\sum_{\lambda}\frac{\partial \mathcal{U}}{\partial \mathcal{B}_{\mu\lambda}}\mathcal{B}_{\nu\lambda} \tag{12.33}$$

are the instantaneous atom-based internal kinetic energy and virial tensors, and $\mathcal{V}$ and $\mathcal{U}$ being the instantaneous volume and total potential energy of the system, $\underline{\mathcal{B}}$ the box matrix introduced in Sec. 3.5 and $\dot{\mathbf{r}}_i$ the internal velocities. The corresponding isotropic (scalar) quantities are related to the tensor quantities through

$$\mathcal{K}^* = Tr[\underline{\mathcal{K}}^*], \mathcal{W}^* = Tr[\underline{\mathcal{W}}^*], \mathcal{P}^* = (1/3)Tr[\underline{\mathcal{P}}^*], \tag{12.34}$$

where Tr returns the trace of a matrix, $\mathcal{K}^*$ is equivalent to Eq. 2.6, and $\mathcal{W}$ is defined as

$$\mathcal{W}^* = \frac{3\mathcal{V}}{2}\frac{\partial \mathcal{U}}{\partial \mathcal{V}}. \tag{12.35}$$

One can show that:[102,120] (1) the contribution to the atom-based virial tensor of a potential energy term that solely depends on the scalar products or determinants defined by a set of interatomic vectors is symmetric; (2) the contribution to the atom-based virial tensor of a potential energy term that solely depends on the angles defined by a set of vectors is (in addition) traceless. The first observation implies that all covalent (bond stretching or constraint, bond-angle bending, proper and improper dihedral angle), and pairwise nonbonded force field terms lead to a symmetric contribution to the atom-based virial. The second observation implies that covalent bond-angle bending as well as proper and improper dihedral angle (but not bond stretching or constraint and pairwise nonbonded) terms lead to a traceless contribution to the atom-based virial (i.e., no contribution to the scalar atom-based pressure). However, these results are generally not valid for the corresponding group-based tensor (see below).

In the special case of a pairwise-additive interaction term $\mathcal{U}_p$ depending on minimum-image interatomic distances and without explicit dependence on the box dimensions (bond stretching or constraint and pairwise nonbonded terms; but not reciprocal-space lattice-sum interactions[118,119] see Sec. 7.4), Eq. 12.33 leads to a virial contribution

$$\mathcal{W}^*_p = -\tfrac{1}{2}\sum_{i=1}^{N}\sum_{j>i}^{N}\mathbf{f}_{p,ij}\otimes\overline{\mathbf{r}}_{ij}, \tag{12.36}$$

where $\mathbf{r}_{ij} = \mathbf{r}_i - \mathbf{r}_j$ is the vector connecting j to i, $\overline{\mathbf{r}}_{ij}$ the corresponding minimum-image vector, and $\mathbf{f}_{p,ij}$ the pairwise force exerted by atom j on atom i. This equation is easily generalized to interaction terms involving more than two atoms (bond-angle bending, proper and improper dihedral-angle terms). The atom based virial contribution of all covalent (including bond constraints) and nonbonded (excluding reciprocal-space lattice-sum interactions) terms is calculated using Eq. 12.36 or one of its generalizations. Note that MD++ internally stores the virial without the prefactor $-\frac{1}{2}$.

The GROMOS implementation includes the possibility of using a group-based pressure definition (corresponding to any arbitrary partitioning of atoms into virial groups), instead of the atom-based one. In this case, the intragroup contribution to the kinetic energy as well as the contribution of intragroup forces to the virial are removed from the pressure definition (which affects the fluctuations of this quantity, but not its average value). As shown elsewhere[118,119] (the equations reported therein should be altered by halving the virial and replacing $\mathbf{r}_{ij}$ by $-\mathbf{r}_{ij}$ to match the present conventions), the group-based virial tensor can be calculated from the corresponding atom-based tensor by adding a simple correction term, which depends on the overall atomic forces and on the pressure group definitions. More precisely, the group-based virial tensor is given by

$$\underline{\mathcal{W}} = \underline{\mathcal{W}}* + \tfrac{1}{2}\sum_{I\alpha}\mathbf{f}_{I\alpha}\otimes\mathbf{d}_{\mathbf{I}\alpha}, \tag{12.37}$$

where $I\alpha$ denotes atom α in pressure group I, $\mathbf{f}_{I\alpha}$ the overall force on atom $I\alpha$, and $\mathbf{d}_{\mathbf{I}\alpha}$ the coordinate vector of atom $I\alpha$ relative to the center of mass of the gathered pressure group I containing this atom. The *gathered* representation of the pressure group is generated by following the atoms as they drift throughout the periodic system. The group-based pressure tensor is then calculated as

$$\underline{\mathcal{P}} = \frac{2}{\mathcal{V}}(\underline{\mathcal{K}} - \underline{\mathcal{W}}) \tag{12.38}$$

where $\underline{\mathcal{K}}$ is the group-based internal kinetic energy tensor, defined as

$$\underline{\mathcal{K}} = \tfrac{1}{2}\sum_{I=1}^{N_s}\left(\sum_{\alpha=1}^{N_\alpha(I)} m_i\right)^{-1}\left(\sum_{\alpha=1}^{N_\alpha(I)} m_i\dot{\mathbf{r}}_i\right)\otimes\left(\sum_{\alpha=1}^{N_\alpha(I)} m_i\dot{\mathbf{r}}_i\right) \tag{12.39}$$

where N_s is the number of pressure groups and $N_\alpha(I)$ the number of atoms in pressure group I.

Although the atom-based pressure tensor $\underline{\mathcal{P}}*$ is typically symmetric, this is generally not the case for the group-based pressure tensor $\underline{\mathcal{P}}$ (although the antisymmetric contribution to this tensor should vanish upon time averaging). When applying a barostat algorithm, the antisymmetric component of $\underline{\mathcal{P}}$ should induce an overall rotation of the computational box (which would alter the box angular momentum), while the symmetric component results in a deformation of the box (which conserves the box angular momentum). In practice, the overall rotation of the box is rather a nuisance, and is avoided by symmetrizing the tensor ($\underline{\mathcal{P}} \rightarrow [\underline{\mathcal{P}} + {}^T\underline{\mathcal{P}}]$) prior to application of the barostat algorithm[121] where the T presuperscript indicates the transpose of the matrix.

12.5. Pressure scaling

For compatibility with experiment, it is often desirable to sample configurations from the isothermal-isobaric ensemble (constant temperature and pressure). Thermostat algorithms have been described in Sec. 12.2. A modification of the basic MD scheme with the purpose of maintaining the pressure constant (on average) is called a barostat algorithm. The various methods for carrying out MD at constant pressure are based on the same principles as the constant temperature schemes with the role of temperature played by the pressure and the role of the atomic velocities played by the atomic positions.

The use of a barostat is only applicable to simulations under periodic boundary conditions. In the GROMOS implementation, the various options for the variations for the box parameters (and the associated scaling of atomic coordinates) involved in the use of a barostat are: (1) no variations of the box parameters; (2) isotropic scaling, that is, identical relative variations of the box-edge lengths only; (3) semi-anisotropic scaling, that is, two box-edge lengths are scaled identically (or left constant) while the third box-edge length is scaled individually (or left constant); (4) partially anisotropic scaling, that is, independent relative variations of the box-edge lengths only; (5) fully anisotropic scaling, that is, independent variations of all box parameters (box-edge lengths, box angles, and Euler angles). For a truncated-octahedral box, only the first two options are allowed. For a rectangular box, only the first four options are allowed. For a triclinic box, all options are allowed. In the latter case, variations in the box shape are accompanied by variations in the box Euler angles, so as to guarantee that the barostat does not introduce a rigid-body rotational component to the box orientation. Note, however, that the location of the box center of mass is affected by any type of coordinate scaling. Like in the temperature scaling the *weak-coupling method* (Berendsen barostat[11]) is again very simple.

The atomic equations of motion are modified such that the net result on the system is a first-order relaxation of the pressure $\mathcal{P}$ towards the preset reference value P_0

$$\frac{d\mathcal{P}(t)}{dt} = \tau_P^{-1}[P_0 - \mathcal{P}(t)] \tag{12.40}$$

As described in Sec. 12.4 the hydrostatic pressure tensor can be calculated with Eq. 12.38 using the virial theorem,

$$\mathcal{P}_{\alpha\beta}(t) = 2[\mathcal{K}_{\alpha\beta}(t) - \mathcal{W}_{\alpha\beta}(t)]/\mathcal{V}(t) \tag{12.41}$$

where $\alpha = x, y$ or z and $\beta = x, y$ or z, $\underline{\mathcal{W}}(t)$ is the virial tensor (Sec. 12.4) and $\mathcal{V}$ (t) is the volume of the computational box. For a rectangular box we have (Sec. 4.4.2.1)

$$\mathcal{V}(t) = a(t)b(t)c(t) \tag{12.42}$$

with a, b and c the lengths of the x-, y- and z-axes of the computational box. For a truncated octahedron we have Sec. 4.4.2.2

$$\mathcal{V}(t) = \tfrac{1}{2}a^3(t). \tag{12.43}$$

and for a triclinic box (Sec. 4.4.1.3)

$$\begin{aligned}\mathcal{V}(t) &= a(t)b(t)c(t)[1 - \cos^2\alpha(t) - \cos^2\beta(t) - \cos^2\gamma(t) \\ &+ 2\cos\alpha(t)\cos\beta(t)\cos\gamma(t)]^{1/2}\ .\end{aligned} \tag{12.44}$$

The pressure components along the x-, y- and z-axes, that is, the diagonal elements $\mathcal{P}_{xx}$, $\mathcal{P}_{yy}$ and $\mathcal{P}_{zz}$ can be defined correspondingly,

$$\mathcal{P}_{\alpha\alpha}(t) = 2[\mathcal{K}_{\alpha\alpha}(t) - \mathcal{W}_{\alpha\alpha}(t)]/\mathcal{V}(t) \tag{12.45}$$

where $\alpha = x, y$ or z. The isotropic hydrostatic pressure $\mathcal{P}$ can then be calculated with

$$\mathcal{P}(t) = \frac{1}{3}(\mathcal{P}_{xx}(t) + \mathcal{P}_{yy}(t) + \mathcal{P}_{zz}(t)) \tag{12.46}$$

as described in Eq. 12.34. The isothermal compressibility κ_T will relate a change in pressure $\Delta\mathcal{P}$ at constant temperature to a change in volume $\Delta\mathcal{V}$,

$$\Delta\mathcal{P}(t) = \frac{-\Delta\mathcal{V}(t)}{\kappa_T \mathcal{V}(t)} \tag{12.47}$$

and a change in volume can be obtained by scaling the atomic coordinates and the edges of the computational box with a factor μ,

$$\Delta\mathcal{V}(t) = [(\mu(t))^3 - 1]\mathcal{V}(t). \tag{12.48}$$

Discretizing Eq. 12.40 using the MD time step Δt and solving the *pressure scaling factor* $\mu(t)$ from Eq. 12.40 and Eq. 12.46, Eq. 12.47 yields

$$\mu(t) = \left[1 - \kappa_{_T}\frac{\Delta t}{\tau_p}[P_0 - \mathcal{P}(t)]\right]^{\frac{1}{3}} \tag{12.49}$$

in the isotropic case,

$$\mu_\alpha(t) = \left[1 - \kappa_{_T}\frac{\Delta t}{\tau_p}[P_{0,\alpha\alpha} - \mathcal{P}_{\alpha\alpha}(t)]\right]^{\frac{1}{3}} \tag{12.50}$$

in case the x-, y- and z-dimensions are scaled separately and

$$\mu_{\alpha\beta}(t) = \left[\delta_{\alpha\beta} - \kappa_{_T}\frac{\Delta t}{\tau_p}[P_{0,\alpha\beta} - \mathcal{P}_{\alpha\beta}(t)]\right]^{\frac{1}{3}} \tag{12.51}$$

in case of fully anisotropic scaling. In the case of semi anisotropic scaling where two axes α and β are scaled with the same scaling factor

$$\mu_{\alpha,\beta}(t) = \left[1 - \kappa_{_T}\frac{\Delta t}{\tau_p}[(P_{0,\alpha\alpha} - \mathcal{P}_{\alpha\alpha}(t)) + (P_{0,\beta\beta} - \mathcal{P}_{\beta\beta}(t)))/2]\right]^{\frac{1}{3}}. \tag{12.52}$$

The elements of $P_{0,\alpha\beta}$ can be set separately. This is done with a reference pressure tensor PRES0(,) in the PRESSURESCALE block.

The scaling of the atomic coordinates $\mathbf{r}_i(t)$ and the box edges $\mathbf{a}(t)$, $\mathbf{b}(t)$ and $\mathbf{c}(t)$ with the factor $\mu(t)$ at each MD step will make the pressure $\mathcal{P}(t)$ or the components $\mathcal{P}_{\alpha\beta}(t)$ relax towards $\mathcal{P}_0$ (or $\mathcal{P}_{0,\alpha\beta}$), the relaxation rate being controlled by the ratio of the isothermal compressibility κ_T of the system and the chosen *pressure relaxation time* τ_P. The value of κ_T may not be accurately known, but this is no problem, since τ_P is an adjustable parameter. The values of the isothermal compressibility of water at a pressure of 1atm = 1.01325 Bar = 0.0610184 kJ mol^{-1}nm^{-3} and a temperature of 293K is for example κ_T = 45.91 10^{-6} Bar^{-1} = 76.24 10^{-5} (kJmol^{-1}nm^{-3})$^{-1}$**[122]**. The compressibility of proteins is about 10 to 20% of that of water**[123]**. So, for a system consisting of half protein half water we find an estimated value of $\kappa_{_T}$ = 45.75 10^{-5} (kJmol^{-1}nm^{-3})$^{-1}$. The switch to set the compressibility κ_T is called COMP. The value of τ_P, TAUP, should be chosen sufficiently small (strong coupling) to achieve the required average pressure, but on the other hand sufficiently large (weak coupling) to avoid disturbance of the properties of the system by the coupling to the pressure bath.**[11]** Since the definition of the pressure, Eqs. 12.41, 12.45), depends on the kinetic energy, the pressure coupling should not be stronger than the temperature coupling,

$$\tau_p > \tau_{_T}. \tag{12.53}$$

Typical values for τ_P are 0.4-0.5 ps.**[11]**

The following switches of the PRESSURESCALE block in MD++ have not been described yet (see Vol. 4):
The switch COUPLE is used to control the pressure scaling: COUPLE=off(0), no pressure calculation or scaling
COUPLE=calc(1), pressure calculation, but no scaling

COUPLE=scale(2), pressures calculation and scaling.
The switch SCALE chooses the scaling applied:
SCALE=off(0), no pressure scaling
SCALE=iso(1), isotropic pressure scaling
SCALE=aniso(2), anisotropic pressure scaling (x-, y-, z-axes, no angle deformation)
SCALE=full(3), fully anisotropic pressure scaling
SCALE=semianiso(4), semi-anisotropic pressure scaling
SEMI(1..3) gives the settings for the semi anisotropic pressure scaling. The 3 numbers can have values 0, 1 or 2 and represent the x-, y- and z-axes. If one of the numbers is 0, the according axis is not scaled. If two have the same number, they are scaled together.

12.6. MD algorithms

The *algorithm for* MD *simulation* based on the leap-frog integration scheme, which may include coupling to a temperature bath (indicated by the symbol T) and a pressure bath (indicated by the symbol P), and which may include the application of distance constraints (indicated by the symbol C) using one of the constraining methods described in Chap. 10 can be summarized by the following steps. The application of periodic boundary conditions is indicated by the symbol B. Writing data to file is indicated by the symbol W.

0. The positions $\mathbf{r}_i(t_n)$ and velocities $\mathbf{v}_i(t_n - \Delta t/2)$ for all atoms are given. Calculate the kinetic energies $\mathcal{K}(t_n - \Delta t/2)$, and the temperatures $T(t_n - \Delta t/2)$. The initial step number is zero, $n = 0$.

0P. The box lengths $\mathbf{a}(t_n),\ \mathbf{b}(t_n),\ \mathbf{c}(t_n)$ are given.

0C. The mentioned positions satisfy the constraints and the mentioned velocities, temperatures and kinetic energies do not contain components along the constraints.

0B. The solvent molecules may not be split by the periodic boundaries, they must be covalently connected. The same condition must hold for the atoms of a solute charge group.

1. Calculate the translational ($\mathcal{K}_{tr}(t_n - \Delta t/2)$) and rotational ($\mathcal{K}_{ir}(t_n - \Delta t/2)$) kinetic energy for the relevant temperature groups, using Eq. 12.6 and Eq. 12.7. Calculate the relative positions $d_{i\alpha}$, for solute and solvent as preparation for the virial calculation (Eq. 12.37).

1B. If required, apply the periodic boundary conditions to put the solute charge groups and solvent molecules in the central computational box (see Sec. 4.4.1.2).

2. Calculate the (unconstrained) forces from the potential energy function $\mathcal{V}(\boldsymbol{r}(t))$

$$\mathbf{f}_i(t_n) \quad = \quad -\frac{\partial \mathcal{V}(\boldsymbol{r}(t_n))}{\partial \mathbf{r}_i} \tag{12.54}$$

(Eq. 12.54)) using the nearest image convention in case of periodic boundary conditions, and at the same time

2P. calculate the atomic or group-based virial $\mathcal{W}^*(t_n)$ or $\mathcal{W}(t_n)$.

3C. If required, apply positions constraints (see Sec. 10.2), *i.e.* set forces and velocities to zero.

4. Determine the (unconstrained) velocities $\mathbf{v}_i(t_n + \Delta t/2)$ from Eq. 12.1.

5T. In case the group-based translational kinetic energy and the internal, rotational kinetic energy are jointly coupled to a temperature bath, scale the velocities $\mathbf{v}_i(t_n + \Delta t/2)$ of the atoms that are coupled to a temperature bath with the appropriate temperature scaling factor $\lambda(t_n - \Delta t/2)$ based on the relevant contributions to $\mathcal{K}(t_n - \Delta t/2)$. The calculation of the scaling factors is dependent on the thermostat chosen, see Sec. 12.2.

6. Determine the (unconstrained) positions $\mathbf{r}_i(t_n + \Delta t)$ from Eq. 12.2.

7C. Make the positions satisfy the constraints (see Sec. 10.3.1)

$$C(\boldsymbol{r}(t_n); \boldsymbol{r}(t_n + \Delta t); \boldsymbol{r}(t_n + \Delta t)) \tag{12.55}$$

8C. Calculate the constrained velocities

$$\mathbf{v}(t_n + \Delta t/2) \quad = \quad [\boldsymbol{r}(t_n + \Delta t) - \boldsymbol{r}(t_n)]/\Delta t \tag{12.56}$$

9. Calculate the kinetic energies $\mathcal{K}(t_n + \Delta t/2)$ to determine the scaling factors $\lambda(t_n + \Delta t/2)$ and the temperatures $T(t_n + \Delta t/2)$.

10P. Calculate the volume of the periodic box $\mathcal{V}(t_n)$, and calculate the atomic or group-based pressure tensor $\mathcal{P}(t_n)$ from Eq. 12.41 and Eq. 12.45 using the appropriate kinetic energy $\mathcal{K}_{tr}$ calculated in step 1 and the virial from step 2P.

11P. Scale the atomic positions $\mathbf{r}_i(t_n + \Delta t)$ and the box lengths $\mathbf{a}(t_n)$, $\mathbf{b}(t_n)$, $\mathbf{c}(t_n)$ to obtain $\mathbf{a}(t_n + \Delta t)$, $\mathbf{b}(t_n + \Delta t)$, $\mathbf{c}(t_n + \Delta t)$ with the appropriate pressure scaling factor $\mu(t_n)$, Eq. 12.48, using the pressure (components) from step 10P. If atoms are positionally restrained or kept fixed (Sec. 10.2), scale their reference positions also with the pressure scaling factor.

12. In case of perturbation (see Sec. 14.6), possibly change λ-values and update the masses and individual λ-values.

13. Calculate the total energies and update the energy averages. The kinetic energy at t_n is calculated as the average of the kinetic energies at $t_n - \frac{1}{2}\Delta t$ and $t_n + \frac{1}{2}\Delta t$[124].

14W. At the end of a MD step print the energies (ENERGY block at time t_n), pressure and volume (PRESSURE block) and scaling data (MULTIBATHCOUPLING block and PCOUPLE block), replica data (REMD block). Write the configuration $\boldsymbol{r}(t_n + \Delta t)$ to the trajectory file.

15W. If at the end of the run, write the final configuration $\boldsymbol{r}(t_n + \Delta t)$ and velocities $\mathbf{v}(t_n + \Delta t/2)$ to a single configuration file and write perturbation data: energy derivatives with respect to λ at time t_n, λ-values at time $t_n + \Delta t$, atom-atom distance restraints data at t_n, ^3J-coupling constant restraints data at t_n, S^2-order parameter restraints data at t_n, local-elevation data at t_n, replica data at t_n, X-ray scaling constants at t_n and R-values at t_n.

15. Increase the time to $t_{n+1} = t_n + \Delta t$ and the step number n to *n+1*.

When a set of atoms is to be kept fixed, their positions $\mathbf{r}_i$ are kept equal to their reference positions and the forces $\mathbf{f}_i$ on them and their velocities $\mathbf{v}_i$ are kept equal to zero at each MD step. Their inverse masses are set to zero in order to immobilize these atoms when their position might be up for resetting by the constraint procedure in case a fixed atom is involved in a constraint to a non-fixed atom.

12.7. Initialization, equilibration and sampling

An MD simulation starts with initial atomic positions and velocities. Although the results should be independent of these, it is good practice to choose the initial configuration as representative for the molecular system in equilibrium as possible. *Strain* in the configuration *should be removed* by a short (10-100 steps) energy minimization in order to avoid conversion of the strain energy into kinetic energy leading to a high temperature which will induce unsollicited barrier crossings, dihedral angle transitions, etc. The reading of the initial configuration in GROMOS is controlled in the block INITIALISE. If no *velocities* are available, they can be taken *from a Maxwell distribution* of a temperature T_i (TEMPI)

$$P(\mathbf{v}_j) \quad = \quad [2\pi k_B T_i/m_j]^{-\frac{3}{2}} exp[-m_j \mathbf{v}_j^2/(2k_B T_i] \tag{12.57}$$

where $P(\mathbf{v}_j)$ is the probability of occurrence of velocity $\mathbf{v}_j$ of atom j. Mathematically, this velocity distribution has the form of a product of 3 Gaussian distributions for the components v_{xj}, v_{yj} and v_{zj} with the standard deviation σ given by

$$\sigma \quad = \quad [k_B T_i/m_j]^{\frac{1}{2}} \tag{12.58}$$

Given the atomic masses, Boltzmann's constant, the initial temperature (TEMPI) and a random number generator seed (IG), Maxwellian initial velocities $\mathbf{v}_i(t_0 - \Delta t/2)$ can be generated if the variable NTIVEL = 1. If NTIVEL = 0 the initial velocities will be read from single-configuration file. This option is required to continue an MD simulation without a discontinuity in the trajectory.

The initial configuration and velocities may not satisfy the solute or solvent constraints. Besides, the atoms of charge groups of the solute may be split by the periodic box, Sec. 4.4.1.2. In the block INITIALISE shaking of the initial configuration is controlled with the switch NTISHK:

NTISHK	=	0:	initial coordinates $\boldsymbol{r}(t_0)$ and velocities $\boldsymbol{v}(t_0 - \Delta t/2)$ will not be shaken.
	=	1:	initial coordinates $\boldsymbol{r}(t_0)$ will be shaken.
	=	2:	initial velocities $\boldsymbol{v}(t_0 - \Delta t/2)$ will be shaken.
	=	3:	initial coordinates $\boldsymbol{r}(t_0)$ and velocities $\boldsymbol{v}(t_0 - \Delta t/2)$ will be shaken; the solute charge groups are reassembled if necessary.

By using the switch NTICOM the translational motion of and the rotational motion about the centre of mass can be removed from the initial velocities:

NTICOM	=	0:	initial centre of mass motion will not be removed.
	=	1:	initial translational motion of the centre of mass will be removed.
	=	2:	in addition, initial rotational motion about the centre of mass will be removed.

The *removal of centre of mass* motion during MD simulation is controlled within the COMTRANSROT block with variable NSCM:

NSCM	=	0:	centre of mass motion will not be removed.
	<	0:	centre of mass translation and rotation will be removed every NSCM steps.
	>	0:	centre of mass translation will be removed every NSCM steps.

For long MD simulations removal of the centre of mass motion should be regularly (every 10-100 ps) done. If atoms are kept fixed in a simulation, the centre of mass motion is not removed. For an in vacuo simulation without centre of mass translation or rotation, NDFMIN = 6 degrees of freedom should be subtracted from the total number of degrees of freedom when calculating the temperature from the kinetic energy. For a simulation using periodic boundary conditions without centre of mass translation, NDFMIN = 3 should be used. For a simulation using an extended wall region of positionally restrained or fixed atoms, NDFMIN = 0 should be used. Alternatively, the simulation can be performed under rototranslational constraints, as described in Sec. 10.7.

In order to *continue an* MD *simulation* the single-configuration file must contain the appropriate data for a continuation run:

- atomic coordinates at time t_0,
- atomic velocities at time $t_0 - \Delta t/2$,
- dimensions of the periodic box,
- setting for lattice shift vectors,
- perturbation data (cumulative energy derivatives at time $t_0 - \Delta t$, λ-values at time t_0),
- atom-atom distance restraint data (averages at time $t_0 - \Delta t$),
- ^3J-coupling constant restraint data (averages at time $t_0 - \Delta t$),
- S^2-order parameter restraint data (averages at time $t_0 - \Delta t$),
- local-elevation data (conformations visited so far, at time $t_0 - \Delta t$),
- setting of positions and orientations for roto-translational constraints,
- replica data,
- X-ray scaling constants and R-values (averages at time $t_0 - \Delta t$).

These data are written after the last (NSTLIM-th) step to a single-configuration file in order to allow for further continuation simulation.

The number of MD time steps of size Δt (DT) is to be specified in NSTLIM within the block STEP. The initial time point t_0 may be specified in the variable T for administrative purposes. It does not play a role in the algorithm, which only counts steps. Before the first step the non-bonded interaction charge group pair list must be generated. It will be regenerated every NSNB (5-10) steps (PAIRLIST block).

In order to *start the simulation* in a gentle way, the initial velocities can be taken from a *Maxwell distribution of low temperature* (say 50K) and subsequently the reference temperature can be raised after short

simulation periods (few ps) in a few steps (100K, 200K) to room temperature. At the same time *harmonic position restraining* can be applied to parts, e.g. the solute of the system in order to prevent possible distortions due to the release of strain present in the initial configuration, e.g. due to bad solute-solvent contacts. The *coupling to the* temperature and pressure *baths can be made strong* ($\tau_T \approx 0.01$ps, $\tau_\mathcal{P} \approx 0.05$ps) during the initial stage (few ps) of a simulation in order to allow for a rapid transfer of excess heat and pressure to the respective baths.

Ideally, the *equilibration period* of a simulation should be longer than the relaxation time of the system in order to secure equilibration. It will depend on the relaxation time of the property one is interested in. Some properties, such as the kinetic energy, require short (picoseconds) equilibration times, whereas others, such as dielectric properties, may require longer times, of the order of hundreds of picoseconds. During a simulation a number of *quantities*, such as the kinetic energy, the potential energy and the various terms contributing to it, the diffusion away from the initial structure, can be *monitored* to obtain a picture of the stability of a simulation.

At every NTPR-th time step a number of quantities are printed. In the TIMESTEP block MD time step number and time at the current MD step are given. In the ENERGIES block the following quantites are printed at time t:

`E_Total`	= total energy of the molecular system
`E_Kinetic`	= total kinetic energy of the molecular system
`E_Potential`	= total potential energy of the molecular system
`E_Covalent`	= total energy of covalent terms (solutes)
`E_Bonds`	= total energy of bond-stretching terms (solutes)
`E_Angles`	= total energy of bond-angle bending terms (solutes)
`E_Improper`	= total energy of improper (harmonic) dihedral angle terms (solutes)
`E_Dihedral`	= total energy of (trigonometric) dihedral angle terms (solutes)
`E_Crossdihedral`	= total energy of cross-dihedral angle terms (solutes)
`E_Non-bonded`	= total energy of nonbonded terms (solutes)
`E_Vdw`	= total energy of van der Waals interaction terms (at time t)
`E_El (RF)`	= total energy of the electrostatic interaction terms, $\mathcal{V}^{(ele)}$, in the *reaction-field* electrostatic scheme
`E_El (LS)`	= total energy of the electrostatic interaction terms, $\mathcal{V}^{(ele)}$, in the *lattice sum* electrostatic scheme
`E_El (pair)`	= pairwise potential energy contribution, $\mathcal{V}^{(ele,pws)}$, to the total electrostatic energy interaction term $\mathcal{V}^{(ele)}$
`E_El (real-space)`	= real-space pairwise potential energy contribution to $\mathcal{V}^{(ele,pws)}$ in the *lattice sum* electrostatic scheme
`E_El (k-space)`	= reciprocal-space pairwise potential energy contribution to $\mathcal{V}^{(ele,pws)}$ in the *lattice sum* electrostatic scheme
`E_El (A term)`	= A-term potential energy contribution to $\mathcal{V}^{(ele,pws)}$ in the *lattice sum* electrostatic scheme

E_El (lattice sum self)
= self potential energy contribution, $\mathcal{V}^{(ele,slf)}$, to the total electrostatic energy interaction term $\mathcal{V}^{(ele)}$

E_El (surface term)
= surface potential energy contribution, $\mathcal{V}^{(ele,srf)}$, to the total electrostatic energy interaction term $\mathcal{V}^{(ele)}$

E_Polarisation self
= total energy of polarisation self term

E_Special = total energy of special terms

E_SASA = total energy of SASA terms

E_Volume = total energy of SASA volume term

E_Constraints = total energy due to constraints in the molecular system

E_Distanceres = total energy of atom-atom distance restraint term

E_Disfieldres = total energy of distance-field restraint

E_Dihrest = total energy of dihedral restraining term

E_Posrest = total energy of atom position restraining term

E_EDS reference = total energy of EDS reference state

E_Jrest = total energy of ^3J-value restraining term

E_X-ray restraints = total energy of X-ray restraining term

E_Local elevation = total energy of local elevation term

E_Order-parameter rest.
= total energy of S^2-order parameter restraining term

E_RDCrest = total energy of RDC restraints

E_Symmetry restraints
= total energy of symmetry restraints

E_EDS reference = EDS reference energy

E_Entropy = total entropy term

E_QM = total energy of QM/MM interactions

When a free energy perturbation calculation is performed, the free energy perturbation parameter λ and the derivatives of the terms listed above with respect to λ are also written out.

In the TEMPERATURES block active temperature baths coupled to temperature groups in the system are given. For each temperature bath the total kinetic energy (EKIN), translational kinetic energy (EKIN-MOL-TR), sum of internal and rotational kinetic energy (EKIN-MOL-IR) and the corresponding temperatures (T, T-MOL-TR and T-MOL-IR) as well as the temperature scaling factors (SCALE) are printed for the degrees of freedom that are coupled to each bath.

In the PRESSURE block molecular kinetic energies, virial, pressure tensor, volume of the periodic box and total pressure are printed.

The centre of mass motion is regularly printed, and a least-squares fit of the total energy as function of the step number to a straight line is also regularly carried out and printed. This allows an examination of the

conservation of translational and rotational momentum and of the total energy. The latter should be conserved in MD simulations without coupling to temperature and pressure baths, without time-averaging and local-elevation terms, without fixed atoms, and in the absence of cut-off noise and noise due to constraints. If in addition no atoms are positionally restrained, the translational momentum should also be conserved. If in addition no periodic boundary conditions are used, the rotational momentum should also be conserved. The dihedral-angle transitions are not printed to the output file but to a special trajectory (see Vol. 5).

The switch array NTF[1..6] controls the presence (=1) or absence (=0) in Eq. 3.5 of the different terms of the GROMOS force field, $\mathcal{V}^{(phys)}$ in Eq. 3.4:

NTF[1]: bond-stretching interaction

NTF[2]: bond-angle bending interaction

NTF[3]: improper (harmonic) dihedral-angle bending interaction

NTF[4]: (trigonometric) dihedral-angle torsion interaction

NTF[5]: non-bonded interaction involving charges

NTF[6]: non-bonded interaction

The special terms $V^{special}$ in Eq. 3.4 are controlled by separate switches, which were discussed in Chap. 9.

NTPOR: atom position restraining or fixing

NTDIR: atom-atom distance restraining

NTDFR: distance-field restraining

NTDLR: dihedral-angle restraining

NTJVR: ^3J-coupling constant restraining

NTOPR: S^2-order parameter restraining

At the end of a simulation the averages and root-mean-square fluctuations of the quantities mentioned above are printed together with the average temperatures and pressure and their r.m.s. fluctuations. The final configuration and velocities and other quantities that are needed to continue the simulation are saved (see Vol. 4).

The *sampling period* or analysis period of a simulation should be long enough to allow for an appropriate sampling of the property of interest, that is, the sampling period should be longer than the relaxation time of the property of interest.[125] The results are generally analyzed by taking time averages over the simulation or parts of a simulation. By monitoring the time averages as a function of the length of the averaging period it can be tested whether the time averages are converging.[126]

In the WRITETRAJ block there are several switches which control writing of trajectories of data (coordinates, velocities, forces, energies and free energies). The switches NTWX and NTWSE control the writing of configurations. For NTWX $>$ 0 solute and solvent coordinates are printed every NTWX steps, beginning at step n = 0 and ending at step n = NSTLIM-|NTWX|. For NTWX $<$ 0 only solute coordinates are printed, which may reduce disk space requirements. When searching conformational space, one would rather save low energy configurations than configurations at regular intervals. For NTWSE = 0 normal coordinate trajectory is written out and for NTWSE $>$ 0 a minimum-energy coordinate and energy trajectory is written out. The switch NTWV controls the writing of velocities. If NTWV $>$ 0 solute and solvent velocities are written out, beginning at step n = 0, and ending at step n = NSTLIM - |NTWV|. If NTWV $<$ 0 only solute velocities are written out. The switch NTWF controls writing of the force trajectory. For NTWF $>$ 0 the FREEFORCERED and CONSFORCERED blocks (see Vol. 4) are written out every NTWF steps, for NTWF $<$ 0 only solute forces are written out. The switch NTWE controls the writing of energy, pressure and volume data. If NTWE $>$ 0, every NTWE-th time step the ENERGY03 and VOLUMEPRESSURE03 blocks (see Vol. 4) are saved, beginning at step n = 0, and ending at step n = NSTLIM - NTWE. The switch

NTWG controls the writing of free energy data. If NTWG > 0 every NTWG-th time step the FREEENERDERIVS03 block (see Vol. 4) is saved, beginning at step n = 0, and ending at step n = NSTLIM - NTWG. The switch NTWB controls writing of a block-averaged energy trajectory. If NTWB > 0 block-averaged energies and free energies (if NTWG > 0) are printed every NTWB steps.

CHAPTER 13

Stochastic Dynamics

13.1. Introduction

Stochastic dynamics (SD) simulation with an empirical energy function such as Eq. 3.4 is also much used to study the equilibrium structural, dynamic and thermodynamic properties of molecules. It is an extension of MD simulation, a frictional force and a randomly fluctuating force are added to the forces derived from $\mathcal{V}^{(phys)}(\mathbf{r})$ and $\mathcal{V}^{(spec)}(\mathbf{r})$, which leads to the Langevin equations of motion Eq. 2.13, as discussed in Sec. 2.4. These additional forces approximate partly the effect of degrees of freedom that are not explicitly treated in the simulation on the explicitly treated degrees of freedom. A major application is the replacement of explicit solvent molecules in an MD simulation of a (macro)molecule in solution by (implicit) stochastic and frictional forces on the (macro)molecule in a SD simulation. SD simulation is also a useful method for searching conformational space for low energy conformers. Due to the random components in the forces, it may search a wider part of space than a comparable MD simulation. A third type of application of SD simulation is in conjunction with the extended wall region boundary condition (Sec. 4.3). The motion of the positionally restrained atoms of the wall region may be treated by the Langevin equation, so that it gets randomized and the wall region can exchange heat with the hypothetical environment (vacuum) outside the extended wall region. SD simulation may also be used to control the temperature, *i.e.* as a Langevin thermostat.[127]

Here, we only consider the differences of SD simulation with respect to MD simulation. In the first three applications of SD simulation mentioned above the application of periodic boundary conditions (Sec. 4.4) would not make much sense. However, it is possible to use periodic boundary conditions within SD. In case of using periodic boundary conditions it has to be considered that the calculations of the virial and pressure are incomplete. Thus, SD simulation at constant pressure, means coupling to a pressure bath, is impossible. The possibility to use weak coupling to a temperature bath is maintained for the following reason. Application of SD simulation with non-zero atomic friction coefficients γ_i implies an atomic coupling to a temperature T_{ref} (TEMPSD) in Eq. 2.15. However, atoms for which $\gamma_i = 0$ feel no random and no frictional force, so are not coupled to the temperature bath at T_{ref}. The combination of weak temperature coupling to a temperature bath at T_0, as discussed in Sec. 12.2, with SD simulation is a, be it not very elegant, option to redress the temperature of atoms for which $\gamma_i = 0$ and which are subject to noise. Therefore, only a simplified version of weak temperature coupling can be combined with SD.

The leap-frog SD algorithm is given in Sec. 13.2. The choice of the atomic friction coefficients γ_i is discussed in Sec. 13.3.

13.2. Leap-frog SD algorithm

Apart from a mean-force term, Langevin's equation of motion Eq. 2.13 differs from Newton's equation Eq. 2.8 by the occurrence of a stochastic force $\mathbf{f}_i^{st}(t)$ and a frictional force $-m_i\gamma_i\mathbf{v}_i(t)$. These extra terms make the SD version of the leap-frog scheme more complicated than the MD one[128]. The solution of Eq. 2.13 in terms of $\mathbf{v}_i(t)$ around time $t = t_n$ is

$$\begin{aligned}\mathbf{v}_i(t) &= \mathbf{v}_i(t_n)exp[-\gamma_i(t-t_n)] \\ &+ m_i^{-1}exp[-\gamma_i(t-t_n)]\int_{t_n}^{t} exp[-\gamma_i(t_n-t')][\mathbf{f}_i(t')+\mathbf{f}_i^{st}(t')]dt' \end{aligned} \tag{13.1}$$

Since the stochastic properties of the random force $\mathbf{f}_i^{st}(t')$ are given (postulated), the stochastic properties of the integral over $\mathbf{f}_i^{st}(t')$ can be obtained directly. The integral over the force $\mathbf{f}_i(t')$ is, as in Sec. 12.1 for

MD, obtained by expanding $\mathbf{f}_i(t')$ in a Taylor series around $t = t_n$ and omitting all terms beyond third order in the time step Δt in the positions, beyond second order in the velocities, and beyond first order in the forces. The SD equivalent of the *leap-frog velocity formula* Eq. 12.1 then becomes[128]

$$\begin{aligned} \mathbf{v}_i(t_n + \Delta t/2) &= \mathbf{v}_i(t_n - \Delta t/2)exp(-\gamma_i \Delta t) \\ &+ m_i^{-1}\mathbf{f}_i(t_n)\Delta t[1 - exp(-\gamma_i \Delta t)]/(\gamma_i \Delta t) \\ &- exp[-\gamma_i \Delta t]\mathbf{V}_i(t_n; -\Delta t/2) + \mathbf{V}_i(t_n; \Delta t/2) \end{aligned} \tag{13.2}$$

where

$$\mathbf{V}_i(t_n; \Delta t/2) \equiv m_i^{-1} exp(-\gamma_i \Delta t/2) \int_{t_n}^{t_n + \Delta t/2} exp[-\gamma_i(t_n - t')]\mathbf{f}_i^{st}(t')dt' \tag{13.3}$$

The equivalent of the *leap-frog position formula* Eq. 12.2 is obtained by integrating Eq. 2.9 using Eq. 13.1 for the velocity[128]

$$\begin{aligned} \mathbf{r}_i(t_n + \Delta t) &= \mathbf{r}_i(t_n) \\ &+ \mathbf{v}_i(t_n + \Delta t/2)\Delta t[exp(\gamma_i \Delta t/2) - exp(-\gamma_i \Delta t/2)]/(\gamma_i \Delta t) \\ &- \mathbf{R}_i(t_n + \Delta t/2; -\Delta t/2) + \mathbf{R}_i(t_n + \Delta t/2; \Delta t/2) \end{aligned} \tag{13.4}$$

where

$$\mathbf{R}_i(t_n; \Delta t/2) \equiv (m_i \gamma_i)^{-1} \int_{t_n}^{t_n + \Delta t/2} [1 - exp[\gamma_i(t_n + \Delta t/2 - t')]]\mathbf{f}_i^{st}(t')dt'. \tag{13.5}$$

When the friction coefficient γ_i tends to zero, the SD *leap-frog scheme* Eq. 13.2 and Eq. 13.4 reduces to the MD *leap-frog scheme* Eq. 12.1 and Eq. 12.2. Due to condition Eq. 2.15, which connects the stochastic force $\mathbf{f}_i^{st}$ with the friction coefficient γ_i, the *stochastic integrals* Eq. 13.3 and Eq. 13.5 tend to zero for γ_i tending to zero.

When using the SD leap-frog integration scheme Eq. 13.2 and Eq. 13.4 it must be noted that the stochastic variable $V_i(t_n; -\Delta t/2)$ is correlated with the stochastic variable $\mathbf{R}_i(t_n - \Delta t/2; \Delta t/2)$, since they are different integrals of the stochastic force $\mathbf{f}_i^{st}(t')$ over the same time interval $(t_n - \Delta t/2, t_n)$. The same observation holds for the stochastic variables $\mathbf{R}_i(t_n + \Delta t/2; -\Delta t/2)$ and $\mathbf{V}_i(t_n; \Delta t/2)$, which are integrals over $\mathbf{f}_i^{st}(t')$ over the same time interval $(t_n, t_n + \Delta t/2)$. This means that these correlated stochastic variables must be sampled in a correlated manner[128]

The probability distribution for the x-, y-, z-components of $\mathbf{R}_i(t_n - \Delta t/2; \Delta t/2)$, irrespective the value of $\mathbf{V}_i(t_n; -\Delta t/2)$, is

$$P(R_{ix}) = [2\pi\sigma_1^2]^{-\frac{1}{2}} exp[-R_{ix}^2/(2\sigma_1^2)], \tag{13.6}$$

and the conditional probability distribution for the x-, y-, z-components of $\mathbf{V}_i(t_n; -\Delta t/2)$, given the specific value $\mathbf{R}_i(t_n - \Delta t/2; \Delta t/2)$ sampled from Eq. 13.6, is

$$P(V_{ix}|R_{ix}) = [2\pi\sigma_2^2]^{-\frac{1}{2}} exp[-(V_{ix} - \sigma_3 R_{ix})^2/(2\sigma_2^2)] \tag{13.7}$$

where

$$\sigma_1^2 \equiv k_B T_{ref} m_i^{-1} C(\gamma_i \Delta t/2)/\gamma_i^2, \tag{13.8}$$

$$\sigma_2^2 \equiv k_B T_{ref} m_i^{-1} B(\gamma_i \Delta t/2)/C(\gamma_i \Delta t/2), \tag{13.9}$$

$$\sigma_3 \equiv \gamma_i D(\gamma_i \Delta t/2)/C(\gamma_i \Delta t/2), \tag{13.10}$$

with

$$B(\gamma_i \Delta t/2) \equiv \gamma_i \Delta t[exp(+\gamma_i \Delta t) - 1] - 4[exp(+\gamma_i \Delta t/2) - 1]^2, \tag{13.11}$$

$$C(\gamma_i \Delta t/2) \equiv \gamma_i \Delta t - 3 + 4exp(-\gamma_i \Delta t/2) - exp(-\gamma_i \Delta t) \tag{13.12}$$

and

$$D(\gamma_i \Delta t/2) \equiv 2 - exp(+\gamma_i \Delta t/2) - exp(-\gamma_i \Delta t/2). \tag{13.13}$$

The probability distribution for the x-, y-, z-components of $\mathbf{V}_i(t_n; \Delta t/2)$, irrespective the value of $\mathbf{R}_i(t_n + \Delta t/2; -\Delta t/2)$, is

$$P(V_{ix}) = [2\pi\rho_1^2]^{-\frac{1}{2}} exp[-V_{ix}^2/(2\rho_1^2)], \tag{13.14}$$

and the conditional probability distribution for the x-, y-, z-components of $\mathbf{R}_i(t_n + \Delta t/2; -\Delta t/2)$, given the specific value $\mathbf{V}_i(t_n; \Delta t/2)$ sampled from Eq. 13.14, is

$$P(R_{ix}|V_{ix}) = [2\pi\rho_2^2]^{-\frac{1}{2}} exp[-(R_{ix} - \rho_3 V_{ix})^2/(2\rho_2^2)] \tag{13.15}$$

where

$$\rho_1^2 \equiv k_B T_{ref} m_i^{-1}[1 - exp(-\gamma_i \Delta t)], \tag{13.16}$$

$$\rho_2^2 \equiv k_B T_{ref} m_i^{-1} B(-\gamma_i \Delta t/2)/[\gamma_i^2[1 - exp(-\gamma_i \Delta t)]], \tag{13.17}$$

$$\rho_3 \equiv D(-\gamma_i \Delta t/2)/[-\gamma_i[1 - exp(-\gamma_i \Delta t)]]. \tag{13.18}$$

The *algorithm for* SD *simulation* based on the leap-frog integration scheme, which may include weak coupling to a temperature bath of temperature T_0 (indicated by the symbol T), and which may include the application of distance constraints (indicated by the symbol C) using one of the constraining methods described in Chap. 10 can be summarized in the following steps.

0. The positions $\mathbf{r}_i(t_n)$ and velocities $\mathbf{v}_i(t_n - \Delta t/2)$ for all atoms are given. Calculate the kinetic energies $\mathcal{K}(t_n - \Delta t/2)$, and the temperatures $T(t_n - \Delta t/2)$. The initial step number is zero, $n = 0$.

0C. The mentioned positions satisfy the constraints and the mentioned velocities, temperatures and kinetic energies do not contain components along the constraints.

1. Remove the centre of mass motion: Calculate the molecular centre of mass positions for the temperature groups and the translational ($\mathcal{K}^{tr}(t_n - \Delta t/2; \mathcal{G}_T)$) and rotational $\mathcal{K}^{ir}(t_n - \Delta t/2; \mathcal{G}_T)$) kinetic energy. Calculate the relative positions $d_{i\alpha}(t_n)$, for use in Eq. 12.37.

1B. If required, apply the periodic boundary conditions (not for vacuum simulation).

2. Calculate the (unconstrained) forces from the potential energy function $\mathcal{V}(\boldsymbol{r})$

$$\mathbf{f}_i(t_n) = -\frac{\partial \mathcal{V}(\boldsymbol{r}(t_n)}{\partial \mathbf{r}_i} \tag{13.19}$$

3C. If required, apply positions constraints (see Sec. 10.2).

4. Sample the x-, y-, z-components of a vector $\mathbf{V}_i$ from a Gaussian distribution with zero mean and width σ_2^2 and determine

$$\mathbf{V}_i(t_n; -\Delta t/2) = \sigma_3 \mathbf{R}_i(t_n - \Delta t/2; \Delta t/2) + \mathbf{V}_i^{'} \tag{13.20}$$

5. Sample the x-, y-, z-components of a vector $\mathbf{V}_i(t_n; \Delta t/2)$ from a Gaussian distribution with zero mean and width ρ_1^2.

6. Determine the (unconstrained) velocities $\mathbf{v}_i(t_n + \Delta t/2)$ from Eq. 13.2.

7. Calculate the new positions excluding the contributions of the stochastic integrals in Eq. 13.4

$$\mathbf{r}_i(t_n + \Delta t) = \mathbf{r}_i(t_n) + \mathbf{v}_i(t_n + \Delta t/2)\Delta t E(\gamma_i \Delta t/2) \tag{13.21}$$

where

$$E(\gamma_i \Delta t/2) \equiv [exp(\gamma_i \Delta t/2) - exp(-\gamma_i \Delta t/2)]/(\gamma_i \Delta t) \tag{13.22}$$

8T. Scale the velocities $\mathbf{v}_i(t_n + \Delta t/2)$ of the atoms that are coupled to a temperature bath with the appropriate temperature scaling factor $\lambda(t_n - \Delta t/2)$, belonging to the groups of degrees of freedom that are jointly coupled to the bath (Sec. 12.2). The scaling factors are based on $\mathcal{K}(t_n - \Delta t/2)$ and depend on the thermostat chosen.

9C. Make the velocities satisfy the constraints by the following two steps. Perform

$$C(\boldsymbol{r}(t_n); \boldsymbol{r}(t_n + \Delta t); \boldsymbol{r}(t_n + \Delta t)) \tag{13.23}$$

Calculate the constrained velocities

$$\mathbf{v}(t_n + \Delta t/2) = [\mathbf{r}_i(t_n + \Delta t) - \mathbf{r}_i(t_n)]/[\Delta t E(\gamma_i \Delta t/2)] \tag{13.24}$$

10. Calculate the kinetic energies $\mathcal{K}(t_n + \Delta t/2)$ to determine the scaling factors $\lambda(t_n + \Delta t/2)$ and the temperatures $T(t_n + \Delta t/2)$.

11. Sample the x-, y-, z-components of a vector $\mathbf{R}_i^{'}$ from a Gaussian distribution with zero mean and width ρ_2^2 and determine

$$\mathbf{R}_i(t_n + \Delta t/2; -\Delta t/2) = \rho_3 \mathbf{V}_i(t_n; \Delta t/2) + \mathbf{R}_i^{'} \tag{13.25}$$

12. Sample the x-, y-, z-components of $\mathbf{R}_i(t_n + \Delta t/2;\ \Delta t/2)$ from a Gaussian distribution with zero mean and width σ_1^2.

13. Add the stochastic integrals from Eq. 13.4 to obtain the (unconstrained) positions

$$\begin{aligned} \mathbf{r}_i(t_n + \Delta t) &= \mathbf{r}_i(t_n + \Delta t) - \mathbf{R}_i(t_n + \Delta t/2; -\Delta t/2) \\ &+ \mathbf{R}_i(t_n + \Delta t/2; \Delta t/2) \end{aligned} \tag{13.26}$$

14C. Make the positions satisfy the constraints

$$C(\boldsymbol{r}(t_n); \boldsymbol{r}(t_n + \Delta t); \boldsymbol{r}(t_n + \Delta t)) \tag{13.27}$$

15. In case of perturbation (see Sec. 14.6), possibly change λ-values and update the masses and individual λ-values.

16. Calculate the total energies and update the energy averages. The kinetic energy at t_n is calculated as the average of the kinetic energies at $t_n - \Delta t/2$ and $t_n + \Delta t/2$[124].

17W. At the end of an MD step print the energies (ENERGY block at time t_n), stochastic integrals $\mathbf{R}_i(t_n + \Delta t/2; \Delta t/2)$, scaling data (MULTIBATHCOUPLING block), replica data (REMD block). Write the configuration $\mathbf{r}_i(t_n + \Delta t)$ to the trajectory file.

18W. If at the end of the run, write the final configuration $\mathbf{r}_i(t_n + \Delta t)$ and velocities $\mathbf{v}_i(t_n + \Delta t/2)$ to a single configuration file and write perturbation data (energy derivatives with respect to λ at time t_n, the λ-values at time $t_n + \Delta t$), atom-atom distance restraints data at $\mathbf{t}_n$, ^3J-coupling constant restraints data at t_n, S^2-order parameter restraints data at t_n, local-elevation data at t_n, replica data at t_n, X-ray scaling constants at t_n and R-values at t_n.

18. Increase the time to $t_{n+1} = t_n + \Delta t$ and the step number $\mathcal{N}_t$ to $\mathcal{N}_t + 1$.

When computing the coefficients involving exponents of $\gamma\Delta t$, for small values of $\gamma_i\Delta t$ the numerical accuracy of the expressions is not guaranteed. Using an 48-bit mantissa they are only accurate to better than $1{:}10^6$ when $\gamma_i\Delta t > 0.05$. For $\gamma_i\Delta t < 0.05$ series expansion expressions are used.[128]

When weak coupling to a temperature bath is used, its temperature T_0(TEMP0m) should be taken equal to the SD reference temperature T_{ref} (TEMPSD).

13.3. Choice of atomic friction coefficient

When performing a SD simulation, atomic friction coefficients γ_i must be given. In the case of a solute in a stochastic solvent, the γ_i of the solute atoms should be proportional to the fraction ω_i of the atomic surface that is accessible to solvent and to the friction coefficient γ_{solv} of the solvent molecules,

$$\gamma_i(t) = \gamma_{solv}\omega_i(t) \tag{13.28}$$

An approximate value for γ_{solv} can be obtained from the experimental solvent viscosity η_{solv} using Stokes' law

$$\gamma_{solv} = 6\pi R_{solv}\eta_{solv}/m_{solv} \tag{13.29}$$

where R_{solv} is the Stokes radius and m_{solv} the mass of a solvent molecule. In this way a friction coefficient $\gamma_{solv} = 91$ ps^{-1} for H_2O and $\gamma_{solv} = 24$ ps^{-1} for CCl_4 was derived (T = 300K)[129]. The calculation of an exact solvent accessible surface area for each atom is an expensive task. Since the stochastic model of the solvent effects is anyway not correct in atomic detail, it makes no sense to accurately determine the ω_i. Therefore, one may use the approximate formula

$$\omega_i(t) = maximum(0, 1 - N_i^{nb}(t)/N^{nbref}) \tag{13.30}$$

in which the number of neighbour atoms of atom i at time t within a 3D sphere of radius R^{nbref}(RCUTF) is denoted by $N_i^{nb}(t)$ and N^{nbref}(NBREF) should be chosen equal to the number of neighbours at which atom i looses its contact with the solvent. For example, for $R^{nbref} = 0.3$ nm we use $N^{nbref} = 6$[129]. The atomic solvent accessible area weight factors $\omega_i(t)$ need not be calculated at every time step, since they should be a slowly varying function of the solute conformation. They will be recalculated every NSFR (100-1000) steps (if NTFR = 3).

An alternative is to specify the atomic friction coefficients GAM[i] in an atomic friction coefficients file, see Vol. 4, or to take them all equal to one value, CFRIC. This input variable also serves as overall weight factor. The switch NTFR controls the application of stochastic dynamics:

NTFR = 0, no SD simulation
= 1, SD simulation with γ_i = CFRIC
= 2, SD simulation with γ_i = CFRIC * GAM[i] and GAM[1..NR] is read from an atomic friction coefficients file
= 3, SD simulation with γ_i = CFRIC * ω_i from Eq. 13.30

CHAPTER 14

Free Energy Determination

14.1. Introduction

Several methods exist for calculating the free energy difference between two states A and B of a molecular system or between two molecular systems A and B, which are based on statistical mechanics.[130] In the so-called coupling parameter approach, the Hamiltonian Eq. 3.1 is made an analytical function of the coupling parameter λ,

$$\mathcal{H}(\boldsymbol{p},\boldsymbol{r};\lambda) = \mathcal{K}(\boldsymbol{p};\lambda)+\mathcal{V}(\boldsymbol{r};\lambda) \tag{14.1}$$

such that

$$\mathcal{H}(\boldsymbol{p},\boldsymbol{r};\lambda_A) = \mathcal{H}_A(\boldsymbol{p},\boldsymbol{r}) \tag{14.2}$$
$$\mathcal{H}(\boldsymbol{p},\boldsymbol{r};\lambda_B) = \mathcal{H}_B(\boldsymbol{p},\boldsymbol{r}) \tag{14.3}$$

where the Hamiltonians $\mathcal{H}_A$ and $\mathcal{H}_B$ characterize states or systems A and B. In order to keep the notation concise, we omit in the formulae of this chapter the explicit dependence of the Hamiltonian (terms) on the force-field parameters $\mathbf{s}$, the masses m and the box matrix $\underline{\mathcal{B}}$. Using the $\lambda-$dependent Hamiltonian Eq. 14.1, the (Helmholtz) free energy $\mathcal{F}$ becomes a function of λ,

$$\mathcal{F}(\lambda) = -k_BT\ln\mathcal{Z}(\lambda), \tag{14.4}$$

where the (λ-dependent) canonical partition function of the system of $\mathcal{N}_a$ atoms is given by

$$\mathcal{Z}(\lambda) = [h^{3\mathcal{N}_a}\mathcal{N}_a!]^{-1}\int\int e^{-\mathcal{H}(\boldsymbol{p},\boldsymbol{r};\lambda)/k_BT}d\boldsymbol{p}d\boldsymbol{r}. \tag{14.5}$$

where h is Planck's constant, and the factor $(\mathcal{N}_a!)^{-1}$ should be omitted when the atoms of the system are distinguishable. The free energy difference $\Delta\mathcal{F}_{BA}$ then reads

$$\begin{aligned}
\Delta\mathcal{F}_{BA} &= \mathcal{F}(\lambda_B)-\mathcal{F}(\lambda_A)\\
&= -k_BT\ln\left(\frac{\mathcal{Z}(\lambda_B)}{\mathcal{Z}(\lambda_A)}\right)\\
&= -k_BT\ln\left(\int\int e^{-[\mathcal{H}(\boldsymbol{p},\boldsymbol{r};\lambda_B)-\mathcal{H}(\boldsymbol{p},\boldsymbol{r};\lambda_A)]/k_BT}P(\boldsymbol{p},\boldsymbol{r};\lambda_A)d\mathbf{p}d\mathbf{r}\right)\\
&= -k_BT\ln\left(\left\langle e^{-[\mathcal{H}(\lambda_B)-\mathcal{H}(\lambda_A)]/k_BT}\right\rangle_{\lambda_A}\right).
\end{aligned} \tag{14.6}$$

The probability of the configuration $\boldsymbol{r}$ with momenta $\boldsymbol{p}$ in the (canonical) ensemble is defined as

$$P(\boldsymbol{p},\boldsymbol{r};\lambda) \equiv \frac{e^{-\mathcal{H}(\boldsymbol{p},\boldsymbol{r};\lambda)/k_BT}}{\int\int e^{-\mathcal{H}(\boldsymbol{p},\boldsymbol{r};\lambda)/k_BT}d\boldsymbol{p}d\boldsymbol{r}} \tag{14.7}$$

and the brackets $\langle ...\rangle_\lambda$ denote an ensemble average over an ensemble generated using the Hamiltonian $\mathcal{H}(\boldsymbol{p},\boldsymbol{r};\lambda)$. Eq. 14.6 is called the *free energy perturbation formula*, since the average involved will converge slowly unless the difference between the states described by $\mathcal{H}(\lambda_A)$ and $\mathcal{H}(\lambda_B)$ is small. The free energy difference $\Delta\mathcal{F}_{BA}$ can also be expressed as an ensemble average at $\lambda=\lambda_B$,

$$\Delta\mathcal{F}_{BA} = +k_BT\ln\left(\left\langle e^{-[\mathcal{H}(\lambda_A)-\mathcal{H}(\lambda_B)]/k_BT}\right\rangle_{\lambda_B}\right). \tag{14.8}$$

Formulae Eq. 14.6 and Eq. 14.8 can also be written as a perturbation formula for a change of Hamiltonian characterized by $\pm\Delta\lambda$,

$$\begin{aligned} \Delta\mathcal{F}_{\lambda\pm\Delta\lambda} &\equiv \mathcal{F}(\lambda\pm\Delta\lambda) - \mathcal{F}(\lambda) \\ &= -k_B T \ln\left(\left\langle e^{-[\mathcal{H}(\lambda\pm\Delta\lambda)-\mathcal{H}(\lambda)]/k_B T}\right\rangle_\lambda\right). \end{aligned} \tag{14.9}$$

Taking the derivative of $\mathcal{F}(\lambda)$ with respect to λ one finds

$$\mathcal{F}'(\lambda) \equiv \frac{\partial\mathcal{F}(\lambda)}{\partial\lambda} = \left\langle \frac{\partial\mathcal{H}(\lambda)}{\partial\lambda}\right\rangle_\lambda \tag{14.10}$$

which leads to the *thermodynamic integration formula*

$$\Delta\mathcal{F}_{BA} = \int_{\lambda_A}^{\lambda_B} \mathcal{F}'(\lambda)d\lambda = \int_{\lambda_A}^{\lambda_B} \left\langle \frac{\partial\mathcal{H}(\lambda)}{\partial\lambda}\right\rangle_\lambda d\lambda. \tag{14.11}$$

The formulae given above concern the canonical ensemble, so are applicable to trajectories from (N,V,T) simulations and give (Helmholtz) free energy differences. The corresponding formulae for (N,P,T) simulations giving Gibbs free energy or free enthalpy differences can be found in ref.[131].

In standard free energy perturbation calculations the *atomic masses* $m(\lambda)$ and *force-field parameters* $\mathbf{s}(\lambda)$ are made a function of the *coupling parameter* λ. The dependence of the Hamiltonian $\mathcal{H}(\boldsymbol{p},\boldsymbol{r};\lambda)$ on λ is given in Sec. 14.2.

When constraints are applied (Chap. 10), these appear formally as parameters in the Hamiltonian.[130] So, changing a distance constraint $\sigma_k(\boldsymbol{r};\lambda)$, Sec. 10.3.1, as a function of λ may lead to a change in free energy. Formulae for obtaining free *energy differences* due to differences in *distance constraints* (bond lengths) are given in Sec. 14.3.

Technical and *practical issues* with respect to the choice of pathway and of states A and B are discussed in Sec. 14.4. The use of the thermodynamic integration formula is discussed in Sec. 14.6 and that of the perturbation formula in Sec. 14.7.

In Sec. 14.8 it is briefly indicated how the various restraining functions of $\mathcal{V}^{(spec)}(\boldsymbol{r};\mathbf{s})$ can be used to bias the sampling along a chosen reaction coordinate R to obtain the free energy $\mathcal{F}(R)$ as a function of R using *umbrella sampling techniques*.[130,132] Sec. 14.9, finally, discusses a special use of the perturbation formula, in terms of enveloping distribution sampling.

14.2. Parameterization of the Hamiltonian

In free energy perturbation, the Hamiltonian $\mathcal{H}$ depends on the coupling parameter λ

$$\mathcal{H}(\mathbf{p},\mathbf{r};\lambda) = \mathcal{K}(\mathbf{p},\mathbf{r};\lambda) + \mathcal{V}(\mathbf{r};\lambda). \tag{14.12}$$

The parameter λ controls the change from state A to state B,

$$\begin{aligned} &\lambda = \lambda_A = 0: && \texttt{state A} \\ &\lambda = \lambda_B = 1: && \texttt{state B} \end{aligned} \tag{14.13}$$

Under these conditions we may write

$$\begin{aligned} \mathcal{H}(\mathbf{p},\mathbf{r};\lambda) &= \mathcal{K}(\mathbf{p},\mathbf{r};\lambda) + \mathcal{V}^{(b)}(\mathbf{r};\lambda) + \mathcal{V}^{(\theta)}(\mathbf{r};\lambda) + \mathcal{V}^{(\xi)}(\mathbf{r};\lambda) \\ &+ \mathcal{V}^{(\varphi)}(\mathbf{r};\lambda) + \mathcal{V}^{(nbd)}(\mathbf{r};\lambda) \\ &+ \mathcal{V}^{(Jr)}(\mathbf{r}) + \mathcal{V}^{(le)}(\mathbf{r}) + \mathcal{V}^{(pr)}(\mathbf{r}) \\ &+ \mathcal{V}^{(dr)}(\mathbf{r};\lambda) + \mathcal{V}^{(tr)}(\mathbf{r};\lambda) \end{aligned} \tag{14.14}$$

Of the last five terms, which are the special interaction terms described in Chap. 9, only $\mathcal{V}^{(dr)}$ (Sec. 9.3) and $\mathcal{V}^{(tr)}$ (Sec. 9.6) can be made $\lambda-$dependent, see Secs. 14.2.10 and Sec. 14.2.11.

We note that atom position fixing (Sec. 10.2) should not be used in a free energy perturbation calculation.

When distance constraints are applied, the kinetic energy $\mathcal{K}(\mathbf{p},\mathbf{r};\lambda)$ depends on the atomic coordinates $\mathbf{r}$. Using SHAKE, the momenta $\mathbf{p}$ will depend on the coordinates $\mathbf{r}$, since the velocities are calculated from shaken positions (Eq. 12.56 and Eq. 13.24). The $\lambda-$dependent kinetic energy is

$$\mathcal{K}(\mathbf{p},\mathbf{r};\lambda) \quad = \quad \sum_{i=1}^{\mathcal{N}_a} \tfrac{(\mathbf{p}_i)^2}{2m_i(\lambda)} = \sum_{i=1}^{\mathcal{N}_a} \tfrac{1}{2} m_i(\lambda)(\mathbf{v}_i)^2 \tag{14.15}$$

with

$$m_i(\lambda) = (1-\lambda)m_i^A + \lambda m_i^B. \tag{14.16}$$

The mass of atom i in state A is m_i^A and in state B it is m_i^B. For the derivatives with respect to λ (using $\mathcal{K}$ as a function of $\mathbf{p}$, not of $\mathbf{v}$) one finds[133]

$$\frac{\partial \mathcal{K}(\mathbf{p},\mathbf{r};\lambda)}{\partial \lambda} = -\sum_{i=1}^{\mathcal{N}_a} \tfrac{1}{2}(m_i^B - m_i^A)(\mathbf{v}_i)^2 \tag{14.17}$$

The corresponding expression for use in the perturbation formula Eq. 14.9 is, assuming that $\mathbf{p}$ and $\mathbf{r}$ correspond to λ,

$$\mathcal{K}(\mathbf{p},\mathbf{r};\lambda \pm \Delta\lambda) - \mathcal{K}(\mathbf{p},\mathbf{r};\lambda) = \mp\Delta\lambda \sum_{i=1}^{\mathcal{N}_a} \tfrac{1}{2}(m_i^B - m_i^A)\tfrac{m_i(\lambda)}{m_i(\lambda\pm\Delta\lambda)}(\mathbf{v}_i)^2 \tag{14.18}$$

We note that the mass of a positionally fixed atom (Sec. 10.3.6) cannot be made $\lambda-$dependent.

14.2.1. Covalent bond forces. The $\lambda-$dependent version of the quartic potential-energy function term describing the covalent bond-stretching interaction (Sec. 5.1) is obtained by making the force constant $k_n^{(b,q)}$ and the ideal bond length b_n^0 linearly dependent on λ,

$$\begin{aligned}
&V^{(b,q)}(\mathbf{r};\lambda) = \sum_{n=1}^{N^{(b)}} {V^{(b,q)}}_n(b_n;\lambda) \\
&= \sum_{n=1}^{N^{(b)}} \tfrac{1}{4}\Big[(1-\lambda)k_n^{(b,q)\,A} + \lambda k_n^{(b,q)\,B}\Big]\Big[\ {b_n}^2 - \big[\ (1-\lambda)b_n^{0\,A} + \lambda b_n^{0\,B}\big]^2\Big]^2 \\
&= \sum_{n=1}^{N^{(b)}} \tfrac{1}{4}k_n^{(b,q)\,A}\big[\ {b_n}^2 - (b_n^{0\,A})^2\big]^2 \\
&\quad + \sum_{n=1}^{N^{(b)}} \tfrac{1}{4}\lambda\Big\{ -2k_n^{(b,q)\,A}\big[\ b_n^{0\,B} - b_n^{0\,A}\big]\big[\ 2b_n^{0\,A} + \lambda(b_n^{0\,B} - b_n^{0\,A})\big]\big[({b_n}^2 - (b_n^{0\,A})^2\big] \\
&\quad + \lambda k_n^{(b,q)\,A}\big[\ b_n^{0\,B} - b_n^{0\,A}\big]^2\big[\ 2b_n^{0\,A} + \lambda(b_n^{0\,B} - b_n^{0\,A})\big]^2 \\
&\quad + \Big[\ k_n^{(b,q)\,B} - k_n^{(b,q)\,A}\Big]\Big[\ {b_n}^2 - \big[\ b_n^{0\,A} + \lambda(b_n^{0\,B} - b_n^{0\,A})\big]^2\Big]^2\Big\} \\
&= V^{(b,q)}(\mathbf{r};\lambda=\lambda_A=0) + \Delta V^{(b,q)\,A}(\mathbf{r};\lambda)
\end{aligned} \tag{14.19}$$

The forces $\mathbf{f}^{(b,q)\,A}_{i}$ and $\mathbf{f}^{(b,q)\,A}_{j}$ in state A ($\lambda = \lambda_A = 0$) on atoms i and j due to the n-th term in Eq. 5.1 are given by expressions Eq. 17.1 and Eq. 17.2, using $k_n^{(b,q)} = k_n^{(b,q)\,A}$ and using $b_n^0 = b_n^{0\,A}$. The forces on atoms i and j due to the n-th term of the energy difference $\Delta V^{(b,q)\,A}(\mathbf{r};\lambda)$ are

$$\begin{aligned}
\mathbf{f}^{(b,q)\,\Delta A}_{i} &= -\frac{\partial \Delta V^{(b,q)\,A}_{n}}{\partial {b_n}^2}\frac{\partial {b_n}^2}{\partial \mathbf{r}_i} \\
&= \lambda\Big\{\, k_n^{(b,q)\,A}\,\big[\, b_n^{0\,B} - b_n^{0\,A}\big]\,\big[\, 2b_n^{0\,A} + \lambda(b_n^{0\,B} - b_n^{0\,A})\big] \\
&\quad - \Big[\, k_n^{(b,q)\,B} - k_n^{(b,q)\,A}\Big]\,\big[\, {b_n}^2 - [b_n^{0\,A} + \lambda(b_n^{0\,B} - b_n^{0\,A})]^2\big]\,\Big\}\mathbf{r}_{ij}
\end{aligned} \tag{14.20}$$

and

$$\mathbf{f}^{(b,q)\,\Delta A}_{j} = -\mathbf{f}^{(b,q)\,\Delta A}_{i}. \tag{14.21}$$

The derivative with respect to λ of the energy $V^{(b,q)}(\mathbf{r};\lambda)$ and of the energy difference $\Delta V^{(b,q)\,A}(\mathbf{r};\lambda)$ with respect to state A is

$$\begin{aligned}
\frac{\partial V^{(b,q)}(\mathbf{r};\lambda)}{\partial \lambda} &= \frac{\partial \Delta V^{(b,q)\,A}(\mathbf{r};\lambda)}{\partial \lambda} \\
&= \sum_{n=1}^{N^{(b)}} \tfrac{1}{4}\Big\{ -4\Big[\, k_n^{(b,q)\,A} + \lambda(k_n^{(b,q)\,B} - k_n^{(b,q)\,A})\Big]\,\big[\, b_n^{0\,B} - b_n^{0\,A}\big] \\
&\quad \cdot \big[\, b_n^{0\,A} + \lambda(b_n^{0\,B} - b_n^{0\,A})\big]\,\big[\, {b_n}^2 - [b_n^{0\,A} + \lambda(b_n^{0\,B} - b_n^{0\,A})]^2\big] \\
&\quad + \Big[\, k_n^{(b,q)\,B} - k_n^{(b,q)\,A}\Big]\,\big[\, {b_n}^2 - [b_n^{0\,A} + \lambda(b_n^{0\,B} - b_n^{0\,A})]^2\big]^2\Big\}.
\end{aligned} \tag{14.22}$$

The corresponding expression for use in the perturbation formula Eq. 14.9 is

$$V^{(b,q)}(\mathbf{r};\lambda \pm \Delta\lambda) - V^{(b,q)}(\mathbf{r};\lambda) \tag{14.23}$$

which can easily be obtained from Eq. 14.19.

The $\lambda-$dependent version of the harmonic potential-energy function term describing the covalent bond-stretching (Sec. 5.1) is obtained by making the force constant $k_n^{(b,h)}$ and the ideal bond length b_n^0 linearly dependent on λ,

$$\begin{aligned}
V^{(b,h)}(\mathbf{r};\lambda) &= \sum_{n=1}^{N^{(b)}} V^{(b,h)}(b_n;\lambda) \\
&= \sum_{n=1}^{N^{(b)}} \tfrac{1}{2}\Big[(1-\lambda)k_n^{(b,h)\,A} + \lambda k_n^{(b,h)\,B}\Big]\,\big[b_n - [(1-\lambda)b_n^{0\,A} + \lambda b_n^{0\,B}]\big]^2 \\
&= \sum_{n=1}^{N^{(b)}} \tfrac{1}{2}k_n^{(b,h)\,A}[b_n - b_n^{0\,A}]^2 \\
&\quad + \sum_{n=1}^{N^{(b)}} \tfrac{1}{2}\lambda\Big\{ -k_n^{(b,h)\,A}\,\big[\, b_n^{0\,B} - b_n^{0\,A}\big]\,\big[\, 2[b_n - b_n^{0\,A}] - \lambda[b_n^{0\,B} - b_n^{0\,A}]\big] \\
&\quad + \Big[\, k_n^{(b,h)\,B} - k_n^{(b,h)\,A}\Big]\,\big[\, b_n - b_n^{0\,A} - \lambda b_n^{0\,B} - b_n^{0\,A})\big]^2\Big\} \\
&= V^{(b,h)}(\mathbf{r};\lambda = \lambda_A = 0) + \Delta V^{(b,h)\,A}(\mathbf{r};\lambda).
\end{aligned} \tag{14.24}$$

The forces $\mathbf{f}^{(b,h)\,A}_{i}$ and $\mathbf{f}^{(b,h)\,A}_{j}$ in state A ($\lambda = \lambda_A = 0$) on atoms i and j due to the n-th term in Eq. 5.6 are given by expressions Eq. 17.3 and Eq. 17.4, using $k_n^{(b,h)} = k_n^{(b,h)\,A}$ and $b_n^0 = b_n^{0\,A}$.

The forces on atoms i and j due to the n-th term in the energy difference $\Delta V^{(b,h)\,A}(\mathbf{r};\lambda)$ are

$$\begin{aligned}
\mathbf{f}^{(b,h)\,\Delta A}_{i} &= -\frac{\partial \Delta V^{(b,h)\,A}_{n}}{\partial b_n}\frac{\partial b_n}{\partial \mathbf{r}_i} \\
&= \lambda \Big\{ \; k_n^{(b,h)\,A}[b_n^{0\,B} - b_n^{0\,A}] \\
&\quad - \Big[k_n^{(b,h)\,B} - k_n^{(b,h)\,A}\Big] \; \big[\; b_n - b_n^{0\,A} - \lambda(b_n^{0\,B} - b_n^{0\,A})\big] \Big\} \; \frac{\partial b_n}{\partial \mathbf{r}_i}
\end{aligned} \tag{14.25}$$

and

$$\mathbf{f}^{(b,h)\,\Delta A}_{j} = -\mathbf{f}^{(b,h)\,\Delta A}_{i} \tag{14.26}$$

The derivative with respect to λ of the energy $V^{(b,h)}(\mathbf{r};\lambda)$ and of the energy difference $\Delta V^{(b,h)\,A}$ with respect to the state A is:

$$\begin{aligned}
&\tfrac{\partial V^{(b,h)}(\mathbf{r};\lambda)}{\partial \lambda} = \tfrac{\partial \Delta V^{(b,h)\,A}(\mathbf{r};\lambda)}{\partial \lambda} \\
&= \sum_{n=1}^{N^{(b)}} \tfrac{1}{2} \Big\{ \; -2 \Big[\; k_n^{(b,h)\,A} + \lambda(k_n^{(b,h)\,B} - k_n^{(b,h)\,A}) \Big] \; \big[\; b_n^{0\,B} - b_n^{0\,A}\big] \\
&\quad \big[\; b_n - b_n^{0\,A} - \lambda(b_n^{0\,B} - b_n^{0\,A})\big] \\
&\quad + \Big[\; k_n^{(b,h)\,B} - k_n^{(b,h)\,A}\Big] \; \big[\; b_n - b_n^{0\,A} - \lambda(b_n^{0\,B} - b_n^{0\,A})\big]^2 \Big\} .
\end{aligned} \tag{14.27}$$

The expression for use in the perturbation formula Eq. 14.9 is

$$V^{(b,h)}(\mathbf{r};\lambda \pm \Delta\lambda) - V^{(b,h)}(\mathbf{r};\lambda) \tag{14.28}$$

which can easily be obtained from Eq. 14.24.

14.2.2. Covalent bond forces (soft potential energy function). When the perturbation involves the breaking of a bond numerical instabilities occur in $\frac{\partial V^{(b,h)}(\mathbf{r};\lambda)}{\partial \lambda}$ because the distance b between the formerly bonded atoms becomes large in the state where the bond stretching force constant is 0. This can be avoided by using a modified, "soft" bond stretch potential energy function, introducing a softness term $S(b,\lambda)$. Wang et al[134] formulate the contribution to the potential energy due to a soft harmonic bond b with force constant $k^{(b,h)}$ and target value b^0 that is broken at $\lambda = 0$ and has its full strength at $\lambda = 1$ as follows:

$$V(b,\lambda) = \frac{1}{2} K \lambda (b - b^0)^2 \frac{1}{S(b,(1-\lambda))} \tag{14.29}$$

where

$$S(b,\lambda) = 1 + \alpha_b \lambda (b - b^0)^2$$

and α_b is a positive number that can be adjusted to maximize the phase space overlap between neighbouring λ windows.[134]

In GROMOS a more general form of the soft harmonic bond stretch potential energy function is implemented, which allows the bond in either of the two states to be broken and the bond lengths in the two states to be different. In analogy to Eq. 14.24:

$$\begin{aligned} V^{(bs,h)}(\mathbf{r};\lambda) &= \sum_{n=1}^{N^{(bs)}} V^{(bs,h)}(b_n;\lambda) \\ &= \sum_{n=1}^{N^{(bs)}} \tfrac{1}{2}\left[(1-\lambda)\tfrac{k_n^{(b,h)\,A}}{S_n^A(b_n,\lambda)} + \lambda\tfrac{k_n^{(b,h)\,B}}{S_n^B(b_n,1-\lambda)}\right]\left[b_n - b_n^0(\lambda)\right]^2 \end{aligned} \tag{14.30}$$

where $N^{(bs)}$ is the number of soft bonds and $S_n^X(b_n,\lambda)$ the softness term for state X

$$S_n^X(b_n,\lambda) \;=\; 1+\alpha_b\lambda(b_n - b_n^{0\,X})^2 \tag{14.31}$$

and

$$b_n^0(\lambda) \;=\; (1-\lambda)b_n^{0\,A} + \lambda b_n^{0\,B}$$

The forces on atoms i and j due to the n-th term in the energy $V^{(bs,h)}(\mathbf{r};\lambda)$ are

$$\begin{aligned} \mathbf{f}^{(bs,h)}{}_i &= -\frac{\partial V^{(bs,h)}{}_n}{\partial b_n}\frac{\partial b_n}{\partial \mathbf{r}_i} \\ &= -\left[\frac{(1-\lambda)k_n^{(b,h)\,A}}{S_n^A(b_n,\lambda)^2} + \frac{\lambda k_n^{(b,h)\,B}}{S_n^B(b_n,1-\lambda)^2}\right]\left[b_n - b_n^0(\lambda)\right]\frac{\partial b_n}{\partial \mathbf{r}_i} \\ &= -\left[\frac{(1-\lambda)k_n^{(b,h)\,A}}{S_n^A(b_n,\lambda)^2} + \frac{\lambda k_n^{(b,h)\,B}}{S_n^B(b_n,1-\lambda)^2}\right]\left[b_n - b_n^0(\lambda)\right]\frac{\mathbf{r}_{ij}}{r_{ij}} \end{aligned} \tag{14.32}$$

and

$$\mathbf{f}^{(bs,h)}{}_j \;=\; -\mathbf{f}^{(bs,h)}{}_i \tag{14.33}$$

The derivative with respect to λ of the energy $V^{(bs,h)}(\mathbf{r};\lambda)$ is:

$$\begin{aligned} &\frac{\partial V^{(bs,h)}(\mathbf{r};\lambda)}{\partial\lambda} = \\ &= \sum_{n=1}^{N^{(bs)}} \frac{1}{2}(b_n - b_n^0(\lambda))^2\left[\frac{k_n^{(b,h)\,A}}{S_n^A(b_n,\lambda)^2}(-X1+X2) + \frac{k_n^{(b,h)\,B}}{S_n^B(b_n,1-\lambda)^2}(X1+X2)\right] \\ &-(b_n - b_n^0(\lambda))(b_n^{0\,B} - b_n^{0\,A})\left[\frac{(1-\lambda)k_n^{(b,h)\,A}}{S_n^A(b_n,\lambda)} + \frac{\lambda k_n^{(b,h)\,B}}{S_n^B(b_n,1-\lambda)}\right] \end{aligned} \tag{14.34}$$

with

$$\begin{aligned} X1 &= 1+\alpha(b_n - b_n^0(\lambda))^2 \\ X2 &= 2\alpha\lambda(1-\lambda)(b_n - b_n{}^0(\lambda))(b_n^{0\,B} - b_n^{0\,A}) \end{aligned} \tag{14.35}$$

14.2.3. Covalent bond-angle forces. The $\lambda-$dependent version of the potential-energy function describing the covalent bond-angle bending interaction, which is harmonic in the cosine of the bond angles (Sec. 5.2 , Eq. 5.7) is obtained by making the force constant $k_n^{(\theta,c)}$ and the cosine of the ideal bond angle θ_n linearly dependent on λ,

$$
\begin{aligned}
V^{(\theta,c)}(\mathbf{r};\lambda) &= \sum_{n=1}^{N^{(\theta)}} {V^{(\theta,c)}}_n(\theta_n;\lambda) \\
&= \sum_{n=1}^{N^{(\theta)}} \tfrac{1}{2}\Big[(1-\lambda)k_n^{(\theta,c)A} + \lambda k_n^{(\theta,c)B}\Big]\big[\cos\theta_n - [(1-\lambda)\cos\theta_n^{0\,A} + \lambda\cos\theta_n^{0\,B}]\big]^2 \\
&= \sum_{n=1}^{N^{(\theta)}} \tfrac{1}{2}k_n^{(\theta,c)A}\big[\,\cos\theta_n - \cos\theta_n^{0\,A}\big]^2 \\
&+ \sum_{n=1}^{N^{(\theta)}} \tfrac{1}{2}\lambda\Big\{\,-k_n^{(\theta,c)A}[\cos\theta_n^{0\,B} - \cos\theta_n^{0\,A}]\,\big[\,2[\cos\theta_n - \cos\theta_n^{0\,A}] - \lambda[\cos\theta_n^{0\,B} - \cos\theta_n^{0\,A}]\big] \\
&+[k_n^{(\theta,c)B} - k_n^{(\theta,c)A}]\big[\,\cos\theta_n - \cos\theta_n^{0\,A} - \lambda[\cos\theta_n^{0\,B} - \cos\theta_n^{0\,A}]\big]^2\Big\} \\
&= V^{(\theta,c)}(\mathbf{r};\lambda=\lambda_A=0) + \Delta V^{(\theta,c)A}(\mathbf{r};\lambda).
\end{aligned}
\tag{14.36}
$$

The forces $\mathbf{f}_{\,i}^{(\theta,c)A}$, $\mathbf{f}_{\,j}^{(\theta,c)A}$ and $\mathbf{f}_{\,k}^{(\theta,c)A}$ in state A ($\lambda=\lambda_A=0$) on atoms i, j and k due to the n-th term in Eq. 5.7 are given by expressions Eq. 17.5, Eq. 17.6 and Eq. 17.7 using $k_n^{(\theta,c)} = k_n^{(\theta,c)A}$ and $\theta_n^0 = \theta_n^{0\,A}$.

The forces on atoms i, j and k due to the n-th term in the energy difference $\Delta V^{(\theta,c)A}(\boldsymbol{r};\lambda)$ are

$$
\begin{aligned}
\mathbf{f}_{\,i}^{(\theta,c)\Delta A} &= -\frac{\partial \Delta V^{(\theta,c)A}_{\;\;n}}{\partial\cos\theta_n}\frac{\partial\cos\theta_n}{\partial\mathbf{r}_i} \\
&= \lambda\Big\{\,k_n^{(\theta,c)A}[\cos\theta_n^{0\,B} - \cos\theta_n^{0\,A}] \\
&\quad -\Big[\,k_n^{(\theta,c)B} - k_n^{(\theta,c)A}\Big]\,\big[\,\cos\theta_n - \cos\theta_n^{0\,A} - \lambda[\cos\theta_n^{0\,B} - \cos\theta_n^{0\,A}]\big]\Big\}\frac{\partial\cos\theta_n}{\partial\mathbf{r}_i}
\end{aligned}
\tag{14.37}
$$

$$
\mathbf{f}_{\,k}^{(\theta,c)\Delta A} = -\frac{\partial \Delta V^{(\theta,c)A}_{\;\;n}}{\partial\cos\theta_n}\frac{\partial\cos\theta_n}{\partial\mathbf{r}_k} \tag{14.38}
$$

and

$$
\mathbf{f}_{\,j}^{(\theta,c)\Delta A} = -\mathbf{f}_{\,i}^{(\theta,c)\Delta A} - \mathbf{f}_{\,k}^{(\theta,c)\Delta A}. \tag{14.39}
$$

The derivative with respect to λ of the energy $V^{(\theta,c)}(\mathbf{r};\lambda)$ and of the energy difference $\Delta V^{(\theta,c)A}(\mathbf{r};\lambda)$ with respect to state A is

$$
\begin{aligned}
\frac{\partial V^{(\theta,c)}(\mathbf{r};\lambda)}{\partial\lambda} &= \frac{\partial \Delta V^{(\theta,c)A}(\mathbf{r};\lambda)}{\partial\lambda} \\
&= \sum_{n=1}^{N^{(\theta)}} \tfrac{1}{2}\Big\{\,-2\Big[k_n^{(\theta,c)A} + \lambda(k_n^{(\theta,c)B} - k_n^{(\theta,c)A})\Big]\,\big[\,\cos\theta_n^{0\,B} - \cos\theta_n^{0\,A}\big] \\
&\quad \big[\,\cos\theta_n - \cos\theta_n^{0\,A} - \lambda(\cos\theta_n^{0\,B} - \cos\theta_n^{0\,A})\big] \\
&\quad +\Big[\,k_n^{(\theta,c)B} - k_n^{(\theta,c)A}\Big]\,\big[\,\cos\theta_n - \cos\theta_n^{0\,A} - \lambda(\cos\theta_n^{0\,B} - \cos\theta_n^{0\,A})\big]^2\Big\}.
\end{aligned}
\tag{14.40}
$$

The corresponding expressions for use in the perturbation formula Eq. 14.9 are

$$V^{(\theta,c)}(\mathbf{r};\lambda \pm \Delta\lambda) - V^{(\theta,c)}(\mathbf{r};\lambda) \tag{14.41}$$

which can easily be obtained from Eq. 14.36.

The $\lambda-$dependent version of the harmonic potential-energy function describing the covalent bond-angle bending interaction (Eq. 5.11) is obtained by making the force constant $k_n^{(\theta,h)}$ and the ideal bond angle θ_n^0 linearly dependent on λ,

$$\begin{aligned}
V^{(\theta,h)}(\mathbf{r};\lambda) &= \sum_{n=1}^{N^{(\theta)}} {V^{(\theta,h)}}_n(\theta_n;\lambda) \\
&= \sum_{n=1}^{N^{(\theta)}} \tfrac{1}{2}\Big[(1-\lambda)k_n^{(\theta,h)A} + \lambda k_n^{(\theta,h)B}\Big]\big[\theta_n - [(1-\lambda)\theta_n^{0\,A} + \lambda\theta_n^{0\,B}]\big]^2 \\
&= \sum_{n=1}^{N^{(\theta)}} \tfrac{1}{2}k_n^{(\theta,h)A}\big[\theta_n - \theta_n^{0\,A}\big]^2 \\
&\quad + \sum_{n=1}^{N^{(\theta)}} \tfrac{1}{2}\lambda\Big\{ -k_n^{(\theta,h)A}[\theta_n^{0\,B} - \theta_n^{0\,A}]\,\big[\,2[\theta_n - \theta_n^{0\,A}] - \lambda[\theta_n^{0\,B} - \theta_n^{0\,A}]\big] \\
&\quad + [k_n^{(\theta,h)B} - k_n^{(\theta,h)A}]\big[\,\theta_n - \theta_n^{0\,A} - \lambda[\theta_n^{0\,B} - \theta_n^{0\,A}]\big]^2\Big\} \\
&= V^{(\theta,h)}(\mathbf{r};\lambda = \lambda_A = 0) + \Delta V^{(\theta,h)A}(\mathbf{r};\lambda).
\end{aligned} \tag{14.42}$$

The forces $\mathbf{f}_i^{(\theta,h)A}$, $\mathbf{f}_j^{(\theta,h)A}$ and $\mathbf{f}_k^{(\theta,h)A}$ in state A ($\lambda = \lambda_A = 0$) on atoms i, j and k due to Eq. 5.11 are given by expressions Eq. 17.8, Eq. 17.9 and Eq. 17.10 using $k_n^{(\theta,h)} = k_n^{(\theta,h)A}$ and $\theta_n^0 = \theta_n^{0\,A}$.

The forces on atoms i, j and k due to the n-th term in the energy difference $\Delta V^{(\theta,h)A}(\mathbf{r};\lambda)$ are

$$\begin{aligned}
\mathbf{f}_i^{(\theta,h)\Delta A} &= -\frac{\partial \Delta {V^{(\theta,h)A}}_n}{\partial\theta_n}\frac{\partial\theta_n}{\partial\mathbf{r}_i} \\
&= \lambda\Big\{ k_n^{(\theta,h)A}[\theta_n^{0\,B} - \theta_n^{0\,A}] \\
&\quad - \Big[\,k_n^{(\theta,h)B} - k_n^{(\theta,h)A}\Big]\,\big[\,\theta_n - \theta_n^{0\,A} - \lambda(\theta_n^{0\,B} - \theta_n^{0\,A})\big]\Big\}\frac{\partial\theta_n}{\partial\mathbf{r}_i}
\end{aligned} \tag{14.43}$$

$$\mathbf{f}_k^{(\theta,h)\Delta A} = -\frac{\partial \Delta {V^{(\theta,h)A}}_n}{\partial\theta_n}\frac{\partial\theta_n}{\partial\mathbf{r}_k} \tag{14.44}$$

and

$$\mathbf{f}_j^{(\theta,h)\Delta A} = -\mathbf{f}_i^{(\theta,h)\Delta A} - \mathbf{f}_k^{(\theta,h)\Delta A}. \tag{14.45}$$

The derivative with respect to λ of the energy $V^{(\theta,h)}(\mathbf{r};\lambda)$ and of the energy difference $\Delta V^{(\theta,h)A}(\mathbf{r};\lambda)$ with respect to state A is

$$\begin{aligned}
\frac{\partial V^{(\theta,h)}(\mathbf{r};\lambda)}{\partial\lambda} &= \frac{\partial \Delta V^{(\theta,h)A}(\mathbf{r};\lambda)}{\partial\lambda} \\
&= \sum_{n=1}^{N^{(\theta)}} \tfrac{1}{2}\Big\{ -2\Big[\,k_n^{(\theta,h)A} + \lambda(k_n^{(\theta,h)B} - k_n^{(\theta,h)A})\Big]\,\big[\,\theta_n^{0\,B} - \theta_n^{0\,A}\big] \\
&\quad \big[\,\theta_n - \theta_n^{0\,A} - \lambda(\theta_n^{0\,B} - \theta_n^{0\,A})\big] \\
&\quad + \Big[\,k_n^{(\theta,h)B} - k_n^{(\theta,h)A}\Big]\,\big[\,\theta_n - \theta_n^{0\,A} - \lambda(\theta_n^{0\,B} - \theta_n^{0\,A})\big]^2\Big\}.
\end{aligned} \tag{14.46}$$

The expression for use in the perturbation formula Eq. 14.9 is

$$V^{(\theta,h)}(\mathbf{r};\lambda \pm \Delta\lambda) - V^{(\theta,h)}(\mathbf{r};\lambda) \tag{14.47}$$

which can easily be obtained from Eq. 14.42.

14.2.4. Covalent bond-angle forces (soft potential energy function). When a bond is broken also the force constants of affected bond angles should go to zero and numerical instabilities are - even though weaker than in the bond-stretching term (see Sec. 14.2.2) - also apparent in the λ derivatives of the bond-angle bending term $\frac{\partial V^{(\theta,c)}(\mathbf{r};\lambda)}{\partial\lambda}$. A soft potential energy function $V^{(\theta s,c)}(\mathbf{r};\lambda)$ and the corresponding λ derivative $\frac{\partial V^{(\theta s,c)}(\mathbf{r};\lambda)}{\partial\lambda}$ can be used analogous to Eq. 14.30 and Eq. 14.34, simply substituting b with $\cos\theta$.

The forces on atoms i, j, and k of the n-th soft angle are then:

$$\begin{aligned}
\mathbf{f}^{(\theta s,c)}{}_i &= -\frac{\partial V_n^{(\theta s,c)}}{\partial\cos\theta_n}\frac{\partial\cos\theta_n}{\partial\mathbf{r}_i} \qquad (14.48)\\
&= -\left[\frac{(1-\lambda)k_n^{(\theta,c)A}}{S_n^A(\cos\theta_n,\lambda)^2} + \frac{\lambda k_n^{(\theta,c)B}}{S_n^B(\cos\theta_n,1-\lambda)^2}\right]\left[\cos\theta_n - \cos\theta_n^0(\lambda)\right]\frac{\partial\cos\theta_n}{\partial\mathbf{r}_i}\\
&= -\left[\frac{(1-\lambda)k_n^{(\theta,c)A}}{S_n^A(\cos\theta_n,\lambda)^2} + \frac{\lambda k_n^{(\theta,c)B}}{S_n^B(\cos\theta_n,1-\lambda)^2}\right]\left[\cos\theta_n - \cos\theta_n^0(\lambda)\right]\left[\frac{\mathbf{r}_{kj}}{r_{kj}} - \frac{\mathbf{r}_{ij}}{r_{ij}}\cos\theta_n\right]\frac{1}{r_{ij}}\\
\mathbf{f}^{(\theta s,c)}{}_k &= -\frac{\partial V_n^{(\theta s,c)}}{\partial\cos\theta_n}\frac{\partial\cos\theta_n}{\partial\mathbf{r}_k}\\
&= -\left[\frac{(1-\lambda)k_n^{(\theta,c)A}}{S_n^A(\cos\theta_n,\lambda)^2} + \frac{\lambda k_n^{(\theta,c)B}}{S_n^B(\cos\theta_n,1-\lambda)^2}\right]\left[\cos\theta_n - \cos\theta_n^0(\lambda)\right]\left[\frac{\mathbf{r}_{ij}}{r_{ij}} - \frac{\mathbf{r}_{kj}}{r_{kj}}\cos\theta_n\right]\frac{1}{r_{kj}}\\
\mathbf{f}^{(\theta s,c)}{}_j &= -\mathbf{f}^{(\theta s,c)}{}_i - \mathbf{f}^{(\theta s,c)}{}_k
\end{aligned}$$

with

$$S_n^X(\cos\theta_n,\lambda) = 1 + \alpha_\theta\lambda(\cos\theta_n - \cos\theta_n^{0\,X})^2 \tag{14.49}$$

and

$$\cos\theta_n^0(\lambda) = (1-\lambda)\cos\theta_n^{0\,A} + \lambda\cos\theta_n^{0\,B}. \tag{14.50}$$

14.2.5. Improper dihedral-angle forces. The $\lambda-$dependent version of the harmonic improper dihedral-angle bending interaction (Sec. 5.3) is obtained by making the force constant $k_n^{(\xi)}$ and the ideal improper

dihedral-angle ξ_n^0 linearly dependent on λ,

$$
\begin{aligned}
V^{(\xi)}(\mathbf{r};\lambda) &= \sum_{n=1}^{N^{(\xi)}} V^{(\xi)}{}_n(\xi_n;\lambda) \\
&= \sum_{n=1}^{N^{(\xi)}} \tfrac{1}{2}\left[(1-\lambda)k_n^{(\xi)\,A} + \lambda k_n^{(\xi)\,B}\right]\left[\,\xi_n - [(1-\lambda)\xi_n^{0\,A} + \lambda\xi_n^{0\,B}]\right]^2 \\
&= \sum_{n=1}^{N^{(\xi)}} \tfrac{1}{2}k_n^{(\xi)\,A}[\xi_n - \xi_n^{0\,A}]^2 \\
&\quad + \sum_{n=1}^{N^{(\xi)}} \tfrac{1}{2}\lambda\Big\{ -k_n^{(\xi)\,A}\left[\,\xi_n^{0\,B} - \xi_n^{0\,A}\right]\left[\,2[\xi_n - \xi_n^{0\,A}] - \lambda[\xi_n^{0\,B} - \xi_n^{0\,A}]\right] \\
&\quad + \left[\,k_n^{(\xi)\,B} - k_n^{(\xi)\,A}\right]\left[\,\xi_n - \xi_n^{0\,A} - \lambda(\xi_n^{0\,B} - \xi_n^{0\,A})\right]^2\Big\} \\
&= V^{(\xi)}(\mathbf{r};\lambda = \lambda_A = 0) + \Delta V^{(\xi)\,A}(\mathbf{r};\lambda).
\end{aligned}
\tag{14.51}
$$

The forces ${\mathbf{f}^{(\xi)}}_i^A$, ${\mathbf{f}^{(\xi)}}_j^A$, ${\mathbf{f}^{(\xi)}}_k^A$ and ${\mathbf{f}^{(\xi)}}_l^A$ in state A ($\lambda = \lambda_A = 0$) on atoms i, j, k and l due to the n-th term in Eq. 5.13 are given by expressions Eq. 17.11, Eq. 17.12, Eq. 17.13 and Eq. 17.14 using $k_n^{(\xi)} = k_n^{(\xi)\,A}$ and $\xi_n^0 = \xi_n^{0\,A}$.

The forces on atoms i, j, k and l due to the n-th term in the energy difference $\Delta V^{(\xi)\,A}(\mathbf{r};\lambda)$ are

$$
\begin{aligned}
{\mathbf{f}^{(\xi)}}_i^{\Delta A} &= -\frac{\partial \Delta {V^{(\xi)}}_n^A}{\partial \xi_n}\frac{\partial \xi_n}{\partial \mathbf{r}_i} \qquad (14.52)\\
&= \lambda\Big\{\,k_n^{(\xi)\,A}[\xi_n^{0\,B} - \xi_n^{0\,A}] \\
&\quad - \left[\,k_n^{(\xi)\,B} - k_n^{(\xi)\,A}\right]\left[\,\xi_n - \xi_n^{0\,A} - \lambda(\xi_n^{0\,B} - \xi_n^{0\,A})\right]\Big\}\frac{\partial \xi_n}{\partial \mathbf{r}_i}
\end{aligned}
$$

$$
{\mathbf{f}^{(\xi)}}_j^{\Delta A} = -\frac{\partial \Delta {V^{(\xi)}}_n^A}{\partial \xi_n}\frac{\partial \xi_n}{\partial \mathbf{r}_j} \tag{14.53}
$$

$$
{\mathbf{f}^{(\xi)}}_l^{\Delta A} = -\frac{\partial \Delta {V^{(\xi)}}_n^A}{\partial \xi_n}\frac{\partial \xi_n}{\partial \mathbf{r}_l} \tag{14.54}
$$

and

$$
{\mathbf{f}^{(\xi)}}_k^{\Delta A} = -{\mathbf{f}^{(\xi)}}_i^{\Delta A} - {\mathbf{f}^{(\xi)}}_j^{\Delta A} - {\mathbf{f}^{(\xi)}}_l^{\Delta A}. \tag{14.55}
$$

The derivative with respect to λ of the energy $V^{(\xi)}(\mathbf{r};\lambda)$ and of the energy difference $\Delta V^{(\xi)}(\mathbf{r};\lambda)$ with respect to state A is

$$\begin{aligned}
&\frac{\partial V^{(\xi)}(\mathbf{r};\lambda)}{\partial\lambda} = \frac{\partial \Delta V^{(\xi)\,A}(\mathbf{r};\lambda)}{\partial\lambda} \\
&= \sum_{n=1}^{N^{(\xi)}} \frac{1}{2}\Big\{ -2\Big[\, k_n^{(\xi)\,A} + \lambda(k_n^{(\xi)\,B} - k_n^{(\xi)\,A})\Big]\,\big[\,\xi_n^{0\,B} - \xi_n^{0\,A}\big] \\
&\quad \big[\,\xi_n - \xi_n^{0\,A} - \lambda(\xi_n^{0\,B} - \xi_n^{0\,A})\big] \\
&\quad + \Big[\, k_n^{(\xi)\,B} - k_n^{(\xi)\,A}\Big]\,\big[\,\xi_n - \xi_n^{0\,A} - \lambda(\xi_n^{0\,B} - \xi_n^{0\,A})\big]^2\Big\}.
\end{aligned} \tag{14.56}$$

The expression for use in the perturbation formula Eq. 14.9 is

$$V^{(\xi)}(\mathbf{r};\lambda \pm \Delta\lambda) - V^{(\xi)}(\mathbf{r};\lambda) \tag{14.57}$$

which can easily be obtained from Eq. 14.51.

14.2.6. Improper dihedral-angle forces (soft potential energy function). A soft potential energy function, analogous to the ones for the bond stretching and bond-angle bending terms can also be applied to the improper dihedrals to reduce numerical instabilities when a bond is broken. A soft potential energy $V^{(\xi s)}(\mathbf{r};\lambda)$ and the corresponding λ derivative $\frac{\partial V^{(\xi s)}(\mathbf{r};\lambda)}{\partial\lambda}$ are defined as in Eq. 14.30 and Eq. 14.34, simply substituting b with ξ.

The forces on atoms i, j, k and l of the n-th soft improper dihedral angle are then:

$$\begin{aligned}
\mathbf{f}^{(\xi s)}{}_i &= -\frac{\partial V^{(\xi s)}{}_n}{\partial\xi_n}\frac{\partial\xi_n}{\partial\mathbf{r}_i} \\
&= -\left[\frac{(1-\lambda)k_n^{(\xi)\,A}}{S_n^A(\xi_n,\lambda)^2} + \frac{\lambda k_n^{(\xi)\,B}}{S_n^B(\xi_n,1-\lambda)^2}\right]\big[\xi_n - \xi_n^0(\lambda)\big]\,\frac{\partial\xi_n}{\partial\mathbf{r}_i} \\
&= -\left[\frac{(1-\lambda)k_n^{(\xi)\,A}}{S_n^A(\xi_n,\lambda)^2} + \frac{\lambda k_n^{(\xi)\,B}}{S_n^B(\xi_n,1-\lambda)^2}\right]\big[\xi_n - \xi_n^0(\lambda)\big]\,\frac{r_{kj}}{r_{mj}^2}\mathbf{r}_{mj} \\
\mathbf{f}^{(\xi s)}{}_l &= -\frac{\partial V^{(\xi s)}{}_n}{\partial\xi_n}\frac{\partial\xi_n}{\partial\mathbf{r}_l} \\
&= -\left[\frac{(1-\lambda)k_n^{(\xi)\,A}}{S_n^A(\xi_n,\lambda)^2} + \frac{\lambda k_n^{(\xi)\,B}}{S_n^B(\xi_n,1-\lambda)^2}\right]\big[\xi_n - \xi_n^0(\lambda)\big]\,\frac{r_{kj}}{r_{nk}^2}\mathbf{r}_{nk} \\
\mathbf{f}^{(\xi s)}{}_j &= -\frac{\partial V^{(\xi s)}{}_n}{\partial\xi_n}\frac{\partial\xi_n}{\partial\mathbf{r}_j} \\
&= \left[\frac{\mathbf{r}_{ij}\cdot\mathbf{r}_{kj}}{r_{kj}^2} - 1\right]\mathbf{f}^{(\xi s)}{}_i - \frac{\mathbf{r}_{kl}\cdot\mathbf{r}_{kj}}{r_{kj}^2}\mathbf{f}^{(\xi s)}{}_l \\
\mathbf{f}^{(\xi s)}{}_k &= -\mathbf{f}^{(\xi s)}{}_i - \mathbf{f}^{(\xi s)}{}_j - \mathbf{f}^{(\xi s)}{}_l
\end{aligned} \tag{14.58}$$

where

$$S_n^X(\xi_n,\lambda) = 1 + \alpha_\xi\lambda(\xi_n - \cos\xi_n^{0\,X})^2, \tag{14.59}$$

$$\xi_n^0(\lambda) = (1-\lambda)\xi_n^{0\,A} + \lambda\xi_n^{0\,B} \tag{14.60}$$

and

$$\begin{aligned}
\mathbf{r}_{mj} &= \mathbf{r}_{ij} \times \mathbf{r}_{kj} \\
\mathbf{r}_{nk} &= \mathbf{r}_{kj} \times \mathbf{r}_{kl} \\
r_{mj} &= (\mathbf{r}_{mj} \cdot \mathbf{r}_{mj})^{1/2} \\
r_{nk} &= (\mathbf{r}_{nk} \cdot \mathbf{r}_{nk})^{1/2}.
\end{aligned}$$

14.2.7. Dihedral-angle torsion forces. The $\lambda-$dependent version of the trigonometric dihedral-angle torsion interaction (Sec. 5.4) is obtained by applying a linear combination of the interaction function at states A and B,

$$\begin{aligned}
V^{(\varphi,s)}(\mathbf{r};\lambda) &= \sum_{n=1}^{N^{(\varphi)}} V^{(\varphi,s)}{}_n(\varphi_n;\lambda) \\
&= \sum_{n=1}^{N^{(\varphi)}} (1-\lambda) k_n^{(\varphi,s)\,A}[1+\cos(\varphi_n^{0\,A})\cos(m_n^{(\varphi)\,A}\varphi_n)] + \lambda k_n^{(\varphi,s)\,B}[1+\cos(\varphi_n^{0\,B})\cos(m_n^{(\varphi)\,B}\varphi_n)] \\
&= \sum_{n=1}^{N^{(\varphi)}} k_n^{(\varphi,s)\,A}[1+\cos(\varphi_n^{0\,A})\cos(m_n^{(\varphi)\,A}\varphi_n)] + \sum_{n=1}^{N^{(\varphi)}} \lambda \Big\{ k_n^{(\varphi,s)\,B}[1+\cos(\varphi_n^{0\,B})\cos(m_n^{(\varphi)\,B}\varphi_n)] \\
&\quad - k_n^{(\varphi,s)\,A}[1+\cos(\varphi_n^{0\,A})\cos(m_n^{(\varphi)\,A}\varphi_n)] \Big\} \\
&= V^{(\varphi,s)}(\mathbf{r};\lambda=\lambda_A=0) + \Delta V^{(\varphi,s)\,A}(\mathbf{r};\lambda).
\end{aligned} \tag{14.61}$$

The forces $\mathbf{f}^{(\varphi,s)\,A}_{\;\;i}$, $\mathbf{f}^{(\varphi,s)\,A}_{\;\;j}$, $\mathbf{f}^{(\varphi,s)\,A}_{\;\;k}$ and $\mathbf{f}^{(\varphi,s)\,A}_{\;\;l}$ in state A ($\lambda = \lambda_A = 0$) on atoms i, j, k and l due to the n-th term in Eq. 5.18 are given by expressions Eq. 17.16, Eq. 17.18, Eq. 17.19 and Eq. 17.20 using $k_n^{(\varphi,s)} = k_n^{(\varphi,s)\,A}$, $\varphi_n^0 = \varphi_n^{0\,A}$ and $m_n^{(\varphi)} = m_n^{(\varphi)\,A}$.

The forces on atoms i, j, k and l due to the n-th term in the energy difference $\Delta V^{(\varphi,s)\,A}(\mathbf{r};\lambda)$ are

$$\begin{aligned}
\mathbf{f}^{(\varphi,s)\,\Delta A}_{\;\;\;\;i} &= -\frac{\partial \Delta V^{(\varphi,s)\,A}_{\;\;\;\;n}}{\partial \cos\varphi_n} \frac{\partial \cos\varphi_n}{\partial \mathbf{r}_i} \\
&= -\lambda \left\{ k_n^{(\varphi,s)\,B} \cos(\varphi_n^{0\,B}) \frac{\partial \cos(m_n^{(\varphi)\,B}\varphi_n)}{\partial \cos\varphi_n} \right. \\
&\qquad \left. - k_n^{(\varphi,s)\,A} \cos(\varphi_n^{0\,A}) \frac{\partial \cos(m_n^{(\varphi)\,A}\varphi_n)}{\partial \cos\varphi_n} \right\} \frac{\partial \cos\varphi_n}{\partial \mathbf{r}_i}
\end{aligned} \tag{14.62}$$

$$\mathbf{f}^{(\varphi,s)\,\Delta A}_{\;\;\;\;j} = -\frac{\partial \Delta V^{(\varphi,s)\,A}_{\;\;\;\;n}}{\partial \cos\varphi_n} \frac{\partial \cos\varphi_n}{\partial \mathbf{r}_j} \tag{14.63}$$

$$\mathbf{f}^{(\varphi,s)\,\Delta A}_{\;\;\;\;l} = -\frac{\partial \Delta V^{(\varphi,s)\,A}_{\;\;\;\;n}}{\partial \cos\varphi_n} \frac{\partial \cos\varphi_n}{\partial \mathbf{r}_l} \tag{14.64}$$

and

$$\mathbf{f}^{(\varphi,s)\,\Delta A}_{\;\;\;\;k} = -\mathbf{f}^{(\varphi,s)\,\Delta A}_{\;\;\;\;i} - \mathbf{f}^{(\varphi,s)\,\Delta A}_{\;\;\;\;j} - \mathbf{f}^{(\varphi,s)\,\Delta A}_{\;\;\;\;l}. \tag{14.65}$$

The derivative with respect to λ of the energy $V^{(\varphi,s)}(\mathbf{r};\lambda)$ and of the energy difference $\Delta V^{(\varphi,s)\,A}(\mathbf{r};\lambda)$ with respect to state A is

$$\begin{aligned}
\frac{\partial V^{(\varphi,s)}(\mathbf{r};\lambda)}{\partial\lambda} &= \frac{\partial \Delta V^{(\varphi,s)\,A}(\mathbf{r};\lambda)}{\partial\lambda} \\
&= \sum_{n=1}^{N^{(\varphi)}} \Big\{ k_n^{(\varphi,s)\,B} \Big[1+\cos(\varphi_n^{0\,B})\cos(m_n^{(\varphi)\,B}\varphi_n)\Big] \\
&\qquad -k_n^{(\varphi,s)\,A}\Big[1+\cos(\varphi_n^{0\,A})\cos(m_n^{(\varphi)\,A}\varphi_n)\Big]\Big\}.
\end{aligned} \tag{14.66}$$

The corresponding expression for use in the perturbation formula Eq. 14.9 is

$$V^{(\varphi,s)}(\mathbf{r};\lambda\pm\Delta\lambda) - V^{(\varphi,s)}(\mathbf{r};\lambda) \tag{14.67}$$

which can easily be obtained from Eq. 14.61.

The generalized $\lambda-$dependent version of the trigonometric dihedral-angle torsion interaction (Sec. 5.4) is obtained in a similar way,

$$\begin{aligned}
V^{(\varphi,g)}(\mathbf{r};\lambda) &= \sum_{n=1}^{N^{(\varphi)}} V^{(\varphi,g)}{}_n(\varphi_n;\lambda) \\
&= \sum_{n=1}^{N^{(\varphi)}} (1-\lambda)k_n^{(\varphi,g)\,A}[1+\cos(m_n^{(\varphi)\,A}\varphi_n-\varphi_n^{0\,A})] + \lambda k_n^{(\varphi,g)\,B}[1+\cos(m_n^{(\varphi)\,B}\varphi_n-\varphi_n^{0\,B})] \\
&= \sum_{n=1}^{N^{(\varphi)}} k_n^{(\varphi,g)\,A}[1+\cos(m_n^{(\varphi)\,A}\varphi_n-\varphi_n^{0\,A})] + \sum_{n=1}^{N^{(\varphi)}} \lambda\Big\{ k_n^{(\varphi,g)\,B}[1+\cos(m_n^{(\varphi)\,B}\varphi_n-\varphi_n^{0\,B})] \\
&\quad -k_n^{(\varphi,g)\,A}[1+\cos(m_n^{(\varphi)\,A}\varphi_n-\varphi_n^{0\,B})]\Big\} \\
&= V^{(\varphi,g)}(\mathbf{r};\lambda=\lambda_A=0) + \Delta V^{(\varphi,g)\,A}(\mathbf{r};\lambda).
\end{aligned} \tag{14.68}$$

The forces $\mathbf{f}^{(\varphi,g)\,A}_{i}$, $\mathbf{f}^{(\varphi,g)\,A}_{j}$, $\mathbf{f}^{(\varphi,g)\,A}_{k}$ and $\mathbf{f}^{(\varphi,g)\,A}_{l}$ in state A ($\lambda=\lambda_A=0$) on atoms i, j, k and l due to the n-th term in Eq. 5.18 are given by expressions Eq. 17.21, Eq. 17.23, Eq. 17.25 and Eq. 17.26 using $k_n^{(\varphi,g)}=k_n^{(\varphi,g)\,A}$, $\varphi_n^0=\varphi_n^{0\,A}$ and $m_n^{(\varphi)}=m_n^{(\varphi)\,A}$.

The forces on atoms i, j, k and l due to the n-th term in the energy difference $\Delta V^{(\varphi,g)\,A}(\mathbf{r};\lambda)$ are

$$\begin{aligned}
\mathbf{f}^{(\varphi,g)\,\Delta A}_{i} &= -\frac{\partial \Delta V^{(\varphi,g)\,A}_{n}}{\partial\varphi_n}\frac{\partial\varphi_n}{\partial\mathbf{r}_i} \\
&= -\lambda\Big\{ k_n^{(\varphi,g)\,B} m_n^{(\varphi)\,B} sin(m_n^{(\varphi)\,B}\varphi_n-\varphi_n^{0\,B}) \\
&\qquad -k_n^{(\varphi,g)\,A} m_n^{(\varphi)\,A} sin(m_n^{(\varphi)\,A}\varphi_n-\varphi_n^{0\,A})\frac{\partial\varphi_n}{\partial\mathbf{r}_i}
\end{aligned} \tag{14.69}$$

$$\mathbf{f}^{(\varphi,g)\,\Delta A}_{j} = -\frac{\partial \Delta V^{(\varphi,g)\,A}_{n}}{\partial\varphi_n}\frac{\partial\varphi_n}{\partial\mathbf{r}_j} \tag{14.70}$$

$$\mathbf{f}^{(\varphi,g)\,\Delta A}_{l} = -\frac{\partial \Delta V^{(\varphi,g)\,A}_{n}}{\partial\varphi_n}\frac{\partial\varphi_n}{\partial\mathbf{r}_l} \tag{14.71}$$

and

$$\mathbf{f}^{(\varphi,g)\,\Delta A}_{k} = -\mathbf{f}^{(\varphi,g)\,\Delta A}_{i} - \mathbf{f}^{(\varphi,g)\,\Delta A}_{j} - \mathbf{f}^{(\varphi,g)\,\Delta A}_{l}. \tag{14.72}$$

The derivative with respect to λ of the energy $V^{(\varphi,g)}(\mathbf{r};\lambda)$ and of the energy difference $\Delta V^{(\varphi,g)A}(\mathbf{r};\lambda)$ with respect to state A is

$$\begin{aligned}\frac{\partial V^{(\varphi,g)}(\mathbf{r};\lambda)}{\partial\lambda} &= \frac{\partial \Delta V^{(\varphi,g)A}(\mathbf{r};\lambda)}{\partial\lambda} \\ &= \sum_{n=1}^{N^{(\varphi)}} \Big\{ k_n^{(\varphi,g)B}\Big[\,1+\cos(m_n^{(\varphi)B}\varphi_n-\varphi_n^{0\,B})\Big] \\ &\qquad -k_n^{(\varphi,g)A}\Big[\,1+\cos(m_n^{(\varphi)A}\varphi_n-\varphi_n^{0\,A})\Big]\Big\}. \end{aligned} \tag{14.73}$$

The corresponding expression for use in the perturbation formula Eq. 14.9 is

$$V^{(\varphi,g)}(\mathbf{r};\lambda\pm\Delta\lambda)-V^{(\varphi,g)}(\mathbf{r};\lambda) \tag{14.74}$$

which can easily be obtained from Eq. 14.68.

14.2.8. Non-bonded forces. The $\lambda-$dependent version of the non-bonded (van der Waals and electrostatic) interaction (Sec. 3.3, Eqs. 6.6 and 6.7) to be a non-linear function of λ. Both the soft-core radius and the strength of the interaction depend non-linearly on λ in order to allow for a smooth change of real atoms to dummy atoms and vice versa[26]. The $\lambda-$dependent non-bonded interaction is only implemented for reaction field electrostatics and reads

$$\begin{aligned}&\mathcal{V}^{(nbd)}(\mathbf{r};\lambda)= \\ &\sum_{\substack{nonbonded\\ perturbed\\ pairs(i,j)}} \Big\{ \Big[\,\lambda^n\mathcal{V}^{(nbd)}(\mathbf{r}_{ij};B;(1-\lambda)) \;+(1-\lambda)^n\mathcal{V}^{(nbd)}(\mathbf{r}_{ij};A;\lambda)\Big]\;\Big\}\end{aligned} \tag{14.75}$$

with $n=$ integer >0, and for reaction field electrostatics,

$$\begin{aligned}&\mathcal{V}^{(nbd)}(\mathbf{r}_{ij};X;\lambda)=\mathcal{V}^{(vdw)}(\mathbf{r}_{ij};X;\lambda) \\ &\quad +\mathcal{V}^{(ele)}(\mathbf{r}_{ij};q_i^X,q_j^X,X;\lambda)\end{aligned} \tag{14.76}$$

$$\begin{aligned}&=\frac{1}{[\alpha_{LJ}(i,j)(\lambda^2)C_{126}^X(i,j)+(r_{ij})^6]}\cdot\Big[\,\frac{{C_{12}}^X(i,j)}{[\alpha_{LJ}(i,j)(\lambda^2)C_{126}^X(i,j)+(r_{ij})^6]}-{C_6}^X(i,j)\Big] \\ &\quad +\frac{q_i^Xq_j^X}{4\pi\varepsilon_0\varepsilon_1}\left[\frac{1}{[\alpha_c(i,j)(\lambda^2)+(r_{ij})^2]^{\frac{1}{2}}}-\frac{\frac{1}{2}C_{rf}(r_{ij})^2}{[\alpha_c(i,j)(\lambda^2)+{R_{rf}}^2]^{\frac{3}{2}}}-\frac{(1-\frac{1}{2}C_{rf})}{R_{rf}}\right]\end{aligned} \tag{14.77}$$

where the interaction parameters that are different in states A and B are indicated by the superscript X ($=A$ or B):

$$\begin{aligned} q_i^X &= \text{partial charge of atom i in state } X(A \text{ or } B) \\ {C_{12}}^X(i,j) &= r^{12} \text{ vdW parameter for atom pair } (i,j) \text{ in state } X(A \text{ or } B) \\ {C_6}^X(i,j) &= r^6 \text{ vdW parameter for atom pair } (i,j) \text{ in state } X(A \text{ or } B)\end{aligned} \tag{14.78}$$

and

$$\begin{aligned} C_{126}^X(i,j) &= \frac{{C_{12}}^X(i,j)}{{C_6}^X(i,j)} \qquad \text{if} \quad {C_6}^X(i,j)\neq 0 \\ &= 0 \qquad\qquad\qquad\quad \text{if} \quad {C_6}^X(i,j)=0\end{aligned} \tag{14.79}$$

The reaction field parameters R_{rf} and C_{rf} are defined in Sec. 2-7.3.

Softcore parameters $\alpha_{LJ}(i,j)$ and $\alpha_C(i,j)$ are determined based on input parameters ALPHLJ and ALPHC in the input block PERTURB and may be multiplied by atom specific weights specified in the perturbation topology ISCLJ[i] and ISCC[i]. We distinguish the following cases

- Both atoms i and j are listed in the perturbation topology
  $\alpha_{LJ}(i,j)$ = ALPHLJ * ([ISCLJ[i] + ISCLJ[j])/2
  $\alpha_C(i,j)$ = ALPHC * (ISCC[i] + ISCC[j])/2

- Only atom i is listed in the perturbation topology
  $\alpha_{LJ}(i,j)$ = ALPHLJ * ISCLJ[i]
  $\alpha_C(i,j)$ = ALPHC * ISCC[i]
- Only atom j is listed in the perturbation topology
  $\alpha_{LJ}(i,j)$ = ALPHLJ * ISCLJ[j]
  $\alpha_C(i,j)$ = ALPHC * ISCC[j]

The *summation* in Eq. 14.75 runs *over all pairs* of atoms with sequence numbers i and j and *which involve at least one perturbed atom*. Atoms are considered to be perturbed when they are occurring in the perturbation molecular topology file (see Sec. 4-3.3). As discussed in Sec. 2.3, a number of pairs is excluded from the summation in Eq. 14.75:

- excluded neighbour atom pairs (Sec. 2.3), for these pairs, however, the reaction-field and self-interaction terms corresponding to Eq. 7.11 and Eq. 7.12 are evaluated accordingly.
- atom pairs not included in the charge group pair list (cut-off R_{cp}) or in the long-range non-bonded interaction (cut-off R_{cl}).

The non-bonded interaction between *not-perturbed atoms* is evaluated using Eq. 6.1 and Eq. 7.10-Eq. 7.12. This implies that for such atom pairs no soft-core interaction can be invoked. In other words, for a conformational search simulation involving soft-core atoms, the soft-core atoms can only be selected using the perturbation topology file.

We note that for $n > 1$ in Eq. 14.75 or $\alpha_{LJ} \neq 0$ or $\alpha_C \neq 0$ in Eq. 14.76 the path connecting $\mathcal{V}^{(nbd)}(A)$ and $\mathcal{V}^{(nbd)}(B)$ is non-linear. This implies that even when the end states are chosen to be identical, $A = B$, the path connecting them is $\lambda-$dependent. For example, considering only a $\lambda-$dependence between state A ($\lambda = 0$) and state B ($\lambda = 1$) taken equal to A, we have $\mathcal{V}^{(nbd)}(\lambda = 0) = \mathcal{V}^{(nbd)}(\lambda = 1) \neq \mathcal{V}^{(nbd)}(0 < \lambda < 1)$.

The forces on atoms i and j due to the (i,j)-th term in formula Eq. 14.75 are

$$\begin{aligned} \mathbf{f}^{(nbd)}{}_i &= -\frac{\partial \mathcal{V}^{(nbd)}}{\partial \mathbf{r}_i} \\ &= -\lambda^n \frac{\partial \mathcal{V}^{(nbd)}(\mathbf{r}_{ij};B;(1-\lambda))}{\partial \mathbf{r}_i} - (1-\lambda)^n \frac{\partial \mathcal{V}^{(nbd)}(\mathbf{r}_{ij};A;\lambda)}{\partial \mathbf{r}_i} \end{aligned} \tag{14.80}$$

and

$$\mathbf{f}^{(nbd)}{}_j = -\mathbf{f}^{(nbd)}{}_i \tag{14.81}$$

with

$$\begin{aligned} &\frac{\partial \mathcal{V}^{(nbd)}(\mathbf{r}_{ij};X;\lambda)}{\partial \mathbf{r}_i} = \\ &\frac{-6(r_{ij})^4}{\left[\ \alpha_{LJ}(i,j)(\lambda^2) C^X_{126}(i,j) + (r_{ij})^6\right]^2} \cdot \left[\frac{2{C_{12}}^X(i,j)}{\left[\ \alpha_{LJ}(i,j)(\lambda^2) C^X_{126}(i,j) + (r_{ij})^6\right]} - {C_6}^X(i,j) \right] \cdot \mathbf{r}_{ij} \\ &-\frac{q_i^X q_j^X}{4\pi\varepsilon_0\varepsilon_1} \left[\frac{1}{\left[\ \alpha_c(i,j)(\lambda^2) + (r_{ij})^2\right]^{\frac{3}{2}}} + \frac{C_{rf}}{\left[\ \alpha_c(i,j)(\lambda^2) + {R_{rf}}^2\right]^{\frac{3}{2}}} \right] \cdot \mathbf{r}_{ij}. \end{aligned} \tag{14.82}$$

The derivative with respect to λ of the non-bonded interaction is

$$\begin{aligned} &\frac{\partial \mathcal{V}^{(nbd)}}{\partial \lambda} = \\ &\sum_{\substack{nonbonded \\ perturbed \\ pairs(i,j)}} \Big\{ n\lambda^{n-1} \mathcal{V}^{(nbd)}(\mathbf{r}_{ij};B;(1-\lambda)) + \lambda^n \frac{\partial \mathcal{V}^{(nbd)}(\mathbf{r}_{ij};B;(1-\lambda))}{\partial \lambda} \\ &-n(1-\lambda)^{n-1} \mathcal{V}^{(nbd)}(\mathbf{r}_{ij};A;\lambda) + (1-\lambda)^n \frac{\partial \mathcal{V}^{(nbd)}(\mathbf{r}_{ij};A;\lambda)}{\partial \lambda} \Big\} \end{aligned} \tag{14.83}$$

with

$$\frac{\partial \mathcal{V}^{(nbd)}(\mathbf{r}_{ij};X;\lambda)}{\partial\lambda} =$$

$$\frac{-2\lambda\alpha_{LJ}(i,j)C^X_{126}(i,j)}{\left[\ \alpha_{LJ}(i,j)(\lambda^2)C^X_{126}(i,j)+(r_{ij})^6\right]^2}\cdot\left[\ \frac{2C_{12}{}^X(i,j)}{\left[\ \alpha_{LJ}(i,j)(\lambda^2)C^X_{126}(i,j)+(r_{ij})^6\right]}-C_6{}^X(i,j)\right] \tag{14.84}$$

$$-\frac{q^X_i q^X_j}{4\pi\varepsilon_0\varepsilon_1}\cdot\lambda\alpha_c(i,j)\cdot\left[\ \frac{1}{\left[\ \alpha_c(i,j)(\lambda^2)+(r_{ij})^2\right]^{\frac{3}{2}}}-\frac{\frac{3}{2}C_{rf}(r_{ij})^2}{\left[\ \alpha_c(i,j)(\lambda^2)+R_{rf}{}^2\right]^{\frac{5}{2}}}\right]$$

and

$$\frac{\partial \mathcal{V}^{(nbd)}(\mathbf{r}_{ij};X;(1-\lambda))}{\partial\lambda} = -\frac{\partial \mathcal{V}^{(nbd)}(\mathbf{r}_{ij};X;\lambda)}{\partial\lambda} \tag{14.85}$$

The corresponding expression for use in the perturbation formula Eq. 14.9 is

$$\mathcal{V}^{(nbd)}(\mathbf{r}_{ij};\lambda\pm\Delta\lambda)-\mathcal{V}^{(nbd)}(\mathbf{r}_{ij};\lambda) \tag{14.86}$$

which can easily be obtained from Eq. 14.75 and Eq. 14.76.

14.2.9. Polarization. For free energy calculations using the coupling parameter approach (Sec. 14.1) the Hamiltonian of the system has to be made dependent on a coupling parameter λ. Free energy differences between two states A ($\lambda=0$) and B ($\lambda=1$) are then obtained from a thermodynamic integration over the averages of the derivative of the Hamiltonian with repect to λ. Several terms will change compared to the non-polarisable case[45].

The λ-dependent V^{coul} is

$$\begin{aligned}
\mathcal{V}^{coul}(\boldsymbol{r}^N,\boldsymbol{r}'^N;\lambda) &= \frac{1}{4\pi\epsilon_0\epsilon_{cs}}\sum_{i=1}^{N-1}\sum_{\substack{j>i\\ j\ inside\ cut-off\ i\\ (i,j)\ not\ excluded}}^{N}\Bigg[\\
&\quad (1-\lambda)^n\Bigg\{(q^A_i-q^{A,v}_i)(q^A_j-q^{A,v}_j)\left(\frac{1}{(|\mathbf{r}_i-\mathbf{r}_j|^2+\alpha_C\lambda^2)^{1/2}}\right)\\
&+ (q^A_i-q^{A,v}_i)q^A_j\left(\frac{1}{(|\mathbf{r}_i-\mathbf{r}'_j|^2+\alpha_C\lambda^2)^{1/2}}\right)\\
&+ q^{A,v}_i(q^A_j-q^{A,v}_j)\left(\frac{1}{(|\mathbf{r}'_i-\mathbf{r}_j|^2+\alpha_C\lambda^2)^{1/2}}\right)\\
&+ q^{A,v}_i q^{A,v}_j\left(\frac{1}{(|\mathbf{r}'_i-\mathbf{r}'_j|^2+\alpha_C\lambda^2)^{1/2}}\right)\Bigg\}\\
&+ \lambda^n\Bigg\{(q^B_i-q^{B,v}_i)(q^B_j-q^{B,v}_j)\left(\frac{1}{(|\mathbf{r}_i-\mathbf{r}_j|^2+\alpha_C(1-\lambda)^2)^{1/2}}\right)\\
&+ (q^B_i-q^{B,v}_i)q^B_j\left(\frac{1}{(|\mathbf{r}_i-\mathbf{r}'_j|^2+\alpha_C(1-\lambda)^2)^{1/2}}\right)\\
&+ q^{B,v}_i(q^B_j-q^{B,v}_j)\left(\frac{1}{(|\mathbf{r}'_i-\mathbf{r}_j|^2+\alpha_C(1-\lambda)^2)^{1/2}}\right)\\
&+ q^{B,v}_i q^{B,v}_j\left(\frac{1}{(|\mathbf{r}'_i-\mathbf{r}'_j|^2+\alpha_C(1-\lambda)^2)^{1/2}}\right)\Bigg\}\Bigg]
\end{aligned} \tag{14.87}$$

and the λ-dependent V^{rf} is

$$\begin{aligned}
V^{rf}(\boldsymbol{r}^N,\boldsymbol{r}'^N;\lambda) &= -\frac{1}{4\pi\epsilon_0\epsilon_{cs}}\sum_{i=1}^{N-1}\sum_{\substack{j>i\\ j\ inside\ cut-off\ i}}^{N}\Bigg[\\
&\quad (1-\lambda)^n\Bigg\{(q^A_i-q^{A,v}_i)(q^A_j-q^{A,v}_j)\left(C_{rf,aux}(\lambda)|\mathbf{r}_i-\mathbf{r}_j|^2+\frac{1-\frac{1}{2}C_{rf}}{R_{rf}}\right)
\end{aligned}$$

$$
\begin{aligned}
&+ \quad (q_i^A - q_i^{A,v})q_j^A \left(C_{rf,aux}(\lambda)|\mathbf{r}_i - \mathbf{r}'_j|^2 + \frac{1-\frac{1}{2}C_{rf}}{R_{rf}} \right) \\
&+ \quad q_i^{A,v}(q_j^A - q_j^{A,v}) \left(C_{rf,aux}(\lambda)|\mathbf{r}'_i - \mathbf{r}_j|^2 + \frac{1-\frac{1}{2}C_{rf}}{R_{rf}} \right) \\
&+ \quad q_i^{A,v}q_j^{A,v} \left(C_{rf,aux}(\lambda)|\mathbf{r}'_i - \mathbf{r}'_j|^2 + \frac{1-\frac{1}{2}C_{rf}}{R_{rf}} \right) \Bigg\} \\
&+ \quad \lambda^n \Bigg\{ (q_i^B - q_i^{B,v})(q_j^B - q_j^{B,v}) \left(C_{rf,aux}(1-\lambda)|\mathbf{r}_i - \mathbf{r}_j|^2 + \frac{1-\frac{1}{2}C_{rf}}{R_{rf}} \right) \\
&+ \quad (q_i^B - q_i^{B,v})q_j^B \left(C_{rf,aux}(1-\lambda)|\mathbf{r}_i - \mathbf{r}'_j|^2 + \frac{1-\frac{1}{2}C_{rf}}{R_{rf}} \right) \\
&+ \quad q_i^{B,v}(q_j^B - q_j^{B,v}) \left(C_{rf,aux}(1-\lambda)|\mathbf{r}'_i - \mathbf{r}_j|^2 + \frac{1-\frac{1}{2}C_{rf}}{R_{rf}} \right) \\
&+ \quad q_i^{B,v}q_j^{B,v} \left(C_{rf,aux}(1-\lambda)|\mathbf{r}'_i - \mathbf{r}'_j|^2 + \frac{1-\frac{1}{2}C_{rf}}{R_{rf}} \right) \Bigg\} \Bigg] \\
&- \quad \frac{1}{4\pi\epsilon_0\epsilon_{cs}} \sum_{i=1}^{N} [(1-\lambda)^n (q_i^A)^2 + \lambda^n (q_i^B)^2] \frac{1}{2} \frac{(1-\frac{1}{2}C_{rf})}{R_{rf}}
\end{aligned}
\tag{14.88}
$$

where

$$
C_{rfaux}(\lambda) = \frac{\frac{1}{2}C_{rf}}{({R_{rf}}^2 + \alpha_C \lambda^2)^{3/2}} \tag{14.89}
$$

is an auxilary function to simplify the formula, $q_i^{A(B)}$ is the charge on atom i in state $A(B)$, α_C is the soft core parameter, and C_{rf} defined by Eq. 7.126. The derivatives with respect to λ are then

$$
\begin{aligned}
\frac{\partial V^{coul}}{\partial \lambda} &= \frac{1}{4\pi\epsilon_0\epsilon_{cs}} \sum_{i=1}^{N-1} \sum_{\substack{j \ inside \ cut-off \ i \\ (i,j) \ not \ excluded}}^{N} \Bigg[-(1-\lambda)^n \lambda \alpha_C \\
&\quad \Bigg\{ (q_i^A - q_i^{A,v})(q_j^A - q_j^{A,v}) \left(\frac{1}{(|\mathbf{r}_i - \mathbf{r}_j|^2 + \alpha_C\lambda^2)^{3/2}} \right) \\
&+ \quad (q_i^A - q_i^{A,v})q_j^A \left(\frac{1}{(|\mathbf{r}_i - \mathbf{r}'_j|^2 + \alpha_C\lambda^2)^{3/2}} \right) \\
&+ \quad q_i^{A,v}(q_j^A - q_j^{A,v}) \left(\frac{1}{(|\mathbf{r}'_i - \mathbf{r}_j|^2 + \alpha_C\lambda^2)^{3/2}} \right) + q_i^{A,v}q_j^{A,v} \left(\frac{1}{(|\mathbf{r}'_i - \mathbf{r}'_j|^2 + \alpha_C\lambda^2)^{3/2}} \right) \Bigg\} \\
&+ \quad \lambda^n(1-\lambda)\alpha_C \\
&\quad \Bigg\{ (q_i^B - q_i^{B,v})(q_j^B - q_j^{B,v}) \left(\frac{1}{(|\mathbf{r}_i - \mathbf{r}_j|^2 + \alpha_C(1-\lambda)^2)^{3/2}} \right) \\
&+ \quad (q_i^B - q_i^{B,v})q_j^B \left(\frac{1}{(|\mathbf{r}_i - \mathbf{r}'_j|^2 + \alpha_C(1-\lambda)^2)^{3/2}} \right) \\
&+ \quad q_i^{B,v}(q_j^B - q_j^{B,v}) \left(\frac{1}{(|\mathbf{r}'_i - \mathbf{r}_j|^2 + \alpha_C(1-\lambda)^2)^{3/2}} \right) + q_i^{B,v}q_j^{B,v} \left(\frac{1}{(|\mathbf{r}'_i - \mathbf{r}'_j|^2 + \alpha_C(1-\lambda)^2)^{3/2}} \right) \Bigg\} \\
&- \quad n(1-\lambda)^{n-1} \\
&\quad \Bigg\{ (q_i^A - q_i^{A,v})(q_j^A - q_j^{A,v}) \left(\frac{1}{(|\mathbf{r}_i - \mathbf{r}_j|^2 + \alpha_C\lambda^2)^{1/2}} \right) + (q_i^A - q_i^{A,v})q_j^A \left(\frac{1}{(|\mathbf{r}_i - \mathbf{r}'_j|^2 + \alpha_C\lambda^2)^{1/2}} \right) \\
&+ \quad q_i^{A,v}(q_j^A - q_j^{A,v}) \left(\frac{1}{(|\mathbf{r}'_i - \mathbf{r}_j|^2 + \alpha_C\lambda^2)^{1/2}} \right) + q_i^{A,v}q_j^{A,v} \left(\frac{1}{(|\mathbf{r}'_i - \mathbf{r}'_j|^2 + \alpha_C\lambda^2)^{1/2}} \right) \Bigg\} \\
&+ \quad n\lambda^{n-1} \\
&\quad \Bigg\{ (q_i^B - q_i^{B,v})(q_j^B - q_j^{B,v}) \left(\frac{1}{(|\mathbf{r}_i - \mathbf{r}_j|^2 + \alpha_C(1-\lambda)^2)^{1/2}} \right) \\
&+ \quad (q_i^B - q_i^{B,v})q_j^B \left(\frac{1}{(|\mathbf{r}_i - \mathbf{r}'_j|^2 + \alpha_C(1-\lambda)^2)^{1/2}} \right) \\
&+ \quad q_i^{B,v}(q_j^B - q_j^{B,v}) \left(\frac{1}{(|\mathbf{r}'_i - \mathbf{r}_j|^2 + \alpha_C(1-\lambda)^2)^{1/2}} \right) \\
&+ \quad q_i^{B,v}q_j^{B,v} \left(\frac{1}{(|\mathbf{r}'_i - \mathbf{r}'_j|^2 + \alpha_C(1-\lambda)^2)^{1/2}} \right) \Bigg\} \Bigg]
\end{aligned}
\tag{14.90}
$$

and

$$
\begin{aligned}
\frac{\partial V^{rf}}{\partial \lambda} &= \frac{1}{4\pi\epsilon_0\epsilon_{cs}} \sum_{i=1}^{N-1} \sum_{\substack{j>i \\ j\ inside\ cut-off\ i}}^{N} \Bigg[-(1-\lambda)^n \lambda \alpha_C \\
&\quad \Bigg\{ (q_i^A - q_i^{A,v})(q_j^A - q_j^{A,v}) \left(-\frac{\frac{3}{2} C_{rf} |\mathbf{r}_i - \mathbf{r}_j|^2}{(R_{rf}^2 + \alpha_C \lambda^2)^{5/2}} \right) + (q_i^A - q_i^{A,v}) q_j^A \left(-\frac{\frac{3}{2} C_{rf} |\mathbf{r}_i - \mathbf{r}'_j|^2}{(R_{rf}^2 + \alpha_C \lambda^2)^{5/2}} \right) \\
&+ q_i^{A,v}(q_j^A - q_j^{A,v}) \left(-\frac{\frac{3}{2} C_{rf} |\mathbf{r}'_i - \mathbf{r}_j|^2}{(R_{rf}^2 + \alpha_C \lambda^2)^{5/2}} \right) + q_i^{A,v} q_j^{A,v} \left(-\frac{\frac{3}{2} C_{rf} |\mathbf{r}'_i - \mathbf{r}'_j|^2}{(R_{rf}^2 + \alpha_C \lambda^2)^{5/2}} \right) \Bigg\} \\
&+ \lambda^n (1-\lambda) \alpha_C \\
&\quad \Bigg\{ (q_i^B - q_i^{B,v})(q_j^B - q_j^{B,v}) \left(-\frac{\frac{3}{2} C_{rf} |\mathbf{r}_i - \mathbf{r}_j|^2}{(R_{rf}^2 + \alpha_C (1-\lambda)^2)^{5/2}} \right) + (q_i^B - q_i^{B,v}) q_j^B \left(-\frac{\frac{3}{2} C_{rf} |\mathbf{r}_i - \mathbf{r}'_j|^2}{(R_{rf}^2 + \alpha_C (1-\lambda)^2)^{5/2}} \right) \\
&+ q_i^{B,v}(q_j^B - q_j^{B,v}) \left(-\frac{\frac{3}{2} C_{rf} |\mathbf{r}'_i - \mathbf{r}_j|^2}{(R_{rf}^2 + \alpha_C (1-\lambda)^2)^{5/2}} \right) + q_i^{B,v} q_j^{B,v} \left(-\frac{\frac{3}{2} C_{rf} |\mathbf{r}'_i - \mathbf{r}'_j|^2}{(R_{rf}^2 + \alpha_C (1-\lambda)^2)^{5/2}} \right) \Bigg\} \\
&- n(1-\lambda)^{n-1} \\
&\quad \Bigg\{ (q_i^A - q_i^{A,v})(q_j^A - q_j^{A,v}) \left(-C_{rf,aux}(\lambda) |\mathbf{r}_i - \mathbf{r}_j|^2 - \frac{1 - \frac{1}{2} C_{rf}}{R_{rf}} \right) \\
&+ (q_i^A - q_i^{A,v}) q_j^A \left(-C_{rf,aux}(\lambda) |\mathbf{r}_i - \mathbf{r}'_j|^2 - \frac{1 - \frac{1}{2} C_{rf}}{R_{rf}} \right) \\
&+ q_i^{A,v}(q_j^A - q_j^{A,v}) \left(-C_{rf,aux}(\lambda) |\mathbf{r}'_i - \mathbf{r}_j|^2 - \frac{1 - \frac{1}{2} C_{rf}}{R_{rf}} \right) \\
&+ q_i^{A,v} q_j^{A,v} \left(-C_{rf,aux}(\lambda) |\mathbf{r}'_i - \mathbf{r}'_j|^2 - \frac{1 - \frac{1}{2} C_{rf}}{R_{rf}} \right) \Bigg\} \\
&+ n\lambda^{n-1} \\
&\quad \Bigg\{ (q_i^B - q_i^{B,v})(q_j^B - q_j^{B,v}) \left(-C_{rf,aux}(1-\lambda) |\mathbf{r}_i - \mathbf{r}_j|^2 - \frac{1 - \frac{1}{2} C_{rf}}{R_{rf}} \right) \\
&+ (q_i^B - q_i^{B,v}) q_j^B \left(-C_{rf,aux}(1-\lambda) |\mathbf{r}_i - \mathbf{r}'_j|^2 - \frac{1 - \frac{1}{2} C_{rf}}{R_{rf}} \right) \\
&+ q_i^{B,v}(q_j^B - q_j^{B,v}) \left(-C_{rf,aux}(1-\lambda) |\mathbf{r}'_i - \mathbf{r}_j|^2 - \frac{1 - \frac{1}{2} C_{rf}}{R_{rf}} \right) \\
&+ q_i^{B,v} q_j^{B,v} \left(-C_{rf,aux}(1-\lambda) |\mathbf{r}'_i - \mathbf{r}'_j|^2 - \frac{1 - \frac{1}{2} C_{rf}}{R_{rf}} \right) \Bigg\} \Bigg] \\
&- \frac{1}{4\pi\epsilon_0\epsilon_{cs}} \sum_{i=1}^{N} ([-n(1-\lambda)^{n-1} (q_i^A)^2 + n\lambda^{n-1} (q_i^B)^2] \frac{1}{2} \frac{(1 - \frac{1}{2} C_{rf})}{R_{rf}}
\end{aligned}
\tag{14.91}
$$

Using for the λ-dependence of the polarisability $\alpha_i(\lambda)$

$$\alpha_i(\lambda) = (1-\lambda)^m \alpha_i^A + \lambda^m \alpha_i^B,$$

the λ-dependence of the electric field $\mathbf{E}_i(\lambda)$ is

$$
\begin{aligned}
\mathbf{E}_i^{coul}(\lambda) &= \frac{1}{4\pi\epsilon_0\epsilon_{cs}} \sum_{\substack{j>i \\ j\ inside\ cut-off\ i \\ (i,j)\ not\ excluded}}^{N} \Bigg\{ (1-\lambda)^n \\
&\quad \left[\frac{(q_j^A - q_j^{A,v})(\mathbf{r}_i - \mathbf{r}_j)}{(|\mathbf{r}_i - \mathbf{r}_j|^2 + \alpha_C \lambda^2)^{3/2}} + \frac{q_j^{A,v}(\mathbf{r}_i - \mathbf{r}'_j)}{(|\mathbf{r}_i - \mathbf{r}'_j|^2 + \alpha_C \lambda^2)^{3/2}} \right] \\
&\quad + \lambda^n \left[\frac{(q_j^B - q_j^{B,v})(\mathbf{r}_i - \mathbf{r}_j)}{(|\mathbf{r}_i - \mathbf{r}_j|^2 + \alpha_C (1-\lambda)^2)^{3/2}} + \frac{q_j^{B,v}(\mathbf{r}_i - \mathbf{r}'_j)}{(|\mathbf{r}_i - \mathbf{r}'_j|^2 + \alpha_C (1-\lambda)^2)^{3/2}} \right] \Bigg\}
\end{aligned}
\tag{14.92}
$$

and

$$
\mathbf{E}_i^{rf}(\lambda) = \frac{C_{rf}}{4\pi\epsilon_0\epsilon_{cs}} \sum_{\substack{j>i \\ j\ inside\ cut-off\ i}}^{N} \Bigg\{ (1-\lambda)^n
$$

$$\left[\frac{(q_j^A - q_j^{A,v})(\mathbf{r}_i - \mathbf{r}_j)}{(R_{rf}^2 + \alpha_C\lambda^2)^{3/2}} + \frac{q_j^{A,v}(\mathbf{r}_i - \mathbf{r}'_j)}{(R_{rf}^2 + \alpha_C\lambda^2)^{3/2}}\right]$$
$$+\lambda^n\left[\frac{(q_j^B - q_j^{B,v})(\mathbf{r}_i - \mathbf{r}_j)}{(R_{rf}^2 + \alpha_C(1-\lambda)^2)^{3/2}} + \frac{q_j^{B,v}(\mathbf{r}_i - \mathbf{r}'_j)}{(R_{rf}^2 + \alpha_C(1-\lambda)^2)^{3/2}}\right]\Bigg\} \tag{14.93}$$

and one gets for the λ-dependent $V^{self,i}$

$$\begin{aligned} V^{self,i} & & (14.94)\\ &= \frac{1}{2}\alpha_i(\lambda)(E_i(\lambda))^2 && for\ E_i(\lambda) \le E_{0,i}\\ &= \frac{1}{2}\alpha_i(\lambda)(E_{0,i})^2 &&\\ &+ \frac{\alpha_i(\lambda)(E_{0,i})^2}{p_i(p_i-1)}\left[-p_i^2 + (p_i^2-1)\left(\frac{E_i(\lambda)}{E_{0,i}}\right) + \left(\frac{E_{0,i}}{E_i(\lambda)}\right)^{p_i-1}\right] && for\ E_i(\lambda) > E_{0,i}. \end{aligned}$$

The λ-derivative of this perturbed self polarisation potential energy is

$$\begin{aligned} \frac{\partial V^{self,i}}{\partial\lambda} & & (14.95)\\ &= \frac{1}{2}m(\lambda^{m-1}\alpha_i^B - (1-\lambda)^{m-1}\alpha_i^A)(\mathbf{E}_i(\lambda))^2 + \alpha_i(\lambda)\mathbf{E}_i(\lambda)\cdot\frac{\partial\mathbf{E}_i(\lambda)}{\partial\lambda} && for\ E_i(\lambda) \le E_{0,i}\\ &= m(\lambda^{m-1}\alpha_i^B - (1-\lambda)^{m-1}\alpha_i^A)(E_{0,i})^2 &&\\ &\left(\frac{1}{2} + \frac{1}{p_i(p_i-1)}\left[-p_i^2 + (p_i^2-1)\left(\frac{E_i(\lambda)}{E_{0,i}}\right) + \left(\frac{E_{0,i}}{E_i(\lambda)}\right)^{p_i-1}\right]\right) &&\\ &+\frac{\alpha_i(\lambda)E_{0,i}}{p_i}\left[(p_i+1) - \left(\frac{E_{0,i}}{E_i(\lambda)}\right)^{p_i}\right]\frac{\partial E_i(\lambda)}{\partial\lambda} && for\ E_i(\lambda) > E_{0,i}. \end{aligned}$$

with

$$\frac{\partial E_i(\lambda)}{\partial\lambda} = \frac{\mathbf{E}_i(\lambda)\cdot\frac{\partial\mathbf{E}_i(\lambda)}{\partial\lambda}}{(\mathbf{E}_i(\lambda)\cdot\mathbf{E}_i(\lambda))^{1/2}} \tag{14.96}$$

14.2.10. Perturbed atom-atom distance restraints. The $\lambda-$dependent version of the atom-atom distance restraining term (Sec. 9.3) is obtained by making the restraining force constant ${k^{(dr)}}_k$ and the (repulsive or attractive) distance restraint k with length ${\mathbf{r}^0}_k$ between atoms i and i' dependent on λ,

$$\mathcal{V}^{(dr)}(\mathbf{r};\lambda) = \sum_{k=1}^{N^{(dir)}} 2^{n+m}\lambda^n(1-\lambda)^m{\mathcal{V}^{(dr)}}_k^{AB}(\mathbf{r}_{ii'}; {k^{(dr)}}_k^A, {k^{(dr)}}_k^B; {\mathbf{r}^0}_k^A, {\mathbf{r}^0}_k^B, \Delta r^h) \tag{14.97}$$

The pre-factor $2^{n+m}\ \lambda^n\ (1-\lambda)^m$ with user-specified exponents n and m is added to make the use of perturbed distance restraints possible without restraining the system in the end states,[100] using the so-called hidden restraints.

For a perturbed *attractive* distance restraint, ${\mathcal{V}^{(dr)}}_k^{AB}$ reads

$${\mathcal{V}^{(dr)}}_k^{AB}(\mathbf{r}_{ii'}, {k^{(dr)}}_n^A, {k^{(dr)}}_k^B, {\mathbf{r}^0}_k^A, {\mathbf{r}^0}_k^B, \Delta r^h) = 0$$

$$for\ 0 < r_{ii'} < (1-\lambda){\mathbf{r}^0}_k^A + \lambda\ {\mathbf{r}^0}_k^B$$

$$= \tfrac{1}{2}((1-\lambda){k^{(dr)}}_k^A + \lambda{k^{(dr)}}_k^B)[r_{ii'} - (1-\lambda){\mathbf{r}^0}_k^A - \lambda{\mathbf{r}^0}_k^B]^2$$

$$for\ (1-\lambda){\mathbf{r}^0}_k^A + \lambda{\mathbf{r}^0}_k^B < r_{ii'} < (1-\lambda){\mathbf{r}^0}_k^A + \lambda{\mathbf{r}^0}_k^B + \Delta r^h$$

$$= ((1-\lambda){k^{(dr)}}_k^A + \lambda{k^{(dr)}}_k^B)[r_{ii'} - (1-\lambda){\mathbf{r}^0}_k^A - \lambda{\mathbf{r}^0}_k^B - \tfrac{1}{2}\Delta r^h]\Delta r^h$$

$$for\ (1-\lambda){\mathbf{r}^0}_k^A - \lambda{\mathbf{r}^0}_k^B + \Delta r^h < r_{ii'} \tag{14.98}$$

and the forces on atom i and i' due to ${\mathcal{V}^{(dr)}}_k^{AB}$ in Eq. 14.98 are

$$\mathbf{f}^{(dir)}{}_i = -2^{n+m}\lambda^n(1-\lambda)^m \frac{\partial {\mathcal{V}^{(dr)}}_k^{AB}}{\partial r_{ii'}} \frac{\partial r_{ii'}}{\partial \mathbf{r}_i} \tag{14.99}$$

with

$$\begin{aligned}
&\frac{\partial {\mathcal{V}^{(dr)}}_k^{AB}}{\partial r_{ii'}} \frac{\partial r_{ii'}}{\partial \mathbf{r}_i} = 0 \\
&\qquad\qquad for\ 0 < r_{ii'} < (1-\lambda){\mathbf{r}^0}_k^A - \lambda {\mathbf{r}^0}_k^B \\
&= ((1-\lambda){k^{(dr)}}_k^A + \lambda {k^{(dr)}}_k^B)[r_{ii'} - (1-\lambda){\mathbf{r}^0}_k^A - \lambda {\mathbf{r}^0}_k^B] \cdot \frac{\mathbf{r}_i}{r_{ii'}} \\
&\qquad\qquad for\ (1-\lambda){\mathbf{r}^0}_k^A - \lambda {\mathbf{r}^0}_k^B < r_{ii'} < (1-\lambda){\mathbf{r}^0}_k^A - \lambda {\mathbf{r}^0}_k^B + \Delta r^h \\
&= ((1-\lambda){k^{(dr)}}_k^A + \lambda {k^{(dr)}}_k^B) \cdot \Delta \mathbf{r}^h \cdot \frac{\mathbf{r}_i}{r_{ii'}} \\
&\qquad\qquad for\ (1-\lambda){\mathbf{r}^0}_k^A - \lambda {\mathbf{r}^0}_k^B + \Delta r^h < r_{ii'}
\end{aligned} \tag{14.100}$$

and

$$\mathbf{f}^{(dir)}{}_{i'} = -\mathbf{f}^{(dir)}{}_i \tag{14.101}$$

For a perturbed *repulsive* distance restraint, ${\mathcal{V}^{(dr)}}_k^{AB}$ reads

$$\begin{aligned}
&{\mathcal{V}^{(dr)}}_k^{AB}(r_{ii'}, {k^{(dr)}}_k^A, {k^{(dr)}}_k^B, {\mathbf{r}^0}_k^A, {\mathbf{r}^0}_k^B, \Delta r^h) \\
&= ((1-\lambda){k^{(dr)}}_k^A + \lambda {k^{(dr)}}_k^B)[r_{ii'} - (1-\lambda){\mathbf{r}^0}_k^A - \lambda {\mathbf{r}^0}_k^B - \tfrac{1}{2}\Delta r^h]\Delta r^h \\
&\qquad\qquad for\ 0 < r_{ii'} < (1-\lambda){\mathbf{r}^0}_k^A - \lambda {\mathbf{r}^0}_k^B - \Delta r^h \\
&= \tfrac{1}{2}((1-\lambda){k^{(dr)}}_k^A + \lambda {k^{(dr)}}_k^B)[r_{ii'} - (1-\lambda){\mathbf{r}^0}_k^A - \lambda {\mathbf{r}^0}_k^B]^2 \\
&\qquad\qquad for\ (1-\lambda){\mathbf{r}^0}_k^A - \lambda {\mathbf{r}^0}_k^B - \Delta r^h < r_{ii'} < (1-\lambda){\mathbf{r}^0}_k^A - \lambda {\mathbf{r}^0}_k^B \\
&= 0 \\
&\qquad\qquad for\ (1-\lambda){\mathbf{r}^0}_k^A - \lambda {\mathbf{r}^0}_k^B < r_{ii'}
\end{aligned} \tag{14.102}$$

and the forces on atom i and i' due to ${\mathcal{V}^{(dr)}}_k^{AB}$ in Eq. 14.102 are calculated from Eq. 14.99 with

$$\begin{aligned}
&\frac{\partial {\mathcal{V}^{(dr)}}_k^{AB}}{\partial r_{ii'}} \frac{\partial r_{ii'}}{\partial \mathbf{r}_i} = ((1-\lambda){k^{(dr)}}_k^A + \lambda {k^{(dr)}}_k^B) \cdot \Delta r^h \cdot \frac{\mathbf{r}_i}{r_{ii'}} \\
&\qquad\qquad for\ 0 < r_{ii'} < (1-\lambda){\mathbf{r}^0}_k^A - \lambda {\mathbf{r}^{0\,0,B}}_k - \Delta r^h
\end{aligned}$$

$$= ((1-\lambda)k^{(dr)}{}_k^A + \lambda k^{(dr)}{}_k^B) \cdot [r_{ii'} - (1-\lambda)\mathbf{r}^0{}_k^A - \lambda \mathbf{r}^0{}_k^B] \cdot \frac{\mathbf{r}_i}{r_{ii'}}$$

$$for\ (1-\lambda)\mathbf{r}^0{}_k^A - \lambda \mathbf{r}^0{}_k^B - \Delta r^h < r_{ii'} < (1-\lambda)\mathbf{r}^0{}_k^A - \lambda \mathbf{r}^0{}_k^B$$

$$= 0$$

$$for\ (1-\lambda)\mathbf{r}^0{}_k^A - \lambda \mathbf{r}^0{}_k^B < r_{ii'} \tag{14.103}$$

and

$$\mathbf{f}^{(dir)}{}_{i'} = -\mathbf{f}^{(dir)}{}_i \tag{14.104}$$

The $\lambda-$derivative of $\mathcal{V}^{(dr)}(\mathbf{r};\lambda)$ reads

$$\frac{\partial \mathcal{V}^{(dr)}(\mathbf{r};\lambda)}{\partial \lambda} = \sum_{k=1}^{N^{(dir)}} 2^{n+m}[(n\lambda^{n-1}(1-\lambda)^m - m\lambda^n(1-\lambda)^{m-1})$$

$$\cdot\ \mathcal{V}^{(dr)}{}_k^{AB}(r_{ii'}, k^{(dr)}{}_k^A, k^{(dr)}{}_k^B, \mathbf{r}^0{}_k^A, \mathbf{r}^0{}_k^B, \Delta r^h)$$

$$+\lambda^n(1-\lambda)^m \frac{\partial \mathcal{V}^{(dr)}{}_k^{AB}(r_{ii'}, k^{(dr)}{}_k^A, k^{(dr)}{}_k^B, \mathbf{r}^0{}_k^A, \mathbf{r}^0{}_k^B, \Delta r^h)}{\partial \lambda}] \tag{14.105}$$

In case of an *attractive* distance restraint,

$$\frac{\partial \mathcal{V}^{(dr)}{}_k^{AB}(r_{ii'}, k^{(dr)}{}_k^A, k^{(dr)}{}_k^B, \mathbf{r}^0{}_k^A, \mathbf{r}^0{}_k^B, \Delta r^h)}{\partial \lambda} = 0$$

$$for\ 0 < r_{ii'} < (1-\lambda)\mathbf{r}^0{}_k^A + \mathbf{r}^0{}_k^B$$

$$= \tfrac{1}{2}(k^{(dr)}{}_k^B - k^{(dr)}{}_k^A)[r_{ii'} - (1-\lambda)\mathbf{r}^0{}_k^A - \lambda \mathbf{r}^0{}_k^B]^2$$

$$+((1-\lambda)k^{(dr)}{}_k^A + \lambda k^{(dr)}{}_k^B)[r_{ii'} - (1-\lambda)\mathbf{r}^0{}_k^A - \lambda \mathbf{r}^0{}_k^B] \cdot (\mathbf{r}^0{}_k^A - \mathbf{r}^0{}_k^B)$$

$$for\ (1-\lambda)\mathbf{r}^0{}_k^A + \lambda \mathbf{r}^0{}_k^B < r_{ii'} < (1-\lambda)\mathbf{r}^0{}_k^A + \lambda \mathbf{r}^0{}_k^B + \Delta r^h$$

$$= (k^{(dr)}{}_k^B - k^{(dr)}{}_k^A)(r_{ii'} - (1-\lambda)\mathbf{r}^0{}_k^A - \lambda \mathbf{r}^0{}_k^B - \tfrac{1}{2}\Delta r^h)\Delta r^h$$

$$+((1-\lambda)k^{(dr)}{}_k^A + \lambda k^{(dr)}{}_k^B)\Delta r^h(\mathbf{r}^0{}_k^A - \mathbf{r}^0{}_k^B)$$

$$for\ (1-\lambda)\mathbf{r}^0{}_k^A + \lambda \mathbf{r}^0{}_k^B + \Delta r^h < r_{ii'} \tag{14.106}$$

In case of a *repulsive* distance restraint,

$$\frac{\partial \mathcal{V}^{(dr)}{}_k^{AB}(r_{ii'}, k^{(dr)}{}_k^A, k^{(dr)}{}_k^B, \mathbf{r}^0{}_k^A, \mathbf{r}^0{}_k^B, \Delta r^h)}{\partial \lambda}$$

$$= -[(k^{(dr)}{}_k^B - k^{(dr)}{}_k^A)(r_{ii'} - (1-\lambda)\mathbf{r}^0{}_k^A - \lambda \mathbf{r}^0{}_k^B - \tfrac{1}{2}\Delta r^h)\Delta r^h$$

$$+((1-\lambda)k^{(dr)\,A}_k + \lambda k^{(dr)\,B}_k)\Delta r^h(\mathbf{r}^{0\,A}_k - \mathbf{r}^{0\,B}_k)]$$

$$for\ 0 < r_{ii'} < (1-\lambda)\mathbf{r}^{0\,A}_k - \lambda\mathbf{r}^{0\,B}_k - \Delta r^h$$

$$= \tfrac{1}{2}(k^{(dr)\,B}_k - k^{(dr)\,A}_k)[r_{ii'} - (1-\lambda)\mathbf{r}^{0\,A}_k - \lambda\mathbf{r}^{0\,B}_k]^2$$

$$+((1-\lambda)k^{(dr)\,A}_k + \lambda k^{(dr)\,B}_k)[r_{ii'} - (1-\lambda)\mathbf{r}^{0\,A}_k - \lambda\mathbf{r}^{0\,B}_k]\cdot(\mathbf{r}^{0\,A}_k - \mathbf{r}^{0\,B}_k)$$

$$for\ 0 < r_{ii'} < (1-\lambda)\mathbf{r}^{0\,A}_k - \lambda\mathbf{r}^{0\,B}_k - \Delta r^h$$

$$= 0$$

$$for\ (1-\lambda)\mathbf{r}^{0\,A}_k + \lambda\mathbf{r}^{0\,B}_k < r_{ii'} \tag{14.107}$$

14.2.11. Perturbed dihedral angle restraints. Similar to distance restraining, a λ dependence can be introduced to the dihedral-angle restraints to enforce conformational sampling along a pathway from state A to state B

$$\mathcal{V}^{(tr)}(\boldsymbol{r},\lambda) = \sum_{k=1}^{\mathcal{N}^{(tr)}} 2^{n+m}\lambda^n\,(1-\lambda)^m\,\mathcal{V}^{(tr)\,AB}(\phi_k; k^{(tr)\,A}, k^{(tr)\,B}; \phi^{0A}_k, \phi^{0B}_k, \delta\phi^h_k,), \tag{14.108}$$

The pre-factor $2^{n+m}\lambda^n(1-\lambda)^m$ with user-specified exponents n and m is added to make use of perturbed dihedral restraints possible without restraining the system in the end states, using so-called hidden restraints.[100]

For a perturbed dihedral angle restraint, $\mathcal{V}^{(tr)\,AB}$ reads

$$\begin{array}{ll}
\mathcal{V}^{(tr)\,AB}(\phi; k^{(tr)\,A}, k^{(tr)\,B}; \phi^{0A}_k, \phi^{0B}_k, \delta\phi^h_k) = & \\
-[(1-\lambda)k^{(tr)\,A} + \lambda k^{(tr)\,B}](\Delta\phi_k + 1/2\Delta\phi^h)\Delta\phi^h & \Delta\phi_k < -\Delta\phi^h \\
1/2[(1-\lambda)k^{(tr)\,A} + \lambda k^{(tr)\,B}](\Delta\phi_k)^2 & -\Delta\phi^h \le \Delta\phi_k \le \Delta\phi^h \\
[(1-\lambda)k^{(tr)\,A} + \lambda k^{(tr)\,B}](\Delta\phi_k - 1/2\Delta\phi^h)\Delta\phi^h & \Delta\phi_k > \Delta\phi^h
\end{array} \tag{14.109}$$

where

$$\Delta\phi_k = \phi_k - (1-\lambda)\phi^{0A}_k - \lambda\phi^{0B}_k + 2m\pi. \tag{14.110}$$

and m is chosen such that ϕ_k is within the range $[(1-\lambda)\phi^{0A}_k - \lambda\phi^{0B}_k + \delta_k - 2\pi, (1-\lambda)\phi^{0A}_k - \lambda\phi^{0B}_k + \delta_k]$. Using this dihedral angle restraint formulation δ_k determines at which position the direction of the rotation around the dihedral angle inverts. Typically, δ_k is set to 180^o. The force on atom i is

$$\mathbf{f}_i \;=\; -2^{n+m}\lambda^n\,(1-\lambda)^m\,\frac{\partial\mathcal{V}^{(tr)\,AB}}{\partial\Delta\phi_k}\frac{\partial\phi_k}{\partial\mathbf{r}_i}$$

where

$$\begin{array}{ll}
\dfrac{\partial\mathcal{V}^{(tr)\,AB}}{\partial\Delta\phi_k} = & \\
-[(1-\lambda)k^{(tr)\,A} + \lambda k^{(tr)\,B}]\Delta\phi^h\dfrac{\partial\phi_k}{\partial\mathbf{r}_i} & \Delta\phi_k < -\Delta\phi^h \\
[(1-\lambda)k^{(tr)\,A} + \lambda k^{(tr)\,B}]\Delta\phi_k\dfrac{\partial\phi_k}{\partial\mathbf{r}_i} & -\Delta\phi^h \le \Delta\phi_k \le \Delta\phi^h \\
[(1-\lambda)k^{(tr)\,A} + \lambda k^{(tr)\,B}]\Delta\phi^h\dfrac{\partial\phi_k}{\partial\mathbf{r}_i} & \Delta\phi_k > \Delta\phi^h
\end{array} \tag{14.111}$$

and $\frac{\partial\phi_k}{\partial\mathbf{r}_i}$ is equivalent to the expression used for the physical dihedral angle potential term.

The λ-derivative of $\mathcal{V}^{(tr)}(\boldsymbol{r},\lambda)$ reads

$$\begin{aligned}\frac{\partial \mathcal{V}^{(tr)}(\boldsymbol{r},\lambda)}{\partial \lambda} &= \sum_{k=1}^{\mathcal{N}^{(tr)}} 2^{n+m}[n\lambda^{n-1}(1-\lambda)^m - m\lambda^n(1-\lambda)^m)\mathcal{V}^{(tr)\,AB} \\ &\quad +\lambda^n(1-\lambda)^m \frac{\partial \mathcal{V}^{(tr)\,AB}}{\partial \lambda}\end{aligned} \tag{14.112}$$

where

$$\begin{aligned}\frac{\partial \mathcal{V}^{(tr)\,AB}}{\partial \lambda} &= \\ &\Delta\phi^h\Big((k^{(tr)}{}^B_k - k^{(tr)}{}^A_k)\left(\Delta\phi_{k\lambda} - 1/2\phi^0_{lin}\right) \\ &+ \Big((1-\lambda)k^{(tr)}{}^A_k + \lambda k^{(tr)}{}^B_k\Big)\Big(\phi^{0,A}_k - \phi^{0,B}_k\Big)\Big), \qquad \Delta\phi_k < -\Delta\phi^h \\ &1/2\Big(-(k^{(tr)}{}^B_k - k^{(tr)}{}^A_k)(\Delta\phi_{k\lambda})^2 \\ &+ 2\Big((1-\lambda)k^{(tr)}{}^A_k + \lambda k^{(tr)}{}^B_k\Big)\Delta\phi_k\Big(\phi^{0,A}_k - \phi^{0,B}_k\Big)\Big), \quad -\Delta\phi^h \le \Delta\phi_k \le \Delta\phi^h \\ &\Delta\phi^h\Big((k^{(tr)}{}^B_k - k^{(tr)}{}^A_k)\left(\Delta\phi_k - 1/2\Delta\phi^h\right) \\ &+ \Big((1-\lambda)k^{(tr)}{}^A_k + \lambda k^{(tr)}{}^B_k\Big)\Big(\phi^{0,A}_k - \phi^{0,B}_k\Big)\Big). \qquad \Delta\phi_k > \Delta\phi^h\end{aligned}$$

14.2.12. Perturbed distance-field distance restraints. The DF restraint can also be made dependent on a coupling parameter λ, making it more broadly applicable. In this case, the force constant and reference value of a DF restraint at a certain λ-value can be obtained with

$$l^0_{AB}(\lambda) = (1-\lambda)l^0_A + \lambda l^0_B \tag{14.113}$$

$$k^{(df)}_{AB}(\lambda) = (1-\lambda)k^{(df)}_A + \lambda k^{(df)}_B \tag{14.114}$$

Here, l^0_A and l^0_B are the reference values in two states A and B, respectively. Similarly, $k^{(df)}_A$ and $k^{(df)}_B$ represent the force constants for the DF restraint in states A and B, respectively. The potential energy can be calculated with

$$\mathcal{V}^{(df)}(\lambda) = 2^{n+m}\lambda^n(1-\lambda)^m\mathcal{V}^{(df)}(l_{ij}, k^{(df)}_{AB}(\lambda), l^0_{AB}(\lambda), \Delta l^h) \tag{14.115}$$

with $\mathcal{V}^{(df)}(l_{ij}, k^{(df)}_{AB}(\lambda), l^0_{AB}(\lambda), \Delta l^h)$ calculated according to Eq. 9.139. Here, we have introduced the prefactor term with variables m and n to be able to create so called hidden restraints.[100] Depending on the choice of these variables, the restraint is not present in one or both of the end states. The energy derivative can now be calculated using Eq. 14.116 and Eq. 14.117:

$$\begin{aligned}\frac{\partial \mathcal{V}^{(df)}(\lambda)}{\partial \lambda} &= 2^{n+m}[n\lambda^{n-1}(1-\lambda)^m - m\lambda^n(1-\lambda)^{m-1}]\mathcal{V}^{(df)}(l_{ij}, k^{(df)}_{AB}(\lambda), l^0_{AB}(\lambda), \Delta l^h) \\ &+ 2^{n+m}\lambda^n(1-\lambda)^m \frac{\partial \mathcal{V}^{(df)}(l_{ij}, k^{(df)}_{AB}(\lambda), l^0_{AB}(\lambda), \Delta l^h)}{\partial \lambda}\end{aligned} \tag{14.116}$$

with

$$\begin{aligned}&\frac{\partial \mathcal{V}^{(df)}(l_{ij}, k^{(df)}_{AB}(\lambda), l^0_{AB}(\lambda), \Delta l^h)}{\partial \lambda} \\ &= -(k^{(df)}_B - k^{(df)}_A)[l_{ij} - l^0_{AB}(\lambda) + \tfrac{1}{2}\Delta l^h]\tfrac{1}{2}\Delta l^h + k^{(df)}_{AB}(\lambda)(l^0_B - l^0_A)\Delta l^h && l_{ij} \le l^0 - \Delta l^h \\ &= \tfrac{1}{2}(k^{(df)}_B - k^{(df)}_A)[l_{ij} - l^0_{AB}(\lambda)]^2 - k^{(df)}_{AB}(\lambda)[l_{ij} - l^0_{AB}(\lambda)](l^0_B - l^0_A) && l^0 - \Delta l^h < l_{ij} \le l^0 + \Delta l^h \\ &= (k^{(df)}_B - k^{(df)}_A)[l_{ij} - l^0_{AB}(\lambda) - \tfrac{1}{2}\Delta l^h]\tfrac{1}{2}\Delta l^h - k^{(df)}_{AB}(\lambda)(l^0_B - l^0_A)\Delta l^h && l_{ij} > l^0 + \Delta l^h\end{aligned} \tag{14.117}$$

The forces are calculated similar as for the non-perturbed DF restraint:

$$\mathbf{f}_j(\lambda) = 2^{n+m}\lambda^n(1-\lambda)^m\mathbf{f}^{AB}_j(\lambda) \tag{14.118}$$

and $\mathbf{f}^{AB}_j(\lambda)$ is calculated using Eq. 9.140, replacing $k^{(df)}$ with $k^{(df)}_{AB}(\lambda)$ and l^0 with $l^0_{AB}(\lambda)$.

The current implementation allows for applications of DF in normal MD simulations, in free energy calculations or in combination with enhanced sampling methods like local elevation (LE, see Sec. 9.13.1) or Hamiltonian replica exchange (REMD, see Sec. 16.3).

14.3. Constraints

When constraints are applied in a simulation (Chap. 10), these appear formally as parameters in the Hamiltonian[130,133]. If the distance constraint Sec. 10.3 is dependent on the coupling parameter λ,

$$\sigma_k(\mathbf{r};\lambda) \equiv \mathbf{r}^2_{k_1k_2} - {d^0}^2_{k_1k_2}(\lambda) = 0 \qquad with\ k = 1,2,...,N^{(c)} \tag{14.119}$$

the constraint forces at time t (Sec. 10.3.8)

$$\begin{aligned} {\mathbf{f}^{(c)}}_i(t) &= -\sum_{k=1}^{N^{(c)}} l_k(\lambda;t)\frac{\partial\sigma_k(\mathbf{r}(t);\lambda)}{\partial\mathbf{r}_i(t)} \\ &= -2\sum_{k=1}^{N^{(c)}} l_k(\lambda;t)(\delta_{ik_1}-\delta_{ik_2})\mathbf{r}_{k_1k_2}(t) \end{aligned} \tag{14.120}$$

and the Lagrange multipliers $l_k(\lambda;t)$ will also depend on λ. The $\lambda-$dependent version of the distance constraints is taken linear in the distance constraint lengths ${d^0}_{k_1k_2}$,

$${d^0}_{k_1k_2}(\lambda) = (1-\lambda){d^0}^A_{k_1k_2} + \lambda {d^0}^B_{k_1k_2}. \tag{14.121}$$

Following the derivation in Sec. 10.3 the set of $N^{(c)}$ quadratic equations from which the $N^{(c)}$ multipliers $l_k(\lambda;t)$ are to be solved and used to obtain the constrained positions $\mathbf{r}(t+\Delta t)$ through Eq. 10.7 and Eq. 10.8 become also $\lambda-$dependent,

$$\begin{aligned} &\big[\ {\mathbf{r}^{uc}}_{k_1k_2}(t+\Delta t) - 2l_k(\lambda;t)(m_{k_1}^{-1}+m_{k_2}^{-1})\mathbf{r}_{k_1k_2}(t)\cdot(\Delta t)^2\big]^2 \\ &\quad -\big[\ (1-\lambda){d^0}^A_{k_1k_2} + \lambda{d^0}^B_{k_1k_2}\big]^2 = 0 \qquad with\ k = 1,2,...,N^{(c)} \end{aligned} \tag{14.122}$$

After linearization of Eq. 14.122 the $\lambda-$dependent expressions for the Lagrange multipliers and the corrections to the unconstrained positions become

$$l_k(\lambda;t) = \frac{((1-\lambda){d^0}^A_{k_1k_2} + \lambda{d^0}^B_{k_1k_2})^2 - ({\mathbf{r}^{uc}}_{k_1k_2}(t+\Delta t))^2}{-4(\Delta t)^2(m_{k_1}^{-1}+m_{k_2}^{-1})(\mathbf{r}_{k_1k_2}(t)\cdot{\mathbf{r}^{uc}}_{k_1k_2}(t+\Delta t))}. \tag{14.123}$$

$$\begin{aligned} \Delta{\mathbf{r}^{uc}}_{k_1}(t+\Delta t) &= -2(\Delta t)^2 m_{k_1}^{-1} l_k(\lambda;t)\mathbf{r}_{k_1k_2}(t) \\ &= m_{k_1}^{-1} g_k(\lambda;t)\mathbf{r}_{k_1k_2}(t) \end{aligned} \tag{14.124}$$

and

$$\begin{aligned} \Delta{\mathbf{r}^{uc}}_{k_2}(t+\Delta t) &= +2(\Delta t)^2 m_{k_2}^{-1} l_k(\lambda;t)\mathbf{r}_{k_1k_2}(t) \\ &= -m_{k_2}^{-1} g_k(\lambda;t)\mathbf{r}_{k_1k_2}(t). \end{aligned} \tag{14.125}$$

Since the atoms may be involved in more than one constraint, the set of equations Eq. 14.122 is solved in linearized form iteratively by the procedure SHAKE, that is, SHAKE as discussed in Sec. 10.3.1 changes the atomic positions $\mathbf{r}^{uc}(t+\Delta t)$ iteratively, such that at the end of the iterative process they satisfy the constraints, and can be returned as $\mathbf{r}(t+\Delta t)$. The number of iterations N_{sh} is determined as discussed in Sec. 10.3. At the n-th iteration step, for each constraint k = 1, 2, ..., $N^{(c)}$ the quantities

$$g_k(\lambda;t;n) = -2(\Delta t)^2 l_k(\lambda;t;n) \tag{14.126}$$

are calculated from Eq. 14.123 and the atomic positions $\mathbf{r}^{uc}(t+\Delta t)$ changed by applying the current (n-th) approximation of the constraint force Eq. 14.120

$${\mathbf{r}^{uc}}_{k_2}(t+\Delta t;n) = {\mathbf{r}^{uc}}_{k_2}(t+\Delta t;n-1) - m_{k_2}^{-1} g_k(\lambda;t;n)\mathbf{r}_{k_1k_2}(t). \tag{14.127}$$

$${\mathbf{r}^{uc}}_{k_1}(t+\Delta t;n) = {\mathbf{r}^{uc}}_{k_1}(t+\Delta t;n-1) + m_{k_1}^{-1} g_k(\lambda;t;n)\mathbf{r}_{k_1k_2}(t) \tag{14.128}$$

The Lagrange multipliers at time t become

$$l_k(\lambda;t) = \sum_{n=1}^{N_{sh}} l_k(\lambda;t;n) \tag{14.129}$$

or

$$g_k(\lambda;t) = \sum_{n=1}^{N_{sh}} g_k(\lambda;t;n). \tag{14.130}$$

The contribution of the constraints Eq. 14.119 to the derivative of the free energy $\mathcal{F}(\lambda)$ with respect to λ at time t is[130]

$$\begin{aligned} \frac{\partial \mathcal{F}^{(c)}(\lambda;t)}{\partial \lambda} &= \frac{\partial}{\partial \lambda} \sum_{k=1}^{N^{(c)}} l_k(\lambda;t)\sigma_k(\mathbf{r}(t);\lambda) \\ &= \sum_{k=1}^{N^{(c)}} l_k(\lambda;t) \frac{\partial \sigma_k(\mathbf{r}(t);\lambda)}{\partial \lambda} \\ &= \sum_{k=1}^{N^{(c)}} \frac{\partial \mathcal{F}_k^{(c)}(\lambda;t)}{\partial \lambda} \end{aligned} \tag{14.131}$$

in which the contribution of the k-th constraint is

$$\begin{aligned} \frac{\partial \mathcal{F}_k^{(c)}(\lambda;t)}{\partial \lambda} &= -2l_k(\lambda;t)d^0{}_{k_1k_2}(\lambda)(d^{0B}{}_{k_1k_2} - d^{0A}{}_{k_1k_2}) \\ &= (\Delta t)^{-2} g_k(\lambda;t)[(1-\lambda)d^{0A}{}_{k_1k_2} + \lambda d^{0B}{}_{k_1k_2}](d^{0B}{}_{k_1k_2} - d^{0A}{}_{k_1k_2}). \end{aligned} \tag{14.132}$$

The corresponding expression for use in the perturbation formula Eq. 14.9 is, assuming that $\mathbf{r}$ corresponds to λ,

$$\begin{aligned} &\sum_{k=1}^{N^{(c)}} l_k(\lambda)[\sigma_k(\mathbf{r};\lambda \pm \Delta\lambda) - \sigma_k(\mathbf{r};\lambda)] \\ &= -\sum_{k=1}^{N^{(c)}} l_k(\lambda)[d^{02}{}_{k_1k_2}(\lambda \pm \Delta\lambda) - d^{02}{}_{k_1k_2}(\lambda)] \\ &= -\sum_{k=1}^{N^{(c)}} l_k(\lambda)\Delta\lambda(d^{0B}{}_{k_1k_2} - d^{0A}{}_{k_1k_2}) \cdot \left[\ \Delta\lambda(d^{0B}{}_{k_1k_2} - d^{0A}{}_{k_1k_2}) \pm 2(d^{0A}{}_{k_1k_2} + \lambda(d^{0B}{}_{k_1k_2} - d^{0A}{}_{k_1k_2}))\right] \\ &= \sum_{k=1}^{N^{(c)}} \tfrac{1}{2}(\Delta t)^{-2} g_k(\lambda) \left[\ d^{02}{}_{k_1k_2}(\lambda \pm \Delta\lambda) - d^{02}{}_{k_1k_2}(\lambda)\right]. \end{aligned} \tag{14.133}$$

14.4. Assigning different $\lambda-$dependences for specific groups of atoms

The Hamiltonian, as described in Sec. 14.1 and Sec. 14.2 was made dependent on a global coupling parameter λ, for which the value is set via the RLAM variable in the PERTURBATION block of the MD input file (Chap. 4-8). MD++ additionally offers the possibility to introduce (via the LAMBDAS block in the MD input file, Chap. 4-8) for specific types of interactions that involve atoms of two energy groups i and j a coupling parameter Λ_{ij}, which is related to the global coupling parameter λ via the polynomial

$$\Lambda_{ij} = a_{ij}\lambda^4 + b_{ij}\lambda^3 + c_{ij}\lambda^2 + d_{ij}\lambda + e_{ij}, \tag{14.134}$$

where the polynomial coefficients $a_{ij}, b_{ij}, c_{ij}, d_{ij}$ and e_{ij} are constants and specified by the user in the LAMBDAS block as well. When specifying a coupling parameter Λ_{ij} involving covalent, special interactions or masses, i should be equal to j, and covalent or special interactions are only perturbed using Λ_{ii} when

the first atom given in the topology (or restraining) file to specify the atom-atom distance or covalent bond, angle or (im)proper dihedral, is part of energy group i. Λ_{ij} can only be specified for covalent interactions listed in the perturbation topology, or for masses and nonbonded interaction involving atoms listed in the perturbation topology.

For any perturbed interaction that is not specified the LAMBDAS block of the MD input file, a_{ij}, b_{ij}, c_{ij} and e_{ij} in Eq. 14.134 can be considered to have a zero value, and $d_{ij} = 1$ in Eq. 14.134.

The use of Λ_{ij} for perturbing specific interactions implies the following for the expressions for the perturbed Hamiltonian. λ in the expressions for the atomic masses, kinetic energy and covalent interactions and forces as given in Sec. 14.2 is replaced by $\Lambda_{ij}(=\Lambda_{ii})$ and the right-hand side of the equations Eq. 14.17, Eq. 14.22, Eq. 14.27, Eq. 14.40, Eq. 14.46, Eq. 14.56, Eq. 14.66 and Eq. 14.73 for the λ-derivatives of the kinetic and covalent interaction energy terms (in which λ is to be changed with $\Lambda_{ij}(=\Lambda_{ii})$ as well) have to be multiplied by $\frac{\partial \Lambda_{ij}}{\partial \lambda}$. From equation Eq. 14.134

$$\frac{\partial \Lambda_{ij}}{\partial \lambda} = 4a_{ij}\lambda^3 + 3b_{ij}\lambda^2 + 2c_{ij}\lambda + d_{ij} \tag{14.135}$$

Expressions Eq. 14.75 and Eq. 14.76 for the perturbed non-bonded interaction is to be replaced by

$$\begin{aligned}
&\mathcal{V}^{(nbd)}(\mathbf{r};\lambda) = \\
&\sum_{\substack{nonbonded\\ perturbed\\ pairs(i,j)}} \Big\{ \Big[(\Lambda_{ij}^{(vdw)})^n \mathcal{V}^{(vdw)}(\mathbf{r}_{ij}; B; (1-\Lambda_{ij}^{(sl)})) + (1-\Lambda_{ij}^{(vdw)})^n \mathcal{V}^{(vdw)}(\mathbf{r}_{ij}; A; \Lambda_{ij}^{(sl)}) \Big] \\
&+ [((\Lambda_{ij}^{(ele)})^n \mathcal{V}^{(ele)}(\mathbf{r}_{ij}; B; (1-\Lambda_{ij}^{(sc)}))) + (1-\Lambda_{ij}^{(ele)})^n \mathcal{V}^{(ele)}(\mathbf{r}_{ij}; A; (1-\Lambda_{ij}^{(sc)}))\Big] \Big\}
\end{aligned} \tag{14.136}$$

where four different interaction-specific coupling parameters Λ_{ij} can be specified:

- $\Lambda_{ij}^{(vdw)}$ scales the Lennard-Jones interactions
- $\Lambda_{ij}^{(sl)}$ determines the softness in the Lennard-Jones interactions
- $\Lambda_{ij}^{(ele)}$ scales the electrostatic interactions
- $\Lambda_{ij}^{(sc)}$ determines the softness in the electrostatic interactions.

In equation Eq. 14.136, $\mathcal{V}^{(vdw)}$ and $\mathcal{V}^{(ele)}$ for state X reads as:

$$\begin{aligned}
&\mathcal{V}^{(vdw)}(\mathbf{r}_{ij}; X; \Lambda_{ij}^{(sl)}) = \frac{1}{[\alpha_{LJ}(i,j)(\Lambda_{ij}^{(sl)})^2 C_{126}^X(i,j) + (r_{ij})^6]} \\
&\cdot \left[\frac{{C_{12}}^X(i,j)}{[\alpha_{LJ}(i,j)(\Lambda_{ij}^{(sl)})^2 C_{126}^X(i,j) + (r_{ij})^6]} - {C_6}^X(i,j) \right]
\end{aligned} \tag{14.137}$$

and

$$\mathcal{V}^{(ele)}(\mathbf{r}_{ij};X;\Lambda_{ij}^{(sc)}) =$$

$$\frac{q_i^X q_j^X}{4\pi\varepsilon_0\varepsilon_1}\left[\frac{1}{[\alpha_c(i,j)(\Lambda_{ij}^{(sc)})^2+(r_{ij})^2]} - \frac{\frac{1}{2}C_{rf}(r_{ij})^2}{[\alpha_c(i,j)(\Lambda_{ij}^{(sc)})+(R_{rf})^2]^{\frac{3}{2}}} - \frac{(1-\frac{1}{2}C_{rf})}{R_{rf}}\right] \tag{14.138}$$

The forces on atoms i and j due to the (i,j)-th term in Eq. 14.136 are

$$\begin{aligned}\mathbf{f}^{(nbd)}{}_i = (\Lambda_{ij}^{(vdw)})^n\ \frac{\partial\mathcal{V}^{(vdw)}(\mathbf{r}_{ij};B;(1-\Lambda_{ij}^{(sl)}))}{\partial\mathbf{r}_i} + (1-\Lambda_{ij}^{(vdw)})^n\frac{\partial\mathcal{V}^{(vdw)}(\mathbf{r}_{ij};A;\Lambda_{ij}^{(sl)})}{\partial\mathbf{r}_i}\\ +(\Lambda_{ij}^{(ele)})^n\frac{\partial\mathcal{V}^{(ele)}(\mathbf{r}_{ij};B;(1-\Lambda_{ij}^{(sc)}))}{\partial\mathbf{r}_i} + (1-\Lambda_{ij}^{(ele)})^n\frac{\partial\mathcal{V}^{(ele)}(\mathbf{r}_{ij};A;(1-\Lambda_{ij}^{(sc)}))}{\partial\mathbf{r}_i}\end{aligned} \tag{14.139}$$

and

$$\mathbf{f}^{(nbd)}{}_j = -\mathbf{f}^{(nbd)}{}_i \tag{14.140}$$

with

$$\begin{aligned}\frac{\partial\mathcal{V}^{(vdw)}(\mathbf{r}_{ij};X;\lambda)}{\partial\mathbf{r}_i} &= \frac{-6(r_{ij})^4}{[\alpha_{LJ}(i,j)(\Lambda_{ij}^{(sl)})^2C_{126}^X(i,j)+(r_{ij})^6]^2}\\ &\cdot\left[\frac{C_{12}{}^X(i,j)}{[\alpha_{LJ}(i,j)(\Lambda_{ij}^{(sl)})^2C_{126}^X(i,j)+(r_{ij})^6]} - C_6{}^X(i,j)\right]\cdot\mathbf{r}_{ij}\end{aligned} \tag{14.141}$$

and

$$\frac{\partial\mathcal{V}^{(ele)}(r_{ij};X;\lambda)}{\partial\mathbf{r}_i} = \frac{q_i^X q_j^X}{4\pi\varepsilon_0\varepsilon_1}\left[\frac{1}{[\alpha_c(i,j)(\Lambda_{ij}^{(sc)})^2+(r_{ij})^2]^{\frac{3}{2}}} + \frac{C_{rf}}{[\alpha_c(i,j)(\Lambda_{ij}^{(sc)})^2+(R_{rf})^2]^{\frac{3}{2}}}\right]\cdot\mathbf{r}_{ij} \tag{14.142}$$

The $\lambda-$derivative of the right-hand side of equation Eq. 14.136 reads

$$\begin{aligned}\frac{\partial\mathcal{V}^{(nbd)}(\mathbf{r};\lambda)}{\partial\lambda} = \{&n(\Lambda_{ij}^{(vdw)})^{n-1}\mathcal{V}^{(vdw)}(\mathbf{r}_{ij};B;(1-\Lambda_{ij}^{(sl)}))\frac{\partial\Lambda_{ij}^{(vdw)}}{\partial\lambda}\\ &+(\Lambda_{ij}^{(vdw)})^n\frac{\partial\mathcal{V}^{(vdw)}(\mathbf{r}_{ij};B;(1-\Lambda_{ij}^{(sl)}))}{\partial\Lambda_{ij}^{(sl)}}\frac{\partial\Lambda_{ij}^{(sl)}}{\partial\lambda} - n(1-\Lambda_{ij}^{(vdw)})^n\mathcal{V}^{(vdw)}(\mathbf{r}_{ij};A;\Lambda_{ij}^{(sl)})\frac{\partial\Lambda_{ij}^{(vdw)}}{\partial\lambda}\\ &+(1-\Lambda_{ij}^{(vdw)})^n\frac{\partial\mathcal{V}^{(vdw)}(\mathbf{r}_{ij};A;\Lambda_{ij}^{(sl)})}{\partial\Lambda_{ij}^{(sl)}}\frac{\partial\Lambda_{ij}^{(sl)}}{\partial\lambda} + n(\Lambda_{ij}^{(ele)})^{n-1}\mathcal{V}^{(ele)}(\mathbf{r}_{ij};B;(1-\Lambda_{ij}^{(sc)}))\frac{\partial\Lambda_{ij}^{(ele)}}{\partial\lambda}\\ &+(\Lambda_{ij}^{(ele)})^n\frac{\partial\mathcal{V}^{(ele)}(\mathbf{r}_{ij};B;(1-\Lambda_{ij}^{(sc)}))}{\partial\Lambda_{ij}^{(sc)}}\frac{\partial\Lambda_{ij}^{(sc)}}{\partial\lambda} - n(1-\Lambda_{ij}^{(ele)})^{n-1}\mathcal{V}^{(ele)}(\mathbf{r}_{ij};A;\Lambda_{ij}^{(sc)})\frac{\partial\Lambda_{ij}^{(ele)}}{\partial\lambda}\\ &+(1-\Lambda_{ij}^{(ele)})^n\frac{\partial\mathcal{V}^{(ele)}(\mathbf{r}_{ij};A;\Lambda_{ij}^{(sc)})}{\partial\Lambda_{ij}^{(sc)}}\frac{\partial\Lambda_{ij}^{(sc)}}{\partial\lambda}\end{aligned} \tag{14.143}$$

In Eq. 14.143, the $\frac{\partial \Lambda_{ij}^{X}}{\partial \lambda}$ terms are evaluated according to equation Eq. 14.135, and

$$\frac{\partial \mathcal{V}^{(vdw)}(\mathbf{r}_{ij};X;\Lambda_{ij}^{(sl)})}{\partial \Lambda_{ij}^{(sl)}} = \frac{-2\Lambda_{ij}^{(sl)}\alpha_{LJ}(i,j)C_{126}^{X}(i,j)}{\left[\ \alpha_{LJ}(i,j)(\Lambda_{ij}^{(sl)})^2 C_{126}^{X}(i,j)+(r_{ij})^6\right]^2}\left[\frac{2{C_{12}}^{X}(i,j)}{\left[\alpha_{LJ}(i,j)(\Lambda_{ij}^{(sl)})^2 C_{126}^{X}(i,j)+(r_{ij})^6\right]} - {C_6}^{X}(i,j)\right] \tag{14.144}$$

$$\frac{\partial \mathcal{V}^{(ele)}(\mathbf{r}_{ij};X;\Lambda_{ij}^{(sc)})}{\partial \Lambda_{ij}^{(sc)}} = -\frac{q_i^X q_j^X}{4\pi\varepsilon_0\varepsilon_1}\cdot\Lambda_{ij}^{(sc)}\alpha_c(i,j) \cdot\left[\frac{1}{\left[\alpha_c(i,j)(\Lambda_{ij}^{(sc)})^2+(r_{ij})^2\right]^{\frac{3}{2}}} - \frac{\frac{3}{2}C_{rf}(r_{ij})^2}{\left[\alpha_c(i,j)(\Lambda_{ij}^{(sc)})^2+(R_{rf})^2\right]^{\frac{5}{2}}}\right] \tag{14.145}$$

and

$$\frac{\partial \mathcal{V}^{(nbd)}(\mathbf{r};X;(1-\Lambda_{ij}^{(sl/sc)}))}{\partial \Lambda_{ij}^{(sl/sc)}} = -\frac{\partial \mathcal{V}^{(nbd)}(\mathbf{r};X;\Lambda_{ij}^{(sl/sc)})}{\partial \Lambda_{ij}^{(sl/sc)}} \tag{14.146}$$

14.5. Choice of pathway and states A and B

Technical aspects of specifying the states A and B are discussed in Sec. 4-3.3. The *molecular topology*, as described in Sec. 4-3.2, the so-called unperturbed topology, corresponds to *state A*. Since atoms cannot be created or destroyed, only their interaction with other atoms can be modified or perturbed, the unperturbed topology corresponding to state A must contain all atoms involved in the perturbation as either real or dummy (i.e. non-interacting) atoms. So, state B has the same number of atoms as state A. The *difference between state B and A* is specified in a *perturbation molecular topology* (Sec. 4-3.3). In Sec. 4-3.3 *eight points of interest* are listed, which should be kept in mind when constructing both, molecular and perturbation, topology files for use in a free energy calculation.

General considerations and *indications* with respect to the *choice of pathways* in free energy calculations have been discussed in refs.[130,131,135]. Here, we shall only list the most important issues.

1. *Choice of thermodynamic cycle and its four end states.*
   In most free energy calculations the concept of a thermodynamic cycle is used. Since the free energy $\mathcal{F}$ is a state function, a change in free energy, $\Delta\mathcal{F}$, will be independent of the path connecting the end states, as long as the system is in equilibrium and is changed in a reversible way. In that case, along a closed pathway or cycle we have $\Delta\mathcal{F} = 0$. This result implies that there are many possibilities of obtaining $\Delta\mathcal{F}$ between two end states A and B. One may calculate $\Delta\mathcal{F}$ directly using a pathway connecting states A and B, or one may design a cycle of which a pathway from state A to state B is only one part, and calculate the $\Delta\mathcal{F}$ of the remaining part of the cycle. The power of the thermodynamic cycle technique resides in the fact that *pathways* and *cycles* may correspond to *non-chemical processes*, and so may be chosen such as to optimize the accuracy of the calculation. Generally, equilibration and sampling are optimized by *keeping the differences between states A and B minimal*. Secondly, the *end states A and B* should be *structurally well characterized* in order to avoid excessively long equilibration and sampling periods[130]. The end states and the connecting pathway should be chosen such that the relaxation time of the system with respect to the change in Hamiltonian and the time required to sample the ensemble are both minimized. This implies that the most direct or chemical path is not necessarily the most efficient[136,137]. As only terms in the Hamiltonian that are modified, *i.e.* depend on λ, contribute to the change in free energy, the number of λ dependences should be minimized. The introduction of additional or removal of degrees of freedom should be avoided: generally, when changing a real atom into a dummy atom or vice versa, only non-bonded interactions should be modified, bonded terms such as bond-length, bond-angle and dihedral-angle terms should remain unchanged. This avoids the additional work required to modify the associated force constants and the additional sampling required as the atom

gains degrees of freedom. Perturbations should be defined such that an atom does not become fully uncoupled from the rest of the system. If possible, the mass of an atom should remain unperturbed.

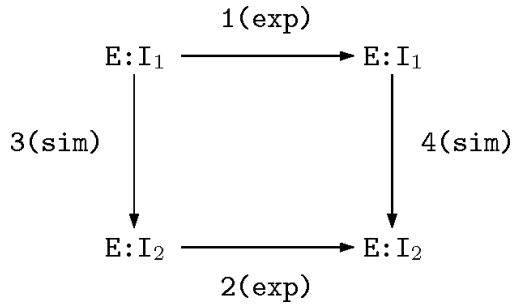

FIGURE 14.1. Thermodynamic cycle with respect to the relative binding of two inhibitors I_1 and I_2 to an enzyme E. The symbol ':' indicates complexation.[138]

2. *Choice of boundary conditions.*
   Thermodynamic cycles allow for the cancellation of systematic errors occurring in parallel legs of a cycle. For example, errors in processes 3 and 4 in Fig. 14.1 may cancel when $\Delta\Delta\mathcal{F}_{43} = \Delta\mathcal{F}_4 - \Delta\mathcal{F}_3$ is calculated. However, cancellation may only happen when the *simulation conditions* along the *parallel legs* are chosen *as similar as possible*: the simulations along legs 3 and 4 should not involve different box shapes, different spatial boundary conditions (e.g. periodic versus extended wall) or different thermodynamic boundary conditions (e.g. (N,V,T) versus (N,P,T)).

3. *Absence and presence of force field terms.*
   In a thermodynamic cycle the contribution of given force-field terms may be equal along parallel legs, and so might be ignored. Great care is required, however, when selecting force-field or Hamiltonian terms to be neglected. For example, the work done increasing or decreasing a charge during a simulation will depend on the dielectric permittivity of the medium. Long-range electrostatic contributions can only be ignored if the dielectric properties of the environments on both legs of the thermodynamic cycle are equivalent. This is not the case when one leg corresponds to the low dielectric interior of a protein or non-polar solvent and the other to a high dielectric medium such as water[139]. Whether bonded force terms can be ignored is also questionable: if the conformational freedom of (part of) the molecular system is different along parallel legs of a cycle, bonded force terms will make a different contribution along the different legs which must be explicitly calculated. Finally, we note that the *terms in the Hamiltonian* Eq. 14.14 *that do not depend on* λ *should be kept identical along (parallel) legs of a cycle*: position restraining, atom-atom distance restraining, dihedral-angle restraining, ^3J-coupling constant restraining interactions, etc. should not be different along different legs of a cycle. Switches for force field terms, such as NTF[1..10] (Sec. 12.7), should also not be different. Local-elevation interaction and time-averaging distance or ^3J-value restraining or S^2-order parameter restraining should not be used at all, since they involve changing the Hamiltonian as a function of time.

4. *Choice of atomic masses.*
   Due to the factor m_i^{-1} in the equations of motion Eq. 2.8 and Eq. 2.13, the mass of an atom should not be chosen equal to zero.
5. *Atoms without non-bonded interactions.*
   The van der Waals and Coulomb potential energy terms contain a singularity when the interatomic distance r becomes zero. For fully interacting atom pairs this singularity is never sampled in a simulation due to the repulsive term in the van der Waals interaction. This singularity in $\mathcal{V}^{(nbd)}$, $\frac{\partial\mathcal{V}^{(nbd)}}{\partial\mathbf{r}}$ or $\frac{\partial\mathcal{V}^{(nbd)}}{\partial\lambda}$ will be sampled if the non-bonded interaction is defined to be zero in state A or state B (presence of dummy atoms), leading to numerical instabilities in the simulation[26]. When the effective non-bonded interaction radius of an atom becomes smaller than the length of flight of the atom per (finite) MD time step, very high energy regions of the potential energy will be sampled. To avoid such problems, a soft-core interaction should be selected for atoms without non-bonded interaction (i.e. dummy atoms) in one of the end states B and A[26].

14.6. Thermodynamic integration

In the early applications of the thermodynamic integration (TI) Eq. 14.11 the coupling parameter λ was made a function of time t, $\lambda(t)$, and the integral was integrated in small time steps Δt during an MD simulation of $\mathcal{N}_t$ steps

$$\Delta\mathcal{F}_{BA} = \sum_{n=1}^{\mathcal{N}_t} \frac{\partial\mathcal{H}}{\partial\lambda}\frac{\partial\lambda}{\partial t}\Delta t. \tag{14.147}$$

This technique is called continuous change of λ, or *slow growth* or single-configuration TI. It suffers from a number of disadvantages[135]. The system is never truly in equilibrium, but lags behind the changing Hamiltonian. This results in excess work being done on the system and a systematic overestimation of the free energy change. Attempting to correct for this overestimation by averaging results for the forward and reverse change from short simulations is an unreliable procedure. A necessary but not sufficient condition to obtain a reliable free energy change is that the difference between forward and reverse processes or hysteresis is small. A small hysteresis, however, indicates only the degree of reversibility. It indicates neither that the system is in equilibrium nor that a representative ensemble has been sampled for each value of λ. If a change of $\mathcal{H}(\lambda)$ is carried out much faster than the system can respond, the system will remain trapped in a (non-representative) local state. If this state is adequately sampled during the simulation, the change will appear reversible and a small hysteresis will be observed. The calculated free energy change will, however, be dependent on the precise starting configuration and as the length of the simulation is increased, the apparent hysteresis will also increase[140]. In practice, slow growth procedures should only be used to bring the system gradually from one $\lambda-$value to another.

An alternative use of the thermodynamic integration formula Eq. 14.11 is to compute ensemble averages at a few, $\mathcal{N}_\lambda$, fixed $\lambda-$values and perform the integration numerically using interpolation formulae for the integrand,

$$\Delta\mathcal{F}_{BA} = \sum_{n=1}^{\mathcal{N}_\lambda} \left\langle \frac{\partial\mathcal{H}}{\partial\lambda} \right\rangle_{\lambda_n} w(\lambda_n), \tag{14.148}$$

where the weight factors of the numerical integration formula that is used are denoted by $w(\lambda_n)$. This technique is called TI *with numerical quadrature* or multi-configurational TI. It has a number of practical advantages. Effects due to the equilibration of the system with respect to the change in Hamiltonian and those depending on the extent of sampling can be largely separated. The convergence of the ensemble average $\langle ... \rangle_{\lambda_n}$ at fixed λ_n-value can be monitored as a function of the simulation time. If the integrand turns out to vary rapidly as a function of λ, more intermediate λ-values can be added into the numerical integration[140]. Simple numerical integration methods such as the trapezoidal rule, Simpson's rule or cubic spline integration may be used to integrate over λ.

To estimate the *precision of* $\langle \partial\mathcal{H}/\partial\lambda \rangle_{\lambda_n}$, the following formula can be used for the standard deviation on the mean[139],

$$\sigma\left(\left\langle \frac{\partial\mathcal{H}}{\partial\lambda} \right\rangle_{\lambda_n} \right) = \left(\frac{S_{\lambda_n}}{\mathcal{N}_{conf}} \right)^{\frac{1}{2}} \sigma\left(\frac{\partial\mathcal{H}}{\partial\lambda} \right), \tag{14.149}$$

where $\mathcal{N}_{conf}$ denotes the number of configurations over which the ensemble average at $\lambda = \lambda_n$ is taken, and $\sigma(\partial\mathcal{H}/\partial\lambda)$ is calculated as the square root of the variance over the ensemble

$$\sigma^2\left(\frac{\partial\mathcal{H}}{\partial\lambda} \right) = \frac{1}{\mathcal{N}_{conf}} \sum_{t=1}^{\mathcal{N}_{conf}} \left[\frac{\partial\mathcal{H}}{\partial\lambda} - \left\langle \frac{\partial\mathcal{H}}{\partial\lambda} \right\rangle_{\lambda_n,\mathcal{N}_{conf}} \right]^2. \tag{14.150}$$

To calculate the statistical inefficiency, S_{λ_n}, the total simulation time at $\lambda = \lambda_n$ is divided into M blocks of length b, and $\mathcal{N}_b$ configurations are taken from each block such that $M \cdot \mathcal{N}_b = \mathcal{N}_{conf}$.

The variance in the mean is then calculated for each possible block length b as

$$\sigma^2\left(\left\langle \frac{\partial\mathcal{H}}{\partial\lambda} \right\rangle_{\lambda_n,b} \right) = \frac{1}{M} \sum_{m=1}^{M} \left[\left\langle \frac{\partial\mathcal{H}}{\partial\lambda} \right\rangle_{\lambda_n,\mathcal{N}_b,m} - \left\langle \frac{\partial\mathcal{H}}{\partial\lambda} \right\rangle_{\lambda_n,\mathcal{N}_{conf}} \right]^2, \tag{14.151}$$

where $< ... >_{\lambda_n,\mathcal{N}_b,m}$ denotes the ensemble average at $\lambda = \lambda_n$ over $\mathcal{N}_b$ sample configurations of the m-th block. S_{λ_n} is then calculated as

$$S_{\lambda_n} = \lim_{\mathcal{N}_b \to \infty} \frac{\mathcal{N}_b \sigma^2 \left(\left\langle \frac{\partial \mathcal{H}}{\partial \lambda} \right\rangle_{\lambda_n, b} \right)}{\sigma^2 \left(\frac{\partial \mathcal{H}}{\partial \lambda} \right)}. \tag{14.152}$$

Effectively, only one configuration of every S_{λ_n} configurations used contributes new information to the average. The simulation periods needed to obtain a given degree of convergence of $\langle \partial \mathcal{H}/\partial \lambda \rangle_{\lambda_n}$ may be quite different for different λ_n-values[139, 141].

To estimate the *precision of the numerical quadrature*, one may assume that the integrand is Gaussian distributed with a mean $\langle \partial \mathcal{H}/\partial \lambda \rangle_{\lambda_n}$ and a width given by Eq. 14.149. Assuming no correlation between the distributions at different λ_n points, the standard deviation on $\Delta \mathcal{F}_{BA}$ becomes[139]

$$\sigma(\Delta \mathcal{F}_{BA}) = \left[\sum_{n=1}^{\mathcal{N}_\lambda} w(\lambda_n) \sigma^2 \left(\left\langle \frac{\partial \mathcal{H}}{\partial \lambda} \right\rangle_{\lambda_n} \right) \right]^{1/2}. \tag{14.153}$$

Additional tests of the reliability of the obtained free energy difference $\Delta \mathcal{F}_{BA}$ can and should be carried out[130].

1. The *addition of extra λ -values* in the numerical integration over λ in Eq. 14.147 should not dramatically change the $\Delta \mathcal{F}_{BA}$-value obtained so far[140].
2. When carrying out more than one change of a system, e.g. from state A to state B and from A to C, the quality of the equilibration, sampling and integration over λ can be tested by performing the change from state B to C, which *closes a cycle*[140]
$$\Delta \mathcal{F}_{BA} + \Delta \mathcal{F}_{CB} + \Delta \mathcal{F}_{AC} = 0 \tag{14.154}$$
3. Repetition of individual simulations with *different initial* equilibrium *configurations* or *velocities* should yield the same result.
4. *Small changes* in the *computational procedure* should not affect the obtained $\Delta \mathcal{F}_{BA}$-value[142].

14.7. Thermodynamic perturbation and extrapolation

The perturbation formulae Eq. 14.6, Eq. 14.8 and Eq. 14.9 can also be used to compute free energy differences. In the limit of infinite sampling or when the ensembles corresponding to $\mathcal{H}(\lambda)$ and $\mathcal{H}(\lambda \pm \Delta\lambda)$ overlap perfectly the perturbation formula Eq. 14.9 will yield the exact $\Delta \mathcal{F}_{\lambda \pm \Delta\lambda}$ value. In practice, these conditions are never fulfilled. If the ensembles corresponding to states A and B do not overlap closely, calculations based on the perturbation formula must be split into a number of steps between intermediate systems along the pathway connecting states A and B that are sufficiently similar to allow for the use of Eq. 14.9, and then $\Delta \mathcal{F}_{BA}$ is just the sum of the $\Delta \mathcal{F}$ values for all intermediate steps,

$$\begin{aligned} \Delta \mathcal{F}_{BA} &= \sum_{n=0}^{\mathcal{N}_\lambda - 1} -k_B T \ln \left\langle e^{-[\mathcal{H}(\lambda_{n+1}) - \mathcal{H}(\lambda_n)]/k_B T} \right\rangle_{\lambda_n} \\ &= \sum_{n=1}^{\mathcal{N}_\lambda} +k_B T \ln \left\langle e^{-[\mathcal{H}(\lambda_{n-1}) - \mathcal{H}(\lambda_n)]/k_B T} \right\rangle_{\lambda_n}. \end{aligned} \tag{14.155}$$

We note that the sampling and convergence properties of the thermodynamic integration formula Eq. 14.147 and the perturbation formula Eq. 14.155 are different.[143] The requirement of closely overlapping ensembles for neighbouring λ-values in Eq. 14.155 does not apply to the TI formula Eq. 14.147, since the latter is based on the assumption of the smoothness of $\mathcal{F}'(\lambda)$, which is different from the assumption of overlapping ensembles for λ and $\lambda \pm \Delta\lambda$[135]. For the TI formula the convergence of the ensemble average does not depend on the magnitude of the change $\Delta\lambda$ in λ, as it does for the perturbation formula. Therefore, the TI formula offers the better opportunity to reduce and monitor errors in practice.[139]

Free energy calculations based on Eq. 14.147 or Eq. 14.155 are computationally very expensive. If one would like to obtain the relative free energy differences of a number (M) of end states B_1, B_2, ..., B_M with respect to state A, $M \cdot \mathcal{N}_\lambda$ converged simulations, at the various $\lambda-$points along the different pathways from A to B_1, B_2, ..., B_M, are required. This number could be reduced to 1 if one could use the perturbation formula Eq. 14.6 directly, that is, without intermediate λ-values between states A and B_m. One would use state A as reference state, the ensemble of which is used to *extrapolate the behaviour of* $\Delta \mathcal{F}_{\lambda_A + \Delta\lambda}$ *to* $\Delta\lambda = \lambda_{B_m} - \lambda_A$, *i.e.* state B_m. This approach has two advantages.

1. Only a single reference state A ($\lambda = \lambda_A$) need be considered and simulated.
2. The fluctuations in this reference state A are only dependent on λ_A not on the λ_{B_m}, that is, not on the λ changes to be considered.

The question is, however, whether the changes in free energy, $\Delta\mathcal{F}_{B_m A}$ can be accurately estimated for physically relevant states A and B_m. This is the case when the following two concepts are used[143,144] (see Eq. 14.155).

1. Eq. 14.6 gives incorrect results, if the configurations sampled in the reference state A ($\lambda = \lambda_A$) do not correspond to low energy configurations in the end states B_m. This is especially the case when real atoms are changed into dummy atoms or vice versa. A remedy is *to introduce soft-core non-bonded interactions* such as Eq. 14.75 - Eq. 14.77 in state A at positions where real atoms are to be changed into dummy atoms or vice versa. In this way the sampling of this new *reference state* A' is biased such that it encompasses the parts of configuration space accessible to the system in state A *and* in the end states B_m. So, a *non-physical state* A' is simulated which is chosen such that the accuracy of the free energy differences $\Delta\mathcal{F}_{AA'}$ and $\Delta\mathcal{F}_{B_m A'}$ (m = 1,2, ..., M) calculated using Eq. 14.6 is optimized.
2. The *difference* in free energy between the various *physical states* A and B_m can then be determined as

$$\Delta\mathcal{F}_{B_m A} = \Delta\mathcal{F}_{B_m A'} - \Delta\mathcal{F}_{A' A} \qquad with\ m = 1, 2, ..., M. \tag{14.156}$$

Use of the perturbation formula in combination with soft-core non-bonded interaction sites and a non-physical reference state that is simulated makes estimation of a series of free energy differences based on a single simulation possible.

The *energetic contribution* $\Delta\mathcal{U}_{BA}$ and the *entropic contribution* $T\cdot\Delta\mathcal{S}_{BA}$ to the total free energy difference $\Delta\mathcal{F}_{BA}$ can be obtained using the formulae[143,145]

$$\begin{aligned} \Delta\mathcal{U}_{BA} &= \langle\mathcal{H}(\lambda_B)\rangle_{\lambda_B} - \langle\mathcal{H}(\lambda_A)\rangle_{\lambda_A} \\ &= \left\langle\mathcal{H}(\lambda_B) e^{+[\Delta\mathcal{F}_{BA} - [\mathcal{H}(\lambda_B) - \mathcal{H}(\lambda_A)]]/k_B T}\right\rangle_{\lambda_A} - \langle\mathcal{H}(\lambda_A)\rangle_{\lambda_A} \end{aligned} \tag{14.157}$$

and

$$T\Delta\mathcal{S}_{BA} = \Delta\mathcal{U}_{BA} - \Delta\mathcal{F}_{BA}. \tag{14.158}$$

Program dg_ener can be used to obtain free energy differences $\Delta\mathcal{F}_{\lambda_A+\Delta\lambda}$ from the time series of the Hamiltonian in a reference state A′ (molecular topology) and in states A, B_m. It calculates a perturbation formula free energy difference Eq. 14.9. Because only the difference of the Hamiltonian is included in this equation, only those terms in the Hamiltonian that are different in states A, B_m from state A' need to be re-evaluated from a molecular trajectory (e.g. using program ener, or by performing an analysis running over an existing stimulation (block READTRAJ, see Chap. 4-8).

14.8. Umbrella sampling

The TI and perturbation formulae are very powerful when a change in free energy is associated with a change of chemical composition of the molecular system. In some cases, one wishes to consider the free energy as a function of a given geometrical parameter $\mathcal{Q}$, the reaction coordinate, e.g. the distance r_{ij} between reactants i and j in a chemical reaction or a torsional angle φ_n in case of a conformational change. The free energy as a function of $\mathcal{Q}$, $\mathcal{F}$ ($\mathcal{Q}$), is called a potential of mean force or a free energy profile. It is defined as[130]

$$\mathcal{F}(\mathcal{Q}') = -k_B T \ln\left[\frac{\int\int \delta(\mathcal{Q}(\boldsymbol{r}) - \mathcal{Q}') e^{-\frac{\mathcal{H}}{k_B T}} d\boldsymbol{p} d\boldsymbol{r}}{\int\int e^{-\frac{\mathcal{H}}{k_B T}} d\boldsymbol{p} d\boldsymbol{r}}\right] \tag{14.159}$$

$$= -k_B T \ln P(\mathcal{Q}') \tag{14.160}$$

where the function $\mathcal{Q}(\boldsymbol{r})$ defines the reaction coordinate in terms of the atomic coordinates $\boldsymbol{r}$, δ is the Dirac delta function and the probability to find the system at $\mathcal{Q} = \mathcal{Q}'$ is $P(\mathcal{Q}')$. If during a single simulation the sampling along the whole range of $\mathcal{Q}'$-values has been sufficient, $\mathcal{F}$ ($\mathcal{Q}'$) can be directly calculated from the probability distribution $P(\mathcal{Q}')$ as obtained from the trajectory. However, if there are free energy barriers

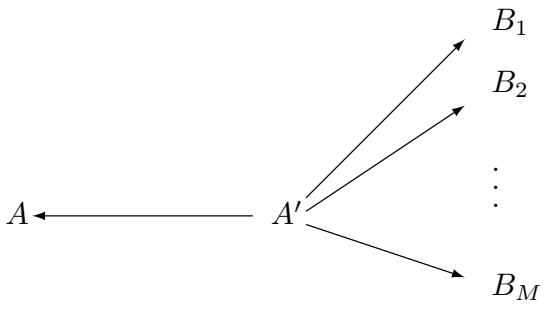

FIGURE 14.2. The free energy differences $\Delta\mathcal{F}_{B_m A}$ between the physical states A and B_1, B_2, ...B_m are obtained by using an ensemble for the non-physical state A′ ($\lambda = \lambda_{A'}$) which should contain soft-core non-bonded interaction sites for all atoms that have a different non-bonded interaction between states A and B_M ($m = 1, 2, ..., M$), and applying the perturbation formula between $\lambda = \lambda_{A'}$ and to $\lambda = \lambda_A$ and $\lambda = \lambda_{B_m}$ ($m = 1, 2, ..., M$), and Eq. 14.156.

much higher than k_BT along $\mathcal{Q}\,'$, these may inhibit a proper sampling along $\mathcal{Q}\,'$. In that case, the sampling may be improved by applying a biasing function.

In the so-called *umbrella-sampling technique* (US)[88] an auxiliary potential energy term $\mathcal{V}^{(spec)}(\mathcal{Q}(\boldsymbol{r}))$ is added to the Hamiltonian of the system, which *biases the sampling*. Simulation including the umbrella potential energy term then yields the biased probability distribution $P^{bias}(\mathcal{Q}')$, from which the unbiased probability distribution $P(\mathcal{Q}')$ can be obtained through the relation[130]

$$P(\mathcal{Q}') = P^{bias}(\mathcal{Q}')\frac{e^{+\frac{\mathcal{V}^{(spec)}(\mathcal{Q}')}{k_BT}}}{< e^{+\frac{\mathcal{V}^{(spec)}(\mathcal{Q}')}{k_BT}} >} \tag{14.161}$$

where $< ... >$ denotes an average over the simulations. The umbrella sampling technique can in principle be applied with any kind of biasing potential energy term $\mathcal{V}^{(spec)}(\mathcal{Q}'$, however mainly two types of umbrella potential energy functions are used.

1. Umbrella potential energy functions constructed to obtain uniform or quasi-uniform sampling. These functions typically will have to be created through an adaptive procedure, e.g. LE and LEUS. This is further explained in (Sec. 9.13.1).
2. Windowing umbrella potential energy functions, where the umbrella potential energy function is constructed to sample a specific range of $\mathcal{Q}$.

In the windowing umbrella sampling method a restraining potential energy function is added $\mathcal{V}^{(spec)} = \mathcal{V}^{(res)}(\mathcal{Q}_0)$ which *restrains the sampling* to within a given range of the reaction coordinate $\mathcal{Q}'$ around a given value $\mathcal{Q}' = \mathcal{Q}_0$. For the free energy profile $\mathcal{F}(\mathcal{Q}';\mathcal{Q}_0)$ around $\mathcal{Q}_0$ we then find

$$\begin{aligned}\mathcal{F}(\mathcal{Q}';\mathcal{Q}_0) &= -k_BT\ln P^{bias}(\mathcal{Q}';\mathcal{Q}_0) - \mathcal{V}^{(res)}(\mathcal{Q}';\mathcal{Q}_0) \\ &\quad +k_BT\ln < e^{+\frac{\mathcal{V}^{(res)}(\mathcal{Q};\mathcal{Q}_0)}{k_BT}} >_{\mathcal{Q}_0} -k_BT\ln\mathcal{Z} \\ &= -k_BT\ln P^{restr}(\mathcal{Q}';\mathcal{Q}_0) - \mathcal{V}^{(res)}(\mathcal{Q}';\mathcal{Q}_0) + C(\mathcal{Q}_0)\end{aligned} \tag{14.162}$$

where the (unknown) partition function of the molecular system is indicated by $\mathcal{Z}$. Since the last two terms in the first part of Eq. 14.162 do not depend on $\mathcal{Q}'$, they can be written as a constant depending only on $\mathcal{Q}_0$, $C(\mathcal{Q}_0)$. So using Eq. 14.162 the free energy profile within a given range around $\mathcal{Q}_0$ can be determined up to a constant. The overall free energy profile $\mathcal{F}(\mathcal{Q}')$ can then be obtained by a series of umbrella simulations restrained around the values $\mathcal{Q}_0, \mathcal{Q}_1, \mathcal{Q}_2, \ldots$ and by adding different constants $C(\mathcal{Q}_i)$ to the local free energy profiles $\mathcal{F}(\mathcal{Q}';\mathcal{Q}_i)$ so that the resulting free energy profile $\mathcal{F}(\mathcal{Q}')$ is a continuous function of the reaction coordinate $\mathcal{Q}'$[61,62,132,146].

The atom-atom *distance restraining* function Eq. 9.3, $\mathcal{V}^{(dr)}$, discussed in Sec. 9.3 or the *dihedral-angle restraining* function Eq. 9.60, $\mathcal{V}^{(tr)}$, discussed in Sec. 9.6 are suitable for use as umbrella potential energy terms. The force constants $k^{(pr)}$ in Eq. 9.4 or $k^{(tr)}$ in Eq. 9.60 should be chosen sufficiently large to focus the sampling around r_m or φ_n, but not too big in order to avoid too narrow probability distributions around the points $\mathcal{Q}_i = r_m$ or $\mathcal{Q}_i = \varphi_n$, in which case many simulations would be required to cover the whole range of $\mathcal{Q}$ -values.[61,132]

Alternatively, the free energy difference between two conformations, separated by high energy barriers may be elegantly calculated using hidden, perturbed distance restraints or hidden, perturbed dihedral angle restraints, as explained in Sec. 14.2.10 and Sec. 14.2.11.

14.9. Enveloping Distribution Sampling

Enveloping distribution sampling (EDS) is an alternative approach to calculating the free energy difference between various pairs of states A and B

$$\Delta\mathcal{F}_{BA} = \mathcal{F}_B - \mathcal{F}_A = -\beta^{-1} \ln\left(\frac{\mathcal{Z}_B}{\mathcal{Z}_A}\right). \tag{14.163}$$

This free energy difference can be calculated from the energy difference distributions

$$\begin{aligned} \rho_A\left(\Delta\mathcal{V}; \Delta\mathcal{V}_{BA}\right) &= \left\langle \delta\left[\Delta\mathcal{V} - \left(\mathcal{V}_B - \mathcal{V}_A\right)\right]\right\rangle_A \\ \rho_B\left(\Delta\mathcal{V}; \Delta\mathcal{V}_{BA}\right) &= \left\langle \delta\left[\Delta\mathcal{V} - \left(\mathcal{V}_B - \mathcal{V}_A\right)\right]\right\rangle_B, \end{aligned} \tag{14.164}$$

where $\langle ... \rangle_X$ indicates an average over an ensemble sampled at state X, $\mathcal{V}_X(\boldsymbol{r})$ is the potential energy part of the Hamiltonian $\mathcal{H}_X(\boldsymbol{p}, \boldsymbol{r}) = \mathcal{K}_X(\boldsymbol{p}) + \mathcal{V}_X(\boldsymbol{r})$, and $\Delta\mathcal{V}_{BA}(\boldsymbol{r}) = \mathcal{V}_B(\boldsymbol{r}) - \mathcal{V}_A(\boldsymbol{r})$. In the following the kinetic part of the Hamiltonian $\mathcal{K}_X(\boldsymbol{p})$ is omitted for simplicity. The free energy difference can be expressed as[147–149]

$$\rho_B\left(\Delta\mathcal{V}; \Delta\mathcal{V}_{BA}\right) e^{-\beta\Delta\mathcal{F}_{BA}} = \rho_A\left(\Delta\mathcal{V}; \Delta\mathcal{V}_{BA}\right) e^{-\beta\Delta\mathcal{V}}, \tag{14.165}$$

indicating that the free energy difference $\Delta\mathcal{F}_{BA}$ is the energy difference $\Delta\mathcal{V}$ where the two energy difference distributions intersect. Sampling of both $\rho_A\left(\Delta\mathcal{V}; \Delta\mathcal{V}_{BA}\right)$ and $\rho_B\left(\Delta\mathcal{V}; \Delta\mathcal{V}_{BA}\right)$ in a single simulation can be achieved by construction of a reference state R that envelopes the two states of interest. The free energy difference is then estimated as

$$\Delta\mathcal{F}_{BA} = -\beta^{-1} \ln \frac{\left\langle e^{-\beta\left(\mathcal{V}_B - \mathcal{V}_R\right)}\right\rangle_R}{\left\langle e^{-\beta\left(\mathcal{V}_A - \mathcal{V}_R\right)}\right\rangle_R}. \tag{14.166}$$

A reference state Hamiltonian which allows sampling of both $\rho_A\left(\Delta\mathcal{V}; \Delta\mathcal{V}_{BA}\right)$ and $\rho_B\left(\Delta\mathcal{V}; \Delta\mathcal{V}_{BA}\right)$ reads[150–152]

$$\mathcal{V}_R(\boldsymbol{r}) = -\beta^{-1} \ln\left\{e^{-\beta\left(\mathcal{V}_A(\mathbf{r}) - E_A^R\right)} + e^{-\beta\left(\mathcal{V}_B(\mathbf{r}) - E_B^R\right)}\right\}, \tag{14.167}$$

where E_A^R and E_B^R are energy offset parameters. If the important parts of configuration space of A and B lie far apart, regions of phase space important to A and to B will be separated by a high barrier on the potential energy surface of the reference state.

14.9.1. EDS with smoothness parameter s. To lower the energy barrier between the states, a dimensionless smoothness parameter $s > 0$ can be introduced:[153]

$$\mathcal{V}_R(\boldsymbol{r}) = -\left(\beta s\right)^{-1} \ln\left\{e^{-\beta s\left(\mathcal{V}_A(\mathbf{r}) - E_A^R\right)} + e^{-\beta s\left(\mathcal{V}_B(\mathbf{r}) - E_B^R\right)}\right\}, \tag{14.168}$$

In practice, the statistical efficiency[154] strongly depends on the chosen smoothness parameter s.[155] In order to ensure efficient sampling of the regions of phase space important to state A and those important to state B, the barrier can be decreased by lowering s ($s > 0$).

In order to estimate multiple free energy differences from a single simulation the reference state Hamiltonian has to be generalized to multiple EDS states. Currently three different ways of doing this are implemented in MD++. All presented Hamiltonians reduce to Eq. 14.167 for two EDS states. A generalized reference state that uses a single smoothness parameter reads[150–153]

$$\mathcal{V}_R(\boldsymbol{r}) = -\left(\beta s\right)^{-1} \ln\left\{\sum_{i=1}^{\mathcal{N}^{(s)}} e^{-\beta s\left(\mathcal{V}_i(\mathbf{r}) - E_i^R\right)}\right\}, \tag{14.169}$$

where $\mathcal{N}^{(s)}$ is the number of EDS states. The corresponding equations of motion read

$$\dot{\boldsymbol{r}}_k(t) = m^{-1}\boldsymbol{p}_k(t) \tag{14.170}$$

$$\begin{aligned}
\dot{\boldsymbol{p}}_k(t) &= \boldsymbol{f}_k(t) = \left(-\frac{\partial \mathcal{V}_R(\boldsymbol{r})}{\partial \boldsymbol{r}_k}\right) \\
&= \sum_{i=1}^{\mathcal{N}^{(s)}} \left\{ \frac{e^{-\beta s\left(\mathcal{V}_i(\boldsymbol{r})-E_i^R\right)}}{\sum_{j=1}^{\mathcal{N}^{(s)}} e^{-\beta s\left(\mathcal{V}_j(\boldsymbol{r})-E_j^R\right)}} \left(-\frac{\partial \mathcal{V}_i(\boldsymbol{r})}{\partial \boldsymbol{r}_k}\right) \right\} \\
&= \sum_{i=1}^{\mathcal{N}^{(s)}} \left\{ \left[\sum_{j=1, j\neq i}^{\mathcal{N}^{(s)}} e^{-\beta s\left(\Delta\mathcal{V}_{ji}(\boldsymbol{r})-\Delta E_{ji}^R\right)} + 1 \right]^{-1} \left(-\frac{\partial \mathcal{V}_i(\boldsymbol{r})}{\partial \boldsymbol{r}_k}\right) \right\},
\end{aligned} \tag{14.171}$$

with $\Delta\mathcal{V}_{ji}(\boldsymbol{r}) = \mathcal{V}_j(\boldsymbol{r}) - \mathcal{V}_i(\boldsymbol{r})$ and $\Delta E_{ji}^R = E_j^R - E_i^R$. Employing a single smoothness parameter s can be problematic if the important parts of phase space of some states lie far apart (requiring a low s parameter) and that of others are close (allowing a higher s parameter). Therefore, a generalized reference state that employs $\mathcal{N}^{(s)}(\mathcal{N}^{(s)}-1)/2$ pairwise smoothness parameters s_{ij} can be defined[156]

$$\mathcal{V}_R(\boldsymbol{r}) = -\frac{1}{\beta}\ln\left\{ \left[\sum_{i=1}^{\mathcal{N}^{(s)}-1} \sum_{j>i}^{\mathcal{N}^{(s)}} \left(e^{-\beta s_{ij}\left(\mathcal{V}_i(\boldsymbol{r})-E_i^R\right)} + e^{-\beta s_{ij}\left(\mathcal{V}_j(\boldsymbol{r})-E_j^R\right)} \right)^{\frac{1}{s_{ij}}} \right] \frac{1}{\mathcal{N}^{(s)}-1} \right\}, \tag{14.172}$$

with the corresponding equations of motion

$$\dot{\boldsymbol{r}}_k(t) = m^{-1}\boldsymbol{p}_k(t) \tag{14.173}$$

$$\begin{aligned}
&\dot{\boldsymbol{p}}_k(t) = \boldsymbol{f}_k(t) = \left(-\frac{\partial \mathcal{V}_R(\boldsymbol{r})}{\partial \boldsymbol{r}_k}\right) \\
&= \sum_{i=1}^{\mathcal{N}^{(s)}-1} \sum_{j>i}^{\mathcal{N}^{(s)}} \left\{ \frac{\left(e^{-\beta s_{ij}\left(\mathcal{V}_i(\boldsymbol{r})-E_i^R\right)} + e^{-\beta s_{ij}\left(\mathcal{V}_j(\boldsymbol{r})-E_j^R\right)} \right)^{\frac{1}{s_{ij}}}}{\sum_{l=1}^{\mathcal{N}^{(s)}-1} \sum_{m>l}^{\mathcal{N}^{(s)}} \left(e^{-\beta s_{lm}\left(\mathcal{V}_l(\boldsymbol{r})-E_l^R\right)} + e^{-\beta s_{lm}\left(\mathcal{V}_m(\boldsymbol{r})-E_m^R\right)} \right)^{\frac{1}{s_{lm}}}} \right.
\end{aligned}$$

$$\left. \cdot \left[\frac{\left(-\partial \mathcal{V}_i(\boldsymbol{r})/\partial \boldsymbol{r}_k\right)}{1 + e^{-\beta s_{ij}\left(\Delta\mathcal{V}_{ji}(\boldsymbol{r})-\Delta E_{ji}^R\right)}} + \frac{\left(-\partial \mathcal{V}_j(\boldsymbol{r})/\partial \boldsymbol{r}_k\right)}{1 + e^{+\beta s_{ij}\left(\Delta\mathcal{V}_{ji}(\boldsymbol{r})-\Delta E_{ji}^R\right)}} \right] \right\}. \tag{14.174}$$

However, only $(\mathcal{N}^{(s)}-1)$ s_{ij} parameters are necessary to connect all states with each other. Imagine that the "closest path" from A to C is via B. Then it would suffice to adapt s_{AB} and s_{BC} instead of introducing a (possibly very low) s_{AC}. This idea has been pursued in the third reference state Hamiltonian[156]

$$\mathcal{V}_R(\mathbf{r}) = -\frac{1}{\beta}\ln\left\{ \left[\sum_{\substack{(\mathcal{N}^{(s)}-1) \\ i,j\ pairs}} \left(e^{-\beta s_{ij}\left(\mathcal{V}_i(\boldsymbol{r})-E_i^R\right)} + \quad e^{-\beta s_{ij}\left(\mathcal{V}_j(\boldsymbol{r})-E_j^R\right)} \right)^{\frac{1}{s_{ij}}} \right] \frac{\mathcal{N}^{(s)}}{2(\mathcal{N}^{(s)}-1)} \right\}, \tag{14.175}$$

with the corresponding equations of motion

$$\dot{\boldsymbol{r}}_k(t) = m^{-1}\boldsymbol{p}_k(t) \tag{14.176}$$

$$\begin{aligned}
&\dot{\boldsymbol{p}}_k(t) = \boldsymbol{f}_k(t) = \left(-\frac{\partial \mathcal{V}_R(\boldsymbol{r})}{\partial \boldsymbol{r}_k}\right) \\
&= \sum_{\substack{(\mathcal{N}^{(s)}-1) \\ i,j\ pairs}} \left\{ \frac{\left(e^{-\beta s_{ij}\left(\mathcal{V}_i(\boldsymbol{r})-E_i^R\right)} + e^{-\beta s_{ij}\left(\mathcal{V}_j(\boldsymbol{r})-E_i^R\right)} \right)^{\frac{1}{s_{ij}}}}{\sum_{\substack{(\mathcal{N}^{(s)}-1) \\ l,m\ pairs}} \left(e^{-\beta s_{lm}\left(\mathcal{V}_l(\boldsymbol{r})-E_l^R\right)} + e^{-\beta s_{lm}\left(\mathcal{V}_m(\boldsymbol{r})-E_m^R\right)} \right)^{\frac{1}{s_{lm}}}} \right.
\end{aligned}$$

$$\cdot \left[\frac{(-\partial \mathcal{V}_i(\boldsymbol{r})/\partial \boldsymbol{r}_k)}{1+e^{-\beta s_{ij}\left(\Delta\mathcal{V}_{ji}(\boldsymbol{r})-\Delta E^R_{ji}\right)}} + \frac{(-\partial \mathcal{V}_j(\boldsymbol{r})/\partial \boldsymbol{r}_k)}{1+e^{+\beta s_{ij}\left(\Delta\mathcal{V}_{ji}(\boldsymbol{r})-\Delta E^R_{ji}\right)}} \right] \Bigg\} . \tag{14.177}$$

Here, the sum is only performed over $(\mathcal{N}^{(s)}-1)$ pairs. The $(\mathcal{N}^{(s)}-1)$ pairs are chosen from all $\mathcal{N}^{(s)}(\mathcal{N}^{(s)}-1)/2$ pairs such that a maximum spanning tree of s_{ij} parameters is obtained. That is, only those EDS end states that show the closest "distance" in phase space (i.e. allow for the largest s_{ij}) are directly connected.

Although the three reference state Hamiltonians (Eq. 14.169, Eq. 14.172, Eq. 14.175) are of increasing complexity, the computational effort in an MD simulation employing these Hamiltonians is comparable. This is due to the fact that the bottleneck of the computation is not the combination of the end state energies and forces to obtain the reference state potential energy (Eq. 14.169, Eq. 14.172, Eq. 14.175) and forces (Eq. 14.171, Eq. 14.174, Eq. 14.177), respectively, but the computation of these end state energies and forces themselves.

In order to limit the computational effort, the unperturbed interactions are calculated only once at each time step, i.e. are not unnecessarily recalculated for each of the $\mathcal{N}^{(s)}$EDS Hamiltonian terms. Only the perturbed interactions are calculated at every time step for each of the $\mathcal{N}^{(s)}$EDS Hamiltonian terms. The overhead of an EDS calculation compared to a single, standard MD simulation is, therefore, determined by the size of the perturbed part of the system. If the number of unperturbed interactions is larger than the number of perturbed interactions, an EDS simulation of $\mathcal{N}^{(s)}$ states will take less computing time than $\mathcal{N}^{(s)}$ independent non-EDS molecular dynamics simulations. If the number of perturbed interactions is very large, the number of states is small, and the conformational changes involved in the perturbations are big, standard staging methods such as thermodynamic integration (see Sec. 14.6) would be the method of choice. EDS will work also in these cases but is not likely to be more efficient than standard approaches. However, often one is interested in perturbations involving many states, with a rather small number of perturbed interactions, and rather local conformational changes. A prototypical example would be the binding of many distinct ligands to a common receptor. Here, the number of perturbed interactions is much smaller than the number of unperturbed interactions and performing an EDS simulation will be more efficient than performing all simulations independently. Unlike in staging approaches such as TI no simulations at "unphysical" intermediate states are performed. Although the reference state itself is an "unphysical" intermediate state, it is constructed such that the sampling is focused on configurations which are of importance to the end states.

14.9.2. Accelerated EDS. Since modification of $\mathcal{V}_R(\boldsymbol{r})$ with the smoothness parameter s leads to distortion of the original energy minima with respect to the coordinates,[153] a different approach based on Accelerated MD[157,158] can be chosen to lower large potential energy barriers between end-states. The continuous accelerated EDS Hamiltonian $\mathcal{V}^*_R(\boldsymbol{r})$ smoothened with a harmonic potential energy function which preserves local energy minima reads[159,160]

$$\mathcal{V}^*_R(\boldsymbol{r}) = \begin{cases} \mathcal{V}_R(\boldsymbol{r}) - \frac{E_{max}-E_{min}}{2}, & \text{for } \mathcal{V}_R(\boldsymbol{r}) \geq E_{max} \\ \mathcal{V}_R(\boldsymbol{r}) - \frac{1}{2(E_{max}-E_{min})}\left(\mathcal{V}_R(\boldsymbol{r})-E_{min}\right)^2, & \text{for } E_{max} > \mathcal{V}_R(\boldsymbol{r}) > E_{min} \\ \mathcal{V}_R(\boldsymbol{r}), & \text{for } \mathcal{V}_R(\boldsymbol{r}) \leq E_{min} \end{cases} \tag{14.178}$$

where $\mathcal{V}_R(\boldsymbol{r})$ is the non-accelerated EDS Hamiltonian given by Eq. 14.167, E_{max} and E_{min} are the maximum and minimum borders of the accelerated region of the EDS Hamiltonian, respectively. The accelerated EDS equations of motion read

$$\dot{\boldsymbol{r}}_k(t) = m^{-1}\boldsymbol{p}_k(t) \tag{14.179}$$

$$\begin{aligned} \dot{\boldsymbol{p}}_k(t) &= \boldsymbol{f}_k(t) = \left(-\frac{\partial \mathcal{V}^*_R(\boldsymbol{r})}{\partial \boldsymbol{r}_k}\right) \\ &= \begin{cases} -\frac{\partial \mathcal{V}_R(\boldsymbol{r})}{\partial \boldsymbol{r}_k}\left(\frac{E_{max}-\mathcal{V}_R(\boldsymbol{r})}{E_{max}-E_{min}}\right), & \text{for } E_{max} > \mathcal{V}_R(\boldsymbol{r}) > E_{min} \\ -\frac{\partial \mathcal{V}_R(\boldsymbol{r})}{\partial \boldsymbol{r}_k}, & \text{for } \mathcal{V}_R(\boldsymbol{r}) \geq E_{max}, \mathcal{V}_R(\boldsymbol{r}) \leq E_{min} \end{cases} \end{aligned} \tag{14.180}$$

where $-\frac{\partial \mathcal{V}_R(\boldsymbol{r})}{\partial \boldsymbol{r}_k}$ is the negative derivative of the non-accelerated EDS Hamiltonian given by Eq. 14.171 with a smoothness parameter $s = 1$.

Adequate accelerated EDS parameters E_{max}, E_{min} and energy offset parameters E_i^R can be determined simultaneously during a non-equilibrium parameter search simulation in which the EDS Hamiltonian is explored freely and EDS parameters are adjusted on-the-fly. An end-state is currently sampled by the EDS Hamiltonian if its energy $\left(\mathcal{V}_i(\mathbf{r}) - E_i^R\right)$ is minimal. If an end-state is sampled, its average energy $\overline{\mathcal{V}_i(\mathbf{r}) - E_i^R}$ and standard deviaton of the energy $\sigma_{\mathcal{V}_i(\mathbf{r})}$ are calculated. Moreover, the average of the maximum transition energy between states within a state-visit period (a state-visit period is defined as having seen all states at least once), $E_{max}^{\ddagger}$, is calculated. The maximum potential energy barrier between any end-states is now given by

$$\Delta E_{max} = E_{max}^{\ddagger} - \min\left(\overline{\mathcal{V}_i(\mathbf{r}) - E_i^R}\right). \tag{14.181}$$

The upper border for the accelerated region of the EDS Hamiltonian is $E_{max}^{\ddagger}$

$$E_{max} = E_{max}^{\ddagger} \tag{14.182}$$

and the lower border for the accelerated region is calculated such that the maximum potential energy barrier in an accelerated EDS Hamiltonian $\mathcal{V}_R^*(\boldsymbol{r})$ is reduced to a value ΔE_{max}^*. This value can be chosen to be a multiple of the standard deviation $\sigma_{\mathcal{V}_i(\mathbf{r})}$ of the energy of the end-state with the lowest average energy $\min\left(\overline{\mathcal{V}_i(\mathbf{r}) - E_i^R}\right)$.**[160]** The lower border E_{min} reads

$$E_{min} = 2\left\{\min\left(\overline{\mathcal{V}_i(\mathbf{r}) - E_i^R}\right) + \Delta E_{max}^*\right\} - E_{max}^{\ddagger}. \tag{14.183}$$

If E_{min} calculated according to Eq. 14.183 is smaller than $\min\left(\overline{\mathcal{V}_i(\mathbf{r}) - E_i^R}\right)$, it is given by

$$E_{min} = \frac{2E_{max}^{\ddagger}\Delta E_{max}^* + 2E_{max}^{\ddagger}\min\left(\overline{\mathcal{V}_i(\mathbf{r}) - E_i^R}\right) - \left(E_{max}^{\ddagger}\right)^2 - \min\left(\overline{\mathcal{V}_i(\mathbf{r}) - E_i^R}.\right)^2}{2\Delta E_{max}^*}. \tag{14.184}$$

The EDS energy offset parameters E_i^R are calculated explicitly from the free-energy differences between the single end-states with accelerated Hamiltonians $\mathcal{V}_i^*(\boldsymbol{r})$**[160]** which read

$$\mathcal{V}_i^*(\boldsymbol{r}) = \begin{cases} \mathcal{V}_i(\boldsymbol{r}) - \frac{E_{max}-E_{min}}{2}, & \text{for } \mathcal{V}_i(\boldsymbol{r}) \geq E_{max} + E_i^R \\ \mathcal{V}_i(\boldsymbol{r}) - \frac{1}{2(E_{max}-E_{min})}\left(\mathcal{V}_i(\boldsymbol{r}) - E_{min} - E_i^R\right)^2, & \text{for } E_{max} + E_i^R > \mathcal{V}_i(\boldsymbol{r}) > E_{min} + E_i^R \\ \mathcal{V}_i(\boldsymbol{r}), & \text{for } \mathcal{V}_i(\boldsymbol{r}) \leq E_{min} + E_i^R \end{cases} \tag{14.185}$$

The energy offset of the first state is arbitrarily set to zero ($E_1^R = 0$) and all other energy offset parameters $E_{i\neq 1}^R$ are calculated by free energy perturbation given in Eq. 14.6

$$E_{i\neq 1}^R = -k_B T \ln\left(\left\langle e^{-[\mathcal{V}_{i\neq 1}^*(\boldsymbol{r}) - \mathcal{V}_R^*(\boldsymbol{r})]/k_B T}\right\rangle_R\right) + k_B T \ln\left(\left\langle e^{-[\mathcal{V}_1^*(\boldsymbol{r}) - \mathcal{V}_R^*(\boldsymbol{r})]/k_B T}\right\rangle_R\right). \tag{14.186}$$

To allow for faster adjustment of the energy offset parameters during the parameter search simulation, a *memory relaxation time* $\tau_{\Delta\mathcal{V}}$**[58]** is implemented for the exponential averages of the potential energy differences in analogy to the time-averaged distance restraining function described in Eq. 9.14. The exponential potential energy differences with a characteristic memory decay time $\tau_{\Delta\mathcal{V}}$ read

$$\begin{aligned} \langle e^{-[\mathcal{V}_i^*(\boldsymbol{r}) - \mathcal{V}_R^*(\boldsymbol{r})]/k_B T}\rangle_t &= \left(1 - e^{-\Delta t/\tau_{\Delta\mathcal{V}}}\right) e^{-[\mathcal{V}_i^*(\boldsymbol{r}) - \mathcal{V}_R^*(\boldsymbol{r})]/k_B T}(t) \\ &+ e^{-\Delta t/\tau_{\Delta\mathcal{V}}} \langle e^{-[\mathcal{V}_i^*(\boldsymbol{r}) - \mathcal{V}_R^*(\boldsymbol{r})]/k_B T}\rangle_{t-\Delta t}, \end{aligned} \tag{14.187}$$

where t is the simulation time and Δt the simulation time-step. In MD++, the memory decay time $\tau_{\Delta\mathcal{V}}$ can be linearly interpolated over time between two values $\tau^A_{\Delta\mathcal{V}}$ at the beginning of the simulation run and $\tau^B_{\Delta\mathcal{V}}$ at the end of the simulation run:

$$\tau_{\Delta\mathcal{V}} = \tau^A_{\Delta\mathcal{V}} + \left(\tau^B_{\Delta\mathcal{V}} - \tau^A_{\Delta\mathcal{V}}\right)\frac{t}{t_{tot}}. \tag{14.188}$$

Here, t_{tot} is the total simulation time of the run. This is especially useful for systems in which the energy offset parameters are very large. In such cases, $\tau^A_{\Delta\mathcal{V}}$ can be set to a small value to allow for rapid adjustment of the energy offset parameters at the beginning of the parameter search simulation, while more statistics are used upon convergence of the energy offset parameters towards the end of the parameter search simulation.

14.9.3. Twin-system EDS. A drawback of the thermodynamic cycle shown in Fig. 14.1 is that the accuracy of $\Delta\Delta\mathcal{F}_{43} = \Delta\Delta\mathcal{F}_{21}$ can be low if two large, almost equal numbers, are subtracted, e.g. due to a change in charge state or partial charges between I_1 and I_2. This problem can be avoided by an alternative choice of the thermodynamic cycle, shown in Fig. 14.3, in which (i) one state combines the free state and computational box for one ligand with the bound state and computational box for the other ligand, and (ii) the two processes of changing ligand I_1 into I_2 in these free and bound states are carried out in opposite directions.[161] This process directly yields $\Delta\Delta\mathcal{F}_{21}$ and may lead to a smaller change of the energy of the combined state. In Fig. 14.3, the round brackets denote a periodic computational box with a particular ligand in water (free) or with a particular ligand bound to the protein in water (bound). The rectangular brackets denote that the two computational boxes are to be combined into one state or Hamiltonian,

$$\begin{aligned}\mathcal{H}_A &= \mathcal{H}\left(I_2; free\right) + \mathcal{H}\left(E; I_1; bound\right) \\ \mathcal{H}_B &= \mathcal{H}\left(I_1; free\right) + \mathcal{H}\left(E; I_2; bound\right)\end{aligned} \tag{14.189}$$

Using EDS this process can be simulated for a pair of states A and B and two computational boxes 1 and 2, employing the reference state Hamiltonian

$$\mathcal{V}_R\left(\boldsymbol{r}\right) = -\left(\beta s\right)^{-1}\ln\left\{e^{\left[-\beta s\left(\mathcal{V}_{A1}(\mathbf{r})+\mathcal{V}_{A2}(\mathbf{r})-E^R_A\right)\right]} + e^{\left[-\beta s\left(\mathcal{V}_{B1}(\mathbf{r})+\mathcal{V}_{B2}(\mathbf{r})-E^R_B\right)\right]}\right\}, \tag{14.190}$$

where $\mathcal{V}_{Xi}\left(\boldsymbol{r}\right)$ is the potential energy part corresponding to box i of the Hamiltonian $\mathcal{H}_X\left(\boldsymbol{p},\boldsymbol{r}\right)$. The corresponding equations of motion read

$$\dot{\boldsymbol{r}}_k(t) = m^{-1}\boldsymbol{p}_k(t) \tag{14.191}$$

$$\begin{aligned}\dot{\boldsymbol{p}}_k(t) &= \boldsymbol{f}_k(t) = \left(-\frac{\partial\mathcal{V}_R(\boldsymbol{r})}{\partial\boldsymbol{r}_k}\right) \\ &= \left[e^{-\beta s\left(\mathcal{V}_{B1}(\mathbf{r})+\mathcal{V}_{B2}(\mathbf{r})-\left(\mathcal{V}_{A1}(\mathbf{r})+\mathcal{V}_{A2}(\mathbf{r})\right)-\Delta E^R_{BA}\right)}+1\right]^{-1}\left(-\frac{\partial\left(\mathcal{V}_{A1}(\boldsymbol{r})+\mathcal{V}_{A2}(\boldsymbol{r})\right)}{\partial\boldsymbol{r}_k}\right) \\ &\quad + \left[e^{+\beta s\left(\mathcal{V}_{B1}(\mathbf{r})+\mathcal{V}_{B2}(\mathbf{r})-\left(\mathcal{V}_{A1}(\mathbf{r})+\mathcal{V}_{A2}(\mathbf{r})\right)-\Delta E^R_{BA}\right)}+1\right]^{-1}\left(-\frac{\partial\left(\mathcal{V}_{B1}(\boldsymbol{r})+\mathcal{V}_{B2}(\boldsymbol{r})\right)}{\partial\boldsymbol{r}_k}\right).\end{aligned} \tag{14.192}$$

Because the potential energy of box 1 does not depend on the configurations in box 2 and vice versa,

$$\begin{aligned}\frac{\partial\mathcal{V}_{A2}(\boldsymbol{r})}{\partial\boldsymbol{r}_k} = \frac{\partial\mathcal{V}_{B2}(\boldsymbol{r})}{\partial\boldsymbol{r}_k} = 0 \qquad &\text{for particles } k \text{ in system 1} \\ \frac{\partial\mathcal{V}_{A1}(\boldsymbol{r})}{\partial\boldsymbol{r}_k} = \frac{\partial\mathcal{V}_{B1}(\boldsymbol{r})}{\partial\boldsymbol{r}_k} = 0 \qquad &\text{for particles } k \text{ in system 2}\end{aligned} \tag{14.193}$$

Therefore, the coupling of the two boxes only occurs via the prefactors.

14.9.4. Configurational EDS. The EDS method can also be used to obtain the relative free energy of different conformations or configurational states. Assume we wish to calculate the free enthalpy difference between two conformations, α and β, of a molecule, and one or both of them is not the most stable one of the molecule. We may use the EDS technique to obtain the free enthalpy difference by defining the EDS reference Hamiltonian as follows. Two restraining energy function terms are defined which restrain the molecular conformations to conformation α or to conformation β, *i.e.*, $\mathcal{V}^{rest}_X(\boldsymbol{r}^N; K^{rest}_X, \boldsymbol{r}^N_{0,\xi})$ where X = A or B and $\boldsymbol{r}^N_{0,\xi}$ is the set of parameters which characterizes the conformation ξ, $\xi = \alpha$ or β, *e.g.*,

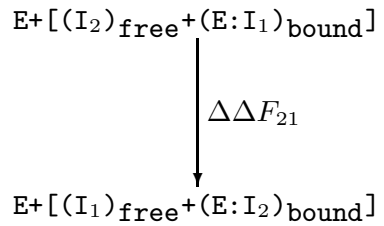

FIGURE 14.3. Alternative thermodynamic cycle with respect to the relative binding of two inhibitors I_1 and I_2 to an enzyme E. The symbol ':' indicates complexation.

through particular hydrogen-bond distance ranges or torsional-angle ranges, and K_X^{rest} is the restraining force constant. Thus, the resulting Hamiltonian for the end state X is

$$\mathcal{V}_X(\boldsymbol{r}^N) = \mathcal{V}_X^{rest}(\boldsymbol{r}^N; k_X^{rest}, \boldsymbol{r}_{0\xi}^N) + \mathcal{V}^{(phys)}(\boldsymbol{r}^N) \tag{14.194}$$

where $\mathcal{V}^{(phys)}(\boldsymbol{r}^N)$ is the interaction function of a particular force field. Then, we may construct an EDS reference-state Hamiltonian:

$$\begin{aligned} \mathcal{V}_R(\boldsymbol{r}^N; s, E_{BA}^R) &= -\beta^{-1}s^{-1}\ln\left\{e^{-\beta s(\mathcal{V}_A^{rest}(\boldsymbol{r}^N)-E_A^R)} + e^{-\beta s(\mathcal{V}_B^{rest}(\boldsymbol{r}^N)-E_B^R)}\right\} + \mathcal{V}^{(phys)}(\boldsymbol{r}^N) \\ &= \mathcal{V}^{\mathrm{EDS},rest}(\boldsymbol{r}^N; s, E_{BA}^R) + \mathcal{V}^{(phys)}(\boldsymbol{r}^N) \end{aligned} \tag{14.195}$$

where s is a smoothness parameter and $E_B^R - E_A^R = E_{BA}^R$ is an energy offset parameter difference, which are chosen such as to optimize the sampling of both end states A and B. In the original EDS implementation, the configurations $\boldsymbol{r}^N$ that are sampled by the reference Hamiltonian $\mathcal{H}_R$, *i.e.*, $\mathcal{V}_R$, are not assigned to any conformational states. They are considered[90] to belong to state A if

$$\mathcal{V}_A^{rest}(\boldsymbol{r}^N) - E_A^R) < (\mathcal{V}_B^{rest}(\boldsymbol{r}^N) - E_B^R) \tag{14.196}$$

In the case considered here, configurations must be separated into different sets, *i.e.*, different conformational states: they belong to set α if

$$\mathcal{V}_A^{rest}(\boldsymbol{r}^N) \leq E_\alpha^{thres} \text{ and } \mathcal{V}_B^{rest}(\boldsymbol{r}^N) > E_\beta^{thres} \tag{14.197}$$

they belong to set β if

$$\mathcal{V}_A^{rest}(\boldsymbol{r}^N) > E_\alpha^{thres} \text{ and } \mathcal{V}_B^{rest}(\boldsymbol{r}^N) \leq E_\beta^{thres} \tag{14.198}$$

or they may belong to neither of them, called sets γ and δ with set γ defined by

$$\mathcal{V}_A^{rest}(\boldsymbol{r}^N) > E_\alpha^{thres} \text{ and } \mathcal{V}_B^{rest}(\boldsymbol{r}^N) > E_\beta^{thres} \tag{14.199}$$

and set δ defined by

$$\mathcal{V}_A^{rest}(\boldsymbol{r}^N) \leq E_\alpha^{thres} \text{ and } \mathcal{V}_B^{rest}(\boldsymbol{r}^N) \leq E_\beta^{thres} \tag{14.200}$$

Generally, set δ should contain no or only a few configurations in order to make a meaningful distinction between sets α and β. Here, the configurations that belong to sets α and β are defined via an energy threshold criterion E_ξ^{thres}, which maps configurations $\boldsymbol{r}^N$ onto an energy $\mathcal{V}_X^{rest}(\boldsymbol{r}^N)$ using the same function $\mathcal{V}_X^{rest}(\boldsymbol{r}^N)$ that is used in the reference Hamiltonian. This means that the configurations that belong to sets α and β are defined through Eqs. 14.197 and 14.198, respectively. We note that these sets α and β differ from the conformational ensembles A and B that are through the end-state Hamiltonians defined by Eq. 14.194. Alternatively, the conformational sets α and β could be defined using a geometric measure such as an atom-positional root-mean-square deviation (RMSD) from a given configuration, either in Cartesian

or in internal torsional coordinates, instead of using the restraining functions $\mathcal{V}_X^{rest}$ and threshold energies E_ξ^{thres}. Configurations then belong to set α if

$$\mathrm{RMSD}(\boldsymbol{r}^N, \boldsymbol{r}_\alpha^N) \leq \mathrm{RMSD}_\alpha^{thres} \text{ and } \mathrm{RMSD}(\boldsymbol{r}^N, \boldsymbol{r}_\beta^N) > \mathrm{RMSD}_\beta^{thres} \tag{14.201}$$

they belong to set β if

$$\mathrm{RMSD}(\boldsymbol{r}^N, \boldsymbol{r}_\alpha^N) > \mathrm{RMSD}_\alpha^{thres} \text{ and } \mathrm{RMSD}(\boldsymbol{r}^N, \boldsymbol{r}_\beta^N) \leq \mathrm{RMSD}_\beta^{thres} \tag{14.202}$$

or they belong to neither of them, called sets γ and δ:

$$\gamma : \mathrm{RMSD}(\boldsymbol{r}^N, \boldsymbol{r}_\alpha^N) > \mathrm{RMSD}_\alpha^{thres} \text{ and } \mathrm{RMSD}(\boldsymbol{r}^N, \boldsymbol{r}_\beta^N) > \mathrm{RMSD}_\beta^{thres} \tag{14.203}$$

$$\delta : \mathrm{RMSD}(\boldsymbol{r}^N, \boldsymbol{r}_\alpha^N) \leq \mathrm{RMSD}_\alpha^{thres} \text{ and } \mathrm{RMSD}(\boldsymbol{r}^N, \boldsymbol{r}_\beta^N) \leq \mathrm{RMSD}_\beta^{thres} \tag{14.204}$$

Again, the thresholds $\mathrm{RMSD}_\xi^{thres}$ should be chosen such that set δ contains no or only a few configurations. In the procedure and expressions used in the optimization of the parameters s and $E_B^R = E_{BA}^R$ (E_A^R is standardly set to zero in two-state EDS), configurations that belong to sets γ and δ can be ignored. Thus, we get for updating the energy offset E_B^R (corresponds to eq 13 of ref[155]):

$$E_B^R(new) = -\frac{1}{\beta} \ln \left\langle \left\{ e^{-\beta(\mathcal{V}_A^{rest} - \mathcal{V}_B^{rest} + E_B^R(old))} + 1 \right\}^{-1} \right\rangle_{R,not\gamma,not\delta} + E_B^R(old) \tag{14.205}$$

where configurations of sets γ and δ are excluded when calculating the ensemble average over the ensemble of the reference state R. For updating or rather choosing a new s parameter, we calculate

$$s_A = -\left\{ \ln \left\langle e^{-\beta(|\mathcal{V}_B^{rest} - \mathcal{V}_A^{rest}| - E_{BA}^R)} \right\rangle_A \right\}^{-1} \tag{14.206}$$

and

$$s_B = -\left\{ \ln \left\langle e^{-\beta(|\mathcal{V}_A^{rest} - \mathcal{V}_B^{rest}| + E_{BA}^R)} \right\rangle_B \right\}^{-1} \tag{14.207}$$

and take the lowest s value as the new s

$$s = \min(s_A, s_B) \tag{14.208}$$

which corresponds to eq 14 of ref[155]. Ensembles A and B are obtained by reweighting the configurations generated using the reference state R to the corresponding end state A or B. For a quantity $Q(\boldsymbol{r}^N)$, which is a function of the coordinates $\boldsymbol{r}^N$, we have

$$\langle Q \rangle_X = \frac{\int Q(\boldsymbol{r}^N) e^{-\beta \mathcal{V}_X(\boldsymbol{r}^N)} d\boldsymbol{r}^N}{\int e^{-\beta \mathcal{V}_X(\boldsymbol{r}^N)} d\boldsymbol{r}^N} \tag{14.209}$$

or using the ensemble R

$$\langle Q \rangle_X = \frac{\left\langle Q e^{-\beta(\mathcal{V}_X - \mathcal{V}_R)} \right\rangle_R}{\left\langle e^{-\beta(\mathcal{V}_X - \mathcal{V}_R)} \right\rangle_R} \tag{14.210}$$

Subsequently, the ensemble averaging in Eq. 14.210 could be restricted to the sets α and β. In that case, these restricted ensemble averages can be written as

$$\langle Q \rangle_A = \frac{\left\langle Q e^{-\beta(\mathcal{V}_A - \mathcal{V}_R)} \right\rangle_{R,not\gamma,not\delta}}{\left\langle e^{-\beta(\mathcal{V}_A - \mathcal{V}_R)} \right\rangle_{R,not\gamma,not\delta}} \tag{14.211}$$

$$= \frac{\left\langle Q e^{-\beta\left(\mathcal{V}_A^{rest}-\mathcal{V}^{\mathrm{EDS},rest}(s,E_{BA}^R)\right)}\right\rangle_{R,not\gamma,not\delta}}{\left\langle e^{-\beta\left(\mathcal{V}_A^{rest}-\mathcal{V}^{\mathrm{EDS},rest}(s,E_{BA}^R)\right)}\right\rangle_{R,not\gamma,not\delta}}$$

and

$$\langle Q\rangle_B = \frac{\left\langle Q e^{-\beta(\mathcal{V}_B-\mathcal{V}_R)}\right\rangle_{R,not\gamma,not\delta}}{\left\langle e^{-\beta(\mathcal{V}_B-\mathcal{V}_R)}\right\rangle_{R,not\gamma,not\delta}} \tag{14.212}$$

$$= \frac{\left\langle Q e^{-\beta\left(\mathcal{V}_B^{rest}-\mathcal{V}^{\mathrm{EDS},rest}(s,E_{BA}^R)\right)}\right\rangle_{R,not\gamma,not\delta}}{\left\langle e^{-\beta\left(\mathcal{V}_B^{rest}-\mathcal{V}^{\mathrm{EDS},rest}(s,E_{BA}^R)\right)}\right\rangle_{R,not\gamma,not\delta}}$$

In this way, erratic irrelevant energy values due to irrelevant configurations not belonging to sets α and β are excluded from influencing the parameter optimization for sampling of sets α and β. Furthermore, configurations which belong to set δ that have low $\mathcal{V}_X^{rest}$ values are excluded too. The free enthalpy difference between two end-state Hamiltonians B and A in the EDS simulation is evaluated through[155]

$$\Delta G_{BA} = G_B - G_A = \Delta G_{BR} - \Delta G_{AR} = -\frac{1}{\beta}\ln\frac{\left\langle e^{-\beta(\mathcal{H}_B-\mathcal{H}_R)}\right\rangle_R}{\left\langle e^{-\beta(\mathcal{H}_A-\mathcal{H}_R)}\right\rangle_R} \tag{14.213}$$

The expression used to obtain the free enthalpy difference between conformational sets β and α from an ensemble generated using the reference-state Hamiltonian $\mathcal{V}_R(\boldsymbol{r}^N; s, E_{BA}^R)$ reads

$$\Delta G_{\beta\alpha} = G_\beta - G_\alpha == -\frac{1}{\beta}\ln\left\{\frac{N_\beta(\mathcal{V}^{(phys)})}{N_\alpha(\mathcal{V}^{(phys)})}\right\} \tag{14.214}$$

where $N_\xi(\mathcal{V}^{(phys)})$ is the number of configurations belonging to set ξ in an ensemble generated using $\mathcal{V}^{(phys)}$. In terms of the ensemble R generated using the reference-state potential energy $\mathcal{V}_R$, we get

$$\Delta G_{\beta\alpha} = -\frac{1}{\beta}\ln\left\{\frac{\left\langle e^{+\beta\mathcal{V}^{\mathrm{EDS},rest}}\right\rangle_{R,set\beta}}{\left\langle e^{+\beta\mathcal{V}^{\mathrm{EDS},rest}}\right\rangle_{R,set\alpha}} \times \frac{N_\beta(\mathcal{V}_R)}{N_\alpha(\mathcal{V}_R)}\right\} \tag{14.215}$$

In other words, the ensemble R that was generated using the biasing potential energy function $\mathcal{V}^{EDS,rest}$ is reweighted using Eq. 14.215, and the configurations of the sets α and β are used in the averaging via their relative populations in the ensemble R, *i.e.*, $N_\alpha(\mathcal{V}_R)$ and $N_\beta(\mathcal{V}_R)$

$$\frac{N_\beta(\mathcal{V}_R)}{N_\alpha(\mathcal{V}_R)} = \frac{\left\langle\delta(\boldsymbol{r}^N-\boldsymbol{r}_\beta^N)\right\rangle_R}{\langle\delta(\boldsymbol{r}^N-\boldsymbol{r}_\alpha^N)\rangle_R} \tag{14.216}$$

Eq. 14.215 can be simply rewritten as

$$\Delta G_{\beta\alpha} = -\frac{1}{\beta}\ln\frac{N_\beta(\mathcal{V}_R)}{N_\alpha(\mathcal{V}_R)} - \frac{1}{\beta}\ln\left\langle e^{+\beta\mathcal{V}^{\mathrm{EDS},rest}}\right\rangle_{R,set\beta} + \frac{1}{\beta}\ln\left\langle e^{+\beta\mathcal{V}^{\mathrm{EDS},rest}}\right\rangle_{R,set\alpha} \tag{14.217}$$

Eq. 14.217 is equivalent to the expression used in conformational state-specific one-step perturbation.[162] In other words, the EDS reference-state Hamiltonian can be used as the reference state in one-step perturbation, ensuring sufficient sampling of the conformational end states, which is reached by optimizing the parameters s and E_{BA}^R . If simulations based on the end state potential energy functions $\mathcal{V}_X(\boldsymbol{r}^N)$, see Eq. 14.194, are

available, these ensembles X = A and X = B can also be used to obtain the free enthalpy difference between conformational sets β and α:[163]

$$\Delta G_{\beta\alpha} = -\frac{1}{\beta} \ln \left\{ \frac{\left\langle e^{+\beta \mathcal{V}_B^{rest}} \right\rangle_{B,set\beta}}{\left\langle e^{+\beta \mathcal{V}_A^{rest}} \right\rangle_{A,set\alpha}} \times \frac{\langle 1 \rangle_{B,set\beta}}{\langle 1 \rangle_{A,set\alpha}} \times \frac{\left\langle e^{-\beta(\mathcal{V}_M - \mathcal{V}_A)} \right\rangle_A}{\left\langle e^{-\beta(\mathcal{V}_M - \mathcal{V}_B)} \right\rangle_B} \right\} \tag{14.218}$$

in which $\mathcal{V}_M$ is an intermediate state connecting two end states. If we use the EDS reference-state Hamiltonian as the intermediate state, the ensemble averages in the last factor of Eq. 14.218 can be written as

$$\left\langle e^{-\beta(\mathcal{V}_M - \mathcal{V}_X)} \right\rangle_X = \left\langle e^{-\beta(\mathcal{V}^{\mathrm{EDS},rest}(s, E_{BA}^R) - \mathcal{V}_X^{rest})} \right\rangle_X \tag{14.219}$$

In[164] it is shown that this type of EDS can be efficiently used to obtain the relative free energy of a rather unstable conformation or fold.

CHAPTER 15

QM/MM simulation

15.1. Introduction

In the combined quantum-mechanical/molecular-mechanical (QM/MM) methodology, the simulated system is divided spatially into a region that is treated quantum-chemically, e.g. the reactive center of a protein, and a region that is described by a molecular-mechanical force field, e.g. the remaining residues of the protein and the solvent.

In this chapter, the following notation is used: a subscript denotes the subsystem or region, QM or MM, that is described while a superscript indicates the type of the Hamiltonian, quantum-mechanical (QM) or classial-mechanical (CM).

15.2. Hamiltonian

The Hamiltonian, $\hat{\mathcal{H}}$, of the simulated system can be written as the sum of the Hamiltonians of the individual QM and MM subsystems and an additional term, $\hat{\mathcal{V}}_{QM/MM}$ describing the interactions between them,

$$\hat{\mathcal{H}} = \hat{\mathcal{H}}_{QM} + \mathcal{H}_{MM} + \hat{\mathcal{V}}_{QM/MM}, \tag{15.1}$$

where $\hat{\mathcal{H}} = \hat{\mathcal{K}} + \hat{\mathcal{V}}$, with $\hat{\mathcal{K}}$ the kinetic energy and $\hat{\mathcal{V}}$ the potential energy term. Here, the quantum operator $\hat{\mathcal{H}}_{MM}$ which contains a function $\mathcal{H}_{MM}$ and the unity operator will be simply denoted as $\mathcal{H}_{MM}$.

The Hamiltonian of the quantum subsystem can be expressed as the sum of a quantum term $\hat{\mathcal{H}}_{QM}^{QM}$ and a classical term $\mathcal{H}_{QM}^{CM}$,

$$\hat{\mathcal{H}}_{QM} = \hat{\mathcal{H}}_{QM}^{QM} + \mathcal{H}_{QM}^{CM}. \tag{15.2}$$

Accordingly, the coupling term, $\hat{\mathcal{V}}_{QM/MM}$, can be written as

$$\hat{\mathcal{V}}_{QM/MM} = \hat{\mathcal{V}}_{QM/MM}^{QM} + \mathcal{V}_{QM/MM}^{CM}. \tag{15.3}$$

It typically takes into account bonded as well as nonbonded interactions between the QM and MM subsystems. *However, the current implementation[165] only holds for noncovalent interactions at the QM/MM boundary.* To evaluate the electrostatic interactions between the QM and MM regions, $\hat{\mathcal{V}}_{QM/MM}^{QM}$, the MM atoms a are included in the QM Hamiltonian as positionally fixed external point charges (electrostatic embedding scheme). When applying the Born–Oppenheimer approximation, the resulting QM Hamiltonian (in atomic units) of the system reads

$$\begin{aligned}
\hat{\mathcal{H}}^{QM} &= \hat{\mathcal{H}}_{QM}^{QM} + \hat{\mathcal{V}}_{QM/MM}^{QM} \\
&= \Big(\sum_e -\tfrac{1}{2}\nabla_e^2 + \sum_e \sum_{e'>e} \tfrac{1}{|\mathbf{r}_{ee'}|} - \sum_n \sum_e \tfrac{Z_n}{|\mathbf{r}_e - \mathbf{R}_n|} \\
&+ \sum_n \sum_{n'>n} \tfrac{Z_n Z_{n'}}{|\mathbf{R}_{nn'}|}\Big) \\
&+ \Big(\sum_n \sum_a \tfrac{Z_n Z_a}{|\mathbf{R}_{na}|} - \sum_e \sum_a \tfrac{Z_a}{|\mathbf{r}_e - \mathbf{R}_a|}\Big),
\end{aligned} \tag{15.4}$$

where e and e' run over QM treated electrons, n and n' run over QM nuclei, Z is the charge of the QM nuclei and MM atoms, respectively and a runs over all MM atoms within a given cutoff $\mathrm{R_{QM/MM}}$ around the QM region or solute. This Hamiltonian is expressed using the standard (non-SI) units commonly used

in the quantum chemistry community. Van der Waals interactions between the QM nuclei and MM atoms, $\mathcal{V}^{CM}_{QM/MM}$ or $\mathcal{V}^{vdW}_{QM/MM}$, are treated on the basis of classical mechanics.

The classical potential energy term of the system is given by

$$\begin{aligned}
\mathcal{V}^{CM}(\mathbf{r}^n,\mathbf{r}^a) &= \mathcal{V}^{CM}_{MM}(\mathbf{r}^a)+\mathcal{V}^{vdW}_{QM/MM}(\mathbf{r}^n,\mathbf{r}^a)+\mathcal{V}^{vdW}_{QM}(\mathbf{r}^n)\\
&= \Big(\textstyle\sum_{\text{bonds i}}\frac{1}{2}K^b_i[b_i-b^0_i]^2+\sum_{\text{bond angles i}}\frac{1}{2}K^\theta_i[\theta_i-\theta^0_i]^2\\
&+ \textstyle\sum_{\text{torsions i}}K^\varphi_i[1+cos[m_i\varphi_i-\delta_i]]+\sum_{\text{improper torsions i}}\frac{1}{2}K^\zeta_i[\zeta_i-\zeta^0_i]^2\\
&+ \textstyle\sum_a\sum_{a'>a}4\epsilon_{aa'}\left[\left(\frac{\sigma_{aa'}}{r_{aa'}}\right)^{12}-\left(\frac{\sigma_{aa'}}{r_{aa'}}\right)^{6}\right]+\sum_a\sum_{a'>a}\frac{1}{4\pi\epsilon_0\epsilon_{cs}}\frac{q_aq'_a}{r_{aa'}}\\
&+ \textstyle\sum_a\sum_{a'>a}\frac{q_aq_{a'}}{4\pi\epsilon_0\epsilon_{cs}}\frac{(-\frac{1}{2}C_{rf}r^2_{aa'})}{R^3_{rf}}+\sum_a\sum_{a'>a}\frac{q_aq_{a'}}{4\pi\epsilon_0\epsilon_{cs}}\frac{(\frac{1}{2}C_{rf}-1)}{R_{rf}}\Big)\\
&+ \left(\textstyle\sum_n\sum_a 4\epsilon_{na}\left[\left(\frac{\sigma_{na}}{r_{na}}\right)^{12}-\left(\frac{\sigma_{na}}{r_{na}}\right)^{6}\right]\right)\\
&+ \left(\textstyle\sum_n\sum_{n'}4\epsilon_{nn'}\left[\left(\frac{\sigma_{nn'}}{r_{nn'}}\right)^{12}-\left(\frac{\sigma_{nn'}}{r_{nn'}}\right)^{6}\right]\right),
\end{aligned} \tag{15.5}$$

where the first four terms describe covalent, bonded interactions with K denoting the particular force constant and the index ^{0} indicating an ideal bond length, angle or torsional angle value[166,167]. The next four terms describe the classical nonbonded interactions within the MM region, namely the van der Waals interactions in the form of a Lennard-Jones term, the electrostatic Coulomb interactions between (partial) atomic charges q, and the distance-dependent and distance-independent interaction terms for the reaction field with R_{rf} being the reaction field cutoff radius. The ninth term accounts for the aforementioned van der Waals interactions between the nuclei of the QM region and the atoms of the MM region and the last term specifies the van der Waals interactions between the nuclei of the QM region.

For the integration of Newton's equations of motion in molecular dynamics simulations, the force on each particle, i, is determined from the gradient of the total potential energy of the system at the position of particle i, where i can be either a QM nucleus or a MM atom,

$$\mathbf{f}_i=-\frac{\partial}{\partial\mathbf{r}_i}\mathcal{V}(\mathbf{r}^n,\mathbf{r}^a). \tag{15.6}$$

Using Eq. 15.4 and Eq. 15.5, the total force on particle i can be written as the sum of the different contributions from the QM and CM Hamiltonians, respectively,

$$\mathbf{f}_i=-\frac{\partial}{\partial\mathbf{r}_i}\mathcal{V}^{QM}(\mathbf{r}^n,\mathbf{r}^a)-\frac{\partial}{\partial\mathbf{r}_i}\mathcal{V}^{CM}(\mathbf{r}^n,\mathbf{r}^a), \tag{15.7}$$

where $\mathcal{V}^{\mathrm{QM}}$ is given by

$$\mathcal{V}^{QM}=\frac{\left\langle\Psi|\hat{\mathcal{H}}^{QM}_{QM}+\hat{\mathcal{V}}^{QM}_{QM/MM}|\Psi\right\rangle}{\langle\Psi|\Psi\rangle}. \tag{15.8}$$

The implementation of the GROMOS QM/MM scheme[165] is based on direct communication between GROMOS and the particular quantum-chemical program via code-integrated interfaces that execute system calls to the particular QM executable of MNDO[168] or TURBOMOLE[169], respectively. A general description of the object-oriented C++ architecture of the GROMOS software can be found in[170]. The QM/MM functionality of GROMOS was implemented in the new class, `QMMM_Interaction`, within the namespace *interaction*. At every MD step, single-point full-SCF calculations are carried out by the specified QM program, MNDO or TURBOMOLE. The GROMOS software automatically generates the program specific input files for the QM calculation including information about the type and position of the QM atoms as well as the position and charges of the MM atoms to be included in the QM Hamiltonian as external point charges. If periodic boundary conditions are applied, the system is gathered beforehand, with respect to the first atom of the list of QM atoms, in order to determine the MM atoms within the specified QM/MM cutoff radius for evaluation of the electrostatic interactions. The charge group based QM/MM cutoff radius is a variable input parameter (*RCUTQ*). Subsequent to the QM calculation, the QM energies and gradients are

extracted from the corresponding output files and converted to SI-like units which are generally used in the GROMOS data files.

15.3. Initialization, simulation and analysis

Preliminary to a GROMOS QM/MM simulation the following change with respect to a conventional GROMOS topology is needed: explicit hydrogen atoms are to be added for the part of the system to be treated quantum-mechanically (no united atoms). During the course of a GROMOS QM/MM simulation GROMOS topological information considering bonded and electrostatic interactions of atoms that are part of the defined QM region will not be used (see Eq. 15.5).

To apply the GROMOS QM/MM functionality the switch $NTQMMM$ has to be set to 1 with $NTQMSW$ being either 0 (MNDO) or 1 (TURBOMOLE). In QM/MM simulation the timestep should be chosen smaller (e.g. 0.5 fs) than in classical MD simulation. If $NTQMMM = 1$, an additional QMMM specification file has to be provided. This file has to contain the specific input parameters for the quantum-chemical program package to be used as well as the paths to their executables.

Analysis of the GROMOS QM/MM trajectories can be performed straightforward using the GROMOS++ program package.

CHAPTER 16

Replica Exchange (RE) Molecular Dynamics

16.1. Introduction

Replica exchange method (REMD)[171–174,175] is developed to enhance sampling of the conformational space. With this technique, a number of replicas of a system that do not interact with each other are simulated simultaneously. These replicas may represent different thermodynamic state points (T-REMD) or different Hamiltonians ($\mathcal{H}$-REMD).

For a system of $\mathcal{N}_a$ atoms of mass m_k (k = 1,...,$\mathcal{N}_a$) with coordinate $\boldsymbol{q} \equiv \{\boldsymbol{q}_1, ..., \boldsymbol{q}_{\mathcal{N}_a}\}$ and momentum vectors $\boldsymbol{p_q} \equiv \{\mathbf{p}_1, ..., \mathbf{p}_{\mathcal{N}_a}\}$, the Hamiltonian $\mathcal{H}(\boldsymbol{q}, \boldsymbol{p_q})$ is the sum of the kinetic energy $\mathcal{K}(\boldsymbol{p_q})$ and the potential energy $\mathcal{V}$ $(\boldsymbol{q})$:

$$\mathcal{H}(\boldsymbol{q}, \boldsymbol{p_q}) = \mathcal{K}(\boldsymbol{p_q}) + \mathcal{V}(\boldsymbol{q}) \tag{16.1}$$

where

$$\mathcal{K}(\boldsymbol{p_q}) = \sum_{k=1}^{\mathcal{N}_a} \frac{\mathbf{p}_k^2}{2m_k} \tag{16.2}$$

In the canonical ensemble of a REMD simulation, the state is specified as

$$\mathrm{X} = \{..., x_m^i, ..., x_n^j, ...\} \tag{16.3}$$

where $x \equiv (\boldsymbol{q}, \boldsymbol{p_q})$, x_m^i the ith replica simulated at the mth condition. The average kinetic energy at temperature T is given by

$$< \mathcal{K}(\boldsymbol{p_q}) >_T \; =< \sum_{k=1}^{\mathcal{N}_a} \frac{\mathbf{p}_k^2}{2m_k} >= \frac{3}{2}\mathcal{N}_a k_B T \tag{16.4}$$

The weight factors for this state is given by the product of Boltzmann factor for individual non-interacting replicas,

$$\mathrm{W_{RE}(X)} = exp\{-\sum_{i=1}^{M} \beta_{m(i)} \mathcal{H}_m(\boldsymbol{q}^{[i]}, \boldsymbol{p_q}^{[i]})\} \tag{16.5}$$

During the simulations, after a predefined time interval, a Monte Carlo exchange between two replicas s' and s'' is attempted with exchange probability

$$P(s' \leftrightarrow s'') = \frac{\mathrm{W}(S'')}{\mathrm{W}(S')} = \frac{\mathrm{w}(S' \leftrightarrow S'')}{\mathrm{w}(S'' \leftrightarrow S')} = exp(-\Delta) \tag{16.6}$$

where Δ is defined as:

T-REMD:

$$\Delta = ((k_B T_{s'})^{-1} - (k_B T_{s''})^{-1})(U(x) - U(x)) \tag{16.7}$$

$\mathcal{H}$-REMD:

$$\Delta = [(U(x_{s''}; \lambda_{s'}) - U(x_{s'}; \lambda s')) - (U(x_{s''}; \lambda_{s''}) - U(x_{s'}; \lambda s''))]/(k_B T) \tag{16.8}$$

16.2. Temperature replica exchange MD

Using T-REMD, N independent copies (replicas) of the systems are propagated simultaneously at different fixed temperatures. At regular time intervals, pairs of replicas at successive temperatures are exchanged according to a Metropolis criterion allowing individual replicas to sample a range of temperatures. At higher temperatures the increased thermal energy facilitates the exploration of conformational space and allows the system to cross barriers that are difficult to cross at the temperature of interest on a given time scale.

Of the *M non-interacting* copies (or replicas) of the original system in the canonical ensemble (NVT) at M different temperatures T_m (m=1,...,M), there is a one-to-one correspondence between replicas (i=1,...,M) and temperatures (m=1,...,M),

$$\mathrm{X} = (x_1^{[i(1)]}, ..., x_M^{[i(M)]}) = (x_{m(1)}^{[1]}, ..., x_{m(M)}^{[M]}) \tag{16.9}$$

where X stands for a "state" in this generalized ensemble, and $x_m^{[i]}$ the replica i at the temperature T_m, and

$$x_m^{[i]} \equiv (\boldsymbol{q}^{[i]}, \boldsymbol{p_q}^{[i]})_m \tag{16.10}$$

We can write a permutation function to show the one-to-one correspondence:

$$\begin{cases} i = i(m) \equiv f(m); \\ m = m(i) \equiv f^{-1}(i) \end{cases} \tag{16.11}$$

Since the replicas are non-interacting, the weight factor for the state X is given by the product of Boltzmann factors for each replica (or at each temperature):

$$\mathrm{W_{RE}(X)} = exp\{-\sum_{m=1}^{M} \beta_{m(i)} H(\boldsymbol{q}^{[i]}, \boldsymbol{p_q}^{[i]})\} = exp\{-\sum_{i=1}^{M} \beta_m H(\boldsymbol{q}^{[i(m)]}, \boldsymbol{p_q}^{[i(m)]})\} \tag{16.12}$$

For the exchange of a pair of replicas i (at T_m) and j (at T_n),

$$\mathrm{X} = (..., x_m^{[i]}, ..., x_n^{[j]}, ...) \rightarrow \mathrm{X'} = (..., x_m^{[j]'}, ..., x_n^{[i]'}, ...) \tag{16.13}$$

The new permutation function f' is:

$$\begin{cases} i = f(m) \rightarrow j = f'(m); \\ j = f(n) \rightarrow i = f'(n) \end{cases} \tag{16.14}$$

In detail, the two exchanged replicas are

$$\begin{cases} x_m^{[i]} \equiv (\boldsymbol{q}^{[i]}, \boldsymbol{p_q}^{[i]})_m \rightarrow x_m^{[j]'} \equiv (\boldsymbol{q}^{[j]}, \boldsymbol{p_q}^{[j]'})_m \\ x_n^{[j]} \equiv (\boldsymbol{q}^{[j]}, \boldsymbol{p_q}^{[j]})_n \rightarrow x_n^{[i]'} \equiv (\boldsymbol{q}^{[i]}, \boldsymbol{p_q}^{[i]'})_n \end{cases} \tag{16.15}$$

This is equal to the exchange of a pair of temperatures T_m and T_n for the corresponding replicas i and j:

$$\begin{cases} x_m^{[i]} \equiv (\boldsymbol{q}^{[i]}, \boldsymbol{p_q}^{[i]})_m \rightarrow x_n^{[i]'} \equiv (\boldsymbol{q}^{[i]}, \boldsymbol{p_q}^{[i]'})_n \\ x_n^{[j]} \equiv (\boldsymbol{q}^{[j]}, \boldsymbol{p_q}^{[j]})_n \rightarrow x_m^{[j]'} \equiv (\boldsymbol{q}^{[j]}, \boldsymbol{p_q}^{[j]'})_m \end{cases} \tag{16.16}$$

where

$$\begin{cases} \boldsymbol{p_q}^{[i]'} \equiv \sqrt{\frac{T_n}{T_m}} \boldsymbol{p_q}^{[i]}) \\ \boldsymbol{p_q}^{[j]'} \equiv \sqrt{\frac{T_m}{T_n}} \boldsymbol{p_q}^{[j]}) \end{cases} \tag{16.17}$$

This means that the velocities of all atoms in the replicas will be uniformly rescaled by a factor defined by the square root of the ratio of the two temperatures.

To ensure the convergence of this exchange process towards an equilibrium distribution, a detailed balance condition is imposed on the transition probability $\mathrm{w(X \rightarrow X')}$:

$$\mathrm{W_{RE}(X)\ w(X \rightarrow X') = W_{RE}(X')\ w(X' \rightarrow X)} \tag{16.18}$$

then

$$\begin{aligned} \tfrac{\mathrm{w(X \rightarrow X')}}{\mathrm{w(X' \rightarrow X)}} &= exp\{-\beta_m[\mathcal{K}(\boldsymbol{p_q}^{[j]'}) + \mathcal{V}(\boldsymbol{q}^{[j]})] - \beta_n[\mathcal{K}(\boldsymbol{p_q}^{[i]'}) + \mathcal{V}(\boldsymbol{q}^{[i]})] \\ &\quad +\beta_m[\mathcal{K}(\boldsymbol{p_q}^{[i]}) + \mathcal{V}(\boldsymbol{q}^{[i]})] + \beta_n[\mathcal{K}(\boldsymbol{p_q}^{[j]}) + \mathcal{V}(\boldsymbol{q}^{[j]})]\} \\ &= exp[-(\beta_n - \beta_m)(\mathcal{V}_i - \mathcal{V}_j)] \\ &= exp(-\Delta) \end{aligned} \tag{16.19}$$

and i, j, m, n are related by the permutation function before the exchange

$$i = f(m), j = f(n) \tag{16.20}$$

This can be satisfied by the usual Metropolis criterion:

$$\mathrm{w}(\mathrm{X} \to \mathrm{X}') \equiv \mathrm{w}(x_m^{[i]} \mid x_n^{[j]}) = \begin{cases} 1, & for \Delta \leq 0 \\ exp(-\Delta) & for \Delta > 0 \end{cases} \tag{16.21}$$

By driving replicas to explore temperature space, T-REMD allows the system to cross energetic barriers and access regions of the conformational space difficult to reach at low temperatures.

In order to ensure a uniform exchange probability the temperatures were chosen according to the relation:

$$T_i = T_0 \; exp(i \; c) \tag{16.22}$$

where T_0 and c can be varied to give a desired exchange ratio.

Assuming $\beta_1 < \beta_2 < ... < \beta_M$, a T-REMD simulation is then done by alternately performing the two steps:

1. each replica in canonical ensemble of the fixed temperature T_m is simulated simultaneously and independently for a certain number of MC or MD steps;
2. a pair of replicas at neighboring temperatures, say $x_m^{[i]}$ and $x_{m+1}^{[j]}$, are exchanged with the probability $\mathrm{w}(x_m^{[i]} \mid x_n^{[j]})$.

For optimal performance of T-REMD, it is necessary to choose an appropriate temperature distribution. This can be done through an iterative procedure.

For the average at any intermediate temperature of R independent simulations, one can use the multiple-histogram reweighting techniques (WHAM), and the average of a physical quantity A at any intermediate temperature $T = 1/k_B\beta$ is given by

$$< A >= \frac{\sum\limits_{\mathcal{V}} A(\mathcal{V}) P(\mathcal{V}; \beta)}{\sum\limits_{\mathcal{V}} P(\mathcal{V}; \beta)} \tag{16.23}$$

where

$$P(\mathcal{V}; \beta) = \frac{\sum\limits_{m=1}^{R} g_m^{-1} N_m(\mathcal{V}) e^{-\beta \mathcal{V}}}{\sum\limits_{m=1}^{R} n_m g_m^{-1} e^{f_m - \beta_m \mathcal{V}}} \tag{16.24}$$

and

$$e^{-f_m} = \sum_E P(\mathcal{V}; \beta_m) \tag{16.25}$$

Here $g_m = 1+2\tau_m$, and τ_m is the integrated autocorrelation time at temperature T_m. $N_m(\mathcal{V})$ and n_m are the energy histogram and the total number of samples obtained in the mth run, respectively. In T-REMD $n_m = N_{sim}$. $P(\mathcal{V}; \beta)$ in Eqs. 16.24 and 16.25 are solved self-consistently by iteration.

16.2.1. Simulation checks. To examine whether a replica-exchange simulation indeed performed properly, there are three points to check:[171]

- whether the temperatures are optimally distributed;
  the optimal temperature distributions imply that all the acceptance ratios are the same, resulting in a free random walk in the replica temperature space.
- whether the number of replica temperatures is sufficient;
  the number of replica temperatures is sufficient if the acceptance ratios are not too small, say, greater than 0.1.
- whether the highest temperature is sufficiently high so that no trapping in a local energy-minimum occurs;

16.2.2. Factors determining the efficiency. T-REMD has been shown to be efficient at the lowest temperature, and meanwhile it provides converged distributions over the range of temperatures used in T-REMD simulations.[175] The efficiency and convergence are determined by the mixing/sorting of the replicas, which is the source of the main gain of this method, and can also bring false precision and be misinterpreted as true convergence or increased sampling efficiency.[176].

A sensible choice of intervals between exchange trials, ideally equal to the correlation time of the potential energy following an exchange, strongly depends on the size of the system. For small systems, the exchanges were mainly determined by the fluctuations within the solvent rather than the conformation of the solute, which is not the case for large systems, and for large systems, the conformation of the solute may require much longer time to reach the convergence.[127]

16.3. Hamiltonian replica exchange MD

Hamiltonian replica exchange MD can be realized by means of perturbation of the force field. Hamiltonians can be perturbed in different ways, see Sec. 14.2. In GROMOS, Hamiltonian replica exchange MD is performed by assigning different values of the coupling parameter λ to the different replicas. Note that the use of individual λ-values (Sec. 14.4) offers additional flexibility in this definition. For example, simulations may be set in which the replicas differ only in the softness of specific interactions, but not in the nonbonded interaction parameters.[174]

Use of $\mathcal{H}$-REMD in free-energy calculations using e.g. thermodynamic integration can improve the convergence, in particular when slow relaxation of some degrees of freedom is to be expected.[177] A condition for improved convergence is that the barriers leading to slow relaxation are absent in at least one replica. By using individual λ-values, such a replica may be explicitly designed. Furthermore, to improve the chances of relaxation in this replica, multiple replicas at the same value of λ may be included.[174]

While in T-REMD the optimal distribution of temperatures may be derived using the iterative procedures outlined above, this may be more cumbersome for $\mathcal{H}$-REMD. Using some preliminary simulations, one may design a mimicking approach from which the optimal sampling efficiency may be obtained.[178]

16.4. Initialization, simulation and analysis

In GROMOS, REMD is implemented through the program `repex_mpi`. This will start the replicas as separate MPI processes and control all the file handling and exchanges.

16.4.1. Set up of a RE simulation. The time between replica-exchange switches is set by the switch NSTLIM in the STEP block. Specific settings for the REMD simulation are defined in the REPLICA block. To do a T-REMD, the total number of temperatures is defined by the switch NRET and the temperature of each replica by RET:

`NRET`	number of replica exchange temperatures
`RET(1..NRET)`	temperature for each replica

and the scaling of temperature can be achieved by the switch LRESCALE:

`LRESCALE`	0: don't scale temperatures after exchange trial 1: scale temperatures after exchange trial

To do $\mathcal{H}$-REMD, one needs to define the number of λ-values by NRELAM, and the λ-value of each replica by RELAM. In addition, the timestep for each λ-replica can be specified separately, to allow for changes in the grain-level between the replicas:[51]

`NRELAM`	number of replica exchange lambda values
`RELAM(1..NRELAM)`	lambda value for each lambda-replica
`RETS(1..NRELAM)`	timestep of every λ-replica

Furthermore, the following switches in the REPLICA block control the REMD simulation

`NRETRIAL`	number of overall exchange trials
`NREQUIL`	number of exchange periods to equilibrate; no switches are performed in the first NREQUIL exchange periods
`CONT`	specifies if the simulation is a continuation from a previous REMD simulation. 0: input coordinates for all replicas are read from a single file 1: input coordinates for all replicas are read from separate files (see below)

Replica exchanges are attempted every NSTLIM steps. In `repex_mpi`, switches are only attempted between neighbouring replicas (in T for T-REMD, or in λ for $\mathcal{H}$-REMD). At odd trial attempts (i.e. after NSTLIM, 3xNSTLIM, 5xNSTLIM, ... timesteps), switches are attempted between replica pairs (1,2), (3,4), etc. At even trial attempts (i.e. after 2xNSTLIM, 4xNSTLIM, ... timesteps) switches are attempted between replica pairs (2,3), (4,5), etc.

The simulation may start with a single structure as the starting coordinates for all replicas, or each replica with a specified structure individually. If CONT = 0 in the REPLICA block, `repex_mpi` will read a single coordinate file as starting structure for all replicas. If CONT = 1 in the REPLICA block, `repex_mpi` will take the input parameter specified for the `@conf` flag, add the replica number to the filename and try to read the structure for every replica individually.

16.4.2. Analysis of a RE **trajectory.** For all output files, `repex_mpi` takes the filename as specified by the appropriate option and adds the replica number to the specified filename. Standard output for the individual replicas is written to files, specified by the `@repout` option. Furthermore, through the `@repdata` option an additional output-file is specified, which gives an overview of the switching attempts, the relevant energies, switching probabilities and switching acceptances.

The configurations generated in a REMD simulation of M replicas can be analyzed to obtain equilibrium averages for a target distribution P, where we can further derive an equilibrium property with eq. Eq. 16.23. Note that the trajectory files written out by `repex_mpi` contain the data pertaining to a single state of the simulation (temperature or λ-value), i.e. the coordinates and velocities are not continuous in time.

It is also possible to obtain kinetic information from a REMD simulation.[179] Due to the discontinuous feature of REMD simulations, it is necessary to use short-time propagators for the analysis, concerning that it is possible to calculate short-time correlation functions accurately with REMD. For a replica in $T-$REMD or $\mathcal{H}-$REMD, the maximum time scale is given by the simulation time between two accepted exchanges. In the sense of conformational transitions, a master equation may be constructed by dividing the whole space into N states,

$$\frac{dP_i(t)}{dt} = \sum_{j=1}^{N}[k_{ij}P_j(t) - k_{ji}P_i(t)] \tag{16.26}$$

where $P_i(t)$ the population of state i, $k_{ij} \geq 0$ the transition rate from states j to i.

The Eq. 16.26 may be rewriten as

$$\frac{d\mathbf{P}(t)}{dt} = \mathbf{K}\mathbf{P}(t) \tag{16.27}$$

where $\mathbf{K}$ is the transition rate matrix, and its diagonal elements are

$$k_{ii} = -\sum_{j\neq i} k_{ji} < 0 \tag{16.28}$$

The propagators are defined as the probability of being in state i at time 0 and j at time t and have the form

$$p(j,t|i,0) = [exp(\mathbf{K}t)]_{ji} \tag{16.29}$$

The elements of the matrix $\mathbf{K}$ may be estimated from a maximum-likelihood procedure. First the number of transitions N_{ji} from state i to j is determined within a time interval Δt, then the coefficients of the master

equation may estimated from the likelihood maximization,[180] where the logarithm of likelihood is defined as

$$ln\Lambda = \sum_{i=1}^{N}\sum_{j=1}^{N} N_{ji} ln\ p(j, \Delta t|i, 0) \tag{16.30}$$

The above approach has been used to study the transition rates of a helical peptide in water between its microscopic conformational states or between folding and unfolding.[179]

CHAPTER 17

Derivatives of the force-field terms

17.1. Bond stretching force-field term

Quartic case: the forces on atoms i and j due to formula (Eq. 5.5) are

$$\begin{aligned} \mathbf{f}_i &= -\frac{\partial V_n^{bond,q}}{\partial b_n^2}\,\frac{\partial b_n^2}{\partial \mathbf{r}_i} \\ &= -K_{b_n}\,[b_n^2 - b_{0_n}^2]\mathbf{r}_{ij} \end{aligned} \tag{17.1}$$

and

$$\mathbf{f}_j = -\mathbf{f}_i\ . \tag{17.2}$$

Harmonic case: the forces on atoms i and j due to formula (Eq. 5.6) are

$$\begin{aligned} \mathbf{f}_i &= -\frac{\partial V_n^{bond}}{\partial b_n}\,\frac{\partial b_n}{\partial \mathbf{r}_i} \\ &= -K_{b_n}^{harm}\,[b_n - b_{0_n}]\frac{\mathbf{r}_{ij}}{r_{ij}} \end{aligned} \tag{17.3}$$

and

$$\mathbf{f}_j = -\mathbf{f}_i. \tag{17.4}$$

17.2. Bond-angle bending force-field term

Cosine-harmonic form:

The forces on atoms i, j and k due to the n-th term in Eq. 5.11 are

$$\begin{aligned} \mathbf{f}_i &= -\frac{\partial V^{(\theta,c)}}{\partial \cos\theta_n}\,\frac{\partial \cos\theta_n}{\partial \mathbf{r}_i} \\ &= -k_n^{(\theta,c)}\ [\ \cos\theta_n - \cos\theta_{0_n}\ ]\ \left[\ \frac{\mathbf{r}_{kj}}{r_{kj}} - \frac{\mathbf{r}_{ij}}{r_{ij}}\ \cos\theta_n\ \right]\ \frac{1}{r_{ij}} \end{aligned} \tag{17.5}$$

and

$$\begin{aligned} \mathbf{f}_k &= -\frac{\partial V^{(\theta,c)}}{\partial \cos\theta_n}\,\frac{\partial \cos\theta_n}{\partial \mathbf{r}_k} \\ &= -k_n^{(\theta,c)}\ [\ \cos\theta_n - \cos\theta_{0_n}\ ]\ \left[\ \frac{\mathbf{r}_{ij}}{r_{ij}} - \frac{\mathbf{r}_{kj}}{r_{kj}}\ \cos\theta_n\ \right]\ \frac{1}{r_{kj}} \end{aligned} \tag{17.6}$$

and

$$\mathbf{f}_j\ =\ -\mathbf{f}_i\ -\mathbf{f}_k \tag{17.7}$$

Angle-harmonic form:

For harmonic bond angles the forces on atoms i, j and k due to the n-th term in Eq. 5.12 are

$$\mathbf{f}_i = k_n^{(\theta,h)} \cdot \frac{\theta - \theta_0}{\sin\theta} \cdot \frac{1}{r_{ij}} \left(\frac{\mathbf{r}_{kj}}{r_{kj}} - \frac{\mathbf{r}_{ij}}{r_{ij}} \cos\theta \right) \tag{17.8}$$

and

$$\mathbf{f}_k = k_n^{(\theta,h)} \cdot \frac{\theta - \theta_0}{\sin\theta} \cdot \frac{1}{r_{kj}} \left(\frac{\mathbf{r}_{ij}}{r_{ij}} - \frac{\mathbf{r}_{kj}}{r_{kj}} \cos\theta \right) \tag{17.9}$$

and

$$\mathbf{f}_j = -\mathbf{f}_i - \mathbf{f}_k \tag{17.10}$$

17.3. Improper dihedral-angle bending force-field term

The forces on atoms i, j, k and l due to the n-th term in formula (Eq. 5.17)

$$\begin{aligned} \mathbf{f}_i &= -\frac{\partial V^{(\xi)}}{\partial \xi_n}\ \frac{\partial \xi_n}{\partial \mathbf{r}_i} \\ &= -k_n^{(\xi)}\ [\ \xi_n\ -\xi_{0_n}]\ \frac{r_{kj}}{r_{mj}^2}\ \mathbf{r}_{mj} \end{aligned} \tag{17.11}$$

$$\begin{aligned} \mathbf{f}_l &= -\frac{\partial V^{(\xi)}}{\partial \xi_n}\ \frac{\partial \xi_n}{\partial \mathbf{r}_l} \\ &= +k_n^{(\xi)}\ [\ \xi_n\ -\xi_{0_n}]\ \frac{r_{kj}}{r_{nk}^2}\ \mathbf{r}_{nk} \end{aligned} \tag{17.12}$$

$$\begin{aligned} \mathbf{f}_j &= -\frac{\partial V^{(\xi)}}{\partial \xi_n}\ \frac{\partial \xi_n}{\partial \mathbf{r}_j} \\ &= \left[\frac{(\mathbf{r}_{ij}\ \cdot\ \mathbf{r}_{kj})}{r_{kj}^2}\ -1\right]\ \mathbf{f}_i\ -\frac{(\mathbf{r}_{kl}\ \cdot\ \mathbf{r}_{kj})}{r_{kj}^2}\ \mathbf{f}_l \end{aligned} \tag{17.13}$$

and

$$\mathbf{f}_k\ =\ -\mathbf{f}_i\ -\mathbf{f}_j\ -\mathbf{f}_l \tag{17.14}$$

17.4. Proper dihedral-angle torsion force-field term

The cosine expansions in terms of derivatives ($\partial cos(m\varphi)/\partial cos\varphi$):

$$\begin{aligned} &\partial\cos(0\varphi)/\partial\cos\varphi = 0 \\ &\partial\cos(1\varphi)/\partial\cos\varphi = 1 \\ &\partial\cos(2\varphi)/\partial\cos\varphi = 4\cos\varphi \\ &\partial\cos(3\varphi)/\partial\cos\varphi = 12\cos^2\varphi - 3 \\ &\partial\cos(4\varphi)/\partial\cos\varphi = 32\cos^3\varphi - 16\cos\varphi \\ &\partial\cos(5\varphi)/\partial\cos\varphi = 80\cos^4\varphi - 60\cos^2\varphi + 5 \\ &\partial\cos(6\varphi)/\partial\cos\varphi = 192\cos^5\varphi - 192\cos^3\varphi + 36\cos\varphi \end{aligned} \tag{17.15}$$

Symmetric form:

The forces on atoms i, j, k and l due to the n-th term in formula (Eq. 5.22 are

$$\mathbf{f}_i = -\frac{\partial V^{(\varphi,s)}}{\partial\cos(m_n\ \varphi_n)}\ \frac{\partial\cos(m_n\ \varphi_n)}{\partial\cos\varphi_n}\ \frac{\partial\cos\varphi_n}{\partial\mathbf{r}_i} \tag{17.16}$$

$$= -k_n^{(\varphi,s)}\cos(\delta_n)\frac{\partial\cos(m_n\ \varphi_n)}{\partial\cos\varphi_n}\ \left[\frac{\mathbf{r}_{ln'}}{r_{ln'}} - \frac{\mathbf{r}_{im'}}{r_{im'}}\ \cos\varphi_n\right]\ \frac{1}{r_{im'}} \tag{17.17}$$

$$\mathbf{f}_l = -k_n^{(\varphi,s)}\cos(\delta_n)\frac{\partial\cos(m_n\ \varphi_n)}{\partial\cos\varphi_n}\ \left[\frac{\mathbf{r}_{im'}}{r_{im'}}\ -\frac{\mathbf{r}_{ln'}}{r_{ln'}}\cos\varphi_n\right]\frac{1}{r_{ln'}} \tag{17.18}$$

$$\mathbf{f}_j = \left[\frac{(\mathbf{r}_{ij}\ \cdot\ \mathbf{r}_{kj})}{r_{kj}^2}\ -1\right]\ \mathbf{f}_i\ -\frac{(\mathbf{r}_{kl}\ \cdot\ \mathbf{r}_{kj})}{r_{kj}^2}\ \mathbf{f}_l \tag{17.19}$$

and

$$\mathbf{f}_k\ =\ -\mathbf{f}_i\ -\mathbf{f}_j\ -\mathbf{f}_l \tag{17.20}$$

Generalized form:

When doing so, the forces on atoms i, j, k and l due to the n-th term in (Eq. 5.23) are

$$\mathbf{f}_i = -\frac{\partial V^{(\varphi,g)}}{\partial \varphi_n}\frac{\partial \varphi_n}{\partial \mathbf{r}_i} \tag{17.21}$$

$$= k_n^{(\varphi,g)} m_n sin(m_n\varphi_n - \delta_n)\frac{r_{kj}}{r_{mj}^2}\ \mathbf{r}_{mj} \tag{17.22}$$

$$\mathbf{f}_l = -\frac{\partial V^{(\varphi,g)}}{\partial \varphi_n}\frac{\partial \varphi_n}{\partial \mathbf{r}_l} \tag{17.23}$$

$$= -k_n^{(\varphi,g)} m_n sin(m_n\varphi_n - \delta_n)\frac{r_{kj}}{r_{nk}^2}\ \mathbf{r}_{nk} \tag{17.24}$$

$$\mathbf{f}_j = -\frac{\partial V^{(\varphi,g)}}{\partial \varphi_n}\frac{\partial \varphi_n}{\partial \mathbf{r}_j} \tag{17.25}$$

$$= \left[\frac{(\mathbf{r}_{ij}\ \cdot\ \mathbf{r}_{kj})}{r_{kj}^2} - 1\right]\ \mathbf{f}_i - \frac{(\mathbf{r}_{kl}\ \cdot\ \mathbf{r}_{kj})}{r_{kj}^2}\ \mathbf{f}_l$$

and

$$\mathbf{f}_k = -\mathbf{f}_i - \mathbf{f}_j - \mathbf{f}_{ll} \tag{17.26}$$

with $\mathbf{r}_{mj}$ and $\mathbf{r}_{nk}$ calculated according to Eq. 5.15, and

$$sin(m_n\varphi_n - \delta_n) = \text{sign}\ \sqrt{1 - cos^2(m_n\varphi_n - \delta_n)} \tag{17.27}$$

17.5. LJ interaction terms

The forces on atoms i and j due to van der Waals interactions are

$$\mathbf{f}_i^{LJ} = \left[\frac{2C_{12}(i,j)}{\mathbf{r}_{ij}^6} - C_6(i,j)\right]\cdot\frac{6\mathbf{r}_{ij}}{r_{ij}^8} \tag{17.28}$$

and

$$\mathbf{f}_j = -\mathbf{f}_i \quad . \tag{17.29}$$

17.6. Electrostatic interaction terms: Coulomb plus reactive field

The forces on atoms i and j due to Coulomb and reaction field are

$$\mathbf{f}_i^{CRF} = \frac{q_i q_j}{4\pi\epsilon_0\epsilon_{cs}}\left[\frac{1}{r_{ij}^3} + \frac{C_{rf}}{{R_{rf}}^3}\right]\mathbf{r}_{ij} \tag{17.30}$$

and

$$\mathbf{f}_j = -\mathbf{f}_i \quad . \tag{17.31}$$

17.7. Electrostatic interaction terms: lattice sum

The force on atom i corresponding to Eq. 7.44 is given by

$$\mathbf{F}_{\eta,i} = (4\pi\epsilon_0)^{-1}\sum_{j=1\,,\,j\neq i\,,\,\overline{r}_{ij}<R_p\,,\,j\notin Exc(i)}^{N_q} q_i\,q_j\,[\overline{r}_{ij}^{-1}\eta(a^{-1}\overline{r}_{ij}) - a^{-1}\eta'(a^{-1}\overline{r}_{ij})]\overline{r}_{ij}^{-2}\overline{\mathbf{r}}_{ij} \tag{17.32}$$

$$+(4\pi\epsilon_0)^{-1}\sum_{i=1}^{N_q}\sum_{j=1\,,\,j>i\,,\,j\in Exc(i)}^{N_q} q_i\,q_j\,\{\overline{r}_{ij}^{-1}[\eta(a^{-1}\overline{r}_{ij}) - 1] - a^{-1}\eta'(a^{-1}\overline{r}_{ij})\}\overline{r}_{ij}^{-2}\overline{\mathbf{r}}_{ij}\ .$$

The derivatives η' of the switch functions corresponding to the charge-shaping functions implemented are listed in Tab. 7.3.

The force on atom i corresponding to Eq. 7.45 is given by

$$\mathbf{F}_{\gamma,i} = (\epsilon_0 V)^{-1} q_i \sum_{\mathbf{l}\in\mathbb{W}\,,\,l\neq 0} k^{-2}\,\hat{\gamma}(ak)\,\mathbf{k}\,[\,C(\mathbf{k})\sin\mathbf{k}\cdot\mathbf{r}_i - S(\mathbf{k})\cos\mathbf{k}\cdot\mathbf{r}_i\,]\;. \tag{17.33}$$

Eq. 17.33 is rewritten

$$\mathbf{F}_{\gamma,i} = 8(\epsilon_0 V)^{-1} q_i \sum_{\mathbf{l}\in\mathbb{W}'\,,\,l\neq 0} k^{-2}\,\hat{\gamma}(ak)\,\sigma_{\mathbf{k}}\,\underline{\mathbf{D}}\mathbf{k} \tag{17.34}$$

where $\underline{\mathbf{D}}$ is a diagonal matrix with elements

$$\begin{aligned} D_{xx} \;=\;& -c_{x,i,l_x}c_{y,i,l_y}[S_x(\mathbf{k})c_{z,i,l_z} + C_y(\mathbf{k})s_{z,i,l_z}] + s_{x,i,l_x}s_{y,i,l_y}[S_y(\mathbf{k})c_{z,i,l_z} + C_x(\mathbf{k})s_{z,i,l_z}] \\ & -c_{x,i,l_x}s_{y,i,l_y}[C_z(\mathbf{k})c_{z,i,l_z} + S_o(\mathbf{k})s_{z,i,l_z}] + s_{x,i,l_x}c_{y,i,l_y}[C_o(\mathbf{k})c_{z,i,l_z} + S_z(\mathbf{k})s_{z,i,l_z}]\;, \end{aligned} \tag{17.35}$$

$$\begin{aligned} D_{yy} \;=\;& -c_{x,i,l_x}c_{y,i,l_y}[S_y(\mathbf{k})c_{z,i,l_z} + C_x(\mathbf{k})s_{z,i,l_z}] + s_{x,i,l_x}s_{y,i,l_y}[S_x(\mathbf{k})c_{z,i,l_z} + C_y(\mathbf{k})s_{z,i,l_z}] \\ & +c_{x,i,l_x}s_{y,i,l_y}[C_o(\mathbf{k})c_{z,i,l_z} + S_z(\mathbf{k})s_{z,i,l_z}] - s_{x,i,l_x}c_{y,i,l_y}[C_z(\mathbf{k})c_{z,i,l_z} + S_o(\mathbf{k})s_{z,i,l_z}]\;, \end{aligned} \tag{17.36}$$

and

$$\begin{aligned} D_{zz} \;=\;& -c_{x,i,l_x}c_{y,i,l_y}[S_z(\mathbf{k})c_{z,i,l_z} - C_o(\mathbf{k})s_{z,i,l_z}] - s_{x,i,l_x}s_{y,i,l_y}[S_o(\mathbf{k})c_{z,i,l_z} - C_z(\mathbf{k})s_{z,i,l_z}] \\ & -c_{x,i,l_x}s_{y,i,l_y}[C_x(\mathbf{k})c_{z,i,l_z} - S_y(\mathbf{k})s_{z,i,l_z}] - s_{x,i,l_x}c_{y,i,l_y}[C_y(\mathbf{k})c_{z,i,l_z} - S_x(\mathbf{k})s_{z,i,l_z}]\;. \end{aligned} \tag{17.37}$$

The reciprocal-space Ewald contribution to the atomic virial W_μ (corresponding to the energy term E_γ defined by Eqs. 7.26 and evaluated as Eq. 7.45) reads[118]

$$W_{ew,\mu} = -(4\epsilon_0\epsilon_{ls}V)^{-1} \sum_{\mathbf{l}\in\mathbb{W}\,,\,l\neq 0} \hat{\Gamma}_\mu(\mathbf{k})\,[\,C^2(\mathbf{k}) + S^2(\mathbf{k})\,]\;, \tag{17.38}$$

where the $C(\mathbf{k})$ and $S(\mathbf{k})$ functions are given by Eq. 7.46, and

$$\hat{\Gamma}_\mu(\mathbf{k}) = \frac{(k^2 - 2k_\mu^2)\hat{\gamma}(ak) + akk_\mu^2\hat{\gamma}'(ak)}{k^4}\;, \tag{17.39}$$

with $\hat{\gamma}'(\kappa) = \partial\hat{\gamma}(\kappa)/\partial\kappa$ (Tab. 7.5). As discussed in Sec. 7.4.3, an increase in computational efficiency can be obtained by restricting the summation to a half-space and doubling the result, or even, summing over an octant and multiplying the result by eight.

The virial associated with the energy contribution E_γ (Eq. 7.72) can be calculated as

$$\underline{\mathbf{W}}_\gamma = \frac{1}{2}\frac{\partial E_\gamma}{\partial\underline{\mathbf{L}}}\,{}^t\underline{\mathbf{L}}\;. \tag{17.40}$$

Inserting Eq. 7.72 into Eq. 17.40, noting that $\hat{s}_g$ is independent of $\underline{\mathbf{L}}$ when the particle coordinates are scaled together with the box dimensions, and making use of Eq. 4.47, one obtains

$$\underline{\mathbf{W}}_\gamma = -(4\epsilon_0\,V)^{-1} \sum_{\mathbf{l}\in G\,,\,l\neq 0} [\hat{G}_g^\dagger(\mathbf{k_l})\underline{\mathbf{1}} + \widehat{\underline{\mathbf{\Gamma}}}_g^{\,o}(\mathbf{k_l})]\mid\hat{s}_g(\mathbf{k_l})\mid^2 \tag{17.41}$$

where $\hat{G}_g^\dagger(\mathbf{k_l})$ and $\widehat{\underline{\mathbf{\Gamma}}}_g^{\,o}(\mathbf{k_l})$ are defined as in Eqs. 7.69 and 7.70.

CHAPTER 18

Appendices

18.1. Conversion of force constants: bond-stretching and bond-angle bending interactions

In GROMOS the bond-stretching interaction may be chosen harmonic,

$$V_n^{(b,h)}(b_n, k_n^{(b,h)}, b_n^0) = \frac{1}{2} k_n^{(b,h)} (b_n - b_n^0)^2 \tag{18.1}$$

or quartic,

$$V_n^{(b,q)}(b_n, k_n^{(b,q)}, b_n^0) = \frac{1}{4} k_n^{(b,q)} ({b_n}^2 - {b_n^0}^2)^2 = \frac{1}{4} k_n^{(b,q)} (b_n + b_n^0)^2 (b_n - b_n^0)^2 \quad . \tag{18.2}$$

Comparison of the two forms leads to the conversion formula

$$k_n^{(b,h)} = 2 {b_n^0}^2 k_n^{(b,q)} \tag{18.3}$$

because generally $b_n \simeq b_n^0$, and

$$k_n^{(b,q)} = \frac{k_n^{(b,h)}}{2 {b_n^0}^2} \tag{18.4}$$

In GROMOS the bond-angle bending interaction may be chosen harmonic,

$$V_n^{(\theta,h)}(\theta_n; k_n^{(\theta,h)}; \theta_n^0) = \frac{1}{2} k_n^{(\theta,h)} (\theta_n - \theta_n^0)^2 \tag{18.5}$$

or cosine-harmonic,

$$V_n^{(\theta,c)}(\theta_n; k_n^{(\theta,c)}; \theta_n^0) = \frac{1}{2} k_n^{(\theta,c)} (\cos\theta_n - \cos\theta_n^0)^2 \quad . \tag{18.6}$$

The force constants of the two forms can be related by the requirement that for the two angles θ_n for which

$$V_n^{(\theta,h)}(\theta_n; k_n^{(\theta,h)}; \theta_n^0) = V_n^{(\theta,c)}(\theta_n; k_n^{(\theta,c)}; \theta_n^0) \tag{18.7}$$

the average of the energies (Eq. 18.7) for the two angles θ_n should be equal to $\frac{1}{2} k_B T$.

Eq. 18.5 yields for the two θ_n angles

$$\theta_n = \theta_n^0 \pm \left(\frac{k_B T}{k_n^{(\theta,h)}} \right)^{\frac{1}{2}} \tag{18.8}$$

which after insertion into Eq. 18.6 and averaging over the two angles θ_n yields

$$k_n^{(\theta,c)} = \frac{2 k_B T}{\left[\cos\left(\theta_n^0 + \left(\frac{k_B T}{k_n^{(\theta,h)}} \right)^{\frac{1}{2}} \right) - \cos\theta_n^0 \right]^2 + \left[\cos\left(\theta_n^0 - \left(\frac{k_B T}{k_n^{(\theta,h)}} \right)^{\frac{1}{2}} \right) - \cos\theta_n^0 \right]^2} \tag{18.9}$$

Of course if $k_n^{(\theta,h)} = 0$, then $k_n^{(\theta,c)} = 0$ and Eq. 18.9 should not be used. An inverse relation can be derived analogously. Eq. 18.6 yields for the two θ_n angles

$$\theta_n = \begin{cases} \arccos\left(\cos\theta_n^0 \pm \left(\frac{k_B T}{k_n^{(\theta,c)}}\right)^{\frac{1}{2}}\right) & \text{if } -1 \leq \cos\theta_n^0 \pm \left(\frac{k_B T}{k_n^{(\theta,c)}}\right)^{\frac{1}{2}} \leq 1 \\ \begin{cases} \arccos\left(\cos\theta_n^0 + \left(\frac{k_B T}{k_n^{(\theta,c)}}\right)^{\frac{1}{2}}\right) \\ 2\theta_n^0 - \arccos\left(\cos\theta_n^0 + \left(\frac{k_B T}{k_n^{(\theta,c)}}\right)^{\frac{1}{2}}\right) \end{cases} & \text{if } -1 \leq \cos\theta_n^0 + \left(\frac{k_B T}{k_n^{(\theta,c)}}\right)^{\frac{1}{2}} \leq 1 \\ \begin{cases} \arccos\left(\cos\theta_n^0 - \left(\frac{k_B T}{k_n^{(\theta,c)}}\right)^{\frac{1}{2}}\right) \\ 2\theta_n^0 - \arccos\left(\cos\theta_n^0 - \left(\frac{k_B T}{k_n^{(\theta,c)}}\right)^{\frac{1}{2}}\right) \end{cases} & \text{if } -1 \leq \cos\theta_n^0 - \left(\frac{k_B T}{k_n^{(\theta,c)}}\right)^{\frac{1}{2}} \leq 1 \\ \text{not defined} & \text{else} \end{cases} \tag{18.10}$$

which after insertion into Eq. 18.5 and averaging over the two angles θ_n yields

$$k_n^{(\theta,h)} = \frac{2k_B T}{\left[\arccos\left(\cos\theta_n^0 + \left(\frac{k_B T}{k_n^{(\theta,c)}}\right)^{\frac{1}{2}}\right) - \theta_n^0\right]^2 + \left[\arccos\left(\cos\theta_n^0 - \left(\frac{k_B T}{k_n^{(\theta,c)}}\right)^{\frac{1}{2}}\right) - \theta_n^0\right]^2} \tag{18.11}$$

Again if $k_n^{(\theta,c)} = 0$, $k_n^{(\theta,h)} = 0$ and Eq. 18.11 should not be used.

Eq. 18.11 is the physical inverse of Eq. 18.9, *not* the mathematical one.

For $k_B T$ one can chose the values $k_B = 8.3144110^{-3}\,\mathrm{kJ\,mol^{-1}\,K^{-1}}$ and $T = 300\,\mathrm{K}$, leading to $2.494323\,\mathrm{kJ\,mol^{-1}}$ or $0.5961575\,\mathrm{kcal\,mol^{-1}}$.

Bibliography

[1] W.F. van Gunsteren and H.J.C. Berendsen. Computer Simulation of Molecular Dynamics: Methodology, Applications and Perspectives in Chemistry. *Angew. Chem. Int. Ed.*, 29:992–1023, 1990.

[2] W.F. van Gunsteren, D. Bakowies, R. Baron, I. Chandrasekhar, M. Christen, X. Daura, P. Gee, D.P. Geerke, A. Glättli, P.H. Hünenberger, M.A. Kastenholz, C. Oostenbrink, M. Schenk, D. Trzesniak, N.F.A. van der Vegt, and H.B. Yu. Biomolecular modelling: goals, problems, perspectives Angew. Chem ¡strong¿118¡/strong¿ (2006) 4168-4198. *Angew. Chem. Int. Ed.*, 45:4064–4092, 2006.

[3] K. Meier, A. Choutko, J. Dolenc, A.P. Eichenberger, S. Riniker, and W.F. van Gunsteren. Multi-resolution simulation of biomolecular systems: a review of methodological issues. *Angew. Chem. Int. Ed.*, 52:2820–2834, 2013.

[4] H. J. C. Berendsen. *Simulating the Physical World, Hierarchical Modeling from Quantum Mechanics to Fluid Dynamics*. Cambridge University Press, 2007.

[5] W.F. van Gunsteren, T. Huber, and A.E. Torda. Biomolecular Modelling: Overview of Types of Methods to Search and Sample Conformational Space. *European Conference on Computational Chemistry (E.C.C.C 1), American Institute of Physics, Conference Proceedings*, 330:253–268, 1995.

[6] M. Christen and W.F. van Gunsteren. On searching in, sampling of, and dynamically moving through conformational space of biomolecular systems: a review. *J. Comput. Chem.*, 29:157–166, 2007.

[7] P.H. Hünenberger. Thermostat Algorithms for Molecular-Dynamics Simulations. *Adv. Polym. Sci.*, 173:105–149, 2005.

[8] M. Parrinello R. Car. Unified Approach for Molecular Dynamics and Density-Functional Theory. *Phys. Rev. Lett.*, 55:2471–2474, 1985.

[9] H. Yu and W.F. van Gunsteren. Accounting for polarization in molecular simulation. *Comput. Phys. Commun.*, 172:69–85, 2005.

[10] S.R. Billeter, P.M. King, and W.F. van Gunsteren. Can the density maximum of water be found by computer simulation? *J. Chem. Phys.*, 100:6692–6699, 1994.

[11] H.J.C. Berendsen, J.P.M. Postma, W.F. van Gunsteren, A. DiNola, and J.R. Haak. Molecular dynamics with coupling to an external bath. *J. Chem. Phys.*, 81:3684–3690, 1984.

[12] W.F. van Gunsteren, P.M. King, and A.E. Mark. Fundamentals of drug design from a biophysical viewpoint. *Quart. Rev. Biophysics*, 27:435–481, 1994.

[13] T. Huber, A.E. Torda, and W.F. van Gunsteren. Optimization Methods for Conformational Sampling Using a Boltzmann-Weighted Mean Field Approach. *Biopolymers*, 39:103–114, 1996.

[14] W.F. van Gunsteren, H.J.C. Berendsen, F. Colonna, D. Perahia, J.P. Hollenberg, and D. Lellouch. On Searching Neighbours in Computer Simulations of Macromolecular Systems. *J. Comput. Chem.*, 5:272–279, 1984.

[15] H.J.C. Berendsen. Treatment of Long-Range Forces in Molecular Dynamics. In J. Hermans, editor, *Molecular Dynamics and Protein Structure*, pages 18–22. Polycrystal Book Service, Western Springs, Ill, USA, 1985.

[16] J. L. Finney. Long-range forces in molecular dynamics calculations on water. *J. Comput. Chem.*, 28:92–102, 1978.

[17] W. B. Streett; D. J. Tildesley; G. Saville. Multiple time-step methods in molecular dynamics Molecular Physics: An International Journal at the Interface Between Chemistry and Physics. *Mol. Phys.*, 35:639–648, 1978.

[18] P. G. Debenedetti A. A. Chialvo. An automated Verlet neighbor list algorithm with a multiple time-step approach for the simulation of large systems. *Comput. Phys. Commun.*, 70:467–477, 1992.

[19] T. Heinz and P.H. Hünenberger. A fast pairlist construction algorithm for molecular simulations under periodic boundary conditions. *J. Comput. Chem.*, 25:1474, 2004.

[20] H. Bekker, H.J.C. Berendsen, E.J. Dijkstra, S. Achterop, R. v. Drunen, D. v.d. Spoel, A. Sijbers, H. Keegstra, B. Reitsma, and M.K.R. Renardus. GROMACS Method of Virial Calculation Using a Single Sum. In R.A. de Groot and J. Nadrchal, editors, *Proceedings of the 4th Intl. Conference Physics Computing '92*, pages 257–261. World Scientific Publishing Company, Singapore, 1993.

[21] W.F. van Gunsteren and M. Karplus. Protein Dynamics in Solution and in a Crystalline Environment: A Molecular Dynamics Study. *Biochemistry*, 21:2259–2274, 1982.

[22] F. Fraternali and W.F. van Gunsteren. An Efficient Mean Solvation Force Model for Use in Molecular Dynamics Simulations of Proteins in Aqueous Solution. *J. Mol. Biol.*, 256:939–948, 1996.

[23] H. Bekker. Unification of box shapes in molecular simulations. *J. Comput. Chem.*, 18:1930–1942, 1997.

[24] C. Oostenbrink, A. Villa, A.E. Mark, and W.F. van Gunsteren. A biomolecular force field based on the free enthalpy of hydration and solvation: the GROMOS force-field parameter sets 53A5 and 53A6. *J. Comput. Chem.*, 25:1656, 2004.

[25] IUPAC-IUB commission on biochemical nomenclature. Abbreviations and symbols for the description of the conformation of polypeptide chains. Tentative rules (1969). *Biochemistry*, 9:3471–3479, 1970.

[26] T.C. Beutler, A.E. Mark, R.C. van Schaik, P.R. Gerber, and W.F. van Gunsteren. Avoiding singularities and numerical instabilities in free energy calculations based on molecular simulations. *Chem. Phys. Lett.*, 222:529–539, 1994.

[27] W. H. Press; S. A. Teukolsky; W. T. Vetterling; B. P. Flannery. *Numerical Recipes 3rd Edition: The Art of Scientific Computing*. Cambridge University Press, 2007.

[28] P.H. Hünenberger. *Simulation and theory of electrostatic interactions in solution: Computational chemistry, biophysics, and aqueous solution*, chapter Lattice-sum methods for computing electrostatic interactions in molecular simulations. American Institute of Physics, New York, U.S.A., 1999.
[29] P.P. Ewald. Die Berechnung optischer und elektrostatischer Gitterpotentiale. *Ann. Phys.*, 369:253–287, 1921.
[30] R.W. Hockney and J.W. Eastwood. *Computer simulation using particles.* McGraw-Hill, New York, U.S.A., 1981.
[31] E. Wigner. Effect of the electron interaction on the energy levels of electrons in metals. *Trans. Faraday Soc.*, 34:678–685, 1938.
[32] B.U. Felderhof. Wigner solids and diffusion controlled reactions in a regular array of spheres. *Physica A*, 130:34–56, 1985.
[33] B.R.A. Nijboer and T.W. Ruijgrok. On the energy per particle in three- and two-dimensional Wigner lattices. *J. Stat. Phys.*, 53:361–382, 1988.
[34] M. Deserno and C. Holm. How to mesh up Ewald sums. I. A theoretical and numerical comparison of various particle mesh routines. *J. Chem. Phys.*, 109:7678–7693, 1998.
[35] M. Deserno and C. Holm. How to mesh up Ewald sums. II. An accurate error estimate for the particle-particle-particle-mesh algorithm. *J. Chem. Phys.*, 109:7694–7701, 1998.
[36] T. P. Straatsma; J. A. McCammon. Molecular Dynamics Simulations with Interaction Potentials Including Polarization Development of a Noniterative Method and Application to Water. *Mol. Simul.*, 5:181–192, 1990.
[37] P. Drude. *The Theory of Optics*. New York [etc.] Longmans, Green, and Co., 1901.
[38] M. Born K. Huang. *Dynamic Theory of Crystal Lattices*. Oxford University Press , Oxford, UK, 1954.
[39] D.P. Geerke and W.F. van Gunsteren. Calculation of the free energy of polarization: quantifying the effect of explicitly treating electronic polarization on the transferability of force-field parameters. *J. Phys. Chem. B*, 111:6425–6436, 2007.
[40] S. Riniker, A.P.E. Kunz, and W.F. van Gunsteren. On the calculation of the dielectric permittivity of molecular models in the liquid phase. *J. Chem. Theory Comput.*, 7:1469–1475, 2011.
[41] H. Yu, T Hansson, and W.F. van Gunsteren. Development of a Simple, Self-Consistent Polarizable Model for Liquid Water. *J. Chem. Phys.*, 118:221–234, 2003.
[42] Z. Lin, S.J. Bachmann, and W.F. van Gunsteren. GROMOS polarisable charge-on-spring models for liquid urea: COS/U and COS/U2. *J. Chem. Phys.*, 142:094117, 2015.
[43] H. Yu and W.F. van Gunsteren. Charge-on-spring polarizable water models revisited: From water clusters to liquid water to ice. *J. Chem. Phys.*, 121:9549–9564, 2004.
[44] A.P. Kunz and W.F. van Gunsteren. Development of a non-linear classical polarisation model for liquid water and aqueous solutions: COS/D. *J. Phys. Chem. A*, 113:11570–11579, 2009.
[45] S.J. Bachmann and W.F. van Gunsteren. On the compatibility of polarisable and non-polarisable models for liquid water. *Mol. Phys.*, 112:2761–2780, 2014.
[46] A. Glättli, X. Daura, and W.F. van Gunsteren. Derivation of an improved SPC model for liquid water: SPC/A and SPC/L. *J. Chem. Phys.*, 116:9811–9828, 2002.
[47] W.F. van Gunsteren and H.J.C. Berendsen. Algorithms for macromolecular dynamics and constraint dynamics. *Mol. Phys.*, 34:1311–1327, 1977.
[48] S. Riniker and W.F. van Gunsteren. A simple, efficient polarisable coarse-grained water model for molecular dynamics simulations. *J. Chem. Phys.*, 134:084110, 2011.
[49] W. Huang and W.F. van Gunsteren. Challenge of representing entropy at different levels of resolution in molecular simulation. *J. Phys. Chem. B*, 119:753–763, 2015.
[50] S.Riniker, J.R. Allison, and W.F. van Gunsteren. On developing coarse-grained models for biomolecular simulation: a review:. *Phys. Chem. Chem. Phys.*, 14:12423–12430, 2012.
[51] M. Christen and W.F. van Gunsteren. Multigraining: an algorithm for simultaneous fine-grained and coarse-grained simulation of molecular systems. *J. Chem. Phys.*, 124:7, 2006.
[52] S. Riniker and W.F. van Gunsteren. Mixing coarse-grained and fine-grained water in molecular dynamics simulations of a single system. *J. Chem. Phys.*, 137:044120, 2012.
[53] S. Riniker, A.P. Eichenberger, and W.F. van Gunsteren. Structural effects of an atomic-level layer of water molecules around proteins solvated in supra-molecular coarse-grained water. *J. Phys. Chem. B*, 116:8873–8879, 2012.
[54] R. Kaptein, E.R.P. Zuiderweg, R.M. Scheek, R. Boelens, and W.F. van Gunsteren. A Protein Structure from Nuclear Magnetic Resonance Data lac Repressor Headpiece. *J. Mol. Biol.*, 182:179–182, 1985.
[55] W.F. van Gunsteren, R. Boelens, R. Kaptein, R.M. Scheek, and E.R.P. Zuiderweg. An Improved Restrained Molecular Dynamics Technique to Obtain Protein Tertiary Structure from Nuclear Magnetic Resonance Data. In J. Hermans, editor, *Molecular Dynamics and Protein Structure*, pages 92–99. Polycrystal Book Service, Western Springs, Ill, USA, 1985.
[56] A.E. Torda and W.F. van Gunsteren. Molecular Modeling Using Nuclear Magnetic Resonance Data. In K.B. Lipkowitz and D.B. Boyd, editors, *Reviews in Computational Chemistry*, volume III, pages 143–172. VCH Publishers, Inc. New York, 1992.
[57] W.F. van Gunsteren, R.M. Brunne, P. Gros, R.C. van Schaik, C.A. Schiffer, and A.E. Torda. Accounting for Molecular Mobility in Structure Determination Based on Nuclear Magnetic Resonance Spectroscopic and X-Ray Diffraction Data. In T.L. James and N.J. Oppenheimer, editors, *Nuclear Magnetic Resonance*, volume 239 of *Methods in Enzymology*, pages 619–654. Academic Press, New York, 1994.
[58] A.E. Torda, R.M. Scheek, and W.F. van Gunsteren. Time-dependent distance restraints in molecular dynamics simulations. *Chem. Phys. Lett.*, 157:289–294, 1989.
[59] A.E. Torda, R.M. Scheek, and W.F. van Gunsteren. Time-averaged Nuclear Overhauser Effect Distance Restraints Applied to Tendamistat. *J. Mol. Biol.*, 214:223–235, 1990.
[60] A.P. Nanzer, W.F. van Gunsteren, and A.E. Torda. Parametrisation of time-averaged distance restraints in MD simulations. *J. Biomol. NMR*, 6:313–320, 1995.
[61] F. Fraternali and W.F. van Gunsteren. Conformational Transitions of a Dipeptide in Water: Effects of Imposed Pathways Using Umbrella Sampling Techniques. *Biopolymers*, 34:347–355, 1994.

[62] T.C. Beutler, T. Bremi, R.R. Ernst, and W.F. van Gunsteren. Motion and Conformation of Side Chains in Peptides. A Comparison of 2D Umbrella-Sampling Molecular Dynamics and NMR Results. *J. Phys. Chem.*, 100:2637–2645, 1996.
[63] W.R.P. Scott, A.E. Mark, and W.F. van Gunsteren. On using time-averaging restraints in molecular dynamics simulation. *J. Biomol. NMR*, 12:501–508, 1998.
[64] A.E. Torda, R.M. Brunne, T. Huber, H. Kessler, and W.F. van Gunsteren. Structure refinement using time-averaged J-coupling constant restraints. *J. Biomol. NMR*, 3:55–66, 1993.
[65] A.P. Nanzer, A.E. Torda, C. Bisang, C. Weber, J.A. Robinson, and W.F. van Gunsteren. Dynamical Studies of Peptide Motifs in the Plasmodium falciparum Circumsporozoite Surface Protein by Restrained and Unrestrained MD Simulations. *J. Mol. Biol.*, 267:1012–1025, 1997.
[66] B. Keller, M. Christen, C. Oostenbrink, and W.F. van Gunsteren. On using oscillating time-dependent restraints in MD simulation. *J. Biomol. NMR*, 37:1–14, 2007.
[67] A. Pardi, M. Billeter, and K. Wüthrich. Calibration of the angular dependence of the amide proton-Cα proton coupling constants, $^3J_{\mathrm{HN}\alpha}$, in a globular protein. Use of $^3J_{\mathrm{HN}\alpha}$ for identification of helical secondary structure. *J. Mol. Biol.*, 180:741–751, 1984.
[68] A. DeMarco, M. Llinás, and K. Wüthrich. Analysis of the ^{1}H-NMR spectra of ferrichrome peptides. I. The non-amide protons. *Biopolymers*, 17:617–636, 1978.
[69] A. DeMarco, M. Llinás, and K. Wüthrich. ^{1}H-^{1}5N spin-spin couplings in alumichrome. *Biopolymers*, 17:2727–2742, 1978.
[70] V. F. Bystrov. Spin-spin coupling and the conformational states of peptide systems. *Prog. NMR Spectr.*, 10:41–81, 1976.
[71] M. Christen, B. Keller, and W.F. van Gunsteren. Biomolecular structure refinement based on adaptive restraints using local-elevation simulation. *J. Biomol. NMR*, 39:265–273, 2007.
[72] N. Hansen, F. Heller, N Schmid, and W.F. van Gunsteren. Time-averaged order parameter restraints in molecular dynamics simulations. *J. Biomol. NMR*, 60:169–187, 2014.
[73] E.R. Henry and A. Szabo. Influence of vibrational motion on solid state line shapes and NMR relaxation. *J. Chem. Phys.*, 82:4753 – 4761, 1985.
[74] D. Waasmaier and A. Kirfel. New analytical scattering-factor functions for free atoms and ions. *Acta Crystallogr.*, A51:416–431, 1995.
[75] P. Gros, W.F. van Gunsteren, and W.G.J. Hol. Inclusion of Thermal Motion in Crystallographic Structures by Restrained Molecular Dynamics. *Science*, 249:1149–1152, 1990.
[76] T. A. Jones, J. Y. Zuo, S. W. Cowan, and M. Kjeldgaard. Improved methods for building protein models in electron density maps and the location of errors in these models. *Acta Crystallogr.*, 47A:110–119, 1991.
[77] M. S. Chapman. Restrained real-space macromolecular atomic refinement using a new resolution-dependent electron-density function. *Acta Crystallogr.*, A51:69–80, 1995.
[78] A. de Ruiter and C. Oostenbrink. Protein-ligand binding from distancefield distances and Hamiltonian replica exchange simulations. *J. Chem. Theor. Comput.*, 9:883 – 892, 2012.
[79] E. W. Dijkstra. A note on two problems in connexion with graphs. *Numer. Math.*, 1:269–271, 1959.
[80] B. Tidor. Simulated annealing on free energy surfaces by a combined molecular dynamics and Monte Carlo approach. *J. Phys. Chem.*, 97:1069–1073, 1993.
[81] Z. Liu and B.J. Berne. Method for accelerating chain folding and mixing. *J. Chem. Phys.*, 99:6071–6077, 1993.
[82] X. Kong and C.L. Brooks III. λ-dynamics: A new approach to free energy calculations. *J. Chem. Phys.*, 105:2414–2423, 1996.
[83] H. Hansen and P.H. Hünenberger. Ball-and-stick local elevation umbrella sampling: molecular simulations involving enhanced sampling within conformational or alchemical subspaces of low internal dimensionalities, minimal irrelevant volumes and problem-adapted geometries. *J. Chem. Theory Comput.*, 6:2622–2646, 2010.
[84] H. Hansen, X. Daura, and P.H. Hünenberger. Enhanced conformational sampling in molecular dynamics simulations of solvated peptides: Fragment-based local elevation umbrella sampling. *J. Chem. Theory Comput.*, 6:2598–2621, 2010.
[85] T. Huber, A.E. Torda, and W.F. van Gunsteren. Local elevation: A method for improving the searching properties of molecular dynamics simulation. *J. Comput. Aided Mol. Des.*, 8:695–708, 1994.
[86] O. Engkvist and G. Karlström. A method to calculate the probability distribution for systems with large energy barriers. *Chem. Phys.*, 213:63–76, 1996.
[87] A. Laio and M. Parrinello. Escaping free-energy minima. *Proc. Natl. Acad. Sci. USA*, 99:12562–12566, 2002.
[88] G.M. Torrie and J.P. Valleau. Nonphysical sampling distributions in Monte Carlo free-energy estimation: Umbrella sampling. *J. Comput. Phys.*, 23:187–199, 1977.
[89] H.S. Hansen and P.H. Hünenberger. Using the local elevation method to construct optimized umbrella sampling potentials: calculation of the relative free energies and interconversion barriers of glucopyranose ring conformers in water. *J. Comput. Chem.*, 31:1–23, 2010.
[90] C.D. Christ and W.F. van Gunsteren. Enveloping Distribution Sampling: A method to calculate free energy differences from a single simulation. *J. Chem. Phys.*, 126:184110, 2007.
[91] A. Barducci, G. Bussi, and M. Parrinello. Well-tempered metadynamics: A smoothly converging and tunable free-energy method. *Phys. Rev. Lett.*, 100:020603/1–020603/4, 2008.
[92] I.G. Tironi, R.M. Brunne, and W.F. van Gunsteren. On the relative merits of flexible versus rigid models for use in computer simulations of molecular liquids. *Chem. Phys. Lett.*, 250:19–24, 1996.
[93] W.F. van Gunsteren and M. Karplus. Effect of Constraints on the Dynamics of Macromolecules. *Macromolecules*, 15:1528–1544, 1982.
[94] W.F. van Gunsteren. Constrained dynamics of flexible molecules. *Mol. Phys.*, 40:1015–1019, 1980.
[95] J.-P. Ryckaert, G. Ciccotti, and H.J.C. Berendsen. Numerical Integration of the Cartesian Equations of Motion of a System with Constraints: Molecular Dynamics of n-Alkanes. *J. Comput. Phys.*, 23:327–341, 1977.
[96] S. Miyamoto and P. A. Kollman. SETTLE: An Analytical Version of the SHAKE and RATTLE Algorithm for Rigid Water Models. *J. Comput. Chem.*, 13(8):952–962, 1992.

[97] V. Kräutler, W.F. van Gunsteren, and P.H. Hünenberger. A Fast SHAKE Algorithm to Solve Distance Constraint Equations for Small Molecules in Molecular Dynamics Simulations. *J. Comput. Chem.*, 22:501–508, 2001.
[98] B. Hess, H. Bekker, H.J.C. Berendsen, and J.G.E.M. Fraaije. LINCS: A Linear Contstraint Solver for Molecular Simulations. *J. Comput. Chem.*, 18:1463–1472, 1997.
[99] M. Christen and W.F. van Gunsteren. An approximate but fast method to impose flexible distance constraints in molecular dynamics simulations. *J. Chem. Phys.*, 122:144106, 2005.
[100] M. Christen, A.-P.E. Kunz, and W.F. van Gunsteren. Sampling of rare events using hidden restraints. *J. Phys. Chem. B*, 110:8488–8498, 2006.
[101] R.C. van Schaik, H.J.C. Berendsen, A.E. Torda, and W.F. van Gunsteren. A Structure Refinement Method Based on Molecular Dynamics in Four Spatial Dimensions. *J. Mol. Biol.*, 234:751–762, 1993.
[102] H. Bekker, H.J.C. Berendsen, and W.F. van Gunsteren. Force and virial of torsional-angle dependent potentials. *J. Comput. Chem.*, 16:527–533, 1995.
[103] W.F. van Gunsteren, S.R. Billeter, A.A. Eising, P.H. Hünenberger, P. Krüger, A.E. Mark, W.R.P. Scott, and I.G. Tironi. *Biomolecular Simulation: The GROMOS96 Manual and User Guide*. Vdf Hochschulverlag AG an der ETH Zürich, Zürich, Switzerland, 1996.
[104] C. L. Brooks III D. J. Tobias. Molecular-dynamics with internal coordinate constraints. *J. Chem. Phys.*, 89:5115–5127, 1988.
[105] A. Amadei, G. Chillemi, M. A. Ceruso, A. Grottesi, and A. Di Nola. Molecular dynamics simulations with constrained roto-translational motions: Theoretical basis and statistical mechanical consistency. *J. Chem. Phys.*, 112:9–23, 2000.
[106] R. Fletcher and C.M. Reeves. Function minimization by conjugate gradients. *Comput. J.*, 7:149–154, 1964.
[107] W.F. van Gunsteren and M. Karplus. A Method for Constrained Energy Minimization of Macromolecules. *J. Comput. Chem.*, 1:266–274, 1980.
[108] W.F. van Gunsteren and H.J.C. Berendsen. Computer Simulation as a Tool for Tracing the Conformational Differences between Proteins in Solution and in the Crystalline State. *J. Mol. Biol.*, 176:559–564, 1984.
[109] J. Lautz, H. Kessler, R. Kaptein, and W.F. van Gunsteren. Molecular dynamics simulations of cyclosporin A: The crystal structure and dynamic modelling of a structure in apolar solution based on NMR data. *J. Comput. Aided Mol. Des.*, 1:219–241, 1987.
[110] Polak E. and G. Ribiére. Note sur la convergence de méthodes de directions conjuguées. *Rev. Fr. Inform. Rech. O.*, 3(R1):35–43, 1969.
[111] W.F. van Gunsteren, A.P. Nanzer, and A.E. Torda. Molecular simulation methods for generating ensembles or trajectories consistent with experimental data. In K. Binder and G. Ciccotti, editors, *Monte Carlo and Molecular Dynamics of Condensed Matter Systems*, volume 49 of *Proceedings of the Euroconference*, pages 777–788. SIF, Bologna, Italy, 1996.
[112] L.V. Woodcock. Isothermal molecular dynamics calculations for liquid salts. *Chem. Phys. Lett.*, 10:257–261, 1971.
[113] M.P. Allen and D.J. Tildesley. *Computer simulation of liquids*. Oxford University Press, New York, USA, 1987.
[114] S. Nosé. A molecular dynamics method for simulations in the canonical ensemble. *Mol. Phys.*, 52:255–268, 1984.
[115] S. Nosé. A unified formulation of the constant temperature molecular dynamics methods. *J. Chem. Phys.*, 81:511–519, 1984.
[116] W.G. Hoover. Canonical dynamics: Equilibrium phase-space distributions. *Phys. Rev. A*, 31:1695–1697, 1985.
[117] G.J. Martyna, M.L. Klein, and M. Tuckerman. Nosé-Hoover chains: The canonical ensemble via continuous dynamics. *J. Chem. Phys.*, 97:2635–2643, 1992.
[118] P.H. Hünenberger. Calculation of the group-based pressure in molecular simulations: I. A general formulation including Ewald and particle-particle-particle-mesh electrostatics. *J. Chem. Phys.*, 116:6880–6897, 2002.
[119] B. Oliva and P.H. Hünenberger. Calculation of the group-based pressure in molecular simulations: II. Numerical tests and application to liquid water. *J. Chem. Phys.*, 116:6898–6909, 2002.
[120] H. Bekker and P. Ahlström. The Virial of Angle Dependent Potentials in Molecular Dynamics Simulations. *Mol. Simul.*, 13:367–374, 1994.
[121] E. Paci and M. Marchi. Constant-pressure molecular dynamics techniques applied to complex molecular systems and solvated proteins. *J. Phys. Chem.*, 100:4314–4322, 1996.
[122] G. S. Kell. Precise representation of volume properties of water at 1 atmosphere. *J. Chem. Eng. Data*, 12:66–69, 1967.
[123] B. Gavish, E. Gratton, and C. J. Hardy. Adiabatic compressibility of globular proteins. *PNAS*, 80:750–754, 1983.
[124] M.A. Cuendet and W.F. van Gunsteren. On the calculation of velocity-dependent properties in molecular dynamics simulations using the leap-frog integration algorithm. *J. Chem. Phys.*, 127:184102, 2007.
[125] W.F. van Gunsteren, P.H. Hünenberger, A.E. Mark, P.E. Smith, and I.G. Tironi. Computer simulation of protein motion. *Comput. Phys. Commun.*, 91:305–319, 1995.
[126] P.H. Hünenberger, A.E. Mark, and W.F. van Gunsteren. Fluctuation and Cross-Correlation Analysis of Protein Motions Observed in Nanosecond Molecular Dynamics Simulations. *J. Mol. Biol.*, 252:492–503, 1995.
[127] Z. Lin and W.F. van Gunsteren. On the use of a weak-coupling thermostat in replica-exchange molecular dynamics simulations. *J. Chem. Phys.*, 143:034110, 2015.
[128] W.F. van Gunsteren and H.J.C. Berendsen. A leap-frog algorithm for stochastic dynamics. *Mol. Simul.*, 1:173–185, 1988.
[129] Shi Yun-yu, Wang Lu, and W.F. van Gunsteren. On the approximation of solvent effects on the conformation and dynamics of cyclosporin A by stochastic dynamics simulation techniques. *Mol. Simul.*, 1:369–383, 1988.
[130] W.F. van Gunsteren, T.C. Beutler, F. Fraternali, P.M. King, A.E. Mark, and P.E. Smith. Computation of free energy in practice: choice of approximations and accuracy limiting factors. In W.F. van Gunsteren, P.K. Weiner, and A.J. Wilkinson, editors, *Computer Simulation of Biomolecular Systems, Theoretical and Experimental Applications*, volume 2, pages 315–348. Escom Science Publishers, Leiden, The Netherlands, 1993.
[131] W.F. van Gunsteren. The role of computer simulation techniques in protein engineering. *Protein Eng.*, 2:5–13, 1988.
[132] T.C. Beutler and W.F. van Gunsteren. The computation of a potential of mean force: Choice of the biasing potential in the umbrella sampling technique. *J. Chem. Phys.*, 100:1492–1497, 1994.

[133] W.F. van Gunsteren. Methods for calculation of free energies and binding constants: Successes and problems. In W.F. van Gunsteren and P.K. Weiner, editors, *Computer Simulation of Biomolecular Systems, Theoretical and Experimental Applications*, pages 27–59. Escom Science Publishers, Leiden, The Netherlands, 1989.

[134] L. Wang, Y. Deng, Y. Wu, B. Kim, D.N. LeBard, D. Wandschneider, M. Beachy, R.A. Friesner, and R. Abel. Accurate Modeling of Scaffold Hopping Transformations in Drug Discovery. *J. Chem. Theory Comput.*, 13(1):42–54, 2017.

[135] A.E. Mark and W.F. van Gunsteren. Free Energy Calculations in Drug Design: A Practical Guide. In P.M. Dean, G. Jolles, and C.G. Newton, editors, *New Perspectives in Drug Design*, Proceedings of the 9th Intl. Roundtable, pages 185–200. Academic Press Ltd., 1995.

[136] A.E. Mark, W.F. van Gunsteren, and H.J.C. Berendsen. Calculation of Relative Free Energy via Indirect Pathways. *J. Chem. Phys.*, 94:3808–3816, 1991.

[137] Z. Lin and W.F. van Gunsteren. A comparison of pathway independent and pathway dependent methods in the calculation of conformational free enthalpy differences. *Protein Sci.*, 2015.

[138] J. A. Tembe, B. L.; McCammon. A simple theoretical approach is outlined for calculating differences in the free energy of binding of related ligand-receptor pairs. *Computers & Chemistry*, 8:281–283, 1984.

[139] X. Daura, P.H. Hünenberger, A.E. Mark, E. Querol, F.X. Avilés, and W.F. van Gunsteren. Free Energies of Transfer of Trp Analogs from Chloroform to Water: Comparison of Theory and Experiment and the Importance of Adequate Treatment of Electrostatic and Internal Interactions. *J. Am. Chem. Soc.*, 118:6285–6294, 1996.

[140] A.E. Mark, S.P. van Helden, P.E. Smith, L.H.M. Janssen, and W.F. van Gunsteren. Convergence Properties of Free Energy Calculations: Alpha-Cyclodextrin Complexes as a Case Study. *J. Am. Chem. Soc.*, 116:6293–6302, 1994.

[141] T.C. Beutler, D.R. Béguelin, and W.F. van Gunsteren. Free energy of cavity formation in solvent: Computational, methodological and physical aspects. *J. Chem. Phys.*, 102:3787–3793, 1995.

[142] Shi Yun-yu, A.E. Mark, Wang Cun-xin, Huang Fuhua, H.J.C. Berendsen, and W.F. van Gunsteren. Can the stability of protein mutants be predicted by free energy calculations? *Protein Eng.*, 6:289–295, 1993.

[143] H. Liu, A.E. Mark, and W.F. van Gunsteren. Estimating the Relative Free Energy of Different Molecular States with Respect to a Single Reference State. *J. Phys. Chem.*, 100:9485–9494, 1996.

[144] A.E. Mark, Y. Xu, H. Liu, and W.F. van Gunsteren. Rapid non-empirical approaches for estimating relative binding free energies. *Acta Biochim. Polonica*, 42:525–536, 1995.

[145] C. Peter, C. Oostenbrink, A. van Dorp, and W.F. van Gunsteren. Estimating entropies from molecular dynamics simulations. *J. Chem. Phys.*, 120:2652–2661, 2004.

[146] T.C. Beutler and W.F. van Gunsteren. Umbrella sampling along linear combinations of generalized coordinates Theory and application to a glycine dipeptide. *Chem. Phys. Lett.*, 237:308–316, 1995.

[147] K. S. Shing and K. E. Gubbins. The Chemical-Potential In Dense Fluids And Fluid Mixtures Via Computer-Simulation. *Mol. Phys.*, 46(5):1109–1128, 1982.

[148] J. G. Powles, W. A. B. Evans, and N. Quirke. Non-Destructive Molecular-Dynamics Simulation Of The Chemical-Potential Of A Fluid. *Mol. Phys.*, 46(6):1347–1370, 1982.

[149] G. Jacucci and N. Quirke. Free-Energy Calculations For Crystals. *Lect. Notes Phys.*, 166:38–57, 1982.

[150] K. K. Han. A New Monte-Carlo Method For Estimating Free-Energy And Chemical-Potential. *Phys. Lett. A*, 165(1):28–32, 1992.

[151] K. K. Han. Multiensemble sampling: An alternative efficient Monte Carlo technique. *Phys. Rev. E*, 54(6):6906–6910, 1996.

[152] Y. G. Chen and G. Hummer. Slow conformational dynamics and unfolding of the calmodulin C-terminal domain. *J. Am. Chem. Soc.*, 129(9):2414–2415, 2007.

[153] C. D. Christ and W. F. van Gunsteren. Multiple free energies from a single simulation: Extending enveloping distribution sampling to nonoverlapping phase-space distributions. *J. Chem. Phys.*, 128(17):174112, 2008.

[154] J. D. Chodera, W. C. Swope, J. W. Pitera, C. Seok, and K. A. Dill. Use of the weighted histogram analysis method for the analysis of simulated and parallel tempering simulations. *J. Chem. Theory Comput.*, 3(1):26–41, 2007.

[155] C.D. Christ and W.F. van Gunsteren. Simple, efficient, and reliable computation of multiple free energy differences from a single simulation: a reference Hamiltonian parameter update scheme for enveloping distribution sampling (EDS). *J. Chem. Theory Comput.*, 5:276–286, 2009.

[156] C.D. Christ and W.F. van Gunsteren. Comparison of three enveloping distribution sampling Hamiltonians for the estimation of multiple free energy differences from a single simulation. *J. Comput. Chem.*, 30:1664–1679, 2009.

[157] D. Hamelberg, J. Mongan, and J.A. McCammon. Accelerated molecular dynamics: A promising and efficient simulation method for biomolecules. *J. Chem. Phys.*, 120:11919 – 11929, 2004.

[158] Y. Miao, V.A. Feher, and J.A. McCammon. Gaussian accelerated molecular dynamics: Unconstrained enhanced sampling and free energy calculation. *J. Chem. Theory Comput.*, 11:3584 – 3595, 2015.

[159] J.W. Perthold and C. Oostenbrink. Accelerated enveloping distribution sampling: Enabling sampling of multiple end states while preserving local energy minima. *J. Phys. Chem. B*, 122:5030 – 5037, 2018.

[160] D. Petrov J.W. Perthold and C. Oostenbrink. Toward automated free energy calculation with accelerated enveloping distribution sampling (a-eds). *J. Chem. Inf. Model.*, XXX:XXX – XXX, 2020.

[161] N. Hansen, P.H. Hünenberger, and W.F. van Gunsteren. Efficient combination of environment change and alchemical perturbation within the enveloping distribution sampling (EDS) scheme: twin system EDS and application to the determination of octanol-water partition coefficients. *J. Chem. Theory Comput.*, 9:1334–1346, 2013.

[162] Z. Lin, J.Kornfeld, M. Mächler, and W.F. van Gunsteren. Prediction of folding equilibria of differently substituted peptides using one-step perturbation. *J. Am. Chem. Soc.*, 132:7226–7278, 2010.

[163] Z. Lin, H. Liu, S. Riniker, and W.F. van Gunsteren. On the use of enveloping distribution sampling (EDS) to compute free enthalpy differences between different conformational states of molecules: application to 3_{10}-, α, and π helices. *J. Chem. Theory. Comput.*, 7:3884–3897, 2011.

[164] Z. Lin, C. Necula, and W.F. van Gunsteren. Using enveloping distribution sampling to compute the folding free enthalpy of a β-peptide with a very unstable folded conformation in solution: The advantage of focused sampling using EDS. *Chem. Phys.*, 428:156–163, 2014.
[165] K. Meier, N. Schmid, and W.F. van Gunsteren. Interfacing the GROMOS (bio)molecular simulation software to quantum-chemical program packages. *J. Comput. Chem.*, 2012, DOI: 10.1002/jcc.23047.
[166] M. Christen, P. H. Hünenberger, D. Bakowies, R. Baron, R. Bürgi, D. P. Geerke, T. N. Heinz, M. A. Kastenholz, V. Kräutler, C. Oostenbrink, C. Peter, D. Trzesniak, and W. F. van Gunsteren. The GROMOS software for biomolecular simulation: GROMOS05. *J. Comput. Chem.*, 26:1719–1751, 2005.
[167] W. F. van Gunsteren et al. http://www.gromos.net.
[168] W. Thiel. MNDO99 v. 6.1 ed., Max-Planck-Institut für Kohlenforschung: Mülheim an der Ruhr, Germany, 2003.
[169] R. Ahlrichs et. al. http://www.cosmologic.de/turbomole.html.
[170] N. Schmid, C.D. Christ, M.Christen, A.P. Eichenberger, and W.F. van Gunsteren. Architecture and implementation and parallelization of the GROMOS software for biomolecular simulation. *Comput. Phys. Commun.*, 183:890–903, 2012.
[171] Y. Sugita and Y. Okamoto. Replica-exchange molecular dynamics method for protein folding. *Chem. Phys. Lett.*, 314:141–151, 1999.
[172] Y. Okamoto. Generalized-ensemble algorithms: enhanced sampling techniques for Monte Carlo and molecular dynamics simulations. *J. Mol. Graph. Mod.*, 22:425–439, 2004.
[173] D.; Meng Y. Sindhikara and A. E. Roitberg. Exchange frequency in replica exchange molecular dynamics. *J. Chem. Phys.*, 128:024103, 2008.
[174] J. Hritz and C. Oostenbrink. Hamiltonian replica exchange molecular dynamics using soft-core interactions. *J. Chem. Phys.*, 128:144121, 2008.
[175] X. Periole and A.E. Mark. Convergence and sampling efficiency in replica exchange simulations of peptide folding in explicit solvent. *J. Chem. Phys.*, 126:10, 2007.
[176] A.P.E. Kunz and W.F. van Gunsteren. Enhancing the configurational sampling of ions in aqueous solution using adiabatic decoupling with translational temperature scaling. *J. Phys. Chem. B*, 115:2931–2936, 2011.
[177] D. Steiner, C. Oostenbrink, F. Diederich, M. Zürcher, and W.F van Gunsteren. Calculation of Binding Free Energies of Inhibitors to Plasmepsin II. *J. Comput. Chem.*, 32:1801–1812, 2011.
[178] J. Hritz and C. Oostenbrink. Optimization of replica exchange molecular dynamics by fast mimicking. *J. Chem. Phys.*, 127:204104, 2007.
[179] N.-V. Buchete and G. Hummer. Peptide folding kinetics from replica exchange molecular dynamics. *Phys. Rev. E*, 77:030902(R), 2008.
[180] N.-V. Buchete and G. Hummer. Coarse Master Equations for Peptide Folding Dynamics. *J. Phys. Chem. B*, 112:6057–6069, 2008.

Symbols

Symbol	Meaning
	Common names and abbreviations
GROMOS	The GROMOS software package
MD++	The MD++ simulation engine in C++
GROMOS++	The GROMOS++ analysis package in C++
GROMOS96	The GROMOS96 simulation package (1996)
3D	abbreviation for three dimensions
AA	Atomistic (All Atom) models
BD	Brownian Dynamics simulation
B&S – LEUS	Ball and stick local elevation umbrella sampling
CG	Coarse Grained models
CGEM	Conjugate gradient method for energy minimization
FRCG	Fletcher-Reeves conjugate gradient method for energy minimization
PRCG	Polak-Ribiére conjugate gradient method for energy minimization
COG	Center of geometry
COS	Charge On Spring approach
CP	Car Parrinello approach
DF	Distancefield
DOF	Degrees of freedom (abbreviation)
DPD	Diffusive Particle Dynamics simulation
`doxygen`	Documentation platform
EM	Energy minimisation
EDS	Enveloping distribution sampling
FBC	Fixed boundary conditions
HBC	Hyper-spherical boundary conditions
LE	Local elevation
LEUS	Local elevation umbrella sampling
LS	Lattice-sum method
MC	Monte Carlo sampling
MD	Molecular Dynamics simulation
NOE	Nuclear Overhauser Effect
PBC	Periodic boundary conditions
PPPM	Particle-particle–particle-mesh (P^3M) method
QM	Quantum Mechanical models
QMD	Quantum Molecular Dynamics simulation
RDF	Radial distribution function
RE	Replica Exchange
REMD	Replica Exchange Molecular Dynamics simulation
RF	Reaction-field method
RMSD	Root-mean-square difference
RMSF	Root-mean-square fluctuation
SD	Stochastic Dynamics simulation
SDEM	Steepest descent method for energy minimization
TI	Thermodynamic integration
US	Umbrella sampling

Symbol	Meaning
VBC	Vacuum boundary conditions
	Physical constants
h	Planck's constant [0.3990313 kJ mol^{-1} ps]
$\hbar$	Planck's constant divided by 2π [0.06350780 kJ mol^{-1} ps]
$N_{\rm Av}$	Avogadro's number [6.02214 $\times 10^{23}$]
k_B	Boltzmann's constant [1.380662 $\times 10^{-26}$ kJ K^{-1})]
R	Ideal gas constant ($N_{\rm Av} \times k_B$)
c	Speed of light [2.99792458 $\times 10^5$ nm ps^{-1}]
	Degrees of freedom and system configuration
$\mathcal{N}_d$	Number of degrees of freedom of a system
$\mathcal{N}_a$	Number of particles in a system of particles ($\mathcal{N}_d$ =3$\mathcal{N}_a$)
$\mathcal{N}_a^{solu}$	Number of particles the solute consists of
$\boldsymbol{q}$	$3\mathcal{N}_a$-dimensional generalized coordinate vector of a system of particles
$\boldsymbol{p_q}$	$3\mathcal{N}_a$-dimensional generalized momentum vector of a system of particles
$\boldsymbol{r}$	$3\mathcal{N}_a$-dimensional Cartesian coordinate vector of a system of particles
$\boldsymbol{p}$	$3\mathcal{N}_a$-dimensional Cartesian momentum vector of a system of particles
$\boldsymbol{f}$	$3\mathcal{N}_a$-dimensional Cartesian force vector of a system of particles
$\overline{\boldsymbol{f}}$	$3\mathcal{N}_a$-dimensional Cartesian mean force vector of a system of particles
$\boldsymbol{f}^{st}$	$3\mathcal{N}_a$-dimensional Cartesian stochastic force vector of a system of particles
$\mathbf{f}_i^{st}$	$3\mathcal{N}_a$-dimensional Cartesian stochastic force vector of a system of particles
$\boldsymbol{v}$	$3\mathcal{N}_a$-dimensional Cartesian velocity vector of a system of particles
$\mathbf{r}$	3-dimensional Cartesian coordinate vector of a particle
$\mathbf{p}$	3-dimensional Cartesian momentum vector of a particle
$\mathbf{f}$	3-dimensional Cartesian force vector of a particle
$\mathbf{v}$	3-dimensional Cartesian velocity vector of a particle
Ψ $[\Psi(\boldsymbol{r})]$	Wavefunction (position representation; configuration of a quantum-mechanical system of $\mathcal{N}_a$ particles)
$\{$ $\boldsymbol{r}$,$\boldsymbol{p}$ $\}$	Phase-space point (Cartesian coordinates; configuration of a classical system of $\mathcal{N}_a$ particles)
	(Statistical) thermodynamics
$\mathcal{F}$	Free energy
G	Gibbs free energy
H	Enthalpy
$\mathcal{U}$	Energy of a system
$\mathcal{S}$	Entropy of a system
$\mathcal{Z}$	Partition function
$\mathcal{T}$	Instantaneous temperature
$\mathcal{T}_o$	Reference temperature
$\mathcal{K}$	Instantaneous kinetic energy of a system
$\mathcal{K}_{tr}$	Instantaneous translational kinetic energy
$\mathcal{K}_{ir}$	Instantaneous internal+rotational kinetic energy
$\mathcal{U}$	Instantaneous total potential energy of a system
$\mathcal{W}$	Instantaneous virial of a system
$\mathcal{P}$	Instantaneous pressure of a system
$\mathcal{V}$	Instantaneous volume of a system
ρ_J	Number particle density of particles J
	Miscellaneous

Symbol	Meaning
t	Time
Δt	discrete time step
$\mathcal{N}_t$	Number of MD steps
P	Probability
m	Mass of a particle
M	Mass of the whole system
$\underline{\mathbf{m}}$	Diagonal mass matrix of a system of $\mathcal{N}_a$ particles
γ	Friction coefficient of a particle
$\underline{\gamma}$	Diagonal friction coefficient matrix of a system of $\mathcal{N}_a$ particles
T	Absolute temperature
β	prefactor: $1/k_BT$
τ_T	relaxation time for the coupling to a temperature bath
$\mathbf{s}$	Vector denoting the collection of all force-field parameters
λ	Coupling parameter Lambda for a lambda dependent Hamiltonian
$\mathcal{N}_\lambda$	Number of λ-values in a TI simulation
H	Heaviside function defined as $H(x) = 0 \; \forall \; x < 0$ and $H(x) = 1 \; \forall \; x > 0$
sign	Sign function: $\text{sign}(x) = 1 \; \forall \; x > 0$ and $\text{sign}(x) = -1 \; \forall \; x < 0$
i	imaginary number, $i^2 = -1$
δ_{ij}	general Kronecker delta
σ	Standard deviation
σ^2	Variance
$\mathcal{N}_{conf}$	Number of configurations in an ensemble
D	Diffusion constant
R_{gyr}	radius of gyration
η	the viscosity of a system
$g(r)$	radial distribution function
s	Smoothness parameter in EDS simulations
E^R	Energy offset parameter in EDS simulations
$\mathcal{N}^{(s)}$	Number of states in EDS simulations
Spatial boundary conditions	
$\underline{\mathcal{B}}$	3×3-matrix of the box-edge vectors (columns) in the reference Cartesian coordinate system (PBC)
$\hat{\mathbf{e}}$	Unit vector
$\mathbf{a}$	First edge vector of a (triclinic) box (in the reference coordinate system)
$\mathbf{b}$	Second edge vector of a (triclinic) box (in the reference coordinate system)
$\mathbf{c}$	Third edge vector of a (triclinic) box (in the reference coordinate system)
a	length of first edge of a (triclinic) box
b	length of second edge of a (triclinic) box
c	length of third edge of a (triclinic) box
$\mathbf{T}$	Position vector of the reference corner of a triclinic box (components in the reference coordinate system and vector relative to the origin of this system)
$\underline{\mathbf{L}}$	Computational box matrix (columns defined by the components of edge vectors $\mathbf{a}$, $\mathbf{b}$ and $\mathbf{c}$ in the reference coordinate system)
$\underline{\mathbf{B}}$	Edge length matrix (diagonal, elements a, b and c)
α	First edge angle a triclinic box (between $\mathbf{b}$ and $\mathbf{c}$)
β	Second edge angle a triclinic box (between $\mathbf{a}$ and $\mathbf{c}$)
γ	Third edge angle a triclinic box (between $\mathbf{a}$ and $\mathbf{b}$)
ϕ	First Euler angle of a triclinic box

Symbol	Meaning
θ	Second Euler angle of a triclinic box
ψ	Third Euler angle of a triclinic box
$\check{\mathbf{r}}$	Oblique coordinates of a real-space vector (with reference to the box-edge vectors)
$\check{\mathbf{r}}$	Oblique fractional coordinates of a real-space vector (with reference to the box-edge vectors)
$\check{\mathbf{k}}$	Oblique coordinates of a reciprocal-space vector
$\check{\mathbf{k}}$	Oblique fractional coordinates of a reciprocal-space vector
$\mathbf{l}$	Lattice vector (three-dimensional vector with integer components)
$\mathbf{k}$	Reciprocal-lattice vector ($\mathbf{k} = 2\pi\underline{\mathbf{L}}^{-1}\mathbf{l}$)
$\underline{\mathbf{S}}$	Transformation matrix
$\underline{\mathbf{R}}$	Transformation matrix
$\underline{\mathbf{T}}$	Transformation matrix
Representation of the interaction	
$\hat{\mathcal{H}}$	Hamiltonian operator describing the interaction for quantum-mechanical degrees of freedom
$\hat{\mathcal{K}}$	Kinetic energy operator (kinetic energy contribution to the quantum-mechanical Hamiltonian operator)
$\hat{\mathcal{V}}$	Potential energy operator (potential energy contribution to the quantum-mechanical Hamiltonian operator)
$\mathcal{H}$ $[\mathcal{H}(\boldsymbol{r},\boldsymbol{p})]$	Hamiltonian function describing the interaction for classical degrees of freedom
$\mathcal{K}$ $[\mathcal{K}(\boldsymbol{p})]$	Kinetic energy contribution to the classical Hamiltonian function
$\mathcal{V}$ $[\mathcal{V}(\boldsymbol{r})]$	Potential energy contribution to the classical Hamiltonian function
$\overline{\mathcal{V}}$ $[\overline{\mathcal{V}}(\boldsymbol{r})]$	Potential of mean force contribution to the classical Hamiltonian function
Physical interactions	
φ [Proper dihedral-angle term]	
$\mathcal{V}^{(phys)}$ $[\mathcal{V}^{(phys)}(\boldsymbol{r};\underline{\mathcal{B}};\mathbf{s})]$	Physical potential energy contribution to $\mathcal{V}$
$\mathcal{V}^{(cov)}$ $[\mathcal{V}^{(cov)}(\boldsymbol{r};\underline{\mathcal{B}};\mathbf{s})]$	Covalent potential energy contribution to $\mathcal{V}^{(phys)}$
$\mathcal{V}^{(nbd)}$ $[\mathcal{V}^{(nbd)}(\boldsymbol{r};\underline{\mathcal{B}};\mathbf{s})]$	Non-bonded potential energy contribution to $\mathcal{V}^{(phys)}$
$\mathcal{V}^{(b)}$ $[\mathcal{V}^{(b)}(\boldsymbol{r};\underline{\mathcal{B}};\mathbf{s})]$	Bond stretching potential energy contribution to $\mathcal{V}^{(cov)}$
$\mathcal{V}^{(\theta)}$ $[\mathcal{V}^{(\theta)}(\boldsymbol{r};\underline{\mathcal{B}};\mathbf{s})]$	Bond-angle bending potential energy contribution to $\mathcal{V}^{(cov)}$
$\mathcal{V}^{(\xi)}$ $[\mathcal{V}^{(\xi)}(\boldsymbol{r};\underline{\mathcal{B}};\mathbf{s})]$	Improper dihedral-angle bending potential energy contribution to $\mathcal{V}^{(cov)}$
$\mathcal{V}^{(\varphi)}$ $[\mathcal{V}^{(\varphi)}(\boldsymbol{r};\underline{\mathcal{B}};\mathbf{s})]$	Proper dihedral-angle torsion potential energy contribution to $\mathcal{V}^{(cov)}$
$\mathcal{V}^{(vdw)}$ $[\mathcal{V}^{(vdw)}(\boldsymbol{r};\underline{\mathcal{B}};\mathbf{s})]$	Van der Waals potential energy contribution to $\mathcal{V}^{(nbd)}$
$\mathcal{V}^{(ele)}$ $[\mathcal{V}^{(ele)}(\boldsymbol{r};\underline{\mathcal{B}};\mathbf{s})]$	Electrostatic potential energy contribution to $\mathcal{V}^{(nbd)}$
$\mathcal{V}^{(LJCRF)}$	Sum of the non-bonded potentials $\mathcal{V}^{(vdw)}$ and $\mathcal{V}^{(ele)}$
Physical force-field terms	
$V^{(b)}$ $[V^{(b)}(b;k^{(b)},b^0)]$	Potential energy function associated with the stretching of a single covalent bond (quartic: $V^{(b,q)}$; harmonic: $V^{(b,h)}$; soft harmonic: $V^{(bs,h)}$)
$V_n^{(b)}$ $[V^{(b)}(b_n;k_n^{(b)},b_n^0)]$	Potential energy function associated with the stretching of the nth single covalent bond (quartic: $V_n^{(b,q)}$; harmonic: $V_n^{(b,h)}$; soft harmonic: $V_n^{(bs,h)}$)
$\mathbf{f}^{(b,q)}$	Force due to the bond stretching potential (quartic)
$\mathbf{f}^{(b,h)}$	Force due to the bond stretching potential (harmonic)
$\mathbf{f}^{(bs,h)}$	Force due to the bond stretching potential (soft harmonic)
$N^{(b)}$	Number of covalent bonds in the molecular system
$N^{(bs)}$	Number of soft covalent bonds in the molecular system
$M_n^{(b)}$	Bond type code associated with covalent bond term n

Symbol	Meaning
$b_n \quad [b_n(\boldsymbol{r}, \underline{\mathcal{B}})]$	Length of covalent bond n in the considered configuration
$b_n^0 \quad [b^0(M_n^{(b)}, \mathbf{s})]$	Reference length of covalent bond term n
$k_n^{(b,q)}$	Force constant of stretching for covalent bond term n (quartic potential)
$k_n^{(b,h)}$	Force constant of stretching for covalent bond term n (harmonic potential)
$V^{(\theta)} \quad [V^{(\theta)}(\theta; k^{(\theta)}, \theta^0)]$	Potential energy function associated with the bending of a single covalent bond angle (cosine-harmonic: $V^{(\theta,c)}$; soft cosine-harmonic: $V^{(\theta s,c)}$; angle-harmonic: $V^{(\theta,h)}$)
$V_n^{(\theta)} \quad [V_n^{(\theta)}(\theta_n; k_n^{(\theta)}, \theta_n^0)]$	Potential energy function associated with the bending of the nth covalent bond angle (cosine-harmonic: $V_n^{(\theta,c)}$; soft cosine-harmonic: $V_n^{(\theta s,c)}$; angle-harmonic: $V_n^{(\theta,h)}$)
$\mathbf{f}^{(\theta,c)}$	Force due to the bond angle potential (cosine-harmonic)
$\mathbf{f}^{(\theta s,c)}$	Force due to the bond angle potential (soft cosine-harmonic)
$\mathbf{f}^{(\theta,h)}$	Force due to the bond angle potential (angle-harmonic)
$N^{(\theta)}$	Number of covalent bond angles in the molecular system
$M_n^{(\theta)}$	Bond-angle type code associated with covalent bond-angle term n
$\theta_n \quad [\theta_n(\boldsymbol{r}, \underline{\mathcal{B}})]$	Value of covalent bond angle n in the considered configuration
$\theta_n^0 \quad [\theta^0(M_n^{(\theta)}, \mathbf{s})]$	Reference angle of covalent bond-angle term n
$k_n^{(\theta,c)}$	Force constant of bending for covalent bond-angle term n (cosine-harmonic potential)
$k_n^{(\theta s,c)}$	Force constant of bending for covalent bond-angle term n (soft cosine-harmonic potential)
$k_n^{(\theta,h)}$	Force constant of bending for covalent bond-angle term n (angle-harmonic potential)
$V^{(\xi)} \quad [V^{(\xi)}(\xi; k^{(\xi)}, \xi^0)]$	Potential energy function associated with the bending of a single covalent improper dihedral angle
$V^{(\xi s)} \quad [V^{(\xi s)}(\xi; k^{(\xi)}, \xi^0)]$	Potential energy function associated with the bending of a single covalent improper dihedral angle
$\mathbf{f}^{(\xi)}$	Force due to the improper dihedral-angle potential
$\mathbf{f}^{(\xi s)}$	Force due to the soft improper dihedral-angle potential
$N^{(\xi)}$	Number of covalent improper dihedral angles in the molecular system
$N^{(\xi s)}$	Number of covalent improper dihedral angles in the molecular system
$M_n^{(\xi)}$	Improper dihedral-angle type code associated with covalent improper dihedral-angle term n
$\xi_n \quad [\xi_n(\boldsymbol{r}, \underline{\mathcal{B}})]$	Value of covalent improper dihedral angle n in the considered configuration
$\xi_n^0 \quad [\xi^0(M_n^{(\xi)}, \mathbf{s})]$	Reference angle of covalent improper dihedral-angle term n
$k_n^{(\xi)}$	Force constant of bending for covalent improper dihedral-angle term n
$V^{(\varphi)} \quad [V^{(\varphi)}(\varphi; k^{(\varphi)}, \varphi^0)]$	Potential energy function associated with the torsion of a single covalent proper dihedral angle (symmetric potential: $V^{(\varphi,s)}$; generalized: $V^{(\varphi,g)}$)
$\mathbf{f}^{(\varphi,s)}$	Force due to the symmetric proper dihedral-angle potential
$\mathbf{f}^{(\varphi,g)}$	Force due to the generalized proper dihedral-angle potential
$N^{(\varphi)}$	Number of covalent proper dihedral angles in the molecular system
$M_n^{(\varphi)}$	Proper dihedral-angle type code associated with covalent proper dihedral-angle term n
$\varphi_n \quad [\varphi_n(\boldsymbol{r}, \underline{\mathcal{B}})]$	Value of covalent proper dihedral angle n in the considered configuration
$\varphi_n^0 \quad [\varphi^0(M_n^{(\varphi)}, \mathbf{s})]$	Reference angle (phase shift) of covalent proper dihedral-angle term n
$m_n^{(\varphi)} \quad [m_n^{(\varphi)}(M_n^{(\varphi)}, \mathbf{s})]$	Multiplicity of covalent proper dihedral-angle term n
$k_n^{(\varphi,s)}$	Force constant of torsion for covalent proper dihedral-angle term n (symmetric potential; $\varphi_n^0 = 0, \pi$; $m_n^{(\varphi)} \leq 6$)

Symbol	Meaning
$k_n^{(\varphi,g)}$	Force constant of torsion for covalent proper dihedral-angle term n (generalized potential; $\varphi_n^0 \in [0, 2\pi[$)
q	Partial charge of an atom or site
C_{12}	Van der Waals (Pauli) repulsion coefficient of an atom or site (Lennard-Jones function)
C_6	Van der Waals (London) dispersion coefficient of an atom or site (Lennard-Jones function)
C_{126}	Ratio of Van der Waals coefficients $\frac{C_{12}}{C_6}$ (Lennard-Jones function)
α_{LJ}	Lennard-Jones soft-core switching parameter
α_C	Coulomb soft-core switching parameter
$\mathcal{V}^{(ele,pws)}$ $[\mathcal{V}^{(ele,pws)}(\boldsymbol{r};\underline{\mathcal{B}};\mathbf{s})]$	Pairwise potential energy contribution to $\mathcal{V}^{(ele)}$
$\mathcal{V}^{(ele,slf)}$ $[\mathcal{V}^{(ele,slf)}(\underline{\mathcal{B}};\mathbf{s})]$	Self potential energy contribution to $\mathcal{V}^{(ele)}$
$\mathcal{V}^{(ele,srf)}$ $[\mathcal{V}^{(ele,srf)}(\boldsymbol{r};\underline{\mathcal{B}};\mathbf{s})]$	Surface potential energy contribution to $\mathcal{V}^{(ele)}$
$\mathbf{f}^{(nbd)}$	Force due to the non-bonded forces
$\Psi_{ij}^{(ele)}$ $[\Psi_{ij}^{(ele)}(\boldsymbol{r};\underline{\mathcal{B}};\mathbf{s})]$	Electrostatic influence function associated with the particle pair $i-j$
$\delta_{ij}^{(exc)}$ $[\delta_{ij}^{(exc)}(\mathbf{s})]$	Indicator of non-bonded exclusion for the particle pair $i-j$
$\Psi^{(ele,slf)}$ $[\Psi^{(ele,slf)}(\underline{\mathcal{B}})]$	Electrostatic self influence function
$\psi^{(RF)}$ $[\psi^{(RF)}(\mathrm{x})]$	Influence function at distance x of a particle in RF electrostatics
H $[H(\mathrm{x})]$	Heaviside step function (one if x is positive, zero otherwise)
R_C	Cutoff distance (truncation)
R_{cp}	Short-range cut-off
R_{cl}	Long-range cut-off
R^{cg}	radius of a charge group
N_{cg}	number of atoms belonging to a charge group
R_{RF}	Cutoff distance (onset of the RF continuum; usually set equal to R_C)
ϵ_{RF}	Relative dielectric permittivity of the RF continuum (usually set equal to that of the solvent)
κ_{RF}	Inverse Debye screening length of the RF continuum (usually set to zero)
C_{RF}	Constant characterizing the effect of the RF continuum
$\overline{\mathbf{R}}_{ij}$ $[\overline{\mathbf{R}}_{ij}(\boldsymbol{r})]$	Vector (FBC) or minimum-image vector (PBC) connecting the center of the CG containing particle j to the center of the CG containing particle i (norm $\overline{R}_{ij}$)
$\mathcal{V}^{(ele,pws,RF-CB)}$ $[\mathcal{V}^{(ele,pws,RF-CB)}(\boldsymbol{r};\underline{\mathcal{B}};\mathbf{s})]$	Coulombic pairwise potential energy contribution to $\mathcal{V}^{(ele,pws)}$ (RF electrostatics)
$\mathcal{V}^{(ele,pws,RF-RF)}$ $[\mathcal{V}^{(ele,pws,RF-RF)}(\boldsymbol{r};\underline{\mathcal{B}};\mathbf{s})]$	Distance-dependent pairwise potential energy contribution to $\mathcal{V}^{(ele,pws)}$ (RF electrostatics)
$\mathcal{V}^{(ele,pws,RF-RC)}$ $[\mathcal{V}^{(ele,pws,RF-RC)}(\boldsymbol{r};\underline{\mathcal{B}};\mathbf{s})]$	Distance-independent pairwise potential energy contribution to $\mathcal{V}^{(ele,pws)}$ (RF electrostatics)
$\Psi_{ij}^{(ele,LS-RS)}$ $[\Psi_{ij}^{(ele,LS-RS)}(\boldsymbol{r};\underline{\mathcal{B}};\mathbf{s})]$	Real-space component of electrostatic influence function $\Psi_{ij}^{(ele)}$ (LS electrostatics)
$\Psi_{ij}^{(ele,LS-KS)}$ $[\Psi_{ij}^{(ele,LS-KS)}(\boldsymbol{r};\underline{\mathcal{B}};\mathbf{s})]$	Reciprocal-space component of the electrostatic influence function $\Psi_{ij}^{(ele)}$ (LS electrostatics)
$\mathcal{V}^{(ele,pws,LS-RS)}$ $[\mathcal{V}^{(ele,pws,LS-RS)}(\boldsymbol{r};\underline{\mathcal{B}};\mathbf{s})]$	Real-space pairwise potential energy contribution to $\mathcal{V}^{(ele,pws)}$ (LS electrostatics)
$\mathcal{V}^{(ele,pws,LS-KS)}$ $[\mathcal{V}^{(ele,pws,LS-KS)}(\boldsymbol{r};\underline{\mathcal{B}};\mathbf{s})]$	Reciprocal-space pairwise potential energy contribution to $\mathcal{V}^{(ele,pws)}$ (LS electrostatics)
$\psi^{(LS)}$ $[\psi^{(LS)}(\mathbf{x})]$	Influence function at position $\mathbf{x}$ relative to a particle in LS electrostatics
a	Width of the charge-shaping function
γ $[\gamma(\mathrm{x})]$	Charge-shaping function

Symbol	Meaning
$\hat{\gamma}$ $[\hat{\gamma}\ (\mathrm{x})]$	Fourier transformed charge-shaping function
$\mathbf{E}$	Electric field
$\boldsymbol{\mu}$	Dipole
$\boldsymbol{J}$	
α	Electronic polarisability
$\mathbf{P}$	Polarisation
ϵ	Dielectric permittivity
γ^{pol}	γ to calculate position of off site charge
k^{ho}	harmonic force constant in the COS model
ϕ	Electrostatic potential
Unphysical force-field terms	
$\mathcal{V}^{(spec)}$	Unphysical potential energy
$\mathcal{V}^{(res)}$	Restraint energy
$\mathcal{V}^{(pr)}$	Position restraining potential energy contribution to $\mathcal{V}^{(phys)}$
$\mathbf{f}^{(c)}$	Force due to the position constraints
$k^{(pr)}$	Force constant of an unphysical position-restraining term
$\mathcal{N}^{(pr)}$	number of positionally restrained atoms
l	Lagrange multiplier for position constraints
$\mathcal{V}^{(dr)}$	Distance restraining potential energy contribution to $\mathcal{V}^{(phys)}$
$\mathbf{f}^{(dir)}$	Force due to the atom-atom distance restraints
$k^{(dr)}$	Force constant of an unphysical distance-restraining term
$\mathbf{r}^0$	Equilibrium distance of distance restraint
$N^{(dir)}$	Number of atom-atom distance restraints
d_{CH}	carbon-hydrogen distance
d_{CC}	carbon-carbon distance
τ_{dr}	decay time for time-averaged distance restraining
$\mathcal{V}^{(tr)}$	Dihedral-angle restraining potential energy contribution to $\mathcal{V}^{(phys)}$
$k^{(tr)}$	Force constant of an unphysical dihedral-angle restraining term
$\mathcal{N}^{(tr)}$	number of restrained dihedral angles
$\mathcal{V}^{(Jr)}$	^3J-restraining potential energy contribution to $\mathcal{V}^{(phys)}$
$k^{(Jr)}$	Force constant of an unphysical ^3J-value restraining term
^3J	J-value or J-coupling constant
$^3J^0$	experimental J-value
J	general representation of a J-value
J^0	experimental J-value
ΔJ^0	width of flat-bottom for J-value restraining
a	a in Karplus relation
b	b in Karplus relation
c	c in Karplus relation
τ^s_{Jr}	period of scaling in periodically-scaled J-value restraining
Δt_ω	time period for which scaling is suspended in periodically-scaled J-value restraining
N_{le}	number of bins in J-value local elevation biasing
$w_{\zeta ni}$	weight of gaussian in J-value LE
$\mathcal{V}^{(Fxr)}$	$\mid F \mid$-restraining potential energy contribution to $\mathcal{V}^{(phys)}$
$\mathcal{V}^{(exr)}$	ρ-restraining potential energy contribution to $\mathcal{V}^{(phys)}$
$\mathcal{V}^{(sxr)}$	symmetry restraining potential energy contribution to $\mathcal{V}^{(phys)}$

Symbol	Meaning
k^{xr}	(harmonic) force constant for the crystallographic restraining
k^{sym}	harmonic force constant for the crystallographic symmetry restraining
F	Structure factor amplitude
ρ	Electron density
S	space group of a crystal
N_{sym}	Number of symmetry operations of a space group
$\mathbb{S}$	Symmetry operator $\mathbb{S} = \mathbf{R}\mathbf{r} + \mathbf{t}$
$\mathbf{R}$	Rotation matrix of a symmetry operator
$\mathbf{t}$	Translation vector of a symmetry operator
$\mathcal{V}^{(Sr)}$	S^2-restraining potential energy contribution to $\mathcal{V}^{(phys)}$
$k^{(Sr)}$	Force constant of an unphysical S^2-value restraining term
S^2	S^2-order parameter
$S^{2,0}$	experimental S^2-value
S	general representation of a S^2-value
S^0	experimental S^2-value
$\mathcal{V}^{(df)}$	Distancefield restraining potential energy contribution to $\mathcal{V}^{(phys)}$
$\mathbf{f}^{(df)}$	Force due to the atom-atom distance restraints
$k^{(df)}$	Force constant of an unphysical distance-restraining term
l^0	Equilibrium distance of distance restraint
g_s	Distancefield grid distance
$\mathcal{V}^{(le)}$	Local elevation (LE) energy
$\mathcal{V}^{(bias)}$	bias energy
γ	LE basis function
$k^{(le)}$	LE force constant
$\mathbf{r}^{uc}$	unconstrained atomic positions
N_c	Number of constraints
N_{sh}	number of iterations of the SHAKE algorithm
d^0	constraint length
$\mathbf{f}^{uc}$	unconstrained atomic forces